QUANTUM MECHANICAL CALCULATIONS FOR REARRANGEMENT COLLISIONS OF ELECTRONS, ATOMS, AND MOLECULES

Thesis by
Donald Gene Truhlar

In Partial Fulfillment of the Requirements

For the Degree of
Doctor of Philosophy

California Institute of Technology
Pasadena, California
1970
(Submitted December 1, 1969)

To

Jane

ACKNOWLEDGMENTS

I thank Prof. Aron Kuppermann for acting as research advisor for the work reported here and for his continued interest in my progress in graduate school. In his role as research advisor, he helped me with many discussions.

I thank Dr. David C. Cartwright for his collaboration on "Rearrangement Collisions: Effect of Core Terms, Nonorthogonality, and Conservation of Particle Flux on Approximate Theories" and "Differential and Integral Cross Sections for Excitation of the $2\,^1P$ State of Helium by Electron Impact", Dr. James K. Rice for collaboration on the theoretical study of electron-hydrogen molecule scattering, and Dr. Nicholas W. Winter for his invaluable help and advice on the numerical mathematics and use of the finite difference approximation. I also thank them for their help and discussions on other problems.

I thank Prof. William A. Goddard III, Prof. Vincent McKoy, all the members during the past three years of their research groups and Prof. Kuppermann's research group, Dr. Sandor Trajmar, and Prof. Edward F. Greene for freely providing help and discussions of various aspects of my work. But I want to especially single out from among these helpers Dr. Christopher A. Parr, Prof. Dennis J. Diestler, and Dr. Thomas H. Dunning, Jr., for very important assistance.

Most of all, I thank my wife Jane Truhlar for her patience and understanding, for her help with my work, and for her heroic aid in putting together this thesis.

Much of the work reported here was supported by the Atomic Energy Commission as part of the project "Studies of Chemical Dynamics and Radiation Chemistry" on which Prof. Kuppermann is principal investigator and by the Division of Chemistry and Chemical Engineering of the California Institute of Technology. Much of the preparation of the thesis was supported by the author. The author is grateful for the fellowships, traineeship, and assistantships he received.

The expert typing of part one of the thesis was performed by Mrs. Joan Schuetz of Azusa.

ABSTRACT

Quantum mechanical calculations are presented of approximate scattering cross sections for elastic and inelastic collisions, including rearrangements, for several processes involving electrons, hydrogen (H), helium (He), and potassium (K) atoms, and hydrogen (H_2) and hydrogen halide (HX) molecules. In addition to their interest in terms of the processes themselves, the results are intercompared and compared with previous experimental and theoretical results in such a way as to provide tests of the general usefulness of the various methods used.

Electron scattering is treated using the Born, polarized Born, and Vainshtein-Presnyakov-Sobelman approximations for the direct scattering and thirteen different methods for the exchange scattering. The transitions treated are 1s-1s, 1s-2s, and 2s-2s in H, $1\ ^1S - 2\ ^1P$, $1\ ^1S - 3\ ^1P$, and $1\ ^1S - 2\ ^1S$ in He, and elastic scattering and rovibrational excitation of the ground state of H_2. Most emphasis is placed on impact energies less than about 100 eV but higher energies are also treated. We draw conclusions concerning the accuracy of the various methods for treating the exchange scattering and for calculating integral cross sections and the angular dependences of differential cross sections for small and medium scattering angles. A version of the distorted wave approximation which should often be useful is presented. Some of the results and discussions for scattering off H and for excitation of the $2\ ^1P$ state of He have been presented in two articles and a long abstract which are summarized and referred to in the text.

The statistical phase space theory of Light, Pechukas, and Nikitin is used to calculate cross sections and rate constants for

the reactions H + HX (including two isotopes of H) and K + HCl. The H + HX calculations presented here supplement those already published. The probability of reaction is studied as a function of the incident translational energy and impact parameter and the internal states of the products. A generalized nonstatistical phase space theory is presented which is adiabatic in one limit and equivalent to the statistical theory of Light, Pechukas, and Nikitin in another. Some sample calculations using the new theory on H + HBr reactions are also given.

We present numerical solutions of the three-body Schroedinger equation for the collinear $H + H_2$ and $D + D_2$ chemical reactions on an assumed potential energy surface. The parametrized analytic surface is based on the calculations of Shavitt and coworkers and is thought to be the most accurate surface available. Calculations are performed in one mathematical dimension by the conservation-of-vibrational-energy and vibrational-adiabaticity models. Calculations are presented in two mathematical dimensions which are essentially exact for the collinear collision. The calculations include vibrationally excited reactants and products. The calculations are compared and their relation to and implications for the usual tunneling approximations are discussed.

TABLE OF CONTENTS

PART ONE

ELECTRON-ATOM AND ATOM-MOLECULE COLLISIONS

PART TWO

ELECTRON SCATTERING BY H_2 WITH AND WITHOUT VIBRATIONAL EXCITATION

PART ONE

ELECTRON-ATOM AND ATOM-MOLECULE COLLISIONS

I. INTRODUCTION TO COLLISION THEORY

This chapter contains a brief review of some of the methods and techniques used in collision theory. References to some more detailed discussions and derivations are included. More elementary introductions to scattering theory may be found in many classical mechanics and quantum mechanics texts. There are also many texts and review articles concerned with more advanced aspects of the theory and with applications. Later sections of this thesis describe applications of collision theory to calculate scattering cross sections for processes involving electrons, atoms, molecules, and ions. The purpose of the present section is to provide the background necessary for placing these calculations in perspective in terms of some of the other more and less rigorous methods available for such calculations.

In general we are interested in many-body phenomena. Usually the first step, before applying collision theory, is to reformulate the many-body problem in terms of a few composite particles (or, more esoterically, quasiparticles). When we can neglect the internal structure of these quasiparticles we have achieved an important simplification. However, when the few-quasiparticle model causes appreciable error in the calculation, we want to be able to systematically remove the error by accounting for the internal structure of the quasiparticles. As an example, let us consider the collision of a deuterium atom (D) and a protium molecule (H_2). Let $\vec{r}_{p1}'$, $\vec{r}_{p2}'$, $\vec{r}_{p3}'$, $\vec{r}_{n}'$, $\vec{r}_{e1}'$, $\vec{r}_{e2}'$, and $\vec{r}_{e3}'$ represent the space and spin coordinates of the protons, the neutron, and the electrons, respectively, and let the corresponding symbols without primes denote the space coordinates only. Further let $\underset{\sim}{r}_e' \equiv \vec{r}_{e1}', \vec{r}_{e2}', \vec{r}_{e3}'$. The problems of conversion from the laboratory frame of reference to the center-of-mass coordinate system do not concern us here and

we will refer all these coordinates to the center of mass of the seven-particle system. The wave function for the system can be represented to arbitrary accuracy by the expansion

$$\Psi = \sum_{ijk\ell moq} c_{ijk\ell moq}\, \psi_i(\vec{r}_{p1}')\, \psi_j(\vec{r}_{p2}')\, \psi_k(\vec{r}_{p3}')\, \psi_\ell(\vec{r}_n')\, \psi_m(\vec{r}_{e1}')\, \psi_o(\vec{r}_{e2}')\, \psi_q(\vec{r}_{e3}') \tag{1}$$

where $\{\psi_i\}$ is a complete set of functions. This wave function satisfies the Schroedinger equation

$$(H_7 - E)\,\Psi = 0 \tag{2}$$

where H_7 is the seven-particle Hamiltonian (this development is at least partly formal since the nuclear interaction is not well enough understood to be able to write down the Hamiltonian rigorously). At energies below the MeV range it is a good approximation to consider the deuteron as a quasiparticle without internal structure. Then we rewrite (1) as

$$\Psi = \sum_{ijmoqst} c_{ijmoq,st}\, \psi_i(\vec{r}_{p1}')\, \psi_j(\vec{r}_{p2}')\, \psi_s(\vec{r}_d)\, \psi_m(\vec{r}_{e1}')\, \psi_o(\vec{r}_{e2}')\, \psi_q(\vec{r}_{e3}')\, \psi_t^d(\vec{r}_{p3} - \vec{r}_d,\ \vec{r}_n - \vec{r}_d,\ s_{p3},\ s_n) \tag{3}$$

where s_{p3} and s_n are spin coordinates, $\vec{r}_d$ is the coordinate of the center of mass of the deuteron, and $\{\psi_t^d\}$ are the stationary state eigenfunctions of the deuteron. The advantage of (3) is that the problem reduces to a 6-body problem if we assume

$$c_{ijmoq,\,st} = 0 \qquad \text{if } t \neq 1 \tag{4}$$

which corresponds to the deuteron being in its ground state. For the 6-body problem the Hamiltonian is

$$H_6(\vec{r}_{p1}', \vec{r}_{p2}', \vec{r}_d', \underset{\sim}{r}_e') = \langle \psi_1^d(\vec{r}_{p3} - \vec{r}_d, \vec{r}_n - \vec{r}_d, s_{p3}, s_n) \,| \tag{5}$$

$$H_7(\vec{r}_{p1}', \vec{r}_{p2}', \vec{r}_{p3}', \vec{r}_n', \underset{\sim}{r}_e')| \, \psi_1^d(\vec{r}_{p3} - \vec{r}_d, \vec{r}_n - \vec{r}_d, s_{p3}, s_n)\rangle_{\vec{r}_{p3}, \vec{r}_n}$$

where the subscripts indicate the variables over which the integration is carried out. The 6-body wave function may be rewritten as

$$\Psi = \sum_{ijvu} c_{ijvu}\, \psi_i(\vec{r}_{p1}')\, \psi_j(\vec{r}_{p2}')\, \psi_v(\vec{r}_d')\, \psi_u^{e\ell}(\underset{\sim}{r}_e'; \vec{r}_{p1}', \vec{r}_{p2}', \vec{r}_d') \tag{6}$$

where $\{\psi_u^{e\ell}\}$ are any set of functions which completely span the coordinate and spin space of the three electrons. Note that $\psi_u^{e\ell}$ depends parametrically on the coordinates of the nuclei. Because of the light mass of the electrons relative to the nuclei, the motion of the electrons bound coulombicly to the nuclei is much faster than the nuclear motion except at very large nuclear velocities (corresponding to energies of at least 10 keV). Thus in many low energy atomic and molecular collision processes not involving free electrons the electronic motion adjusts adiabatically to changes in the nuclear positions. Then it is useful to use for the $\psi_u^{e\ell}$ the electronically adiabatic states which are the eigenfunctions defined by

$$(H_3^{e\ell} - E^{e\ell})\, \psi_u^{e\ell} = 0 \tag{7}$$

where

$$H_3^{e\ell} = H_6 - T_{p1} - T_{p2} - T_d \tag{8}$$

and T_a is the kinetic energy operator for particle a. With this set of functions we can often assume that c_{ijvu} is nonzero only for the lowest one or lowest few values of u. The 6-body problem is reduced to a 3-body problem (H_2D) if we assume that

$$c_{ijvu} = 0 \qquad \text{if} \quad u \neq 1 \tag{9}$$

and

$$\begin{aligned} \vec{r}_{H1} &= \vec{r}_{p1} \\ \vec{r}_{H2} &= \vec{r}_{p2} \\ \vec{r}_D &= \vec{r}_d \quad . \end{aligned} \tag{10}$$

[Assumptions with a smaller error than that involved in (9) - (10) can be made by defining appropriate reduced masses but for most cases of interest this is merely a small correction.] The wave function for motion of these three quasiparticles satisfies the Schroedinger equation

$$(H_3 - E)\,\Psi = 0 \tag{11}$$

where

$$H_3(\vec{r}_{H1}, \vec{r}_{H2}, \vec{r}_D) = \langle \psi_1^{el}(\vec{r}_{\sim e}'; \vec{r}_{p1}', \vec{r}_{p2}', \vec{r}_d\,) \,|H_6|\, \psi_1^{el}(\vec{r}_e'; \vec{r}_{p1}', \vec{r}_{p2}', \vec{r}_d\,)\rangle_{\vec{r}_{\sim e}'} \tag{12}$$

and

$$\Psi = \sum_{ijs} c_{ijs}\ \psi_i(\vec{r}_{H1}')\,\psi_j(\vec{r}_{H2}')\,\psi_p(\vec{r}_D'). \tag{13}$$

The assumption of electronic adiabaticity for atomic collisions has been made here in about the simplest possible way. More discussion is given in Appendix 1. Classical mechanics is usually not a good approximation for bound intranuclear motion or bound electronic motion but it sometimes is useful for atomic motion.* Thus we might obtain an approximate solution of the scattering problem by using classical mechanics to solve the 3-body problem with Hamiltonian (12). The classical equations of motion, however, have no provision for changes in the internal energy and structure of the composite particles and the assumption of electronic adiabaticity could not be systematically removed within this semiclassical model. By the quantum mechanical close coupling approximation we can treat the three-composite-body problem (5) - (6) in such a way that we can systematically either make or not make the assumption (9).

It is possible to reduce the D + H - H example problem further to a two-composite-particle problem (D + H_2). This might be useful for the study of nonrearrangement collisions. If, however, we are

---

* Classical mechanics has also been applied to electron scattering, sometimes with surprisingly good success (see, e.g., Gr59, Ba69, Ma69, and references therein).

interested in the chemical reaction to form HD or the dissociation reaction to form 3 atoms, then the problem is a rearrangement and is intrinsically a three-body problem (in this case, three composite bodies). The scattering theory for rearrangement collisions is more difficult than that for nonrearrangement collisions and some of the problems have not been solved even formally. Technically, even the elastic scattering of D from H_2 or the vibrational excitation of H_2 caused by a collision with D involve rearrangement collisions because the electrons may exchange during the collision. However, if it is a good approximation to treat the collision in terms of one or a few electronically adiabatic electronic states then this exchange effect can be included in the calculation of the potential energy surface [i.e., during the solution of eq. (7)] and need not be included explicitly in the scattering problem. Then we do not need to use the theory of rearrangement collisions for such problems.

We next consider in more detail the close coupling method of describing scattering problems. We also discuss a.) how various simpler methods such as first order perturbation theory, the semiclassical theory of scattering, and the optical model arise as approximations to the complete quantum mechanical theory which are valid under special circumstances, b.) the relation of the close coupling theory to the direct numerical solution of the Schroedinger equation, c.) nonrearrangement and rearrangement collisions for the case where the (composite) particles are distinguishable, d.) special effects on the scattering theory due to the quantum mechanical indistinguishability of identical particles.

A. Distinguishable Particles

In this section we will treat all the particles as if they are distinguishable. The changes which must be made in the theory when this is not the case are considered in the next section.

1. State Expansion Methods for Nonrearrangements and General Discussion

Let us first consider the cases of elastic and inelastic nonrearrangement collisions such as the collision of the composite particles A and B. The wavefunction for this system can be expanded as

$$\Psi = \sum_{ij} F_{ij}(\vec{R})\ \psi_i^A(\underset{\sim}{a})\ \psi_j^B(\underset{\sim}{b}) \tag{14}$$

where $\vec{R} \equiv \vec{r}_A - \vec{r}_B$; $\vec{r}_A$ and $\vec{r}_B$ are the coordinates of the centers of mass of the A and B particles; and $\underset{\sim}{a}(\underset{\sim}{b})$ indicates the whole set of internal coordinates of the component particles of A(B) referred to the center of mass of A(B) as origin, i.e., $\underset{\sim}{a} = \vec{r}_1 - \vec{r}_A$, $\vec{r}_2 - \vec{r}_A$, . . . where $\vec{r}_1$, $\vec{r}_2$, etc., are the coordinates of these component particles. The summation sign in (14) indicates summations over the discrete values of the indices and integrations over the continuous ranges, if any. $\{\psi_i^A\}$ and $\{\psi_j^B\}$ are complete sets of functions chosen for their convenience as expansion basis sets. They are further discussed below. If particle B has no internal structure, then $\psi_i^B = 1$. This is the case, for example, in electron scattering; in that case the wavefunction (14) has (except for the lack of an antisymmetrizer) the form of the configuration interaction

wave function which is commonly used in electronic bound state calculations on atoms and molecules. The difference is that in the case of (14) one of the orbitals satisfies scattering boundary conditions instead of vanishing at infinity. For the general cases, we decompose the Hamiltonian H as

$$H(\underset{\sim}{a}, \underset{\sim}{b}, \vec{R}) = T_o(\vec{R}) + H_o(\underset{\sim}{a}, \underset{\sim}{b}) + V(\underset{\sim}{a}, \underset{\sim}{b}, \vec{R}) \tag{15}$$

where $T_o(\vec{R})$ is the kinetic energy operator for relative A - B motion and

$$H_o(\underset{\sim}{a}, \underset{\sim}{b}) \equiv \lim_{R \to \infty} [H(\underset{\sim}{a}, \underset{\sim}{b}, \vec{R}) - T_o(\vec{R})] \tag{16}$$

I.e., H_o is the Hamiltonian of non-interacting A and B and could be written as $H^A(\underset{\sim}{a}) + H^B(\underset{\sim}{b})$. A useful set of functions ψ_i^A, ψ_j^B to use in eq. (14) is the set of eigenfunctions of the separated composite particles. These complete, orthonormal sets of functions satisfy the equations

$$H_o(\underset{\sim}{a}, \underset{\sim}{b})\, \psi_i^A(\underset{\sim}{a})\, \psi_j^B(\underset{\sim}{b}) = (E_i^A + E_j^B)\, \psi_i^A(\underset{\sim}{a})\, \psi_j^B(\underset{\sim}{b}) . \tag{17}$$

Substituting (15) and (17) into

$$(H - E)\, \Psi = 0 , \tag{18}$$

multiplying from the left in turn by each of the products $\psi_i^A\, \psi_j^B$ and integrating over $\underset{\sim}{a}$ and $\underset{\sim}{b}$ we obtain the infinite set of coupled differential equations

$$\langle \psi_i^A \psi_j^B | T_o + H_o - E | \psi_i^A \psi_j^B \rangle_{\underset{\sim}{a},\underset{\sim}{b}} F_{ij}(\vec{R}) = - \sum_{k\ell} \langle \psi_i^A \psi_j^B | V | \psi_k^A \psi_\ell^B \rangle_{\underset{\sim}{a},\underset{\sim}{b}} F_{k\ell}(\vec{R}) . \tag{19}$$

The summation sign again indicates summations of the discrete eigenfunction terms and integration over the continuum ones. Equation (19) is also the equation that is obtained for the functions $F_{k\ell}(\vec{R})$ by applying the Kohn variational method, i.e., the scattering amplitudes calculated from the wavefunction (14) will be stationary to second order in small variations if the expansion functions are solutions of (19) (see, e.g., Ma 65, Chapter XIV, § 2). If we choose our units so that $\hbar = 1$, then

$$E = E_i^A + E_j^B + \langle F_{ij}^o | T_o | F_{ij}^o \rangle_{\vec{R}} \tag{20}$$

$$= E_i^A + E_j^B + (2\mu)^{-1} k_{ij}^2 \tag{21}$$

where $F_{ij}^o = \lim_{R \to \infty} F_{ij}$ and the reduced mass is given by

$$\mu = \frac{m_A m_B}{(m_A + m_B)} \tag{22}$$

in terms of the masses of the colliding particles. Also k_{ij} is the wave number vector of relative motion when the separated particles are in states i and j ($\hbar \vec{k}_{ij} = \mu \vec{v}_{ij}$, where $\vec{v}_{ij}$ is the relative velocity) and the total energy is E. Using (21), we can rewrite the coupled channels eqs. (19) as (see Bu 61, p. 379)

$$(-2\mu\, T_o - k_{ij}^2)\, F_{ij}(\vec{R}) = \sum_{k\ell} U_{ij,\, k\ell}\, F_{k\ell}(\vec{R}) \tag{23}$$

where

$$U_{ij,\, k\ell} = 2\mu \langle \psi_i^A \psi_j^B |V| \psi_k^A \psi_\ell^B \rangle_{\underset{\sim}{a},\, \underset{\sim}{b}} \tag{24}$$

If the initial conditions are particle A in state m approaching particle B in state n with the relative motion in the k_{mn} direction, then the coupled eqs. (19) or (23) must be solved with the boundary conditions (or asymptotic conditions; see, e.g., Me 61, p. 835, Ba 61, p. 381)

$$F_{ij}^{(\pm)}(\vec{k}_{mn}, \vec{R}) \underset{R \text{ large}}{\sim} e^{i\vec{k}_{ij} \cdot \vec{R}}\, \delta_{mn,\, ij} + f_{ij}^{mn}(\vec{k}_{mn}, \hat{R})\, \frac{e^{\pm i k_{ij} R}}{R} \tag{25}$$

where $\hat{R}$ is the unit vector in the $\vec{R}$ direction. Note that the channels are open or closed depending upon whether k_{ij}^2 as computed from (21) is positive or negative. The other conditions on the solution are that Ψ (or, equivalently, each $F_{ij}(\vec{R})$) be finite and continuous everywhere and have a continuous first derivative. The solution (14) with boundary conditions (25) is denoted $\Psi_{mn}^{(\pm)}(\vec{k}_{mn})$. In terms of the asymptotic behavior of the solution the differential cross section for scattering with scattering angles θ, φ (measured from $\hat{k}_{mn}$) and a transition from the states $i = m$, $j = n$ to the states $i = o$, $j = p$ is

given by

$$I_{mn,op} = \frac{v_{op}}{v_{mn}} \left| f_{op}^{mn} (\vec{k}_{mn}, \hat{k}_{op}) \right|^2 \tag{26}$$

where $\hat{k}_{op}$ is a unit vector in the θ, φ direction. The scattering amplitude f_{op}^{mn} can be determined from the asymptotic form of the wave function as in (25) or from (see, for example, Me 61, Chapter XIX, § 19)

$$f_{op}^{mn} (\theta, \varphi) = -\frac{\mu}{2\pi} \langle \psi_o^A(\underset{\sim}{a}) \psi_p^B(\underset{\sim}{b}) e^{i\vec{k}_{op} \cdot \vec{R}} |V| \Psi_{mn}^{(+)}(\vec{k}_{mn}) \rangle \tag{27}$$

$$= -\frac{\mu}{2\pi} \langle \Psi_{op}^{(-)}(\vec{k}_{op}) |V| \psi_m^A(\underset{\sim}{a}) \psi_n^B(\underset{\sim}{b}) e^{i\vec{k}_{mn} \cdot \vec{R}} \rangle \tag{28}$$

The interaction V can be replaced by (H - E) in these two equations if desired. The lack of a subscript after the ket symbol implies an integration over all the coordinates ($\underset{\sim}{a}$, $\underset{\sim}{b}$, and $\vec{R}$). Eq. (27) is called the post interaction formulation and eq. (28) is called the prior interaction formulation.

It is of interest to consider the partial wave expansion for this general two composite body case (Bl 52a). A partial wave expansion is often the first step in a practical calculation. Many different angular momentum coupling schemes are possible. We will consider only one general one as an example. We define the total system angular momentum K and its component K_z which are conserved quantities during the collision. We vectorially add the internal (rotational, electronic, spin) angular momenta I_1 and I_2 of the particles A and B to give a total internal angular momentum S with component S_z and we denote the coupled wave function $\chi_{SS_z}^{\alpha}$

where α denotes remaining quantum numbers. In the case where both particles have no internal angular momentum a typical $\chi^{\alpha}_{SS_z}$ might be $\psi^A_i \psi^B_j$. We let L and L_z be the orbital angular momentum quantum numbers for relative motion of A and B. We define the "channel angular function" for a channel with quantum numbers K, K_z, L, and S as (what is here called L is sometimes called ℓ)

$$\Omega^{\alpha K_z}_{KLS} = \sum_{L_z=-L}^{L} \sum_{S_z=-S}^{S} (LSL_zS_z|LSKK_z) Y_L^{L_z}(\hat{R})\, \chi^{\alpha}_{SS_z} \tag{29}$$

where the Clebsch-Gordan vector-addition coefficient is defined in Co 35. Then (14) is replaced by (we need consider only states with $K_z = S_z$ and we label the initial channel $\alpha' L' S'$; see Bl 52a for more details)

$$\Psi = \sum_{K=0}^{\infty} \sum_{S} \sum_{\substack{L=0 \\ \Delta(KSL)}}^{\infty} \sum_{\alpha} \frac{1}{R\, v_\alpha^{1/2}}\, \Omega^{\alpha K_z}_{KLS}\, F^{K\alpha' L' S'}_{\alpha LS}(R) \tag{30}$$

where v_α is the velocity of relative motion and the triangle inequality $\Delta(K_1K_2K_3)$ means the summation over K_3 is restricted to $|K_1 - K_2| \le K_3 \le (K_1 + K_2)$. Now, substituting this expansion into (18), multiplying by the complex conjugates of the channel angular functions and integrating over $\underset{\sim}{a}$, $\underset{\sim}{b}$, and R, we obtain the coupled set of 1-dimensional differential equations for the $F_\alpha(R)$. There is a separate set of coupled equations corresponding to each value of the total angular momentum K of the system. These are to be solved subject to the boundary conditions

$$F^{K\alpha'L'S'}_{\alpha LS}(R) \underset{R\ \text{large}}{\sim} \delta_{\alpha\alpha'}\,\delta_{LL'}\,\delta_{S'S'}\,e^{-i(k_\alpha R - \frac{1}{2}L\pi)} + S^K_{\alpha LS,\ \alpha'L'S'}\,e^{+i(k_\alpha R - \frac{1}{2}L\pi)} \tag{31}$$

where the $S^K_{\alpha LS,\ \alpha'L'S'}$ are elements of the "scattering matrix" (S matrix). In this way the f^{mn}_{mn} are given as sums of products of $(S^K_{\alpha'LS,\ \alpha'L'S'} - 1)$ and angular factors, and the f^{mn}_{ij} are given by sums over products of $(S^K_{\alpha LS,\ \alpha'L'S'})$ and angular factors. The cross sections are given directly in terms of the S matrix elements as (where primes now denote the final state)

$$\sigma_{\alpha SS_z \to \alpha'S'S_z'} = \frac{\pi}{k_\alpha^2}\,\left| q_{\alpha'S'S_z',\ \alpha SS_z} \right|^2 \tag{32}$$

where

$$q_{\alpha'S'S_z',\ \alpha SS_z} = \sum_{K=0}^{\infty} \sum_{\substack{L \\ \Delta(KSL)}} \sum_{\substack{L' \\ \Delta(KS'L')}} i^{L-L'}(2L+1)^{\frac{1}{2}} (LSOS_z \,|\, LSKS_z)\,(L'S'(S_z - S_z')S_z' \,|\, L'S'KS_z) \tag{33}$$

$$(\delta_{\alpha'\alpha}\,\delta_{S'S}\,\delta_{L'L} - S^K_{\alpha'S'L',\ \alpha SL})\,Y^{S_z - S_z'}_{L'}(\theta,\ \varphi)\,.$$

The integral cross section is the integral of the differential cross section over all scattering angles θ and φ. To obtain the observable cross sections for the $\alpha I_1 I_2 \to \alpha' I_1' I_2'$ transition for the case of unpolarized beams, we must sum over final internal angular momentum directions S_z' and average over initial ones S_z to give

$\sigma_{\alpha S \to \alpha' S'}$ and perform the sum and average

$$\sigma_{\alpha I_1 I_2 \to \alpha' I_1' I_2'} = \sum_{\substack{S \\ \Delta(I_1 I_2 S)}} \sum_{\substack{S' \\ \Delta(I_1' I_2' S')}} \frac{2S+1}{(2I_1+1)(2I_2+1)} \sigma_{\alpha S \to \alpha' S'} \tag{34}$$

Alternatively the asymptotic conditions for the regular solutions of the coupled equations can be taken as

$$F^{K \alpha' L' S'}_{\alpha L S}(R) \underset{R \text{ large}}{\sim} \delta_{\alpha\alpha'} \delta_{LL'} \delta_{SS'} \sin\left(k_\alpha R - \tfrac{1}{2} L \pi\right) + R^K_{\alpha LS,\, \alpha' L' S'} \cos\left(k_\alpha R - \tfrac{1}{2} L \pi\right) \tag{35}$$

instead of eq. (31) where the $R^K_{\alpha LS,\, \alpha' L' S'}$ are elements of the "reactance matrix". In this case the scattering matrix elements can be calculated from

$$\underset{\sim}{S} = (\underset{\sim}{1} - i\underset{\sim}{R})^{-1} (\underset{\sim}{1} + i\underset{\sim}{R}) \tag{36}$$

where $\underset{\sim}{1}$ is the unit matrix. This procedure has some advantages for approximate calculations as discussed in Chapters II and IV. We note from eq. (33) that the probability of a process is really determined by the transition matrix

$$\underset{\sim}{T} = \underset{\sim}{1} - \underset{\sim}{S} \tag{37}$$

and that this is given in terms of the reactance matrix by

$$\underset{\sim}{T} = (\underset{\sim}{1} - i\underset{\sim}{R})^{-1} (-2i\underset{\sim}{R}) \ . \tag{38}$$

Notice that $\underset{\sim}{T}$ and $\underset{\sim}{S}$ are complex while $\underset{\sim}{R}$ is real. The constraint that particle flux be conserved (see, e.g., Ma 65, pp. 324 ff.) places the restrictions on the T matrix that the magnitudes of its diagonal elements must be less than or equal to 2 and the magnitudes of off-diagonal elements must be less than or equal to 1.

In addition to the ease of interpretability, the advantage of the expansion (30) is that coupled one-dimensional equations can be solved numerically in a more straightforward and convenient way. The methods used to solve these coupled equations in actual calculations are discussed in Appendix 2. These methods are an important part of solving the scattering problem because the solution of the close coupling equations is a difficult and complicated matter. In fact, the development of practical, accurate methods of solving the equations delayed progress in the field of molecular scattering for a long time.

Often it is impractical timewise or costwise to solve the full set of close coupled equations (including enough states in the expansion for essentially complete convergence of the solution to the exact one). One systematic approximation scheme is to include only a few states in the expansion (14) or (30). In this case the results depend upon which states are included and it may be possible to achieve a better approximation from an incomplete expansion by choosing functions $\psi_{ij}(\underset{\sim}{a}, \underset{\sim}{b}, \vec{R})$ different from the eigenfunctions of the separated subsystems (this is done, for example, in the method of perturbed stationary states, also called the method of molecular states; see Wu 62, pp. 228-231). This complicates the close coupling equations. In any case, for open channels we should have

$$\lim_{R \to \infty} \psi_{ij}(\underset{\sim}{a}, \underset{\sim}{b}, \vec{R}) = \psi_i(\underset{\sim}{a})\,\psi_j(\underset{\sim}{b}) \tag{39}$$

so that scattering boundary conditions can be imposed. When only one or a few states are included in the expansion it is possible to use the method of Fechbach (Fe 58, Fe 58a) to show formally what kind of effects are being neglected. As an example, we consider the nonrearrangement transition mn → op in more detail by rewriting the expansion (14) as

$$\Psi = \Psi^{mn}_{mn} + \Psi^{mn}_{op} + \tilde{\Psi}^{mnop} \tag{40}$$

where

$$\Psi^{mn}_{mn} \underset{R \text{ large}}{\sim} \psi^{A}_{m}(\underset{\sim}{a})\,\psi^{B}_{n}(\underset{\sim}{b})\left[e^{i\vec{k}_{mn}\vec{R}} + f^{mn}_{mn}(\vec{k}_{mn}, R)\frac{e^{ik_{mn}R}}{R}\right] \tag{41}$$

$$\Psi^{mn}_{op} \underset{R \text{ large}}{\sim} \psi^{A}_{o}(\underset{\sim}{a})\,\psi^{B}_{p}(\underset{\sim}{b})\,f^{mn}_{op}(\vec{k}_{mn}, R)\,\frac{e^{ik_{op}R}}{R} \tag{42}$$

$$\langle \psi^{A}_{q}(\underset{\sim}{a})\,\psi^{B}_{r}(\underset{\sim}{b}) \mid \tilde{\Psi}^{mnop} \rangle_{\underset{\sim}{a},\,\underset{\sim}{b}} \underset{R \to \infty}{\to} 0 \tag{43}$$

where qr = mn or op. Let

$$\tilde{\Psi}^{mnop} = \sum_{\alpha} \Psi_{\alpha} \tag{44}$$

where $\{\Psi_{\alpha}\}$ is a complete basis for the two particles in the space orthogonal to the two functions $\psi^{A}_{m}\,\psi^{B}_{n}$ and $\psi^{A}_{o}\,\psi^{B}_{p}$. Each Ψ_{α} satisfies boundary conditions like (42) or represents a bound AB system. Then the infinite set of coupled equations may be rewritten (see Fe 58 and Ha 66)

$$\langle \psi_i^A \psi_j^B | T_o + H_o - E | \psi_i^A \psi_j^B \rangle_{\underset{\sim}{a},\underset{\sim}{b}} F_{ij}(\vec{R})$$

$$= - \sum_{k\ell = mn,\, op} \langle \psi_i^A \psi_j^B | W | \psi_k^A \psi_\ell^B \rangle_{\underset{\sim}{a},\underset{\sim}{b}} F_{k\ell}(\vec{R}) \tag{45}$$

where ij = m n or o p and

$$W = V + \sum_{\alpha\beta} |\Psi_\alpha\rangle (\underset{\sim}{D}^{-1})_{\alpha\beta} \langle \Psi_\beta | V \tag{46}$$

where

$$D_{\alpha\beta} = \langle \Psi_\alpha | E + i\,0^+ - H | \Psi_\beta \rangle \ . \tag{47}$$

(Note that the lack of a subscript after the $\rangle$ in (46) and (47) indicates the corresponding integrations are over all the variables.) W is a nonlocal, complex potential and Im W is negative definite. The imaginary part of W is nonzero only if at least one channel other than the channels explicitly included in the expansion (in the example, the mn and op channels) is open. This can be seen by making the transformation among the Ψ_α necessary to diagonalize the matrix $\underset{\sim}{D}$ (see Fe 58 for further details). In general, for any set of explicitly included channels, we can define (by its matrix representation) a complex, nonlocal potential which can be used so that the finite expansion gives the exact results. If only one state is explicitly included, this potential is called the optical potential and if more states are included it is the generalized potential (for further discussion and references, see Vo 67). Note that the optical or generalized potential depends on what basis is chosen [i.e., on the form of the $\psi_{ij}(\underset{\sim}{a}, \underset{\sim}{b}, \vec{R})$ for all $\vec{R}$]. Although it is not usually possible

to solve for the exact optical or generalized potential, it is sometimes possible to obtain an approximation to it. For example, we can sum a selected part of the series (46) to include specific effects such as resonance compound states of the target and projectile or adiabatic polarization of the target.

Another class of approximation methods can be obtained by substituting into eq. (27) or (28) a wavefunction Ψ obtained other than by solving the close coupling equations. Using for Ψ the solution to the 1-state close coupling equation yields the distorted wave approximation. This neglects any polarization of the bound state wave functions during the scattering event. (The distorted wave approximation will be discussed again in subsection II.A.2.j.). If the distorted wave solution Ψ is further approximated as

$$\Psi_{ij}^{(\pm)}(\vec{k}_{ij}) = e^{i\vec{k}_{ij}\cdot\vec{R}} \; \psi_i^A(\underset{\sim}{a}) \; \psi_j^B(\underset{\sim}{b}) \qquad (48)$$

we obtain the first Born approximation. This formula for the scattering amplitude can also be derived from the Fermi-Wentzel Golden Rule (see, e.g., Go 66) and represents the result of applying first order perturbation theory to the scattering process. The Born approximation is expected to be accurate when the energy is sufficiently high and/or the interaction potential is sufficiently weak (see, e.g., Ko 54 and Wu 62, p. 42) that the perturbation theory provides a good approximation. Some applications of the Born approximation to electron scattering are given in chapter II. Another approximation can be obtained by putting an approximate optical potential for the one-state equation into eq. (27) or (28) and then approximating the solution Ψ of the one-state equation as in eq. (48). An example of this method is

the polarized Born approximation calculations of electron-molecule scattering which are discussed in Chapter II. In this case the optical potential corresponds to approximately summing terms in eq. (46) which correspond to virtual excitation of excited electronic states of the molecule.

Using the invariance of the Hamiltonian under the operation of time reversal we can show that the scattering matrix and the reactance matrix are symmetric and we can obtain a relation between the cross section or probability for a process and that for its reverse (see, e.g., Ro 67, chapter 10). Some approximation methods yield cross sections which satisfy this relation. Other approximation methods do not necessarily yield cross sections which satisfy this relation. We prefer when possible to use the former methods instead of the latter ones.

By use of procedures like the close coupling method we have been treating the scattering problem as a time-independent quantum mechanical problem by imposing scattering boundary conditions on the solution. It is, in fact, possible to formulate any collision problem in terms of time-independent quantum theory. It is also possible to formulate these problems including the time dependence explicitly. This involves the scattering of wave packets. The time-independent formalism is usually preferred for numerical calculations. (Some examples where the wave packet approach has been used for numerical calculations are Ma 59 and Mc 69.) The formal relationship of the two methods has been discussed many times (see, e.g., Go 64 and Ne 66).

An approach to calculations which differs from the close coupling theory is to forsake quantum mechanics for the relative motion of the colliding subsystems at the very beginning. Then their collision trajectory is calculated classically and the change in

internal states of the subsystems is calculated by full time-dependent quantum mechanics (see, e.g., Ba 62, Os 63 or Ke 66) or by the first order (quantum mechanical) time-dependent perturbation theory (see, e.g., Sh 65, Fl 69, and references therein) where the time-dependence of their interaction is calculated from the trajectory. The difficulties with this approach are that it is hard to systematically improve it and to account for the effect back on the trajectory of changes in the internal motion. Nevertheless this method can yield useful and accurate results in some circumstances. Recently, the formalism necessary to account for the effect on the classical trajectory of the quantum transitions of the subsystem has been worked out by Pechukas (Pe 69).

2. Rearrangements

In the last subsection we have outlined the close coupling theory for nonrearrangements. In practical applications it is never possible to solve the infinite set of coupled equations and we must work with the truncated ones involving, say, N coupled differential equations. These equations are equivalent to a set of N coupled integral equations (see, e.g., Ne 66, chapter 16). In the case of the scattering of two elementary particles, the kernels of the untruncated set of integral equations are nonsingular and can be represented to an arbitrarily great accuracy by an expansion in a finite number of functions. This means that arbitrarily accurate solutions of the coupled integral equations or the coupled differential equations may be obtained by solving the truncated equations if enough expansion functions are retained. However, in the equations corresponding to systems of three or more particles, the kernel is badly behaved (not

"compact", not "completely continuous"), the set of equations may not be truncated, and numerical calculations are suspect (see Ne 66, p. 555). The bad behavior of the infinite set of coupled equations is directly due to the integration over the continuum states of the target. In practice, if we expect that the wavefunction can be represented accurately by a sum over discrete bound state eigenfunctions of two composite particles, we generally consider this lack of rigor in the truncated equations to be merely an unimportant formal difficulty. The problem, however, obviously cannot be ignored for rearrangements. By incorporating the exact solutions to all the component two-body problems, the integral equation for the many-body wave function can be rearranged to yield a new integral equation with a compact (completely continuous) kernel. This involves a major change in all the equations and the methods used to solve them. Fadeev (Fa 60, Fa 63) was the first to write down the well-behaved equations and to give a complete discussion in this context; the resulting equations are called the Fadeev equations. These equations are similar to those used earlier by Watson (Wa 53, Wa 57). The Fadeev equation formalism has two complicating features not found in the equations for two-body processes. First, it involves nonlocal potentials. (Since the Fadeev equations are usually written as relations among transition operators in momentum space these show up in that the equations require as input the two-body transition amplitudes off-the-energy-shell.) Nonlocal potentials are a general feature of most treatments of rearrangements; a simple example is the exchange potentials which occur in electronic problems. Second, if there is a real three-body term in the interaction potential, the Fadeev equations are not very useful for calculations. A real three-body term is one which cannot be written as the sum of two-body

interactions. There are no three-body terms in electron-atom scattering, for example. But in chemical collision problems we usually treat the atoms as the composite particles and the interaction potential between atoms cannot be realistically written as the sum of pairwise interactions at least in cases where chemical reactions are possible.

[A possible difficulty in using the Fadeev equations for problems involving Coulomb potentials was mentioned in Tr 68. It has been pointed out by Chen, Chung, and Kramer that this is not really a difficulty (Ch 69b).]

The difficulty actually arises in rearrangements because of the fact that a different coordinate system is appropriate for expressing the boundary conditions in the initial and the rearranged channels. Thus if we use the expansion (14) for the wavefunction for the collision A + B, the boundary conditions in the rearranged channels must be expressed in terms of continuum eigenfunctions of A and B. There is then no straightforward way of incorporating <u>all</u> the boundary conditions into the eqs. (23) or into the corresponding coupled integral equations. We seek a procedure by which the wavefunction in each arrangement channel can be expanded or expressed in terms of the coordinates and functions appropriate to that channel and the complications these functions cause in any other channels can be eliminated. The rearranged integral equations of Fadeev are one way to do this and to incorporate all the scattering boundary conditions. Another way to do this is to use projection operators (Fe 62). The relation of the Feshbach projection operator approach to the Fadeev equation approach has been discussed by Hahn (Ha 68). Although the projectors can be very complicated, their use enables us to describe rearrangement collisions exactly in terms of coupled integrodifferential

equations which can be solved numerically (see, e.g., Mi 64 and Vo 68). The coupled equations involve simultaneously state expansions appropriate to each of the possible arrangement channels. Recently Miller has written the coupled equations for rearrangement scattering in a particularly uncomplicated form where the projectors appear implicitly but not explicitly (Mi 69). When account is taken of the reduced masses, different coordinates, and eigenfunction expansions appropriate in the different channel asymptotic regions, the treatment of the cross section in terms of the asymptotic form of the wave-function in each channel and the S matrix theory is easily generalized from the equations given in the last section (see, e.g., Mo 65, p. 436, Ge 69, section 29).

A third method for incorporating the rearrangement scattering boundary conditions into the solution of the wave equation is to use a special coordinate system. We can define a special set of coordinates for the collision process which is correct in either asymptotic region. For example, for the collision $A + BC \rightarrow AB + C$ in one dimension we can define a reaction coordinate s which passes monotonically from $-\infty$ to $+\infty$ as the reaction proceeds. Then we can write the wave-function as

$$\Psi = \sum_i F_i(s)\, \varphi_i(t, s) \tag{49}$$

where t is measured transverse to s. Then we can easily impose scattering boundary conditions in the unrearranged and rearranged channels. The biggest difficulty with this approach is that the coupled equations for the F_i become very complicated because of the co-ordinate system. A particular coordinate system like this has been suggested by Marcus (Ma 66a) and used by Rankin and Light (Ra 68,

Li 69, Ra 69). This coordinate system has the advantage that the coupled equations are not too complicated but the disadvantage that the coordinate system is not unique (i.e., three possible s, t pairs can sometimes be used to describe the same point) and the results obtained are not rigorously correct. Their hope is that the method will give accurate numerical results if the coordinate system is chosen so that the wavefunction is small in the region where the coordinates are nonunique.

A fourth method by which the boundary conditions for the rearrangement can be incorporated is the method of subtracted asymptotics (Ef 68). This method, like the projection operator formalism, leads to coupled integrodifferential radial equations resembling (but more complicated than) the nonrearrangement close coupling equations.

The fifth and last method we consider here is the direct solution of the Schroedinger equation without a state expansion. The asymptotic behavior of the solutions obtained can be analyzed in each channel's asymptotic region in terms of the separated subsystem eigenfunctions. The solution will not generally have the correct boundary conditions but a solution with the correct boundary conditions can be obtained as a linear combination of a finite number of linearly independent solutions with arbitrary boundary conditions (Di 68, Di 68b). This direct solution method is often but not always prohibitively difficult. It can of course also be applied to nonrearrangements, but it has a real advantage for rearrangements because it enables us to avoid the special difficulties and complications associated with imposing rearrangement boundary conditions on coupled channels expansions. This method of separating into steps the numerical work required to obtain a solution of the Schroedinger equation and the problem of insuring correct scattering conditions is

a direct extension of the numerical methods (discussed in Appendix 2) which are used to solve the close coupling equations. The direct numerical solution of the multidimensional Schroedinger equation without a state expansion is discussed in Appendix 3.

As for nonrearrangements, it is also possible to calculate the scattering amplitudes for rearrangements by using nonoptimized trial functions and expressions like eq. (27) or eq. (28) which yield the scattering amplitude in terms of the trial function. In this case the particles are arranged differently in the initial and final states so that H_o is different before the collision than after the collision. Then the post-collision interaction must be used in (27) and the pre-collision interactions in (28). When an approximation scheme yields a different result from eq. (27) than from eq. (28) for the same process, the former is called the post form and the latter the prior form.

Some other aspects of rearrangement collisions have been reviewed recently by Bransden (Br 65) and Watson (Wa 69).

B. Identical Particles

When identical particles are involved in only one or the other of the scattering composite particles and do not become rearranged from one to the other we need only account for them by constructing the internal wavefunctions with the correct permutation and spin symmetry. This does not concern the scattering theory directly.

When the scattering process itself involves identical particles we must consider the quantum mechanical interference between classically distinguishable events. A rigorous and straightforward way to include the effects of the indistinguishability of identical

particles is to apply the Kohn variational method (Ko 48, Br 58) to a trial function like (14) but with the correct permutation and spin symmetry. This leads to a set of coupled integrodifferential equations which are like the previously considered close coupling equations except for the addition of nonlocal exchange potentials (see, e.g., Sm 62).

In this thesis we consider in detail the quantum mechanics of two scattering processes involving identical particles. One is the collision on a line of a hydrogen atom with a hydrogen molecule. In this case we assume that the particles cannot pass through one another because of their repulsive interaction at small distances of approach. Then the ordering of the particles on the line is unchanged throughout the collision and we treat them as distinguishable (for collisions in more dimensions, we would have to treat them as indistinguishable).

The other problem of identical particles we consider is electron-atom and electron-molecule scattering. This problem can be treated by the close coupling method with inclusion of exchange as described already. This requires the use of antisymmetrized trial functions. Then the incident electron spin quantum numbers I_1 and I_{z1} are coupled to the target spin quantum numbers I_2 and I_{z2} to give total system spin quantum numbers Σ and μ. The last two are conserved quantities. Separate sets of close coupled equations are solved for each value of Σ to yield partial cross sections $\sigma^{\Sigma\mu}_{\alpha\to\alpha'}$ and the total cross section is calculated by averaging over the possible values of (Σ, μ) as in eq. (34):

$$\sigma_{\alpha I_2 I_{z2} \to \alpha' I_2' I_{z2}'} = \sum_{\Sigma = |I_2 - \frac{1}{2}|}^{I_2 + \frac{1}{2}} \frac{2\Sigma + 1}{2(2I_2 + 1)} \sigma^{\Sigma\mu}_{\alpha \to \alpha'} . \quad (50)$$

Another method of including exchange is to calculate an approximate wave function as if there were no exchange between the incident electron and the target electrons. Then we can antisymmetrize the wave function just before calculating the scattering amplitudes from it (by using eq. (27) or (28) or any variationally correct expression for the scattering amplitude with antisymmetrized wave functions). This is the method used in chapter II. The first and simplest example of this second method is due to Oppenheimer (Op 28). By antisymmetrizing eq. (48) for the Born approximation, he obtained what is called the Born-Oppenheimer approximation for including exchange. Ochkur has emphasized that application of this second method to approximate wave functions Ψ computed from the close coupling equations without exchange is an easier alternative to solving the close coupling equations with exchange but that it corresponds to a variational solution in a more restricted class of functions (Oc 65).

In summary, formulas like the Born-Oppenheimer formula for including exchange in calculations using a nonoptimized trial function may be derived using eq. (48) if the partial cross sections are calculated from antisymmetrized versions of the trial function with the spins coupled to give Σ and μ for the total system spin quantum numbers (some examples of this procedure are worked out in Ri 69). Using this method the partial cross sections for different total system spin states are additive according to eq. (50). For example, in electron scattering from a doublet atom ($I_2 = \frac{1}{2}$) the singlet ($\Sigma = 0$) and triplet ($\Sigma = 1$) scattering do not interfere.

By treating the particles as distinguishable we can separately calculate amplitudes for direct scattering (no exchange of the incident electron with a bound one) and exchange scattering. These processes are really indistinguishable and interfere. If we call the direct and exchange scattering amplitudes f and g we find upon using anti-symmetrized, spin-eigenfunction versions of the same trial functions used for f and g that the scattering amplitude for a definite spin state Σ can be expressed

$$f^{\Sigma}_{\alpha'\alpha} = a_1 f + a_2 g \tag{51}$$

where a_1 and a_2 depend on Σ, I_2, I_2', etc. We will later denote the amplitude in (47) as $f^{\Sigma}_{\alpha'\alpha}(a_1, a_2)$. The weighted-average of the partial cross sections for well-defined spin states or the sum of the direct and exchange cross sections and their interference term is denoted the total cross section (or the unpolarized beam cross section). In chapter II we calculate f and g as primary quantities, then calculate total cross sections from eqs. (50) - (51) and

$$\sigma^{\Sigma\mu}_{\alpha\to\alpha'} = \frac{k_{\alpha'}}{k_{\alpha}} \left| f^{\Sigma}_{\alpha'\alpha} \right|^2 . \tag{52}$$

Good discussions of the treatment of identical particles in scattering are given in Go 64 and Ro 67. A general treatment of the close coupling equations (including exchange) for electron-atom scattering is given in Dr 65.

II. ELECTRON SCATTERING

This chapter contains a discussion of some aspects of electron scattering from H, He, and H_2. Many numerical calculations have been done; all these calculations used trial functions that were not functionally optimized by a variational principle. There were several motivations for these studies; the most noteworthy are:

1. There has been recently a lot of new experimental data (see, for example, Ku 68, La 68a, and Wi 69) on differential cross sections for inelastic processes for electron impact energies in the intermediate range (about 10-125 eV). There is a need for a simple quantum mechanical framework for interpreting these results. There is also a need to know how well simple theories (such as the Born approximation) predict qualitative and quantitative properties of these cross sections.

The energy dependence of the integral cross sections for elastic scattering and excitation of various types of states (optically allowed excitations, singlet-triplet transitions, etc.) have been studied many times and many of their qualitative features can be predicted empirically or from physical principles or both. At present, the angular dependencies of the differential cross sections are not understood in detail. We hope by adding the present calculations to the small body of experimental and theoretical data now available for the angular dependencies of differential cross sections that the emergence of a deeper and fuller understanding of this topic will be hastened.

2. Electron exchange collisions are examples of rearrangement collisions which are amenable to systematic quantum mechanical treatment. We can test conceptual and calculational procedures on these collisions and perhaps make use of what we learn in treating more complicated rearrangements like chemical reactions.

Electron exchange collisions are also of great interest for their own sake. In the low and intermediate energy regions of interest here the spin-orbit coupling and other relativistic effects (these are discussed in Ke 69) are generally very small. If we neglect these relativistic effects, then direct electron scattering cannot cause transitions involving a change of spin multiplicity of the target. Such transitions are very important and are caused by electron exchange. Since in these cases the total cross section is equal to the exchange cross section, these exchange cross sections are measured in the laboratory in straightforward ways without using polarized beams or targets. Exchange cross sections for some processes where direct and exchange collisions can both contribute have also been measured in the laboratory. Dehmelt, Novick and Peters and Franken, Sands, and Hobart obtained bounds on cross sections for exchange scattering of thermal electrons by alkali atoms by observing depolarization by free electrons of an alkali gas previously aligned by optical pumping (De 58, No 58, Fr 58). Lichten and Schultz measured the ratio of the exchange integral cross section to the total integral cross section for electron scattering from the hydrogen atom with excitation of the 2s state by crossing a monoenergetic electron beam and a polarized atomic beam and analyzing by the selective quenching action of a magnetic field (Li 59). Rubin, Perel, and Bederson obtained exchange differential cross sections for elastic collisions by crossing a polarized alkali atom beam with a monoenergetic electron beam and measuring the partial depolarization of the atom beam (Ru 60). Rubin, Bederson, Goldstein, and Collins applied the same technique for scattering involving electronic excitation of alkali atoms (Ru 69).

The theory of electron scattering from atoms and molecules is reviewed in detail in many places (two excellent sources of information are Ma 65 and Dr 65). We will be particularly interested in some of the more elementary theories of electron scattering. The quantum mechanical formulas involved in these methods are discussed in the following section.

A. Formulas

1. Calculation of Cross Sections from Scattering Amplitudes

In this subsection we give formulas derived using the procedure given in section I.B for treating scattering involving identical particles. The algebra involved in the derivation is not shown.

a. Electron-Hydrogen Atom Scattering. In this case both the initial (i) and final (f) states of the atom are doublets. The exchange cross section is

$$I_{ij}^{ex} = \frac{k_j}{k_i} |g_{ji}|^2 \qquad (1)$$

in terms of the exchange amplitude g_{ji} and the wave numbers k_i and k_j of the initial and final states. The direct cross section is

$$I_{ij}^{d} = \frac{k_j}{k_i} |f_{ji}|^2 \qquad (2)$$

in terms of the direct amplitude f_{ji}. The total cross section is

$$I_{ij}^{t} = \frac{k_j}{k_i} \left\{ \frac{1}{4} \left| f_{ji}^{0}(1,1) \right|^2 + \frac{3}{4} \left| f_{ji}^{1}(1,-1) \right|^2 \right\} \tag{3}$$

in terms of the amplitudes defined in eq. (I. 51).

b. Electron-Helium Atom and Electron-Hydrogen Molecule Scattering. In these cases the initial states of the targets are two-electron (the number of electrons N with which the incident electron can exchange is 2) closed-shell ground states and the final target states may be these ground states (electronically elastic scattering) or excited singlet or triplet states (electronically inelastic scattering). In the first two cases the final target state is a singlet and the cross sections are

$$I_{ij}^{d} = \frac{k_j}{k_i} \left| f_{ji} \right|^2 \tag{4}$$

$$I_{ij}^{ex} = \frac{k_j}{k_i} \left| \frac{1}{2} N g_{ji} \right|^2 \tag{5}$$

$$I_{ij}^{t} = \frac{k_j}{k_i} \left| f_{ji}^{1/2}\left(1, -\frac{1}{2}N\right) \right|^2 . \tag{6}$$

In the case where the final state of the target is a triplet the cross sections are

$$I_{ij}^{d} = 0 \tag{7}$$

$$I_{ij}^{ex} = \frac{k_j}{k_i} \left| \frac{\sqrt{3}}{2} N g_{ji} \right|^2 \tag{8}$$

$$I_{ij}^{t} = \frac{k_j}{k_i} \left| f_{ji}^{1/2}(0, \frac{\sqrt{3}\,N}{2}) \right|^2 . \qquad (9)$$

2. Calculation of Scattering Amplitudes

In this subsection we consider the calculation of the direct and exchange scattering amplitudes for electron scattering from the ground electronic states of the hydrogen and helium atoms and the hydrogen molecule. Most of the methods have been discussed in detail elsewhere; some of the pertinent references are given here. We shall use the following notation:

I_{ij} the differential cross section for the $i \rightarrow j$ process.

N_A number of nuclei (each of charge Z_n) in the target.

N number of electrons in the target. $N = 1$ or 2.

$\vec{R}_n$ vector to the nth nucleus of the target from the center of mass of the target.

$\vec{R}$ the vector to the scattering electron from the center of mass of the target.

$\vec{r}_s$ the vector to the s-th electron from the center of mass of the target.

I, J the electronic quantum numbers of the target in states i, j.

$\vec{k}_i, \vec{k}_j$ the wave number vectors of the incident and scattered electrons, respectively. $\vec{k}_i = m\vec{v}_i/\hbar$.

m the mass of the electron.

$\vec{v}_i, \vec{v}_j$ the velocities of the incident and scattered electrons, respectively.

E_i^A the energy of the atom or molecule in state i .

E the total energy: $E = E_i^A + \frac{\hbar^2}{2m} k_i^2$.

E_i, E_j the kinetic energy of the scattering electron before and after the collision, respectively. $E_i = E - E_i^A$.

Ψ_i atoms: the spatial electronic wave function in state I; molecules: the spatial electronic wave function times the nuclear motion wave function.

U_i the ionization potential of the atom in state i .

θ the angle of scattering; $\theta = \arccos(\hat{k}_i \cdot \hat{k}_j)$.

$\vec{q}$ $\vec{q} = \vec{k}_i - \vec{k}_j$. The momentum transfer is $\hbar\vec{q}$.

f_{ji} direct scattering amplitude for the process involving an $i \rightarrow j$ transition.

g_{ji} exchange scattering amplitude for the process involving an $i \rightarrow j$ transition.

$d\tau$ the product of the differentials of all the volume elements of spatial electronic (and nuclear motion, if a molecule) internal coordinates of the target.

In the following we shall use hartree atomic units. In these units $\hbar = m = a_o = 1$, the charge on an electron is 1, energy is given in hartrees (1 h = 27.210 eV), and integral and differential cross sections are given in a_o^2 and a_o^2/steradian, respectively. We shall also use many abbreviations for scattering theory approximations. Some of these are summarized in Table I. Sometimes energy is given in rydbergs (Ry); $E_i = (a_o k_i)^2$ Ry .

a. Born Approximation. In the Born approximation (B)

$f_{ji} = f_{ji}^{B}$ and $g_{ji} = 0$ where (Be 30)

$$f_{ji}^{B} = -\frac{2}{q^2} N M_{ji} - \delta_{IJ} \frac{2}{q^2} P_{ji} \tag{10}$$

$$M_{ji} = +\frac{q^2}{4\pi N} \int \psi_j^* e^{-i\vec{k}_j \cdot \vec{R}} \sum_{s=1}^{N} \frac{1}{|\vec{R} - \vec{r}_s|} \psi_i e^{i\vec{k}_i \cdot \vec{R}} \, d\tau \, d\vec{R} \tag{11}$$

$$= \int \psi_j^* e^{i\vec{q} \cdot \vec{r}_1} \psi_i \, d\tau \tag{12}$$

$$P_{ji} = \sum_{n=1}^{N_A} Z_n \int \psi_j^* e^{i\vec{q} \cdot \vec{R}_n} \psi_i \, d\tau \quad . \tag{13}$$

Cross sections calculated in the Born approximation satisfy detailed balance. The Born approximation is discussed in subsection I.A.1 and in many textbooks. It does not take into account the quantum mechanical indistinguishability of the scattering electron from the bound electrons. This indistinguishability of electrons is important except at very high impact energies. In section I.B we discussed how we can take this into account by antisymmetrizing the trial function to give the Born-Oppenheimer approximation.

b. Born-Oppenheimer Approximations. In the Born-Oppenheimer approximation (BO or BOP), $f_{ji} = f_{ji}^{B}$ and $g = g^{BO}$ (prior) or g^{BOP} (post) where (Op 28, Ba 50)

$$g^{BO(P)} = -\frac{1}{2\pi}\int \psi_j^*(\vec{r}_1 \cdots \vec{r}_{N+1}) e^{-i\vec{k}_j\vec{r}_1} V^{BO(P)} \psi_i e^{i\vec{k}_i\vec{r}_{N+1}} d\tau d\vec{r}_{N+1} \tag{14}$$

and

$$V^{BO} = \sum_{s=1}^{N} \frac{1}{|\vec{r}_{N+1} - r_s|} - \sum_{n=1}^{N_A} \frac{Z_n}{|\vec{r}_{N+1} - \vec{R}_n|} \tag{15}$$

$$V^{BOP} = \sum_{s=2}^{N} \frac{1}{|\vec{r}_1 - \vec{r}_s|} - \sum_{n=1}^{N_A} \frac{Z_n}{|\vec{r}_1 - \vec{R}_n|} \; . \tag{16}$$

The prior and post approximations are obtained by applying the method discussed in section I. C with plane wave trial functions using eqs. (28) and (27). The results are the same in both formulations if exact bound state wave functions are used. Cross sections computed in the Born-Oppenheimer approximation satisfy detailed balance if exact bound state wave functions are used or if the prior form is used for one direction of reaction and the post form for the other. The Born-Oppenheimer approximation is known to give cross sections which are much too high (Ba 50). In the Born-Oppenheimer-minus-core-terms approximation (BOMC), $f_{ji} = f_{ji}^{B}$ and $g = g^{BOMC}$ where g^{BOMC} is given by an expression like (14) except that the potential is (Ka 66)

$$V^{BOMC} = \frac{1}{|\vec{r}_1 - \vec{r}_{N+1}|} \; . \tag{17}$$

Cross sections computed with this method satisfy detailed balance. For $N > 1$, other expressions for the potential including some but

not all of the core terms have also been employed (Jo 65, Jo 66, Mi 68). These are also called the BOMC approximation.

c. The First Order Approximation in the Methods of Bates, Bassel, Gerjuoy, and Mittleman. The trial functions for the initial and rearranged states are not orthogonal in the Born-Oppenheimer approximation. It has been stated many times in the published literature that this is at least partly responsible for the BO approximation yielding such inaccurate results. Attempts to correct the formula (14) for this nonorthogonality have led to many new procedures including the BOMC approximation, the first order exchange approximation (Fe 32, Be 63, Br 65), and the first order approximation of Bates, Bassel and Gerjuoy, and Mittleman (Ba 58, Ba 60, Mi 61, Mi 62). The last two methods (E1 and BBGM1) are identical for elastic scattering and differ only slightly for electronically inelastic scattering (Tr 68). The BBGM1 approximation is calculated from an expression like (14) except V^{BO} is replaced by

$$V^{BBGM} = V^{BO} - \int \psi_i^* \, V^{BO} \, \psi_i \, d\tau \, . \qquad (18)$$

It is physically reasonable to subtract the second term in (18) since such an averaged interaction should not lead to rearrangements. Mittleman has considered other methods where even more of the interaction is subtracted like this (Mi 62).

d. The Ochkur Approximations. At high energies, the Born-Oppenheimer approximation can be expanded (for fixed q) in inverse powers of k_i. This yields (Bo 62, Oc 63)

$$g_{ji}^{BO(P)} \sim g_{ji}^{BOMC} + O(k_i^{-6}) \tag{19}$$

and

$$g_{ji}^{BOMC} \sim g_{ji}^{O} + O(k_i^{-3}) \tag{20}$$

where

$$g_{ji}^{O} = -\frac{2}{k_i^2} M_{ji} \ . \tag{21}$$

The notation BO(P) refers to the Born-Oppenheimer approximation in either the prior or the post form. Similarly,

$$f_{ji}^{B} \sim f_{ji}^{B} + \text{exactly } 0 \tag{22}$$

i.e., for the Born direct amplitude, there are no terms of higher orders of smallness at large k_i than the first term but for the Born-Oppenheimer approximation there are such terms. Ochkur proposed that these terms of higher order of smallness correspond to higher order effects which cannot be taken into account in first order perturbation theory and that they should therefore be dropped (Oc 63). Thus the Ochkur approximation (O) consists in taking $f_{ji} = f_{ji}^{B}$ and $g_{ji} = g_{ji}^{O}$. We call this the prior formulation because of its relation to the prior Ochkur-Rudge approximation discussed below.

By making an expansion in k_j^{-1} instead of k_i^{-1} we obtain instead (Oc 63, Go 64, pp. 158, 163)

$$g_{ji}^{BO(P)} \sim g_{ji}^{OP} + O(k_j^{-3}) \tag{23}$$

where

$$g_{ji}^{OP} = -\frac{2}{k_j^2} M_{ji} \quad . \tag{24}$$

Using $f_{ji} = f_{ji}^{B}$ and $g_{ji} = g_{ji}^{OP}$ is called the post Ochkur approximation (OP). Ochkur recommended the use of the prior form for excitation processes and the post form for de-excitation processes since then the expansion is in terms of a smaller parameter. Also it is only this particular combination which yields cross sections satisfying detailed balance (Oc 63).

In the Ochkur approximation the amplitude for a specified total spin state is then (with $a_2' = a_2/N$)

$$f_{ji}^{\Sigma}(a_1, a_2) = \left(\frac{a_1}{q^2} + \frac{a_2'}{k_i^2}\right)(-2NM_{ji}) + \frac{a_1}{q^2}(-2P_{ji}\,\delta_{JI}) \quad . \tag{25}$$

The total cross section for scattering off the hydrogen atom is

$$\begin{aligned} I_{ij} = {} & \frac{k_j}{k_i}\left(\frac{1}{q^4} - \frac{1}{q^2 k_i^2} + \frac{1}{k_i^4}\right)(4M_{ji}^2) \\ & + \frac{k_j}{k_i}\delta_{JI}\left[\frac{1}{q^4}(4P_{ji}^2 + 8M_{ji}P_{ji}) - \frac{1}{q^2 k_i^2}(4M_{ji}P_{ji})\right] . \end{aligned} \tag{26}$$

The total cross section for scattering off the helium atom or hydrogen molecule is

$$I_{ij} = \frac{k_j}{k_i}\left(\frac{1}{q^4} - \frac{1}{q^2 k^2} + \frac{1}{4k_i^2}\right)(16 M_{ji}^2)$$

$$+ \frac{k_j}{k_i}\,\delta_{JI}\left[\frac{1}{q^4}(4 P_{ji}^2 + 16 M_{ji} P_{ji}) - \frac{1}{q^2 k^2}(8 M_{ji} P_{ji})\right] \tag{27}$$

for the final target state a singlet and

$$I_{ij} = \frac{k_j}{k_i}(12 M_{ji}^2) \tag{28}$$

for the final target state a triplet.

e. The Ochkur-Rudge Approximations. Rudge noticed that the Ochkur exchange amplitude cannot be derived from an expression of the form (I. 27) or (I. 28) for a choice of trial function which satisfies the correct boundary conditions for any approximation to the scattering amplitudes at all energies. He found a trial function which gives the Ochkur amplitude in the high energy limit, which is correctly normalized and satisfies the correct scattering boundary conditions at all energies, and which yields in eq. (I. 28) the exchange amplitude (Ru 65, Ru 65a)

$$g_{ji}^{OR} = -\frac{2}{(k_j - i\sqrt{2U_i})^2} M_{ji} \tag{29}$$

$$= -e^{2i\xi_{ij}} \frac{2}{k_j^2 + 2U_i} M_{ji} \tag{30}$$

where

$$\xi_{ij} = \arctan\left(\frac{\sqrt{2U_i}}{k_j}\right) . \tag{31}$$

This is called the (prior) Ochkur-Rudge approximation (OR). Similarly, the post form of this exchange amplitude can be shown to be (Cr 66)

$$g_{ji}^{ORP} = \frac{-2}{(k_i - i\sqrt{2U_j})^2} M_{ji} \tag{32}$$

$$= -e^{2i\xi_{ji}} \frac{2}{k_j^2 + 2U_i} M_{ji} . \tag{33}$$

This is called the post Ochkur-Rudge approximation (ORP). The Ochkur-Rudge approximations are nonoptimized-trial-function methods. Rudge and Morrison and van Blerkom made calculations using a similar trial function to calculate the direct amplitude (Ru 65a, Mo 66a, Mo 67, Va 68). We call the method finally adopted by them the Morrison-Rudge method. We use $f_{ji} = f_{ji}^B$ and $g_{ji} = g_{ji}^{OR}$ (or g_{ji}^{ORP}) and the result is called the prior (or post) Born-Ochkur-Rudge approximation. The prior Born-Ochkur-Rudge approximation was first used in Tr 68 and Be 68. The post Born-Ochkur-Rudge approximation was first used in Tr 69a.

Neither of the Ochkur-Rudge approximations for exchange scattering nor the Born-Ochkur-Rudge approximations for the total scattering satisfy detailed balance. Bely suggested that this be corrected by using the exchange amplitude (Be 66, Be 67)

$$g_{ji}^{ORB.I} = - \frac{2}{k_j^2 + 2U_i} M_{ji} \qquad (34)$$

which we call the symmetrized Ochkur-Rudge exchange amplitude (ORB.I). Bely mentioned that the problem of finding what kind of direct scattering amplitude should be used with $g_{ji}^{ORB.I}$ was unsettled. We have used $f_{ji} = f_{ji}^{B}$ and $g_{ji}^{ORB.I}$ and the result is called the symmetrized Born-Ochkur-Rudge approximation (BORB.I). It satisfies detailed balance. It had not been used prior to the calculations discussed in this thesis. Recently Ochkur has derived a result which is identical to the symmetrized Born-Ochkur-Rudge approximation by applying approximations based on the dynamics of the collision process to the matrix elements involved in the Born-Oppenheimer and Ochkur approximations (Oc 69). While he claimed the Ochkur approximation was a correction of the perturbation theory of the Born-Oppenheimer approximation, he considers the new result is an improvement in which something beyond the perturbation theory is added.

f. Unitarizing Procedures. The scattering amplitudes computed by any of the methods above can be expanded in terms of scattering matrix elements (see chapter I). Since these methods are approximations to the scattering amplitude they can be considered to yield approximations to these scattering matrix elements in a straightforward way. An alternative procedure and a less straightforward one is to consider that they yield approximations to the reactance matrix elements. This procedure is applicable only if the approximate scattering amplitude is real and satisfies detailed balance. Then

it can be analyzed to give approximate elements of a real, symmetric reactance matrix. Equation (I. 36) has the property that a scattering matrix calculated from it and from a real, symmetric reactance matrix will always be unitary and symmetric. The calculated cross sections will therefore satisfy the constraints imposed by conservation of particle flux (see subsection I. A. 1). The procedure for unitarizing the scattering matrix this way was originated by Seaton (Se 61) and has been applied many times to direct scattering in the Born approximation (Va 60, Bu 66a, Sa 61, So 61, So 62, So 63, Fo 66, Fo 67). The result is called the unitarized Born approximation (B. II or UBA). This result was recently rediscovered (Ab 68). Bely applied this method to his modification and extension of the Ochkur-Rudge method to calculate exchange scattering from ions (Be 67). The procedure was first applied to exchange scattering from neutrals by the present author and coworkers and the details have been published (Tr 68). We applied the procedure to the Ochkur approximation to obtain the unitarized Ochkur approximation (O. II) and to the symmetrized Ochkur-Rudge approximation to obtain the unitarized Ochkur-Rudge approximation (ORB. II). The method was applied to elastic scattering and electronic excitation. Since then Sloan and Moore have derived and used a unitarized version of the Born-Oppenheimer approximation for elastic exchange scattering from a neutral target (Sl 68).

The Seaton unitarization procedure requires that we obtain approximations to all the reactance matrix elements in some square subblock of the full R matrix. For example, to unitarize the result for $a \rightarrow b$ transitions we must obtain R_{aa}, R_{ab}, and R_{bb} to use the matrix equation (I. 36). Such a procedure includes allowance for back coupling ($a \rightarrow b \rightarrow a$) and competition among two channels. Thus the sum of the transition probabilities to the two states a and b from

either state a or b does not exceed the maximum possible value allowed for that sum by the conservation of particle flux theorem. Similarly we could include R_{ac}, R_{bc}, R_{ad}, R_{bd}, R_{cd}, R_{cc}, and R_{dd} in the analysis and use a 4×4 subblock of the matrix equation. Such a treatment includes back coupling, successive first order transitions ($a \rightarrow c \rightarrow b$), and competition among four channels.

g. The Method of Vainshtein, Presnyakov, and Sobelman. Presnyakov, Sobelman, Vainshtein, and Opykhtin (Va 63, Va 64, Pr 64) attempted to derive an expression for the cross section that takes account of electron-electron repulsion as much as possible. Their result is called the method of Vainshtein, Presnyakov, and Sobelman (VPS). In this method an attempt is made to treat distortion of the scattering electron wave function. They made several mathematical approximations which have been variously criticized (Mc 65, Mo 68a, Ky 69). However, the method has been shown to give good integral cross sections even at intermediate energies (Va 64, Pr 64, Pr 66). This is an empirical reason for doing calculations by the method. The formulas necessary for the calculations are all given in Pr 64. It turns out that the scattering amplitudes can be written in terms of M_{ji} but they differ from the Ochkur approximation results by additional factors involving q. In addition, by taking the ratio of their exchange and direct scattering amplitudes, we find it yields a relatively simple Ochkur-like relation.* We can use this ratio and the Born direct amplitude to obtain yet another approximation to the exchange

---

*An Ochkur-like relation is a relation between the direct and exchange scattering amplitudes which is independent of the structure of the target (except for number of electrons, spin quantum numbers, etc.).

amplitude. We call this amplitude the Born-transferred VPS method (BTVPS); that is, $f_{ji} = f_{ji}^{B}$ and

$$g_{ji}^{BTVPS} = \frac{g_{ji}^{VPS}}{f_{ji}^{VPS}} f_{ji}^{B} \quad . \tag{35}$$

Some of the errors caused by the mathematical approximations in the VPS method may cancel out in the BTVPS method and help us to understand better why the VPS cross sections have been so accurate.

h. Coulomb Wave Approximation. Another attempt to eliminate the orthogonality difficulties associated with the Born-Oppenheimer approximation for electron exchange collisions is called the symmetric approximation or the Coulomb wave approximation (Bo 53, Bo 56, Ka 67). This method uses Coulomb waves as trial functions. These functions are not optimized in any way for the particular process to be studied. There is some question as to how appropriate they are for first order calculations on electron scattering off neutral systems. The question is not completely answered.

Using approximations to the amplitudes in the Coulomb wave approximation, Kang and Foland derived another Ochkur-like relation, i.e., they found that the ratio of their exchange amplitude to their direct amplitude was a quotient which did not depend on the bound state wave functions (Ka 67). We use this relation and the Born direct amplitude to obtain an exchange amplitude. We use this exchange amplitude with the Born direct amplitude to calculate the cross sections. We call this the transferred Kang-Foland approximation (TKF) for the exchange part of the scattering and the Born-TKF approx. (BTKF) for the total scattering. The result is $f_{ji} = f_{ji}^{B}$ and

$g_{ji} = C_{KF}\, g^{O}_{ji}$ where (Ka 67)

$$C_{KF} = \left(\frac{\gamma}{\alpha}\right)^{i/k_i} \left(\frac{\alpha+\beta}{\alpha}\right)^{i/k_j} \frac{F\left(1-i/k_i,\ 1,\ \dfrac{2i(k_i k_j - \vec{k}_i \cdot \vec{k}_j)}{k_i^2 k_j}\right)}{F(i/k_i,\ i/k_j,\ 1;\ \chi)} \qquad (36)$$

and α, β, γ, and χ are defined in terms of k_i, k_j, q, and $\cos\theta$ in Ka 67. $F(u, v, x)$ and $F(u, v, w; x)$ in eq. (36) denote the confluent hypergeometric function and the hypergeometric function, respectively (Ab 64). In the high energy limit, the complex number C_{KF} approaches 1 and the BTKF approximation is equivalent to the prior and post Ochkur approximations. Since Kang and Foland did not use any high-energy expansions to derive the Ochkur-like relation, they said it is valid at all energies. Of course there are many approximations involved.

i. Including Polarization in the Effective Interaction Potential by the Polarized Born and Born-Ochkur-Rudge Approximations. The scattering of an electron is determined by the elements of the potential matrix $\underset{\sim}{V}(\vec{R})$ which occurs in the close coupling equations. The matrix elements are defined by (see subsection I. A. 1)

$$V_{ji}(\vec{R}) = \int \Psi_j^* \, V \, \Psi_i \, d\tau \qquad (37)$$

where V represents the interaction of the scattering electron at the position $\vec{R}$ with the target. We will briefly consider these matrix elements and their effect on the scattering cross sections (we exclude

elastic scattering near zero energy and inelastic scattering near the threshold from this discussion). Long range potentials cause large, forward-peaked cross sections. Thus the integral cross section for any process $i \to j$ is affected most strongly by that part of the $V_{ji}(\vec{R})$ which has the longest range. The close coupling equations contain, in addition to terms involving the $V_{ji}(\vec{R})$, terms due to the possibility of exchange of the incident electron with one of the bound ones. If we attempt instead to account for this exchange by an effective local potential, the potential will be exponentially decreasing at large R because the bound charge distribution is decreasing exponentially there. This short range "potential" is totally responsible for exchange cross sections and is important for large angle scattering in cases where direct and exchange processes compete. Transitions for which direct scattering can contribute usually have differential cross sections which are more forward peaked than exchange cross sections because the $V_{ji}(\vec{R})$ are long ranged. The range of the V_{ji} depends on the electronic quantum numbers I and J of states i and j (see Se 61, Da 68). Let us consider the potential matrix elements $V^{K}_{jJ\ell', iI\ell}(R)$ which occur in the coupled radial equations resulting from making a partial wave expansion of the close coupling equations. Here K is the total angular momentum and ℓ and ℓ' are the initial and final orbital angular momenta of the scattering electron. We will abbreviate this quantity as V(j, i, R). For atoms if i = j or I and J are both S states, V(j, i, R) decreases exponentially at large R. For molecules, the presence of a permanent dipole moment or quadrupole moment means that $V^{K}_{jI\ell', iI\ell}$ decreases as R^{-2} or R^{-3}, respectively, at large R. If the $I \to J$ transition is optically allowed by electric dipole selection rules, the transition can occur with a change of the orbital angular momentum of the scattering electron equal to $\Delta\ell = \pm 1$.

Then $V(j,i,R)$ decreases as R^{-2} at large R. Other transitions $I \rightarrow J$ which are not forbidden optically by the spin selection rules can occur by direct scattering with $\lambda \equiv |\ell' - \ell| \geq 2$. Then $V(j,i,R)$ is decreasing as $R^{-\lambda-1}$ at large R (Se 61).

Now consider the generalized optical potential method where we consider explicitly only the initial and final states but use the generalized potentials $W(j,i,R)$ instead of $V(j,i,R)$. This method was discussed in subsection I.A.1. The inclusion of the corrections

$$V'(j,i,R) = W(j,i,R) - V(j,i,R) \tag{38}$$

in the 2-state close coupling-like equations makes them yield exact cross sections for the $i \rightarrow i$, $i \rightarrow j$, and $j \rightarrow j$ processes. A discussion of how these corrections account for virtual and real transitions to other states is given in subsection I.A.1. The charge of the incident electron induces a dipole moment in the target. This mechanism is responsible for the fact that $V'(j,i,R) \sim a_{\ell'\ell}\,\alpha_{ji}/2R^4$ at large R where $a_{\ell'\ell}$ is a constant and α_{ji} can be computed by second order perturbation theory (see, e.g., Pu 63, Da 68). This result is based on the adiabatic approximation (assumption that the electron velocity relative to the target is slow compared to the velocities of the bound electrons) which is accurate at large R even at high energy (E > 100 eV). But for $E_i > 100$ eV, the adiabatic theory may begin to overestimate the polarization even at long distances. At even higher energies (say 10 keV) the polarization effect becomes negligible. If the first order approximations which are used to derive the Born approximation from the close coupling equations are applied instead to the generalized optical potential method coupled equations we obtain a plane wave approximation just like the Born approximation except that the

generalized potential replaces the direct potential $V_{ji}(\vec{R})$. This too was discussed in subsection I. A. 1. We can thus sometimes obtain better results by adding a correction term V' to the usual potential. We have used this approximation where V' is based entirely on considerations of the dipole polarization of the target by the electron charge.* The resulting theory is called the dipole polarized Born approximation or simply the polarized Born approximation. We can also include an exchange amplitude in the calculation. When this is done using the prior Ochkur-Rudge exchange approximation, the result is called the polarized Born-Ochkur-Rudge approximation.

Now consider when the use of the polarized Born approximation (B/P) is expected to provide important qualitative differences from the Born approximation (B). For $S \rightarrow P$ transitions in atoms

$$V(j, i, R) \sim O(R^{-2})$$

$$V'(j, i, R) \sim a_{\ell'\ell}\alpha_{ji}/2R^4 .$$

Since we include the longest range effects without including the polarization, we expect the B theory to give the correct angular dependence at small scattering angles. For $S \rightarrow S$ transitions in atoms $V'(j, i, R)$

---

* The charge of the electron induces monopole, dipole, quadrupole, octupole, and higher order momenta in the target. These moments lead, respectively, to effective interactions which at large R are decreasing exponentially and as R^{-4}, R^{-6}, R^{-8}, and so forth. The induced dipole moment is thus the most important term for small angle scattering and integral cross sections.

is longer range than $V(j, i, R)$. Thus we expect that the experimental differential cross section for $S \rightarrow S$ transitions will have a larger forward peak than is predicted by the B theory and the B theory will be more accurate for $S \rightarrow P$ transitions than for $S \rightarrow S$ transitions. We should use the B/P theory for $S \rightarrow S$ transitions. For elastic scattering from S state atoms, the direct potential is short range and it is necessary to include polarization. For example, it has long been known that it is necessary to include polarization for a qualitatively correct description of elastic electron scattering from the helium atom (Kh 64, Kh 65). For elastic scattering from homonuclear diatomic molecules, the longest range part of the potential $V_{ji}(\vec{R})$ in the static approximation is the asymmetric R^{-3} potential due to the charge-quadrupole interaction. The polarization leads to an R^{-4} effective potential $V_{ji}(\vec{R})$ with symmetric and asymmetric parts. Since the asymmetric potentials average to zero and the symmetric potentials do not, it turns out (as is shown in part two of this thesis) that the inclusion of polarization is necessary for a qualitatively correct description of the scattering in this case also.

Further discussion of and details of the use of the polarized Born and polarized Born-Ochkur-Rudge approximations are given in part two of this thesis.

j. The Restricted sp-Distorted Wave Approximation and the Polarized Restricted sp-Distorted Wave Approximation. The partial waves corresponding to the lowest orbital angular momenta ℓ of the scattering electron are the ones which semiclassically correspond to the smallest impact parameters. Because of the centrifugal potential the higher partial waves do not penetrate as close to the center of the target (where the interaction is generally very strong)

as the s and p partial waves do. Thus the s and p waves are the ones where distortion is most likely to be important. Calculations including the effects of distortion are usually done in a partial wave expansion. At higher energies and at medium energies when long range potentials are present many partial waves will be required. Since the calculations are complicated it is usual to include only the lowest partial waves where the scattering probability is high. The small probability of scattering in each of many higher partial waves can have an important effect on the small angle differential cross sections and the integral cross sections. The calculations including distortion are often corrected for this by adding the results of Born calculations for some of the higher partial waves (see, e.g., Bu 63, Sc 65, and Tr 69a). The Born approximation is more accurate for these higher partial waves for which the interaction is small than for the partial waves with smaller ℓ. However, it is more difficult to carry out the plane wave approximation calculations in a partial wave expansion than by using the unexpanded plane waves (which include all the partial waves). To take into account only distortion of the lowest two partial waves it is easier to compute the whole Born approximation amplitude, subtract that part of it due to scattering with $\ell = 0$ and $\ell = 1$, and add the contribution from $\ell = 0$ and $\ell = 1$ in a distorted wave approximation. A procedure for doing this in electron-homonuclear diatomic molecule scattering (the procedure could be used for electron-atom scattering by considering it to be a special case) is given in this thesis in part two, section I.C. This particular procedure uses the restricted distorted wave approximation (Ta 54, see Cu 69) as discussed there. It is expected that this procedure will cure one of the most glaring weaknesses of the Born, Ochkur, and Born-Ochkur-Rudge approximations and their

polarized versions. This weakness is that these theories often predict differential cross sections which are too small at large scattering angles by more than an order of magnitude.

k. Close Coupling Approximation and Discussion of Methods. The close coupling approximation is discussed in chapter I. The close coupling approximation using the atomic eigenfunctions is very slowly convergent for many electron scattering processes (see, e.g., Bu 62c, Bu 63, Bu 63a). The reason that the close coupling approximation with inclusion of only a few target eigenstates is bad is the difficulty of adequately representing the target polarization and the electron-target correlation in terms of only a few eigenstates. Various methods of improving the close coupling approximation to correct these deficiencies have been suggested and tried (Ga 64, Ga 65, Ga 65a, Bu 66, Ta 67, Da 68, Pe 68, Bu 69a). While these methods are promising, close coupling calculations will remain complicated and difficult. Since some of the methods which are easier to apply give better agreement with experiment than close coupling calculations (see, e.g., Cr 65, Ru 65a, Tr 69a) it is worthwhile to study them in detail, not only because of their empirical value, but also to attempt to understand their success in physical and mathematical terms.

While it is not possible to completely separate the various effects involved in the scattering, it is interesting when discussing the methods given in sections a through i to make an approximate separation. The 1-state close coupling approximation is called the static approximation if exchange of the incident electron is neglected and the exchange approximation if it is included. The static approximation includes distortion and back coupling but does not include

polarization of the target or strong coupling of other states. In a plane wave calculation we neglect distortion. In the other calculations using nonoptimized trial functions we account for it in only a very approximate way. By the 1-state unitarization procedure we account approximately for back coupling. We can account approximately for polarization by adding a polarization potential to the potential in the single channel equation or to the potential in the nonoptimized trial function calculation. By actually solving the close coupling equations including the excited target states responsible for the polarization we can more easily account for the nonlocality of the polarization potential. Further, if these excited states are open channels, the close coupling method also includes the effects of strong coupling. We can approximately include the effects of strong coupling in calculations which do not use close coupling by using the n-state unitarization procedure (where $n \geq 2$) as discussed in subsection II.A.2.f. In close coupling calculations including exchange the effects of exchange on the distortion and polarization and the effects of distortion and polarization on exchange are fully included. In the calculations using nonoptimized trial functions these second order effects are not easily included. They can sometimes be important. Another effect which is included in a close coupling calculation is electron correlation. By electron correlation we mean the representation in the wave function of the effects of the Pauli principle and the electron repulsion on the detailed electronic motion when all the electrons are near the atom (or molecule); this includes, for example, the cusp in the many electron wave function when the coordinates of two electrons are equal. Most of the unoptimized trial function methods treat electron correlation very incompletely and indirectly, if at all.

We have performed many calculations using the methods discussed in this subsection (subsection II.A.2). In section II.B we summarize some of the conclusions concerning these methods' usefulness which we have been able to draw from these calculations.

3. Generalized Oscillator Strengths for the Helium Atom

The scattering amplitudes for electron-hydrogen atom scattering were evaluated analytically (see Tr 68). For the calculations on electron-hydrogen molecule scattering the scattering amplitudes were evaluated using both analytic and numerical techniques and some of the results were fit to power series (see part two of this thesis). The methods used to obtain the scattering amplitudes for electron-helium atom scattering are described in the rest of this subsection.

All of the electron-helium scattering calculations were done using the generalized oscillator strengths. The generalized oscillator strength for electron scattering off the ground state g of helium with excitation of the excited singlet state j is (see, e.g., Be 30, Mi 57, Bu 61, p. 397)

$$\varphi_{gj}(q) = \frac{8}{q^2} (E_j^A - E_g^A) \, |M_{jg}(q)|^2 . \qquad (39)$$

This quantity has been computed as a function of q many times in the past. For excitation of the $2\,^1P$, $3\,^1P$, and $2\,^1S$ states, Kim and Inokuti (Ki 68a) computed very accurate values by using the 52-54 term configuration interaction wave functions (including explicit r_{12} dependence) of Weiss (We 67). For $q \leq 2$, they estimated their generalized oscillator strengths are accurate within 1% for the $2\,^1P$

and $2\,^1S$ excitations and 3% for the $3\,^1P$ excitations. For higher q their values are slightly less accurate. Their best sets of generalized oscillator strengths will be labelled KI. Bell, Kennedy, and Kingston (Be 68) used the 6-term configuration interaction wave function (including explicit r_{12} dependence) of Stewart and Webb for the ground state (St 63) and a single-configuration, minimum-basis-set, hydrogenic-exponent wave function for the $3\,^1P$ state to calculate generalized oscillator strengths for the $1\,^1S - 3\,^1P$ transition. Their results using eq. (12) will be called the BKK set of generalized oscillator strengths.

Since the calculations require many values of $\varphi_{gj}(q)$ at irregular values of q, we found it convenient to fit $\varphi_{gj}(q)$ to a power series. Lassettre pointed out that a Maclaurin series in q is not convergent for all possible q and suggested an alternative form which is convergent in the entire physical domain for atomic $S \rightarrow S$ transitions. The form is (La 65a, Vr 67, Vr 68)

$$\varphi_{gj}(q) = \frac{x}{(1+x)^6}\left[c_o + \sum_{m=0}^{\infty} c_m \left(\frac{x}{1+x}\right)^m\right] \tag{40}$$

where

$$c_o = \lim_{q \rightarrow 0}\left[\frac{\alpha^2 \varphi_{gj}(q)}{q^2}\right] \tag{41}$$

$$x = q^2/\alpha^2 \tag{42}$$

and

$$\alpha = (2U_g)^{1/2} + [2(U_g + E_j^A - E_g^A)]^{1/2} . \tag{43}$$

The convergence properties require α be known only approximately. Similarly for atomic S → P transitions the appropriate form is (Vr 67, Vr 68)

$$\varphi_{gj}(q) = \frac{\varphi_{gj}(0)}{(1+x)^6} \left[1 + \sum_{m=1}^{\infty} c_m \left(\frac{x}{1+x} \right)^m \right] \qquad (44)$$

where x is again given by eqs. (42) and (43). We used these series with the sums truncated to M terms and selected the c_m for $m \geq 1$ to give best agreement over some range of q with one of the available sets of generalized oscillator strengths. For the fitting process we used p values of q in the range q_1 to q_p. The fitting process was well-conditioned but more so for S → P transitions than S → S transitions. Some of the resulting fits are given in Table XV.

B. Electron-Atom Scattering

We have written an article "Rearrangement Collisions: Effect of Core Terms, Nonorthogonality, and Conservation of Particle Flux on Approximate Theories" which is already published. In this article we discussed in detail the Born-Oppenheimer approximation with and without the core term, the first order method of Bates, Bassel and Gerjuoy, and Mittleman, the prior Ochkur and Ochkur-Rudge approximations, the symmetrized Ochkur-Rudge approximation, and the unitarized Ochkur and Ochkur-Rudge approximations for electron exchange scattering. Many calculations using these methods for differential and integral cross sections were presented for the 1s - 1s, 1s - 2s, and 2s - 2s processes of electron-hydrogen atom exchange scattering and they were compared to calculations using optimized

trial functions and to experimental results. There had been no previous accurate calculation of the differential cross sections for the BO, BOMC, BBGM1, O.II, and ORB.II methods. We also discussed the application of these methods to other processes and the application of other methods to the electron exchange problem.

Additional calculations, especially in the unitarized Ochkur and unitarized Ochkur-Rudge approximations, have been performed and the results are summarized in Tables II, III, IV, V, and VI. Additional calculations of exchange cross sections from optimized trial function results of previous workers have been performed and these are compared in Figs. 1-8 with the present results.

Some of the more important conclusions which can be drawn from the article and from the calculations in the tables and figures are:

1. The Born-Oppenheimer approximation without the core term gives integral exchange cross sections and angular dependences which are worse than the ones calculated from the full Born-Oppenheimer approximation. The inclusion of the core term is evidently necessary for consistency in a plane wave calculation.

2. The first order method of Bates, Bassel, Gerjuoy, and Mittleman gives integral exchange cross sections which are better than those in the Born-Oppenheimer approximation but are still in poor agreement with experiment for impact energies below about 20 eV. Since the maxima in the inelastic exchange cross sections occur very near to threshold (the threshold energy is 10.2 eV for the 1s - 2s transition in the hydrogen atom) the BBGM1 method, like the BO and BOMC methods, greatly overestimates the cross section in the region of its maximum.

3. The BO and BBGM1 approximations predict the angular dependence of the exchange differential cross sections much more accurately than the BOMC approximation does.

4. The Ochkur and Ochkur-Rudge methods predict integral exchange cross sections more accurately than the BO, BOMC, or BBGM1 methods. Thus it is not merely spurious contributions to the Born-Oppenheimer amplitude from core terms and nonorthogonality of the plane waves which makes the Ochkur and Ochkur-Rudge approximations work so well; the physical reason, if any, for their success is still not clear. The Ochkur-Rudge method is more accurate than the Ochkur method. However, neither of these methods predict accurate angular dependences of the exchange differential cross sections. The exchange differential cross sections they predict are very similar to those predicted by the BOMC approximation. Evidently the BOMC, O, and ORB.I methods do not treat the interactions responsible for the exchange scattering in a consistent way at least at low and intermediate energies. The differential cross sections thus serve as a sensitive test of whether the O and OR methods predict relatively accurate integral cross sections for the wrong reasons.

5. The unitarized Ochkur-Rudge approximation predicts remarkably accurate integral exchange cross sections but neither it nor the unitarized Ochkur approximation predicts more accurate angular dependencies than their nonunitary versions. The shapes of the differential cross sections as a function of angle are not much changed by unitarization.

We have also calculated the total scattering (direct and exchange scattering and their interference) for the 1s - 2s transition in the hydrogen atom. The methods used for these calculations were the same as those used and described in Tr 68 and Tr 70. For electron-hydrogen atom scattering we evaluate the amplitudes analytically

using exact bound state wave functions. One report of this work "Cross Sections for Excitation of the $2\,^2S$ State of Hydrogen By Electron Impact" has already been published (Tr 69a). This long abstract emphasized the integral cross sections. New calculations were reported using the Born approximation, the Born-Oppenheimer approximation with and without the core term, the prior and post Born-Ochkur and Born-Ochkur-Rudge approximations, the symmetrized Born-Ochkur-Rudge approximation, the Born approximation with exchange correction by the first order method of Bates, Bassel, Gerjuoy, and Mittleman, the method of Vainshtein, Presnyakov, and Sobelman, the Born-transferred Vainshtein-Presnyakov-Sobelman approximation, and the Born-transferred Kang-Foland approximation. The cross sections were compared with other calculations and with experiment. Some other results for the total scattering cross section for the 1s - 1s elastic scattering and the 1s - 2s excitation of the hydrogen atom are given in Tables VII, VIII, IX, X, XI, XII, and XIII.

We have also done many calculations on the excitation of three of the lowest energy excited singlet states of the helium atom -- the $2\,^1S$, $2\,^1P$, and $3\,^1P$ states. The calculations were carried out in the B, O, OP, BOR, BORP, BORB.I, VPS, BTVPS, and BTKF approximations. The methods used for these calculations and the most important results for the excitation of the $2\,^1P$ state are given in an article "Differential and Integral Cross Sections for Excitation of the $2\,^1P$ State of Helium by Electron Impact" which has been accepted for publication (Tr 70). The article also includes experimental results by Rice, Trajmar, and Kuppermann. In the article the new and all the previously available theoretical and experimental data on the excitation of the $2\,^1P$ state of helium are analyzed, discussed, and compared. Further examples of the calculated cross sections for

electron-helium scattering are given in Figs. 9-11 (mostly exchange differential cross sections), 12-17 (mostly total differential cross sections),* and 18-21 (total integral cross sections). In addition some aspects of the ratios of the $2\,^1S$ excitation cross sections to the $2\,^1P$ ones are illustrated by Figs. 22-23 and Table XIV. Calculations have been performed for excitation of the $2\,^1S$ state of helium at all the energies for which there is any experimental data or any previous theoretical calculations. An article discussing the $2\,^1S$ cross sections and the $2\,^1S/2\,^1P$ intensity ratios in more detail is in preparation (Ri 70). This article will compare the calculations to experiments from this laboratory (see, e.g., Ku 68, Ri 69) and elsewhere. Considering all these new results and their comparison with experiment and with each other we can add a few more items to our list of the most important conclusions:

6. The O and BTVPS theories give very similar results for differential and integral cross sections. Hence the BTVPS approximation yields no new results and need not be considered further.

7. The BO, BOMC, BBGM1, OP, and BOR approximations give maximum total integral cross sections larger and in worse agreement with experiment than the Born approximation or some close coupling calculations. The O, BORB.I, and VPS approximations give lower cross sections than the Born approximation and few-state close coupling methods. The BORP and BTKF approximations are

---

*In the semilog plots in Figs. 9-17 many of the cross sections calculated by the O, OP, VPS, BTVPS, and BORB.I methods show sharp, deep dips. These are actually zeroes but do not show up as such on some of these computer-generated figures. They are easily recognized and should not cause any confusion.

sometimes better than and sometimes worse than the B approximation in this respect.

8. The O, BORB.I, and VPS theories and the calculations of Morrison and Rudge (Mo 66a) are in rough agreement with the various experimental total integral cross sections for the 1s - 2s transition in the hydrogen atom. Further clarification of experimental results will be necessary to determine which of these calculations is most accurate in this case. These methods are the most useful for calculating total integral cross sections.

9. The VPS approximation gives better agreement with experiment for the total integral cross sections for electronic excitation of each of the three states of helium than any of the methods we tried (B, O, OP, BOR, BORP, BORB.I, BTKF) which use the Born approximation for the direct amplitude. These results and the previous success of the VPS theory are an empirical justification for using the VPS approximation to calculate integral total cross sections.

10. The BORB.I, O, OP, and VPS methods predict the angular dependencies of total differential cross sections very poorly. A symptom of this is that they sometimes predict a nonphysical zero in the differential cross section. This would not happen if either the direct or exchange scattering amplitude or both were complex (not real).

11. The Born and BOR approximations are in good agreement (better than a factor of 2) with the angular dependence of the experimental total differential cross sections for scattering angles θ less than about 45° for the excitation of the $2\,^1P$ state for impact energies of 34-81.6 eV (81.6 eV is the highest energy for which experimental differential cross sections for scattering angles as large as 45° are available). At the higher energy end of this range where the cross

sections are steeper functions of the scattering angle θ the agreement extends only to smaller θ than it does at lower energies. Evidently the large angle scattering corresponds to such a strong perturbation that these first order theories fail. Formally this means that distortion of the lowest one or more partial waves is necessary to predict the large angle scattering even qualitatively correctly. Evidence for accuracy and inaccuracy of the plane wave theories' predictions of the angular dependences of the $2\,^1P$ differential cross sections at all energies for which experimental data are available is summarized in Tr 70.

12. The BOR approximation can explain the angular dependence of all the presently available experimental total differential cross section data (within the stated experimental error limits) for excitation of the He $2\,^1P$ state $\theta \leq 20^o$ and $E_i \geq 34$ eV.

13. The BTKF and BORP approximations predict the angular dependence of the $2\,^1P$ excitation total differential cross section in worse agreement with experiment than the Born approximation. This is not complete enough evidence to dismiss them. For example, it is possible that by including distortion in the lowest few partial waves of a BORP or BTKF calculation they would agree better with experiment.

14. No consistent criterion except detailed balance arose so far from the study of electron scattering from H and He to indicate that the BOR, BORP, or BORB. I approximation is more correct in any basic way. The inaccuracies in the first order treatments presented here for the total scattering (including direct and exchange scattering and the interference between them) may be at least partly due to treating the direct and exchange scattering by different methods so that the relative phase of the direct and exchange scattering

amplitudes may be predicted inaccurately. This fault can be corrected by calculating the scattering using antisymmetrized trial functions which are eigenfunctions of the electronic spin of the three-electron system.

15. None of the methods we examined gave even approximately correct angular dependences for the differential cross sections for excitation of the $2\,^1P$ or $2\,^1S$ states of He for $E_i = 26.5$ eV. Evidently this is too close to threshold for these first order methods to work.

16. The ratios of differential cross sections for two processes (e.g., $2\,^1S/2\,^1P$ or $3\,^1P/2\,^1P$ in helium) are much less sensitive to the method of calculation used than are the cross sections themselves. Thus the $2\,^1S/2\,^1P$ cross section ratios computed by the B, O, BOR, BORP, BORB.I, BTKF, VPS, or BTVPS approximations agree within a few per cent for $\theta \leq 60^o$ in the intermediate energy range. The B, BOR, and BTKF approximations to these cross section ratios agree with each other over an even wider angular range.

17. None of the methods we examined is in agreement with the experimental angular dependences of the total differential cross sections for excitation of the $2\,^1S$ state of helium for impact energies in the range 34-55.5 eV. The theoretical cross sections do not fall rapidly enough with increasing θ at small θ, indicating the theory has underestimated the range of the effective potential (as discussed in section A.2.i). Since the first order theory was approximately correct for the angular dependence of the $2\,^1P$ total cross section at small θ (this too was expected as discussed in section A.2.i), the theory does not predict the $2\,^1S/2\,^1P$ intensity ratios accurately. The polarized Born approximation or polarized Born-Ochkur-Rudge approximation should be applied to $S \rightarrow S$ transitions. The calculations without polarization are in better agreement with the $2\,^1S$

excitation total differential cross sections at E_i = 81.6 eV than at the lower energies. This could be an accidental result of several effects including distortion or perhaps the energy is high enough so that polarization is less important or there is more experimental error.

C. Electron-Molecule Scattering

In part two of this thesis we present the methods used for polarized Born and polarized Born-Ochkur-Rudge calculations of electron-hydrogen molecule scattering. Calculated cross sections for elastic scattering and vibrational excitation are included. These calculations are much more complicated than the calculations on electron-atom scattering. In chapter I of part two of the thesis we also compare the calculations for elastic scattering to some previous ones and to low energy and high energy experimental data for elastic scattering. Table XVI gives additional calculations of the elastic integral cross sections (these include elastic scattering plus pure rotational excitation) in the intermediate energy range. Figure 24 compares low energy elastic differential cross sections with the very recent theoretical results of Henry and Lane (He 69) and Hara (Ha 69a) and with the experiments of Ehrhardt and Linder (Eh 68). The calculations of Henry and Lane and Hara include distortion and higher order effects, but the present results are in good agreement with them when polarization is included.

In chapter II of part two we present more calculations on low and intermediate energy elastic scattering and comparison with previous theoretical and previous and new experimental results. In chapter III of part two we present more calculations on vibrational excitation

cross sections at low and intermediate energies and compare with previous theoretical and previous and new experimental results.

TABLE I

Abbreviations for Exchange Scattering Theories[a]

BO	Born-Oppenheimer approximation (prior)
BOP	Born-Oppenheimer approximation (post)
BOMC	Born-Oppenheimer approximation without core term(s)
O	Ochkur approximation (prior)
O.II n x n	Unitarized Ochkur approximation (prior) including n states
OP	Ochkur approximation (post)
OR	Ochkur-Rudge approximation (prior)
ORP	Ochkur-Rudge approximation (post)
ORB.I	Symmetrized Ochkur-Rudge approximation
ORB.II n x n	Unitarized Ochkur-Rudge approximation including n states
ORB.III, ORB.IV	Approximately unitarized Ochkur-Rudge approximations
BBGM1	First order approximation of Bates, Bassel and Gerjuoy, and Mittleman
E1	First order exchange approximation
KF	Kang-Foland approximation to the Coulomb wave approximation
TKF	Transferred KF approximation
VPS	Vainshtein-Presnyakov-Sobelman approximation
TVPS	Transferred VPS approximation
PO	Polarized orbital method
B/P	Polarized Born approximation
BOR/P	Polarized Born-Ochkur-Rudge approximation (prior)

[a]The abbreviations used to name theories for exchange scattering are listed in this table. The Born approximation for direct scattering is called B and the prefix B used with an abbreviation for the exchange amplitude is used to indicate a calculation of the total scattering (direct plus exchange). For the various forms of the Born-Oppenheimer and Ochkur theories, however, the direct scattering is always calculated in the Born approximation and thus the B is omitted from the abbreviation.

TABLE II

Scattering angles (deg) at the positions of the highest peaks of the calculated differential cross sections for electron exchange scattering off the hydrogen atom with excitation from the ground state to the 2s state.

E	Method							
(eV)	BOMC	BO	O	OR	BBGM1	BSS[a]	O. II[b]	OR. II[b]
13.6	80	0	85	85	0	180	85	85
19.6	55	180	60	60	180	180	60	60
30.6	45	180	45	45	45	0	45	45
54.4	30	30	30	30	30	0	35	35

[a] 1s - 2s - 2p close coupling calculations (Bu 63)

[b] 2 x 2 matrix equation used for unitarization

TABLE III

Integral exchange cross sections for electron scattering off the ground state of the hydrogen atom in the 1 and 2-state unitarized Ochkur and Ochkur-Rudge approximations. The exchange elastic scattering and the exchange excitation of the 2s state are given.

	1s - 1s				1s - 2s	
E_i(eV)	O. II 1 x 1	O. II 2 x 2	ORB. II 1 x 1	ORB. II 2 x 2	O. II 2 x 2	ORB. II 2 x 2
1.20	151.46		28.72			
1.36	134.16		27.07			
1.80	102.21		23.29			
2.20	83.91		20.57			
2.60	71.03		18.35			
3.00	61.41		16.51			
3.40	53.87		14.95			
4.20	43.01		12.47			
5.44	32.01		9.73			
7.00	23.40		7.42			
9.52	15.15		5.08			
10.50	12.99	12.98	4.45	4.34	0.00	0.09
11.00	12.04	11.98	4.17	4.01	0.01	0.14
12.00	10.39	10.16	3.67	3.49	0.10	0.23
13.00	9.01	8.68	3.25	3.09	0.20	0.27
13.60	8.28	7.95	3.03	2.88	0.23	0.27
14.00	7.85	7.52	2.90	2.75	0.24	0.27
15.00	6.86	6.57	2.59	2.47	0.25	0.26
16.00	6.03	5.78	2.32	2.22	0.24	0.24
17.00	5.31	5.10	2.09	2.00	0.23	0.22
19.59	3.89	3.75	1.62	1.56	0.20	0.18
22.00	2.97	2.88	1.29	1.26	0.16	0.14
25.00	2.17	2.11	1.00	0.98	0.13	0.11
30.61	1.28	1.26	0.65	0.64	0.08	0.07
40.00	0.61	0.61	0.35	0.35	0.04	0.04
45.00	0.44	0.44	0.26	0.26	0.03	0.03
54.42	0.25	0.25	0.16	0.16	0.02	0.02
70.00	0.12	0.12	0.09	0.08	0.01	0.01
100.00	0.04	0.04	0.03	0.03	0.00	0.00

TABLE IV

Integral cross sections (a_o^2) for exchange elastic scattering off the 2s state of the hydrogen atom in the 1 and 2-state unitarized Ochkur and Ochkur-Rudge approximations.

	2s - 2s			
E_i (eV)	O.II 1 x 1	O.II 2 x 2	ORB.II 1 x 1	ORB.II 2 x 2
1.80	200.22	198.73	40.09	38.96
2.80	80.00	78.59	19.38	18.85
3.40	48.83	47.78	13.45	13.11
3.80	36.39	35.55	10.84	10.57
4.80	18.95	18.46	6.70	6.54
5.80	10.99	10.69	4.44	4.34
6.80	6.93	6.72	3.11	3.04
9.39	2.70	2.61	1.40	1.43
11.80	~1.39	~1.34	0.84	0.82

TABLE V

Integral cross sections (a_o^2) for exchange elastic scattering of electrons off the ground state of the hydrogen atom calculated using various methods. For calculations with the reactance matrix, the size of the block of the matrix used in the equation for the scattering matrix is indicated in the column heading.

E_i (eV)	BO	BOMC	BBGM1	BSS 1×1	BSS[a] 2×2	BSS[a] 4×4	O	O. II 1×1	O. II 2×2	OR	ORB. II 1×1	ORB. II 2×2
1.36	239.13	738.53	48.13	-	-	20.85	4166.76	2523.00	-	34.44	22.13	-
5.44	47.15	196.69	4.82	-	-	8.55	166.39	32.01	-	13.58	9.73	-
9.52	13.02	69.66	2.00	-	-	3.23	38.91	15.14	-	6.60	5.08	-
13.60	4.78	29.88	1.85	5.15	4.26	2.86	14.66	8.28	7.95	3.66	3.03	2.88
19.59	1.65	10.95	1.52	2.74	1.73	1.99	5.22	3.89	3.75	1.82	1.62	1.56
30.61	0.54	2.76	0.85	1.38	0.89	0.93	1.43	1.28	1.26	0.68	0.65	0.64
54.42	0.16	0.41	0.25	0.17	0.21	0.23	0.26	0.25	0.25	0.17	0.16	0.16
100.00	0.04	0.06	0.05	-	-	-	0.04	0.04	0.04	0.03	0.03	0.03

[a] 1s-2s-2p close coupling calculations (Bu 62b, Bu 63).

TABLE VI

Integral exchange cross sections (a_o^2) for electron scattering off the hydrogen atom with the 1s → 2s transition calculated using various methods. For calculations with the reactance matrix, the size of the block of the matrix used in the equation for the scattering matrix is indicated in the column heading.

E_i (eV)	BO	BOMC	BBGM1	BSS 2×2	BSS 4×4	VPS	TVPS	TKF	OP	O	O.II 2×2	OR	ORB.II 2×2
13.60	3.017	6.883	1.552	0.623	0.695	0.307	0.590	0.179	9.253	0.578	0.230	0.370	0.269
19.59	0.693	2.641	0.220	0.713	0.360	0.176	0.307	0.057	1.302	0.299	0.195	0.217	0.179
30.61	0.077	0.531	0.029	0.244	0.089	0.062	0.097	0.014	0.212	0.094	0.080	0.076	0.070
54.42	0.011	0.056	0.017	0.018	0.020	0.013	0.018	0.003	0.027	0.018	0.017	0.016	0.016
100.00	0.003	0.006	0.004	-	-	0.002	0.003	0.001	0.004	0.003	0.003	0.003	0.003

TABLE VII

Integral total cross sections (a_0^2) for elastic scattering of electrons from hydrogen atoms (1s). Direct amplitude is from Born approximation and exchange amplitude is from five different approximations. Number in parentheses, if any, is multiplicative power of 10.

E	Cross sections				
(Ry)	BOMC	BO	O	OR	BBGM1
0.1	8.39(2)	1.99(2)	4.39(3)	2.95(1)	3.64(1)
0.3	3.53(2)	6.13(1)	4.01(2)	1.99(1)	1.04(1)
0.4	2.43(2)	3.69(1)	2.10(2)	1.69(1)	8.52
0.7	9.60(1)	1.18(1)	6.01(1)	1.15(1)	8.62
0.8	7.40(1)	9.23	4.49(1)	1.03(1)	8.71
0.9	5.83(1)	7.63	3.48(1)	9.33	8.66
1.0	4.67(1)	6.61	2.79(1)	8.51	8.51
1.3	2.64(1)	5.10	1.64(1)	6.69	7.69
1.44	2.11(1)	4.73	1.34(1)	6.07	7.23
2.0	1.04(1)	3.81	7.37	4.38	5.52
2.25	8.16	3.51	6.04	3.88	4.90
3.0	4.69	2.79	3.83	2.87	3.55
4.0	2.88	2.13	2.54	2.11	2.50
6.0	1.59	1.40	1.50	1.37	1.52
9.0	9.51(-1)	9.07(-1)	9.27(-1)	8.87(-1)	9.39(-1)
20.0	3.89(-1)	3.86(-1)	3.87(-1)	3.83(-1)	3.88(-1)
25.0	3.07(-1)	3.06(-1)	3.06(-1)	3.04(-1)	3.07(-1)
50.0	1.50(-1)	1.50(-1)	1.50(-1)	1.49(-1)	1.50(-1)

TABLE VIII

Peaks in the differential total cross sections for elastic scattering of electrons from hydrogen atoms (1s). Given are all peaks (highest first) among the angles 0(2) 24(6) 60(5) 180. Direct amplitude is from Born approximation and exchange amplitude is from five different approximations. B = 180°. If the minimum value of the differential cross section does not occur at either 0° or B, it is given in parentheses.

E	Peaks				
(Ry)	BOMC	BO	O	OR	BBGM1
0.1	0	B	0	0	B
0.3	0	B	0	0	B, 0(70)
0.4	0	B	0	0	0, B(90)
0.7	0	B, 0(60)	0	0	0, B(125)
0.76	0	B, 0(65)	0	0	0, B(130)
0.8	0	B, 0(65)	0	0	0, B(135)
0.9	0	0, B(75)	0	0	0, B(145)
1.0	0	0, B(80)	0	0	0, B(155)
1.3	0	0, B(95)	0	0	0
1.44	0	0, B(100)	0	0	0
2.0	0	0, B(125)	0	0	0
2.25	0	0, B(135)	0	0	0
3.0	0	0	0	0	0

TABLE IX

Integral total cross sections (a_0^2) for inelastic scattering of electrons from hydrogen atoms for the 1s→2s transition. Direct amplitude from Born approximation and exchange amplitude from five different approximations in the prior formulations. Number in parentheses, if any, is the multiplicative power of 10.

E	Cross sections				
(Ry)	BOMC	BO	O	OR	BBGM1
0.76	2.78	3.15	2.50(-1)	5.70(-1)	2.18
0.80	5.33	5.77	5.17(-1)	1.12	3.94
0.90	6.31	6.22	7.35(-1)	1.44	4.11
1.00	5.63	5.18	7.85(-1)	1.43	3.32
1.30	3.07	2.55	7.18(-1)	1.12	1.57
1.44	2.30	1.89	6.69(-1)	9.87(-1)	1.18
2.00	9.21(-1)	8.09(-1)	5.15(-1)	6.59(-1)	5.88(-1)
2.25	6.95(-1)	6.39(-1)	4.68(-1)	5.74(-1)	4.99(-1)
3.00	4.11(-1)	4.13(-1)	3.68(-1)	4.18(-1)	3.68(-1)
4.00	2.91(-1)	3.00(-1)	2.89(-1)	3.12(-1)	2.86(-1)
6.00	2.00(-1)	2.05(-1)	2.04(-1)	2.11(-1)	2.01(-1)
9.00	1.40(-1)	1.41(-1)	1.41(-1)	1.44(-1)	1.40(-1)
20.00	6.66(-2)	6.67(-2)	6.68(-2)	6.70(-2)	6.66(-2)
25.00	5.38(-2)	5.38(-2)	5.39(-2)	5.40(-2)	5.38(-2)
50.00	2.74(-2)	2.74(-2)	2.74(-2)	2.74(-2)	2.74(-2)

TABLE X

Peaks in the differential total cross sections for excitation of the 2s state of the hydrogen atom from the ground state by electron impact. Given are all peaks (highest first) among the angles 0(1) 12(2) 24(6) 60(5) 180. Direct amplitude calculated is from Born approximation and exchange amplitude is from five different approximations. B = 180°. If the cross section is not a monotonic function of the scattering angle, the position of the minimum is given in parentheses.

E	Peaks				
(Ry)	BOMC	BO	O	OR	BBGM1
0.76	B	0	0	0	0
0.80	B	0	0	0	0
0.90	125(0)	0, B(155)	0	0	0, B(165)
1.00	100(0)	0, B(120)	0	0	0, B(125)
1.30	0, 70(B)	0, B(95)	0	0	0, B(100)
1.44	0	0, B(95)	0	0	0, B(100)
2.00	0	0, B(85)	0	0	0, B(95)
2.25	0	0, B(85)	0	0	0, B(95)
3.00	0	0, B(85)	0	0	0, B(100)
4.00	0	0, B(85)	0	0	0, B(105)
6.00	0	0, B(85)	0	0	0, B(120)
9.00	0	0, B(85)	0	0	0, B(140)
20.00	0	0, B(85)	0	0	0
25.00	0	0, B(85)	0	0	0
50.00	0	0, B(85)	0	0	0

TABLE XI

Differential cross sections (a_0^2/steridian) at 10° for 1s-2s excitation of the hydrogen atom by electron scattering. Direct amplitude is from the Born approximation and exchange amplitude is from five different approximations in the prior interaction formulation. Number in parentheses is the power of 10 by which each cross section is to be multiplied.

E (Ry)	Cross sections				
	BOMC	BO	O	OR	BBGM1
0.76	2.03(-1)	2.83(-1)	2.29(-2)	5.31(-2)	2.01(-1)
0.80	3.48(-1)	6.15(-1)	6.15(-2)	1.29(-1)	4.47(-1)
0.90	3.76(-1)	8.59(-1)	1.37(-1)	2.31(-1)	6.40(-1)
1.00	3.47(-1)	8.83(-1)	2.04(-1)	2.96(-1)	6.71(-1)
1.30	3.21(-1)	7.66(-1)	3.51(-1)	4.19(-1)	6.20(-1)
1.44	3.38(-1)	7.23(-1)	3.99(-1)	4.57(-1)	6.02(-1)
2.00	4.31(-1)	6.46(-1)	5.14(-1)	5.47(-1)	5.82(-1)
2.25	4.66(-1)	6.34(-1)	5.41(-1)	5.68(-1)	5.83(-1)
3.00	5.29(-1)	6.17(-1)	5.80(-1)	5.97(-1)	5.87(-1)
4.00	5.54(-1)	5.97(-1)	5.84(-1)	5.96(-1)	5.80(-1)
6.00	5.29(-1)	5.43(-1)	5.42(-1)	5.48(-1)	5.36(-1)
9.00	4.50(-1)	4.54(-1)	4.55(-1)	4.59(-1)	4.52(-1)
20.00	2.25(-1)	2.25(-1)	2.26(-1)	2.27(-1)	2.25(-1)
25.00	1.66(-1)	1.66(-1)	1.67(-1)	1.67(-1)	1.66(-1)
50.00	4.36(-2)	4.36(-2)	4.36(-2)	4.37(-2)	4.36(-2)

TABLE XII

Differential cross sections (a_0^2/steredian) at 60° for 1s-2s excitation of the hydrogen atom by electron scattering. Calculations are by the Born approximation plus five different methods for exchange. Number in parenthesis is multiplicative power of 10.

E (Ry)	Cross sections				
	BOMC	BO	O	OR	BBGM1
0.76	2.13(-1)	2.64(-1)	2.10(-2)	4.89(-2)	1.85(-1)
0.80	3.97(-1)	5.07(-1)	4.56(-2)	1.05(-1)	3.58(-1)
0.90	4.71(-1)	5.57(-1)	6.71(-2)	1.47(-1)	3.79(-1)
1.00	4.32(-1)	4.55(-1)	7.13(-2)	1.51(-1)	3.01(-1)
1.30	2.59(-1)	1.93(-1)	5.78(-2)	1.13(-1)	1.19(-1)
1.44	2.00(-1)	1.30(-1)	4.92(-2)	9.29(-2)	7.90(-2)
2.00	7.41(-2)	3.37(-2)	2.41(-2)	4.10(-2)	2.27(-2)
2.25	4.96(-2)	2.08(-2)	1.75(-2)	2.88(-2)	1.53(-2)
3.00	1.71(-2)	6.59(-3)	7.17(-3)	1.08(-2)	6.20(-3)
4.00	5.27(-3)	2.09(-3)	2.53(-3)	3.52(-3)	2.39(-3)
6.00	8.50(-4)	3.74(-4)	4.69(-4)	5.97(-4)	5.03(-4)
9.00	1.16(-4)	5.67(-5)	7.09(-5)	8.40(-5)	8.27(-5)
20.00	1.59(-6)	8.98(-7)	1.12(-6)	1.22(-6)	1.39(-6)
25.00	4.52(-7)	2.62(-7)	3.29(-7)	3.52(-7)	4.07(-7)
50.00	8.19(-9)	5.07(-9)	6.47(-9)	6.69(-9)	7.82(-9)

TABLE XIII

Ratio of the electron scattering exchange integral cross section for the 1s → 2s transition in the hydrogen atom to the total integral cross section for the same process.

E_i(Ry)	BSS[a]	MR[b]	BBGM1	BO	BOR
0.80		1.030	0.597	0.672	0.251
0.81	0.744				
1.00	0.612	0.797	0.467	0.583	0.260
1.10		0.706			0.254
1.21	0.546				
1.30		0.556	0.263	0.434	0.236
1.44	0.435		0.186	0.366	0.222
2.00		0.267	0.061	0.168	0.156
2.25	0.178		0.058	0.120	0.133
3.00		0.118	0.067	0.059	0.085
4.00	0.058	0.064	0.059	0.038	0.051
5.00		0.040			0.034
20.00		0.0022	0.0027	0.0024	0.0021
50.00		0.0003	0.0004	0.0004	0.0003

[a] 1s-2s-2p close coupling calculations (Bu 62b, Bu 63).

[b] Morrison and Rudge (Mo 66a).

TABLE XIV

Calculated ratio of the total scattering cross section for excitation of the $2\,^1S$ state of He to that for excitation of the $2\,^1P$ state at an impact energy of 44 eV.

θ (deg)	B	O	BOR	OP	BORP	BORB.I	BTKF	VPS	BTVPS
0	0.09	0.09	0.09	0.09	0.09	0.09	0.09	0.09	0.09
6	0.10	0.10	0.10	0.10	0.10	0.10	0.10	0.10	0.10
12	0.12	0.12	0.12	0.12	0.12	0.12	0.12	0.12	0.12
18	0.17	0.17	0.17	0.17	0.17	0.17	0.17	0.17	0.17
24	0.23	0.23	0.23	0.24	0.23	0.23	0.23	0.23	0.23
30	0.31	0.31	0.31	0.32	0.32	0.31	0.31	0.31	0.31
36	0.41	0.41	0.41	0.42	0.42	0.41	0.41	0.41	0.41
42	0.53	0.53	0.52	0.55	0.54	0.53	0.53	0.52	0.53
48	0.67	0.67	0.66	0.70	0.68	0.67	0.67	0.67	0.67
54	0.84	0.83	0.83	0.91	0.87	0.84	0.84	0.84	0.83
60	1.04	1.03	1.03	1.19	1.08	1.05	1.04	1.04	1.03
70	1.43	1.41	1.41	1.23	1.52	1.44	1.43	1.43	1.41
80	1.87	1.82	1.84	1.52	2.04	1.89	1.87	1.87	1.81
90	2.32	2.19	2.29	2.08	2.61	2.36	2.32	2.32	2.18

TABLE XV

Parameters for series representation of generalized oscillator strengths $\varphi_{gj}(q)$ for electron-helium atom scattering.

j[a]	$2\,^1P^*$	$3\,^1P^*$	$3\,^1P^*$	$2\,^1S^*$	$2\,^1S$
$\varphi_{gj}(q)$	KI	KI	BKK	KI	KI
$\varphi_{gj}(0)$	0.2759	0.0734	0.07671	0.0	0.0
c_0	-	-	-	0.296920	0.296920
α^2	3.391	2.896	2.896	3.551	3.551
p	51	51	20	59	53
q_1	0.224	0.224	0.1	0.224	0.224
q_p	4.4721	4.4721	3.0	10.0	6.32
Accuracy[b](%)	< 0.1	< 0.1	0.04	5	2
M	6	6	5	6	6
c_1	0.456266	2.38487	2.45759	0.185018	0.264769
c_2	0.414351	1.51589	2.17413	2.63492	0.0664954
c_3	-1.74889	3.77057	2.61393	-23.8656	-3.49923
c_4	6.87112	-9.37626	-3.22874	80.2249	18.7459
c_5	-10.0300	16.1137	4.15506	-109.767	-31.6198
c_6	4.99172	-9.66797	-	53.3058	18.0907

[a]The fits marked with asterisks are used for calculations presented in this thesis. The other fit is an alternative one. The differential cross sections presented here are all calculated from the KI sets of generalized oscillator strengths.

[b]This is the accuracy with which the fit reproduces the input $\varphi_{gj}(q)$ in the range q_1-q_p.

TABLE XVI

Electron-H_2 Elastic Scattering Cross Sections
(Atomic Units)

	Polarized Born approximation				Born approximation			
E(eV)	30	50	100	200	30	50	100	200
θ(deg)								
1	19.15	18.88	18.38	17.69	2.22	2.22	2.22	2.21
2	18.22	17.69	16.76	15.51	2.21	2.21	2.20	2.19
3	17.32	16.57	15.26	13.54	2.21	2.20	2.18	2.15
4	16.46	15.51	13.86	11.78	2.20	2.19	2.16	2.10
5	15.64	14.45	12.57	10.18	2.19	2.17	2.12	2.04
10	12.00	10.22	7.52	4.77	2.11	2.04	1.88	1.62
16	8.59	4.80	3.87	1.77	1.95	1.80	1.49	1.06
24	5.38	3.49	1.52	4.73^{-1}	1.69	1.43	9.78^{-1}	4.93^{-1}
30	3.74	2.14	7.50^{-1}	2.14^{-1}	1.47	1.16	6.63^{-1}	2.62^{-1}
36	2.58	1.31	3.93^{-1}	1.21^{-1}	1.26	9.06^{-1}	4.33^{-1}	1.42^{-1}
42	1.78	8.06^{-1}	2.29^{-1}	7.75^{-2}	1.06	6.92^{-1}	2.81^{-1}	8.13^{-2}
48	1.23	5.14^{-1}	1.51^{-1}	5.20^{-2}	8.78^{-1}	5.21^{-1}	1.84^{-1}	5.03^{-2}
54	8.60^{-1}	3.41^{-1}	1.08^{-1}	3.52^{-2}	7.19^{-1}	3.90^{-1}	1.23^{-1}	3.40^{-2}
60	6.13^{-1}	2.40^{-1}	8.09^{-2}	2.52^{-2}	5.85^{-1}	2.93^{-1}	8.56^{-2}	2.49^{-2}
70	3.70^{-1}	1.52^{-1}	5.22^{-2}	1.65^{-2}	4.14^{-1}	1.86^{-1}	5.08^{-2}	1.65^{-2}
80	2.45^{-1}	1.08^{-1}	3.51^{-2}	1.16^{-2}	2.97^{-1}	1.23^{-1}	3.39^{-2}	1.15^{-2}
90	1.77^{-1}	8.09^{-2}	2.52^{-2}	8.09^{-3}	2.18^{-1}	8.56^{-2}	2.49^{-2}	7.98^{-2}
100	1.37^{-1}	6.29^{-2}	1.95^{-2}	5.64^{-3}	1.65^{-1}	6.30^{-2}	1.96^{-2}	5.58^{-3}
110	1.12^{-1}	5.05^{-2}	1.60^{-2}	4.03^{-3}	1.29^{-1}	4.90^{-2}	1.60^{-2}	4.00^{-3}
120	9.45^{-2}	4.16^{-2}	1.35^{-2}	3.02^{-3}	1.05^{-1}	4.01^{-2}	1.35^{-2}	3.00^{-3}
130	8.27^{-2}	3.55^{-2}	1.17^{-2}	2.38^{-3}	8.80^{-2}	3.42^{-2}	1.16^{-2}	2.36^{-3}
140	7.39^{-2}	3.12^{-2}	1.03^{-2}	1.96^{-3}	7.66^{-2}	3.03^{-2}	1.02^{-2}	1.95^{-3}
150	6.80^{-2}	2.84^{-2}	9.30^{-3}	1.70^{-3}	6.90^{-2}	2.78^{-2}	9.18^{-3}	1.69^{-3}
160	6.38^{-2}	2.66^{-2}	8.61^{-3}	1.54^{-3}	6.41^{-2}	2.61^{-2}	8.50^{-3}	1.53^{-3}
170	6.15^{-2}	2.56^{-2}	8.22^{-3}	1.45^{-3}	6.13^{-2}	2.52^{-2}	8.11^{-3}	1.44^{-3}
180	6.08^{-2}	2.52^{-2}	8.09^{-3}	1.42^{-3}	6.04^{-2}	2.49^{-2}	7.98^{-3}	1.41^{-3}
Integral	11.52	7.11	3.64	1.84	5.57	3.53	1.86	0.95

The negative number is the power of ten, if any, by which the number is to be multiplied.

Fig. 1. Calculated elastic differential cross sections (a.u.) for electron exchange scattering by the hydrogen atom in the 1s state:

BBGM1: first order method of Bates, Bassel, Gerjuoy, and Mittleman

BO: Born-Oppenheimer approximation

BOMC: Born-Oppenheimer approximation without the core term

BS: 1s-2s-2p close coupling calculations (Bu 62b)

BSS: 1s-2s-2p close coupling calculations (Bu 63)

E: 1s close coupling calculations (Jo 60, Te 61, Sm 62)

EA: exchange adiabatic approximation (Te 61)

GAILITIS: Gailitis' correlation method calculation (Ga 65)

G-3S: 1s-2s-3s close coupling calculations (Ge 60)

O. II: 1-state unitarized Ochkur approximation

OR: Ochkur-Rudge approximation

ORB. II: 1-state unitarized Ochkur-Rudge approximation

SMF-2S: 1s-2s close coupling calculations (Sm 62)

TL-PO: polarized orbital method (Te 61)

TLS-PO: polarized orbital method (Te 61, Sl 64)

(A)-(B): $E_i = 1.224$ eV

(C): $E_i = 1.360$ eV

(D): $E_i = 2.177$ eV

(E)-(F): $E_i = 3.431$ eV

(G)-(H): $E_i = 5.442$ eV

(I): $E_i = 54.42$ eV

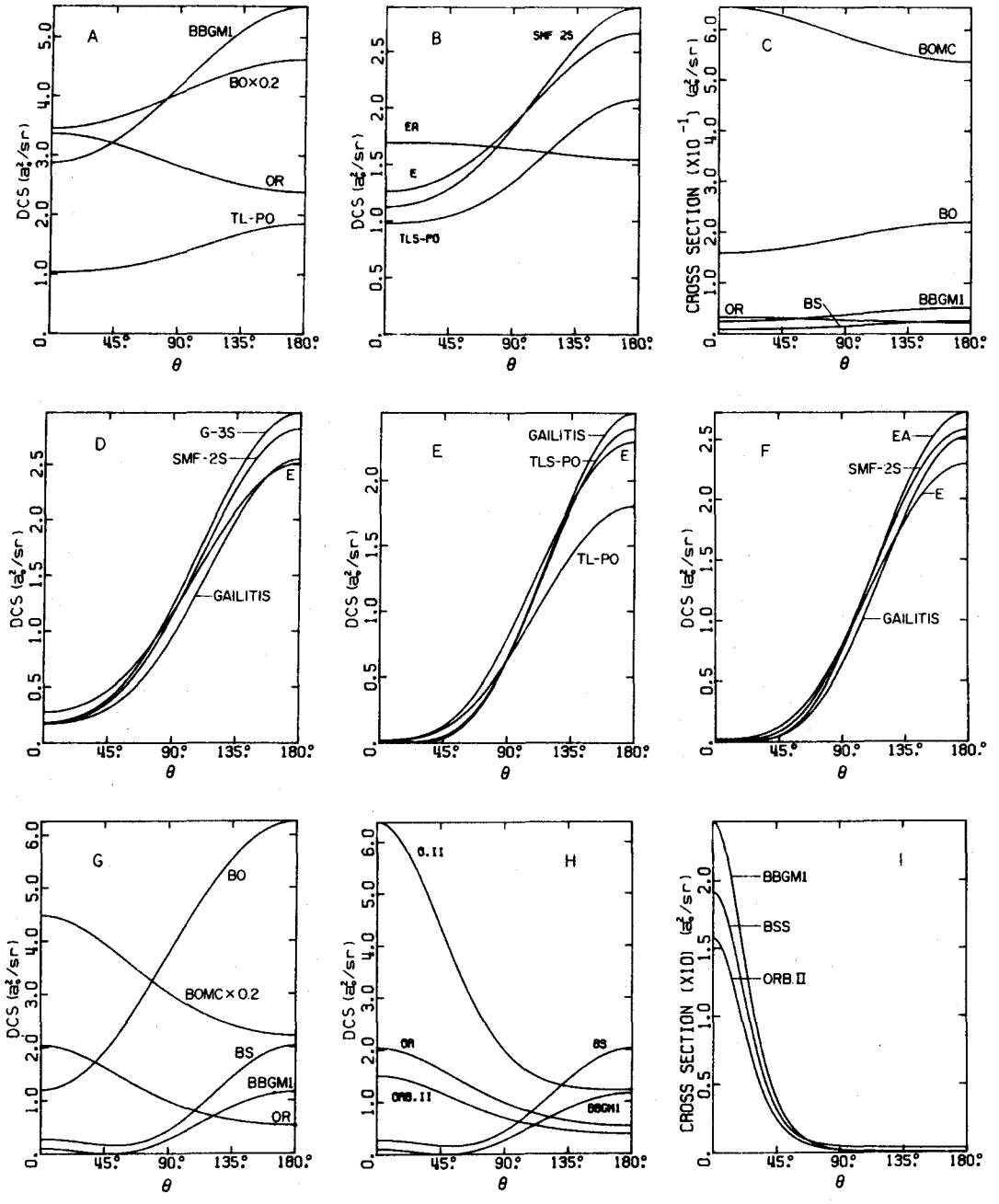
A
BBGM1
BO×0.2
OR
TL-PO
DCS (a.u./sr)
θ
B
SMF 2S
EA
E
TLS-PO
C
BOMC
BO
OR
BS
BBGM1
CROSS SECTION (X10⁻¹) (a.u./sr)
D
G-3S
SMF-2S
E
GAILITIS
E
GAILITIS
TLS-PO
E
TL-PO
F
EA
SMF-2S
E
GAILITIS
G
BO
BOMC×0.2
BS
BBGM1
OR
H
O.II
OR
BS
ORB.II
BBGM1
I
BBGM1
BSS
ORB.II
CROSS SECTION (X10) (a.u./sr)

Fig. 2. Calculated differential cross sections (a.u.) for electron exchange scattering.

(A)-(H): elastic scattering from the 1s state of the hydrogen atom:

BBGM1: first order method of Bates, Bassel, Gerjuoy, and Mittleman

BO: Born-Oppenheimer approximation

BOMC: Born-Oppenheimer approximation without the core term

BS: 1s-2s-2p close coupling calculations (Bu 62b)

BSS: 1s-2s-2p close coupling calculations (Bu 63)

E: 1s close coupling calculations (Jo 60, Te 61, Sm 62)

G-3S: 1s-2s-3s close coupling calculations (Ge 60)

O.II 1 x 1: 1-state unitarized Ochkur approximation

O.II 2 x 2: 2-state unitarized Ochkur approximation

OR: Ochkur-Rudge approximation

ORB.II or ORB.II 1 x 1: 1-state unitarized Ochkur-Rudge approximation

ORB.II 2 x 2: 2-state unitarized Ochkur-Rudge approximation

TL-PO: polarized orbital method (Te 61)

TLS-PO: polarized orbital method (Te 61, Sl 64)

(A)-(B): $E_i = 9.52$ eV

(C)-(F): $E_i = 13.60$ eV

(G)-(H): $E_i = 19.59$ eV

(I): excitation of helium from $1\,^1S$ state to $2\,^1S$ state in the Ochkur approximation. Impact energy (in eV) is indicated.

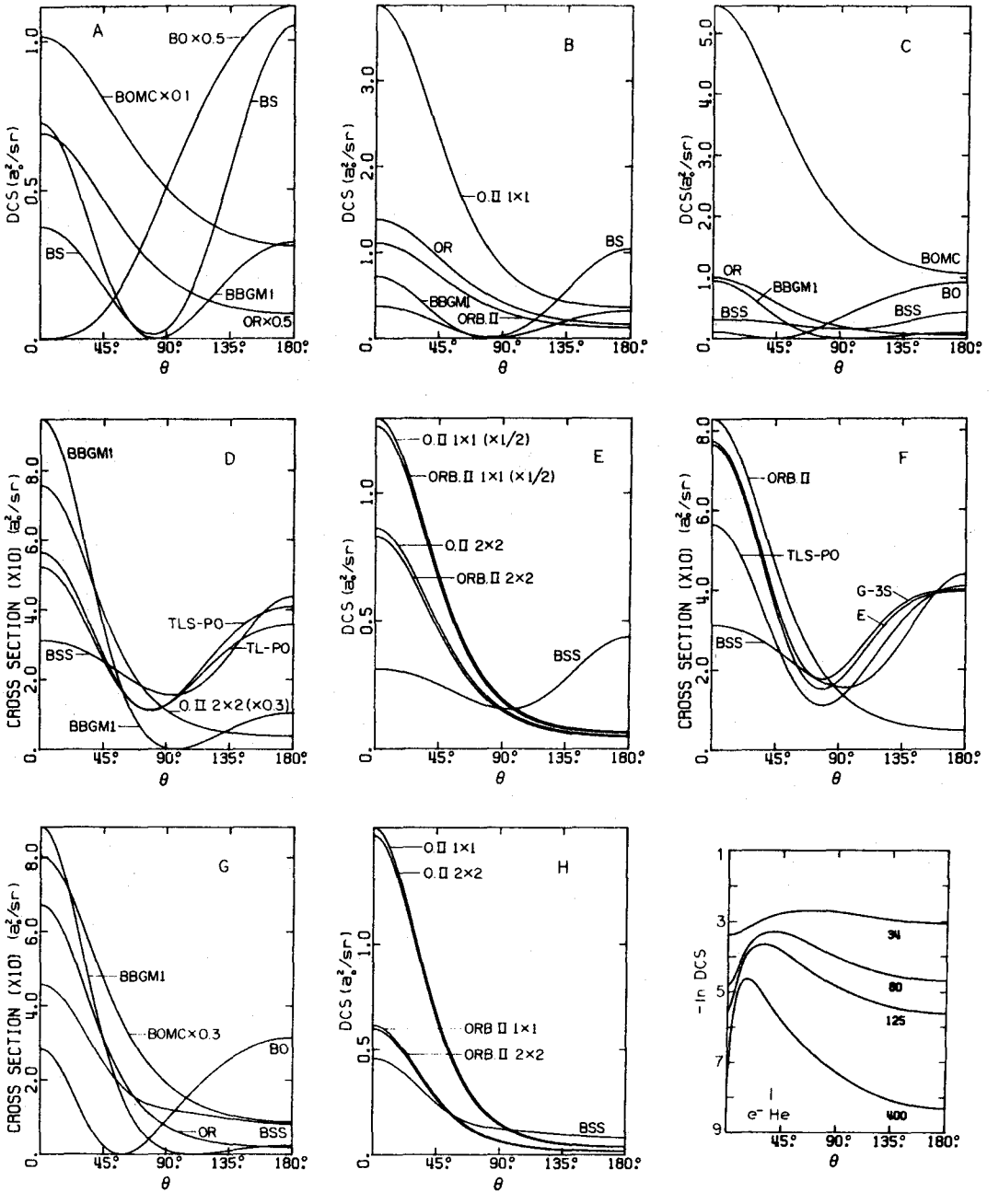
A
BO×0.5
BOMC×0.1
BS
BS
BBGM1
OR×0.5
DCS (a₀²/sr)
θ
B
0.Ⅱ 1×1
OR
BS
BBGM1
ORB.Ⅱ
C
BOMC
OR
BBGM1
BO
BSS
BSS
D
BBGM1
TLS-PO
TL-PO
BSS
0.Ⅱ 2×2(×0.3)
BBGM1
CROSS SECTION (X10) (a₀²/sr)
E
0.Ⅱ 1×1 (×1/2)
ORB.Ⅱ 1×1 (×1/2)
0.Ⅱ 2×2
ORB.Ⅱ 2×2
BSS
F
ORB.Ⅱ
TLS-PO
G-3S
E
BSS
G
BBGM1
BOMC×0.3
BO
OR
BSS
H
0.Ⅱ 1×1
0.Ⅱ 2×2
ORB.Ⅱ 1×1
ORB.Ⅱ 2×2
BSS
-ln DCS
34
80
125
400
e⁻ He

Fig. 3. Calculated differential cross sections (a.u.) for electron scattering:

BBGM1: first order method of Bates, Bassel, Gerjuoy, and Mittleman

BO: Born-Oppenheimer approximation

BOMC: Born-Oppenheimer approximation without the core term

BORB.I: symmetrized Born-Ochkur-Rudge approximation

BTKF: Born-transferred Kang-Foland approximation

BSS: 1s-2s-2p close coupling calculations (Bu 63)

O: prior Ochkur approximation

O.II: 1-state unitarized prior Ochkur approximation

OR, ORB.I: Ochkur-Rudge approximation

ORB.II: unitarized Ochkur-Rudge approximation

TKF: transferred Kang-Foland approximation

VPS: method of Vainshtein, Presnyakov, and Sobelman

(A)-(G): exchange excitation of the 2s state of the hydrogen atom at the impact energies (in eV) indicated.

(H)-(I): exchange (part H and curves labeled E in part I) and total (curves labeled T) excitation of the $2\,^1S$ state of the helium atom at the impact energies (in eV) indicated.

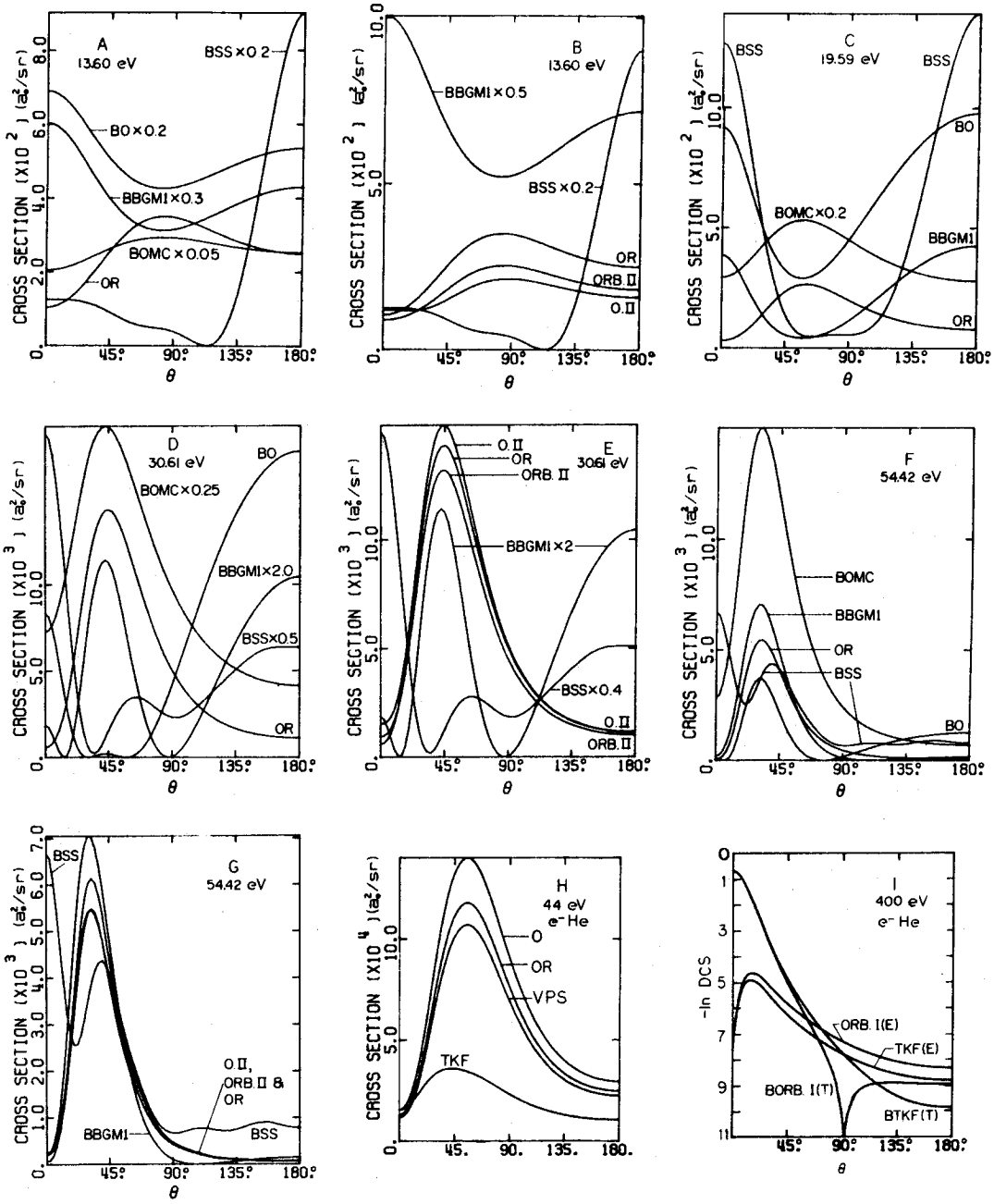
A
13.60 eV
BSS×0.2
BO×0.2
BBGMI×0.3
BOMC×0.05
OR
B
13.60 eV
BBGMI×0.5
BSS×0.2
OR
ORB.II
O.II
C
19.59 eV
BSS
BSS
BO
BOMC×0.2
BBGMI
OR
D
30.61 eV
BO
BOMC×0.25
BBGMI×2.0
BSS×0.5
OR
E
30.61 eV
O.II
OR
ORB. II
BBGMI×2
BSS×0.4
O.II
ORB.II
F
54.42 eV
BOMC
BBGMI
OR
BSS
BO
G
54.42 eV
BSS
O.II,
ORB.II &
OR
BBGMI
BSS
H
44 eV
e⁻ He
O
OR
VPS
TKF
I
400 eV
e⁻ He
ORB. I(E)
TKF(E)
BORB. I(T)
BTKF(T)
CROSS SECTION (X10²) (a₀²/sr)
CROSS SECTION (X10³) (a₀²/sr)
CROSS SECTION (X10⁴) (a₀²/sr)
-ln DCS
θ
45°
90°
135°
180°

Fig. 4. Calculated differential cross sections (a.u.) for electron exchange elastic scattering from the 1s state of the hydrogen atom at an impact energy of 30.61 eV. The methods used are:

BBGM1: first order method of Bates, Bassel, Gerjuoy, and Mittleman

BO: Born-Oppenheimer approximation

BOMC: Born-Oppenheimer approximation without the core term

BSS: 1s-2s-2p close coupling calculations (Bu 63)

G-3S: 1s-2s-3s close coupling calculations (Ge 60)

O.II: unitarized Ochkur approximation

OR: Ochkur-Rudge approximation

ORB.II: unitarized Ochkur-Rudge approximation

Fig. 5. Differential cross sections (a_o^2/ sr) for 1s-1s exchange scattering off the hydrogen atom at E_i = 1.224 eV. The polarized orbital calculations are from Te 61.

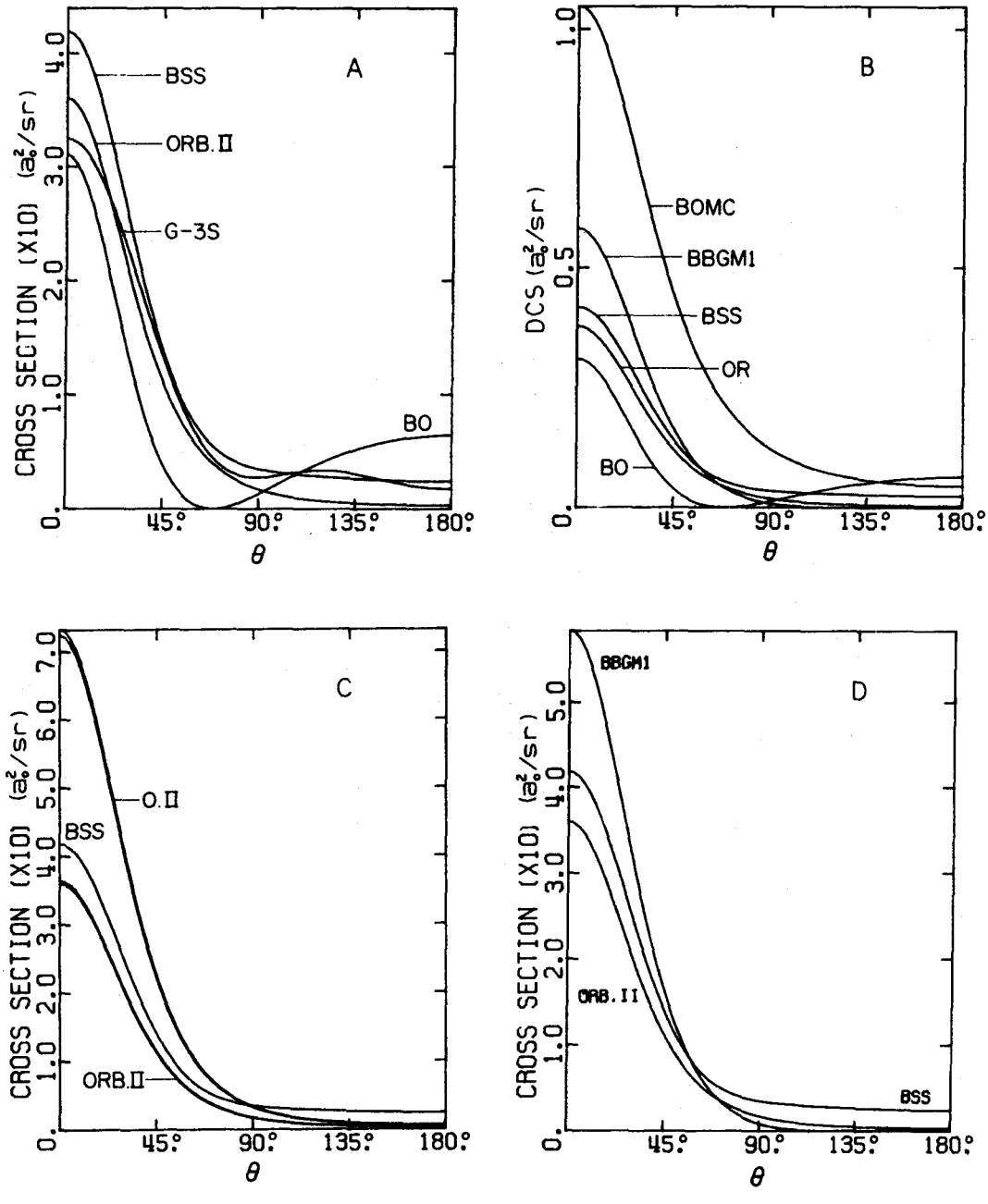
A
BSS
ORB.II
G-3S
BO
CROSS SECTION (X10) (a₀²/sr)
θ
B
BOMC
BBGM1
BSS
OR
BO
DCS (a₀²/sr)
C
O.II
BSS
ORB.II
D
BBGM1
ORB.II
BSS

4

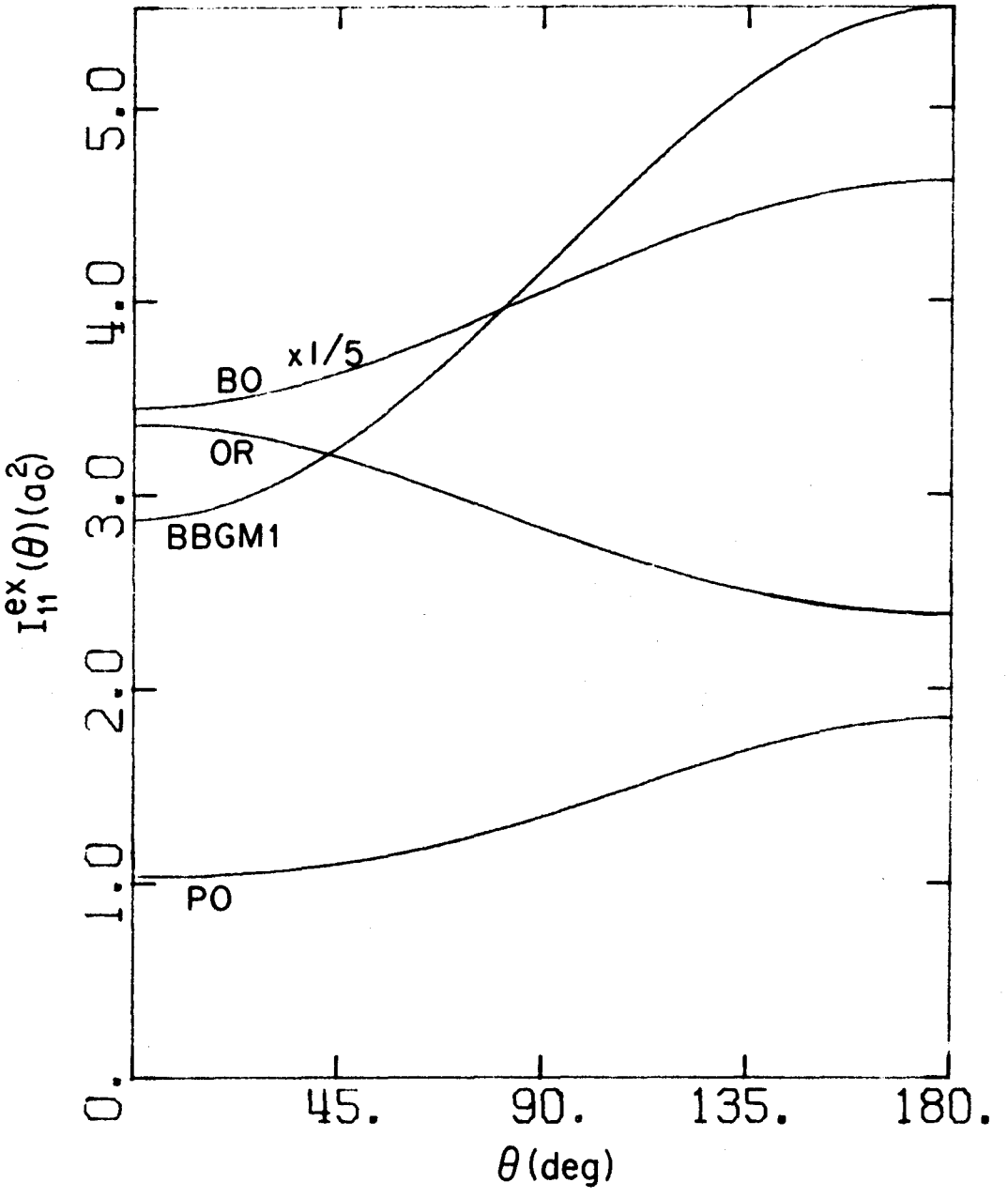
5.0
4.0
3.0
2.0
1.0
0.
45.
90.
135.
180.
θ (deg)
$I_{11}^{ex}(\theta)(a_o^2)$
BO
x1/5
OR
BBGM1
PO

5

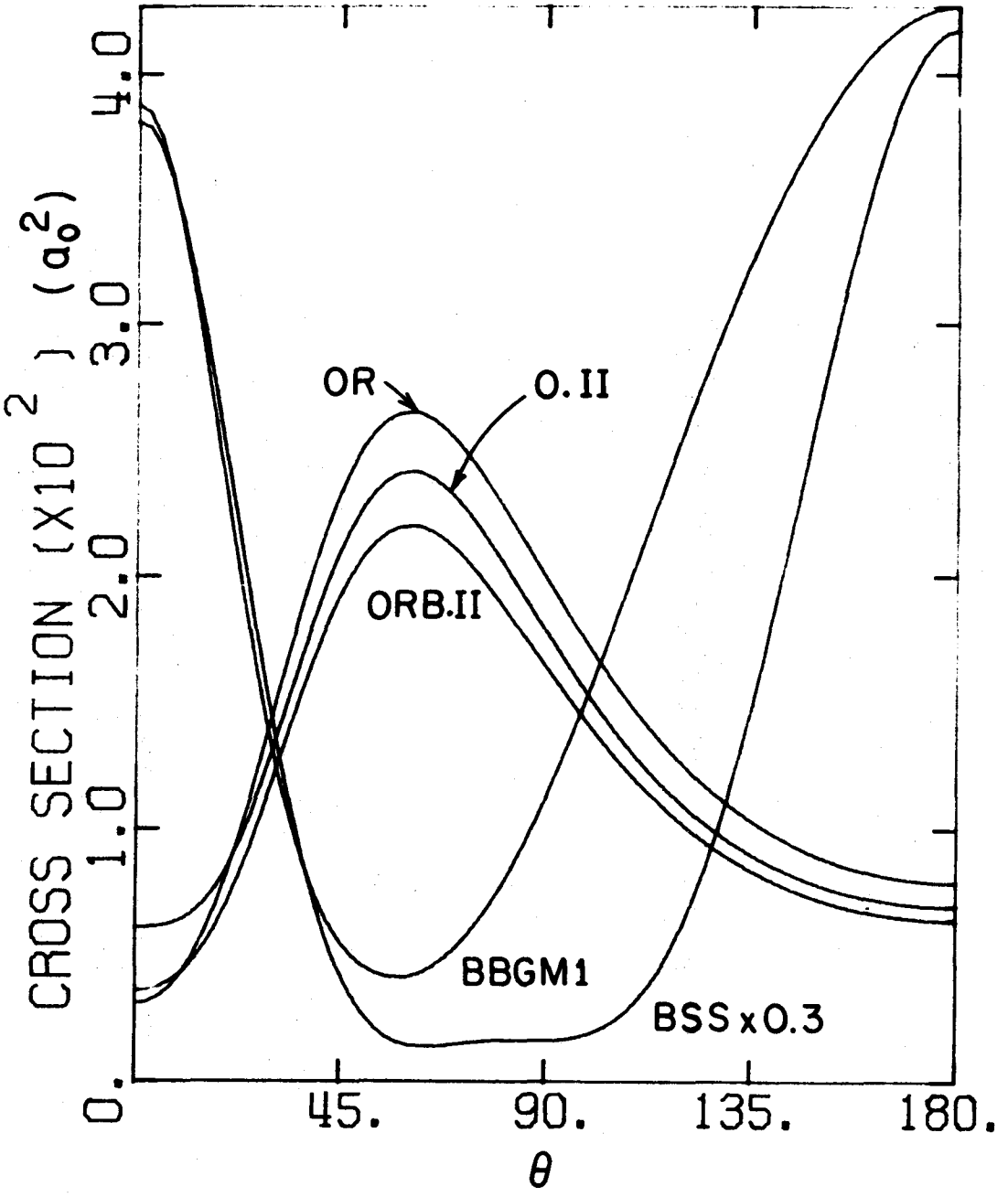

Fig. 6. Angular distribution of exchange scattered electrons for 1s - 2s excitation of H. E = 19.6 eV.

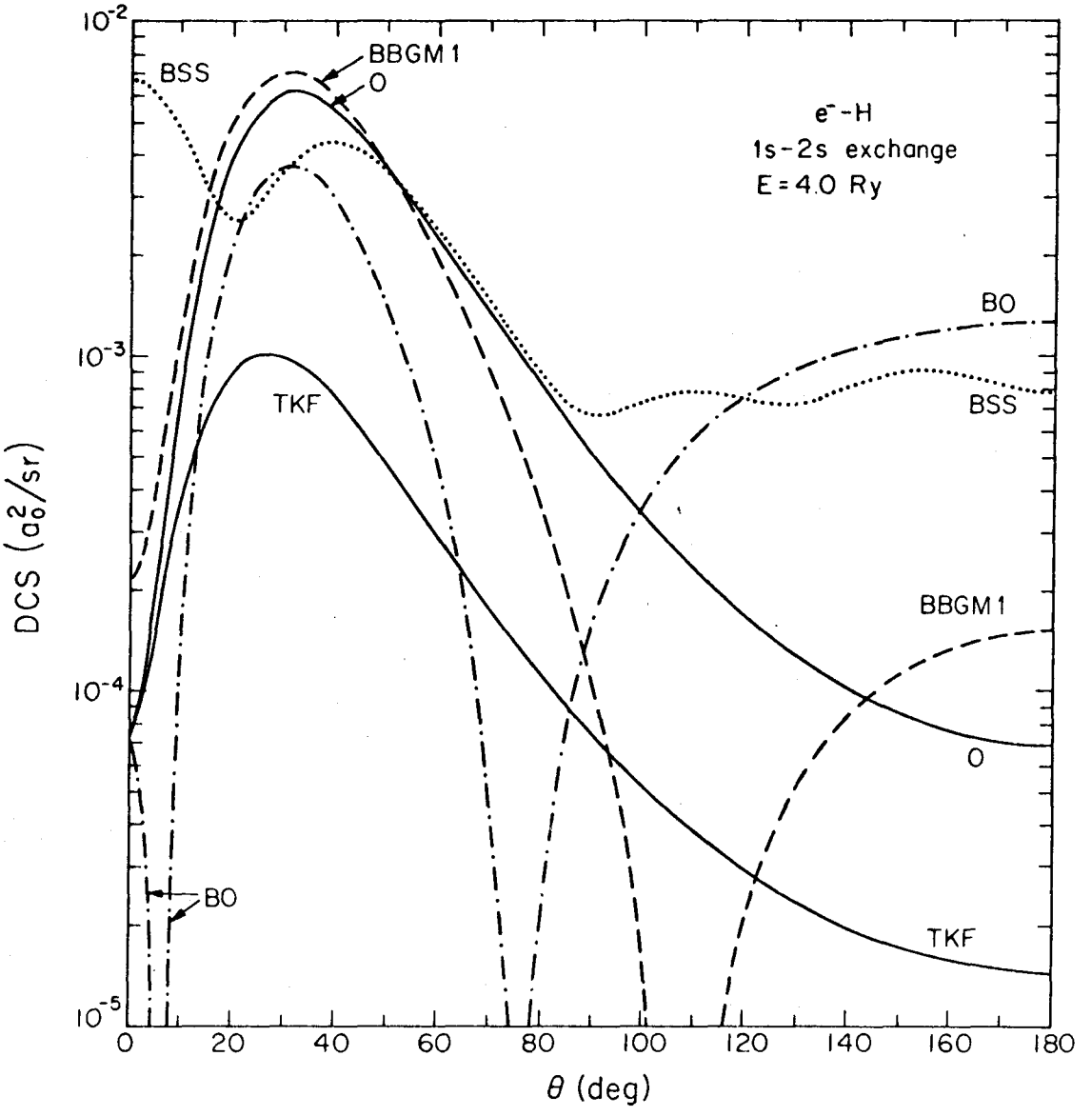

Fig. 7. Differential cross sections (a_o^2/s r) for 1s - 2s exchange scattering off the hydrogen atom at E_i = 54.42 eV. The BSS curve is from Bu 63.

Fig. 8 Integral cross sections (a.u.) vs. impact energy for total scattering of electrons off the ground state of the hydrogen atom with excitation of the 2s state. The present calculations shown are the Born, Born-Oppenheimer, and symmetrized Born-Ochkur-Rudge approximations. The circles are 1s-2s close coupling calculations without exchange (Sm 60). The triangles are 1s-2s-2p close coupling calculations including exchange (Bu 63). Both these calculations are off scale at an impact energy of 13.6 eV. The squares are calculations in a modified version of the Vainshtein-Presnyakov-Sobelman method (Cr 65). The pentagon is from the 6-state close coupling calculations with exchange (Bu 67). The dotted line is the calculation of Morrison and Rudge (Mo 66a). The vertical lines cover the range covered by the three "experimental" results (see Tr 69a for a discussion).

Fig. 9. Calculated differential cross sections (a.u.) for electron scattering by the helium atom.

(A) Total (T) and exchange (E) cross sections for excitation of the $2\,^1S$ and $2\,^1P$ states (S and P, respectively) at $E_i = 26.5$ eV calculated in the BTVPS approximation.

(B)-(I) Exchange cross sections according to the approximations indicated for excitation of the $2\,^1P$ state at the energies indicated.

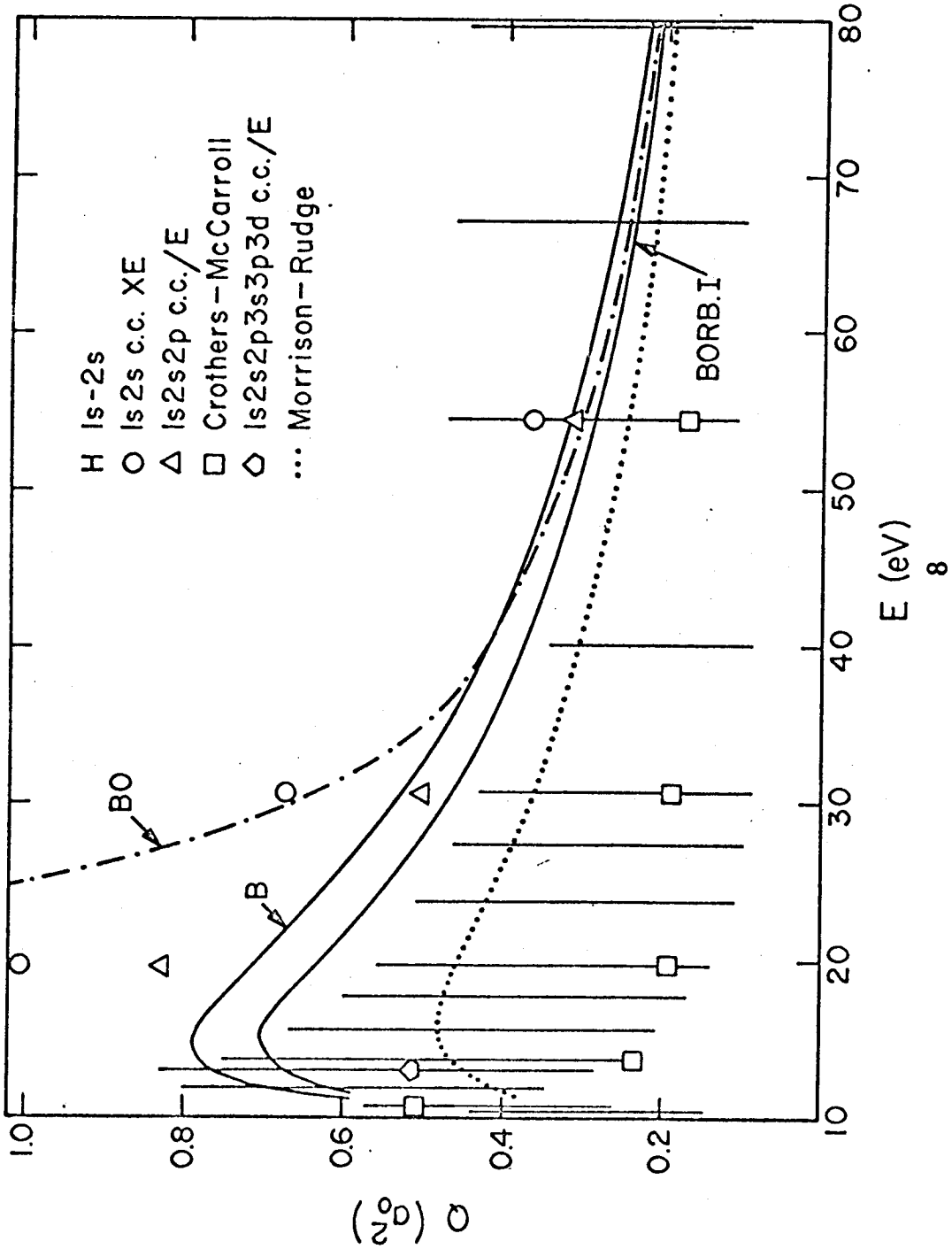
H 1s-2s
1s2s c.c. XE
1s2s2p c.c./E
Crothers-McCarroll
1s2s2p3s3p3d c.c./E
Morrison-Rudge
BORB.I
BO
B
Q (a₀²)
E (eV)
1.0
0.8
0.6
0.4
0.2
10
20
30
40
50
60
70
80

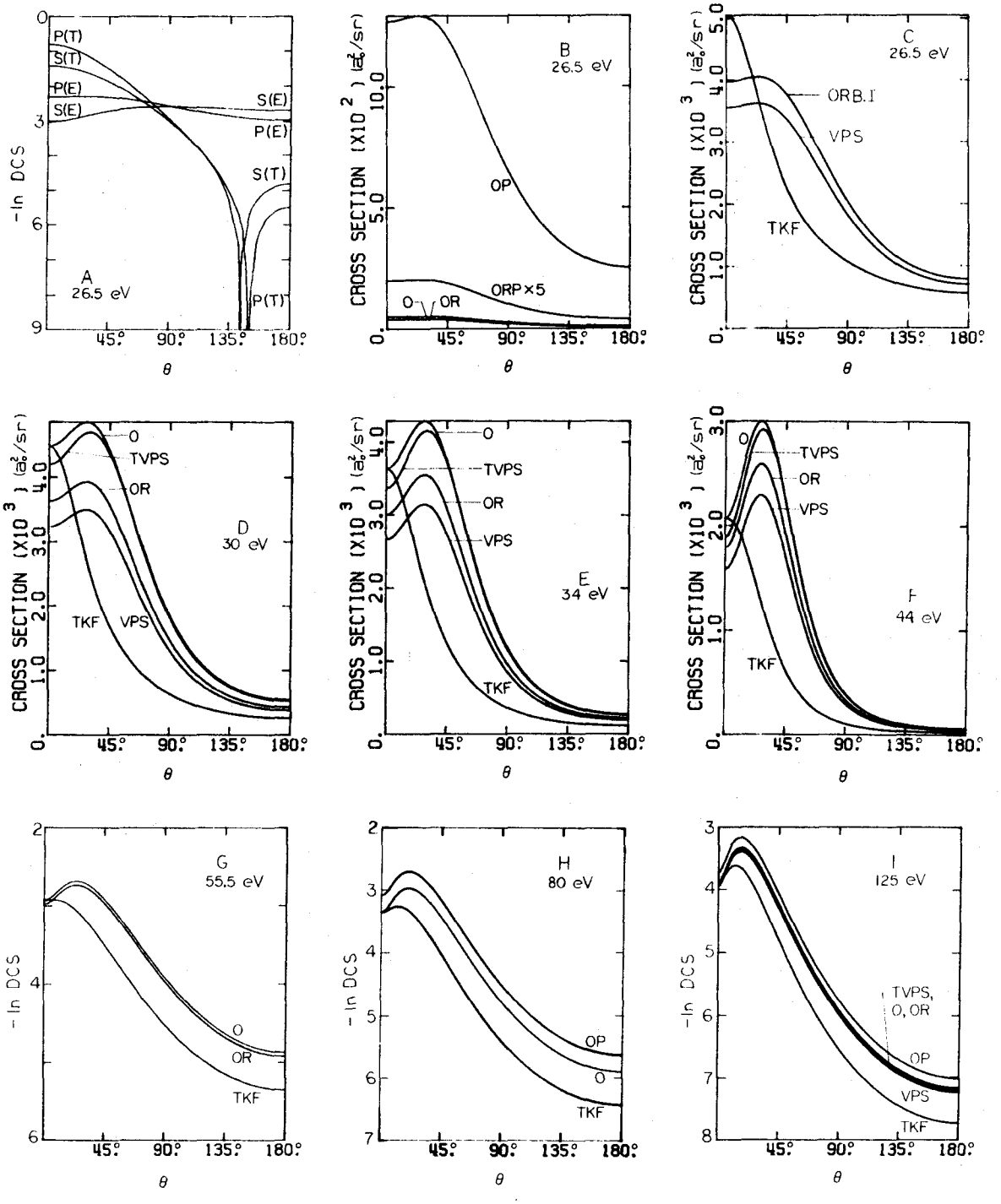
A
26.5 eV
P(T)
S(T)
P(E)
S(E)
-ln DCS
θ
B
26.5 eV
OP
ORP×5
O
OR
CROSS SECTION (X10 2) (a0 2/sr)
C
26.5 eV
ORB.I
VPS
TKF
CROSS SECTION (X10 3) (a0 2/sr)
D
30 eV
O
TVPS
OR
TKF
VPS
E
34 eV
F
44 eV
G
55.5 eV
H
80 eV
I
125 eV
TVPS, O, OR

Fig. 10. Calculated differential cross sections (a.u.) for electron scattering by the helium atom.

(A)-(H) Exchange cross sections for excitation of the $3\,^1P$ state.

(A)-(C) The approximations used and the impact energies are indicated. The O method DCS is greater than the TVPS one at small angles.

(D) E_i = 44 eV. The approximations used are indicated. The O method DCS is not shown because it is too similar to the OR one to be clearly distinguished. The TVPS method DCS is multiplied by 0.1 so it is separated from the OR one.

(E) E_i = 55.5 eV. The approximations used are indicated. The O and TVPS method DCS's are not shown because they are almost parallel to the OR one and within 10% of it over the whole angular range.

(F) E_i = 80 eV. The approximations used are indicated. The O and ORB.I method DCS's are not shown because they are almost indistinguishable from the OR one on the scale of this figure.

(G) O approximation. The impact energies (eV) are indicated.

(H) ORB.I approximation. The impact energies (eV) are indicated.

(I) Total cross sections for excitation of the $2\,^1S$ state of He. The approximations used are indicated. E_i = 125 eV.

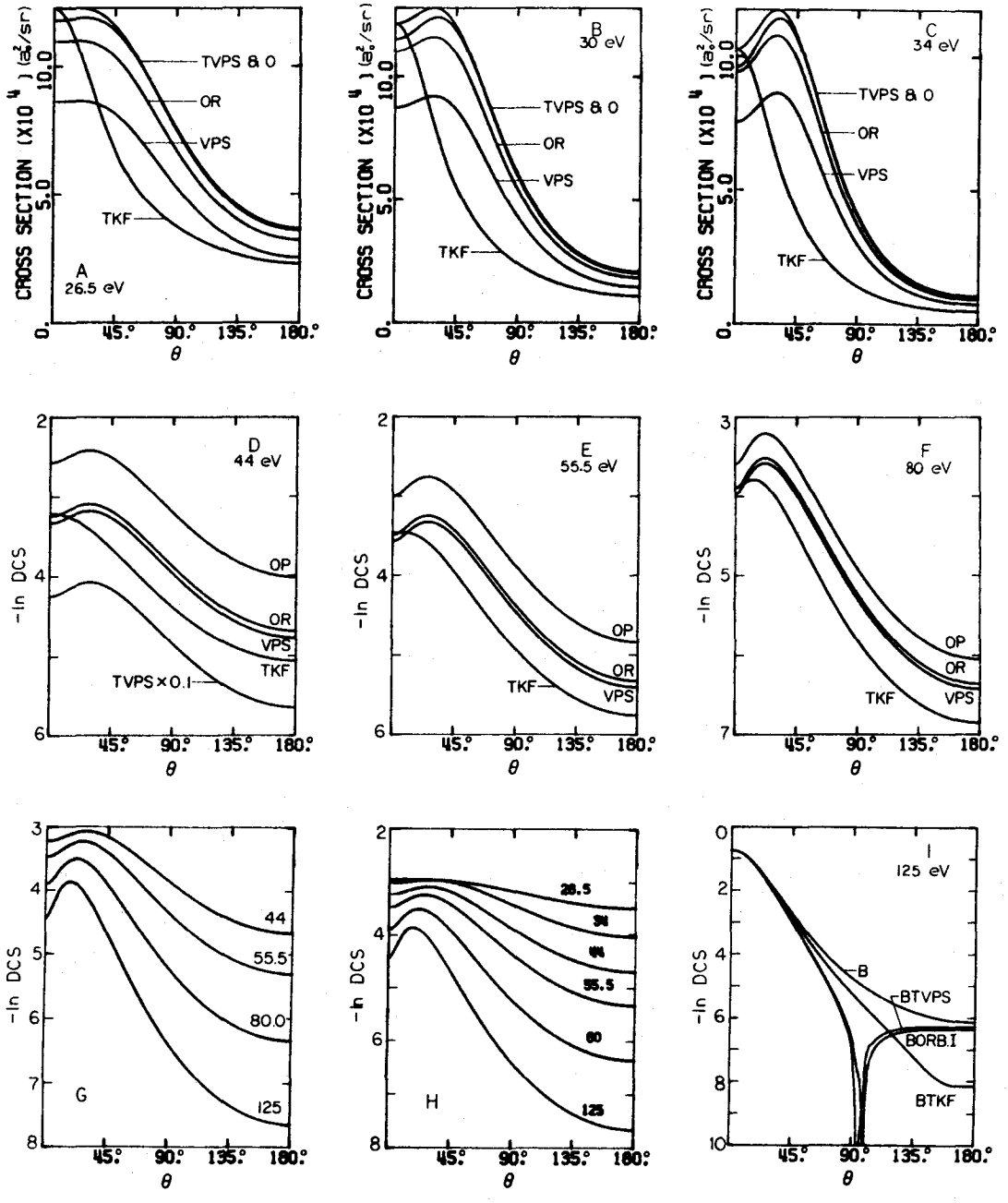
CROSS SECTION (X10^4) (a_o^2/sr)
10.0
5.0
0.
TVPS & O
OR
VPS
TKF
A
26.5 eV
B
30 eV
C
34 eV
45.°
90.°
135.°
180.°
θ
-ln DCS
2
4
6
D
44 eV
OP
OR
VPS
TKF
TVPS×0.1
E
55.5 eV
3
5
7
F
80 eV
G
44
55.5
80.0
125
H
28.5
I
125 eV
B
BTVPS
BORB.I
BTKF
0
8
10

Fig. 11. Calculated exchange differential cross sections (a.u.) for excitation of the $2\,^1S$ state of helium.

(A)-(F): Approximations used and impact energies are indicated. In D the TVPS method DCS is not shown but for $\theta \geq 40^o$ it is greater than the O one but within 2% of it. In E the O, OR, and TVPS method DCS's are not shown but lie everywhere between the OP and VPS ones and within 1% of the latter. In F the O method DCS is not shown because it is between the OP and OR and for $\theta \geq 20^o$ it is within 2% of the TVPS one.

(G)-(I): The impact energies (eV) are indicated. The approximations used are OP in G, OR in H, and TVPS in I.

Fig. 12. Calculated differential cross sections (a.u.) for total scattering of electrons off the ground state of the helium atom with excitation of an $n\,^1P$ state. The impact energies and methods are indicated.

(A)-(F) : $n = 2$

(G)-(I) : $n = 3$

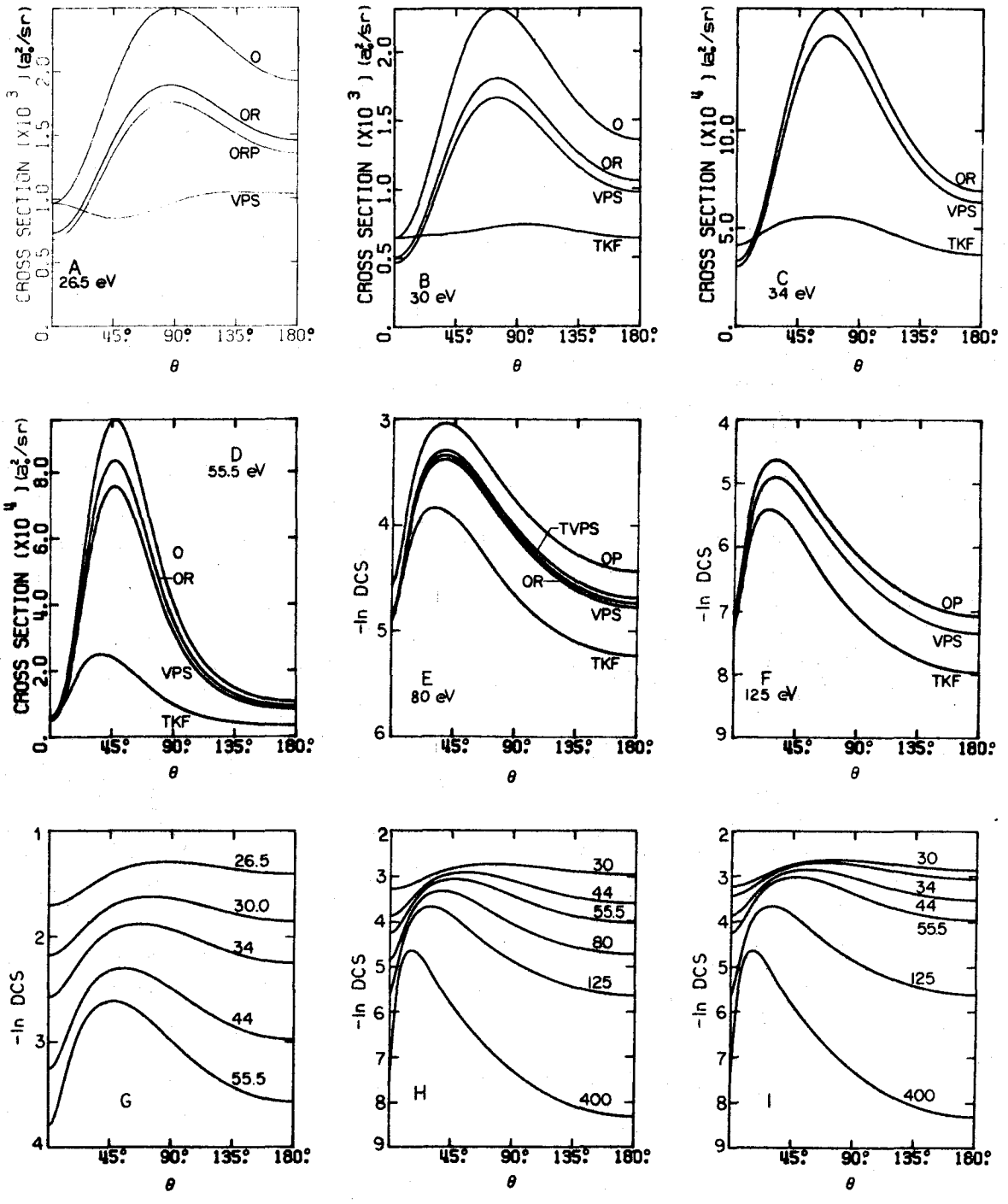
A
26.5 eV
O
OR
ORP
VPS
B
30 eV
TKF
C
34 eV
D
55.5 eV
E
80 eV
TVPS
OP
F
125 eV
G
26.5
30.0
34
44
55.5
H
30
44
55.5
80
125
400
I
CROSS SECTION
-ln DCS
θ

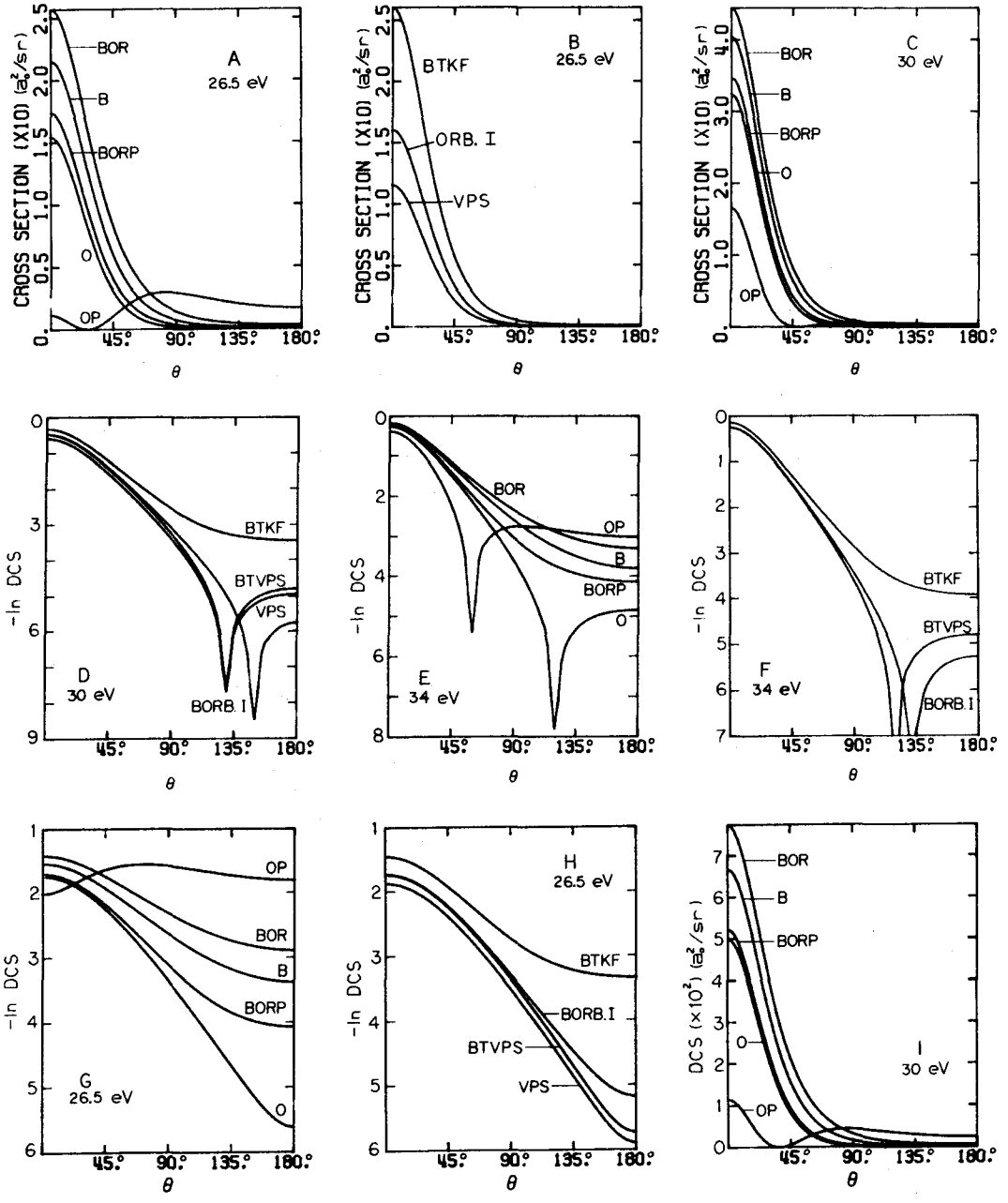
A
26.5 eV
BOR
B
BORP
O
OP
CROSS SECTION (X10) (a₀²/sr)
θ
B
26.5 eV
BTKF
ORB. I
VPS
C
30 eV
D
30 eV
BTVPS
BORB. I
-ln DCS
E
34 eV
F
34 eV
G
26.5 eV
H
26.5 eV
I
30 eV
DCS (×10²) (a₀²/sr)

Fig. 13. Calculated differential cross sections (a.u.) for electron scattering off the ground state of the helium atom.

(A)-(C): Total excitation of $3\,^1P$ state. The impact energies and methods are indicated. The BORB.I curve is less than 7% higher than the BTVPS one at 0^o.

(D): Exchange (E) and total (T) excitation of $3\,^1P$ state according to BTVPS approximation. The impact energies (in eV) are indicated.

(E)-(F): Exchange excitation of $n\,^1P$ state according to OR approximation. The impact energies (in eV) and n are indicated.

(G): Exchange excitation of the states indicated according to OR approximation at an impact energy of 26.5 eV.

(H)-(I): Exchange excitation of $2\,^1S$ state according to OR approximation. The impact energies (in eV) are indicated.

Fig. 14. Calculated differential cross sections (a.u.) for electron scattering off the helium atom with the transition $1\,^1S \rightarrow 2\,^1P$.

(A)-(I), except (F): total scattering. The impact energies and methods are indicated.

(F): Exchange (E) and total scattering at an impact energy of 80 eV. The methods are indicated. For the exchange scattering, the O, OR, ORB.I, VPS, and TVPS cross sections are all the same or practically the same in this case. For the total scattering the VPS cross section is not shown because it is quite similar to the BORB.I and BTVPS ones in this case.

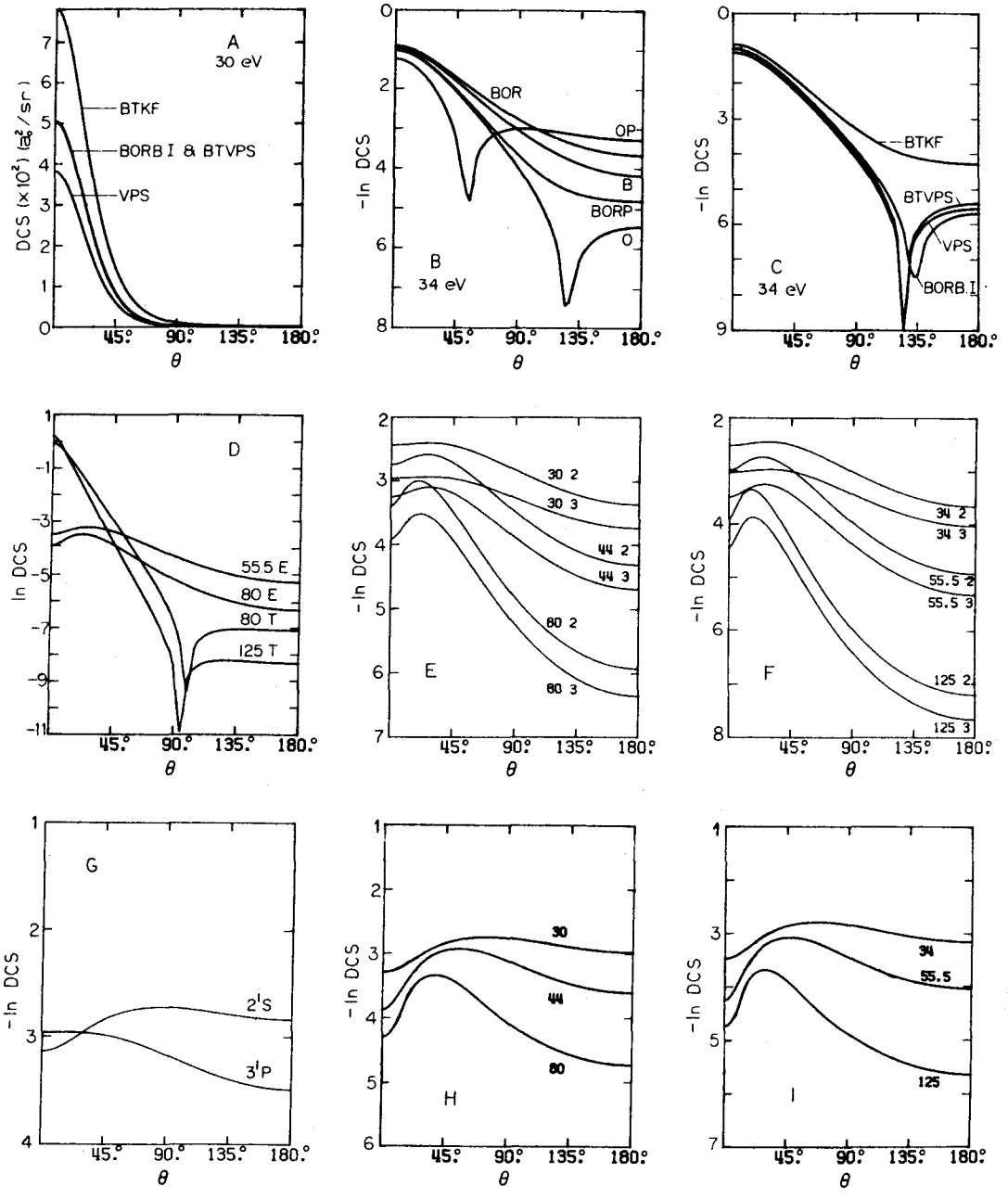
A
30 eV
BTKF
BORB I & BTVPS
VPS
DCS (x10²) (a₀²/sr)
B
34 eV
BOR
OP
B
BORP
O
-ln DCS
C
34 eV
BTKF
BTVPS
VPS
BORB I
D
55.5 E
80 E
80 T
125 T
ln DCS
E
30 2
30 3
44 2
44 3
80 2
80 3
F
34 2
34 3
55.5 2
55.5 3
125 2
125 3
G
2¹S
3¹P
H
30
44
80
I
34
55.5
125
45° 90° 135° 180°
θ

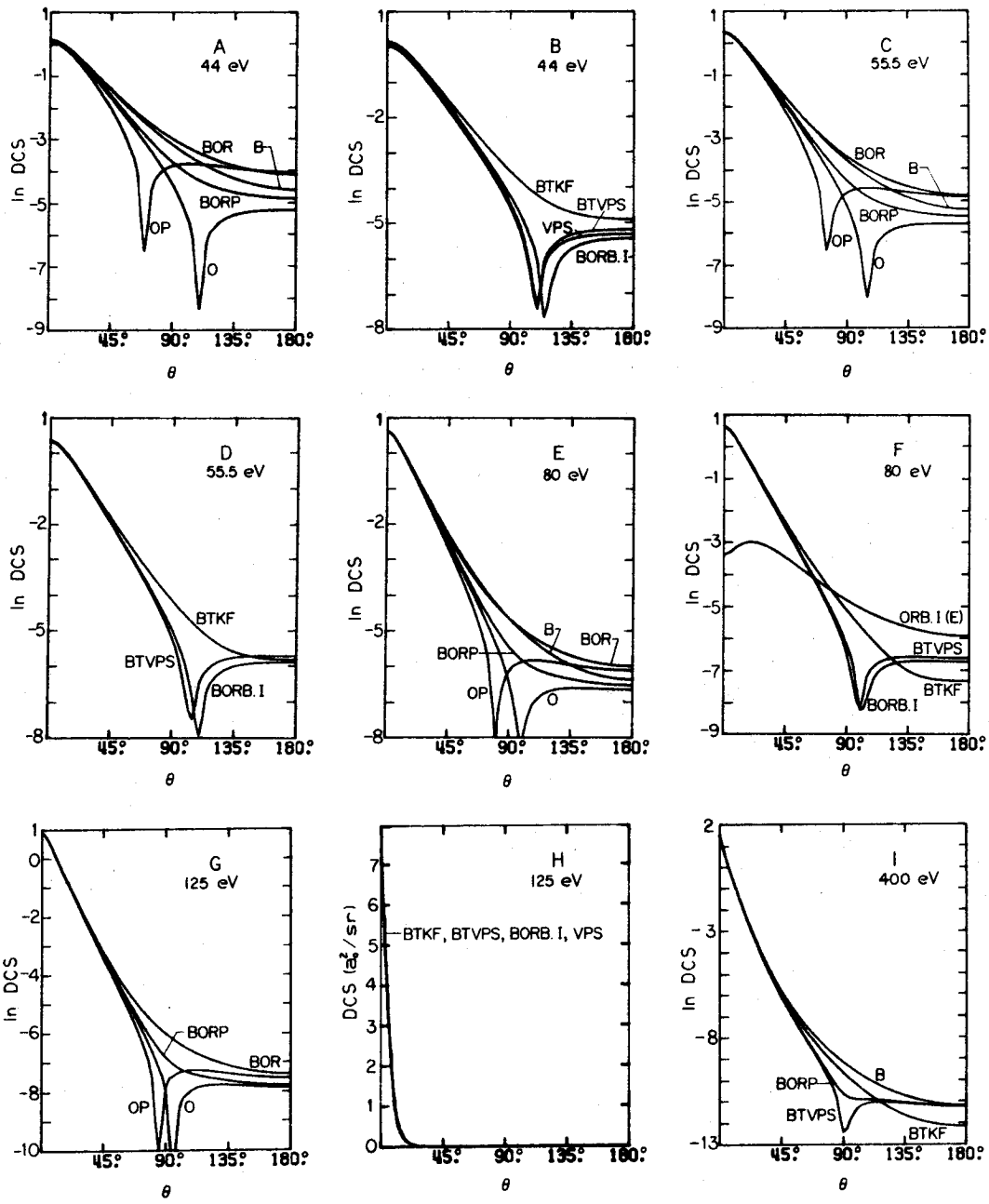
A
44 eV
BOR
B
BORP
OP
O
B
44 eV
BTKF
BTVPS
VPS
BORB.I
C
55.5 eV
BOR
B
BORP
OP
O
D
55.5 eV
BTKF
BTVPS
BORB.I
E
80 eV
B
BOR
BORP
OP
O
F
80 eV
ORB.I (E)
BTVPS
BTKF
BORB.I
G
125 eV
BORP
BOR
OP
O
H
125 eV
BTKF, BTVPS, BORB. I, VPS
I
400 eV
B
BORP
BTVPS
BTKF
ln DCS
DCS (a₀²/sr)
θ
45°
90°
135°
180°

Fig. 15. Calculated differential cross sections (a.u.) for electron total scattering off the helium atom with the transition $1\,^1S \rightarrow n\,^1P$.

(A): VPS approximation. The impact energies (in eV) and n are indicated.

(B)-(I): n = 3. The impact energies and methods are indicated.

(E): The VPS curve (not shown) is lower than but within 23% of the BTVPS one.

(G): The VPS and BTVPS curves are too similar to the BORB.I curve to be shown.

(H): The BTVPS curve (not shown) is within 20% of the VPS one.

Fig. 16. Calculated differential cross sections (a.u.) for electron total scattering off the ground state of the helium atom with excitation of the $2\,^1S$ state. The impact energies and methods are indicated.

Fig. 17. Calculated differential cross sections (a.u.) for electron total scattering off the helium atom with the transition $1\,^1S \rightarrow 2\,^1S$. The impact energies and methods are indicated. In part G, the VPS curve is not shown because the VPS, TVPS, BORB.I, and O curves have very similar shapes and magnitudes over the whole angular range.

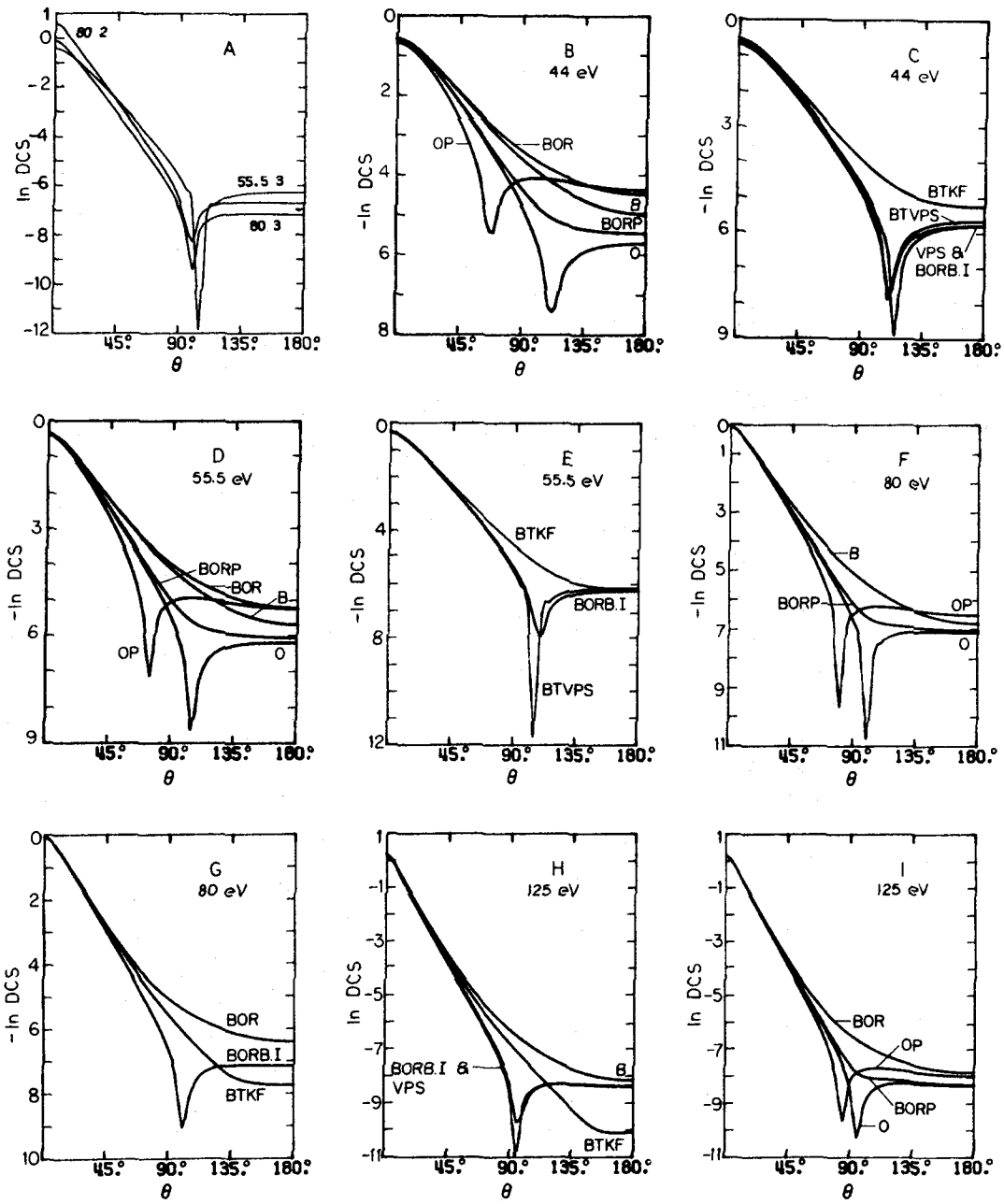
A
80 2
55.5 3
80 3
B
44 eV
OP
BOR
B
BORP
O
C
44 eV
BTKF
BTVPS
VPS &
BORB.I
D
55.5 eV
BORP
BOR
B
OP
O
E
55.5 eV
BTKF
BORB.I
BTVPS
F
80 eV
B
BORP
OP
O
G
80 eV
BOR
BORB.I
BTKF
H
125 eV
BORB.I &
VPS
B
BTKF
I
125 eV
BOR
OP
BORP
O
-ln DCS
ln DCS
θ
45°
90°
135°
180°

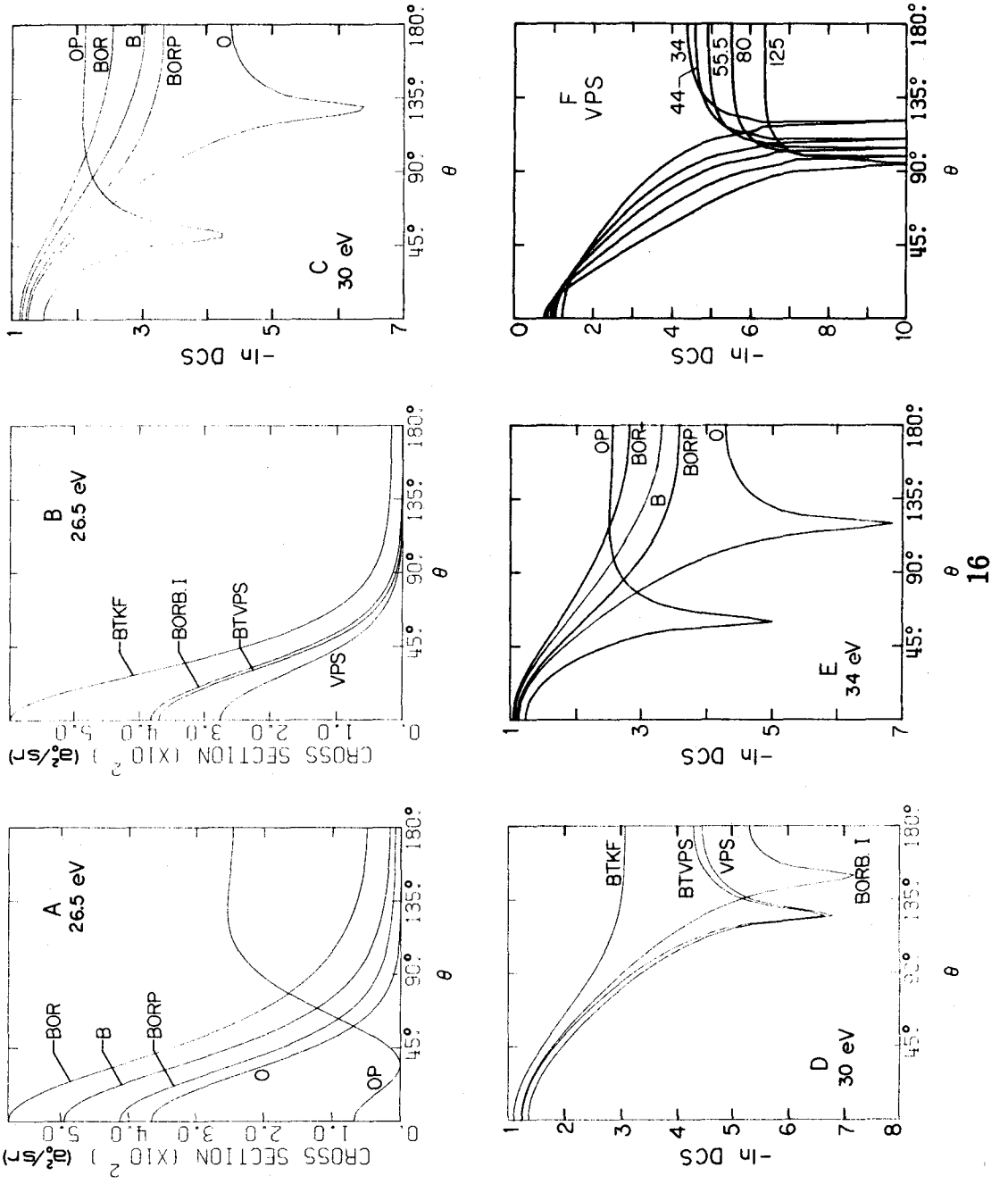
A
26.5 eV
BOR
B
BORP
O
OP
CROSS SECTION (X10 ^{2}) (a$_o^2$/sr)
B
26.5 eV
BTKF
BORB.I
BTVPS
VPS
C
30 eV
OP
BOR
B
BORP
O
-ln DCS
D
30 eV
BTKF
BTVPS
VPS
BORB.I
E
34 eV
F
VPS
44
34
55.5
80
125
θ
45°
90°
135°
180°

16

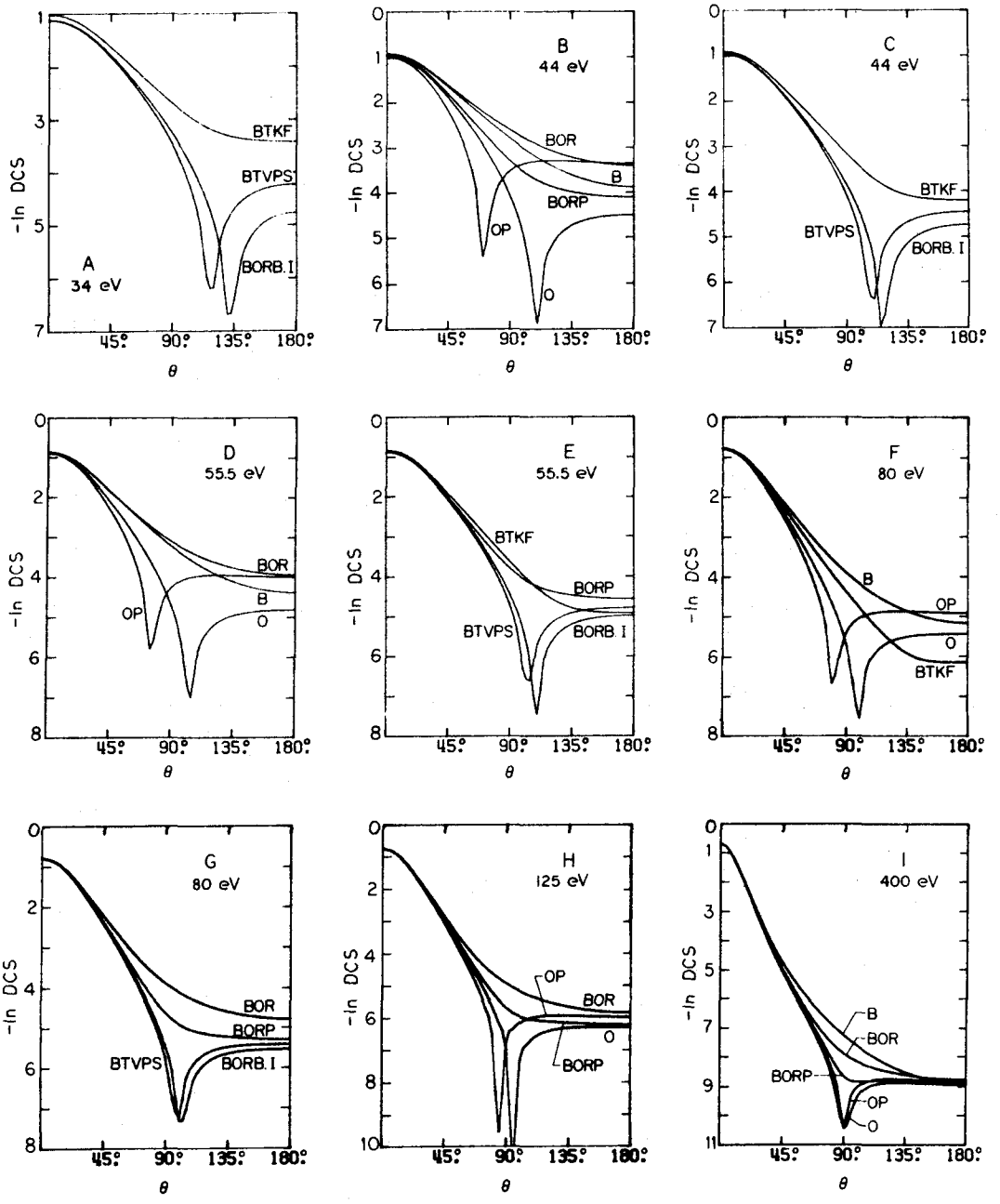
A
34 eV
BTKF
BTVPS
BORB.I
B
44 eV
BOR
B
BORP
OP
O
C
44 eV
BTKF
BTVPS
BORB.I
D
55.5 eV
BOR
B
OP
O
E
55.5 eV
BTKF
BORP
BTVPS
BORB.I
F
80 eV
B
OP
O
BTKF
G
80 eV
BOR
BORP
BTVPS
BORB.I
H
125 eV
OP
BOR
O
BORP
I
400 eV
B
BOR
BORP
OP
O
-ln DCS
θ
45°
90°
135°
180°

Fig. 18. Integral cross sections for electron scattering excitation of the $3\,^1P$ state of helium as functions of impact energy. The methods and sets of generalized oscillator strengths used for the calculations are indicated (see section A. 3). The results of two experimental investigations are also shown. The +'s are from St 64 and the x's are from Mo 69.

Fig. 19. Integral cross sections for electron scattering excitation of the $3\,^1P$ state of helium as functions of impact energy. The methods and sets of generalized oscillator strengths used for the calculations are indicated (see section A. 3).

Fig. 20. Integral cross sections for electron scattering excitation of the $2\,^1S$ state of helium as functions of impact energy. The squares are the experimental results of Richards, Dugan, and Muschlitz (corrected for cascade by the procedure of Gabriel and Heddle; Du 67, Ga 60); the triangles and diamonds are the semi-experimental, semi-theoretical results of Vriens, Simpson, and Mielczarek (Vr 68). The curves are calculated using the methods indicated.

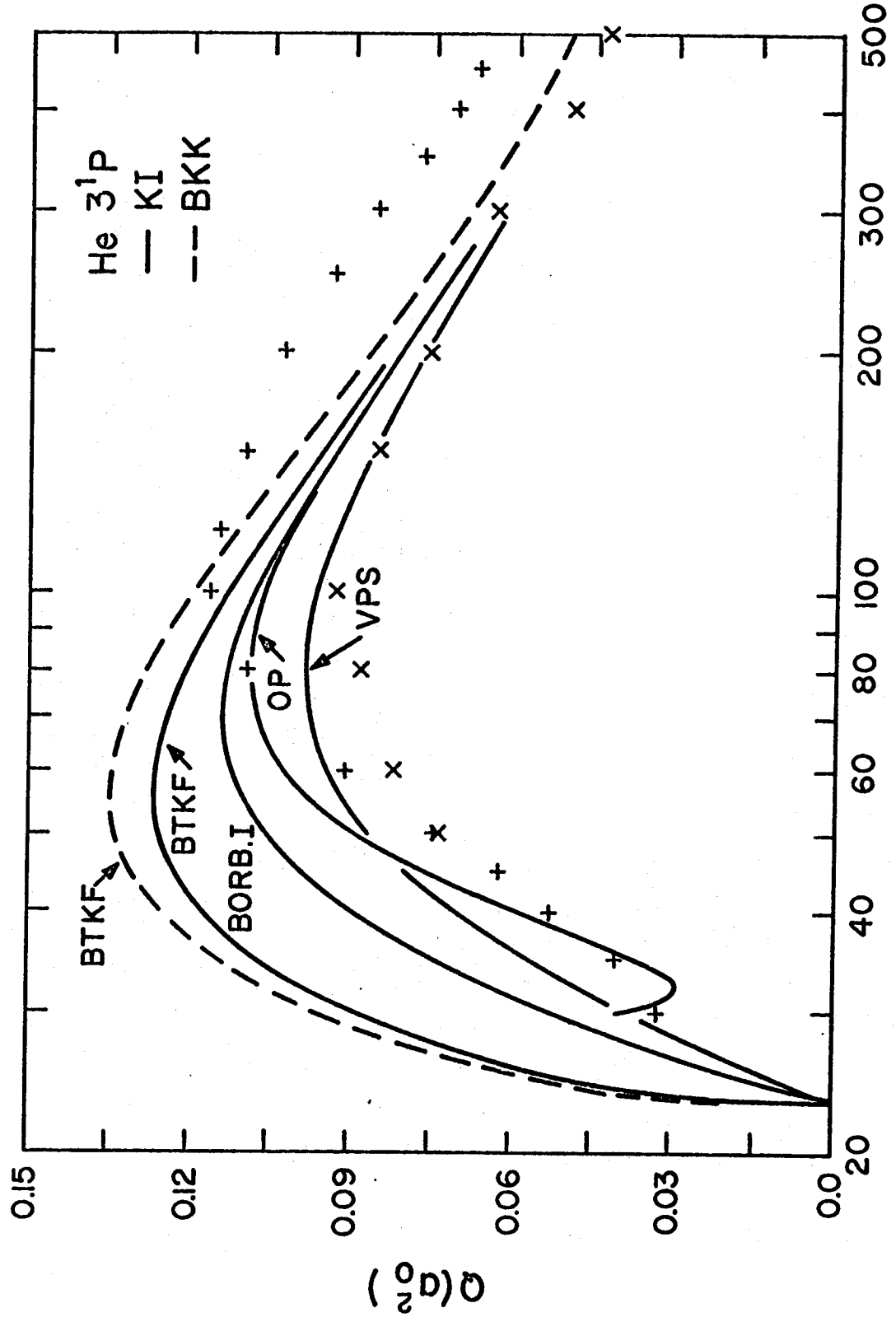
He 3¹P
— KI
-- BKK
BTKF
BTKF
BORB.I
OP
VPS
0.15
0.12
0.09
0.06
0.03
0.0
20
40
60
80
100
200
300
500
Ei(eV)
Q(a₀²)

18

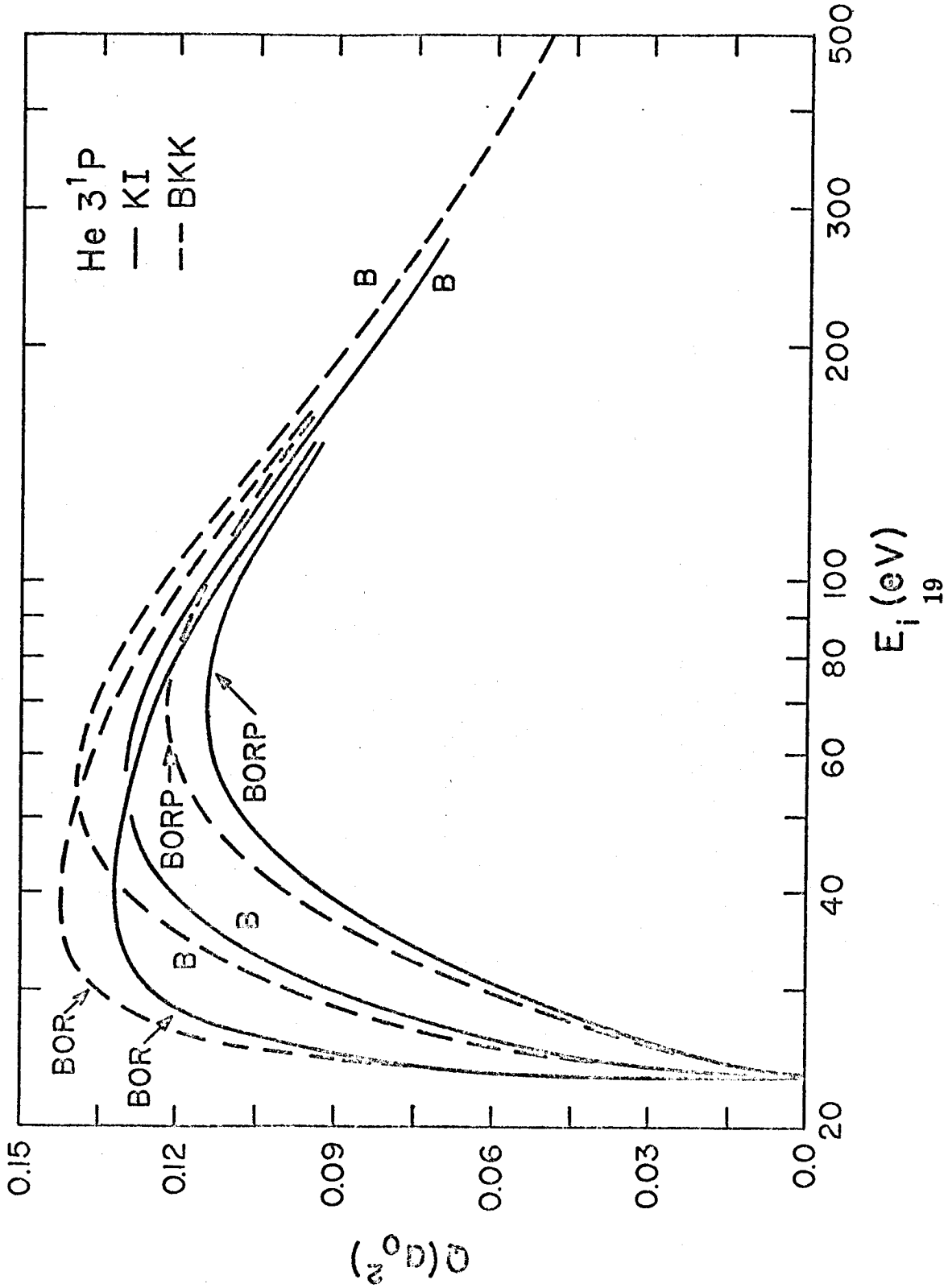
He 3¹P
— KI
-- BKK
B
B
B
B
BORP
BORP
BOR
BOR
0.15
0.12
0.09
0.06
0.03
0.0
20
40
60
80
100
200
300
500
E_i (eV)
19
$Q(D_0^2)$

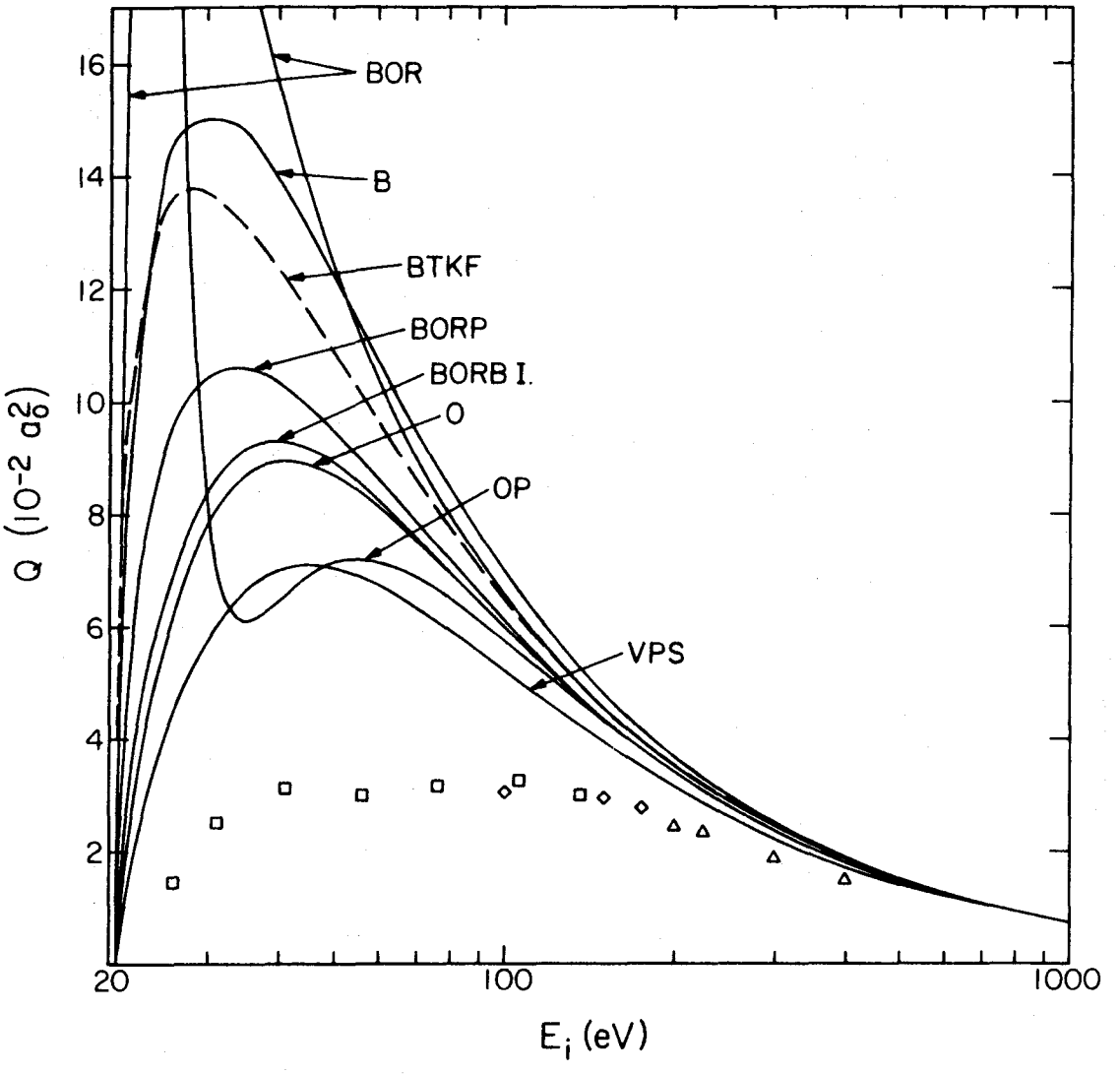
BOR
B
BTKF
BORP
BORB I.
O
OP
VPS
16
14
12
10
8
6
4
2
Q (10-2 a02)
20
100
1000
Ei (eV)

20

Fig. 21. Integral cross sections for electron scattering excitation of the $2\,^1S$ state of helium as functions of impact energy. The square is an experimental result of Dugan, Muschlitz, and Richards (see previous figure caption). The triangles are $1\,^1S$-$2\,^1S$-$2\,^3S$ close coupling calculations including exchange (Ma 64b); the dotted curve is from $1\,^1S$-$2\,^1S$-$2\,^3S$-$2\,^1P$-$2\,^3P$ close coupling calculations including exchange (Bu 65). The other curves are for the methods indicated.

Fig. 22. Ratio of the total scattering differential cross section for the $1\,^1S \rightarrow 2\,^1S$ transition in helium to that for the $1\,^1S \rightarrow 2\,^1P$ transition as a function of scattering angle. The squares with error bars are the experimental results of Rice, Kuppermann, and Trajmar (Ri 68a) at an impact energy of 34 eV; the dotted curve with error bars represents the results of Lassettre, Skerbele, Dillon, and Ross (La 68a) at an impact energy of 48 eV. The solid curves are calculations by the B or BTKF methods (these methods yield results which cannot be distinguished on the scale of this figure). The asterisk is a 46 eV experiment of Doering (Ri 70).

Fig. 23. Ratios of the total scattering differential cross sections for the $1\,^1S \rightarrow 2\,^1S$ transition in helium to those for the $1\,^1S \rightarrow 2\,^1P$ transition as functions of scattering angle for an impact energy of 81.6 eV. The circles are the experimental results of Trajmar, Rice, and Kuppermann (Ri 70); the asterisk is the result of Chamberlain, Heideman, Simpson, and Kuyatt at 80.7 eV (Ch 65); and the curve is calculated in the Born approximation.

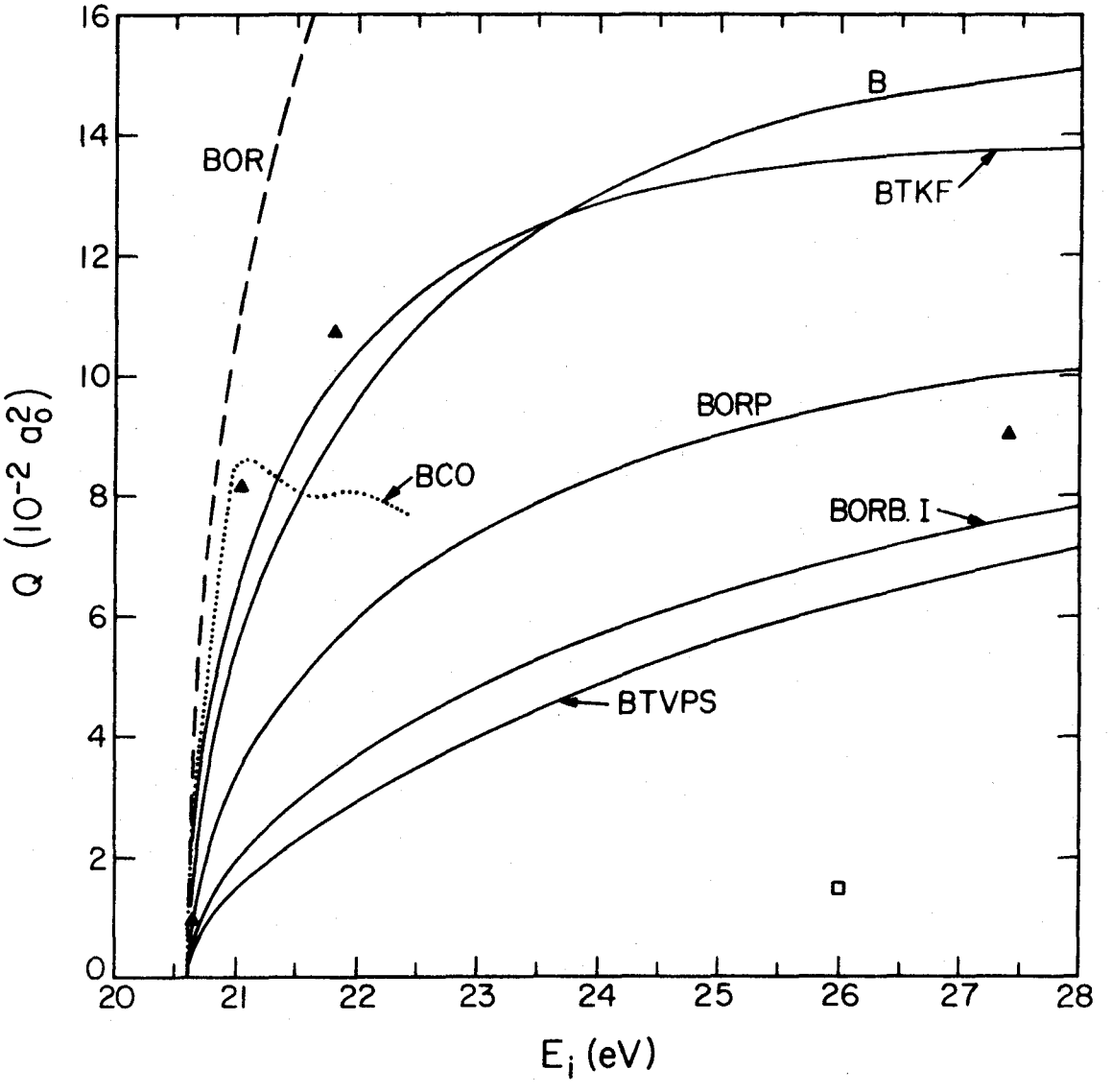
16
14
12
10
8
6
4
2
0
20
21
22
23
24
25
26
27
28
Q (10⁻² a₀²)
E_i (eV)
BOR
B
BTKF
BORP
BCO
BORB. I
BTVPS

21

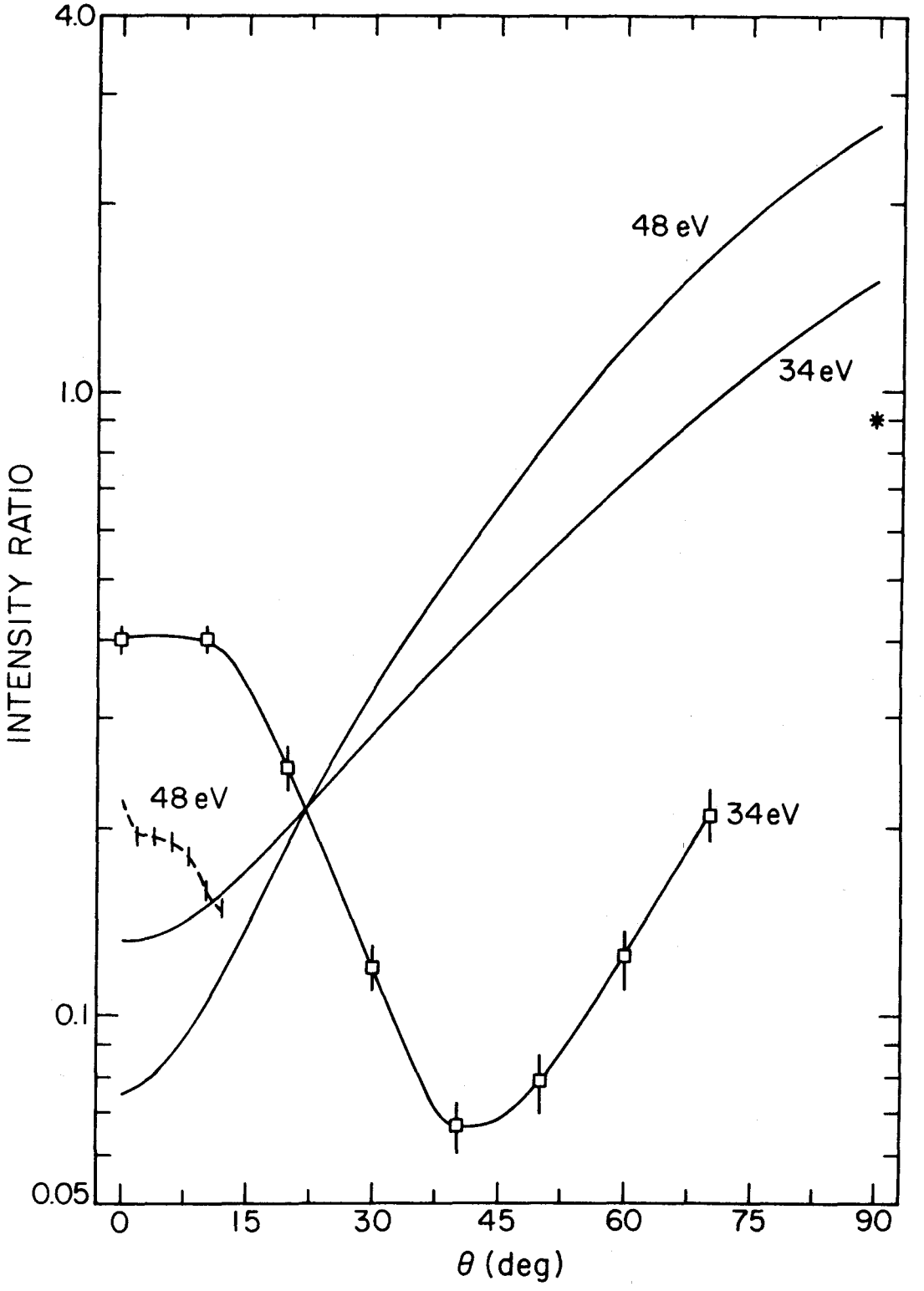
4.0
1.0
0.1
0.05
INTENSITY RATIO
48 eV
34 eV
48 eV
34 eV
*
0
15
30
45
60
75
90
θ (deg)

22

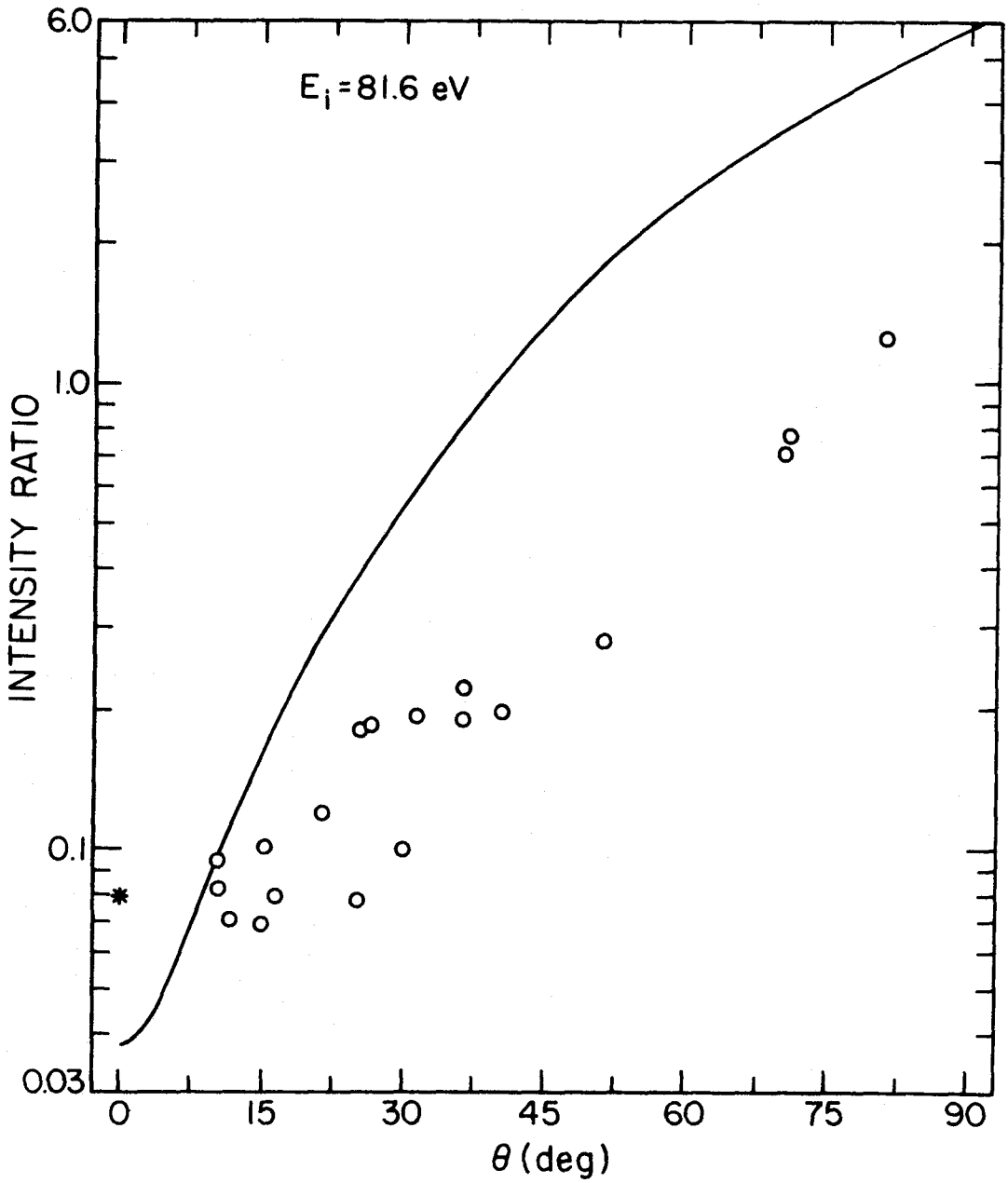

23

Fig. 24. Differential cross sections for elastic scattering of electrons by H_2 at an impact energy of 4.42 eV. All these calculations include electron exchange and the asymmetry of the molecular potential. The HF calculations are in the exchange approximation (discussed in subsection II. A. 2. k) and the HF/P calculations are in the polarized exchange approximation. In addition, these three calculations include some coupling to excited rotational states. The present calculations in the Born-Ochkur-Rudge approximation (labelled BORXP) and the polarized Born-Ochkur-Rudge approximation (BOR/P), the calculations of Hara (H), and the experiments of Ramsauer and Kollath (Ra 32) are for elastic scattering plus rotational excitation. The calculations of Henry and Lane (HL) and the experiments of Ehrhardt and Linder (Eh 68) are for pure elastic scattering. The experiments are normalized arbitrarily for this figure.

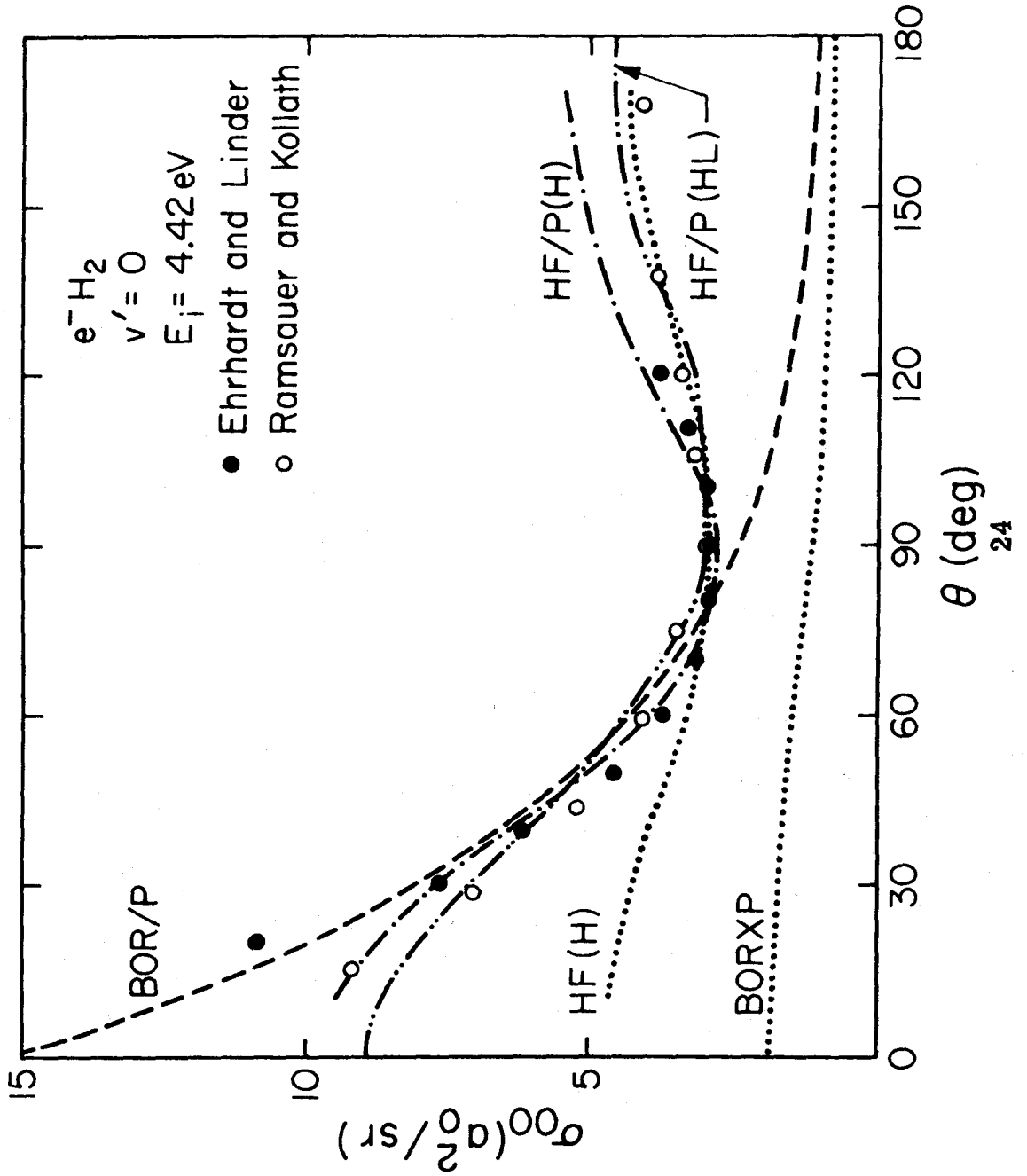
e⁻H₂
v′= 0
E_i= 4.42 eV
● Ehrhardt and Linder
○ Ramsauer and Kollath
BOR/P
HF/P(H)
HF/P (HL)
HF (H)
BORXP
σ00(a₀²/sr)
θ (deg)
15
10
5
0
30
60
90
120
150
180
24

III. PHASE SPACE THEORY OF MOLECULAR COLLISIONS

Because of the large number of eigenstates associated with the internal degrees of freedom of even simple molecules, the exact solution of the close coupled equations (by exact solution we mean the solution of the truncated equations when enough channel states are included so that the truncation error is negligible) for molecular collision processes is not feasible. In fact, except at the lowest energies, it is not possible to even include all the open channels in the wave function expansion. This is not a limitation which will be removed by the next generation of computers, but a fundamental problem. A second difficulty is that there is at present very little accurate knowledge of the potential energy surfaces (see Appendix 1) necessary for solution of the scattering equations. These difficulties in performing rigorous calculations necessitate our using simplified models and approximations. One method of approximation which is useful for calculating cross sections of simple chemical reactions is the phase space theory. This theory assumes that the probability of occurrence of a reaction leading to a set of final states can be calculated directly from a knowledge of only the final states and how much phase space corresponds to them. The details of the theory can be filled in in such a way that it is possible to account for the quantization of the internal energy levels of the reactants and products, for the correct long range force laws governing the probability of collision, and for the exact conservation of any quantities which are constants of the motion (such as the total energy and angular momentum of the collision system). Yet the theory does not require the solution of the full equations of motion. Of course the theory cannot be made exact but it gives estimates of the cross sections for processes for which much more reliable calculations are prohibitively difficult at this time.

The phase space theory will be further defined here as a theory which divides all space into an interaction region and various reactants' and products' channel regions. The dynamics in the channel regions are treated as rigorously as possible but the rigorous quantum mechanical treatment of the interaction region is replaced by the postulate that the probabilities of systems entering and leaving the interaction region to and from the various channels can be calculated from the volume of phase space in each channel. This viewpoint means that the phase space theory is closely related to Keck's variational theory (Ke 58, Ke 67), to Wigner's derivative matrix theory of collisions (Wi 47, Wi 49, La 58, Ni 64, Eu 66, Eu 66a), and to the compound nucleus theory of nuclear reactions (Bu 36).

The statistical theory of Light, Pechukas, and Nikitin (Pe 65, Ni 65, Ni 65a) is a particular example of the phase space theory in which the probability for a system in the interaction region to yield a specific set of final states is taken to be simply proportional to the number of final states. In practice, the channel radii (the channel radius is the distance between subsystems in a channel at which the channel region is connected to the interaction region) have been taken to be large enough so that the only scattering which takes place in the channel region is elastic scattering. The statistical theory is a phenomenological theory which works best when the collisions are hard; but even when it is not strictly applicable it answers the interesting question (Ho 61) of what happens in the limiting case that all degrees of freedom of the interacting system are coupled in the most efficient possible way. The statistical theory, when defined in terms of phase space, is considered here to be the basic raison d'etre for all the phase space theories, and the nonstatistical phase space theories are motivated physically by considering what are the

effects of the system being not quite coupled in the most efficient possible manner. In the terminology of Pechukas and Light (Pe 65), the statistical theory is the limiting form of the phase space theory in which the "weights" of all final states are equal. To see in more detail how the definition in terms of phase space arises from the statistical assumption we will use the S matrix formalism outlined in chapter I (this treatment is applicable to both rearrangements and nonrearrangements provided no 3-body channels are open). The statistical assumption has two parts (see, for a similar partition, Fe 55). The first is that the collision is "sudden" (hard and fast) so that it randomizes all phase information in the wave function (and thus also in the S matrix elements) and also causes nonadiabatic transitions to all quantum states which can be reached without violating conservation of the energy and angular momentum of the total system. Part two of the statistical assumption is that the elements of the S matrix are random except for the constraint that the matrix remains unitary (to insure conservation of particle flux) and symmetric (to insure detailed balancing). Using perturbation theory and the sudden approximation, it can be shown that in the limit where the collisions are hard and fast (potential energy of interaction and relative kinetic energy large compared to energy level separations of the internal states) the S matrix can indeed be taken as an arbitrary unitary matrix (see, e.g., Be 63). This is a physical motivation of the statistical assumption and of the statistical theory of Light, Pechukas, and Nikitin.

In nuclear physics, a model which assumes what we here call part 1 is sometimes called a statistical theory although part 2 is replaced by a different criterion for the scattering amplitudes. We will here call such a model a nonstatistical phase space theory.

In nuclear physics the term "statistical theory" often implies that the scattering wave function is expanded in terms of resonance states and a statistical prescription is used for the distribution of energy levels and widths of these states.

The assumption that the elements of the scattering matrix have random phases means that when we consider an average over a distribution (even a narrow one) of initial conditions or a sum over a group (even a small one) of final conditions, all the interference terms (the cross terms in the square of the sum) in eq. (I. 32) vanish. Then the equation for the differential cross section is the sum of squared terms and is symmetric about 90° (further details may be found in Wo 51 and Ha 52). As mentioned already, conservation of particle flux is expressed by the unitarity of the S matrix

$$\sum_{\alpha'} \sum_{L'} \sum_{S'} \left| S^{K}_{\alpha' L' S',\ \alpha L S} \right|^2 = 1 \ . \tag{1}$$

Part 2 of the statistical assumption as stated above means that

$$\left\langle \left| S^{K}_{\alpha' L' S',\ \alpha L S} \right|^2 \right\rangle_{av} = \frac{1}{N(E, K)} \tag{2}$$

where the average is over all nonzero scattering matrix elements for total angular momentum K and N(E, K) is the number of such nonzero matrix elements, i.e.,

$$N(E, K) = \sum_{\alpha} \sum_{S = |I_1 - I_2|}^{I_1 + I_2} \sum_{\substack{L \\ \Delta(KSL)}} 1 \tag{3}$$

where α includes the specification of all the subsystem quantum numbers including their respective internal angular momenta I_1 and I_2, where the sum over α includes only open channels (at total system energy E), and where the sum over L includes only partial waves which satisfy the criterion for coupling of the channel region to the interaction region. The angular momentum addition triangle $\Delta(J_1 J_2 J_3)$ indicates that the corresponding summation over J_3 is over all J_3 for which $|J_1 - J_2| \leq J_3 \leq (J_1 + J_2)$ (Ro 57, p. 36).

According to eqs. (I.30) and (I.31), an S matrix element $S_{\beta\alpha}$ represents a flux $|S_{\beta\alpha}|^2$ into channel β. Thus in the statistical theory the flux is taken to be the same for any individual channel, i.e., for each quantum state. Semiclassically, each nondegenerate quantum state corresponds to the same amount of phase space (see, e.g., Da 62, Bl 69). Thus counting quantum states and their degeneracies is semiclassically equivalent to integrating over phase space. In this thesis all calculations are fully quantum mechanical and we apply the counting procedure. At higher energies there are too many states for this to be practical and approximation procedures are necessary.

Statistical reaction theories are frequently used in nuclear physics (see, e.g., We 37, Ko 38, Fr 49). The justification for their use there is the long life of the compound nucleus (Be 37). In addition the lack of knowledge of the nuclear forces controlling the reaction dynamics makes a statistical theory particularly appealing. The statistical aspects of the dynamics of nuclear reactions are sometimes augmented by statistical assumptions concerning the distribution of resonance levels of the compound nucleus and the density of states of the nuclei involved. In molecular problems we have more knowledge about the states of the final system. Yet our

knowledge of the intermediate states of the reaction process is often very sketchy because they cannot be experimentally observed in a direct way and the calculation of their properties is an extremely difficult many-body problem. For this reason statistical assumptions often prove useful in molecular problems also.

The statistical assumption is the antithesis of rovibrationally adiabatic theories of reactions. It will fail whenever there is an appreciable probability that the initial state of the system will specifically direct the reaction to proceed to one or a small set of final states.* If the collision complex lasts long enough the system loses its memory of the initial state. This is the basis for the derivation of the statistical theory given by Eu and Ross (Eu 66, Eu 66a) which requires that the eigenlevels of the compound system have a spacing D much greater than their average width $\overline{\Delta E}$. However, this is not a good assumption for many molecular complexes; in fact, the levels probably overlap (Ro 33, Ri 33, Ri 61, Mi 66). Another justification of the statistical theory, not requiring a long-lived complex, is based on the hardness of the collisions as discussed above (and in Li 64, Tr 69, and Li 68). This follows from the sudden approximation, which requires that the incident relative translational energy E_i be much greater than D. In the limit that the levels are effectively degenerate and the interaction is strong, we obtain the statistical theory. In this limit we consider that the interaction V [see eq. (I. 15)] projects the initial state vector $|\, i \,\rangle$ uniformly over the space of all state vectors

---

* Similarly, if there is a barrier on the potential surface between the reactants and products, there is a strong possibility the system will be forced to pass through a col on the surface, i.e., that the reaction path will be guided through a restricted region of phase space. This lessens the probability that the statistical assumption is a good one.

$|\ f\ \rangle$ which are compatible with the conservation laws. Since the level density (1/D) is greater at high energies, we expect the statistical theory to work better at higher energies -- i.e., in the "continuum region" (cf. Bl 52, Section VIII. 7. B, p. 386). One consequence is that at thermal energies the statistical theory is expected to work better for exothermic reactions than for thermoneutral ones because the energy available in the final state for translation and excitation of internal modes is higher for the former class of reactions than for the latter.

Some interesting examples of theoretical calculations in adiabatic-like theories (the reaction proceeds preferentially to one final state) are given in Ch 66, Ma 67, and Bo 68. Real collisions are neither infinitely long-lived nor infinitely hard. These are among the reasons why the statistical assumption is not completely correct. Serauskas and Schlag have proposed corrections to the theory to account for these nonstatistical limitations (Se 66a, Se 66b). Their first correction accounts for the fact that some collisions do not last long enough to form an intermediate state whose internal modes are strongly enough coupled to exchange energy freely. Their second correction comes from the fact that at low velocities the collisions are too soft to effectively broaden the energy levels. In this case the levels do not overlap and energy transfer is less likely. The physics behind these corrections is similar to that involved in the two-state theory of resonant and near-resonant charge transfer. At very low energies there is no probability of charge transfer because the perturbation of the initial state varies too slowly with time. At high energies there is a 50:50 chance of charge transfer because the width of any state is large compared to the separation of interfering states (Li 63). Lichten has a criterion "Q" for the occurrence of this

random process limit which is essentially that the perturbation energy (transition energy) in the strongly coupled region should be much larger than the energy separation of the final states. The effective perturbation energy in the charge transfer problem is larger at higher energies because the system follows the diabatic potential surface (Li 67).

In chemical collisions the long range interaction energy is usually attractive, and we will consider only such cases. The combination of the attractive potential and the repulsive effective potential due to the centrifugal force produces a barrier (the "centrifugal barrier") in the potential energy at large distances R_i^* of separation of the subsystems.* We assume for each orbital angular momentum $L_i \hbar$ of relative motion that systems colliding with enough translational energy E_i to pass classically over the barrier do so and enter the interaction region of configuration space. Systems in the interaction region are called strongly coupled complexes. Sometimes the term "complex" is used elsewhere to mean a system where all the interparticle distances are small (about as small as equilibrium internuclear distances in the separated subsystems) for a time long enough for many vibrations. In the phase space theory, however, we use the term to designate the state of the colliding system during the time when all the particles can interact strongly, but we do not necessarily imply how close the particles are or how long this strong interaction lasts. The configuration of the system at the subsystem separation

---

* In practice we always calculated an R_i^* as independent of subsystem orientation because we used only the spherically symmetric component of the long range potential. Some evidence that this is not a bad approximation is given in Gr 66, p. 147.

R_i^* corresponding to the centrifugal barrier in the initial channel i is the transition state for the association stage of the reaction; there is similarly a transition state in the final channel for the dissociation of the complex. These transition states can be discussed in the language of the theory of unimolecular reactions. Consider the collisional process $A + BC \rightarrow ABC^\dagger$ (the transition state for association to form a complex). If BC can rotate freely in the transition state (this is the case if R_i^* is large enough) it is a loose transition state. If the BC rotation has turned into an $ABC^\dagger$ libration then $ABC^\dagger$ is a tight transition state. When the transition state for association is at the centrifugal barrier, it seems generally to be a loose one; however, a transition state which is determined by the shape of the potential energy surface in a region where bonds are being both made and broken is a tight one (Ma 51, We 62, Ma 65). In all the phase space calculations which have been performed so far the transition state has been treated as a loose one. The collision is considered to be adiabatic up to this transition state so that all vibrational and angular momentum quantum numbers are unchanged. In calculating whether the system can pass over the centrifugal barrier we assume that all the rotational and vibrational energies are unchanged from what they were in the free subsystems. To account for changes in these energy levels or for effects of rigid transition states requires knowledge of the potential energy surfaces. In a rigid transition state the rotations have become bending vibrations and if the collision has been adiabatic during the course of the collision preceding the transition state some energy has been removed from relative translation and put into this rotational-librational motion. This lowers the probability of formation of the complex and is a "steric factor". Free and restricted rotation in transition states

for association to a complex have been discussed in a general way by Marcus (Ma 66, section VII, subsections C and D). If we consider a reaction coordinate s which passes from $-\infty$ to $+\infty$ as the reaction occurs, then the statistical phase space theory assumes the collision is adiabatic up to $s = a$ (where $R_i = R_i^*$), statistical from $s = a$ to $s = b$ (where $R_f = R_f^*$), and adiabatic from $s = b$ to $s = +\infty$. We have used notation where $b \geq a$. If a were equal to b, the reaction would be treated as wholly adiabatic. This is the case in the usual transition state theory of reactions with potential energy barriers and tight transition states (see Ma 67 and references therein). In case such a barrier and tight transition states are important we cannot use the phase space theory with a and b at the centrifugal barriers in the entrance and exit channels. However, for some reactions, especially many ion-molecule reactions, such a barrier is not important and the statistical phase space theory provides a useful means of calculation. For complicated reactions we might consider some of the modes not to be "active" (i.e., statistical) in the interaction region. Such modes would be treated as adiabatic while the others were treated statistically. As a simple example, for $A + BCD \rightarrow AB + CD$ we could treat the CD vibration as adiabatic. When we know more about how strongly various modes of internal motion are coupled during collisions, this mixed-mode calculational method might provide a means of calculating approximate cross sections for polyatomic systems. At present we will consider only triatomic systems. Wolf and Haller (Wo 69) have considered the reaction $H_2^+ + H_2 \rightarrow H_3^+ + H$ using phase space theory. They treated all the modes as statistical in the interaction region.

A. Statistical Theory

1. General Formalism

The quantum mechanical statistical theory for rearrangement collisions in triatomic systems has been derived several times (Pe 65, Ni 65, Ni 65a, Pe 66, Pe 66a, Eu 66, Eu 66a, Li 68). The spin and electronic orbital angular momentum of the atom and the molecule have always been neglected since they are small compared to the rotational angular momentum and the orbital angular momentum of the relative motion of the atom and the molecule. The (generalized) result for the reaction cross section for reactants in state i to produce products in state f is

$$Q_{if} = \frac{\pi \hbar^2}{2\mu_i E_i} \frac{1}{(2M_i + 1)} \sum_{L_i} \zeta_{L_i} \sum_{K} (2K+1) \frac{n(f,K)}{N_{TOT}(K)} \varkappa(i,f) \qquad (4)$$

$$= \frac{\pi \hbar^2}{2\mu_i E_i} \frac{1}{(M_i + 1) g_i^{e\ell}} \sum_{K} (2K+1) \frac{n(i,K)\, n(f,K)}{N_{TOT}(K)} \varkappa(i,f) \qquad (5)$$

where $g_f^{e\ell}$ is the state degeneracy for channel f which is due to electronic and nuclear spin and electronic orbital angular momentum;

$$n(f,K) = \sum_{\substack{L_f \\ \Delta(M_f K L_f)}} g_f^{e\ell}\, \zeta_{L_f} \; ; \qquad (6)$$

$$N_{TOT}(K) = \sum_{f} n(f,K) \; ; \qquad (7)$$

$\varkappa(i,f)$ is a transmission coefficient to be discussed below; ζ_{L_f} is the "sticking probability" (Be 37; Mo 65, chapter XV, § 4), i.e., the probability that a particle incident in channel f with orbital angular momentum of relative motion $L_f\hbar$ will enter the interaction region; i and f are complete sets of quantum numbers [including the chemical identity - electronic quantum numbers I and F, the vibrational quantum numbers n_i and n_f (in this thesis the lowest vibrational state is numbered 0), and the rotational quantum numbers M_i and M_f]; and μ_f is the reduced mass for relative motion in the arrangement channel F. We must take $\varkappa(i,f) = \varkappa(f,i)$ so that the cross sections predicted by (4) and (5) satisfy the principle of detailed balance*

$$g_i\, p_i^{\,2}\, Q_{if} = g_f\, p_f^{\,2}\, Q_{fi} \tag{8}$$

(where g_f and p_f are the total degeneracy and momentum of relative motion, respectively) at constant total energy E and total angular momentum K. However, detailed balance is more manifest in eq. (2) than in eq. (1). The above formulas reduce to the usual statistical theory if

$$\varkappa(i,f) = 1 \tag{9}$$

and

---

* What is here called the principle of detailed balance is often called the principle of microscopic reversibility or the reciprocity theorem.

$$\zeta_{L_f} = \begin{cases} W_f & L_f \leq L_{f\,max} \\ 0 & L_f > L_{f\,max} \end{cases} \qquad (10)$$

where $L_{f\,max}$ is determined by the requirement that the system has enough relative translational energy E_f to pass over the centrifugal barrier and

$$W_f = 1 \qquad (11)$$

in the absence of corrections for reflection and/or steric effects. The statistical theory is valid for completely strong coupling as discussed earlier.

In actual calculations $N_{TOT}(K)$ is a large number. E.g., in some calculations on H + DBr, the maximum $N_{TOT}(K)$ for the case $E_i = 0.012$ eV, $M_i = 3$, $n_i = 0$ was 842 and the maximum $N_{TOT}(K)$ for the case $E_i = 0.063$ eV, $M_i = 3$, $n_i = 0$ was 1192.

2. Specific Applications

Many calculations have been performed using this formalism and its classical mechanics counterpart (a summary of the work done up to the end of 1967 is given in Li 68). Further discussion of the statistical theory, including techniques of calculation, is given in the article "Application of the Statistical Phase-Space Theory to Reactions of Atomic Hydrogen with Deuterium Halides" which has already been published (Tr 69).

In that article we consider the H + DBr, H + DI, and H + HI reactions as examples. We also include some calculations on H + DCl (for which the theory is inapplicable because there is an

important potential energy barrier) to also see what effects are predicted by the statistical theory in a case where it should not be applied. The H + DBr reaction might involve a small potential energy barrier (of the order of magnitude of 1 kcal/mole) and therefore the results for this reaction at low energy might not be strictly comparable with experiment. The iodide reactions do not seem to involve a barrier (Su62) and the treatment may be more appropriate for them. The H + DX(X = halogen) reactions are interesting test cases because of the competition between the endothermic rearrangement channel (HX + D) and the exothermic one (HD + X). In the second rearrangement channel the halogen atom can be produced in an electronically excited state (X*). Tables I, II, and III summarize the predicted cross sections for reactions from a specific initial rotational state (with quantum number M_i) leading to products in their ground electronic state and Tables IV and V summarize the predicted cross sections for the two rearrangement channels for well-defined rotational temperatures. The cross section for the reaction H + DBr → HD + Br, shown in Table IV, is predicted to be decreasing exponentially for $E_i < 0.1$ eV but more slowly than that at higher energies. These cross sections (and others not included in these tables) can be used to calculate the reaction rate constants given in Table VI.

White, Kuppermann, Davis, and Betts have devised experimental methods for determining the fraction of H + DX reactions which lead to abstraction (HD) instead of exchange (HX). Their methods consist in photolyzing DX (containing a small amount of HX impurity) in the presence of excess helium, with monochromatic light of variable wavelength. The atoms produced react by the processes

$$H + DX \rightarrow HX + D$$
$$H + DX \rightarrow HD + X$$
$$D + DX \rightarrow D_2 + X$$
$$X + X \rightarrow X_2$$

Since the ratio α of extinction functions of DX and HX is a very strong function of wavelength for the conditions used, a measurement of the $[HD]/[D_2]$ product ratio can be made as a function of α to determine the abstraction fraction. An extrapolation to infinite rare gas fraction can be made to insure that only thermalized atoms contribute. Persky and Kuppermann have performed further similar experiments. The statistical theory is in fairly good agreement with these experiments (Wh 66, Da 69, Pe 69a) for the ratio of reaction rates into the two rearrangement channels (see Table VII) and for the energy dependence of the ratio. The theory, however, predicts that 10% of the I atoms produced in the H + HI reaction are in the electronically excited $^2P_{1/2}$ state compared to an upper bound on this quantity of $2 \pm 1.5\%$ obtained from different experiments (Ca 68).

In the article we also presented the predictions of the theory for the energy distributions in the vibrational and rotational modes of the products. Some more examples of these product distributions for the H + DBr reaction are given in Tables VIII, IX, X, XI, and XII and Figs. 1 and 2. Table VIII illustrates how the probability of production of vibrationally excited products depends on the initial translational and rotational energy and Tables IX and X show how this probability and some ratios of cross sections for producing different molecules and specific electronic states depend on reactant vibrational energy. Tables XI and XII give reaction cross sections and rate constants for producing vibrationally unexcited and excited molecules for reactions

from the ground vibrational state. They also illustrate the competition between channels and electronic states. Figs. 1 and 2 show typical patterns for the rotational distribution of each product, including the chemically nonreactive one.

As a test of the accuracy of the computer program we checked numerically the detailed balance relation (8) by calculating separately the cross sections for forward and reverse reactions. Some examples are given in Table XIII. They show that relation (8) is adequately satisfied.

The statistical theory has also been applied to the reaction $K + HCl \rightarrow KCl + H$. This reaction is of particular interest because it has been studied in molecular beams* by Greene, Moursund, Ross, and Ackerman (Ac 64, Mo 64, Gr 66) and Odiorne and Brooks (Od 69). By observing the loss of intensity of large angle nonreactive scattering and making a semiclassical analysis, similar to the optical model, the first group of workers was able to determine the probability of reaction P as a function of the initial impact parameter b (Gr 66). Their results are shown in Figs. 3-5. Using the data given in Table XIV and a slightly modified version of the computer program described previously (Tr 69), we calculated the reaction cross section and the probability of reaction as a function of impact parameter for six incident energies E_i. The calculated probability of reaction as a function of impact parameter is given in Figs. 3-6 and the calculated cross sections are given in Fig. 7 and Table XV. Table XV also includes the results for the rotationally inelastic cross section (without chemical reaction) and for the reaction cross sections $Q_{v'}$, into different

* The author is grateful to Prof. E. F. Greene, Dr. A. L. Moursund, and Prof. J. Ross for discussions of this work.

vibrational states $n_F = v'$ of the product KCl. Greene et al. also obtained the integral reaction cross section by the relation

$$Q(KCl) = 2\pi \int P\ b\ db$$

These results are compared to the theoretical results in Fig. 7. Greene et al. could not make useful measurements directly on the scattered KCl because of problems with their detector (Ac 64). Odiorne and Brooks have recently made such measurements (Od 69).

One interesting feature of the comparison of the theoretical and experimental P vs. b curves is the good agreement in shape. Especially at the highest energy considered (E_i = 4.5 kcal/mole), both theory and experiment show a rapid drop of P from about 0.9 to 0 in a small range of b. The systematic difference in the maximum impact parameter for which reaction can occur could be caused by any of the assumptions in the theory or by the experimental errors. For example, the absissa for any experimental point is directly proportional to "r_m" (see Gr 66, the experimental value is 3.3Å). Two parts of the data for the theoretical calculation which strongly affect the maximum impact parameter for which reaction can occur are uncertain. These are the endothermicity and the van der Waal's constant for potential energy in the final state. The endothermicity for the present calculation was taken as E_{thr} = 0.7749 kcal/mole but this could be in error by as much as 1.1 kcal/mole. The endothermicity and the potential energy in the final state are very important for this reaction since the possibility of reaction is limited by the ability of the system to pass over the centrifugal barrier in the final state. (This is to be contrasted to the H + DX cases where reaction was limited by the centrifugal barrier in the initial state. This difference between the systems is due to the differences in the heat of reaction and in the ratio of

reduced masses for relative motion in the initial and final states.). It is interesting that the experiment and the statistical theory agree best for P vs. b at the largest initial energy considered (see Fig. 5). At this energy the effect of any error in E_{thr} on the calculated reaction properties is minimized. The systematic error in the maximum impact parameter for which reaction can occur is the reason for the discrepancy between the theoretical results and the results of Greene et al. for the integral cross sections in Fig. 7.

The break in the experimental P vs. b curves was interpreted by Greene et al. as being due to the opening of a new vibrational excitation channel in the final state. This break does not occur in the theoretical curve although the cross sections for vibrationally excited reaction products (see Table XV) indicate that vibrational excitation of the reaction product is predicted to occur to a noticeable extent.

The statistical theory predicts a large cross section Q_{rot} for the change of rotational state of unreacted HCl (see Table XV). The assumptions in the statistical phase space theory as discussed above are expected to be more valid for rearrangements than for inelastic nonrearrangements. One assumption which can be particularly bad for nonrearrangements is eq. (10). Nevertheless the statistical theory prediction of large rotational excitation is interesting. Since the statistical theory sometimes predicts that some systems will have a small ratio of rotational excitation to chemical reaction, Table XV shows that rotational excitation is especially favored by the kinematics in this case when compared to the endothermic chemical reaction.

B. Nonstatistical Theories

1. Theory of Nonstatistical Corrections

If the full statistical assumption is not made, eqs. (4) - (7) above provide a formally valid approximation if the constraints

$$\zeta_{L_f} \leq 1 \tag{12}$$

$$\varkappa (i, f) \leq 1 \tag{13}$$

are observed. These constraints insure that the conservation of particle flux theorems (Mo 65, Chapter XII, § 1) are satisfied; i.e., the conditions (12) - (13) are necessary to prevent the probability of reaction from exceeding the maximum possible probability of collision.

Part 2 of the statistical assumption is sometimes the weaker part of the statistical phase space theory. The statistical theory of Light, Pechukas, and Nikitin has some formal advantages and also the advantage that it is actually correct in a limit indicated by the sudden approximation derivation (Be 63, Tr 69). However, by changing equations (9) - (11) we can obtain nonstatistical theories which may be more accurate in some practical cases.*

Various methods of assigning values to W_f (leaving the rest of the statistical theory unchanged) lead to one class of

---

*The statistical theory often predicts too much excitation in the products of chemical reaction. A similar result was found in nuclear physics and Wigner conjectured that perhaps the probability is constant per unit energy interval instead of per unit state (Wi 55). This is an example of a nonstatistical phase space theory as defined here.

nonstatistical theories.* The assignment (11) gives the statistical theory of Light, Pechukas, and Nikitin. This choice is implicit in the transition state theory of Wigner and Eyring. For example, the assumption of a loose transition state located at the position of the centrifugal barrier results in a transition state theory rate for the association which is equal to the rate calculated for it by collision theory using (4), (6), (10), and (11) (Jo 62, Jo 66a). This choice is also implicit in the phase space theory of Keck (Ke 67, Li 68). Another possibility is used by Fermi (Fe 50) and Eu and Ross (Eu 66a); they let W_f depend on the asymptotic velocity in channel f, e.g.,

$$W_f = \frac{v_f}{v_o} C_o \tag{14}$$

where v_o is the highest possible velocity in any possible exit channel at energy E and total angular momentum $K\hbar$, and $C_o = C_o(E, K)$ is a constant less than or equal to 1. Serauskas and Schlag (Se 66a, Se 66b) have suggested some nonstatistical modifications of the statistical theory formulas for the case of intermolecular vibrational energy transfer in nonrotating systems. A straightforward attempt to generalize their results to the case of triatomic rearrangements considered here leads to

$$Q_{if} = \frac{\pi\hbar^2}{2\mu_i E_i} \frac{g_f^{e\ell}}{(2M_i+1)} \sum_{L_i=0}^{L_{i\,max}} \sum_{\Delta(M_i L_i K)}^{K} (2K+1) \frac{n^{MSS}(f,K)}{N_{TOT}^{MSS}(K)} \tag{15}$$

*The author is grateful to Dr. F. H. Mies and to Prof. E. F. Greene for discussions of the ideas in this paragraph.

where MSS stands for "modified Serauskas-Schlag",

$$n^{MSS}(f, K) = \sum_{\substack{L_f \\ \Delta(M_f K L_f)}}^{L_{f\,max}} g_F^{e\ell} (1 - e^{-\nu \tau_{fi}}) H(|\Delta E_{w.c.m.}| - h/\tau_{fi}) \qquad (16)$$

in terms of the Heaviside function

$$H(x) = \begin{cases} 1 & x > 0 \\ 1/2 & x = 0 \\ 0 & x < 0 \end{cases} , \qquad (17)$$

$g_F^{e\ell}$ is the electronic state degeneracy of state F, τ_{fi} is the collision time, ν is a characteristic frequency of vibrational energy transfer, and $\Delta E_{w.c.m.}$ is some measure of hard-to-transfer energy (w.c.m. stands for "weakly coupled modes") that must be transferred to effect the transition $i \to f$. The factor in parentheses on the right hand side of (16) is used in the theory to decrease the reaction probability at high velocity because high-velocity collisions are over too rapidly. The next factor decreases the calculated reaction probability at low velocity because low-velocity collisions are too soft. Equations (15) and (16) follow the Serauskas-Schlag renormalization but do not satisfy detailed balance even if $\tau_{fi} = \tau_{if}$. Serauskas and Schlag assumed

$$\tau_{fi} = 2\tau_i \neq \tau_{if} \qquad (18)$$

where τ_i is the half-collision time (time for only either the incoming part of the trajectory or the outgoing part) for a collision in channel i.

Calculations based on (15)- (16) have led us to believe that the Heaviside function used by Serauskas and Schlag is too steep a criterion for the softness-of-collisions corrections and leads to unrealistic results when applied in this way to systems with low vibrational quantum numbers.

2. Generalized Nonstatistical Theory

To obtain a more satisfactory phase space theory of rearrangements incorporating these nonstatistical corrections we take the softness correction to be of the form of an energy denominator. Such energy denominators appear naturally when collision processes are treated from the point of view of perturbation theory or resonance theory (see, e.g., Eu 66, Eu 66a, Le 66, Li 63, Li 67, Mi 66, Mo 65, Chapter XV, § 4, Ro 67, Chapter XII, § 6, Se 55, Chapter VII, § 29). Their appearance is intimately connected with the uncertainty principle and with energy level broadening and they provide a realistic way to incorporate this correction into the model. The basic equation of this new theory becomes

$$Q_{if} = \frac{\pi\hbar^2}{2\mu_i E_i} \frac{1}{(2M_i+1)g_I^e} \sum_K (2K+1) \frac{N_{TOT}(K) n(i,K) n(f,K)}{(DE)^2 + [N_{TOT}(K)]^2} \qquad (19)$$

where $n(i,K)$ and $N_{TOT}(K)$ are again given by eqs. (6) and (7) but

$$\zeta_{L_f} = \begin{cases} 0 & L_f > L_{f\,max} \\ (1 - e^{-\nu\tau_f})W_f & L_f \leq L_{f\,max} \end{cases} \qquad (20)$$

As in the statistical theory, $L_{f\,max}$ is determined by the requirement that the system have enough translational energy to surmount the centrifugal barrier in channel f. In the absence of corrections for other potential energy barriers in the f channel, W_f is given by eq. (11). To ensure detailed balance we take

$$\tau_{fi} = \tau_i + \tau_f \tag{21}$$

where τ_i and τ_f are given by the definition following eq. (18). Finally the correction previously included by the Heaviside function in eq. (16) is now included by taking

$$DE = \frac{\Delta E_{w.c.m.}}{h/\tau_{fi}} N_{SUP}(K) \tag{22}$$

where

$$N_{SUP}(K) = d \sum_f \sum_{\substack{L_f \\ \Delta(M_f K L_f)}}^{L_{f\,max}} g_f^{e\ell} W_f \,. \tag{23}$$

The energy denominator correction DE has the property that the $i \to f$ transition probability is decreased if the collision is too slow or the energy change in the weakly coupled modes is too large. The physical justification of this term from the theories of nonadiabatic processes* that has been given by Serauskas and Schlag (Se 66a) and

---

* Some of these theories have been reviewed in Ma 52, Chapter VII, § 10 and Chapter VIII, § 6. 1, Ni 67, and He 68a.

reviewed above leads to the parameter d having a value of the order of magnitude of 1. For example, in the slow collision time limit ($\tau \to \infty$) for which this DE correction is most important, making the correction using DE with d = 1 decreases the cross section for a given process by a factor of 1/2 for the same value of $\Delta E_{w.c.m.} \times \tau_{fi}/h$ that making the correction with the Heaviside function gives a factor of 1/2 [see eq. (17)]. We can somewhat arbitrarily consider

$$d = 1 \tag{24}$$

to be the nonempirical value for the new theory. If the value can ever later be adjusted to give better agreement of the theory with a particular reaction, that should be considered an empirical adjustment. A better, less arbitrary way to establish a nonempirical value for d is to adjust it to make the calculations agree as much as possible with the calculations performed using the modified Serauskas-Schlag procedure described earlier (note that the new nonstatistical theory is not a special case of the modified Serauskas-Schlag theory and also that the MSS theory is not a special case of the new nonstatistical theory.) Below we will consider how d may be used to give a range of theories with more or less statistical behavior.

It is interesting to note the formal similarity of eq. (19) to Levine's eq. (30) of Le 66, especially if we take

$$|\langle a_j \mid T_i \mid i \rangle|^2 = n(i, K) \tag{25}$$

where the left hand side uses the notation of Le 66. Levine's equation, however, is derived from a different point of view for a different purpose and has a different interpretation.

The energy denominator correction means the new theory has the following interpretation. For very slow collisions even intimate encounters retain a certain amount of wave function phase coherency leading to a special type of nonstatistical breakup of the complex. This special breakup is predominantly elastic scattering but includes contributions from other processes that have small $\Delta E_{w.c.m.}$, i.e., processes that do not require large transfers of energy between weakly coupled modes.

The nonstatistical theory in the above form is obviously not applicable to reactions in which there are appreciable effects due to electronic potential energy barriers (above and beyond the centrifugal and endothermicity barriers). However, the statistical theory has three faults even when applied to reactions without these extra barriers: (i) the absolute values of the cross sections are generally too large; (ii) the theory cannot ever predict an inverted vibrational population in the final state (Li 68); (iii.) the reaction cross section does not fall to zero properly at high energies. Fault (i.) is probably due to the sticking probability being taken as 1 instead of less than 1 and possibly does not have a large effect on the ratios of cross sections for competitive channels of rearranged products. The new sticking probabilities [eq. (20)] are less than 1 and are thus more realistic. Fault (ii.) is a basic failing of the statistical approach. It is possible for the new theory to predict inverted vibrational populations but such a prediction is not probable for many reactions. Fault (iii.) occurs because at high energy the total collision cross section equals (Li 68, Tr 69) the geometrical cross section and strong coupling is still fully allowed for these hard collisions. In the new theory the cross section is reduced at high energy because N_{SUP} becomes larger than N_{TOT} as the energy increases and because of

the factor in eq. (20) which tends to zero as $E \rightarrow \infty$ (and thus τ_i and $\tau_f \rightarrow 0$) since there is not enough time for energy transfer or particle transfer. This correctly mimics the physical reason why the experimental cross section tends toward zero at high energies.

The new theory is not an attempt to provide a fit to every experiment. If ν is fixed by some physical argument concerning the speed of molecular motions in the complex, then the theory provides a framework for a priori calculations of reaction processes which (hopefully) will be accurate and useful for some classes of reactions.

The nonstatistical theory can no longer be given the average S matrix interpretation (Le 68a) and we can no longer define a cross section for formation of a strongly complex or a partially coupled complex. Yet because the theory satisfies the constraints of detailed balance and conservation of particle flux we can define an S matrix (where any S matrix element has no simple relation to the average S matrix element or the average squared S matrix element). Since the theory does not require an interpretation in terms of a complex or in terms of equal accessability of all phase space, it does not imply a symmetric angular distribution in the center-of-mass coordinate system and can be applied to a more general class of compounds. Without additional hypotheses, we cannot calculate angular distribution from the present theory and thus angular distributions cannot be used to test it.

The energy denominator correction in the new nonstatistical theory means that transitions requiring little energy transfer are favored over less adiabatic ones. Thus the theory is part way between adiabatic and statistical. In this respect it is similar to the theory of "statistical adiabaticity" used by Marcus (Ma 68). In both theories the

transitions are restricted to states which are within a small range centered on the "adiabatic" level but are otherwise statistical in some sense. In Marcus' theory the adiabatic levels are defined correctly in terms of their quantum numbers and numerical calculations on real systems are difficult. In the present theory the "adiabatic" levels are defined only crudely in terms of $\Delta E_{w.c.m.}$ but numerical calculations can easily be carried out. We calculate $\Delta E_{w.c.m.}$ from the energy levels of the separated subsystems. It would be preferable to use the value which is effective in the interaction region in which the transition occurs.* This problem has long been recognized in the theory of inelastic collisions involving the "Massey adiabatic criterion" (see, e.g., Ma 49, Ma 52, p. 441, Ra 62, Ha 62, Pa 64, Wa 67, Bo 68). We hope that the error in the cross sections due to this inadequacy of the model is small in this case because so many levels are important and the errors can cancel. Anyway, if we knew the details of the energy separations of the states in the interaction region we could probably do a better calculation than the phase space theory. The spirit of the phase space theory calculations is to see what information we can obtain without using detailed knowledge about the system in the strong interaction region. The nonstatistical theory requires only simple, approximate average properties of the system in the interaction region: the average frequency of intermolecular energy transfer (ν) and the approximate collision duration in any channel (τ_j).

A precise definition cannot be given for the characteristic frequency ν. A similar quantity appears in Slater's theory of

---

*The author is grateful to Dr. R. D. Levine for a discussion of this point.

unimolecular reactions. In the case of unimolecular reactions it can be shown that ν should be the root mean square of the normal frequencies of the complex, weighted with amplitude factors as they affect the crucial coordinate for reaction (Sl 59). Thus a typical value for ν might be 4×10^{13} sec $^{-1}$. A more sophisticated nonstatistical calculation might make ν a function of i, f, and K. We will constrain ν to be a constant.

In the limit that $\tau_{fi} \to 0$ and $\nu \to \infty$ fast enough so that $\nu \tau_{fi} \to \infty$, the nonstatistical theory reduces to the statistical theory. This limit occurs for fast collisions for which the energy transfer in the complex is even faster. We can also obtain the statistical theory at lower velocities by setting the parameters $\nu = \infty$ and $d = 0$. Setting ν equal to any constant gives a whole series of theories depending upon the value of d. For $\nu = \infty$ (which means we neglect the correction for the collision being over too fast for complete energy sharing between the subsystems) we obtain an interesting series ranging from $d = 0$ for the old statistical theory to $d = \infty$ for a very adiabatic theory. If ν is given a value representing the characteristic frequency of energy transfer in the complex, we obtain a set of theories which includes for $d = 1$ the new nonstatistical theory. Recently Bunker and Chang (Bu 69) have also proposed a series of models in which the degree of adiabaticity or statisticality assumed in the treatment may be parametrically varied. In Bunker and Chang's theory, like the present nonstatistical theory, the reaction is adiabatic in regions of the reaction coordinate $s = -\infty$ to $s = a$ and $s = b$ to $s = \infty$ and semistatistical from $s = a$ to $s = b$. In their theory a and b are not necessarily located at the position of the centrifugal barrier. Their treatment does not satisfy detailed balance. Also unlike the present set of theories their models do not reduce to the statistical theory of

Light, Pechukas, and Nikitin in any limit. Both the present set of nonstatistical models and Bunker and Chang's set have the disadvantage that although they span the range of behavior between adiabatic and statistical (or semistatistical) they cannot correctly handle reactions which are not either and are not in the range between these limits. For example, some reactions might proceed preferentially into one or a small bundle of states not centered around the adiabatic one. For example, at very high energy it is sometimes likely that the system will follow one diabatic path.

3. Calculations

Some sample calculations were performed on the H + DBr system using both the modified Serauskas-Schlag theory (MSS) and the new nonstatistical theory. These calculations show what kind of changes can be caused by nonstatistical corrections.

The calculations required estimates of the collision times τ_f. For the MSS calculations these were calculated with classical mechanics and a Lennard-Jones 6-12 potential (no new parameters are required in this case since this potential is uniquely determined by the Van der Waals constant C_F and the hard sphere collision cross section σ_F which already entered the theory). This, of course, is just a model used to calculate characteristic times for each channel and is not meant to imply anything about the true potential. The collision times were calculated by numerical integration and fitted to polynomials. The polynomials were used in the MSS program. In view of the crudity of the model we no longer feel such a complicated treatment is justified and in the new generalized nonstatistical theory calculations we used (Be 60)

$$\tau_f = \max \begin{cases} (R_f^* - \sigma_F)/\nu_f \\ (0.01\, a_o)/\nu_f \end{cases} \tag{26}$$

where R_f^* is the position of the centrifugal barrier and ν_f is the velocity of relative motion. Another possibility for computing the collision time would be to assume the complex is long-lived and to compute τ_{fi} from the internal motion of the complex (see, e.g., Bu 52). We did not attempt this approach.

As an example of the first approach to calculating the collision times, the τ_f in the HBr + D channel for H + DBr with $E_i = 0.04$ eV, $n_i = 0$, and $M_i = 6 - 28$ were in the range 1.5×10^{-14} sec to 1×10^{-12} sec with the mean around 2×10^{-13} sec.

An examination of the normal coordinate frequencies of a semiempirical potential energy surface for HDBr (Pa 69) led us to believe a reasonable value for ν would be 3.6×10^{13} sec^{-1}. With the range of τ_f given in the previous paragraph, this would give a range of $\nu\tau_f = 0.5 - 18$. We also tried various other values to see what would be their effect.

For $\Delta E_{w.c.m.}$ we want a measure of the energy which is hard to transfer. We used

$$\Delta E^{fi}_{w.c.m.} = E_{vib,f} - E_{vib,i} + E^{el}_F - E^{el}_I \tag{27}$$

where the terms on the right hand side are the vibrational energies of the product and reactant and the electronic excitation energies of the product and reactant, respectively. Thus $\Delta E_{w.c.m.}$ is taken to be the difference of the vibronic energies of the initial and final states.

Some typical results of the modified Serauskas-Schlag calculations are given in Tables XVI and XVII for H + DBr reactions with E_i = 0.04 - 0.153 eV. These calculations predicted that there was no vibrational excitation of the reactant or product molecules and that there was no electronic excitation. We expect that this is too drastic a reduction of calculated vibrational excitation and that changing from the Heaviside function correction to the energy denominator correction will give more reasonable results. The calculations also show that ν has only a small effect on the calculated results. This is because $\nu\tau_{ij}$ is usually large at these energies. The correction for a finite frequency of energy flow in the complex would be more important at higher energies.

Some typical results of the new nonstatistical theory are shown in Table XVIII. We note that the characteristic frequency ν has more effect on the cross sections than on their ratios. Table XVIII also shows some statistical calculations for comparison (for these, d = 0 and $\nu = \infty$). We note that the amount of excitation in the reaction products depends on both corrections in a complicated manner but that the nonempirical version (d = 1) of the nonstatistical theory predicts very little excitation. Thus the corrections improve agreement of experiment and theory for excitation of halogen atoms in these reactions. Also the corrections lower the abstraction fraction which is the correct direction for improving the statistical theory to agree with experiment. An effect which is more significant and meaningful, however, is the decrease in the magnitudes of the cross sections. The statistical theory often predicts cross sections (or rate constants) which are too large by a factor of 3 or 4. The nonstatistical corrections, at least for H + DBr, are about of this magnitude.

Clearly more work is required on the nonstatistical corrections to see if they can be used to improve the statistical theory in general or to see under what conditions they are useful.

TABLE I

Reaction cross sections (a_o^2) for H + DCl reaction calculated by statistical theory for the ground vibrational state of DCl

E_i(eV) \ M_i	2	6	10	14	19	26
			Product: HCl + D			
0.012	0.0	0.0	30.8	52.7	63.5	64.4
0.040	0.0	6.4	26.4	36.7	41.8	42.9
0.063	4.8	15.3	28.6	35.0	38.0	39.3
0.087	14.4	21.6	27.6	31.8	33.6	35.3
0.153	21.7	23.6	25.2	27.2	27.3	29.3
0.250	22.7	23.6	23.7	24.3	25.3	26.0
0.370	20.1	20.0	20.5	21.5	22.4	22.8
0.570	17.7	17.9	18.2	18.6	19.1	19.6
			Product: HD + Cl (atom unexcited)			
0.012	129.5	88.6	66.1	56.4	47.3	40.8
0.040	65.1	55.8	45.0	36.8	31.7	28.5
0.063	49.8	46.2	36.8	32.5	29.9	26.9
0.087	38.3	36.3	32.9	30.1	26.6	24.5
0.153	24.0	23.7	23.8	22.7	21.4	21.1
0.250	18.8	18.0	18.9	18.7	19.1	19.5
0.370	13.8	14.4	14.6	15.3	16.4	17.1
0.570	11.4	11.5	12.1	12.5	13.2	14.1

TABLE II

Reaction cross sections (a_o^2) for H + DBr reaction calculated by statistical theory for the ground vibrational state of DBr

E_i(eV) \ M_i	3	6	9	14	21	28
			Product: HBr + D			
0.012	0.0	0.0	3.3	20.4	35.2	42.2
0.040	0.0	2.6	7.4	17.3	26.0	31.7
0.063	3.6	6.2	10.0	16.4	23.0	28.5
0.087	7.0	9.0	11.7	15.8	20.4	25.2
0.153	12.1	12.8	14.0	15.9	18.3	22.4
0.250	13.4	13.6	13.8	14.4	16.9	18.9
0.370	13.6	13.8	14.3	15.5	16.9	18.3
0.570	14.5	14.8	14.9	15.1	16.0	16.7
1.000	14.6	14.7	14.8	15.0	15.4	15.7
			Product: HD + Br (atom unexcited)			
0.012	192.2	186.2	178.5	145.1	120.3	98.5
0.040	133.1	128.7	119.1	102.9	86.6	71.7
0.063	109.6	104.9	99.1	89.1	75.8	64.1
0.087	88.8	85.7	81.6	76.8	65.8	56.4
0.153	65.5	64.9	64.5	61.2	55.2	48.0
0.250	46.3	45.6	44.8	44.0	40.9	37.2
0.370	36.8	36.5	36.1	35.1	34.2	32.7
0.570	24.4	24.4	24.4	24.9	25.0	24.7
1.000	15.7	15.8	15.9	16.3	17.0	17.6

TABLE III

Reaction cross sections (a_o^2) for H + DI reaction calculated by statistical theory for the ground vibrational state of DI

E_i(eV) \ M_i	3	8	13	19	24	33
			Product: HI + D			
0.012	0.0	0.05	8.2	18.6	26.6	40.4
0.040	0.3	3.2	7.8	14.2	18.4	28.0
0.063	2.9	5.0	8.3	13.1	16.4	24.4
0.087	4.7	6.3	8.7	12.0	14.7	21.6
0.153	7.8	8.7	9.9	11.7	14.1	18.8
0.250	9.7	10.2	10.7	12.4	14.0	17.2
0.370	11.3	11.8	12.5	13.6	14.4	16.5
0.570	13.5	13.7	14.1	14.7	15.2	16.2
			Product: HD + I (atom unexcited)			
0.012	249.9	242.2	226.4	204.2	187.2	155.6
0.040	162.6	157.3	149.6	136.7	126.1	105.6
0.063	135.0	132.1	127.4	116.9	107.6	91.4
0.087	113.4	111.1	106.9	100.1	92.3	78.8
0.153	87.8	86.4	84.4	79.7	75.6	65.3
0.250	67.1	66.2	64.7	62.8	59.6	53.4
0.370	53.0	52.7	51.7	50.4	49.1	45.6
0.570	37.4	37.3	37.1	37.0	37.0	36.0

TABLE IV

Reaction cross sections for H + DX reactions calculated by statistical theory for the ground vibrational state of DX and an initial rotational temperature of 300°K

X	E_i (eV)	Cross section (Å^2) HX + D	Cross section (Å^2) HD + I or I*
I	0.012	0.34	74.47
	0.040	0.73	48.53
	0.063	1.29	40.71
	0.087	1.66	34.28
	0.153	2.38	26.97
	0.250	2.82	20.80
	0.370	3.27	16.64
	0.570	3.83	12.08
Br	0.012	0.51	59.39
	0.040	0.93	40.58
	0.063	1.80	33.84
	0.087	2.54	27.73
	0.153	3.62	21.17
	0.250	3.81	15.08
	0.370	3.89	12.31
	0.570	4.11	8.46
	1.000	4.12	5.67
Cl	0.012	1.22	28.49
	0.040	1.87	16.35
	0.063	3.65	13.26
	0.087	5.50	10.91
	0.153	6.47	8.05
	0.250	6.51	6.74
	0.370	5.64	5.39
	0.570	5.01	4.38

TABLE V

Reaction cross sections for H + DI reaction calculated by statistical theory

$T_{rot}(^{o}K)$	E_i(eV)	Cross section ($Å^2$)		
		HI + D	HD + I	HD + I^*
500	0.012	0.95	66.6	6.62
	0.040	1.20	43.5	4.56
	0.063	1.63	36.6	3.82
	0.087	1.91	30.8	3.29
	0.153	2.51	24.0	2.82
	0.250	2.89	18.4	2.30
	0.370	3.35	14.6	1.95
	0.520	3.87	10.4	1.65
700	0.012	1.54	65.2	6.59
	0.040	1.61	42.7	4.53
	0.063	1.93	36.0	3.80
	0.087	2.13	30.4	3.29
	0.153	2.64	23.8	2.82
	0.250	2.98	18.3	2.30
	0.370	3.42	14.6	1.96
	0.570	3.91	10.4	1.66

TABLE VI

Reaction rate constants (cc/sec · molecule) calculated by statistical theory for H + AX for products in specified electronic states

A	X	T(^{o}K)	HX + A	HA + X	HA + X*
D	Cl	300	7.34 (-11)[a]	4.31 (-10)	8.16 (-12)
D	Br	300	3.50 (-11)	8.94 (-10)	1.307 (-10)
		500	8.47 (-11)	9.11 (-10)	1.390 (-10)
		700	12.71 (-10)	9.07 (-10)	1.459 (-10)
D	I	300	2.44 (-11)	11.42 (-10)	1.171 (-10)
		500	5.73 (-11)	11.84 (-10)	1.261 (-10)
		700	8.84 (-11)	12.16 (-10)	1.332 (-10)
H	I	300	7.47 (-11)[b]	11.07 (-10)	1.183 (-10)
		500	11.05 (-10)[b]	11.37 (-10)	1.267 (-10)
		700	14.93 (-10)[b]	12.41 (-10)	1.44 (-10)

[a] The number in parentheses is a power of 10 by which the preceeding number is to be multiplied.

[b] Half the HI yielded by decomposition of the strongly coupled complex is included here as reaction.

TABLE VII

Abstraction fractions (AF) calculated by statistical theory for the H + DBr and H + DI reactions ($T = 300^{o}K$)

X	AF(statistical theory)[a]	AF(experimental)
Br	0.967	0.99[b]
		0.92[c]
I	0.981	0.97[b]
		0.95[c]

[a] For more details see Tr 69.

[b] Da 69.

[c] Pe 69.

TABLE VIII

Cross sections calculated by statistical theory for reaction leading to vibrationally excited species for H + DI reaction

$T_{rot}(^{o}K)$	E_i(eV)	Cross section ($\mathring{A}^2$)		
		$HI^v + D$	$HD^v + I$	$HD^v + I^*$
300	0.012	0.00	38.85	0.72
	0.040	0.00	25.19	0.64
	0.063	0.00	21.33	0.63
	0.087	0.00	18.27	0.62
	0.053	0.00	13.93	0.66
	0.250	0.01	11.19	0.64
	0.370	0.34	9.09	0.62
	0.570	1.15	6.75	0.67
500	0.012	0.00	38.03	0.79
	0.040	0.00	24.88	0.70
	0.063	0.00	21.05	0.67
	0.087	0.00	17.97	0.66
	0.153	0.00	13.87	0.68
	0.250	0.03	11.13	0.66
	0.370	0.40	9.08	0.64
	0.570	1.19	6.76	0.68
700	0.012	0.00	37.27	0.87
	0.040	0.00	24.52	0.76
	0.063	0.00	20.78	0.71
	0.087	0.00	17.73	0.70
	0.153	0.01	13.80	0.70
	0.250	0.07	11.07	0.67
	0.370	0.47	9.06	0.65
	0.570	1.23	6.77	0.69

v indicates vibrationally excited species.

TABLE IX

Statistical theory calculations of ratios of products of the H + DBr reaction (T_{rot} = 500 °K)

E_i (eV)	n_i	Q(HBr) + Q(HD)[a] (a_o^2)	AF[b]	PCE[c] (%)	% vibrational excitation in HBr	% vibrational excitation in HD
0.06300	0	35.22	0.933	13.4	0.0	27.5
0.06300	1	28.10	0.762	17.1	1.3	39.0
0.06300	2	25.50	0.664	19.5	28.8	46.2
0.06300	3	24.15	0.609	21.1	43.8	53.3
0.06300	4	23.43	0.579	22.5	53.6	58.3
0.06300[d]	0	35.22	0.933	13.4	0.0	27.5
0.28983	0	18.06	0.781	16.4	0.8	37.3
0.50969	0	13.82	0.697	18.6	19.6	44.1
0.72256	0	11.62	0.636	20.1	34.2	50.1
0.92846	0	10.33	0.593	21.5	44.6	55.1

[a] Q(P) is the total reaction cross section for production of the product P.

[b] AF = Q(HD)/[Q(HD) + Q(HBr)].

[c] PCE = 100% × $Q(Br^*)/[Q(Br) + Q(Br^*)]$.

[d] The total energies E for rows 6 through 10 are respectively equal to those for rows 1 through 5.

TABLE X

Statistical theory calculations of ratios of products of the H + DBr reaction (T_{rot} = 700 ^{o}K)

E_i (eV)	n_i	Q(HBr) + Q(HD)[a] (a_o^2)	AF[a]	PCE[a]	% vibrational excitation in HBr	% vibrational excitation in HD
0.06300	0	34.86	0.919	13.1	0.1	28.0
0.06300	1	27.91	0.752	17.6	2.9	39.9
0.06300	2	25.34	0.660	19.6	29.7	46.8
0.06300	3	24.09	0.606	21.4	44.2	53.7
0.06300	4	23.35	0.575	22.9	53.9	58.4
0.06300[b]	0	34.86	0.919	13.7	0.1	28.0
0.28983	0	18.04	0.776	16.8	1.8	38.0
0.50969	0	13.85	0.696	18.7	20.6	44.6
0.72256	0	11.69	0.635	20.2	34.6	50.4
0.92846	0	10.39	0.594	21.6	44.9	55.3

[a] Defined in Table X.

[b] The total energies E for rows 6 through 10 are respectively equal to those for rows 1 through 5.

TABLE XI

Statistical theory calculations of abstraction fractions (AF) and per cent of products produced in excited electronic (PCE) and vibrational (PCVE) states for H + DX reaction with $n_i = 0$ and $T_{rot} = 300\ ^{o}K$

X	E_i (eV)	AF	PCE X	PCVE HX	PCVE HD
Cl	0.012	0.959	0.24	0	0
	0.040	0.897	0.87	0	0
	0.063	0.784	2.19	0	0
	0.087	0.665	6.10	0	0
	0.153	0.554	17.28	0	0
	0.250	0.509	23.51	0	0
	0.370	0.489	26.30	0	0
	0.570	0.467	26.04	17	14
Br	0.012	0.992	12.76	0	27
	0.040	0.978	12.37	0	26
	0.063	0.949	13.24	0	27
	0.087	0.916	13.53	0	27
	0.153	0.854	14.13	0	30
	0.250	0.798	15.29	0	35
	0.370	0.760	17.11	29	40
	0.570	0.673	19.02	24	45
	1.000	0.579	21.97	47	57
I	0.012	0.995	8.93	0	53
	0.040	0.985	9.43	0	53
	0.063	0.970	9.44	0	54
	0.087	0.954	9.50	0	55
	0.153	0.919	10.41	0	54
	0.250	0.881	10.95	0	57
	0.370	0.836	11.61	10	58
	0.570	0.759	13.55	30	61

TABLE XII

Statistical theory calculations of reaction rate constants (cc/sec · molecule) for H + AX for vibrationally excited products in specified electronic states[a]

A	X	T (^{o}K)	HX + A	HA + X	HA + X*
D	Cl	300	b	b	b
D	Br	300	b	2.70 (-10)	4.37 (-14)
		500	6.41 (-14)	2.88 (-10)	9.64 (-13)
		700	7.05 (-14)	3.02 (-10)	3.66 (-12)
D	I	300	b	6.53 (-10)	1.65 (-11)
		500	1.50 (-13)	6.83 (-10)	2.24 (-11)
		700	1.23 (-13)	7.07 (-10)	2.74 (-11)
H	I	300		5.78 (-10)	9.60 (-12)
		500		6.02 (-10)	1.57 (-11)
		700		6.68 (-10)	2.08 (-11)

[a] Each number in parentheses is a power of 10 by which the preceding number is to be multiplied.

[b] Less than 1.0 (-15).

TABLE XIII

Checks of how well detailed balance is satisfied for actual computer calculations using the statistical theory

Example	E (a.u.)	f	n_f	M_f	E_f (eV)	F
1	0.00655551	1	0	3	0.0559577	H + DBr
		2	0	6	0.04	H + DBr
	$(2M_1 + 1)E_1 Q_{12} = 1.02167$ eV a_o^2					
	$(2M_2 + 1)E_2 Q_{21} = 1.00268$ eV a_o^2					
	Detailed balance holds within 1.9%.					
2	0.01183338	1	0	3	0.1995771	H + DBr
		2	0	6	0.1836194	H + DBr
	$(2M_1 + 1)E_1 Q_{12} = 1.65456$ eV a_o^2					
	$(2M_2 + 1)E_2 Q_{21} = 1.62740$ eV a_o^2					
	Detailed balance holds within 1.7%.					
3	0.0152144	1	0	2	0.2	$C^+ + D_2$
		2	0	5	0.10944065	$C^+ + D_2^2$
	$(2M_1 + 1)E_1 Q_{12} = 14.125$ eV a_o^2					
	$(2M_2 + 1)E_2 Q_{21} = 14.333$ eV a_o^2					
	Detailed balance holds within 1.4%.					

Example 3 was computed by calculating only every third partial wave directly and interpolating the others.

TABLE XIV

Data for the statistical theory calculations on the reaction $K + H Cl$ [a]

	K	HCl	H	KCl
D_e (eV)		4.6369		4.4373
ω_e (cm^{-1})		2989.74		280.
R_e (a_o)		2.4087		5.2724
R_o (a_o) [b]	6.1		5.8	
$C(e^2 a_o^5)$ [c]	285.		26.	

[a] In addition to these data the calculation requires the masses of all the atoms.

[b] Hard sphere collision radius.

[c] Coefficient of $-R^{-6}$ in long range potential.

TABLE XV

Cross sections for K + HCl collisions; $n_i = 0$, $M_i = 2$.[a]

E_i (kcal/mole)	$E_i - E_{thr}$ (kcal/mole)	$L_{i\,max}$	Cross sections ($\AA^2$)						
			Q_{rot}	Q_0	Q_1	Q_2	Q_3	Q_4	Q(KCl)
1.00	0.23	107	66.5	7.21	0.00	0.00	0.00	0.00	7.21
1.41	0.64	120	58.7	10.56	0.02	0.00	0.00	0.00	10.59
2.29	1.52	141	48.7	11.28	2.64	0.07	0.00	0.00	13.98
2.88	2.11	152	43.9	10.83	3.65	0.81	0.00	0.00	15.31
3.46	2.69	162	41.0	10.27	4.20	1.47	0.25	0.00	16.18
4.468	3.79	176	35.7	9.50	4.58	2.19	0.92	0.24	17.41

[a] All column headings are defined in the text.

TABLE XVI

Calculations on the H + D Br reaction using modified Serauska's - Schlag theory; $n_i = 0$

E_i (eV)	M_i	ν (10^{13} cps)	Cross sections (a_o^2)			$M_{F\,max}$ [a]	
			HBr + D	HD + Br	HD + Br*	HBr	HD
0.040	6	1.0	4.2	133.7	0.0	3	11
		3.6	3.9	134.2	0.0	3	11
		∞	3.9	134.1	0.0	3	11
0.040	14	1.0	26.2	96.6	0.0	9	11
		3.6	24.6	97.7	0.0	9	11
		∞	24.4	97.9	0.0	9	11
0.153	6	1.0	20.7	59.4	0.0	10	12
		3.6	18.8	60.4	0.0	10	12
		∞	18.2	60.8	0.0	10	12
0.153	14	1.0	25.1	55.0	0.0	13	12
		3.6	23.6	55.4	0.0	13	12
		∞	23.0	55.7	0.0	13	12

[a] $M_{F\,max}$ is the maximum rotational quantum number with which product F is produced.

TABLE XVII

Calculations on the H + DBr reaction using the modified Serauskas - Schlag theory; $n_i = 0$, $T_{rot} = 300\ ^{o}K$

E_i	ν	Cross sections ($\AA^2$)			AF
(eV)	($10^{13} sec^{-1}$)	HBr + D	HD + Br	HD + Br*	
0.04	0.1	1.99	36.4	0.0	0.948
	1.0	1.42	37.0	0.0	0.963
	3.6	1.32	37.2	0.0	0.966
	∞	1.31	37.2	0.0	0.966
0.153	0.1	6.17	16.8	0.0	0.731
	1.0	5.84	16.6	0.0	0.740
	3.6	5.30	16.9	0.0	0.761
	∞	5.14	17.0	0.0	0.768

TABLE XVIII

Calculations on H + DBr reaction using new nonstatistical theory; $n_i = 0$

E_i (eV)	M_i	d	ν (sec^{-1})	Cross sections (a_o^2)			$PCVE_3$[a]
				HBr + D	HD + Br	HD + Br*	
0.040	6	1	1.0 (13)[b]	2.2	42.0	7.8 (-3)[b]	0.04
		0	∞	2.6	128.7	1.7 (1)	30.4
0.040	14	1	1.0 (13)	12.4	31.8	5.9 (-3)	0.04
		0	∞	17.3	102.9	1.6 (1)	33.0
0.087	6	1	1.0 (13)	4.5	17.1	6.0 (-3)	0.07
		0.025	∞	9.0	82.5	1.2 (1)	28.7
		0	∞	9.0	85.7	1.3 (1)	31.3
0.087	14	1	1.0 (13)	6.5	15.8	4.9 (-3)	0.07
		0	∞	15.8	76.8	1.2 (1)	34.0
0.153	6	1	0.9 (13)	3.4	7.6	3.3 (-3)	0.09
		1	1.0 (13)	3.7	8.3	4.2 (-3)	0.10
		1	3.6 (13)	8.2	22.2	4.9 (-2)	0.46
		0.5	1.0 (13)	3.7	8.4	1.7 (-2)	0.43
		0.025	1.0 (13)	3.7	11.8	1.7 (0)	29.4
		0	9.0 (10)	0.04	0.2	2.9 (-2)	39.8
		0	9.0 (11)	0.4	1.6	2.9 (-1)	40.1
		0	4.5 (12)	1.9	7.0	1.4 (0)	41.1
		0	1.0 (13)	3.7	14.0	2.8 (0)	40.7
		0	∞	12.8	64.9	1.1 (1)	34.2

[a] $PCVE_3$ is the per cent vibrational excitation in the HD + Br (atom unexcited) channels.

[b] The number in parentheses is a power of 10 by which the preceding number is to be multiplied.

Fig. 1. Rotational distribution. Shown is Q(F; H + DBr, $n_i = 0$, $M_i = 6$, $E_i = 0.087$ eV) vs. M_f for each arrangement channel F. Br indicates Br ($^2P_{3/2}$); Br* indicates Br ($^2P_{1/2}$).

Fig. 2. Rotational distribution. Shown is Q(F; H + DBr, $n_i = 0$, $M_i = 21$, $E_i = 0.370$ eV) vs. M_f for each arrangement channel F.

Fig. 3. Probability of reaction vs. impact parameter for K + HCl. Circles are from Gr 66; curve is result of present statistical calculation.

Fig. 4. Same as Fig. 3.

Fig. 5. Same as Fig. 3.

Fig. 6. Probability of reaction vs. impact parameter for K + HCl from statistical calculations.

Fig. 7. Reaction cross section vs. incident energy for K + HCl from experiment (circles are from Ac 64, square is from Od 69) and theory (X's are from present statistical calculations).

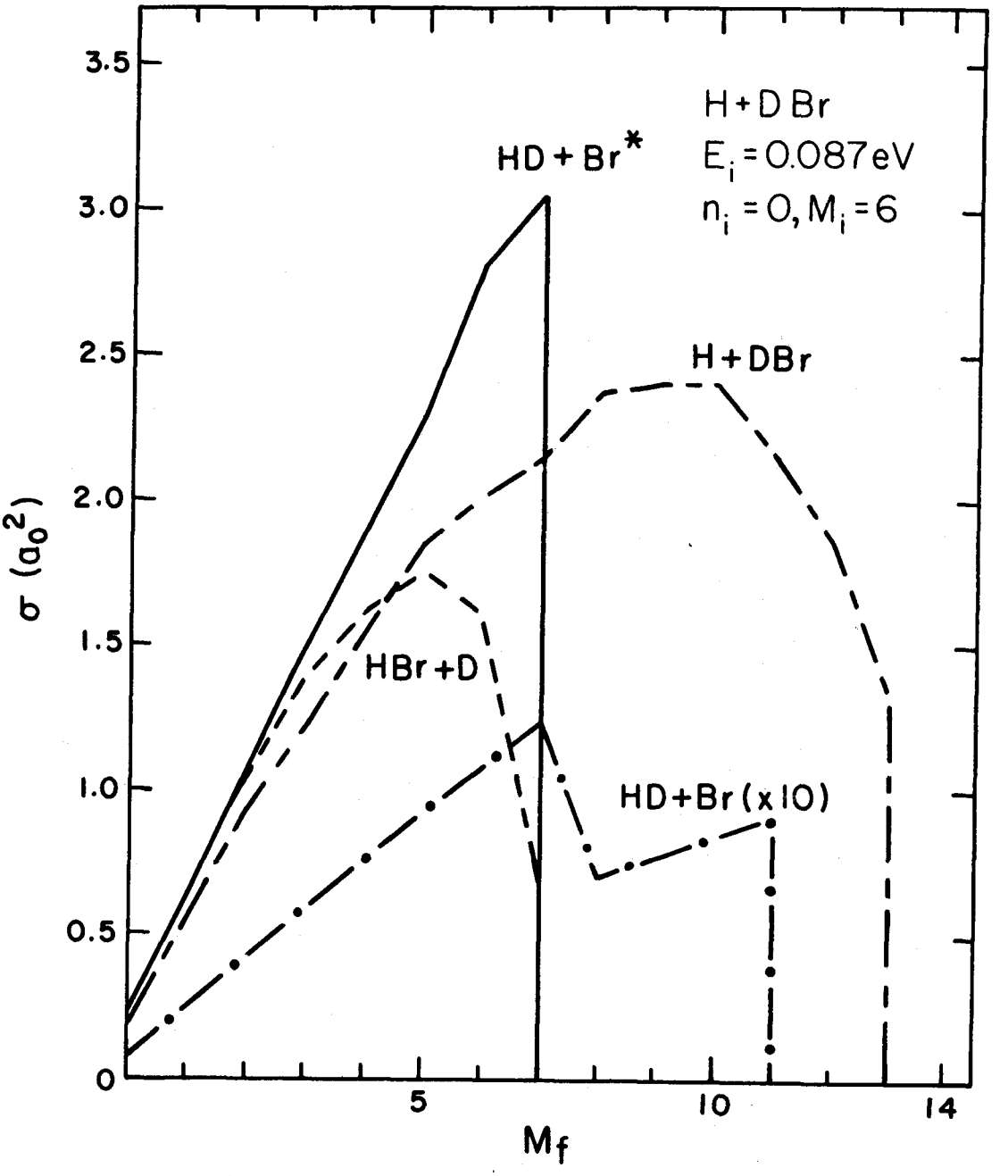
H+D Br
E_i = 0.087 eV
n_i = 0, M_i = 6
HD + Br*
H+DBr
HBr+D
HD+Br (x10)
σ (a_0^2)
M_f
3.5
3.0
2.5
2.0
1.5
1.0
0.5
0
5
10
14

1

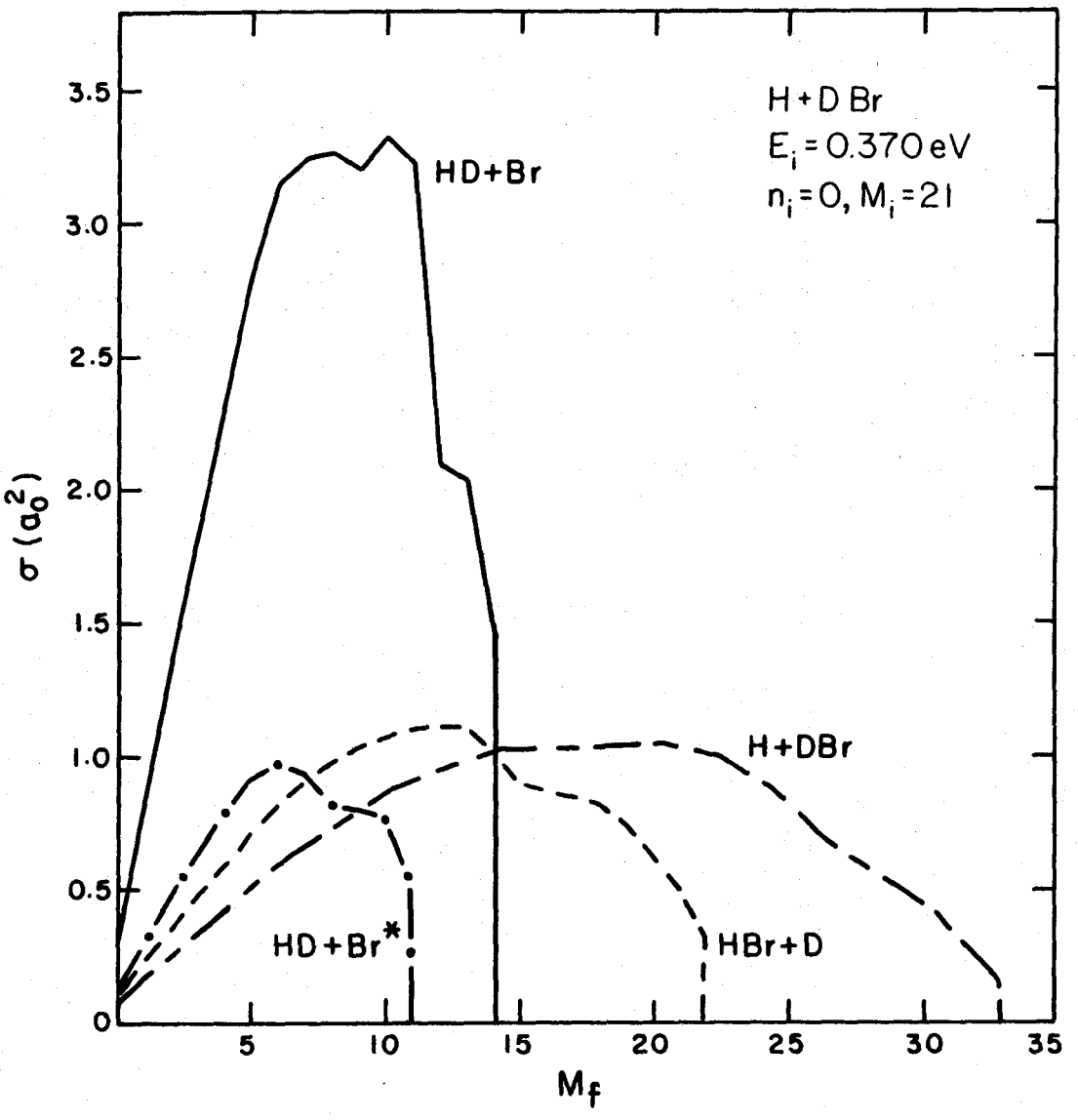
H + D Br
E_i = 0.370 eV
n_i = 0, M_i = 21
HD+Br
H+DBr
HD+Br*
HBr+D
σ (a_0^2)
M_f
0
0.5
1.0
1.5
2.0
2.5
3.0
3.5
5
10
15
20
25
30
35

2

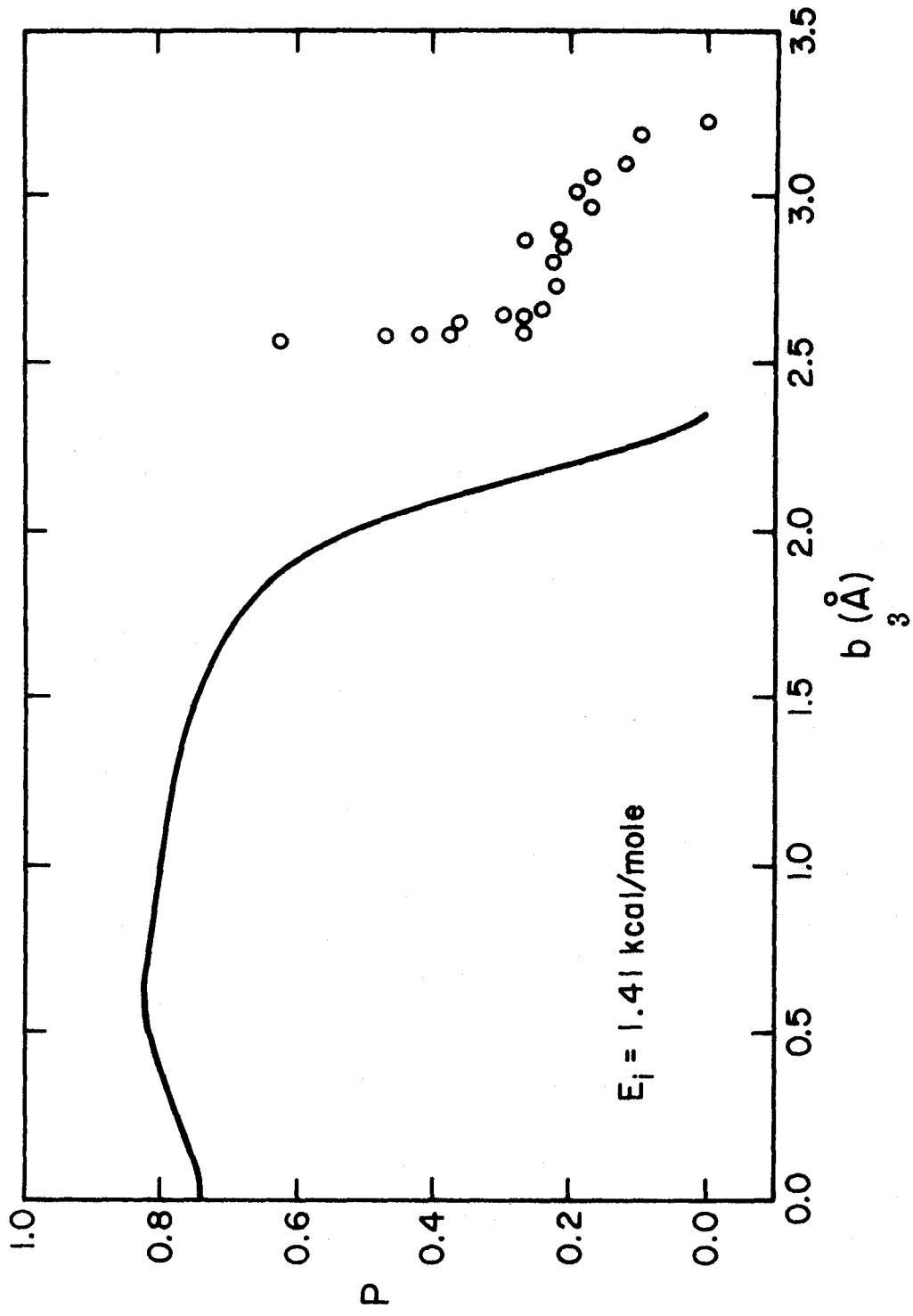
P
1.0
0.8
0.6
0.4
0.2
0.0
0.0
0.5
1.0
1.5
2.0
2.5
3.0
3.5
b (Å)
3
E_i = 1.41 kcal/mole

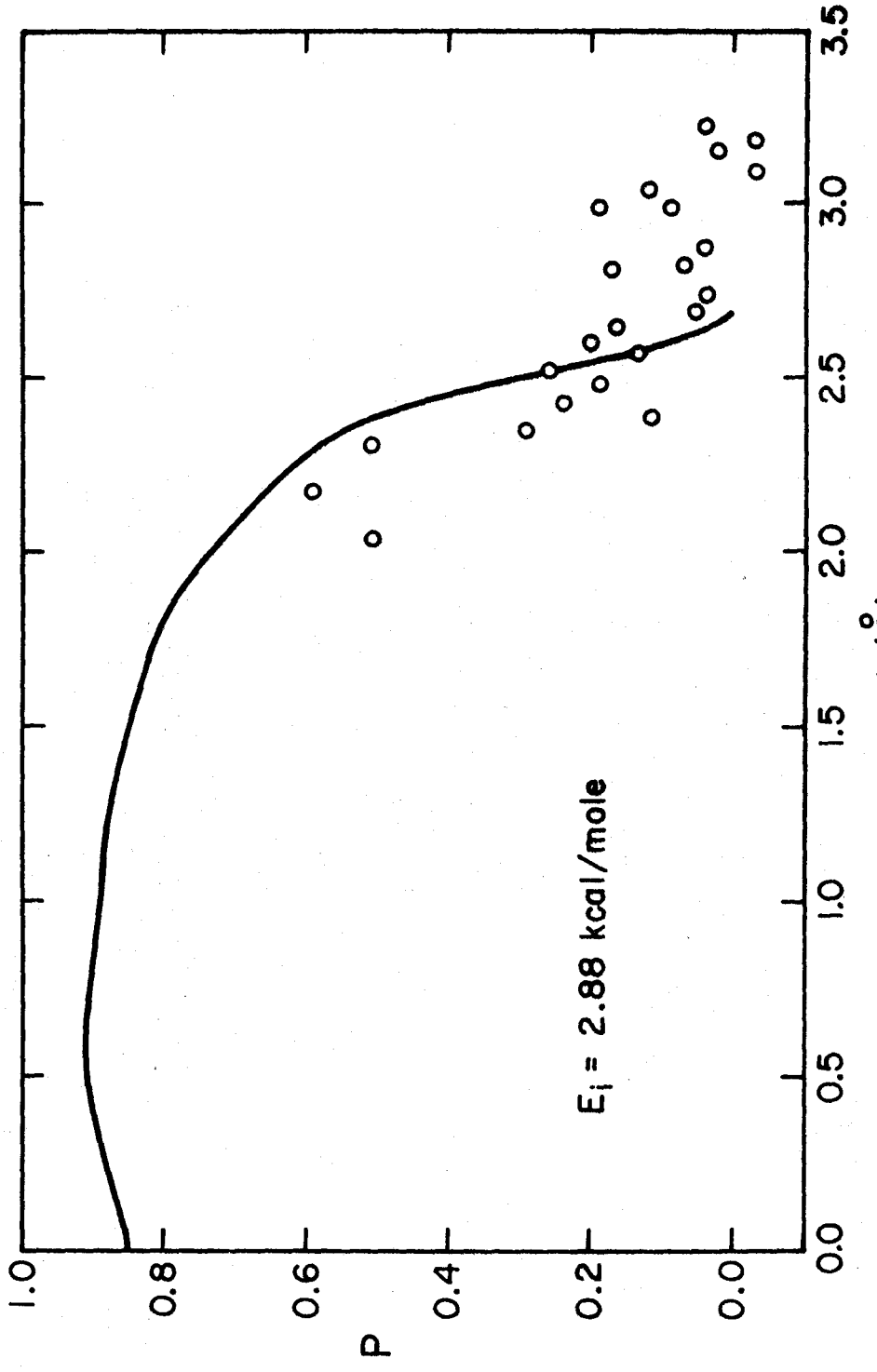

4

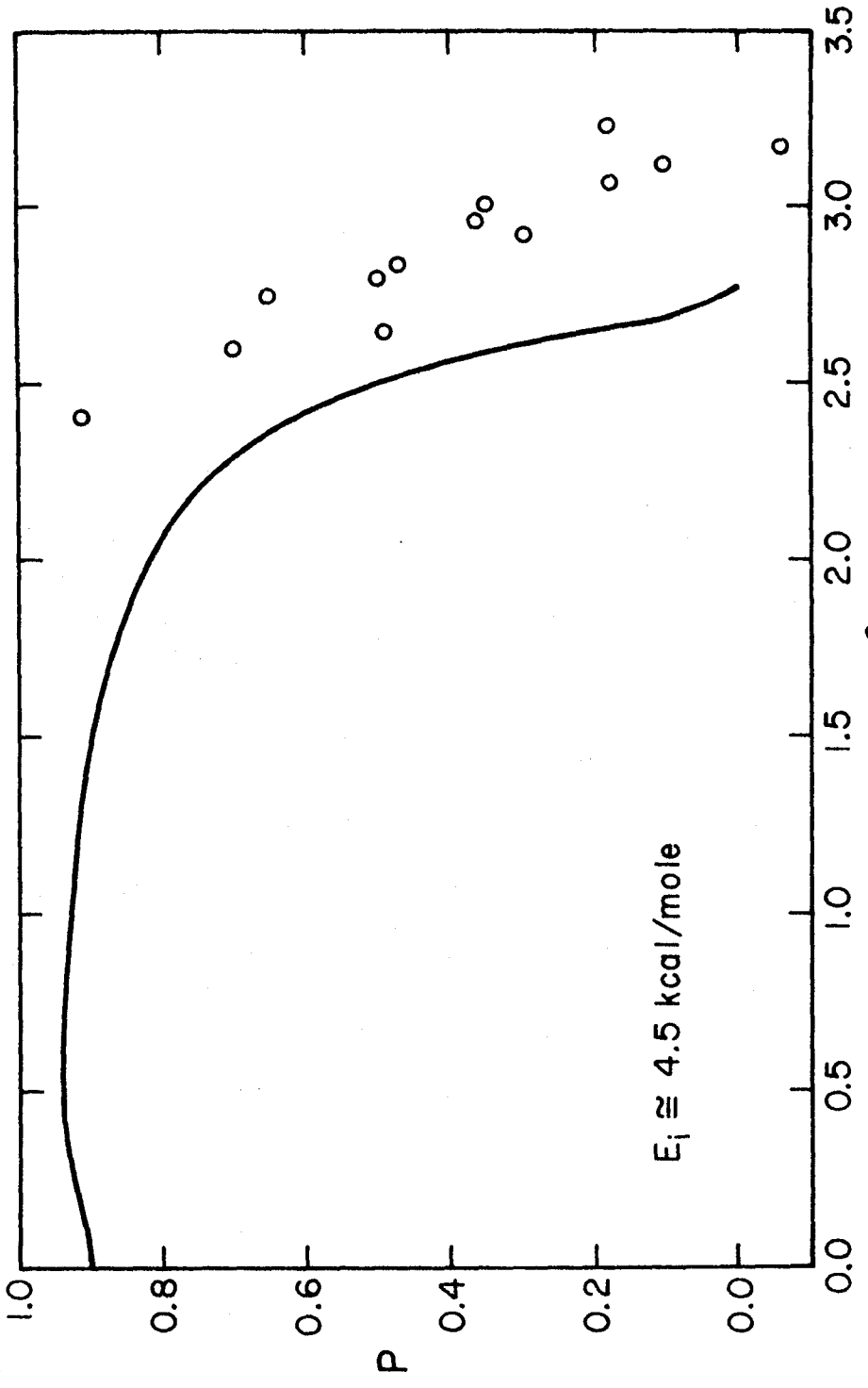

5

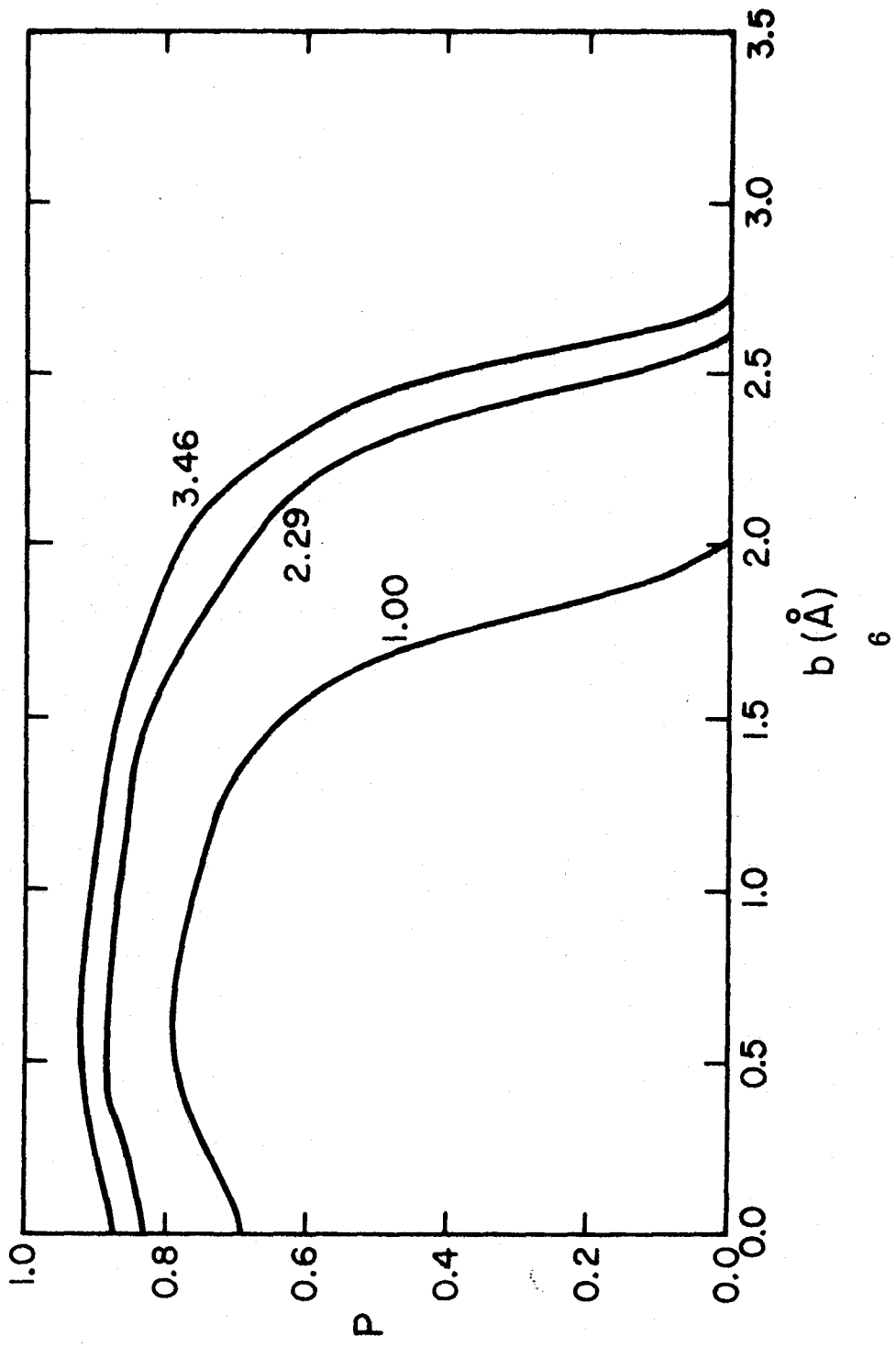

6

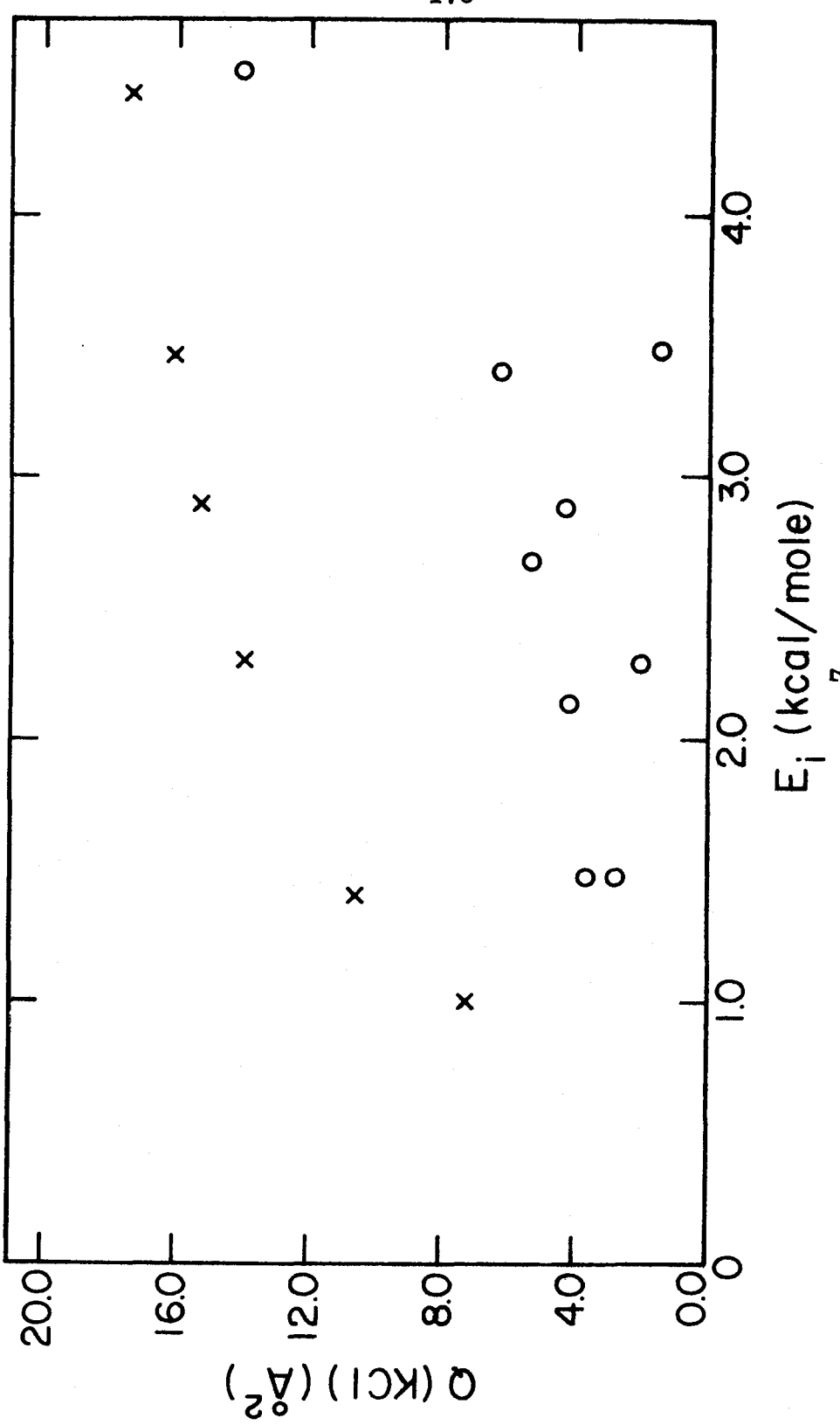
Q (KCl) (Å²)
20.0
16.0
12.0
8.0
4.0
0.0
0
1.0
2.0
3.0
4.0
E_i (kcal/mole)
7

IV. EXACT QUANTUM MECHANICAL CALCULATIONS ON COLLINEAR CHEMICAL REACTIONS

The quantum mechanical theory of rearrangement collisions and the problems encountered in attempting numerical calculations on rearrangements were reviewed in subsection I.A.2 of this thesis. Because the quantum theory of rearrangements is so difficult (see subsection I.A.2), most of our understanding of chemical reactions has come from transition state theory, simplified collision theories such as the statistical phase space theory and hard sphere collision theory with stereochemical corrections, classical trajectory calculations, and other semiclassical chemical models which involve extensive or questionable approximations. Actual calculations using quantum mechanical scattering theory to approximate the wave functions or scattering amplitudes for chemically reactive systems have been performed only a few times (Go 49, Ba 53, Ya 54, Go 54, Ma 59, Mo 62, Mi 65, Ny 65, Su 67, Ka 68, Di 68b, Mo 68, Ta 69, Mc 69). Most of these calculations used either a highly approximate treatment of the scattering or an unrealistic, artificial potential energy surface. Two of the treatments, however, are very significant attempts to treat the $H + H_2 \rightarrow H_2 + H$ reaction quantum mechanically. The most important approximation involved in both is the assumption (made in different ways in the two studies) that the important reactive collisions are approximately linear and can be treated as linear with corrections for nonlinearity added. Karplus and Tang used the distorted wave approximation to treat the $H + H_2$ reaction for relative translational energies in the range 0.25 - 3.3 eV (Ka 68) and Mortensen and Pitzer used a numerical solution of the Schroedinger equation to treat it and three of its isotopic analogues for relative translational energies in the range 0.16 - 0.6 eV (Mo 62, Mo 68). Both these calculations assumed electronic adiabaticity (see Appendix 1) and used semiempirical approximations of the lowest

potential energy surface which are probably fairly accurate. The biggest difficulty in extending these types of calculations to other reactive systems is obtaining an accurate representation of the potential energy surfaces of these systems.

In chapters II and III we felt that it was most important to compare our calculated cross sections with experiment and we felt the scattering treatment was more satisfactory if the calculated results agreed with the experimental ones. Since the quantum mechanical calculation of real reaction cross sections is so difficult, we take a different approach in this chapter. Here we do essentially exact quantum mechanical calculations on simplified models of chemical reactions (in particular, the $H + H_2$ and $D + D_2$ reactions) and compare these to easier, more approximate calculations on the same models. In this way we make progress in the theory of chemical dynamics in the following ways: (1) we develop and improve the techniques for solving the Schroedinger equation for rearrangement collisions; (2) we learn which of the easier, more approximate theories are reliable enough to be applied to the more complicated cases of real chemical reactions where the exact quantum mechanical treatment is too hard; (3) we learn about the real dynamics of collision processes which are models of chemical reactions and thus indirectly learn about the dynamics of real chemical reactions; (4) we learn about the real properties of reaction probabilities in simplified versions of the $H + H_2$ and $D + D_2$ reactions and thus indirectly learn about the properties of the reaction probabilities for the real $H + H_2$ and $D + D_2$ reactions.

Transition state theory (Ey 35, Hi 36, Hi 39) has been very important in the history, understanding, and practical applications of chemical kinetics (transition state theory is also called absolute

reaction rate theory; a recent review of its basic principles is given in Jo 66a). In transition state theory we assume that motion along the direction of a reaction coordinate s can be separated from the other motion of the reacting system and that a potential energy can be defined for motion along this coordinate. This potential as a function of s usually involves a barrier between reactants and products. The effect of quantum mechanical tunneling through this barrier is included in the transmission coefficient which occurs in transition state theory. It usually has a very important effect on the calculated rate constants. In section B, we review the work that has been done on calculating quantum mechanical transmission coefficients for transition state theory. We discuss what is the theoretically most justifiable way of calculating transmission coefficients, and we do numerical calculations the best way and show how much error is introduced by incorrect treatments.

In section C we also consider the collisions of H with H_2 and D with D_2 in one-dimensional space. In this space, assuming electronic adiabaticity and a potential energy surface based on recent a priori calculations (Sh 68), we solve the scattering problem exactly (which requires a treatment in two mathematical dimensions). This is the first exact solution of the $H + H_2$ reaction problem with a realistic potential energy surface for collisions in any number of dimensions (1, 2, or 3). These calculations can provide the basis for testing various approximate theories and for better understanding the dynamics of the collision process. In section C of this chapter we present the results for probabilities of reactions and briefly discuss their interpretation and the comparisons with other theories.

A. An Accurate Analytic Potential Energy Surface

As discussed in Appendix 1 we may consider the $H + H_2$ reaction as proceeding in the ground electronic state with the nuclear motion determined by an effective potential calculated using the Born-Oppenheimer separation of electronic and nuclear motions. This potential has been calculated fairly accurately (using configuration interaction techniques to solve for the electronic wave functions) by Shavitt, Stevens, Minn, and Karplus (Sh 68). Their results confirm the conclusion of many earlier less accurate studies that the lowest energy reaction path for the $H + H_2$ reaction corresponds to a linear collision and that the highest potential energy that must be achieved along this minimum energy path (or reaction path) occurs for the symmetrical configuration where the two bond lengths are equal ($R_{AB} = R_{BC}$ in the notation introduced below). The calculation predicts that this barrier height is 0.477 eV. Shavitt, by an analysis discussed below, estimated that the best guess at the real barrier, as determined by comparing transition state theory to the rate experiments of Westenberg and de Haas (We 67a) and others, is 0.424 eV. He suggested that the barrier in the surface of Shavitt, Stevens, Minn, and Karplus (SSMK) be scaled by a factor (0.424/0.477) = 0.89 along the entire reaction path but that the predicted energy variation not be scaled in directions transverse to this minimum energy path. This scaling can be applied in a straightforward way at the barrier top (which is the transition state saddle point of the potential energy surface) but is ambiguous at other places.

In scattering calculations involving long range potentials, the numerical integration must extend over a large region, including tne whole portion of the configuration space where the potential or its

tail is nonnegligible. In the $H + H_2$ reaction there is a long range potential due to the induced dipole-induced dipole dispersion interaction. This long range interaction means there is a shallow potential well in the surface at large separation of H and H_2. An estimate which is probably accurate within a factor of 2 of the depth of this potential well is the value 0.001 eV obtained from the SSMK calculations (Sh 68). The approximate calculations of Dalgarno, Henry, and Roberts also predict a potential well depth of 0.001 eV (Da 66). This depth is thus at least a factor of a hundred less than the smallest translational energies in which we might be interested for reactive collisions. It is thus not expected to have a significant effect on the scattering considered here and we will neglect it.

Two additional reasons for neglecting this well are that its depth and shape are not known accurately and that including the long range forces makes the calculation more expensive (or for the same cost the numerical approximations are less accurate.)

It is convenient for scattering calculations to have an analytic expression for the potential energy as a function of the internuclear distances involved. Shavitt et al. fit their surface for linear collisions to an expression with 28 linear parameters and 1 nonlinear parameter (Sh 68). This is a fit to the surface before scaling. If we consider only linear collisions, one way to effect the scaling for the whole surface is by adapting to this purpose a procedure developed by Wall and Porter for constructing parametrized potential energy surfaces (Wa 62). This method can be used to construct a surface which has the scaled barrier height, the transition state parameters suggested by Shavitt (Sh 68a; these are the parameters of the SSMK surface except in the direction of the reaction coordinate) and the

correct asymptotic H_2 behavior for R_i or R_f large.* In addition the method still has one as yet undetermined parameter (ℓ in the notation of Wall and Porter). The effect of this parameter is shown schematically in Figure 1. It turns out that this parameter can be chosen so that the contours of the Wall-Porter-type surface with barrier height 0.424 eV are approximately parallel all over the surface to the contours for the SSMK surface with barrier height 0.477 eV. This choice yields $\ell = 3$. Figure 2 is a comparison of the SSMK surface and the Wall-Porter parametrized surface with $\ell = 3$ for the linear H_3 collision. If the shape of the accurate surface (the SSMK surface) had been such that none of the family of surfaces obtainable by the method of Wall and Porter could be made to resemble it, we would have had to use a different method to obtain an analytic representation of the surface.

The Wall-Porter-type fit with $\ell = 3$ to the scaled SSMK surface will simply be called the scaled SSMK surface in the rest of this chapter.

The Wall-Porter method yields a surface which is a generalization of the Morse potential. For $R_{AB} \geq R_o$ and $R_{BC} \leq R_o$ it reduces exactly to a Morse potential in R_{BC}, and for $R_{BC} \geq R_o$ and $R_{AB} \leq R_o$ it reduces exactly to a Morse potential in R_{AB}. For $R_{AB} < R_o$ and $R_{BC} < R_o$ the surface is an elbow-shaped valley which contains a barrier and which connects the two asymptotic regions. In the present case $R_o = 3.620\, a_o$. The following is a FORTRAN IV package containing a double precision function subprogram.

---

*R_i is the distance from A to the center of mass of BC; R_f is the distance from the atom to the center of mass of the molecule in the final state.

```
      BLOCK DATA
      IMPLICIT REAL*8(A-H,O-Z)
      COMMON /DWCOM/ ALFD,A,SN,RN,D,ALFN,ALFDIF,XN,RNMSN,RNMXN,R2T,L
      DATA ALFD,A,SN,D,ALFN,XN/0.70152D0,0.08939D0,1.765D0,109.47D0,1.04
     X435D0,        1.40083D0/
      DATA L,RNMSM/3,1.85630D0/
      END
      SUBROUTINE PREH3
C     THIS SUBPROGRAM SHOULD BE CALLED ONCE BEFORE THE FIRST CALL TO V.
      IMPLICIT REAL*8(A-H,O-Z)
      COMMON /DWCOM/ ALFD,A,SN,RN,D,ALFN,ALFDIF,XN,RNMSN,RNMXN,R2T,L
      RN = RNMSN + SN
      ALFDIF = ALFD - ALFN
      RNMXN = RN - XN
      R2T = 1.4142136D0*RNMSN
      RETURN
      END
      DOUBLE PRECISION FUNCTION V(RAB,RBC)
      IMPLICIT REAL*8(A-H,O-Z)
      LOGICAL RABL,RBCL
      COMMON /DWCOM/ ALFD,A,SN,RN,D,ALFN,ALFDIF,XN,RNMSN,RNMXN,R2T,L
      RABL = RAB.GT.RN
      RBCL = RBC.GT.RN
      IF (RABL.OR.RBCL) GO TO 12
      RNMX = RN - RAB
      THETA =DATAN((RN - RBC)/RNMX)
      STT =DSIN(2.0D0*THETA)
      LM4 = L - 4
      IF (LM4) 3,4,5
    3 STTL = STT**L
      STT4 = STTL*STT**(-LM4)
      GO TO 6
    4 STT4 = STT**4
      STTL = STT4
      GO TO 6
    5 STT4 = STT**4
      STTL = STT4*STT**LM4
    6 GAM = D*(1.0 D0- A*STTL)
      ALF = ALFN + ALFDIF*STT4
      BRACK = R2T - RNMXN
      RCRC = 2.0D0*RN*RN + RAB*RAB + RBC*RBC - 2.0D0*RN*(RAB + RBC)
      SQUIG = BRACK*STT4 + RNMXN -DSQRT(RCRC)
      SQUIG = BRACK*STT4 + RNMXN - RNMX/COS(THETA)
      GO TO 13
   12 GAM = D
      ALF = ALFN
      IF (RABL) SQUIG = RBC - XN
      IF (RBCL) SQUIG = RAB - XN
      IF (RABL.AND.RBCL) SQUIG = SQUIG + RBC - RN
      IF (RABL.AND.RBCL) SQUIG = RAB + RBC - XN - RN
   13 QUAN = 1.0 D0-DEXP(-ALF*SQUIG)
      V = GAM*(QUAN*QUAN - 1.0D0) + D
      V = V/627.71D0
      RETURN
      END
```

The package was written for the IBM 360/75. A call to the function subprogram returns the value of the potential in atomic units.

B. Exact Tunneling Calculations

1. Introduction

We consider the bimolecular reaction

$$A + BC \rightarrow AB + C \tag{1}$$

with a transition state saddle point in the potential energy surface corresponding to linear ABC and with C an isotope of A or the same as A. When B is a light atom and the potential energy barrier height V_c at the transition state is not negligible, we expect that an appreciable contribution to the reaction rate will result from quantum mechanical tunneling through the barrier. Much work has been done [not only for reaction (1) but also for the more general A + BC → AB + C where A, B, and C are general atoms, molecules, or molecular fragments] in an effort to estimate transmission coefficients for transition state theory that account for this tunneling (and sometimes for other effects such as the nonseparability of the reaction path).

The trajectory for a linear atom-diatomic molecular collision occurs in the 2-dimensional configuration space with coordinates

$$R_{AB} = | \vec{r}_A - \vec{r}_B | \tag{2}$$

$$R_{BC} = | \vec{r}_B - \vec{r}_C | \tag{3}$$

where $\vec{r}_A$, $\vec{r}_B$, and $\vec{r}_C$ are the coordinates of the three atoms with respect to the center of mass of the ABC system (see Fig. 3). Most of the tunneling calculations that have been done are based on some effective one-mathematical-dimension (1-MD) approximation (see Fig. 2) but a few treatments (Jo 61, Ma 64c, Ma 65b, Ma 66a) have attempted to consider two-mathematical-dimensional (2-MD) effects. Mortensen and Pitzer (Mo 62, Mo 68) considered the full 2-MD linear collision with approximate corrections for bending. Comparison of the calculations that have been carried out is sometimes difficult because not only the models but also the numerical approximations are different. In this chapter we do not examine the justification for a 1-MD treatment of tunneling but, assuming the 1-MD model, we consider the accuracy with which such 1-MD calculations are made by approximate methods and models. This can be done by numerically computing exact 1-MD scattering solutions of the Schroedinger equation for a typical barrier problem and comparing the results to the results of other numerical methods as applied to this same barrier. In addition, by using the exact numerical solutions for each given model, we can make a legitimate comparison of the models. Further, now that exact 2-MD solutions are becoming practical (see Mo 62, Mo 68, Di 68b, and section C of this chapter), it is interesting to have exact 1-MD calculations for comparison. For this reason we use special methods of reducing the 2-MD barrier to a 1-MD barrier so that the comparison will be more meaningful. Section C presents exact 2-MD solutions of a type that will make this comparison possible.

In subsection 2 we review previous 1-MD treatments of tunneling. In subsection 3 we discuss the transition state theory and consider what is the proper way to make a 1-MD tunneling correction.

2. Previous Treatments of Tunneling in One Mathematical Dimension

There are three basic approaches to the tunneling correction to transition state theory. The first is to consider this as a quantum mechanical correction to the (assumed separable) asymmetric stretch rectilinear reaction normal mode of the transition state (Jo 61, Jo 61a, Jo 62a, Jo 66, pp. 133 ff., 190 ff., 230 ff.). This procedure considers tunneling along path a (see Figs. 3 and 4). The other two approaches consider tunneling along path s (or c). The second approach is to consider the tunneling as a correction to a separable curvilinear reaction coordinate in a modified transition state theory which treats all modes consistently including curvilinear effects (Ma 64c, Ma 64b). This treatment, unlike the first approach, may be applicable even if the de Broglie wavelength for the motion along the potential surface is large compared to the size of the quadratic region of the saddlepoint region. The third approach considers the tunneling correction as a transmission coefficient for the standard rectilinear coordinate transition state theory (as given, e.g., in Jo 66a) but includes in it any estimable effects due to the curvilinear nature of the reaction coordinate or of the nonseparability of the 2-MD problem. Based on these approaches, various models (with different criteria for choosing the parameters) and various numerical methods have been used. In this subsection we review the calculations that have been done. In the next subsection (subsection 3) we will critically discuss the models behind these calculations and in a following subsection (subsection 5) we will consider the numerical methods.

The easiest tunneling correction to apply is the correction factor derived by Wigner (Wi 32) for the case where the reaction

normal mode is separable at the saddle point. This correction factor is for a quadratic barrier and is correct to the second power of Planck's constant. It is[†]

$$1 + \frac{1}{24} \left(\frac{h \nu^*}{k T} \right)^2 \qquad (4)$$

where $\nu^* = | \nu_a |$ and ν_a is the imaginary frequency associated with the reaction coordinate (the asymmetric stretch normal mode at the saddle point) and T is the absolute temperature. This correction factor is only valid when there is only a small amount of tunneling (e.g., at high T) but has found frequent application (Hi 36, Bi 49, Po 55, Bi 59, Sh 59a, Ya 59, Jo 61a, Jo 66a, p. 235). Wigner also derived (Wi 32) an approximation that included a correction for a quartic term in the potential energy at the saddlepoint but this is rarely used (Sh 59a).

Another method is to treat the problem as tunneling through a parabolic barrier or a truncated parabola barrier with the same height and force constant (curvature at the top) as the assumed potential energy surface and to obtain the full quantum mechanical solution for this barrier (Sh 59a, Jo 61a, Jo 61, Ch 63, Ma 64c, Ti 64, Kl 64, Le 68, Sh 68a, Pa 69). At high energies this reduces to the Wigner correction (4), but at lower energies it probably overestimates the tunneling because the barrier is too thin. Various ways to correct this failing by using a parabola with a different force constant have been considered. The parabola may be required to give the "best fit" to the barrier as a function of distance along path c (Sh 62) or to

---

[†]h is Planck's constant and k is the Boltzmann constant.

give the best fit, in the energy range for which tunneling is important, to the barrier along path s (Bi 59). Alternatively it may be chosen as the truncated parabola with the same height and area as the normal mode barrier a (We 59). Or it may be chosen so the truncated barrier gives the same tunneling as another barrier in certain cases (Sc 65a). The analytic mathematical treatment of the parabolic barrier model has been worked out by Bell (Be 59) and others (Hi 53, Bi 59, Sh 62, We 59, We 68, Ma 68a).

Another potential for which, like the untruncated parabola discussed above, an exact analytic solution is possible is the Eckart barrier (Ec 30). For a symmetrical surface (A and C chemically the same although they may be isotopes) this takes the form

$$V = E_c \operatorname{sech}^2 (d\pi\nu^* \sqrt{(2\mu/E_c)}) \qquad (5)$$

where E_c is the barrier height, and μ is the reduced mass, and d is the distance from the top of the barrier. For this potential the force constant F at the top of the barrier (d = 0) is $-(2\pi\nu^*)^2 \mu$ and the range is about $\ell = \sqrt{(E_c/2\mu)}/\nu^*$. This force constant is for the symmetric stretch normal mode of the transition state. There are thus two independent parameters, one of which has always been used to give the correct force constant. Various procedures have been used to assign the other parameter: the barrier can be required to have the correct height V_c (Sh 59a, Jo 61a, Jo 61, Kl 64, Jo 66a, pp. 193 ff., Le 68d, Sh 68a, Sc 65a), the correct height V_a (Jo 61, Jo 62a, Su 63), the height $V_0 = V_c - E_{iz}^{BC}$ where E_{iz}^{BC} is the zero point energy of the reactants (Jo 62, Ch 63, Jo 66a, p. 235, Ki 68b), or the height $V_{00} = V_0 + E_z^+$ where E_z^+ is the zero point energy of the transition state (Ma 64c, Mo 68). The last of these choices is an

attempt to include effects due to the nonseparable nature of the 2-MD problem, and the ideas behind it will be discussed in detail in subsection 3. The Eckart barrier has also been chosen to have the correct 4th derivative at the top (Sh 68a) or to be the best fit over the energy range where tunneling is important to the barrier along path c (Sh 68a). The analytic solutions for transmission across an Eckart barrier have been worked out by Eckart (Ec 30) and others (Jo 61, Jo 62a, Sh 63).

Johnston and Rapp developed an approximation to the 2-MD tunneling which consists in taking a Boltzmann factor-weighted average of Eckart tunneling corrections for several paths parallel to the a path in Fig. 1 (Jo 61). It has been applied frequently (Jo 61, We 59, Ch 63, Kl 64, Ca 64, Wi 65, Jo 66a, pp. 191 ff., 230 ff.). A version of this "2-MD" tunneling correction with a modified definition of the Eckart barriers has also been used (Ki 68b).

3. Transition State Theory

The transition state transmission coefficient is a quantum mechanical correction to the treatment of the reaction coordinate "normal mode." It has been pointed out many times that the transition state theory results if one assumes a Boltzmann distribution of reactants and that all modes of the system, except a separable reaction mode, are adiabatic (Hi 39, Ma 67 and references therein). Denoting progress along the reaction mode coordinate by s (s proceeds from $-\infty$ to $+\infty$ and may be taken to be zero at the top of the barrier), the conserved total energy is then a sum $E = E_s(s) + E_t(s)$ where E_s is the energy in the reaction mode and E_t is the energy in the other modes. Based on the adiabatic hypothesis (the quantum numbers of the t modes do not change), we calculate E_t along the path s (the

path of minimum energy from reactants to products) to find its highest value $E_t^+(s^+)$. Then, classically, reaction occurs for all $E_s(-\infty)$ such that $E_s(s^+) \geq 0$. Thus, as Hirschfelder and Wigner (Hi 39) and Marcus (Ma 67) have pointed out, the potential energy which is responsible for motion of the system along the reaction coordinate is the quantum mechanical adiabatic energy of the other modes of motion of the system (i.e., the energy $E_t(s)$ of the system-minus-the-reaction-mode). Although other interpretations of the transition state theory may be possible, we believe this is the most reasonable one for discussing tunneling corrections. This interpretation disagrees with most of the calculations* described in the previous section and especially with Johnston's statement "the quantum correction for one supposedly separable coordinate does not constitute potential energy for the reaction coordinate" (Jo 66, p. 195). We consider Johnston's statement inconsistent with the proper interpretation of transition state theory.

For a one-dimensional atom-diatomic molecule collision A + BC, the only mode of motion besides motion along the reaction coordinate is the vibrational mode (called the t mode) which is a molecular vibration for the molecule separated from the atom but is the symmetric stretch at the transition state, i.e., it is successively a vibration of BC, a symmetric stretching vibration of ABC, and a vibration of AB. The potential energy for the reaction coordinate mode of motion is the classical potential energy (the potential energy

---

*Marcus (Ma 67) took the point of view of this interpretation but was inconsistent in practice--presumably for the sake of computational expediency--because he took the imaginary asymmetric stretch frequency from the classical potential energy curve instead of the quantum mechanical adiabatic potential curve.

due to treating electronic motion quantum mechanically and adiabatically and neglecting zero point vibrational energy everywhere) plus the adiabatic vibrational energy in mode t. Neglecting the change in energy in this mode (so that the potential energy for the reaction coordinate mode is determined entirely by the classical potential energy) is treating that mode as inactive in Marcus' terminology. It is expected to be a bad approximation. Assuming that the quantum numbers of the vibrational modes transverse to the reaction coordinate do not change is called vibrational adiabaticity.

For a collision in a plane or a collison in three dimensional space we would also have to consider the adiabatic transformation of the rotations of the separated molecule and the orbital motion of A and BC into bending vibrations and rotations at the transition state. For the planar case, the adiabatic energies of the rotations and bends have been worked out by Child (Ch 68a). For the three-dimensional collision, an approximate consideration of this correlation has been worked out by Mortensen and Pitzer for the lowest rotational state of the separated molecule (Mo 62). The adiabatic assumption is not expected to be as good an approximation for these rotations, orbital motions, and bending modes as it is for the vibrational mode of the collinear H + H_2 reaction (Ma 66a, footnote 13). In this chapter we make calculations only for linear collisions.

4. Normal Mode Coordinates

A good discussion of normal mode coordinates for atom-molecule reactions is given in Johnston's book (Jo 66a, chapter 5 and appendix C). The reaction coordinate in transition state theory is a curvilinear coordinate which is tangent to the asymmetric stretch

normal mode coordinate at the transition state but differs from it elsewhere. To compute the transmission coefficient as a quantum mechanical correction to the treatment of the reaction coordinate normal mode, we shall express the reaction coordinate in terms of the transition state normal mode coordinates. Linear scaling of one of the normal mode coordinates by a constant c gives a new set of normal mode coordinates for which the effective mass corresponding to motion along that one normal mode coordinate is multiplied by a factor c^{-2}. We choose that set of normal mode coordinates for which the reduced mass is the same (μ_N) in each normal mode. Then distances appropriate to one-dimensional motion (with reduced mass μ_N) along the reaction coordinate can be computed as curvilinear distances along the reaction coordinate curve in the normal mode coordinate space.

For the H + H_2 or D + D_2 reactions with the transition state at $R_{AB} = R_{BC} = s_o$, the normal coordinates

$$x_1 = \frac{\sqrt{3}}{2} (R_{AB} + R_{BC} - 2s_o) \tag{6}$$

$$x_2 = \frac{1}{2} (R_{BC} - R_{AB}) \tag{7}$$

are coordinates for which the effective mass in any direction is

$$\mu_N = \frac{2}{3} m_A \tag{8}$$

where m_A is the atomic mass* (Sh 68a). We shall refer to the coordinates x_1 and x_2 as simply the normal mode coordinates.

The numerical method used to calculate distances along the curvilinear reaction coordinate in the normal mode space is numerical line integration using points on the reaction path close enough (less than $0.1 a_o$) so that the error involved is negligible.

5. One-Dimensional Potential Energy Barriers, Including the Vibrationally Adiabatic Potential Energy Barrier

Shavitt, Stevens, Minn, and Karplus computed the "minimum energy reaction path" for the $H + H_2$ reaction and also computed a 29-parameter fit to the potential energy surface (Sh 68). The coordinates of some points on this path are given in columns 1 and 2 of Table I. The energy as a function of distance along this path as plotted in the normal coordinate space was used as the best approximation to the barrier by Shavitt (Sh 68a). The correct minimum energy reaction path is the path of steepest descent in the normal mode coordinate space from the transition state (saddle point of the potential energy surface) to the reactants' configuration or, equivalently, the path of steepest ascent from the reactants' configuration to the transition state. This path is different from the path of steepest descent and ascent in the R_{AB}, R_{BC}, space. We computed the minimum energy reaction path in normal coordinate space for the SSMK surface from the 29-parameter fit and obtained a different path

---

*In atomic units, $m_H = 1837.1$ and $m_D = 3671.37$.

from the one given in Sh 68. The path given in Sh 68 was constructed using a different definition of the minimum energy path (not using the normal mode coordinates). The correct path for the SSMK surface is given in columns 3 and 4 of Table I. The minimum energy path for our scaled SSMK surface is given in columns 5 and 6 of Table I. Using these paths we computed the effective one-dimensional barriers for motion (with reduced mass μ_N) along the reaction coordinate. These barriers are given in Tables II and III in the columns labelled V. The barrier from the SSMK surface has been scaled by 0.89. For calculating the tunneling, we fit these barriers to expressions of the form

$$V = b_1 \operatorname{sech}^2(b_3 d^2) + b_2 \exp(-b_4 d^2) + (B - b_1 - b_2) \exp(-4 b_4 d^2) \tag{9}$$

where B is the barrier height, the b_i are determined by least squares fitting, and both B and the b_i are given in Tables II and III. Because of its nonlinear parameters, this form is capable of very accurate fits. This is illustrated in Tables II and III where the numbers in the columns labelled V_{fit} are computed from eq. (9).

From the 29-parameter fit to the SSMK surface and from the analytic expression for our scaled SSMK surface we numerically computed for points on the reaction path in normal coordinate space the second derivative of the potential energy in the direction perpendicular to the reaction path in normal coordinate space. From this, for each point on the reaction path, we computed the force constant and zero point energy of a harmonic oscillator of mass μ_N. These zero point energies are a function ZPE(d), where $d = |s - s_o|$ and

s_o is the position of the barrier along the reaction coordinate. This function is the harmonic approximation to the zero point energy of the motion transverse to the reaction coordinate. If the ZPE(d) function is added to the classical potential energy function V(d) we get a quantum surface $V_q(d)$ for vibrationally adiabatic reactions. (These quantities can also be written as functions of s.) According to the Hirschfelder-Wigner-Marcus interpretation of transition state theory the transmission coefficient should be calculated from a one-dimensional calculation using $V_q(s)$--not V(s). The present work is the first determination ever made of $V_q(s)$ and also the first calculation of scattering off such a potential.

The quantum barrier was computed for two choices of the classical potential energy function V(s). The two choices are the scaled barrier from the SSMK surface (column 5 of Table II) and the barrier from the scaled SSMK surface (column 2 of Table III). The quantum barriers are given in Table IV, which shows they are very similar to each other. Their similarity is an indication of the consistency of our fitting procedure (using the parametrized surface of Wall and Porter). The quantum surfaces were fit to expressions of the form (9) by the least-squares method. The parameters of the fits and some values of the potentials computed from the fits are given in Table IV.

Figure 5 illustrates the V(s) and $V_q(s)$ barriers for the scaled SSMK surface and the Wall-Porter-type $\iota = 3$ surface for linear H_3. The $V_q(s)$ barrier for the strictly linear collisions is 0.274 eV high and is about 0.4 a_o wider at the top than the classical barrier.

One dimensional scattering calculations off the two potentials V(s) and $V_q(s)$ represent two distinct models of the reaction. Use

of the classical potential $V(s)$ assumes conservation of vibrational energy (CVE) in the normal mode for motion transverse to the motion along the reaction coordinate. Use of the "quantum" potential $V_q(s)$ assumes conservation of vibrational quantum number (vibrational adiabaticity or VA) in that mode. The exact numerical solution of the scattering problem for these one dimensional barriers will be discussed in the following subsections.

The simplest interpretation of the vibrational adiabaticity is the one we use here, i.e., to construct the potential $V_q(s)$ by adding the local vibrational energy of the transverse mode to the classical potential energy along the minimum energy reaction path. This is not a strictly correct treatment because the coordinates are nonseparable due to the curvilinear nature of the reaction path. One important effect of the curvature of the minimum energy reaction path and the nonseparability of the Schroedinger equation for the reaction coordinate and the vibrational coordinate is a "centrifugal effect." This and other corrections to the simple scheme used here have been considered by Marcus (Ma 65, Ma 66a), but he has not done numerical calculations like the present ones.

6. Numerical Treatment of One Dimensional Tunneling

The Schroedinger equation is (with $\hbar = 1$)

$$\left[-\frac{1}{2\mu_N} \frac{\delta^2}{\delta s^2} + V(s) - E \right] \psi_k(s) = 0 \qquad (10)$$

where k labels the degenerate solutions. We select a set of N evenly spaced mesh points s_i, $i = 1, 2, \ldots, N$, $s_i < s_{i+1}$, and

approximate the equation for the solution at each of these points in terms of second differences in the standard way. This yields the set of N coupled linear equations

$$\sum_{j=1}^{N} (F_{ij} - \lambda \delta_{ij}) \psi_{jk}^{h} = b_i \quad i = 1, 2, \ldots, N \tag{11}$$

for the approximate values of the solutions $\psi_k^h(s_j)$ at the mesh points. In eq. (11),

$$\lambda = -2h^2 E \tag{12}$$

$$h = s_{i+1} - s_i \tag{13}$$

$$F_{ij} = -2\left[\frac{1}{\mu_N} + h^2 V(s_i)\right] \delta_{ij} + \frac{1}{\mu_N}(\delta_{i,j-1} + \delta_{i,j+1}) \tag{14}$$

$$b_i = \frac{-1}{\mu_N}\left[\psi_k(s_1 - h)\,\delta_{i1} + \psi_k(s_N + h)\,\delta_{iN}\right] . \tag{15}$$

As $h \to 0$, the approximate solutions approach the exact ones, i.e.,

$$\psi_k(s_j) = \lim_{h \to 0} \psi_k^h(s_j) .$$

We choose $s_1 = -s_N$ and s_N to be large enough that $V(s_1)$ is negligible, i.e.,

$$V(s_N) \ll V(0) \tag{16}$$

$$V(s_1) \ll V(0) \tag{17}$$

where $V(0)$ is the height of the barrier. We require two independent solutions with otherwise arbitrary boundary conditions. The first may be obtained with the boundary conditions

$$\psi_1(s_1 - h) = 1 \tag{18}$$

$$\psi_1(s_N + h) = 0 \tag{19}$$

and the second with

$$\psi_2(s_1 - h) = 0 \tag{20}$$

$$\psi_2(s_N + h) = 1 \ . \tag{21}$$

These choices make the wave functions real everywhere. Since we are considering the case where the barrier is symmetrical about $s = 0$, we need not solve for the second solution by solving the set of equations (11) because we can obtain it from the first by reflection through $s = 0$. The asymptotic form of the solutions to the Schroedinger equation is

$$\psi_k(s) \underset{s \to \infty}{\sim} A^{(k)} e^{-ips} + \bar{A}^{(k)} e^{ips} \tag{22}$$

$$\psi_k(s) \underset{s \to -\infty}{\sim} \alpha^{(k)} e^{-ips} + \bar{\alpha}^{(k)} e^{ips} \tag{23}$$

where

$$p = (2\mu_N E)^{1/2} \tag{24}$$

(since $\hbar = 1$) and we do not use the bar to mean complex conjugate. We want to analyze the ψ^h_{jk} for large and small j (corresponding to large $|s|$) in the same way. For large j we set

$$A^{(k)} e^{-ips_j} + \bar{A}^{(k)} e^{ips_j} = \psi^h_{jk} \tag{25}$$

$$A^{(k)} e^{-ips_{j+\ell}} + \bar{A}^{(k)} e^{ips_{j+\ell}} = \psi^h_{j+\ell,\,k} \tag{26}$$

where ℓ is a small integer (ℓ is usually 1 or 2). Solving these equations for $A^{(k)}$ and $\bar{A}^{(k)}$ gives

$$A^{(k)} = (\psi^h_{jk} e^{ips_{j+\ell}} - \psi^h_{j+\ell,\,k} e^{ips_j})/D \tag{27}$$

$$\bar{A}^{(k)} = A^{(k)*} \tag{28}$$

$$D = 2i \sin(p\ell h) . \tag{29}$$

Eq. (28) results from the fact that the ψ^h_{jk} are real. For small j, $\alpha^{(k)}$ and $\bar{\alpha}^{(k)}$ are given by the same equations. We consider the particle to be incident from the right of the barrier. The solution we seek has $A = 1$ and $\bar{\alpha} = 0$, i.e.,

$$\begin{aligned} \psi(s) &\underset{s \to \infty}{\sim} e^{-ips} + \bar{A} e^{iks} \\ \psi(s) &\underset{s \to -\infty}{\sim} \alpha\, e^{-ips} \end{aligned} \tag{30}$$

We can obtain this solution as a linear combination of any two linearly independent solutions. In terms of our approximate solutions we seek the solution with values

$$\psi_j^h = \sum_{k=1}^{2} C_k \psi_{jk}^h \tag{31}$$

where the coefficients are obtained by solving

$$\sum_{k=1}^{2} C_k A^{(k)} = 1 \tag{32}$$

$$\sum_{k=1}^{2} C_k \bar{\alpha}^{(k)} = 0 \ . \tag{33}$$

Equations (32) - (33) can be written in matrix form as

$$\underset{\sim}{A}\ \underset{\sim}{C} = \underset{\sim}{I}' \tag{34}$$

or

$$\begin{pmatrix} A^{(1)} & A^{(2)} \\ \bar{\alpha}^{(1)} & \bar{\alpha}^{(2)} \end{pmatrix} \begin{pmatrix} C_1 \\ C_2 \end{pmatrix} = \begin{pmatrix} 1 \\ 0 \end{pmatrix} \tag{35}$$

The probability of reflection from the barrier (R) and the probability of transmission across it (T) are then obtained from the asymptotic form of the solution with scattering boundary conditions $\{\psi_j^h\}$ as

$$R = \sum_{k=1}^{2} C_k \bar{A}^{(k)} \tag{36}$$

$$T = \sum_{k=1}^{2} C_k \alpha^{(k)} \tag{37}$$

For the case of symmetric potentials the only properties of the second linearly independent solution which we need to obtain R and T are

$$A^{(2)} = \bar{\alpha}^{(1)} \tag{38}$$

$$\bar{A}^{(2)} = \alpha^{(1)} \tag{39}$$

$$\alpha^{(2)} = \bar{A}^{(1)} \tag{40}$$

$$\bar{\alpha}^{(2)} = A^{(1)} \tag{41}$$

The procedure was programmed in FORTRAN IV for the Caltech IBM 7094 computer and the program was checked by computing R and T for the Eckart potential (R and T for the Eckart potential can be obtained analytically as discussed in section IV. B. 2; the analytic solutions are given in Sh 59a and Jo 61). In that case we could obtain R and T to an accuracy of 0. 3% with N = 100 and 0. 04% with N = 400. For the H_3 barriers we used N = 400 and

s_N = 4.0 to 8.0 a_o. The computing time was about 1.0 sec per energy (at one energy we obtain one R and one T; the analysis was usually done at 6 pairs of s_i as a consistency check).

7. Calculation of Boltzmann Transmission Coefficients

The energy of the reacting system A + BC in the center-of-mass coordinate system is

$$E = E_i + E_i^A + E_i^{BC} \tag{42}$$

$$= E_i^+ + E_i^T \tag{43}$$

where E_i is the initial relative translational energy, E_i^A and E_i^{BC} are the initial internal energies of A and BC respectively for the system in state i (i represents the set of all quantum numbers for the separated subsystems), and E_i^+ is the energy available for motion along the reaction coordinate at the transition state if the internal energy at the transition is E_i^T. In the CVE model, $E_i^T = E_i^A + E_i^{BC}$. In the VA model E_i^T is the energy of the system at the transition state for the same quantum numbers i. In either model the tunneling factor (or Boltzmann transmission coefficient) is computed as the average over a Boltzmann distribution of energies of the ratio of the correct quantum mechanical transmission probability to the classical 1-MD transmission probability $T_c(E_i)$. This classical probability is

$$T_c(E_i) = \begin{cases} 1 & E_i^+ \geq 0 \\ 0 & E_i^+ < 0 \end{cases} . \tag{44}$$

The transmission coefficient is (cf. Ma 67)

$$\kappa = \frac{\sum_i \kappa_i \exp(-E_i^T/kT)}{\sum_i \exp(-E_i^T/kT)} \tag{45}$$

where T is the temperature and κ_i is the state-selected transmission coefficient for the reactants in internal states i :

$$\kappa_i = \frac{1}{kT} \int_{-\infty}^{\infty} dE_i^+ \, T(E_i, i) \exp(-E_i^+/kT) \, . \tag{46}$$

$T(E_i, i)$ is the probability of transmission across the barrier for the case where the initial energy is E_i and the initial internal state is i. In eq. (46) we have already performed an integration over $T_c(E_i)$ of eq. (44) to obtain the factor kT in the denominator of eq. (46). The integral in eq. (46) requires the definition

$$T(E_i, i) = 0 \quad \text{if } E_i < 0 \, . \tag{47}$$

We restrict ourselves now to linear $H + H_2$ and $D + D_2$ reactions in the ground electronic state. Then i is v_i, the initial vibrational quantum number. We are interested in the temperature region where only the ground vibrational state of H_2 is appreciably populated and $i = v_i = 0$. Then

$$\kappa \simeq \frac{1}{kT} \int_{-\infty}^{\infty} dE_o^+ \, T(E_o, O) \exp(-E_o^+/kT) \, . \tag{48}$$

Shavitt has shown how the integral (48) can be recast as the sum of two finite range integrals which can be easily integrated (Sh 59). He obtained accurate results (0.01%) using 200 points per integral. We have used his formula [eq. (27) of Sh 59] for the integrals but evaluated them using Gaussian integration. By using 21 points per integral (42 energy points in all) we were able to obtain accuracy usually much better than 1%.

8. Results

In his paper (discussed in section IV. A and subsections IV. B.2 and IV. B.5) on correlation of experimental rate constants with theoretical data on the H_3 potential energy, Shavitt fit an Eckart barrier to the high energy part of the scaled SSMK potential energy barrier (for the reaction path of Sh 68) and calculated the tunneling factors for this potential (Sh 68a). This Eckart barrier had a height of only 0.174 eV and thus H and H_2 are considered to have 0.250 eV (0.424-0.174 = 0.250) of their energy in potential energy at infinite separation. As discussed in subsection IV. B.2, the other parameter of his Eckart barrier was chosen so that it had the correct second derivative at the top. Shavitt reasoned that the amount of transmission is determined by the nature of the potential barrier in the region where $|d|$ is small, i.e., close to the top of the barrier, and that his potential was a good approximation to the barrier in that region. He considered the tunneling factors computed that way to be the best available estimate. By using the method described in subsection IV. B.6 we can compute the transmission functions (and hence the tunneling factors) for any potential barrier and we need not resort to fits with Eckart barriers.

Column 2 of Table V shows the tunneling factors for the $H + H_2$ reaction computed using Shavitt's method (the 0.174 eV high Eckart barrier) and column 3 of Table V shows tunneling factors computed numerically for the fit to the scaled SSMK barrier for the minimum energy path of Sh 68 and Sh 68a (see columns 1-3 of Table II; this barrier will be called SSSMK). Column 4 shows the tunneling factors computed numerically for the fit to the scaled barrier from the SSMK surface for the correct minimum energy path (see columns 4-6 of Table II; this barrier will be called SNSSMK). Columns 2-4 of Table VI show the corresponding tunneling factors for the $D + D_2$ reaction.

Columns 5 of Table V and VI show tunneling factors computed numerically for the fit to the potential energy barrier of the scaled SSMK surface (see Table III; this barrier will be called the NSSSMK barrier).

To check the effect of the small inaccuracies in our fits to the barriers, we also computed the scattering from other fits to these barriers. The differences of the results from those reported here were very small.

For comparison with these attempts to do the problem more accurately than usual, we also computed the tunneling factors using the usual Eckart barrier treatment (see subsection IV. B. 2). This Eckart barrier has the classical barrier height (0.424 eV) and the correct force constant at the transition state. The results are given in column 6 of Table V and column 2 of Table VII.

The tunneling factors given in Tables V and VI and in column 2 of Table VII are based on the conservation-of-vibrational-energy approximation. We also computed tunneling factors using the vibrationally adiabatic quantum barriers of subsection IV. B.5. These tunneling factors are given in columns 3 and 4 of Table VII. The

barrier of column 3 of Table IV is labelled SMSSMK and the barrier of column 6 of Table IV is labelled MSSSMK.

Table VIII reviews the labels used for the different barriers.

9. Discussion

The tunneling factors enter the transition state theory expression for the rate constant as a multiplicative factor. A plot of the logarithm of the tunneling factors vs. the reciprocal temperature gives curves whose ordinates are additive components of the logarithms of the rate constants. When the reaction rate constants are put on an Arrhenius plot (logarithm of reaction rate vs. the reciprocal of the temperature), the fact that the tunneling factors become large at high (1/T) produces curvature on the Arrhenius plots. The curvature in the Arrhenius plots of experimental rates is usually interpreted as evidence of tunneling. The tunneling factors in Tables V, VI, and VII predict that such experimental evidence for tunneling will be most prominent for temperatures below room temperature.

The most important conclusions to be drawn from these tunneling calculations are the following.

1. The tunneling for the SSSMK barrier can be compared to the tunneling for Shavitt's Eckart approximation to it. Because the false bottom on his Eckart barrier (see figure in Sh 68a) makes it too wide at energies much below the highest part, Shavitt's method underestimates the tunneling at low temperature (as expected). However, evidently because its wrong behavior at large d is equivalent to allowing the particle to surmount a large fraction of the barrier with zero reflection, the Shavitt Eckart barrier overestimates the tunneling due to the SSSMK barrier over most of the experimentally

accessible energy range.

2. The standard Eckart barrier overestimates the tunneling as compared to the 1-MD treatment of the real barrier because it is too thin.

3. The tunneling predicted by the NSSSMK and SNSSMK barriers is very similar except at low temperatures. This is another indication of the accuracy of the Wall-Porter parametrized surface in representing the SSMK surface with the energy variation scaled down along the reaction coordinate. The difference between these two sets of tunneling factors at low temperature is due to the Wall-Porter barrier being much thinner near the bottom and thus allowing extra low energy tunneling. For example, at an incident energy of 0.212 eV, the transmission probability for the NSSSMK barrier is 8.0×10^{-5} whereas the transmission probability for the SNSSMK barrier is 2.9×10^{-5}. At lower energies the discrepancy is even greater.

4. The NSSSMK result must be considered the corrected version of Shavitt's model in which two aspects of the computations (the position of the minimum energy path and the evaluation of the transmission functions for the given barrier) are corrected. The NSSSMK tunneling factors are in good agreement with the Shavitt ones except at low temperatures where they are higher. Shavitt's results are in good agreement with experiment except at low temperatures ($T < 300^{o}$ K) where they are as much as 40% too low. Thus the NSSSMK results bring the theoretical and experimental results much closer together.

5. The tunneling factors computed in the vibrationally adiabatic approximations are much different from those computed in the

conservation-of-vibrational-energy approximations. The tunneling factors computed for the wider $V_q(s)$ barriers are much smaller than those computed from the $V(s)$ barriers--as expected. The transmission coefficient according to the VA treatment is sometimes less than 1.0 (i.e., there is more reflection above the barrier than transmission below the barrier for a system with a Boltzmann distribution of relative translational energies). This last fact is a surprising result. It is the first time tunneling factors less than 1.0 have ever been obtained.

6. The tunneling factors have generally been computed on the basis of linear collisions (see subsection IV. B.2). The VA model we used to compute the tunneling factors is the correct model to use with transition state theory for linear collisions (see Hi 39, Ma 65b, Ma 67, and subsection IV. B.3). Since the CVE results do not resemble the VA results, the usual treatment of tunneling appears to be theoretically unjustified and the significance in terms of molecular dynamics of any agreement of theory and experiment using the CVE models (such as point 4 above) is questionable. Including the adiabatic change in the rotational levels for three-dimensional collisions will make the VA barrier resemble the CVE barrier more closely again. However, the amount of agreement of the VA and CVE barriers will then depend on summation and cancellation of at least two factors and the interpretation will still not be straightforward.

The one dimensional calculations will be considered again in section C.

C. Exact Solution of the Linear Collision Problem for $H + H_2$ and $D + D_2$

1. Method

The methods available for solution of the Schroedinger equation for rearrangements have been reviewed in section I. B. The method we use is essentially the method of Diestler and McKoy (Di 68, Di 68b) which is discussed in section I. B and Appendix 3. This is called the finite difference boundary value method. The numerical method used in section IV. B. to solve scattering problems in one mathematical dimension is an application of this method. There are additional complications in applying it to the present problem in two mathematical dimensions.

In the case of collinear collisions $A + BC \rightarrow A + BC$ or $AB + C$, the method consists of the following steps:

i. Select a set of mesh points (each specified by R_{AB} and R_{BC}) which cover a region which includes the interaction region and also parts of both the asymptotic regions (one where R_i is large and one where R_f is large). The interaction region is the region where the potential energy differs from its form in either asymptotic region by an amount which is not negligible when compared with the total energy E or the barrier height. R_i, as defined in chapter I, is the distance from A to the center of mass BC, and R_f is the distance from C to the center of mass of AB.

ii. Use the finite differences method to obtain a number (TNSOL) of linearly independent solutions of the Schroedinger equation at these mesh points. The linearly independent solutions are obtained by specifying a set of linearly independent but otherwise formally

arbitrary boundary conditions in the asymptotic regions. These numerical solutions with arbitrary boundary conditions are called the χ's.

iii. Numerically analyze the solutions in each asymptotic region in terms of a product of an internal eigenfunction of the separated molecule and a travelling wave in the relative motion. The travelling wave has one of the forms $e^{\pm ip_i R_i}$ or a linear combination of both the $\pm$ pair or $e^{\pm i p_f R_f}$ or a linear combination of both of the $\pm$ pair where p_i (p_f) is the momentum in atomic units of relative motion in the i (f) channel.

iv. Based on the analysis of the χ's, take linear combinations of them to form as many scattering solutions as there are open channels. A scattering solution is one that has unit incoming flux in one open channel, no incoming flux in the other open channels, and no components that are increasing with increasing R_f in the closed channels.

v. Analyze the scattering solutions to see how much outgoing flux they have in each channel and from this compute the reaction probabilities.

vi. Repeat steps i through v at several values of the step size h and extrapolate to h = 0.

In the rest of this subsection we discuss the modifications and changes we made in the method of Diestler and McKoy. In subsection 2 we discuss the details of the calculations and present the results. A brief discussion of the results is presented in subsection 3.

The calculations were done using the method just the way it is given in Di 68 or Di 68b except for the following changes and modifications:

1. For the analysis of the χ's (step iii) Diestler and McKoy used the exact analytic solution for the vibrational potential well at R_i or $R_f = \infty$ or they used their best approximation to this exact solution. The integrals involving these functions were evaluated by Simpson's rule. When the exact solution is not available we preferred to use the numerical solution which is obtained with the same finite difference approximation and the same mesh as used for that solution for the χ's and to compute the integrals using the trapezoidal rule (see appendix 4 for further discussion of these numerical solutions). This analysis is more consistent with the particular approximate χ's used and should lead to better behavior of the extrapolation (step vi). Further, unless the functions used for analysis are equal to the exact functions in the limit $h = 0$, the solution will not converge to the exact solution.

2. Diestler and McKoy analyzed their solutions in the asymptotic region in terms of travelling waves. This is equivalent to analyzing the solutions for the approximate elements of the scattering matrix. We analyze our solutions in terms of standing waves. This procedure gives us approximate elements of the reactance matrix. We can compute the scattering matrix from the reactance matrix. The advantages of making approximations to the reactance matrix instead of to the scattering matrix have already been discussed in subsections I. A. 1 and II. A. 2. f. The relation between the scattering matrix and the reactance matrix is discussed in Mo 65, pp. 369-372.

According to the procedure of Diestler and McKoy the probability of reaction from the i state to the j state is expressed as

$$P_{ij} = \frac{k_j}{k_i} \left| \tau_{ji} \right|^2 \tag{49}$$

where

$$\underset{\sim}{\tau} = \underset{\sim}{\bar{A}}\,\underset{\sim}{C} = \underset{\sim}{\bar{A}}\,\underset{\sim}{A}^{-1}\,\underset{\sim}{I}^{D} \tag{50}$$

$$\underset{\sim}{I}^{D} = (\underset{\sim}{I}'\ \underset{\sim}{I}'') \ . \tag{51}$$

The matrices $\underset{\sim}{\bar{A}}$, $\underset{\sim}{C}$, $\underset{\sim}{A}$, and $\underset{\sim}{I}'$ are defined in Di 68 and Di 68b. $\underset{\sim}{C}$ is the coefficient matrix. Each column of $\underset{\sim}{C}$ corresponds to the coefficients of the χ's in one scattering solution of the Schroedinger equation. $\underset{\sim}{I}''$ is just like $\underset{\sim}{I}'$ except for dimensions. For the case where there are N open channels corresponding to A + BC and N' open channels for AB + C, the dimensions of these matrices are (the dimensions in the computer program which performs the analysis must be at least this big)

$\underset{\sim}{\bar{A}}$ is $(N + N') \times$ TNSOL (52)

$\underset{\sim}{A}$ is TNSOL $\times$ TNSOL (53)

$\underset{\sim}{I}'$ is TNSOL $\times$ N (54)

$\underset{\sim}{I}''$ is TNSOL $\times$ N' (55)

$\underset{\sim}{I}^{D}$ is TNSOL $\times$ $(N + N')$ (56)

$\underset{\sim}{C}$ is TNSOL $\times$ $(N + N')$ (57)

$\underset{\sim}{\tau}$ is $(N + N') \times (N + N')$. (58)

This procedure is exactly equivalent to expressing the probabilities in terms of elements of the scattering matrix by the following equations

$$P_{ij} = |S_{ji}|^2 \tag{59}$$

$$\underset{\sim}{S} = - \underset{\sim}{K}^{1/2} \underset{\sim}{\bar{A}} \underset{\sim}{A}^{-1} \underset{\sim}{I}^{D} \underset{\sim}{K}^{-1/2} \tag{60}$$

where $\underset{\sim}{K}$ is the wave number matrix defined by

$$K_{ij} = p_i \delta_{ij} \tag{61}$$

and

$$\underset{\sim}{K} \text{ is } (N + N') \times (N + N') . \tag{62}$$

$\underset{\sim}{S}$ is the scattering matrix and

$$\underset{\sim}{S} \text{ is } (N + N') \times (N + N') . \tag{63}$$

The analysis to obtain reactance matrix elements proceeds just like the analysis of Diestler and McKoy except that the asymptotic form of the χ's is expressed in the notation of Di 68b as

$$\chi_j = \sum_{\ell=1}^{N} \left\{ D_\ell^{(j)} \sin[k_\ell(\alpha x_{12} + x_{23})] + \bar{D}_\ell^{(j)} \cos[k_\ell(\alpha x_{12} + x_{23})] \right\} \varphi_\ell(x_{12})$$

$$+ \sum_{\ell>N} \left\{ B_\ell^{(j)} \exp[-k_\ell(\alpha x_{12} + x_{23})] + \bar{B}_\ell^{(j)} \exp[k_\ell(\alpha x_{12} + x_{23})] \right\} \varphi_\ell(x_{12})$$

$$x_{23} \geq x_{23}^{(0)}$$

$$\chi_j = \sum_{\ell=1}^{N'} \left\{ \delta_\ell^{(j)} \sin[k_\ell'(\beta x_{23} + x_{12})] + \bar{\delta}_\ell^{(j)} \exp[k_\ell'(\beta x_{23} + x_{12})] \right\} \bar{\varphi}_\ell(x_{23})$$

$$+ \sum_{\ell > N'} \left\{ \beta_\ell^{(j)} \exp[-k_\ell(\beta x_{23} + x_{12})] + \bar{\beta}_\ell^{(j)} \exp[k_\ell'(\beta x_{23} + x_{12})] \right\} \bar{\varphi}_\ell(x_{23})$$

$$x_{12} \geq x_{12}^{(0)} \qquad (64)$$

instead of as in eq. (18) of Di 68b. Then we define the matrices $\underset{\sim}{D}$ and $\underset{\sim}{\bar{D}}$ analogous to $\underset{\sim}{A}$ and $\underset{\sim}{\bar{A}}$ where

$$\underset{\sim}{\bar{D}} \text{ is } (N + N') \times \text{TNSOL} \qquad (65)$$

$$\underset{\sim}{D} \text{ is TNSOL} \times \text{TNSOL} . \qquad (66)$$

For example, for the symmetric case with $N = N'$ and $\text{TNSOL} = N + N' + 6$, they are given by

$$D_{ij} = \begin{cases} D_i^{(j)} & i = 1, \ldots, N \\ \bar{B}_i^{(j)} & i = N + 1, \ldots, N + 3 \\ \bar{\delta}_{i-N-3}^{(j)} & i = N + 4, \ldots, 2N + 3 \\ \beta_{i-N-3}^{(j)} & i = 2N + 4, \ldots, 2N + 6 \end{cases} \qquad (67)$$

$$\bar{D}_{ij} = \begin{cases} \bar{D}_i^{(j)} & i = 1, \ldots N \\ \delta_{i-N-3}^{(j)} & i = N + 1, \ldots, 2N . \end{cases} \qquad (68)$$

Then the reactance matrix is given by

$$\underset{\sim}{R} = \underset{\sim}{K}^{1/2} \underset{\sim}{\bar{D}} \underset{\sim}{D}^{-1} \underset{\sim}{I}^{D} \underset{\sim}{K}^{-1/2} \quad . \tag{69}$$

If the scattering matrix is now computed from the reactance matrix by eq. (I. 36) and the reaction probabilities are computed from the scattering matrix by eq. (59), the results will be exactly the same as for the analysis directly in terms of scattering matrix elements. The advantage of the present scheme is that if we symmetrize the $\underset{\sim}{R}$ matrix obtained from (69) the scattering matrix obtained from (I.36) will automatically be symmetric and unitary (see the discussions in chapters I and II). When we have obtained a very accurate numerical solution $\underset{\sim}{S}$ and $\underset{\sim}{R}$ are automatically symmetric to several significant figures and $\underset{\sim}{S}$ is automatically unitary to several significant figures. In less accurate calculations, these properties do not hold. However, we introduce a symmetrized reactance matrix $\underset{\sim}{R}^{S}$ defined by

$$R^{S}_{ij} = \frac{1}{2} (R_{ij} + R_{ji}) \tag{70}$$

The scattering matrix computed from

$$\underset{\sim}{S} = (\underset{\sim}{I} - i \underset{\sim}{R}^{S})^{-1} (\underset{\sim}{I} + i \underset{\sim}{R}^{S}) \tag{71}$$

is then unitary and symmetric. In a similar but less general numerical problem, Delves showed that the transformation (70) is a variationally improved estimate of the reactance matrix

(De 61, the variational principle is discussed in De 62).* We find in practice that, for a given step size, the unitarized result is more accurate than the result calculated by the method of Diestler and McKoy. This does not mean the results obtained using the reactance matrix analysis with symmetrization are necessarily more accurate than those from the scattering matrix analysis for all possible cases. But the reactance matrix analysis with symmetrization is the most convenient way to achieve the desirable property of having all the results satisfy detailed balance and conservation of particle flux.

Finally we consider the method of extrapolation. Diestler and McKoy said that they performed extrapolation to $h = 0$ by fitting their probabilities $P(h)$ computed at different step sizes h to the series

$$P(h) = \sum_{i=1}^{NEX} P_{i-1} h^{i-1} . \qquad (72)$$

It is well known that the local truncation error due to using second central differences (the procedure used here) to approximate elliptic differential operators of the form which occur in the Schroedinger equation for our problem can be expressed as a power series in h which includes only even powers of h. Thus it is possible that the error can be expressed by the series

---

* The author is grateful to Dr. Delves for correspondence concerning his result.

$$P(h) = \sum_{i=1}^{\infty} P_{i-1} h^{2(i-1)} \tag{73}$$

and that we should perform extrapolations to $h = 0$ by using

$$P(h) = \sum_{i=1}^{NEX} P_{i-1} h^{2(i-1)} \quad . \tag{74}$$

We performed extrapolations using eqs. (72) and (74) and found that the extrapolated results obtained using different step sizes and different numbers of step sizes were much more accurate when we used eq. (74). We believe the use of eq. (72) may lead to spurious results except perhaps if NEX is very large. We used eq. (74) to extrapolate to $h = 0$ for all the results reported here. We found that the error component which is proportional to h^2 was almost always the biggest component. So, for example, extrapolations assuming the error had components proportional to h^2, h^3, ... led to results very similar to those which assumed the error components were proportional to h^2, h^4, ... Use of eq. (74) with NEX = 2 is called Richardson's h^2-extrapolation. Use of eq. (74) with NEX = 4 is called Richardson's h^4-extrapolation (see, e.g., Ko 61).

2. Calculations and Results

A number of choices of variables in the numerical method must be made in order to perform numerical calculations. The variables permitted by the numerical method are:

(a) the shape and location of the region over which the mesh is placed;

(b) the number of linearly independent χ's to be obtained and what boundary conditions each χ should satisfy;

(c) the values of R_i and R_f at which the analyses of the χ's are performed;

(d) the number of vibrator functions used to analyze the χ's;

(e) the number of mesh points.

We will now discuss how these choices were made for our calculations on the symmetric cases $H + H_2$ and $D + D_2$ and what values we used for the variables. Our guiding principle was to obtain an accuracy of 1% in the computed scattering probabilities.

(a.) The mesh must cover the classically accessible parts of the interaction region and the near-asymptotic region* and extend far enough into the classically inaccessible region so that it is not too bad an approximation to neglect the tail of the wave function outside the region of the mesh. Diestler and McKoy suggested using a block-L shaped region (in R_{AB}, R_{BC} space) which covers the valley of the reaction path on the potential energy surface and which extends to $R_{AB} = R_{BC} = 0$. A block-L shaped region contains an interior angle greater than 90° and the finite difference treatment of such regions is sometimes inaccurate. We might

---

* The near-asymptotic region is that part of the asymptotic region within about 4-10 step sizes of the interaction region.

expect that this angle is not a serious problem in the present case because the potential surface is high near the position of this angle and the wave function is small there. We verified this numerically by comparing solutions obtained with a block-L shaped region to solutions obtained with a square region obtained by placing mesh points in the upper right corner of the block L. The restriction that the mesh points extend to the origin in the (R_{AB}, R_{BC}) plane was removed and the results were found to be insensitive to changing the small-R boundaries of the grid when they are placed far enough into the classically forbidden region. We also found that extending the arms of the L far into the asymptotic region did not give worthwhile improvement of the results. We finally settled on using a square region for which the boundary values on the wave function are given along the four lines $R_{AB} = 0.3a_o$, $R_{BC} = 0.3a_o$, $R_{AB} = 4.2a_o$, and $R_{BC} = 4.2a_o$. This region was used for all the production runs reported here.

(b.) We obtained NSOL linearly independent χ's with the boundary condition that χ be equal at the $R_{AB} = 4.2a_o$ edge of the mesh region in the A + BC asymptotic region to one of NSOL linearly independent functions and that it be equal to 0 at the other three edges of the mesh region. The NSOL edge functions were taken to be the lowest NSOL eigenfunctions of the BC vibrator. We obtained NSOL more linearly independent χ's by reflection of the first group through the line $R_{AB} = R_{BC}$. This is the same scheme as used by Diestler and McKoy (Di 68, Di 68b). With this scheme we found that accurate results could be obtained in all cases considered by letting NSOL = NOPEN(1) + 3 where NOPEN(1) is the number of open channels for A + BC. Using this many χ's

provided a basis set that was more than good enough since essentially the same results were obtained using NSOL = NOPEN(1) + n for $2 \leq n \leq 5$. We used $n = 3$ for general production runs to be safe from error.

(c.) The analysis of a χ_j is done on two lines across the mesh region at large R_f and on two other lines across the mesh region at large R_i. At each large R edge, we used all six pairs of two lines chosen from among the last four lines of mesh points at that edge. The six analyses should all give the same probabilities if the calculation is accurate. Their deviations from one another are an internal indication of the accuracy of a calculation. We used as the result of a calculation the average of the probabilities determined by the six analyses. The values of the probabilities computed from any one pair of lines usually differed from the average by less than 1%.

(d.) The number of vibrator functions used to analyze the χ's was NSOL + INS where $1 \leq INS \leq 3$. If NSOL is too small, using different values of INS will give different results. We found that the probabilities were almost independent of INS for the values of NSOL and INS we used.

(e.) Once the mesh region is decided upon, the number of mesh points NN determines the step size h. We used square grids with MDM points across the grid. Then $NN = (MDM)^2$ and $h = (3.9a_o)/(MDM + 1)$. Although we could work in the step size region where scattering probabilities at different step sizes agree within 1% with each other, we found by using h^2-extrapolation that these probabilities at even small step sizes were not that accurate. However, we found that extrapolated scattering proba-

bilities which were not as expensive to compute as probabilities from one very large grid were very accurate and were more accurate than those obtained using the largest number of mesh points we could use. The largest number of mesh points we used was 5625 (corresponding to MDM = 75). This is close to the largest size grid we could possibly have run on the IBM 360/75. We determined which step sizes to use for the production runs by first running many step sizes at selected energies in the energy range of the production run. The accuracy of the extrapolated results was ascertained by noting the consistency of results extrapolated from different numbers of runs and from runs with different values of MDM. From the well-studied selected energies we could choose subsets of 2 or 3 values of MDM which seemed reasonably sure to yield accurate extrapolated values at other nearby energies.

We made production runs on $H + H_2$ at energies below that necessary to excite the $v = 1$ vibrational level. For these runs, we made two calculations at each energy and calculated the results by h^2-extrapolation. The grid sizes were MDM = 34 and 49. The compute time* for these two runs was about 3.1 min. The final results of each run are P_{11}^R, the probability of reaction, and P_{11}^V, the probability of reflection. These are given in Figs. 6-9 and in Table IX. We also made production runs on $D + D_2$ at energies below that necessary to excite the $v = 1$ vibrational level. For these runs we followed the same procedure as for $H + H_2$ except we used MDM = 40 and 55. This required 5.3 min. compute time per energy. The results are given in Fig. 10 and in Table X.

---

* All compute times are for the GO step as executed on the IBM 360/75.

We made production runs on $H + H_2$ for energies between the first two vibrational excitation thresholds, i.e., for NOPEN(1) = 2. For these runs we did calculations at three values of MDM (45, 55, and 65) and used eq. (74) with NEX = 3 for extrapolation. These three runs required 13.1 min. compute time per energy. The final results of each run are the probabilities for the system initially in the ground vibrational level to react to give ground state (P_{11}^R) or vibrationally excited (P_{12}^R) product, to scatter with vibrational excitation but no reaction (P_{12}^V), or only to collide elastically (P_{11}^V) and the probabilities of the system initially vibrationally excited to react to give ground state (P_{21}^R) or vibrationally excited product (P_{22}^R), to scatter with vibrational de-excitation but no reaction (P_{21}^V), or only to collide elastically (P_{22}^V). These results are given in Figs. 7-9 and 11-12.

We also numerically computed the vibrational energy levels for the Morse potential which is the separated subsystem limit of the Wall-Porter parametrized potential surface. These calculations were done for the same step sizes used for the scattering calculations and extrapolated the same way the scattering calculations were done (the calculations are described in Appendix 4). These eigenvalues should be used to interpret Figs. 6-11. The resulting zero point energies are 0.2728 eV (H_2) and 0.1938 eV (D_2). The vibrational energies of the first excited vibrational levels are 0.7940 eV (H_2) and 0.5692 eV (D_2). The vibrational energy of the $v = 2$ state of H_2 is 1.2830 eV.

3. Discussion

The reaction probability for energies below the first threshold has the qualitative behavior we expected, i.e., it is a steeply rising function of energy (see Figs. 6-9 and 10). Fig. 9 shows that the results of the 1-MD calculation using the vibrationally adiabatic potential barrier are in qualitative agreement with the 2-MD calculations whereas the calculations using the classical barrier (i.e., the conservation-of-vibrational-energy barrier) are in poor agreement with the 2-MD probabilities. The difference between the two 1-MD treatments is that the vibrationally adiabatic one allows for adiabatic release of the diatomic reagent's vibrational energy into kinetic energy of motion along the reaction coordinate and so it lowers the effective barrier to reaction. Despite the good agreement between the vibrationally adiabatic 1-MD treatment and the 2-MD calculation, there are quantitative discrepancies at low translational energies which mean that the amount of tunneling predicted to occur for a room temperature or lower temperature distribution of relative translational energies could be quite different. Table IX shows that the vibrationally adiabatic 1-MD treatment could predict tunneling factors too low by an order of magnitude and the conservation-of-vibrational-energy 1-MD treatment is even worse. Fig. 10 shows that the conservation-of-vibrational-energy 1-MD calculations are very bad for $D + D_2$ also. These comparisons mean that tunneling factors computed from simple models must be used with extreme caution.

If the H_3 system had zero energy in motion of either the symmetric stretching mode or the reaction coordinate mode, its energy would be 0.424 eV. An $H + H_2$ system with a relative

translational energy of 0.151 eV has a total energy of 0.424 eV. Any reaction at translational energies lower than 0.151 eV is strictly classically forbidden if the reagent has the zero point vibrational energy before the reaction and can be called tunneling in even the strictest interpretation of the term. Table IX shows that this type of tunneling does occur to an important extent.

Figs. 7 and 11 show that the reaction probabilities are predicted to be appreciable in every channel at energies much above the first vibrational excitation threshold. In fact the probabilities show a striking resemblance to those which would be predicted by a statistical phase space theory treatment of $H + H_2$ collisions in 1 physical dimension (the statistical phase space theory is discussed in chapter III). Such a treatment predicts all the probabilities in the energy range between the first two thresholds are 1/4. Yet the oscillations of the probabilities about their mean values (such as the dip in P_{11}^R at a translational energy of 0.63 eV) are not random. Further study of the calculations (such as plotting the scattering wave functions at various energies or comparing the reaction probabilities here with classical mechanical calculations for linear collisions on the same potential energy surface) may reveal a detailed mechanistic interpretation of the maxima and minima in the scattering probability curves. Any such interpretation will have to take into account the competition between all the channels.

It is interesting that in the region between the thresholds $P_{11}^R > P_{12}^R$ and $P_{22}^R > P_{21}^R$, i.e., the reaction probability is greater for the reactive channel in which the vibrational quantum number is conserved than for the channel in which it is changed. Thus even at these higher energies the vibrationally adiabatic model has some merit (the vibrationally adiabatic model predicts the

vibrational quantum number is 100% conserved, i.e., that $P^R_{12} + P^V_{12} = 0$ and $P^R_{21} + P^V_{21} = 0$).

Figs. 11 and 12 show that the probabilities of de-excitation or reaction of vibrationally excited molecules do not rise rapidly from threshold. This is an indication of the difficulty of converting the initial vibrational excitation energy into energy of other modes of motion. Thus at energies up to 0.09 eV above threshold, most of the vibrationally excited molecules simply undergo elastic collisions.

The importance of the energy of the internal degrees of freedom of the reactants for overcoming the barrier to reaction has been discussed recently for the reactions $H_2 + H_2$ and isotopic analogues (Ba 66, Mo 67a, Le 68e) and HI + DI (Ja 69) and for other reactions. In the present case the vibrationally excited H_2 has an energy of 0.794 eV plus its translational energy. The classical barrier height is 0.424 eV. The energy of H_3 at the transition state with zero point energy in the symmetric stretching mode is 0.55 eV plus the kinetic energy of motion along the reaction coordinate.* If the H_3 system has one quantum of vibrational excitation in the symmetric stretching mode at the transition state, its energy is about 0.79 eV plus the kinetic energy of motion along the reaction coordinate. Thus if the vibrational quantum number is conserved so that the effective potential barrier for one-dimensional motion along the reaction coordinate is the quantum mechanically vibrationally adiabatic one, a classical mechanical treatment of that motion predicts a threshold energy near zero. This may explain

---

* In this discussion, remember that the levels are quantized at the transition state only in the approximation of separability of the coordinates. H_3 at the transition state is a short-lived metastable species.

why the reaction probability for vibrationally excited species neither rises very fast from threshold nor has such a large delayed onset for appreciable reaction as the $H + H_2$ reaction (where Fig. 8 shows there is such an onset for a relative translational energy of over 0.20 eV).

It is interesting to make a comparison between the results of our studies of hydrogen atom scattering and electron scattering from the hydrogen molecule. In general we expect a mode of internal motion of the target to adjust adiabaticity to the presence of the incident particle if the mode's characteristic velocity of motion (which determines its relaxation rate) is very large compared to the velocity of the particle. In hydrogen atom scattering the velocities of the electrons are so much greater than the velocities of the protons that electronic adiabaticity is certainly a good approximation (see Appendix 1). But the velocity of internuclear motion in the hydrogen molecule is only about the same as, not an order of magnitude larger than, the relative velocity of the incident hydrogen atom. Yet the calculations show that vibrational adiabaticity is a good approximation. For the scattering of electrons in the intermediate energy range, the velocities of the bound electrons in the target are only about the same as, not an order of magnitude larger than, the relative velocity of the incident electron with respect to the target. But the calculations show that adiabatic polarization of the target by the scattering particle is again a good approximation. At higher initial translational energies the breakdown of the adiabatic approximation is more apparent in both these last two cases (see part two for electron impact energies over 100 eV and notice that $P_{12}^{R} + P_{12}^{V} \neq 0$ in Fig. 7 in this section). The internuclear motion of the H_2 molecule during electron impact

is not at all adiabatic and is well represented by unperturbed vibrational functions. Since the internuclear velocity is much slower than the impinging electron's velocity, this is not unexpected.

The calculations presented in this chapter are the first step in our attempt to understand the $H + H_2$ chemical dynamics. The calculations will be interpreted more fully in future publications. In addition we will report more reaction probability results for collinear collisions for the $H + H_2$ system and its isotopic analogues.

TABLE I

Points on the minimum energy path for the $H + H_2$ reaction. Distances are in atomic units.

SSMK surface		scaled SSMK surface	
R_{AB}	R_{BC}[a]	R_{AB}	R_{BC}[b]
1.765	1.765	1.765	1.765
1.880	1.679	1.784	1.745
1.945	1.640	1.808	1.720
2.020	1.609	1.867	1.671
2.105	1.582	1.925	1.623
2.198	1.559	2.045	1.555
2.300	1.539	2.111	1.525
2.414	1.522	2.162	1.505
2.553	1.507	2.235	1.483
2.694	1.493	2.299	1.467
2.838	1.481	2.409	1.448
2.984	1.470	2.479	1.439
3.192	1.457	2.547	1.432
3.407	1.445	2.614	1.426
3.638	1.435	2.681	1.421
3.872	1.427	2.744	1.417
4.150	1.419	2.822	1.414
4.331	1.412	2.900	1.411
		2.965	1.409
		3.031	1.407
		3.093	1.406
		3.153	1.405
		3.212	1.404
		3.300	1.403
		3.518	1.402
		3.582	1.401

[a] Sh 68, Sh 68a.

[b] Present.

TABLE II

Potential energy barriers from the SSMK surface as a function of distance from the saddle point. The barriers have been scaled by 0.89.

d (a_o)	V^a (eV)	$V_{fit}{}^b$ (eV)	d (a_o)	V^c (eV)	$V_{fit}{}^d$ (eV)
0.000	0.424	0.424	0.000	0.424	0.424
0.104	0.417	0.419	0.044	0.422	0.423
0.160	0.407	0.411	0.099	0.417	0.418
0.226	0.393	0.399	0.152	0.408	0.410
0.301	0.375	0.381	0.257	0.383	0.387
0.385	0.353	0.357	0.314	0.367	0.371
0.478	0.327	0.329	0.358	0.355	0.358
0.585	0.297	0.296	0.424	0.336	0.337
0.717	0.261	0.257	0.482	0.319	0.319
0.852	0.225	0.221	0.583	0.289	0.287
0.990	0.191	0.188	0.649	0.270	0.267
1.131	0.159	0.158	0.714	0.252	0.249
1.332	0.120	0.122	0.843	0.217	0.215
1.542	0.087	0.090	0.904	0.202	0.201
1.768	0.061	0.063	1.056	0.167	0.168
1.998	0.041	0.042	1.186	0.141	0.142
2.274	0.024	0.024	1.306	0.120	0.121
2.500	0.019	0.014	1.424	0.101	0.102
			1.546	0.085	0.085
			1.606	0.078	0.077
			1.671	0.070	0.068

[a] Sh 68a, Sh 68b.

[b] $b_1 = 0.0850$ eV, $b_2 = 0.2520$ eV, $b_3 = 0.25602$, $b_4 = 0.89044$.

[c] Present.

[d] $b_1 = 0.1129$ eV, $b_2 = 0.2294$ eV, $b_3 = 0.30855$, $b_4 = 1.11123$.

TABLE III

Potential energy barrier from the scaled SSMK surface as a function of the distance from the saddle point. The scaled SSMK surface is the parametrized potential energy surface of Wall and Porter with the parameters selected as described in section III. A.

d (a_o)	V (eV)	V_{fit}[a] (eV)
0.000	0.424	0.424
0.043	0.423	0.423
0.098	0.417	0.417
0.151	0.408	0.408
0.256	0.382	0.382
0.312	0.366	0.365
0.358	0.351	0.350
0.421	0.330	0.329
0.479	0.309	0.309
0.581	0.272	0.272
0.644	0.248	0.251
0.706	0.224	0.226
0.832	0.176	0.177
0.894	0.153	0.153
1.046	0.100	0.101
1.175	0.061	0.059
1.299	0.032	0.033
1.418	0.014	0.018
1.542	0.004	0.009
1.603	0.002	0.006
1.668	0.0003	0.004

[a] $b_1 = 0.2691$ eV, $b_2 = 0.0$, $b_3 = 1.01006$, $b_4 = 1.16372$. This barrier could be represented accurately enough by a fit with only 3 parameters.

TABLE IV

Quantum barriers as functions of the distance from the saddle point.

d (a_o)	V_q[a] (eV)	$V_{q,fit}$[b] (eV)	d (a_o)	V_q[c] (eV)	$V_{q,fit}$[d] (eV)
0.000	.277	.277	0.000	.277	.277
0.044	.278	.277	0.043	.277	.277
0.099	.277	.277	0.098	.276	.277
0.152	.279	.276	0.151	.277	.277
0.257	.277	.273	0.256	.275	.276
0.314	.276	.270	0.312	.275	.275
0.358	.276	.268	0.358	.276	.273
0.424	.270	.263	0.421	.272	.269
0.481	.263	.258	0.479	.267	.264
0.583	.247	.247	0.581	.249	.250
0.649	.235	.237	0.644	.235	.237
0.714	.223	.227	0.706	.219	.221
0.778	.210	.215	0.770	.200	.202
0.843	.198	.202	0.832	.180	.180
0.904	.186	.189	0.894	.159	.158
1.056	.157	.156	1.046	.105	.101
1.186	.134	.131	1.115	.061	.058
1.306	.115	.112	1.299	.027	.028
1.424	.098	.097	1.418	.007	.009
1.484	.090	.090	1.481	.001	.002
1.546	.083	.084	1.542	-.002	-.003
1.606	.076	.079	1.603	-.002	-.007
1.671	.072	.074	1.668	-.001	-.010

[a] The sum of the scaled V(d) and the ZPE(d) from the SSMK surface.

[b] $b_1 = 0.1099$ eV, $b_2 = 0.1050$ eV, $b_3 = 0.952810$, $b_4 = 0.178496$, $B^1 = 0.2772$ eV.

[c] The sum of the V(d) and the ZPE(d) from our scaled SSMK surface.

[d] $b_1 = 0.2982$ eV, $b_2 = -0.0224$ eV, $b_3 = 0.941853$, $b_4 = 0.116551$, $B^1 = 0.2772$ eV.

TABLE V

Transmission coefficients for $H + H_2$ reaction computed for four barriers discussed in section IV. B.

T(^{o}K)	Eckart[b]	SSSMK[a]	SNSSMK[a]	NSSSMK[a]
150	502.30			
200	45.00	57.39	83.48	307.32
250	13.13	11.25	14.74	24.10
300	6.49	5.09	6.21	7.95
350	4.17	3.26	3.80	4.44
400	3.11	2.47	2.79	3.12
450	2.53	2.05	2.26	2.48
500	2.17	1.80	1.95	2.11
550	1.93	1.63	1.75	1.87
600	1.77	1.52	1.61	1.71
650	1.65	1.43	1.51	1.59
700	1.56	1.37	1.44	1.50
750	1.48	1.32	1.38	1.43
800	1.43	1.28	1.33	1.38
850	1.38	1.25	1.29	1.34
900	1.34	1.22	1.26	1.30
950	1.31	1.20	1.23	1.27
1000	1.28	1.18	1.21	1.25
1050	1.26	1.16	1.19	1.23
1100	1.24	1.15	1.18	1.21
1150	1.22	1.14	1.16	1.19
1200	1.21	1.13	1.15	1.18
1250	1.19	1.12	1.14	1.17

[a] See text and Table VIII.

[b] $V_c = 0.174$ eV.

TABLE VI

Transmission coefficients for $D + D_2$ reaction computed for four barriers discussed in section IV. B.

T(^{o}K)	Eckart[b]	SSSMK[c]	SNSSMK[c]	NSSSMK[c]	Eckart[a]
150	61.17	60.74	104.91	380.80	
200	10.24	6.91	9.90	14.39	24.45
250	4.52	3.15	4.01	4.89	6.09
300	2.91	2.17	2.58	2.95	3.26
350	2.23	1.75	2.00	2.21	2.33
400	1.88	1.54	1.70	1.85	1.90
450	1.66	1.41	1.53	1.63	1.65
500	1.53	1.32	1.42	1.50	1.50
550	1.43	1.26	1.34	1.40	1.40
600	1.36	1.22	1.28	1.33	1.33
650	1.31	1.18	1.24	1.28	1.28
700	1.27	1.16	1.21	1.24	1.24
750	1.23	1.14	1.18	1.21	1.21
800	1.21	1.12	1.16	1.19	1.18
850	1.19	1.11	1.14	1.17	1.16
900	1.17	1.10	1.13	1.15	1.14
950	1.15	1.09	1.11	1.14	1.13
1000	1.14	1.08	1.10	1.12	1.12
1050	1.13	1.07	1.10	1.11	1.11
1100	1.12	1.07	1.09	1.11	1.10
1150	1.11	1.06	1.08	1.10	1.09
1200	1.10	1.06	1.08	1.09	1.08
1250	1.10	1.05	1.07	1.08	1.08

[a] $V_c = 0.424$ eV.

[b] $V_c = 0.174$ eV.

[c] See text and Table VIII.

TABLE VII

Transmission coefficients for $H + H_2$ reaction computed for three barriers discussed in section IV. B.

T(^{o}K)	Eckart[a]	MSSSMK[b]	SMSSMK[b]
150		4.63	18.53
200	666.25	1.80	1.72
250	44.10	1.35	1.12
300	11.59	1.19	0.98
350	5.61	1.11	0.94
400	3.63	1.07	0.92
450	2.74	1.04	0.91
500	2.25	1.03	0.90
550	1.96	1.01	0.90
600	1.76	1.01	0.90
650	1.62	1.00	0.91
700	1.52	1.00	0.91
750	1.44	0.99	0.91
800	1.39	0.99	0.91
850	1.34	0.99	0.92
900	1.30	0.99	0.92
950	1.27	0.99	0.92
1000	1.24	0.99	0.93
1050	1.22	0.99	0.93
1100	1.20	0.99	0.93
1150	1.18	0.99	0.93
1200	1.17	0.99	0.93
1250	1.15	0.99	0.94

[a] $V_c = 0.424$ eV.

[b] See text and Table VIII.

TABLE VIII

Labels for barriers for $H + H_2$ reaction and $D + D_2$ reaction

SNSSMK	The barrier is computed from the SSMK surface using the correct minimum energy path for this surface in normal coordinate space. Then every point on the barrier is multiplied by 0.89.
NSSSMK	The barrier is computed from the Wall-Porter parametrized surface using the correct minimum energy path for this surface in normal coordinate space. This surface is a fit to the scaled SSMK surface suggested by Shavitt.
SMSSMK	The local zero point energy of the t mode as computed from the SSMK surface is added to the SNSSMK barrier.
MSSSMK	The local zero point energy of the t mode as computed from the Wall-Porter parametrized surface is added to the NSSSMK barrier.

TABLE IX

Low energy transmission probabilities for the collinear $H + H_2$ reaction on the scaled SSMK potential energy surface as computed exactly (2-MD) and by two approximate methods (1-MD) discussed in section IV.B.

2-MD		1-MD			
		VA		CVE	
E_o (eV)	T	E_o (eV)	T	E_o (eV)	T
0.0809	2.79(-5)	0.0798	2.79(-7)	.0706	2.12(-8)
0.1174	1.77(-4)	0.0987	1.11(-6)	.0951	1.04(-7)
0.1572	1.49(-3)	0.1184	3.87(-6)	.1221	5.34(-7)
0.1980	1.49(-2)	0.1386	1.61(-5)	.1510	2.85(-6)
0.2170	4.44(-2)	0.1588	5.77(-5)	.1812	1.53(-5)
0.2361	1.29(-1)	0.1785	2.46(-4)	.2121	8.03(-5)
0.2448	2.02(-1)	0.1974	7.99(-4)	.2430	4.00(-4)
0.2510	2.74(-1)	0.2151	2.57(-3)	.2732	1.84(-3)
0.2578	3.69(-1)	0.2311	9.03(-3)	.3021	7.48(-3)
0.2647	4.78(-1)	0.2451	2.46(-2)	.3291	2.61(-2)
0.2682	5.24(-1)	0.2661	1.10(-1)	.3536	7.45(-2)

The number in parentheses is the power of 10 by which the preceding number should be multiplied.

TABLE X

Low energy transmission probabilities for the collision $D + D_2$ on the scaled SSMK potential energy surface computed numerically.

E_o (eV)	T
0.1327	2.60(-7)
0.1599	2.12(-5)
0.1964	1.70(-5)
0.2143	2.47(-4)
0.2361	9.03(-4)

The number in parentheses is the power of 10 by which the preceding number should be multiplied.

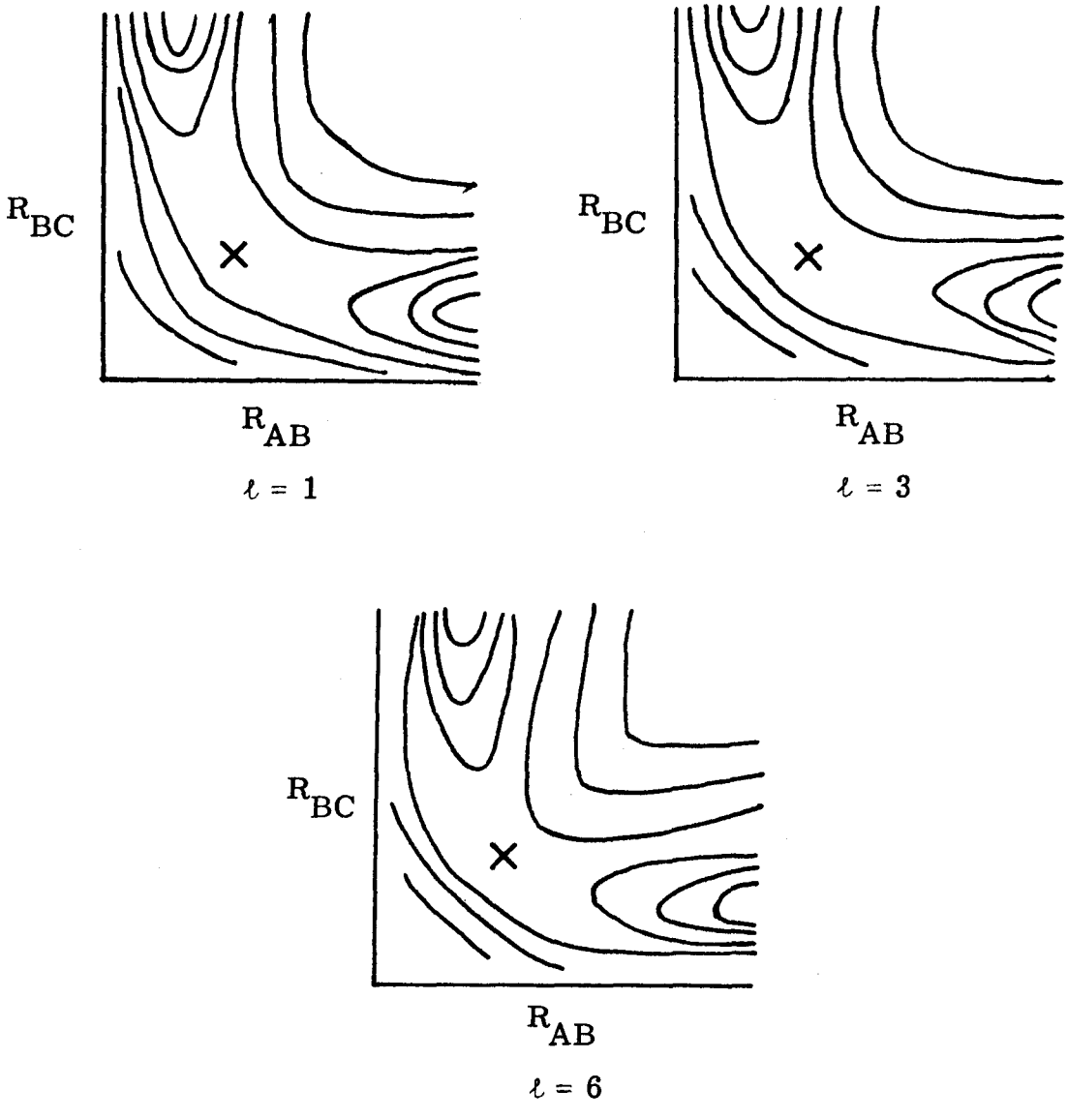

Fig. 1. Wall-Porter-type H_3 potential energy surfaces for various choices of parameter ℓ.

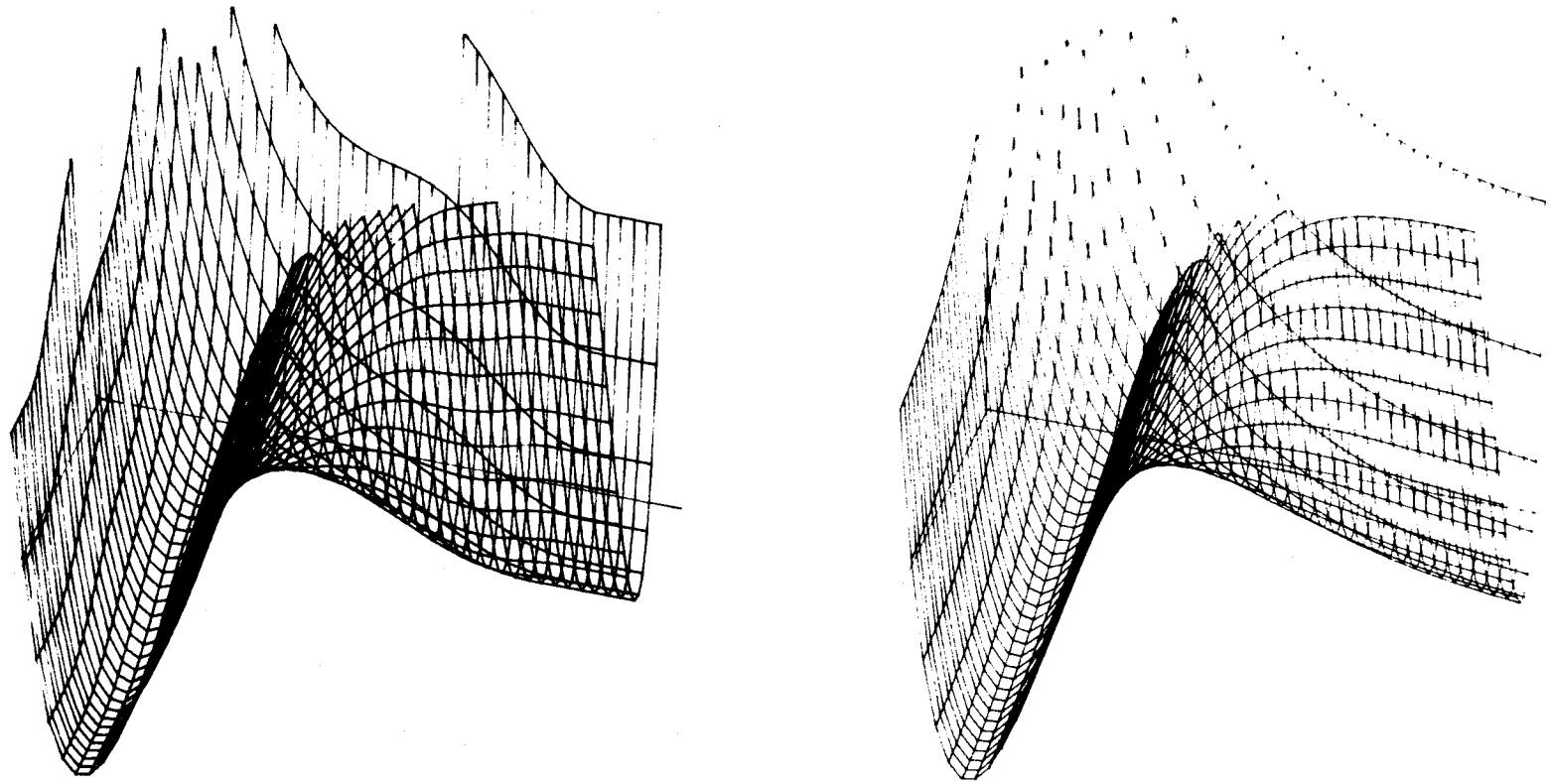

FIG. 2a. Three-dimensional projection views (viewing angles: $\theta = 53°$, $\phi = 16°$) of: left--scaled Wall-Porter type H_3 surface ($\ell = 3$); right--Shavitt-Stevens-Minn-Karplus H_3 surface.

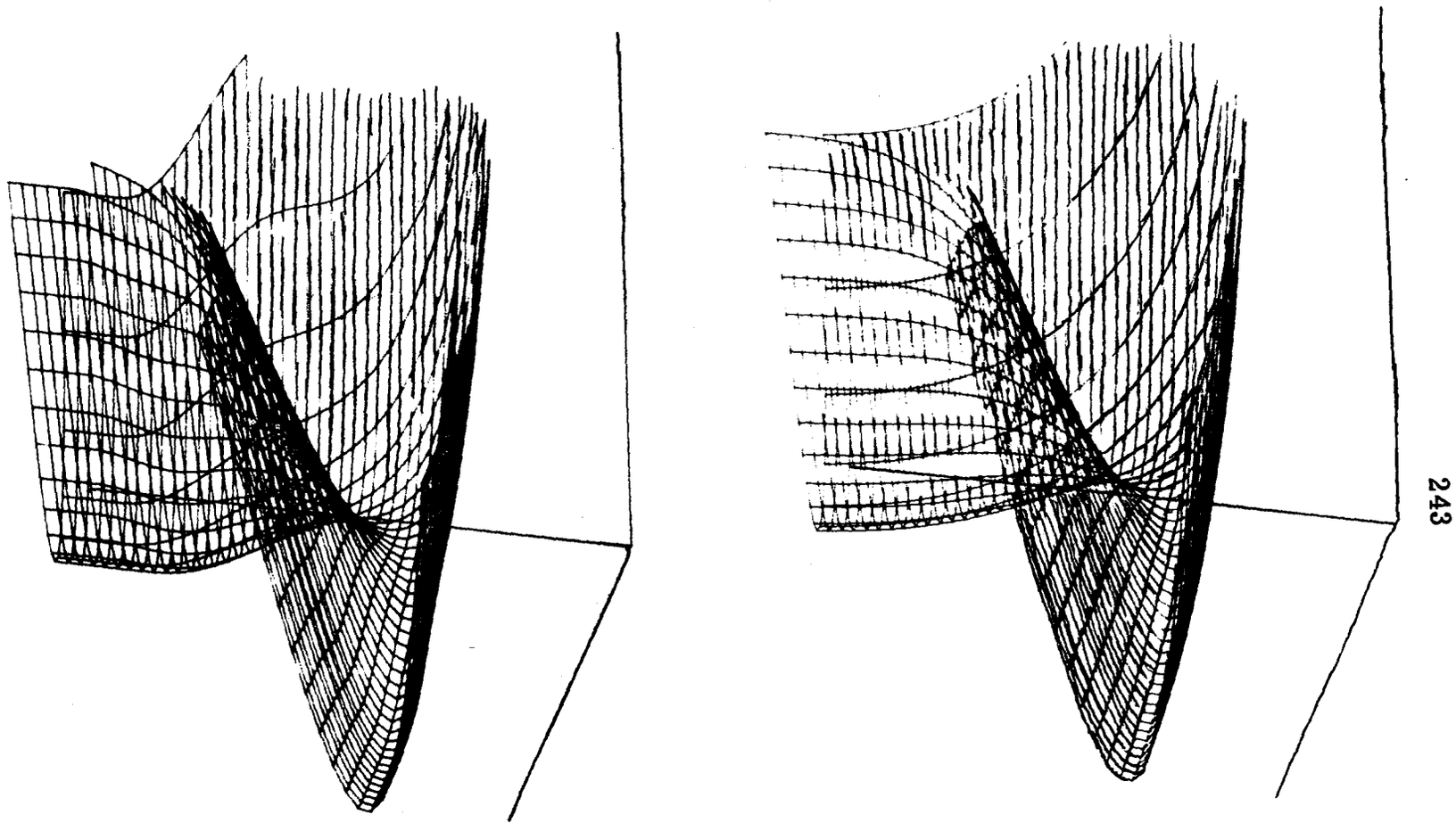

FIG. 2b. Same as Fig. 2a but $\theta = 60^\circ$, $\phi = 104^\circ$.

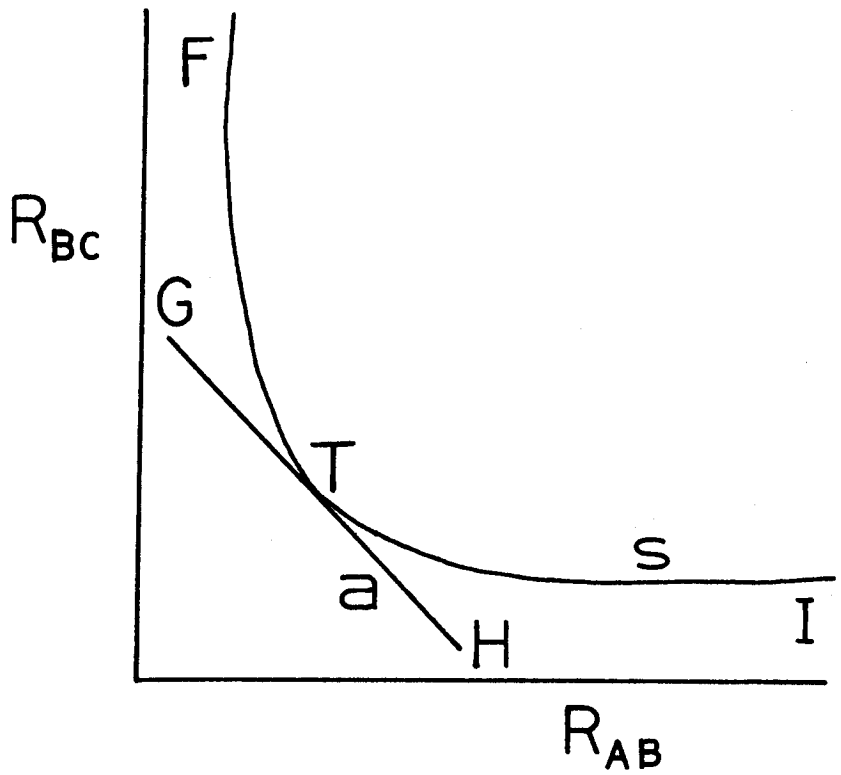

FIG. 3. Two dimensional orthogonal coordinate system for the reaction A + BC → AB + C. The path s from I to F is the path of minimum potential energy. T is the transition state. The path a from H to G corresponds to the asymmetric stretch normal mode of the transition state and is tangential to the reaction path s at the saddle point T.

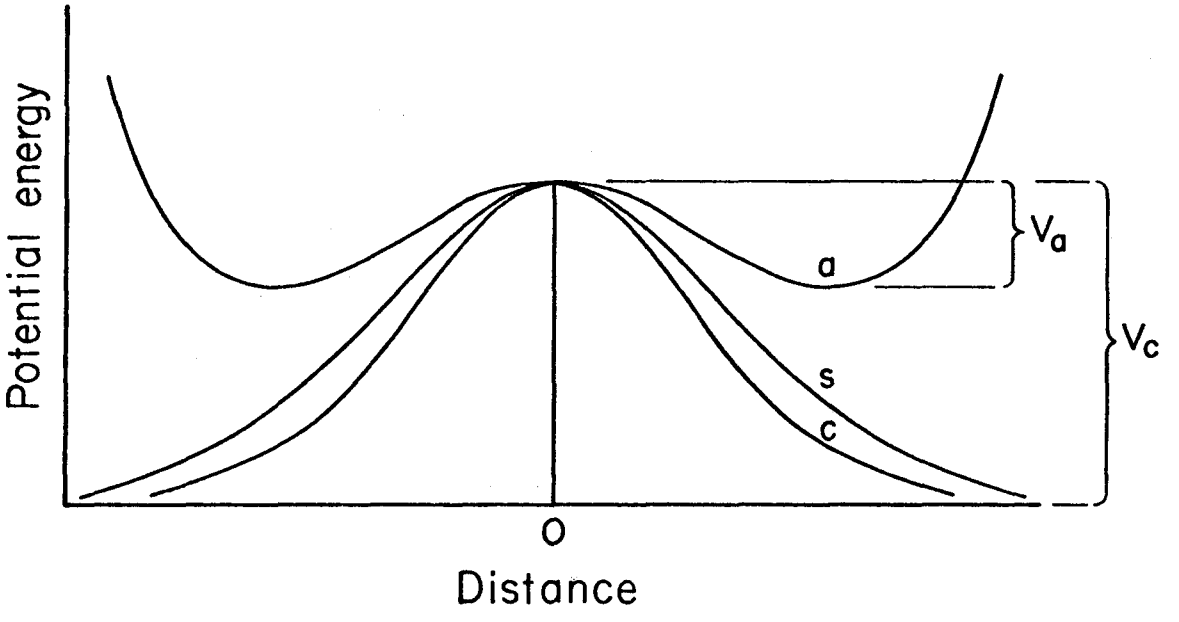

FIG. 4. Barrier along various paths through the potential energy surface. Paths a and s are shown in figure 3. Path c is the path of minimum potential energy in a skewed coordinate system in which the cross term in the kinetic energy vanishes and the reduced mass is the same for motion in all directions (Jo 66a, pp. 336f).

Fig. 5. Potential energy barriers for the collinear $H + H_2$ reaction as described in the text as a function of distance (in the normal coordinate space) from the saddle point of the surface. The barriers are symmetrical so only one half of each barrier is shown. The V barrier is the classical conservation-of-vibrational-energy barrier. The V_q barrier is the quantum mechanical one assuming vibrational adiabaticity. 1 eV = 23.069 kcal/mole.

Fig. 6. Probability of reaction as a function of translational energy for the collinear $H + H_2$ reaction (2-MD calculation).

Fig. 7. Probabilities of reaction and vibrational excitation for the collinear $H + H_2$ system as functions of total energy of the system. The H_2 is initially in the vibrational ground state. The "T" along the abscissa indicates the threshold for vibrational excitation.

Fig. 8. Scattering probabilities for the collinear $H + H_2$ reaction as functions of initial relative translational energy. The H_2 is initially in its ground vibrational state. The "T" along the abscissa indicates the threshold for vibrational excitation.

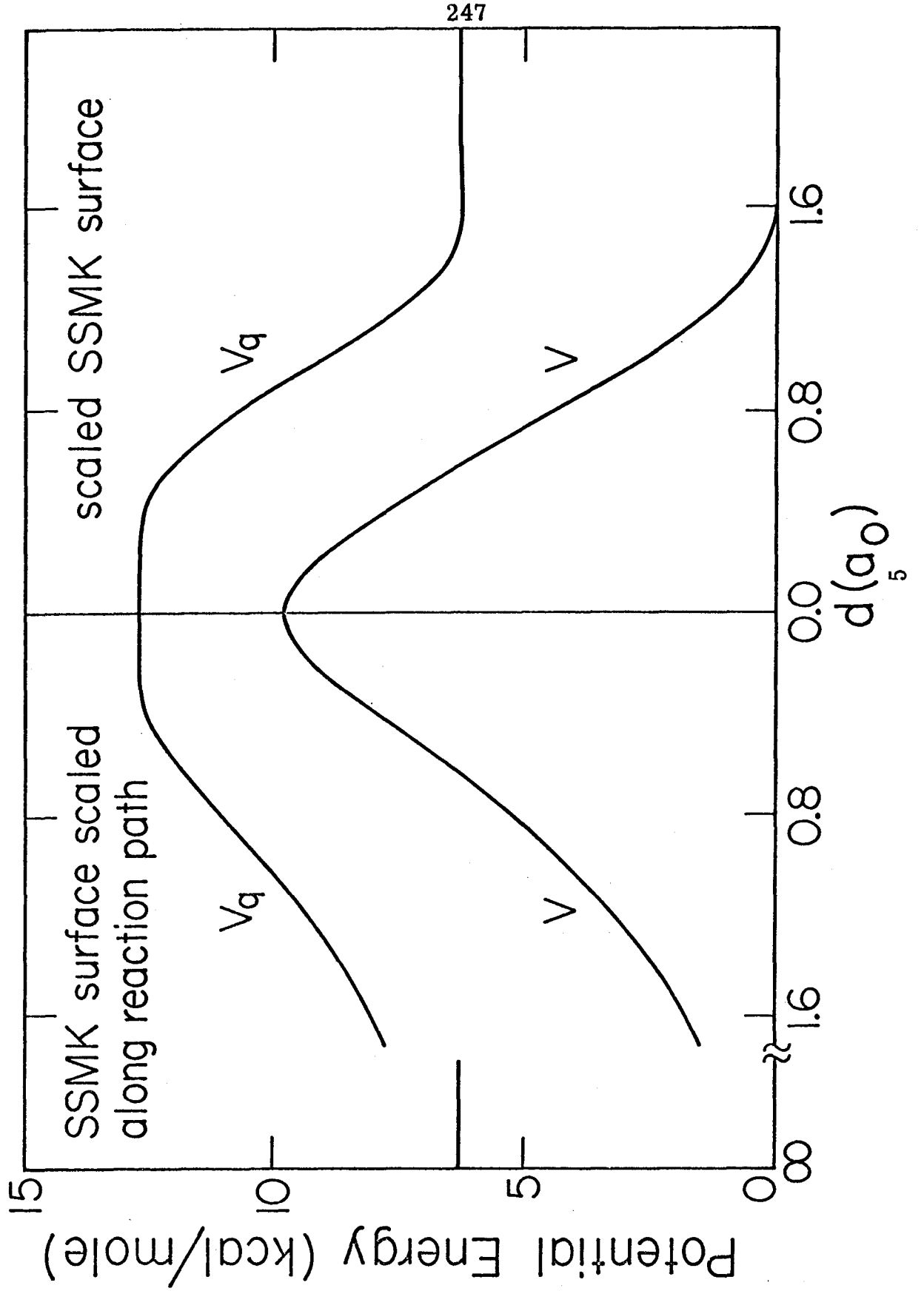
Potential Energy (kcal/mole)
15
10
5
0
SSMK surface scaled
along reaction path
V_q
V
scaled SSMK surface
V_q
V
1.6
0.8
0.0
0.8
1.6
$d(a_0)$
d_5

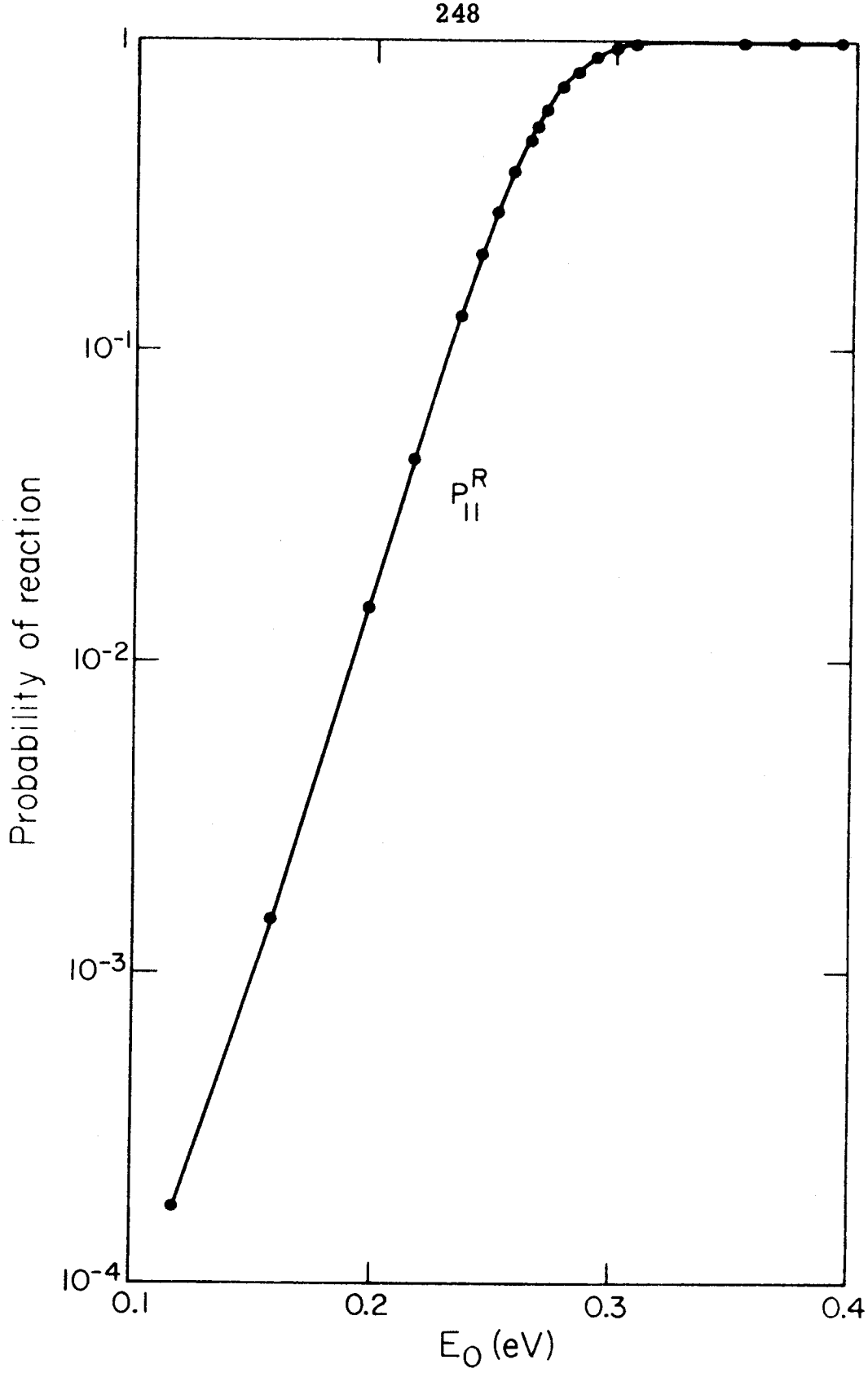
1
10^{-1}
10^{-2}
10^{-3}
10^{-4}
Probability of reaction
P_{11}^{R}
0.1
0.2
0.3
0.4
E_0 (eV)

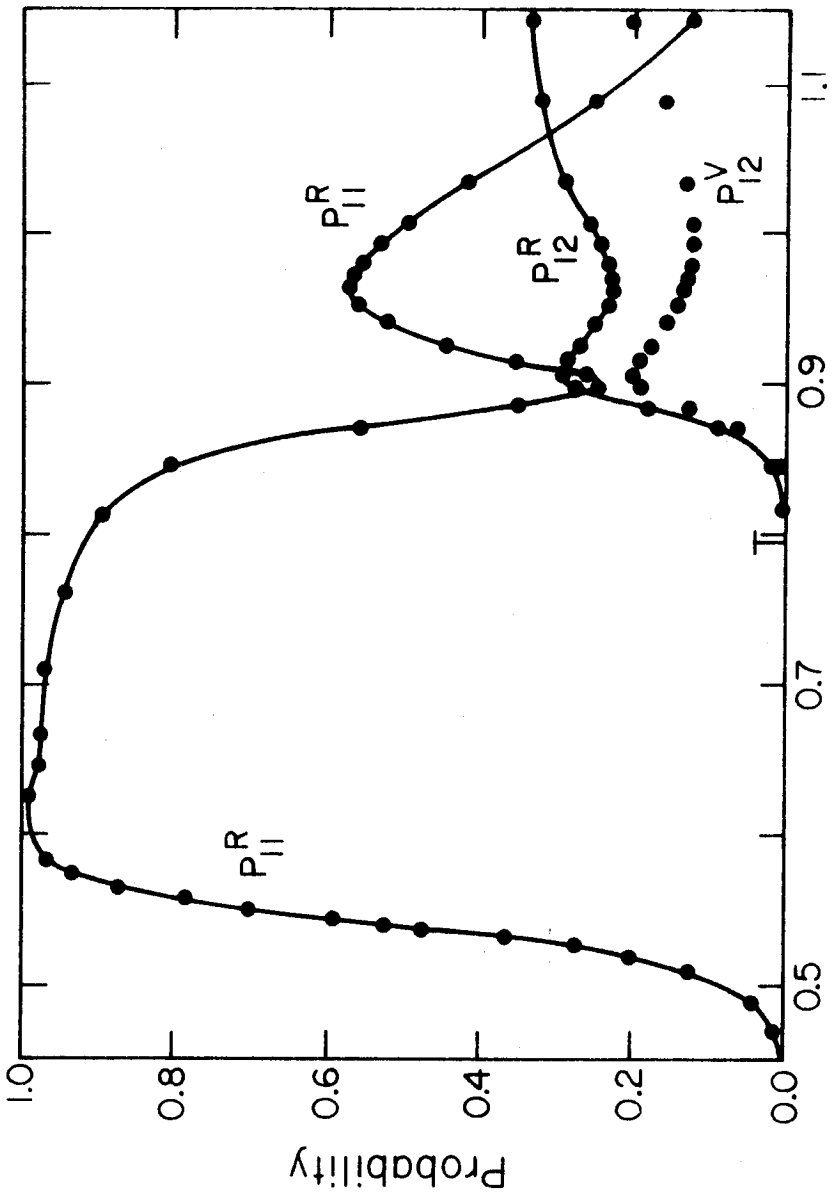
Probability
1.0
0.8
0.6
0.4
0.2
0.0
0.5
0.7
0.9
1.1
E (eV)
P_{11}^R
P_{12}^R
P_{12}^V
P_{11}^R

7

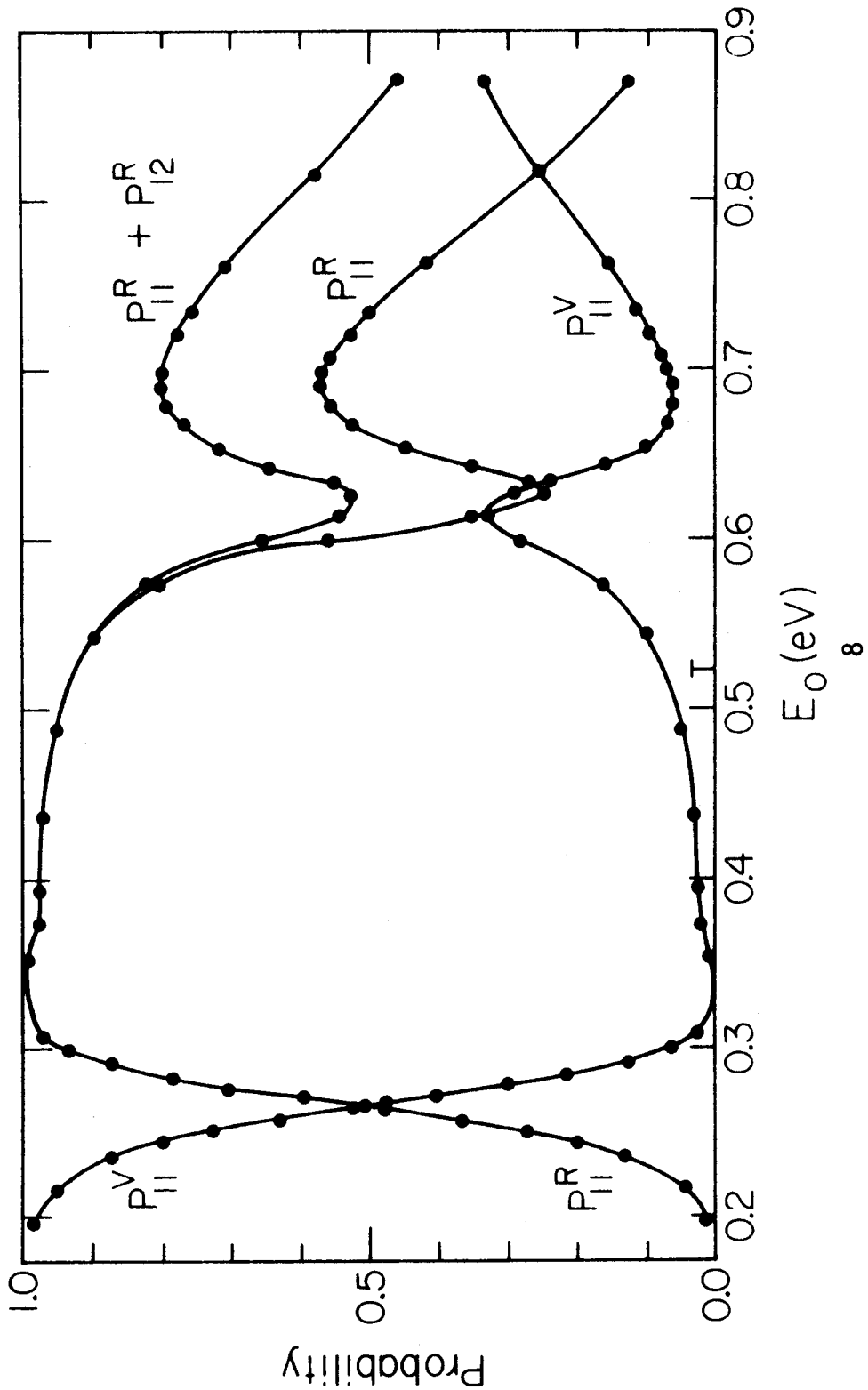
Probability
1.0
0.5
0.0
0.2
0.3
0.4
0.5
0.6
0.7
0.8
0.9
E_0 (eV)
P_{11}^V
P_{11}^R
$P_{11}^R + P_{12}^R$
P_{11}^R
P_{11}^V

Fig. 9. Probabilities of reaction computed for the collinear $H + H_2$ system as functions of initial relative translational energy. These are summed over final vibrational states. The H_2 is initially in the ground vibrational state. The "T" along the abscissa indicates the threshold for vibrational excitation.

Fig. 10. Probabilities of reaction computed for the collinear $D + D_2$ reaction. The results are for total probability of reaction. The left curve is calculated exactly for the scaled SSMK surface. The right curve is calculated by the conservation-of-vibrational-energy model (a treatment in one mathematical dimension) for the SNSSMK barrier defined in Table VIII. The "T" along the abscissa marks the threshold energy for vibrational excitation.

Fig. 11. Probabilities of reaction and vibrational de-excitation for the $H + H_2$ system as functions of total energy of the system. The H_2 is initially vibrationally excited.

Fig. 12. Scattering probabilities for the collinear $H + H_2$ reaction as functions of initial relative translational energy. The H_2 is initially in the $v = 1$ vibrationally excited state.

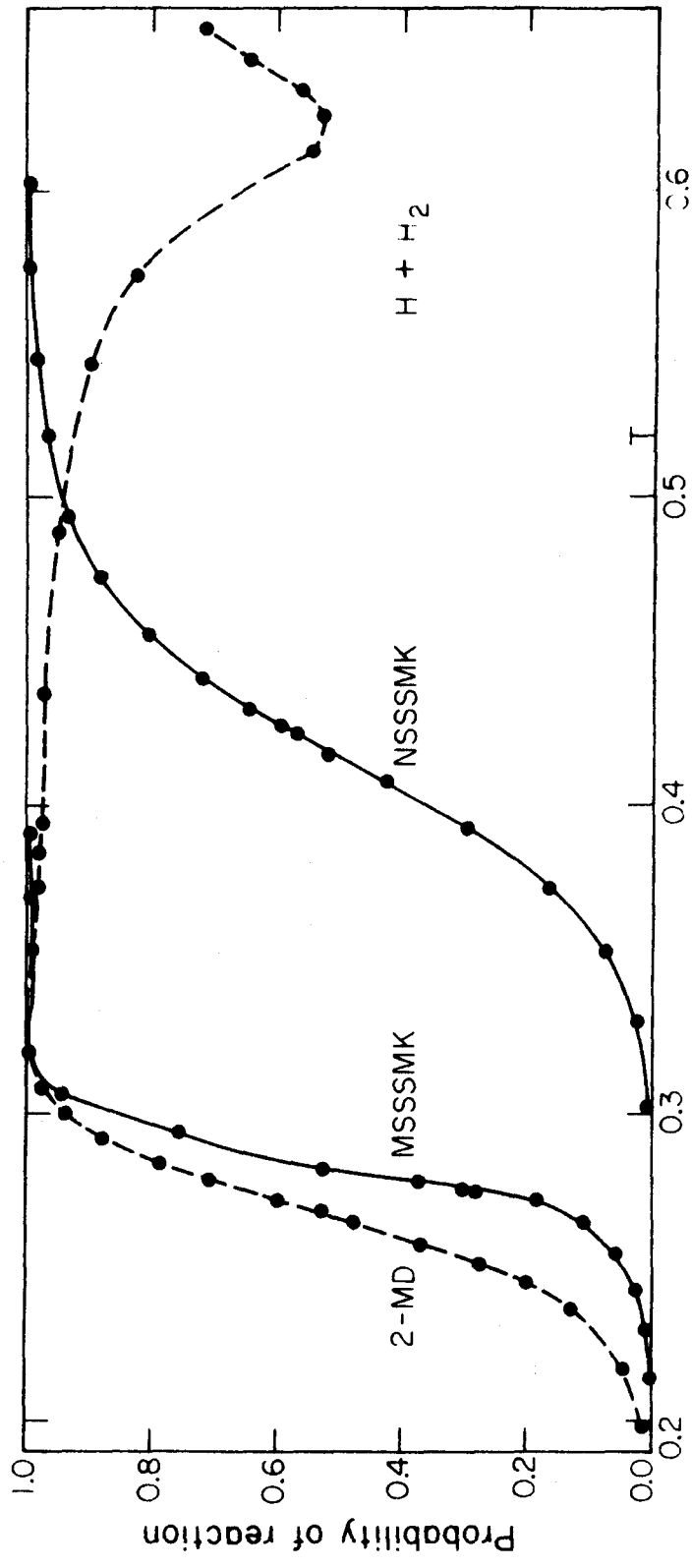
Probability of reaction
1.0
0.8
0.6
0.4
0.2
0.0
0.2
0.3
0.4
0.5
0.6
E_0(eV)
H + H_2
NSSSMK
MSSSMK
2-MD

9

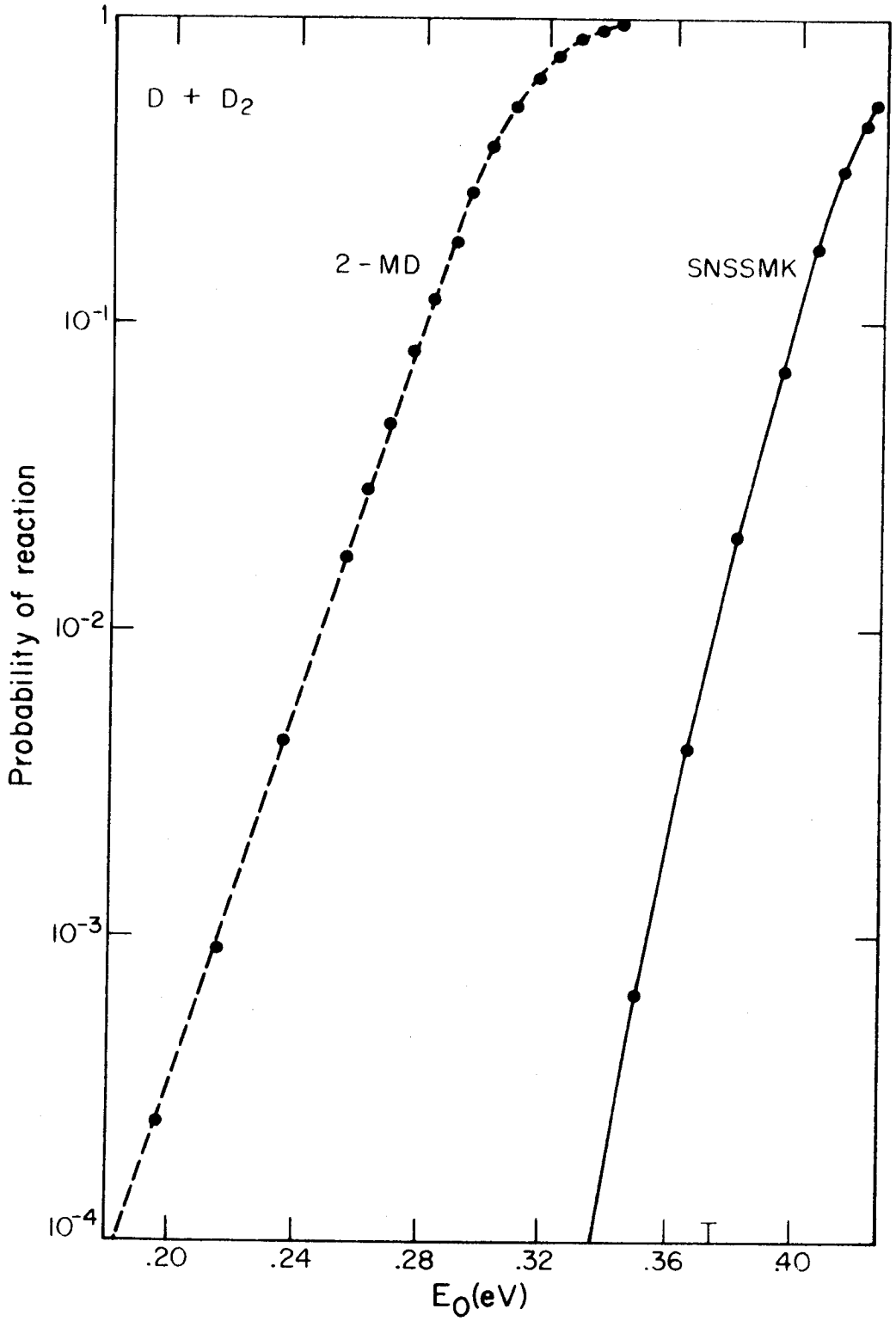
D + D2
2 - MD
SNSSMK
Probability of reaction
1
10-1
10-2
10-3
10-4
.20
.24
.28
.32
.36
.40
E0(eV)

10

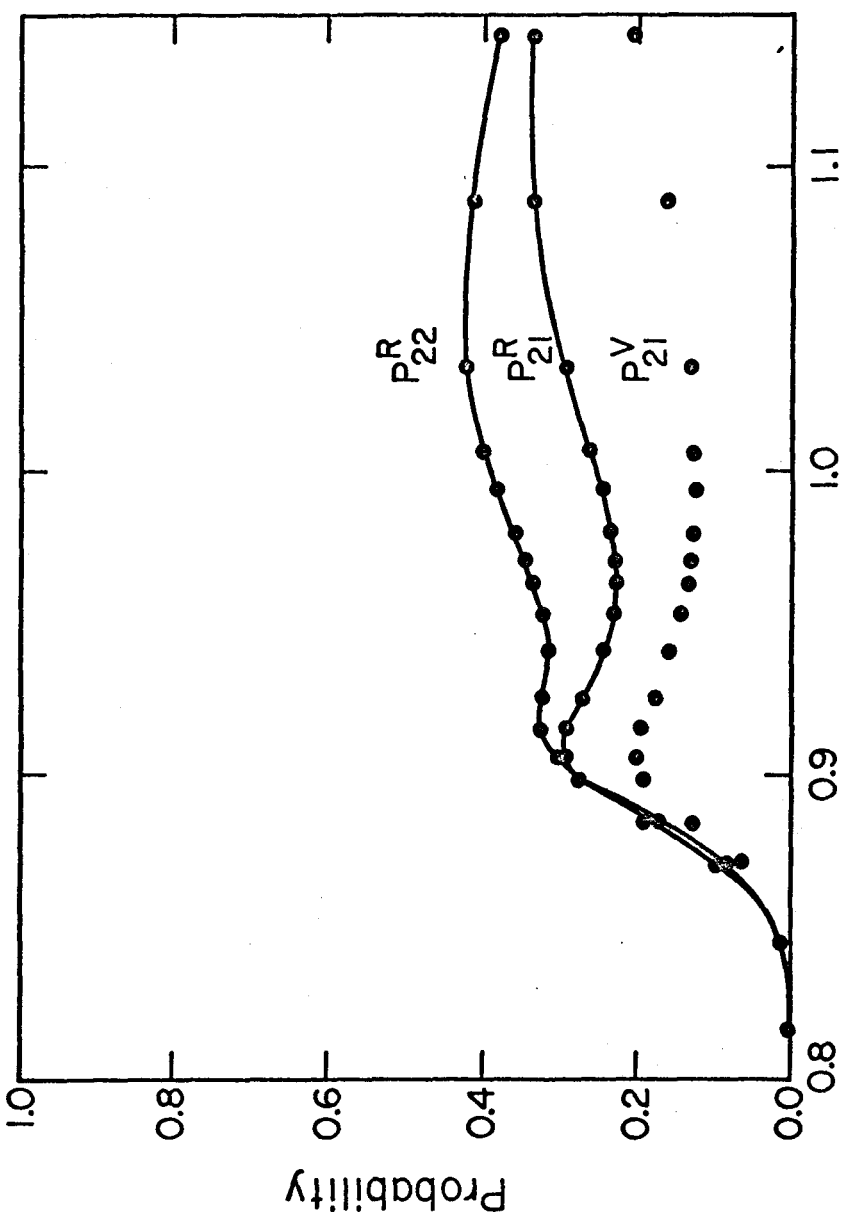

11

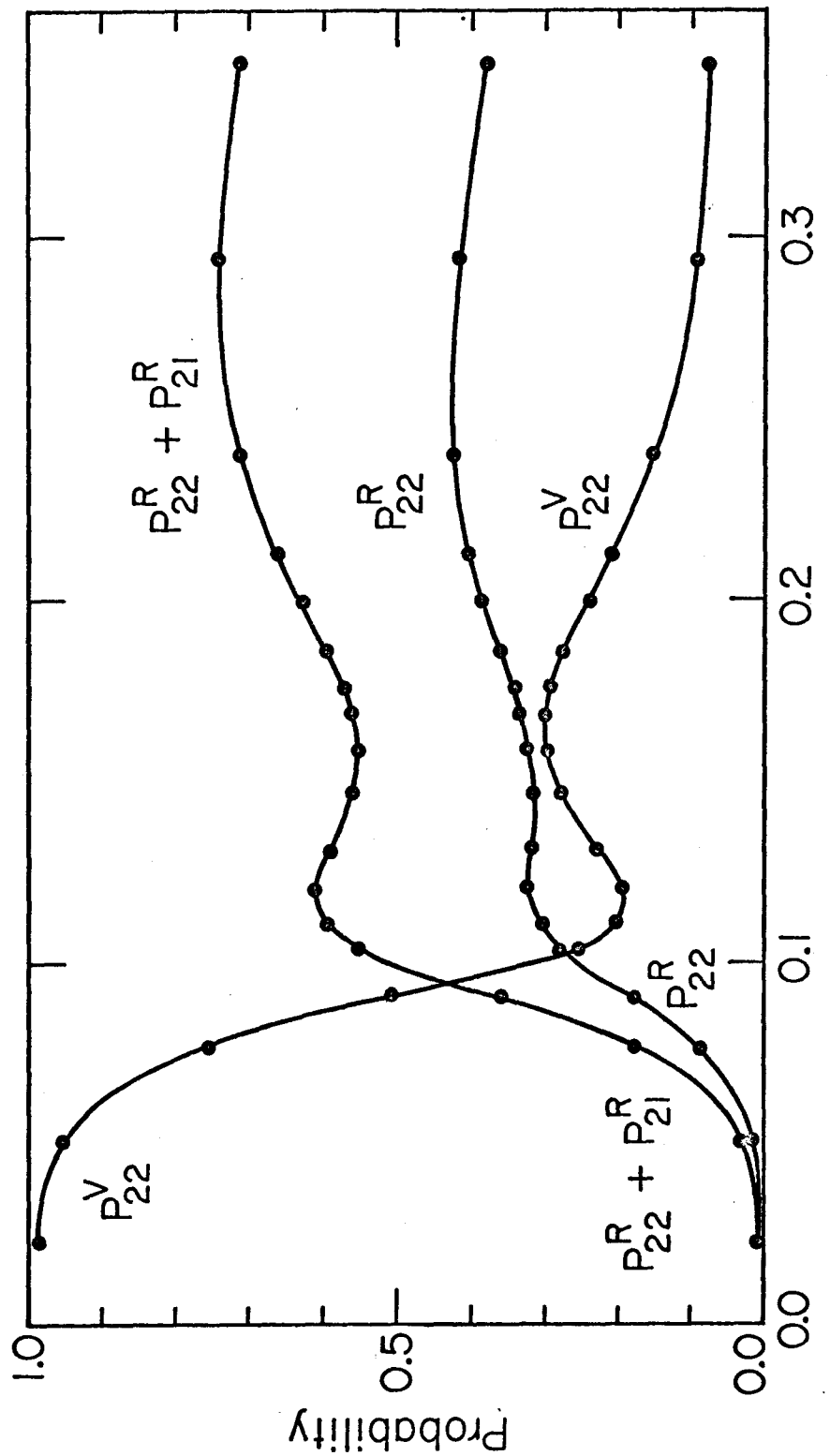
Probability
1.0
0.5
0.0
0.0
0.1
0.2
0.3
E_1 (eV)
P_{22}^V
$P_{22}^R + P_{21}^R$
P_{22}^R
P_{22}^R
P_{22}^V
$P_{22}^R + P_{21}^R$

12

APPENDIX 1

ELECTRONIC ADIABATICITY AND POTENTIAL ENERGY SURFACES FOR MOLECULAR DYNAMICS

It is usual in treating molecular mechanics to make an approximate separation of electronic and nuclear motion (Bo 27, Bo 54). This is possible because of the light mass of the electrons compared to the nuclei. For each fixed set of nuclear coordinates we solve for the energy states of the electronic system. These are the electronically adiabatic energy states so called because the electrons are considered to adjust instantaneously to their appropriate fixed-nuclei distribution for any change in the nuclear coordinates. The energy of each of these electronic states as a function of the nuclei positions can be considered a hypersurface in coordinate-energy space. Each hypersurface is the effective potential energy for motion of the nuclei when the system is in that electronic state. We will generally be interested only in the lowest-energy electronically adiabatic potential energy surface. The theory that chemical reactions occur without changes in the quantum numbers of the electronic system was first discussed by London (Lo 28) and is sometimes called London's adiabatic hypothesis. Although reactions which produce electronically excited species are well known (see, e.g., Th 66, Mo 66), most thermal energy chemical reactions involving reactants in the ground electronic states produce products in their ground electronic states (Th 68).*

---

* The author is grateful to Prof. L. R. Martin for discussions of this subject.

Reactions where the potential surface involves a degenerate state in the separated subsystems limit are one example where many electronic states are likely to be important in the region where the subsystems are interacting strongly. It is important to notice that reaction on the lowest electronically adiabatic surface will usually look like a crossing of surfaces if viewed in terms of electronically diabatic states.* For the low-energy collisions of interest here it is most convenient to use the electronically adiabatic surfaces and we will do this. At higher collision energies (the few eV range) some collisions will be nonadiabatic and the lowest few adiabatic surfaces may be important. In the very high energy range (impact energies greater than about 20 keV) the collisions can be described equally well or better in a diabatic basis.

The potential energy surfaces for systems that are isotopic analogs (e.g., H + DX and H + HX) are exactly the same in this approximation. However, the energetics on them will be different because the zero point energies differ (the zero point energy for any bounded mode of motion is approximately proportional to $\mu^{-1/2}$ where μ is the reduced mass for that mode). Even in the absence of zero point energy differences the difference in reduced mass produces different classical mechanical dynamics and would produce different quantum mechanical dynamics.

---

* This follows by looking at the coefficients of the various structures in a valence bond description (atomic orbital basis description) of the wave function. Before the reaction the coefficient(s) of the structure(s) corresponding to bonding in the bond to be broken is(are) large and the one(s) for the structure(s) corresponding to bonding in the bond to be formed are small. After the reaction, this situation is reversed. See, e.g., Ya 59, Po 69, Ma 40, and Ch 69.

Once the potential energy surfaces corresponding to different electronic states have been determined, the scattering process can be treated by methods discussed elsewhere. If the atomic scattering is treated classically, we must be able to assign one unique potential energy to each set of atomic coordinates. One case where this is possible is when the system remains in one particular total-system electronic state throughout the entire collision event. If the atomic scattering is treated quantum mechanically, the coupling of different electronic states may be included. The close coupling method using an expansion in eigenfunctions of the separated subsystems (see chapter I) can be used for the coupling of the electronically diabatic states. The perturbed stationary state method (see section I.A.1) can be used for the coupling of the electronically adiabatic states. In the latter case the potential energy becomes a differential operator in the matrix close coupling equations and we require both the diagonal and the off-diagonal matrix elements as input. The calculations described in chapter IV are an approximation to this method where only one (the lowest) electronically adiabatic electronic state has been retained so that we require only one diagonal matrix element, i.e., the potential energy. In addition there are even corrections to the fixed-nuclei potential energy diagonal matrix element; we neglect these. This is the Born-Oppenheimer approximation. The corrections to this approximation and the full nonadiabatic treatment of the coupling of Born-Oppenheimer electronic states have been presented by Hirschfelder and Meath (Hi 67).

APPENDIX 2

NUMERICAL SOLUTION OF THE CLOSE COUPLING EQUATIONS

The close coupling approximation involves expanding Ψ as

$$\Psi = \sum_i F_i(R)\, \varphi_i(\underset{\sim}{r}) . \qquad (1)$$

It is described in section I.A, but in this appendix a more simplified notation suffices. R is the distance between the colliding subsystems and $\varphi_i(\underset{\sim}{r})$ are products of their internal eigenfunctions and channel angular functions.

For nonrearrangements, there are two basically different approaches to solving for the close coupling approximation reaction probabilities--one is based on solving for the scattering wave function and the other solves for the transition matrix directly without obtaining the wave function. To solve for the transition probabilities from the wave function requires an analysis in the asymptotic region of an appropriate number of linearly independent solutions of the Schroedinger equation or its truncated matrix equivalent obtained by substituting (1) into $(H - E)\,\Psi = 0$ and successively taking inner products with the φ_i. Such an analysis of linearly independent solutions was used for electron-atom collisions by Bransden and McKee (Br 56), Marriott (Ma 57, Ma 58), Smith and

coworkers (Sm 60, Sm 60a), and many others.* The first application of this method to a molecular problem was by Marriott (Ma 64, Ma 64a, Ma 65a) for atom-spherical vibrator collisions. The method has since been used to solve the close coupling equations for several molecular collision problems: atom-rigid diatomic rotor collisions (Al 67, Le 67, Le 68, Er 68, Ki 68), electron-rigid diatomic rotor collisions (La 67, Ar 68, La 68, Cr 68, It 69, He 69, La 69, atom-atom collisions with transitions among hyperfine levels (Al 69), linear atom-diatomic vibrator collisions (Ri 67, Ch 68) and linear diatomic vibrator-diatomic vibrator collisions (Ri 67, Ri 68). The method of linear combinations of independent solutions has also been applied to solutions of the Schroedinger equation obtained directly by finite difference methods without using a state expansion (Di 68a).

Different methods have been used to obtain the independent solutions. One method is to integrate the differential equation outward as an initial value problem. In order for the expansion (1) to be complete it must include virtuals, i.e., closed channels. When these are included one component of the solution is rising exponentially at large R. If one must integrate out to fairly large R this component may so dominate the wave function as to make it impossible to analyze. To alleviate this difficulty, Smith and Burke developed a method of integrating both outward from R = 0 and inward from the asymptotic region to some intermediate values of

---

* See, for example, Go 62, Bu 62a, and many other papers by P. G. Burke and K. Smith and their coworkers. A particularly clear exposition of the general method is given in Ba 65. For a review of the methods used and references to some other methods of solving the equations, see Bu 62b and Bu 62c. For a recent review of work in this field see Bu 68.

R and there matching the solutions (Sm 61, see also Bu 62b). In some applications to molecular problems it has been possible to simply take a linear combination of solutions that eliminates the rising virtual components (Ri 67, Ri 68, Di 68a). Chan, Light, and Lin transformed at large R to a more truncated basis which neglected virtuals (Ch 68). This could cause a lack of accuracy which has not been evaluated. Johnson and Secrest devised a way to eliminate these computational difficulties by using a modified coordinate system at large R (Jo 67, Jo 68). A version of this method is incorporated into the analysis scheme used in chapter IV.

Another problem which arises when the method of initial value problem with outward integration is used is that at large R the solutions tend to become linearly dependent.* A method of re-orthogonalization to counter this tendency has been developed and successfully employed by Riley and Kuppermann (Ri 68). This method successively recombines the solutions in order to obtain a linearly independent set in the asymptotic region. It is called the DRILL method (for Direct Reduction of ill-conditioning). A simpler way to attain this result is to solve the problem by a boundary value (BV) method instead of an initial value method. This method was apparently first used for coupled equations by Pennell and Delves (Pe 61, see also Bu 62). Diestler and McKoy considered this method but concluded it would be difficult because the finite difference matrix would not be banded (Di 68a). However, this is

---

* This was first noted by Marriott (Ma 64) and is discussed in detail in Ri 67 and Al 69. In some cases, however, this tendency has not been as strong and it was possible just to ignore it (e.g., Le 67, Le 68).

because they did not consider the optimum sequence of equations. A suitable renumbering of finite difference mesh points and equations [i.e., $F_1(R_1)$, $F_2(R_1)$, ..., $F_N(R_1)$, $F_1(R_2)$, $F_2(R_2)$, ..., $F_N(R_{end})$ instead of $F_1(R_1)$, $F_1(R_2)$, ..., $F_1(R_{end})$, $F_2(R_1)$, $F_2(R_2)$, ..., $F_N(R_{end})$]produces a bonded matrix with narrow bandwidth. The DRILL and BV methods can be equivalent if the outward DRILL integration initiates from a null value matrix (e.g., where R is a radial coordinate and the boundary condition is $F_i(0) = 0$). In general the disadvantage of BV methods over initial value (IV) methods of solving differential equations is that they require more computer storage. The BV method has been used by Gutschick et al. (Gu 69).

The molecular c.c. equations have also been solved by methods which solve for the scattering matrix directly (without obtaining the wave functions). A method of this type was first developed by Degasperis (De 64) and the methods have been applied to linear atom-diatomic vibrator collisions (Se 66, Ri 67, Ch 69a), linear diatomic vibrator-diatomic vibrator collisions (Jo 67a, Jo 68, Le 67a, Le 68b, Le 68c).

Either the c.c. method (with a coordinate system of the type used in Ma 66 and Ra 68) or the (no state expansion) finite difference method (see Appendix 2) in any coordinate system can be used to obtain linearly independent solutions for the scattering problem which can then be analyzed by procedures like the one given by Diestler and McKoy (Di 68a) for collinear atom-molecule collisions. Of course various combinations of the c.c. and finite difference (FD) methods are also possible. Also there is a large variety of possible analysis procedures (for example, compare Di 68b with the R matrix analysis in chapter IV of this thesis and compare the asymptotic analysis in terms of complex exponentials with that in terms of spherical Bessel functions).

With regard to combinations of the c.c. IV, c.c. BV, and finite difference BV methods, one might consider using one method for small R and another closer to the asymptotic region. If one obtains a solution χ of the Schroedinger equation for small R using any of the three types of methods, this solution can always be extended by a c.c. method but an FD extension would require solving an elliptic differential equation with Cauchy boundary conditions and is unstable (Mo 53).

APPENDIX 3

NUMERICAL SOLUTION OF THE MULTIDIMENSIONAL SCHROEDINGER EQUATION FOR SCATTERING PROBLEMS

Consider the Schroedinger for two interacting subsystems A and B with composite internal wave function $\psi_i^C(\underset{\sim}{c})$ where i represents all the quantum numbers and $\underset{\sim}{c}$ all the internal coordinates of the subsystems and the coordinates representing their orientation. Then if R is the distance from A to B the wave function can be written

$$\Psi = \sum_{ij} c_{ji} f_j(R) \psi_i^C(\underset{\sim}{c}) \tag{1}$$

where the $f_j(R)$ are a complete set of orthogonal functions. The close coupling (c. c.) method defines

$$F_i(R) = \sum_j c_{ji} f_j(R) \tag{2}$$

so that

$$\Psi = \sum_i F_i(R) \psi_i^C(\underset{\sim}{c}) \tag{3}$$

(cf. eq. (I. 40)) and uses the variational method to derive an equation which is solved numerically for the $F_i(R)$. Thus the close coupling method treats the variation along different coordinates unevenly. The wave function's dependence on the $\underset{\sim}{c}$ coordinates is represented by an expansion in basis functions and its dependence on the R coordinate is solved for numerically.

Depending on the numerical method used for integrating along the R direction, the correspondence between the two representations may be made to appear more or less similar. For example, the three point finite difference scheme is equivalent to applying the variational technique to the subspace of continuous piecewise linear functions (He 68). In case this approximation is used we can consider the close coupling equations to be a variational solution of (1) where the functions ψ_i^C are chosen in one of the standard ways and the functions f_j are all the continuous functions which are separately linear over each interval between adjacent finite difference mesh points.

It is obviously possible to solve for the wave function Ψ in a less asymmetric fashion. One way is to approximate $F_i(R)$ by an expansion in a finite set of functions as in eq. (2) and to solve variationally for the coefficients. This will convert the differential equations problem into an algebraic problem. The input to the algebraic problem consists of integrals over the various expansion functions. This method is called the method of internal functions (Ma 65, chapter VI, § 1) or the Harris method (Ha 67, Mi 67, Ne 68, Ha 69).

Another method of treating the coordinates more symmetrically is to solve numerically in all coordinates as one multidimensional problem. Many standard techniques of numerical analysis may be brought to bear on this problem because the numerical solution of elliptic partial differential equations is a well-studied topic. This is the method used by Mortensen and Pitzer (Mo 62, Mo 68) and Diestler and McKoy (Di 68a, Di 68b) and in chapter IV.

APPENDIX 4

NUMERICAL SOLUTION OF THE ONE DIMENSIONAL SCHROEDINGER EQUATION FOR BOUND STATES

This appendix is concerned with the calculations of vibrational energy eigenvalues and eigenfunctions for diatomic molecules.

A need to compute the nuclear vibrational motion eigenfunctions and eigenvalues for a diatomic molecule arose in two of the projects described in this thesis: the scattering of electrons and hydrogen atoms from hydrogen molecules. The programs used to solve this problem are described in this appendix. The appendix also contains a study of the one dimensional eigenvalue problem for infinite square wells and parabolic wells; this was undertaken in order to determine the accuracy of finite difference approximations in these cases and to estimate what mesh sizes were needed to obtain various levels of accuracy in the eigenfunctions. The latter information was necessary to make an estimate of the feasibility of the $H + H_2$ scattering calculations which were later undertaken. The study also compared some approximations which can be made in solving the problem and showed which procedures are more accurate and should be used for more complicated cases where detailed testing is not feasible.

Denote the positions of the two nuclei in the diatomic molecule as $\vec{R}_1$ and $\vec{R}_2$ (with $R = |\vec{R}_1 - \vec{R}_2|$) and their masses as M_1 and M_2 (with $\mu = M_1M_2/[M_1 + M_2]$). Treating the motion of the electrons as adiabatic with respect to nuclear motion (see appendix 1) and making the usual separation of rotation and vibration we obtain the radial equation for the kth vibrational wave

function of the molecule (in a singlet state and its lowest energy rotational state, see Mo 48, § 23 or La 65, pp. 293-294 for more details):

$$H(R)\,\varphi_k(R) = [T(R) + V(R)]\,\varphi_k(R) = \epsilon_k\,\varphi_k(R) \tag{1}$$

where

$$T(R) = -\frac{1}{2\mu}\,\frac{\delta^2}{\delta R^2} \tag{2}$$

and V(R) is the diatomic molecule's potential energy curve (total fixed-nuclei electronic energy of the molecule minus total electronic energy of the separated atoms). Equation (1) must be solved with the boundary conditions

$$\varphi_k(0) = 0 \tag{3}$$

$$\varphi_k(R) \underset{R \to \infty}{\to} 0\ . \tag{4}$$

The problem is thus equivalent to the case of a single particle moving in one dimension with an infinite potential energy for $R \leq 0$ and the potential energy equal to V(R) for $R > 0$. For most realistic molecular potentials eq. (1) cannot be solved analytically (see, however, Mo 29 and Mu 69). It is then convenient to use numerical integration (an alternative is to use the Rayleigh-Ritz method to obtain the coefficients in an expansion of the solution in terms of a set of known functions; a recent example of this type calculation is given in Ze 67). A common

method of integration is to treat eqs. (1) and (3) as an initial value problem and to integrate outward. The method of Cooley is the most often used procedure of this type (Co 61, Ca 63, Za 63); it uses inward and outward integration with matching of the approximate solutions at intermediate R. The procedure must be iterated until the correct eigenvalue is found. The method described in this appendix is simpler to program and capable of equivalent accuracy. It requires more storage locations but not enough to be a serious problem on most computers. This method has two distinguishing features. First, the system of eqs. (2) - (4) is treated as a boundary value problem. For R_{in} small enough and R_{out} large enough a good approximation to the boundary conditions is that $\varphi_k(R_{in}) = \varphi_k(R_{out}) = 0$. The equation is then solved by making the finite difference approximation. This method is essentially an application to one dimensional problems of a method applied to two dimensional problems by Diestler, Winter, and McKoy (Di 67, Wi 68). Although for these 1-D problems we could use high order difference formulas and a very fine mesh (i.e., a large number of grid points), we were more interested in the model problems in solving the 1-D problem to the same accuracy as the problems which arise in $H + H_2$ scattering. Therefore we used the 3 point difference formula and 10 to 70 points across the well [Diestler (Di 68) had used the 3 point difference formula with 20 to 32 grid points in his scattering calculations and Mortensen (Mo 48) has used 73 to 81 points]. For the problem of vibrational excitation of the hydrogen molecule we found that sufficiently accurate eigenfunctions could be obtained by using the 3 point difference formula and a large number of grid points. Further, the higher order difference formula can be used without extra assumptions only in

the interior of the grid point region for a boundary value problem and extra testing is required to find out the effects of the special approximations which must be used near the boundary. Thus we will not consider the higher order difference formulas.

We now consider the theory of the application of this method to specific cases, the numerical methods used, and the results.

Infinite square well. We use reduced units where $\mu = 1$ and

$$V(R) = \begin{cases} 0 & R \leq \pi \\ \infty & R > \pi \end{cases} \qquad (5)$$

Consider a set of N mesh points (or grid points) R_i evenly spaced between $R = 0$ and $R = \pi$. Then the step size h between mesh points is $\pi/(N + 1)$. Let

$$\varphi_{ik} \equiv \varphi_k(R_i) \qquad (6)$$

and make the finite difference approximation

$$\left.\frac{\delta^2 \varphi_k}{\delta R^2}\right|_{R = R_i} \simeq \frac{1}{h^2}(\varphi_{i-1,k} - 2\varphi_{i,k} + \varphi_{i+1,k}) . \qquad (7)$$

Then the differential equation and its boundary conditions reduce to a set of linear equations for the values of the eigenfunction at the mesh points. These equations can be written in matrix form as

$$\sum_{j=1}^{N} H_{ij} \varphi_{jk} = \epsilon_k \varphi_k \qquad i, k = 1, 2, \ldots, N \tag{8}$$

or more conveniently as

$$\sum_{j=1}^{N} G_{ij} \varphi_{jk} = \lambda_k \varphi_k \qquad i, k = 1, \ldots, N \tag{9}$$

where

$$G_{ij} = -2 \delta_{ij} + \delta_{i,j-1} (1 - \delta_{i1}) + \delta_{i,j+1} (1 - \delta_{iN}) \tag{10}$$

and

$$\epsilon_k = - \lambda_k / 2h^2 \ . \tag{11}$$

As indicated, the finite difference approximation with N grid points across the well yields approximations to the N lowest energy eigenfunctions and eigenvalues. The exact solutions of the differential equation are known in this case and are

$$\epsilon_k = \frac{1}{2} k^2 \qquad k = 1, 2, \ldots \tag{12}$$

$$\varphi_k = \sqrt{2/\pi} \ \sin k R \ . \tag{13}$$

Parabolic well. We consider the case $\mu = 1$. The parabolic well is given by

$$V(R) = - \frac{1}{2} (R - \frac{1}{2} a)^2 \ . \tag{14}$$

The Schroedinger equation is given by (1) or by

$$F(R)\,\varphi_k(R) = [G(R) + U(R)]\,\varphi_k(R) = \lambda_k\,\varphi_k(R) \tag{15}$$

where

$$G(R) = -2h^2\,T(R) \tag{16}$$

$$U(R) = -2h^2\,V(R) \tag{17}$$

$$\lambda_k = -2h^2\,\epsilon_k\ . \tag{18}$$

In matrix notation the equations for the finite difference solution are

$$\sum_{j=1}^{N} F_{ij}\,\varphi_{jk} = \lambda_k\,\varphi_{ik} \tag{19}$$

$$F_{ij} = G_{ij} + \delta_{ij}\,U_{ii} \tag{20}$$

where

$$U_{ii} = U(R_i) = -h^2\left(R_i - \tfrac{1}{2}a\right)^2\ . \tag{21}$$

The almost exact solutions of the differential equation (15) are

$$\epsilon_k = \left(k - \tfrac{1}{2}\right) \quad k = 1,\ 2,\ \ldots \tag{22}$$

and

$$\psi_k = \frac{\pi^{-1/4}}{\sqrt{2^{k-1}(k-1)!}} H_{k-1}(R - \tfrac{a}{2}) e^{-(2R-a)^2/8} \qquad (23)$$

and H_k is a Hermite polynomial. These solutions would be exact if the boundary condition (3) were at $R = -\infty$ instead of $R = 0$. The difference caused by this change in boundary condition is generally small here because we consider large enough values of a.

Hydrogen molecule. In this case we use atomic units. Then $\mu = 919.05$ and V(R) is taken from the accurate calculations of Kolos and Wolniewicz (Ko 65). The matrix equations for the finite difference solutions are then

$$\sum_j F_{ij} \varphi_{jk} = \lambda_k \varphi_{ik} \qquad (24)$$

where

$$F_{ij} = \delta_{ij} [-(2/\mu) + U_{ii}] + 1/\mu [\delta_{i,j-1}(1 - \delta_{i1}) + \delta_{i,j+1}(1 - \delta_{iN})] \qquad (25)$$

$$\lambda_k = -2h^2 \epsilon_k \qquad (26)$$

$$U_{ii} = -2h^2 V(R_i). \qquad (27)$$

For calculations on D_2, the only change is $\mu = 1836.7$.

Numerical methods. The numerical work principally consists in diagonalizing the finite difference matrix to obtain its

eigenvalues and eigenvectors. In all cases we used the Givens-Householder method and single precision arithmetic on the Caltech IBM 7094. The Givens-Householder eigenvalue and eigenvector subroutine was supplied by F. P. Roullard III.

Results for model problems. For the infinite square well the energy eigenvalues could be obtained fairly accurately even for high k. The following table illustrates this:

N	20	30	40	50
k				
1	4.991^{-1}	4.996^{-1}	4.998^{-1}	4.998^{-1}
2	1.985	1.993	1.996	1.997
3	4.425	4.465	4.480	4.487
4	7.764	7.891	7.938	7.960
5	1.193^{1}	1.223^{1}	1.235^{1}	1.240^{1}
8	2.836^{1}	3.029^{1}	3.101^{1}	3.136^{1}
12	5.463^{1}	6.355^{1}	6.707^{1}	6.878^{1}
17	8.160^{1}	1.121^{2}	1.252^{2}	1.318^{2}
23		1.645^{2}	2.027^{2}	2.231^{2}
30		1.942^{2}	2.836^{2}	3.357^{2}
40			3.401^{2}	4.689^{2}

N	60	70	80	90	Exact
k					
1	4.999^{-1}	4.999^{-1}	4.999^{-1}	4.999^{-1}	5.000^{-1}
2	1.998	1.999	1.999	1.999	2.000
3	4.491	4.493	4.495	4.496	4.500
4	7.972	7.979	7.984	7.987	8.000
5	1.243^{1}	1.245^{1}	1.246^{1}	1.247^{1}	1.250^{1}
8	3.155^{1}	3.167^{1}	3.174^{1}	3.180^{1}	3.200^{1}
12	6.974^{1}	7.032^{1}	7.071^{1}	7.098^{1}	7.200^{1}
17	1.355^{2}	1.378^{2}	1.393^{2}	1.404^{2}	1.445^{2}
23	2.350^{2}	2.424^{2}	2.474^{2}	2.509^{2}	2.645^{2}
30	3.673^{2}	3.877^{2}	4.015^{2}	4.112^{2}	4.500^{2}
40	5.542^{2}	6.118^{2}	6.519^{2}	6.807^{2}	8.000^{2}
60	7.535^{2}	9.622^{2}	1.121^{3}	1.242^{3}	1.800^{3}

In this and other tables, the superscript indicates the power of ten by which the number is to be multiplied. For the infinite square well problem, the classically allowed region of the well does not vary with k (for the parabolic well the classically allowed region is wider for higher energy solutions). The results for the square well illustrate the greater difficulty, with increasing k, representing the rapidly oscillating eigenfunction with a finite number of points. We also computed the overlap of the FD solution with the exact solution. This was done two ways - using Simpson's Rule (SR) and using the trapezoidal rule (TR). In each case the FD eigenfunction was normalized using the same method that was to be used for computing the overlap integral. Some typical overlap integrals are given in the table below: in each case the upper of a pair of values is the SR value and the lower is the TR value.

N	20	50	90
k			
1	1.000176	1.000012	1.000002
	1.000000	1.000000	1.000000
4	1.002515	1.000194	1.000034
	1.000000	1.000000	1.000000
7	1.005934	1.000571	1.000105
	1.000000	1.000000	1.000000
16	1.003665	1.002268	1.000504
	1.000000	1.000000	1.000000
25		1.003259	1.001057
		1.000000	1.000000

The agreement obtained using the trapezoidal rule is excellent. It results from the wave functions normalized this way agreeing to more than 6 significant figures with the value of the exact wave function, point-by-point. Likewise the error in the SR case is

due to the SR-normalized wave functions differing (point-by-point) from the exact wave function by about the same amount as the overlap integral differs from 1.0. The conclusion is that solutions obtained using the 3 point difference formula should be normalized using the TR.

We also computed the overlap of the approximate solutions with interpolated values determined from the N = 90, 40, and 30 approximate wave functions. The overlap integrals and conclusions were similar to those above.

For the parabolic binding potential the situation is more complicated because of the exponential tail on the exact wave function. Because of the exponential tail, there is an optimum h for any fixed N. If h is too small, the tail of the wave function is truncated too close in by eq. (4). If h is too large the grid points are being used to obtain an unnecessarily accurate representation of the tail at the expense of a poor representation of the part of the wave function that is large. In our model problem here, $h = a/(N + 1)$. We did calculations with a = 8, 10, 12, 14, and 16. For N = 40, 60 the conclusion concerning the optimum a depends on the level considered and also on whether the eigenvalue or the overlap is used as the criterion of goodness. The following table illustrates this. For each criterion and level listed the table gives the optimum a among those tried (8 - 16):

Criterion	Eigenvalue		Overlap with exact solution	
N	40	60	40	60
k				
1	10	8	8	8
3	10	8	8	8
5	10	8	10	10
7	8	8	10	10
9	10	10	10	10
11	10	10	10	12
13	10	10	12	12
15	10	10	12	12
17	10	12	12	12
19	10	12	12	14
31	10	12		

Even in low energy collision problems one will want a grid capable of giving accurate results even for higher energy solutions because of the importance of virtual states. This table provided a rough guide (after scaling and allowance for anharmonicity) to the optimum spacing of grids for our first attempts at collision problems.

The following table shows how accurately the eigenvalues are predicted. Also listed for the levels shown are the widths of the classically allowed regions (CW = classical width).

		a	10	12	10
	CW				
		N	40	40	60
k					
1	2.00		4.981	4.973	4.992
3	4.47		2.476	2.465	2.489
5	6.00		4.422	4.387	4.465
7	7.21		6.338	6.264	6.428
9	8.25		8.229	8.092	8.386
13	10.00		1.213^{1}	1.159^{1}	1.256^{1}
19	12.17		1.910^{1}	1.653^{1}	2.076^{1}
27	14.56		2.877^{1}	2.256^{1}	3.474^{1}
36	17.09		3.559^{1}	2.905^{1}	5.172^{1}
47	19.29				6.903^{1}

	a	12	14	16	Exact
	N	60	60	60	
k					
1		4.988	4.983	4.978	0.5
3		2.484	2.478	2.472	2.5
5		4.450	4.431	4.410	4.5
7		6.396	6.357	6.312	6.5
9		8.321	8.254	8.176	8.5
13		1.211^{1}	1.012^{1}	1.174^{1}	12.5
19		1.792^{1}	1.729^{1}	1.688^{1}	18.5
27		2.607^{1}	2.415^{1}	2.297^{1}	26.5
36		3.891^{1}	3.212^{1}	2.844^{1}	35.5
47		5.038^{1}	3.983^{1}	3.575^{1}	46.5

The results show that good accuracy can be obtained for the lower levels (which are of primary interest here). The overlaps with the exact eigenfunctions are given in the next table. These were computed with the trapezoidal rule.

a	10	12	10	12	14	16
N	40	40	60	60	60	60
k						
1	1.00000	0.99999	1.00000	1.00000	1.00000	0.99999
3	0.99987	0.99973	0.99997	0.99995	0.99990	0.99983
5	0.99911	0.99809	0.99982	0.99963	0.99931	0.99880
7	0.99641	0.99242	0.99926	0.99857	0.99729	0.99525
9	0.98796	0.97817	0.99664	0.99597	0.99231	0.98643
13	0.83755	0.89417	0.89347	0.98061	0.96401	0.93564
19	-0.24473	0.34522	-0.12813	0.74848	0.82206	0.68343

The only really bad results in these tables occur when the grid does not even cover the full classically allowed region. Of course one would never use such a grid in a real problem. The tables show one can obtain agreement within a few per cent for say the first ten levels using practical sized grids. This means that it is possible to use this method of obtaining vibrational eigenfunctions even in problems involving much vibrational excitation.

Results for H_2. The following table gives the results for H_2 vibrational energy levels using the Kolos and Wolniewicz potentials. The table lists values of R (in a_o) at which the wave function is assumed to vanish, the number N of grid points, the step size h (in a_o), the zero point energy (ZPE), and the amounts of energy needed to excite the first and second vibrationally excited levels. The energy quantities are in atomic units. The last line gives the results of Kolos and Wolniewicz.

Range	N	h	ZPE	ΔE_1	ΔE_2
0.2 - 3.8	17	0.200	0.0094530	0.017219	0.014217
0.2 - 4.2	19	0.200	0.0094530	0.017219	0.014217
0.3 - 4.1	37	0.100	0.0098155	0.018554	0.017171
0.35 - 3.8	68	0.050	0.0098963	0.018861	0.017715
0.35 - 4.05	73	0.050	0.0098963	0.018861	0.017715
0.39 - 4.01	361	0.010	0.0099220	0.0189560	0.0178811
$0.39\dot{3}$ - $4.00\dot{6}$	541	$0.00\dot{6}$	0.0099226	0.0189582	0.0178849
Kolos-Wolniewicz			0.0099291	0.018959	0.017888

The superior dot indicates the digit is continued as a repeating decimal number (e.g., $0.\dot{6} = 2/3$).

REFERENCES

Ab 64 M. Abramowitz and I. A. Stegun, editors, Handbook of Mathematical Functions (National Bureau of Standards, Washington, 1964).

Ab 68 A. Y. Abul-Magd and M. H. Simbel, Z. Physik 215, 121 (1968).

Ac 64 M. Ackerman, E. F. Greene, A. L. Moursund, and J. Ross, J. Chem. Phys. 41, 1183 (1964).

Al 67 A. C. Allison and A. Dalgarno, Proc. Phys. Soc. (London) 90, 609 (1967).

Al 69 D. C. S. Allison and P. G. Burke, J. Phys. B (London) 2, 941 (1969).

Ar 68 R. W. B. Ardill and W. D. Davison, Proc. Roy. Soc. (London) A 304, 465 (1968).

Ba 34 C. E. H. Bawn and G. Ogden, Trans. Faraday Soc. 30, 432 (1934).

Ba 50 D. R. Bates, A. Fundaminsky, J. W. Leech, and H. S. W. Massey, Phil. Trans. Roy. Soc. (London) A243, 93, 117 (1950).

Ba 53 E. Bauer and T.-Y. Wu, J. Chem. Phys. 21, 726 (1953).

Ba 58 D. R. Bates, Proc. Roy. Soc. (London) A247, 294 (1958).

Ba 60 R. H. Bassel and E. Gerjuoy, Phys. Rev. 117, 749 (1960).

Ba 62 D. R. Bates, in Atomic and Molecular Processes, edited by D. R. Bates (Academic Press, New York, 1962), p. 257.

Ba 65 L. L. Barnes, N. F. Lane, and C. C. Lin, Phys. Rev. 137, A388 (1965).

Ba 66 S. H. Bauer and E. Ossa, J. Chem. Phys. 45, 434 (1966).

Ba 69 D. Banks, L. Vriens, and T. F. M. Bonsen, J. Phys. B (London) 2, 976 (1969).

Be 30 H. Bethe, Ann. Physik 5, 325 (1930).

Be 33 R. P. Bell, Proc. Roy. Soc. (London) A139, 466 (1933).

Be 35 R. P. Bell, Proc. Roy. Soc. (London) A148, 241 (1935).

Be 37 H. A. Bethe, Rev. Mod. Phys. 9, 69 (1937), Section IX.

Be 59 R. P. Bell, Trans. Faraday Soc. 55, 1 (1959).

Be 60 S. W. Benson, The Foundations of Chemical Kinetics (McGraw-Hill, New York, 1960), p. 155.

Be 63 R. B. Bernstein, A. Dalgarno, H. Massey, and I. C. Percival, Proc. Roy. Soc. (London) A274, 427 (1963).

Be 63a K. L. Bell and B. L. Moiseiwitsch, Proc. Roy. Soc. (London), A276, 346 (1963).

Be 66 O. Bely, Proc. Phys. Soc. (London) 87, 1010 (1966).

Be 67 O. Bely, Il Nuovo Cimento [10] 49B, 66 (1967).

Be 68 K. L. Bell, D. J. Kennedy, and A. E. Kingston, J. Phys. B (London) 1, 204 (1968).

Bi 49 J. Bigeleisen, J. Chem. Phys. 17, 675 (1949).

Bi 59 J. Bigeleisen, F. S. Klein, R. E. Weston, and M. Wolfsbert, J. Chem. Phys. 30, 1340 (1959).

Bl 52 J. M. Blatt and V. F. Weisskopf, Theoretical Nuclear Physics (John Wiley and Sons, New York, 1952).

Bl 52a J. M. Blatt and L. C. Biedenharn, Rev. Mod. Phys. 24, 258 (1952).

Bl 69 S. M. Blinder, Advanced Physical Chemistry (Macmillan, New York, 1969), Section 20.9.

Bo 27 M. Born and R. Oppenheimer, Ann. Physik 84, 457 (1927).

Bo 36 N. Bohr, Nature 137, 3441 (1936).

Bo 53 S. Borowitz and B. Friedman, Phys. Rev. 89, 441 (1953).

Bo 54 M. Born and K. Huang, Dynamical Theory of Crystal Lattices (Clarendon Press, Oxford, 1954), Section 14.

Bo 56 S. Borowitz and M. M. Klein, Phys. Rev. 103, 612 (1956).

Bo 62 R. A. Bonham, J. Chem. Phys. 36, 3260 (1962).

Bo 68 D. K. Bohme, J. B. Hasted, and P. P. Ong, J. Phys. B (London) 1, 879 (1968).

Br 56 B. H. Bransden and J. S. C. McKee, Proc. Phys. Soc. (London) A69, 422 (1956).

Br 58 B. H. Bransden, A. Dalgarno, T. L. John, and M. J. Seaton, Proc. Phys. Soc. (London) 71, 877 (1958).

Br 65 B. H. Bransden, Adv. At. Mol. Phys. 1, 85 (1965).

Bu 52 M. Burton and J. L. Magee, J. Phys. Chem. 56, 842 (1952).

Bu 61 E. H. S. Burhop, in Quantum Theory: I. Elements, edited by D. R. Bates (Academic Press, New York, 1961), p. 299.

Bu 61a V. M. Burke and M. J. Seaton, Proc. Phys. Soc. (London) 77, 199 (1961).

Bu 62 R. A. Buckingham, in Numerical Solution of Ordinary and Partial Differential Equations, edited by L. Fox (Pergamon Press, Oxford, 1962), p. 184.

Bu 62a P. G. Burke, Y. M. Burke, I. C. Percival and R. McCarroll, Proc. Phys. Soc. (London) 80, 413 (1962).

Bu 62b P. G. Burke and H. M. Schey, Phys. Rev. 126, 147 (1962).

Bu 62c P. G. Burke and K. Smith, Rev. Mod. Phys. 34, 458 (1962).

Bu 63 P. G. Burke, H. M. Schey, and K. Smith, Phys. Rev. 129, 1258 (1963).

Bu 63a P. G. Burke, Proc. Phys. Soc. (London) 82, 443 (1963).

Bu 66 P. G. Burke and A. J. Taylor, Proc. Phys. Soc. (London) 88, 549 (1966).

Bu 67 P. G. Burke, S. Ormonde, W. Whitaker, Proc. Phys. Soc. (London) 92, 319 (1967).

Bu 68 P. G. Burke, The Physics of Electronic and Atomic Collisions: Invited Papers from the Fifth Conference, edited by L. M. Branscomb (J. I. L. A., Boulder, 1968), p. 128.

Bu 69 D. L. Bunker and T. -S. Chang, J. Phys. Chem. 73, 943 (1969).

Bu 69a P. G. Burke, D. F. Gallaher, and S. Geltman, in Sixth International Conference on the Physics of Electronic and and Atomic Collisions: Abstracts of Papers, edited by I. Amdur (M. I. T. Press, Cambridge, 1969), p. 370.

Ca 63 J. K. Cashion, J. Chem. Phys. 39, 1872 (1963).

Ca 64 H. Carmichael and H. S. Johnston, J. Chem. Phys. 41, 1975 (1964).

Ca 68 P. Cadman and J. C. Polanyi, J. Phys. Chem. 72, 3715 (1968).

Ch 63 G. Chiltz, R. Eckling, P. Goldfinger, G. Huybrechts, H. S. Johnston, L. Meyers, and G. Verbeke, J. Chem. Phys. 38, 1053 (1963).

Ch 65 G. E. Chamberlain, H. G. M. Heideman, J. A. Simpson, and C. E. Kuyatt, in Fourth International Conference on the Physics of Electronic and Atomic Collisions: Abstracts of Papers (Science Book Crafters, Hastings-on-Hudson, 1965), p. 378.

Ch 66 M. S. Child, Proc. Roy. Soc. (London) A292, 272 (1966).

Ch 68 S.-K. Chan, J. C. Light, and J.-L. Lin, J. Chem. Phys. 49, 86 (1968).

Ch 68a M. S. Child, Discussions Faraday Soc. 44, 68 (1968).

Ch 69 M. S. Child, Mol. Phys. 16, 313 (1969).

Ch 69a A. S. Cheung and D. J. Wilson, "Quantum Vibrational Transition Probabilities in Atom-Diatomic Molecule Collisions", preprint.

Ch 69b J. C. Y. Chen, K. W. Chung, and P. J. Kramer, Phys. Rev. 184, 64 (1969).

Co 35 E. U. Condon and G. H. Shortley, Theory of Atomic Spectra (Cambridge University Press, Cambridge, 1935).

Co 61 J. W. Cooley, Math. Comp. 15, 363 (1961). See also SHARE Computer Program No. 1072.

Cr 65 D. S. F. Crothers and R. McCarroll, Proc. Phys. Soc. (London) 86, 753 (1965).

Cr 66 D. S. F. Crothers, Proc. Phys. Soc. (London) 87, 1003 (1966).

Cr 68 O. H. Crawford, Chem. Phys. Letters 2, 461 (1968).

Cu 69 C. F. Curtis and R. B. Bernstein, J. Chem. Phys. 50, 1168 (1969).

Da 62 N. Davidson, Statistical Mechanics (McGraw-Hill, New York, 1962), pp. 146-149.

Da 66 A. Dalgarno, R. J. W. Henry, and C. S. Roberts, Proc. Phys. Soc. (London) 88, 611 (1966).

Da 68 R. J. Damburg and S. Geltman, Phys. Rev. Letters 20, 485 (1968).

Da 69 D. R. Davis, J. A. Betts, J. M. White, and A. Kupper - mann, unpublished.

De 58 H. G. Dehmelt, Phys. Rev. 109, 381 (1958).

De 61 L. M. Delves, Nuclear Phys. 26, 136 (1961).

De 62 L. M. Delves, Nuclear Phys. 29, 326 (1962).

De 64 A. Degasperis, Il Nuovo Cimento [10] 34, 1667 (1964).

Di 67 D. J. Diestler and V. McKoy, J. Chem. Phys. 47, 454 (1967).

Di 68 D. J. Diestler, Ph.D. thesis, California Institute of Technology (Pasadena, 1968).

Di 68a D. J. Diestler and V. McKoy, J. Chem. Phys. 48, 2941 (1968).

Di 68b D. J. Diestler and V. McKoy, J. Chem. Phys. 48, 2951 (1968).

Dr 65 G. F. Drukarev, The Theory of Electron-Atom Collisions (Academic Press, London, 1965).

Du 67 J. L. G. Dugan, H. L. Richards, and E. E. Muschlitz, Jr., J. Chem. Phys. 46, 346 (1967).

Ec 30 C. Eckart, Phys. Rev. 35, 1303 (1930).

Ef 68 T. G. Efimenko, B. N. Zakhariev, and V. P. Zhigunov, Ann. Phys. (N.Y.) 47, 275 (1968).

Eh 68 H. Ehrhardt and F. Linder, Phys. Rev. Letters 21, 419 (1968).

Er 68 W. Erlewein, M. von Seggern, and J. P. Toennies, Z. Physik 211, 35 (1968).

Eu 66 B. C. Eu, Ph.D. Thesis, Brown University (Providence, 1966).

Eu 66a B. C. Eu and J. Ross, J. Chem. Phys. 44, 2467 (1966).

Ey 35 H. Eyring, J. Chem. Phys. 3, 107 (1935).

Fa 60 L. D. Fadeev, Zh. Eksperim. i Teor. Fiz. 39, 1459 (1960) [English translation: Soviet Physics-JETP 12, 1014 (1961)].

Fa 63 L. D. Fadeev, Mathematical Problems of the Quantum Theory of Scattering for a Three-Particle System (Trudy Matematicheslogo instituta imeni V. A. Steklova LXIX, U. S. S. R. Academy of Sciences, 1963) [English translation published by Atomic Energy Research Establishment, Harwell, 1964].

Fe 32 E. Feenberg, Phys. Rev. 40, 40 (1932).

Fe 50 E. Fermi, Progr. Theoret. Phys. (Kyoto) 5, 570 (1950).

Fe 55 H. Feshbach, in Statistical Aspects of the Nucleus, a conference held at Brookhaven National Laboratory Jan. 24-26, 1955 (Brookhaven National Laboratory, Upton, 1955), p. 59.

Fe 58 H. Feshbach, Ann. Phys. (N. Y.) 5, 357 (1958).

Fe 58a H. Feshbach, Ann. Rev. Nuc. Sci. 8, 49 (1958).

Fe 62 H. Feshbach, Ann. Phys. (N. Y.) 19, 287 (1962).

Fl 69 M. R. Flannery, J. Phys. B (London) 2, 913 (1969).

Fo 66 M. A. Fox, Proc. Phys. Soc. 88, 65 (1966).

Fo 67 M. A. Fox, Proc. Phys. Soc. 90, 585 (1967).

Fr 49 G. Friedlander, J. W. Kennedy, and J. M. Miller, Nuclear and Radiochemistry, second edition (John Wiley and Sons, New York, 1949), p. 341.

Fr 58 P. Franken, R. Sands, and J. Hobart, Phys. Rev. Letters 1, 52 (1958).

Ga 60 A. H. Gabriel and D. W. O. Heddle, Proc. Roy. Soc. (London) A258, 124 (1960).

Ga 64 M. Gailitis, Zh. Eksperim. i. Teor. Fiz. 47, 160 (1964) [English transl.: Soviet Physics-JETP 20, 107 (1965)].

Ga 65 M. Gailitis, in Effective Cross Sections for Collision of Electrons with Atoms: Atomic Collisions III, edited by V. I. Veldre (Latvian Academy of Sciences, Riga, 1965).

Ga 65a M. Gailitis, in Fourth International Conference on the Physics of Electronic and Atomic Collisions: Abstracts of Papers (Science Bookcrafters, Hastings-on-Hudson, 1965), p. 10.

Ge 60 S. Geltman, Phys. Rev. 119, 1283 (1960).

Ge 69 S. Geltman, Topics in Atomic Collision Theory (Academic Press, New York, 1969).

Go 49 S. Golden and A. M. Peiser, J. Chem. Phys. 17, 630, 842 (1949).

Go 54 S. Golden, J. Chem. Phys. 22, 1938 (1954).

Go 62 A. F. Gorshana and R. Y. Damburg, Opt. i Spektr. 12, 113 (1962) [English transl.: Optics and Spectry. 12, 55 (1962)].

Go 64 M. L. Goldberger and K. M. Watson, Collision Theory (John Wiley and Sons, New York, 1964).

Go 66 K. Gottfried, Quantum Mechanics (W. A. Benjamin, New York, 1966).

Gr 59 M. Grzinski, Phys. Rev. 115, 374 (1959).

Gr 66 E. F. Greene, A. L. Moursund, and J. Ross, Adv. Chem. Phys. 10, 135 (1966).

Gu 69 V. P. Gutschick, V. McKoy, and D. J. Diestler, "A New Boundary Value Technique for Solving the Close Coupled Equations for Inelastic Molecular Collisions," preprint.

Ha 52 W. Hauser and H. Feshbach, Phys. Rev. 87, 366 (1952).

Ha 62 J. B. Hasted and A. R. Lee, Proc. Phys. Soc. (London) 79, 702 (1962).

Ha 66 Y. Hahn, Phys. Rev. 148, 1088 (1966).

Ha 67 F. E. Harris, Phys. Rev. Letters 19, 173 (1967).

Ha 68 Y. Hahn, Phys. Rev. 169, 794 (1968).

Ha 69 F. E. Harris and H. H. Michels, "Expansion Technique for Inelastic Scattering", preprint.

Ha 69a S. Hara, "A Two-Center Approach in Low Energy Electron-H_2 Scattering", preprint.

He 68 R. J. Herbold, Ph.D. Thesis, Case Western Reserve University (Cleveland, 1968).

He 68a B. R. Henry and M. Kasha, Adv. Phys. Chem. 19, 161 (1968).

He 69 R. J. W. Henry and N. F. Lane, Phys. Rev. 183, 221 (1969).

Hi 36 J. O. Hirschfelder, H. Eyring, and B. Topley, J. Chem. Phys. 4, 170 (1936).

Hi 39 J. O. Hirschfelder and E. Wigner, J. Chem. Phys. 7, 616 (1939).

Hi 53 D. L. Hill and J. A. Wheeler, Phys. Rev. 89, 1140 (1953).

Hi 67 J. O. Hirschfelder and W. J. Meath, Adv. Chem. Phys. 12, 3 (1967), Section II.

Ho 61 M. Hoare, Mol. Phys. 4, 465 (1961).

It 69 Y. Itikawa and K. Takayanagi, J. Phys. Soc. Japan 26, 1254 (1969).

Ja 69 S. B. Jaffe and J. B. Anderson, J. Chem. Phys. 51, 1057 (1969).

Jo 60 T. L. John, Proc. Phys. Soc. (London) 76, 532 (1960).

Jo 61 H. S. Johnston and D. Rapp, J. Amer. Chem. Soc. 83, 1 (1961).

Jo 61a H. S. Johnston, Adv. Chem. Phys. 3, 131 (1961).

Jo 62 H. S. Johnston and P. Goldfinger, J. Chem. Phys. 37, 700 (1962).

Jo 62a H. S. Johnston and J. Heicklen, J. Phys. Chem. 66, 532 (1962).

Jo 63 H. S. Johnston and C. Parr, J. Amer. Chem. Soc. 85, 2544 (1963).

Jo 65 C. J. Joachain and M. H. Mittleman, Phys. Rev. 140, A432 (1965).

Jo 66 C. J. Joachain and M. H. Mittleman, Phys. Rev. 151, 7 (1966).

Jo 66a H. S. Johnston, Gas Phase Reaction Rate Theory (The Ronald Press, New York, 1966).

Jo 67 B. R. Johnson, Ph.D. Thesis, University of Illinois (Urbana, 1967).

Jo 67a B. R. Johnson, D. Secrest, W. A. Lester, and R. B. Bernstein, Chem. Phys. Letters, 1, 396 (1967).

Jo 68 B. R. Johnson and D. Secrest, J. Chem. Phys. 48, 4682 (1968).

Ka 66 I.-J. Kang and J. Sucher, Phys. Letters 20, 22 (1966).

Ka 67 I.-J. Kang and W. D. Foland, Phys. Rev. 164, 122 (1967).

Ka 68 M. Karplus and K. T. Tang, Discussions Faraday Soc. 44, 56 (1968).

Ke 58 J. Keck, J. Chem. Phys. 29, 410 (1958).

Ke 66 J. D. Kelley and M. Wolfsberg, J. Chem. Phys. 45, 3881 (1966).

Ke 67 J. C. Keck, Adv. Chem. Phys. 13, 85 (1967).

Ke 69 J. Kessler, Rev. Mod. Phys. 41, 3 (1969).

Kh 64 S. P. Khare and B. L. Moisiewitsch, in Atomic Collision Processes, edited by M. R. C. McDowell (North-Holland, Amsterdam, 1964), p. 49.

Kh 65 S. P. Khare and B. L. Moisewitsch, Proc. Phys. Soc. (London) 85, 821 (1965).

Ki 68 J. L. Kinsey, J. W. Riehl, and J. S. Waugh, J. Chem. Phys. 49, 5268 (1968).

Ki 68a Y.-K. Kim and M. Inokuti, Phys. Rev. 175, 176 (1968).

Ki 68b C. L. Kibby and R. E. Weston, Jr., J. Chem. Phys. 49, 4825 (1968).

Kl 64 F. Klein, A. Persky, and R. E. Weston, J. Chem. Phys. 41, 1799 (1964).

Ko 38 E. J. Konopinski and H. A. Bethe, Phys. Rev. 54, 130 (1938).

Ko 48 W. Kohn, Phys. Rev. 74, 1763 (1948).

Ko 54 W. Kohn, Rev. Mod. Phys. 26, 292 (1954).

Ko 61 Z. Kopal, Numerical Analysis (John Wiley and Sons, New York, 1961), section V-C.

Ko 65 W. Kolos and L. Wolniewicz, J. Chem. Phys. 43, 2429 (1965).

Ku 68 A. Kuppermann, J. K. Rice, and S. Trajmar, J. Phys. Chem. 72, 3894 (1968).

Ky 69 H. L. Kyle and M. R. C. McDowell, J. Phys. B (London) 2, 15 (1969).

La 58 A. M. Lane and R. G. Thomas, Rev. Mod. Phys. 30, 257 (1958).

La 65 L. D. Landau and E. M. Lifshitz, Quantum Mechanics: Nonrelativistic Theory, second edition (Pergamon Press, Oxford, 1965).

La 65a E. N. Lassettre, J. Chem. Phys. 43, 4479 (1965).

La 67 N. F. Lane and S. Geltman, Phys. Rev. 160, 53 (1967).

La 68 N. F. Lane and R. J. W. Henry, Phys. Rev. 173, 183 (1968).

La 68a E. N. Lassettre, A. Skerbele, M. A. Dillon, and K. J. Ross, J. Chem. Phys. 48, 5066 (1968).

La 69 N. F. Lane and S. Geltman, Phys. Rev. 184, 46 (1969).

Le 66 R. D. Levine, J. Chem. Phys. 44, 2046 (1966), especially eqs. (27) - (30).

Le 67 W. A. Lester and R. B. Bernstein, Chem. Phys. Letters 1, 207, 347 (1967).

Le 67a R. D. Levine, B. R. Johnson, J. T. Muckerman, and R. B. Bernstein, Univ. of Wisconsin Technical Report WIS-TCI-272 (1967); J. Chem. Phys. 49, 56 (1968).

Le 68 W. A. Lester and R. B. Bernstein, J. Chem. Phys. 48, 4896 (1968).

Le 68a R. D. Levine, Discussions Faraday Soc. 44, 81 (1968).

Le 68b R. D. Levine, J. Chem. Phys. 44, 51 (1968).

Le 68c R. D. Levine, B. R. Johnson, J. T. Muckerman, and R. B. Bernstein, J. Chem. Phys. 49, 56 (1968).

Le 68d D. J. LeRoy, B. A. Ridley, and K. A. Quickert, Discussions Faraday Soc. 44, 92 (1968).

Le 68e D. Lewis and S. H. Bauer, J. Amer. Chem. Soc. 90, 5390 (1968) .

Li 59 W. Lichten and S. Schultz, Phys. Rev. 116, 1132 (1959).

Li 63 W. Lichten, Phys. Rev. 131, 229 (1963).

Li 64 J. C. Light, J. Chem. Phys. 40, 3221 (1964).

Li 67 W. Lichten, Adv. Chem. Phys. 13, 41 (1967).

Li 68 J. C. Light, Discussions Faraday Soc. 44, 14 (1968).

Li 69 J. C. Light, C. C. Rankin, and D. Russell, Sixth International Conference on the Physics of Electronic and Atomic Collisions: Abstracts of Papers, edited by I. Amdur (M.I.T. Press, Cambridge, 1969), p. 574.

Lo 28 F. London, in Probleme der Modernen Physik : Sommerfeld Festschrift (S. Hirzel, Leipzig, 1928), p. 104.

Ma 40 J. L. Magee, J. Chem. Phys. 8, 687 (1940).

Ma 49 H. S. W. Massey, Rept. Progr. Phys. 12, 248 (1949).

Ma 51 R. A. Marcus, J. Phys. Colloid Chem. 55, 894 (1951).

Ma 52 H. S. W. Massey and E. H. S. Burhop, Electronic and Ionic Impact Phenomena (Clarendon Press, Oxford, 1952).

Ma 57 R. Marriott, Proc. Phys. Soc. (London) A70, 288 (1957).

Ma 58 R. Marriott, Proc. Phys. Soc. (London) 72, 121 (1958).

Ma 59 J. Mazur and R. J. Rubin, J. Chem. Phys. 31, 1395 (1959).

Ma 64 R. Marriott, Proc. Phys. Soc. (London) 83, 159 (1964).

Ma 64a R. Marriott, Proc. Phys. Soc. (London) 84, 877 (1964).

Ma 64b R. Marriott, in Atomic Collision Processes, edited by M. R. C. McDowell (North-Holland, Amsterdam, 1964), p. 114.

Ma 64c R. A. Marcus, J. Chem. Phys. 41, 610 (1964).

Ma 64d R. A. Marcus, J. Chem. Phys. 41, 2614 (1964).

Ma 65 R. A. Marcus, J. Chem. Phys. 43, 2658 (1965).

Ma 65a R. Marriott, Proc. Phys. Soc. (London) 86, 1041 (1965), 88, 83, 617 (1966).

Ma 65b R. A. Marcus, J. Chem. Phys. 43, 1598 (1965).

Ma 66 R. A. Marcus, J. Chem. Phys. 45, 2630 (1966).

Ma 66a R. A. Marcus, J. Chem. Phys. 45, 4493 (1966).

Ma 67 R. A. Marcus, J. Chem. Phys. 46, 959 (1967).

Ma 68 R. A. Marcus, Discussions Faraday Soc. 44, 7 (1968).

Ma 68a R. A. Marcus, Discussions Faraday Soc. 44, 167 (1968).

Ma 69 K. C. Mathur, A. N. Tripathi, and S. K. Joshi, Phys. Rev. 184, 242 (1969).

Mc 65 M. R. C. McDowell, in Fourth International Conference on the Physics of Electronic and Atomic Collisions (Science Bookcrafters, Hudson-on-Hastings, New York, 1965), p. 20.

Mc 69 E. A. McCullough, Jr. and R. E. Wyatt, J. Chem. Phys. 51, 1253 (1969).

Me 61 A. Messiah, Quantum Mechanics, Vol. II (John Wiley and Sons, New York, 1961).

Mi 57 W. F. Miller and R. L. Platzman, Proc. Phys. Soc. (London) 70, 299 (1957).

Mi 61 M. H. Mittleman, Phys. Rev. 122, 1930 (1961).

Mi 62 M. H. Mittleman, Phys. Rev. 130, 373 (1962).

Mi 64 M. H. Mittleman, Ann. Phys. (N. Y.) 28, 430 (1964).

Mi 65 D. A. Micha, Arkiv Fysik 30, 425, 437 (1965).

Mi 66 F. H. Mies and M. Krauss, J. Chem. Phys. 45, 4455 (1966).

Mi 67 H. H. Michels and F. E. Harris, Phys. Rev. Letters 19, 885 (1967).

Mi 68 K. J. Miller and M. Krauss, J. Chem. Phys. 48, 2611 (1968).

Mi 69 W. H. Miller, J. Chem. Phys. 50, 407 (1969).

Mo 29 P. M. Morse, Phys. Rev. 34, 57 (1929).

Mo 48 N. F. Mott and I. N. Sneddon, Wave Mechanics and its Applications (Clarendon Press, Oxford, 1948).

Mo 53 P. M. Morse and H. Feshbach, Methods of Theoretical Physics, Part I (McGraw-Hill, New York, 1953).

Mo 62 E. M. Mortensen and K. S. Pitzer, The Transition State, Chem. Soc. (London), Special Publ. 16, 57 (1962).

Mo 64 A. L. Moursund, Ph.D. Thesis, Brown University, (Providence, 1964).

Mo 65 N. F. Mott and H. S. W. Massey, The Theory of Atomic Collisions, third edition (Clarendon Press, Oxford, 1965).

Mo 66 M. C. Moulton and D. R. Herschbach, J. Chem. Phys. 44, 3010 (1966).

Mo 66a D. J. T. Morrison and M. R. H. Rudge, Proc. Phys. Soc. (London) 89, 45 (1966).

Mo 67 D. J. T. Morrison and M. R. H. Rudge, Proc. Phys. Soc. (London) 91, 565 (1967).

Mo 67a K. Morokuma, L. Pedersen, and M. Karplus, J. Amer. Chem. Soc. 89, 5064 (1967).

Mo 68 E. M. Mortensen, J. Chem. Phys. 48, 4029 (1968).

Mo 68a B. L. Moiseiwitsch and S. J. Smith, Rev. Mod. Phys. 40, 238 (1968).

Mo 69 H. R. Moustafa Moussa, F. J. de Heer, and J. Schutten, Physica 40, 517 (1969).

Mu 69 J. N. Murrell, Mol. Phys. 16, 601 (1969).

Ne 66 R. Newton, Scattering Theory of Waves and Particles (McGraw-Hill, New York, 1966).

Ne 68 R. K. Nesbet, Phys. Rev. 175, 134 (1968).

Ni 64 E. E. Nikitin, Mol. Phys. 8, 473 (1964).

Ni 65 E. E. Nikitin, Teor. i Eksperim. Khim. 1, 135 (1965) [English transl.: Theor. Exptl. Chem. 1, 83 (1965)].

Ni 65a E. E. Nikitin, Teor. i Eksperim. Khim. 1, 428 (1965) [English transl.: Theor. Exptl. Chem. 1, 275 (1965)].

Ni 67 E. E. Nikitin, in Fast Reactions and Primary Processes in Chemical Kinetics, edited by S. Claeson (Almqvist and Wiksell, Stockholm, 1967), p. 165.

No 58 R. Novick and H. E. Peters, Phys. Rev. Letters 1, 54 (1958).

Ny 65 C. Nyeland and T. A. Bak, Trans. Faraday Soc. 61, 1293 (1965).

Oc 63 V. I. Ochkur, Zh. Eksperim. i Teor. Fiz. 45, 734 (1963) [English transl.: Soviet Physics-JETP 18, 503 (1964)].

Oc 65 V. I. Ochkur, Optics and Spectroscopy 19, 258 (1965).

Oc 69 V. I. Ochkur, unpublished talk delivered at the Sixth International Conference on the Physics of Electronic and Atomic Collisions (Boston, 2 Aug. 1969).

Od 69 T. J. Odiorne and P. R. Brooks, "Molecular Beam Reaction of K with HCl: Evidence for an Activation Energy", preprint.

Op 28 J. R. Oppenheimer, Phys. Rev. 32, 361 (1928).

Os 63 A. I. Osipov, Bull. Acad. Sci. USSR Phys. Ser. 27, 1087 (1963).

Pa 64 J. F. Paulson, Ann. Geophys. 20, 75 (1964).

Pa 69 C. A. Parr, Ph.D. Thesis, California Institute of Technology (Pasadena, 1969).

Pe 61 M. M. Pennell and L. M. Delves, Math. Comp. 15, 243 (1961).

Pe 65 P. Pechukas and J. C. Light, J. Chem. Phys. 42, 3281 (1965).

Pe 66 P. Pechukas, J. C. Light, and C. Rankin, J. Chem. Phys. 44, 794 (1966).

Pe 66a P. Pechukas, Ph.D. Thesis, University of Chicago (Chicago, 1966).

Pe 68 J. F. Perkins, Phys. Rev. 173, 164 (1968).

Pe 69 P. Pechukas, Phys. Rev. 181, 174 (1969).

Pe 69a A. Persky and A. Kuppermann, unpublished.

Po 55 J. C. Polanyi, J. Chem. Phys. 23, 1505 (1955).

Po 69 R. N. Porter and L. M. Raff, J. Chem. Phys. 50, 5216 (1969).

Pr 64 L. Presnyakov, I. Sobelman, and L. Vainshtein, in Atomic Collision Processes, edited by M. R. C. McDowell (North Holland, Amsterdam, 1964), p. 243.

Pr 66 L. Presnyakov, I. Sobelman, and L. Vainshtein, Proc. Phys. Soc. (London) 89, 511 (1966).

Pu 63 R. T. Pu, University of California Lawrence Radiation Laboratory Technical Report UCRL-10878 (Berkeley, 1963).

Ra 32 C. Ramsauer and R. Kollath, Ann. Phys. 12, 529 (1932).

Ra 62 D. Rapp and W. E. Francis, J. Chem. Phys. 37, 263 (1962).

Ra 68 C. C. Rankin, Ph.D. Thesis, University of Chicago (Chicago, 1968).

Ra 69 C. C. Rankin and J. C. Light, J. Chem. Phys. 51, 1701 (1969).

Ri 33 O. K. Rice, J. Chem. Phys. 1, 625 (1933).

Ri 61 O. K. Rice, J. Phys. Chem. 65, 1588 (1961).

Ri 67 M. E. Riley, Ph.D. Thesis, California Institute of Technology (Pasadena, 1967).

Ri 68 M. E. Riley and A. Kuppermann, Chem. Phys. Letters 1, 537 (1968).

Ri 68a J. K. Rice, A. Kuppermann, and S. Trajmar, J. Chem. Phys. 48, 945 (1968).

Ri 69 J. K. Rice, Ph.D. Thesis, California Institute of Technology (Pasadena, 1969).

Ri 70 J. K. Rice, D. G. Truhlar, A. Kuppermann, D. C. Cartwright, and S. Trajmar, article in preparation.

Ro 33 N. Rosen, J. Chem. Phys. 1, 319 (1933).

Ro 57 M. E. Rose, Elementary Theory of Angular Momentum (John Wiley and Sons, New York, 1957).

Ro 67 L. S. Rodberg and R. M. Thaler, Introduction to the Quantum Theory of Scattering (Academic Press, New York, 1967).

Ru 60 K. Rubin, J. Perel, and B. Bederson, Phys. Rev. 117, 151 (1960).

Ru 65 M. R. H. Rudge, Proc. Phys. Soc. (London) 85, 607 (1965).

Ru 65a M. R. H. Rudge, Proc. Phys. Soc. (London) 86, 763 (1965).

Ru 69 K. Rubin, B. Bederson, M. Goldstein, and R. E. Collins, Phys. Rev. 182, 201 (1969).

Sa 61 A. Salmona and M. J. Seaton, Proc. Phys. Soc. (London) 77, 617 (1961).

Sc 55 L. I. Schiff, Quantum Mechanics, second edition (McGraw-Hill, New York, 1955).

Sc 65 B. L. Scott, Phys. Rev. 140, A 699 (1965).

Sc 65a W. R. Schulz and D. J. LeRoy, J. Chem. Phys. 42, 3869 (1965).

Se 61 M. J. Seaton, Proc. Phys. Soc. (London) 77, 174 (1961).

Se 66 D. Secrest and B. R. Johnson, J. Chem. Phys. 45, 4556 (1966).

Se 66a R. V. Serauskas, Ph. D. Thesis, Northwestern University (Evanston, 1966).

Se 66b R. V. Serauskas and E. W. Schlag, J. Chem. Phys. 45, 3706 (1966).

Sh 59 I. Shavitt, University of Wisconsin Theoretical Chemistry Laboratory Technical Report WIS-AEC-23 (1959).

Sh 59a I. Shavitt, J. Chem. Phys. 31, 1359 (1959).

Sh 62 T. E. Sharp and H. S. Johnston, J. Chem. Phys. 37, 1541 (1962).

Sh 63 H. Shin, J. Chem. Phys. 39, 2934 (1963).

Sh 65 T. E. Sharp and D. Rapp, J. Chem. Phys. 43, 1233 (1965).

Sh 68 I. Shavitt, R. M. Stevens, F. L. Minn, and M. Karplus, J. Chem. Phys. 48, 2700 (1968).

Sh 68a I. Shavitt, J. Chem. Phys. 49, 4048 (1968).

Sh 68b I. Shavitt, private communication.

Sl 59 N. B. Slater, Theory of Unimolecular Reactions (Cornell University Press, Ithaca, 1959), pp. 57-58.

Sl 64 I. H. Sloan, Proc. Roy. Soc. (London) A281, 151 (1964).

Sl 68 I. H. Sloan and E. J. Moore, J. Phys. B (London) 1, 414 (1968).

Sm 60 K. Smith, W. E. Miller, and A. J. P. Mumford, Proc. Phys. Soc. (London) 76, 559 (1960).

Sm 60a K. Smith, Phys. Rev. 120, 845 (1960).

Sm 61 K. Smith and P. G. Burke, Phys. Rev. 123, 174 (1961).

Sm 62 K. Smith, R. P. McEachran, and P. A. Fraser, Phys. Rev. 125, 553 (1962).

So 61 W. B. Somerville, Proc. Phys. Soc. (London) 78, 695 (1961).

So 62 W. B. Somerville, Proc. Phys. Soc. (London) 80, 806 (1962).

So 63 W. B. Somerville, Proc. Phys. Soc. (London) 82, 446 (1963).

St 63 A. L. Stewart and T. G. Webb, Proc. Phys. Soc. (London) 82, 532 (1963).

St 64 R. M. St. John, F. L. Miller, and C. C. Lin, Phys. Rev. 134, A888 (1964).

Su 62 J. H. Sullivan, J. Chem. Phys. 36, 1925 (1962).

Su 63 J. H. Sullivan, J. Chem. Phys. 39, 3001 (1963).

Su 67 R. J. Suplinskas and J. Ross, J. Chem. Phys. 47, 321 (1967).

Ta 54 K. Takayanagi, Progr. Theor. Phys. 11, 557 (1954).

Ta 67 A. J. Taylor and P. G. Burke, Proc. Phys. Soc. (London) 92, 336 (1967).

Ta 69 K. T. Tang, B. Kleinman, and M. Karplus, J. Chem. Phys. 50, 1119 (1969).

Te 61 A. Temkin and J. C. Lamkin, Phys. Rev. 121, 788 (1961).

Th 66 B. A. Thrush, Chem. in Britain 2, 287 (1966).

Th 68 B. A. Thrush, in Chemische Elementar prozesse, edited by H. Hartmann (Springer-Verlag, Berlin, 1968).

Ti 64 R. B. Timmons and R. E. Weston, J. Chem. Phys. 41, 1654 (1964).

Tr 68 D. G. Truhlar, D. C. Cartwright, and A. Kuppermann, Phys. Rev. 175, 113 (1968).

Tr 69 D. G. Truhlar and A. Kuppermann, J. Phys. Chem. 73, 1722 (1969).

Tr 69a D. G. Truhlar and A. Kuppermann, in Sixth International Conference on the Physics of Electronic and Atomic Collisions: Abstracts of Papers, edited by I. Amdur (M.I.T. Press, Cambridge, 1969), p. 247.

Tr 70 D. G. Truhlar, J. K. Rice, A. Kuppermann, S. Trajmar, and D. C. Cartwright, Phys. Rev.,to be published.

Vo 60 H. Van Regemorter, Mon. Not. Roy. Astron. Soc. 121, 213 (1960).

Va 63 L. Vainshtein, L. Presnyakov, and I. Sobelman, Zh. Eksperim. i Teor. Fiz. 45, 2015 (1963) [English transl.: Soviet Physics-JETP 18, 1383 (1964)] .

Va 64 L. Vainshtein, V. Opykhtin, and L. Presnyakov, Zh. Ekeperim. i Teor. Fiz. 47, 2306 (1964) [English transl.: Soviet Physics-JETP 20, 1542 (1965)].

Va 68 J. van Blerkom, J. Phys. B (London) 1, 423 (1968).

Vo 67 H. C. Volkin, Phys. Rev. 155, 1177 (1967).

Vo 68 H. C. Volkin, Ann. Phys. (N. Y.) 46, 453 (1968).

Vr 67 L. Vriens, Phys. Rev. 160, 100 (1967).

Vr 68 L. Vriens, J. A. Simpson, and S. R. Mielczarek, Phys. Rev. 165, 7 (1968).

Wa 53 K. M. Watson, Phys. Rev. 89, 575 (1953).

Wa 57 K. M. Watson, Phys. Rev. 105, 388 (1957).

Wa 62 F. T. Wall and R. N. Porter, J. Chem. Phys. 36, 3256 (1962).

Wa 67 P. Warneck, J. Chem. Phys. 46, 513 (1967).

Wa 69 K. M. Watson, in Atomic Physics, edited by B. Bederson, V. W. Cohen, and F. M. J. Pichanik (Plenum Press, New York, 1969), p. 333.

We 37 V. Weisskopf, Phys. Rev. 52, 295 (1937).

We 59 R. E. Weston, J. Chem. Phys. 31, 892 (1959).

We 67 A. W. Weiss, J. Res. Natl. Bur. Std. (U.S.) 71A, 163 (1967).

We 67a A. A. Westenberg and N. de Haas, J. Chem. Phys. 47, 1393 (1967).

We 68 R. E. Weston, Discussions Faraday Soc. 44, 163 (1968).

Wh 66 J. M. White, Ph.D. Thesis, University of Illinois (Urbana, 1966).

Wi 32 E. P. Wigner, Z. physik. Chem. (Leipzig) B19, 203 (1932).

Wi 47 E. P. Wigner and L. Eisenbud, Phys. Rev. 72, 29 (1947).

Wi 49 E. P. Wigner, Amer. J. Phys. 17, 99 (1949).

Wi 55 E. P. Wigner, Amer. J. Phys. 23, 371 (1955).

Wi 62 G. M. Wieder and R. A. Marcus, J. Chem. Phys. 37, 1835 (1962).

Wi 65 R. L. Wilkins, J. Chem. Phys. 42, 806 (1965).

Wi 68 N. W. Winter, D. J. Diestler, and V. McKoy, J. Chem. Phys. 48, 1879 (1968).

Wi 69 A. J. Williams III and J. P. Doering, J. Chem. Phys. 51, 2859 (1969).

Wo 51 L. Wolfenstein, Phys. Rev. 82, 690 (1951).

Wo 69 F. A. Wolf and J. L. Haller, "The Statistical Theory of Four-Body, Bimolecular, Resonant Ion-Molecule Reactions", preprint.

Wu 62 T.-Y. Wu and T. Ohmura, Quantum Theory of Scattering (Prentice-Hall, Englewood Cliffs, 1962).

Ya 54 I. Yasumori and S. Sato, J. Chem. Phys. 22, 1938 (1954).

Ya 59 I. Yasumori, Bull. Chem. Soc. Japan 32, 1103, 1110 (1959).

Za 63 R. N. Zare and J. K. Cashion, University of California E. O. Lawrence Radiation Laboratory Technical Report UCRL-10881 (July, 1963).

Ze 67 D. F. Zetik and F. A. Matsen, J. Mol. Spectry. 24, 122 (1967).

PART TWO

ELECTRON SCATTERING BY H_2 WITH AND WITHOUT VIBRATIONAL EXCITATION

I. QUANTUM MECHANICAL THEORY*

---

*This is an expanded version of an article to be published. It was written by D. G. Truhlar and J. K. Rice.

A. INTRODUCTION

An electron that collides with a molecule can leave it in a vibrationally excited state. Although this process has received considerable attention, there has been no previous calculation of the differential scattering cross sections for electron-molecule collisions with vibrational excitation of the ground state.

In this paper, we describe a method that is used for such calculations on the scattering of electrons by molecular hydrogen in a series of papers,[1] of which this is the first. Further we present some results of our calculations for differential and integral cross sections. (The differential cross section--DCS--is differential in the angle of scattering and the integral cross section--Q--is the integral of the DCS over all possible scattering volume elements.)

The most complete previous calculations of the integral cross sections are those of Takayanagi[2] and of Breig and Lin.[3] Using a plane wave approximation, Breig and Lin calculated the scattering due to the long range forces. They obtained the necessary vibrational matrix elements of the electric quadrupole moment and electronic polarizability from experimental data on the intensities of Raman spectra. That data can be used only for one quantum transitions, so in our treatment we have instead obtained the matrix elements by accurate numerical integration using properties calculated by Kolos and Wolniewicz.[4] We have extended Brieg and Lin's scattering treatment to simultaneously include contributions from long range and short range interactions.

The treatment of the short range interactions basically follows that used earlier by Carson.[5] We have used this extended method (a first Born calculation for all important interactions augmented by polarization) to calculate differential and integral cross sections for the elastic scattering and the $0 \rightarrow 1$, $0 \rightarrow 2$, and $0 \rightarrow 3$ vibrational excitations and to study the effects of various parts of the potential on the scattering cross section. We have also examined the inclusion of exchange scattering in the theoretical description and the resulting cross sections by means of the Ochkur-Ridge relation.[6,7]

We have compared our results for elastic scattering at impact energy $E < 20$ eV with some partial wave method calculations of Wilkins and Taylor[8] and Tully and Berry[9] which do not include the polarization, with some partial wave method calculations of Henry and Lane[10] which include all important interactions, with some older theoretical calculations of elastic cross sections,[11-14] and with experiments on the total scattering cross section.[15] We also compare our differential cross sections for elastic scattering to the $E = 3.5$ eV experimental data of Ehrhardt et al.[16] and to the available high-energy experimental data ($E > 100$ eV).[17-20] In papers II and III of this series we compare the theory to all the experimental data (including that of Trajmar et al.[1] and Ehrhardt et al.[16]) for DCS's in the 7-100 eV energy region for elastic scattering and vibrational excitation and to all the experimental data (it is all for $E < 82$ eV) for the magnitudes of the vibrational excitation cross sections. We present in the present paper the first estimates

of the elastic and vibrational excitation integral cross sections for $E \geq 90$ eV. Our predictions of absolute values of elastic scattering and vibrational excitation integral scattering cross sections at lower energies are summarized in papers II and III.

Previous calculations of vibrational excitation cross sections (e.g., Refs. 2-3, 5) were concerned with integral cross sections. In the most recent of those investigations it was shown[3] that it is sufficient to take into account only the long range potentials to obtain cross sections of the right magnitude. We will show that such calculations are not sufficient for calculating the DCS. An improper treatment of the forces at short range can lead to the wrong angular dependence of the cross section at small scattering angle and order of magnitude errors at large scattering angles.

The plane wave approximation used here is expected to be valid at high energies.[21a] We do calculations not only at high energies but also at low and intermediate energies where distortion of the scattering waves might be important. Gerjuoy and Stein[22] argue that when the scattering is dominated by the long range part of the potential the plane wave approximation is valid even at low energy because most of the contribution to the transition integral comes from large electron-molecule separations at low energy. But Takayanagi and Geltman[23] argue that s, p, and d waves (where the partial waves are named according to the orbital angular momentum of the scattering electron with respect to the center-of-mass of the molecule) are also important and that s and p waves are appreciably distorted below about 6 eV (they did

not consider higher energies). In section C we present the extension of our method which is necessary for including some distortion in the s and p waves. A calculation using this method would be a better test of the importance of distortion than previous distorted wave calculations[2] because the present treatment includes the long and short range forces simultaneously and does not completely neglect any partial waves.

B. QUANTUM MECHANICAL THEORY OF ELECTRON-MOLECULE SCATTERING IN THE GROUND ELECTRONIC STATE NEGLECTING DISTORTION

The most complete and straightforward (and usually impractical at present) way to treat electron-molecule scattering is to consider all important molecular states explicitly and solve the full set of coupled equations. Aside from this, several treatments of the nuclear motion in electron-molecule scattering have already been given.[3, 24-33] We treat the problem by computing an approximate local potential $V(\hat{r}, \hat{R})$ representing the interaction of the electron (at position $\hat{r}$ with respect to the center-of-mass of the molecule) with the molecule. This potential depends parametrically upon the nuclear positions ($\hat{R}$ is a vector fixed in the molecule; in particular, $\hat{R}$ is the vector from one nucleus to the other). We treat the scattering problem as the collision of a particle interacting with a rotating vibrator by the interaction potential $V(\hat{r}, \hat{R})$. In this context polarization is treated by modifying the effective potential. Another effective potential can be added to simulate the effects of exchange of the scattering electron and the bound electrons,[14, 34-36] or these effects can be included by using an Ochkur-Bonham-like relation[6, 7] between the exchange and direct scattering amplitudes. In our calculations the latter method was applied. We now consider the interaction potential and the scattering calculation.

1. Potentials

The interaction energy between an electron and a hydrogen molecule can be written

$$V(\underset{\sim}{r}, \underset{\sim}{R}) = V^1(\underset{\sim}{r}, \underset{\sim}{R}) + V^2(\underset{\sim}{r}, \underset{\sim}{R}) \tag{1}$$

where V^1 is the first order potential (i.e., the interaction energy between the electron and the unperturbed molecule) and V^2 is the polarization energy (i.e., the correction to V^1 due to the relaxation of the molecule, in particular its electronic charge distribution, in the presence of the electron). The static potential V^1 is given by[37]

$$V^1(\underset{\sim}{r}, \underset{\sim}{R}) = V^n(\underset{\sim}{r}, \underset{\sim}{R}) + V^e(\underset{\sim}{r}, \underset{\sim}{R}) \tag{2}$$

where

$$V^n(\underset{\sim}{r}, \underset{\sim}{R}) = \int |\Psi_g(\underset{\sim}{r}_1, \underset{\sim}{r}_2; \underset{\sim}{R})|^2 \left(-\frac{1}{r_{0A}} - \frac{1}{r_{0B}}\right) d\underset{\sim}{r}_1 d\underset{\sim}{r}_2 \tag{3}$$

and

$$V^e(\underset{\sim}{r}, \underset{\sim}{R}) = \int |\Psi_g(\underset{\sim}{r}_1, \underset{\sim}{r}_2; \underset{\sim}{R})|^2 \left(\frac{1}{r_{01}} + \frac{1}{r_{02}}\right) d\underset{\sim}{r}_1 d\underset{\sim}{r}_2 \tag{4}$$

Ψ_g is the unperturbed ground state electronic wavefunction of H_2, $\underset{\sim}{r}_1$ and $\underset{\sim}{r}_2$ are the coordinates of the bound electrons, $r_{0i} \equiv |\underset{\sim}{r} - \underset{\sim}{r}_i|$, and r_{0A} and r_{0B} are the distances of the nuclei from the scattering electron. The potential V^1 has been calculated accurately for H_2 at one R by Ardill and Davison.[38] However, we require the dependence of V^1 on R. A simple approximation used by Carson[5] is to calculate

the potential due to two spherically symmetric atomic charge distributions centered at the two nuclei. The atomic charge distributions have R-dependent screening parameters.[39] We call this potential V^C. The first two terms in the multipole expansion of V^C are calculated:

$$V^C(\underset{\sim}{r}, \underset{\sim}{R}) \cong V_0^C(r, R) + V_2^C(r, R)\, P_2(\hat{r}\cdot\hat{R}) \tag{5}$$

Unfortunately, such a charge distribution does not have a quadrupole moment and thus V^C (and every term in its multipole expansion) decreases exponentially in magnitude at large r. In particular, taking the atomic charge density of atom A to be proportional to $e^{-2\,Zr_{0A}}$, we obtain for $r > \frac{R}{2}$:

$$V_0^C(r, R) = \frac{2e^{-Zy}}{ZyR}\left[\, ZR\cosh ZR - (3 + Zy)\sinh ZR\right] \tag{6}$$

and

$$\begin{aligned} V_2^C(r, R) = \frac{10e^{-Zy}}{yR}\Big\{ & R\cosh ZR - y\sinh ZR + \frac{3}{yZR}\left[(y^2+R^2)\cosh ZR\right. \\ & \left. - 3yR\sinh ZR\right] + \frac{3}{y^2Z^2R^2}\left[(R^3+8y^2R)\cosh ZR\right. \\ & \left. - (y^3+8yR^2)\sinh ZR\right] + \frac{3}{(yZR)^3}\left[21y^2R^2\cosh ZR\right. \\ & \left. - 8yR(y^2+R^2)\sinh ZR\right] + \frac{63}{y^2Z^4R^2}\left[R\cosh ZR\right. \end{aligned}$$

$$-y \sinh ZR] - \frac{63}{y^2 Z^5 R^2} \sinh ZR\} \qquad (7)$$

where $y = 2r$. The potentials for $r < \frac{R}{2}$ are given by these expressions with y and R interchanged. For the hydrogen atom exponent Z, we used[40]

$$Z = 1.0 + 0.6875 \exp(-1.0002343\,R). \qquad (8)$$

This is an approximate fit to the results of exponent-optimized minimum basis set calculations on H_2 and is much more accurate than the linear Z(R) dependence which Carson[5] used.

Note that neither V_0^C nor V_2^C can be written as the product of a function of r times a function of R. This is illustrated in Fig. 1, which shows (parts a and d) the change of shape of V_L^C (L = 0, 2) as R varies. V_0^C (r, R_e) agrees quite well with the accurate spherically symmetric potential computed from a one-center wavefunction by Ardill and Davison[38] (cf. Lane and Geltman[35] for a graphical comparison of V_0^C with the potential from a slightly less accurate single-center calculation).

Gerjuoy and Stein[22] have pointed out the importance of the quadrupolar interaction term for electron-molecule collisions causing rotational excitation. We expect that this interaction, because of its long range, is important for vibrational excitation problems also. Thus we have completed the V^1 potential for H_2 by adding to the short range terms (6) and (7) an electron-molecular quadrupole interaction

term

$$V^{Q}(\underset{\sim}{r}, \underset{\sim}{R}) = -\frac{Q(R)}{2r^3} f(r) P_2(\hat{r}\cdot\hat{R}) \tag{9}$$

where Q(R) is the molecular quadrupole moment, a_Q is a "cutoff radius", and f(r) is a "cutoff function" which is 1 for $r > a_Q$. Note that some authors define the quadrupole moment to be a factor of two smaller than the one used here. Four forms for f(r) were considered; for $r < a_Q$ they are: $f^{B'} = (r/a_Q)^3$; $f^{B} = (r/a_Q)^4$; $f^{C} = 0$; $f^{F} = 1$. For the first three, the best a_Q was determined by the criterion that

$$V_2^1(r, R_e) \equiv V_2^C(r, R_e) - \frac{Q(R_e)}{2r^3} f(r) \tag{10}$$

give the smallest average deviation from the accurate $V_2^1(r, R_e)$ published by Ardill and Davison[38] (their potential includes the quadrupole interaction automatically). For the comparison we had to take $Q(R_e) = 0.978$ a.u. and we considered various values of a_Q in increments of $0.1\ a_0$. (For our scattering calculations, we took Q and its dependence on R from the accurate calculations of Kolos and Wolniewicz.[4]) Table I shows how good a fit could be obtained for each form. We will consider scattering off all four forms of the potential to enable us to judge previous work but the B′ potential with $a_Q = 2.0\ a_0$ agrees best with the accurate potential and is considered most theoretically justifiable for use in conjunction with the Carson potential. Figure 1b shows a comparison of this V_2^1 potential with the Ardill-Davison one. The linear dependence of Q on R used by Breig and Lin[3]

for $\Delta v = 1$ transitions (v is the vibrational quantum number) would not give reliable results for $\Delta v > 1$. Figure 1b also shows the R dependence of the theoretically most justifiable V_2^1. Since the shape of the r dependence of V_2^1 depends on R, a product form would not be a good approximation in this case either.

The second order potential V^2 is more difficult to evaluate. However, it was pointed out by Dalgarno and Moffett[27] that polarization is very important for excitation of nuclear motion by electron impact. They considered rotational excitation only. Breig and Lin[3] and Takayanagi[2] pointed out the importance of the polarization potential for vibrational excitation and Breig and Lin showed that it is more important than the quadrupole interaction for vibrational excitation by low energy electrons. A close coupling calculation including excited electronic states would automatically include the polarization. However, we will include the effect as an additional effective potential. The exact form of this potential could be chosen in at least two different ways. We could choose the polarization potential which, when included in our scattering calculation, gives the best agreement with experiment. Or we could choose the polarization potential from a consideration of the electronic interactions. The former approach is unsatisfactory in that adjustment of V^2 could compensate for any inherent inaccuracies of the scattering approximations (see sections 2 and 5 below) used here. Then the "best" polarization potential might have little physical significance. The latter alternative therefore seems likely to lead to better understanding of the scattering process.

In the adiabatic approximation (V^2 calculated for each $\underset{\sim}{r}$ and $\underset{\sim}{R}$ for fixed nuclei and a stationary scattering electron) it is well known that

$$V^2(\underset{\sim}{r}, \underset{\sim}{R}) \underset{r \to \infty}{\sim} -\frac{\alpha(R)}{2r^4} - \frac{\alpha'(R)}{2r^4} P_2(\hat{r} \cdot \hat{R}) \equiv V^2_{aF}(\underset{\sim}{r}, \underset{\sim}{R}) \tag{11}$$

$$V^2_{aF}(\underset{\sim}{r}, \underset{\sim}{R}) = V^2_{0,aF}(r, R) + V^2_{2,aF}(r, R) P_2(\hat{r} \cdot \hat{R}) \tag{12}$$

where α and α' are given in terms of the static dipole polarizability of the molecule parallel ($\alpha_{||}$) and perpendicular ($\alpha_{\perp}$) to the internuclear axis by

$$\alpha = \frac{1}{3}(\alpha_{||} + 2\alpha_{\perp}) \qquad \alpha' = \frac{1}{3}(\alpha_{||} - \alpha_{\perp}) \tag{13}$$

The expression (11) holds for r large enough and E (the scattering electron kinetic energy) low enough. But when r is small a more complicated expression can be obtained for the adiabatic polarization potential which is finite everywhere and nonzero at $r = 0$.[41] Further, except for $r = \infty$, the electron relative velocity is not zero and we must consider effects due to the dynamic polarizability not being equal to the static polarizability. These affects are particularly important when r is small enough that the scattering electron is penetrating the bound electronic charge distribution. Then the increase in electron velocity due to the nuclear attraction is so strong that the first correction to the adiabatic approximation is independent of E. This first correction[42-47,36] amounts essentially to cutting off the potential for small

r. In particular, it has been shown [45,36,48] that coupling of the scattering electron's kinetic energy with the motion of the electrons in the perturbed target leads to an approximate potential which is everywhere repulsive for H and He targets, which exactly cancels the attractive adiabatic polarization potential at $r = 0$, and which decreases asymptotically as r^{-6}. This nonadiabatic cutoff of the polarization potential at small r means that the scattering in the lowest partial waves, which are the ones for which the electron can penetrate appreciably to small r, is treated poorly by the adiabatic approximation at energies above about 20-25 eV.[49,50] In fact, the detailed calculations of Poe and Chang[51] show significant deviation from adiabaticity even in the 5-20 eV range. We will include the nonadiabatic cutoff at small r in our treatment and will also do calculations which show the effect of not including it. Including the nonadiabatic effects (β_1) and also the second leading term in the adiabatic polarization potential, i. e., the quadrupole polarizability (α_q), gives for the long range interaction

$$V_0^2 \underset{r\to\infty}{\sim} -\frac{\alpha}{2r^4} - \left(\frac{\alpha_q}{2} - 3\beta_1\right)\frac{1}{r^6} \tag{14}$$

Since Khare examined the quadrupole polarizability of He and found its inclusion in an elastic scattering calculation to have only a small effect,[52] we will neglect it and we will consider the effect of nonadiabaticity only at small r. That is, we take

$$V^2(\underset{\sim}{r}, \underset{\sim}{R}) = V^2_{0,aF}(r, R)\, g(r)$$

$$+ V_{2,aF}^{2}(r, R)\, g'(r)\, P_2(\hat{r}\cdot\hat{R}) \tag{15}$$

where g and $g' \to 1$ for $r \to \infty$ and they negate the singularity in V_{aF}^2 at small r. Khare and Moisiewitsch argued[49, 13] that a treatment of this type can be used up to very high energies because the force is so long range. This means that much of the cross section comes from higher partial waves for which the long range part of the polarization potential as determined by the static dipole polarizability should be a good approximation. They used the static polarizability in an expression of the form (15) up to an impact energy of 700 eV. Several forms have been commonly used[3] for g(r) and are considered here:

$$g^{A}(r) = r^4(r^2 + a_P^2)^{-2} \tag{16}$$

$$g^{B}(r) = \begin{cases} 1 & r > a_P \\ r^4 a_P^{-4} & r \leq a_P \end{cases} \tag{17}$$

$$g^{C}(r) = \begin{cases} 1 & r > a_P \\ 0 & r \leq a_P \end{cases} \tag{18}$$

$$g^{Dn}(r) = 1 - \exp(-r^n/a_P^n) \tag{19}$$

$$g^{F}(r) = 1$$

The function g' is given similarly but in terms of the cutoff parameter a_P'. Because they do not show the nonadiabatic cutoff to zero, forms

A, B and F are not realistic. (However, making this cutoff might have given in some previous calculations an effective potential which appeared too repulsive because exchange was neglected.[35, 36]) For the same a_p, the Dn form involves a significantly shallower attractive well than the other four. Comparison with the recent nonadiabatic calculation of Lane and Henry[47] for H_2 shows that the nonadiabatic polarization potential resembles the Dn form quite well and may even be more shallow. Because the Dn potentials are found useful here and should be useful for other electron-molecule scattering calculations, we have summarized many of their properties in Appendix A.

It is interesting to note that Sampson and Mjolsness found that their distorted wave calculations of rotational excitation of H_2 by electron impact agreed with swarm experiments if they used form D4 for the polarizability interaction but disagreed if they used form A.[53] Both of these potentials are nonzero at r = 0.

In the spirit of the polarized orbital method,[48] Lane and Henry[47] calculated the polarization potential for $R = R_e$ as the adiabatic one except that, as a correction for nonadiabatic effects, they turned off the interaction of the scattering electron with a bound electron whenever it was closer than the bound electron to the center of positive charge in the molecule. We consider this to be the best available approximation to the real nonadiabatic V^2 for H_2, and we calibrate a Dn potential against the shape of their NP′ potential. Table II gives the position of the minimum (r_{min}), the full-width at half-minimum ($\Delta r_{\frac{1}{2}}$), and the potential at the minimum (in units of the polarizability) of the NP′ potential. Figure 2 shows for which values of a_L ($a_0 \equiv a_p$, $a_2 \equiv a_{p'}$) and n the

Dn potential has the same characteristics. Since we cannot pick a Dn potential which gives all three parameters correctly, we choose as the theoretically most justifiable Dn potentials the ones which give best overall agreement with the shape of the NP′ potential. For the spherically symmetric component this yields n = 5, a_p = 2.1 a_0. For the asymmetric component this yields n = 5, a_p' = 1.8 a_0.[54] These potentials are shown in Fig. 3. The properties of these and some other Dn polarization potentials we will consider are given in Table III. In addition, we have constructed an analytic fit to the NP′ potential which deviates from it by less than 0.1% over the range $1.0 \leq a_0 r \leq 5.0$ and has the correct asymptotic form for large r. We call this the L potential.

One indication of the accuracy of the Lane-Henry polarization potential is that it is in good agreement with the semiempirical polarization potential of Lane and Geltman.[35] Lane and Geltman adjusted the cutoff parameters in their potential so that their close coupling calculations using a realistic static potential and the polarization potential would yield adequate integral elastic cross sections at energies high enough for more than one partial wave to be important.

We obtained the polarizability necessary for the use of equation (15) in scattering calculations from the accurate calculations of Kolos and Wolniewicz.[4]

It is convenient to give special names to certain combinations of choices of cutoff radii. These "data sets" are given in Table IV. Date set 1 (DS1) gives the theoretically most justifiable potential when used in conjunction with the B′ form for f and the D5 form for g and

g′. The cutoff radii in DS1 were chosen to give for these forms of the cutoff functions the best agreement of the analytic potentials with accurate calculations of these potentials as described above. When we refer to DS1 without specifying the forms of the cutoff functions, it should be understood that we mean these. Data set 2 (DS2) similarly gives the best fit of the analytic forms to the accurate potentials when the B′ form is used for f and D7 forms are used for g and g′.

In summary, the overall interaction potential for the electron-H_2 system is taken as

$$V(\underset{\sim}{r}, \underset{\sim}{R}) = V^1(\underset{\sim}{r}, \underset{\sim}{R}) + V^2(\underset{\sim}{r}, \underset{\sim}{R}) \tag{20}$$

$$= V_0(r, R) + V_2(r, R)\, P_2(\hat{r} \cdot \hat{R})$$

where from equations (5), (10), and (15):

$$V_0(r, R) = V_0^C(r, R) - \frac{\alpha(R)}{2r^4}\, g(r) \tag{21}$$

and

$$V_2(r, R) = V_2^C(r, R) - \frac{Q(R)}{2r^3} f(r) - \frac{\alpha'(R)}{2r^4}\, g'(r)\,. \tag{22}$$

The scattering amplitudes for scattering off the five terms on the right-hand sides of Eqs. (21) and (22) will be called S_0, P_0, S_2, Q_2, and P_2, respectively. The exchange scattering amplitude will be called E_0. Figures 1c and 1e show V_0 and V_2 for f, g, g′, n, and a_L as in data set 1. Figure 4 shows the potential surface V for this same data set

as a function of $\underset{\sim}{r}$.

2. Separation of Rotational and Vibrational Motion and the Scattering

For the transition from state p with vibrational quantum number v and rotational quantum numbers J and M to the state p′ (v′, J′, M′) the integral ($Q_{pp'}$) and differential ($\sigma_{pp'}$) cross sections are given by

$$Q_{pp'}(E) = \int \sigma_{pp'}(\theta, E) \sin\theta \, d\theta \, d\varphi \tag{23}$$

$$\sigma_{pp'}(\theta, E) = \frac{k_{p'}}{k_p} \left| f_{p'p}(\theta) \right|^2 \tag{24}$$

in terms of the initial (k_p) and final ($k_{p'}$) momenta[36] of the scattering electron for fixed total energy E_T and the scattering amplitude $f_{p'p}$. In the plane wave approximation (neglecting exchange)

$$f_{p'p}(\theta) = -\left(\frac{1}{2\pi}\right) \int \exp\left[i\underset{\sim}{q} \cdot \underset{\sim}{r} \right] V_{p'p}(\underset{\sim}{r}) \, d\underset{\sim}{r} \tag{25}$$

where $\underset{\sim}{q} \equiv \underset{\sim}{k}_p - \underset{\sim}{k}_{p'}$ and

$$V_{p'p}(\underset{\sim}{r}) = \int \psi^*_{v'J'M'}(\underset{\sim}{R}) \, V(\underset{\sim}{r}, \underset{\sim}{R}) \, \psi_{vJM}(\underset{\sim}{R}) \, d\underset{\sim}{R}, \tag{26}$$

$V(\underset{\sim}{r}, \underset{\sim}{R})$ is the interaction potential between the scattering electron and the molecule discussed in the last section, and ψ_{vJM} is the molecular nuclear coordinate wavefunction for state p. We consider vibrational and rotational motion to be separable and in particular we assume that the vibrational wavefunction can be taken as the one for the J = 0

rotational state. Then

$$\psi_{vJM}(\underset{\sim}{R}) = \psi_v(R)\, Y_{JM}(\hat{R}) \tag{27}$$

Now we consider only the first two terms in the multipole expansion of the potential in (26). Substituting (20) and (27) into (26) and performing the integration over $\hat{R}$ yield[3]

$$V_{p'p}(\underset{\sim}{r}) = V_{0,v'v}(r)\, \delta_{J'J}\, \delta_{M'M} + (-1)^{M-M'} \left(\frac{4\pi}{5}\right)^{\frac{1}{2}} V_{2,v'v}(r)\, C^{(2)}(J'M', JM)\, Y_{2,M-M'}(\hat{r}) \tag{28}$$

where we have chosen the z-axis in the $\underset{\sim}{r}$ coordinate system to be along $\underset{\sim}{R}$. In (28), $C^{(2)}(J'M', JM)$ is the coefficient defined by Brieg and Lin[3]

$$C^{(2)}(J'M', JM) = (4\pi/5)^{\frac{1}{2}} \int Y^*_{J'M'}(\Omega)\, Y_{2,M'-M}(\Omega)\, Y_{JM}(\Omega)\, d\Omega$$

and

$$V_{L,v'v}(r) = \int \psi^*_{v'}(R)\, V_L(r, R)\, \psi_v(R)\, R^2\, dR\,. \tag{29}$$

The error in (29) due to determining ψ_v for the $J = 0$ state (so that, for example, $V_{L,v'v}$ is taken to be the same for $v \rightarrow v'$ transitions with and without concommitant rotational transitions) has been shown to be small in related problems.[55] Note that scattering off the potential (28) strictly implies that $\Delta J = 0, \pm 2$. Thus, for example, there is no difficulty, at any temperature, in applying this procedure to scattering from real hydrogen molecules which exist in ortho and para forms.

Substituting (28) into (24)-(25), summing over M′ and averaging over M we obtain

$$\sigma_{vJ,\,v'J'} = \delta_{J'J}\,\tilde{\sigma}_0 + \mathscr{A}(2J'+1)\begin{pmatrix} J' & 2 & J \\ 0 & 0 & 0 \end{pmatrix}^2 \tilde{\sigma}_2 \tag{30}$$

where

$$\tilde{\sigma}_0 = k_{p'}\, N^2_{v'v}\, q^2/k_p \tag{31}$$

$$N_{v'v} = -(2/q^2) \int \sin q\,r\; V_{0,\,v'v}(r)\; r\; dr \tag{32}$$

$$\mathscr{A} = \begin{cases} 0 & \Delta J \neq 0,\ \pm 2 \\ 0 & J = J' = 0 \\ 1 & \text{Otherwise} \end{cases} \tag{33}$$

$$\tilde{\sigma}_2 = \frac{1}{5}\, k_{p'}\, M^2_{v'v}/k_p \tag{34}$$

$$M_{v'v} = 2 \int V_{2,\,v'v}(r)\; j_2(qr)\; r^2\; dr \tag{35}$$

Here j_2 represents the spherical Bessel function of order 2 and the standard notation[56] is used for the 3-j symbol. It is useful to write (30) in the form

$$\sigma_{vJ,\,v'J} = \tilde{\sigma}_0 + \tilde{\sigma}_2\, \frac{J(J+1)}{(2J-1)(2J+3)} \tag{36}$$

$$\sum_{J' \neq J} \sigma_{vJ,\,v'J'} = \tilde{\sigma}_2\, \frac{3J^2+3J-3}{4J^2+4J-3} \tag{37}$$

We will often be interested in experiments which do not resolve the rotational structure in the excitation spectrum, i. e., we are interested in the sum over all J′ and average over J which is (if we make the approximations $k_p \cong k_{v0} \equiv k_v$)

$$\sigma_{vv'} = \tilde{\sigma}_0 + \tilde{\sigma}_2 . \tag{38}$$

(This is the result for any distribution of J.) The first order calculation which includes the polarization potential will be called the polarized Born approximation (B/P). If we neglect the polarization potential we have just the Born approximation (BXP).

3. Vibrational Matrix Elements

For the computation of equation (29) we require the matrix elements of $V_0^C(r,R)$, $V_2^C(r,R)$, $\alpha(R)$, $\alpha'(R)$, and $Q(R)$ between vibrational wavefunctions. We used vibrational wavefunctions determined numerically for the potential well given by Kolos and Wolniewicz.[57] The numerical method consists in converting the 1-D Schrödinger equation for the problem to a boundary value problem by requiring the wave function to vanish at some points far into the classically inaccessible region. The second derivative is approximated in terms of second differences[58] and the eigenvalues and eigenfunctions of the resulting tridiagonal Hamiltonian matrix are found by the Givens-Householder method.[59] This method is essentially a 1-D analog of the method used for 2-D problems by Diestler, McKoy, and Winter[60] and it was originally programmed for use in atom-molecule scattering problems.[61] A similar method has recently been used for 1-D problems by Rush.[62] For our calculations involving α, α', and Q we used 541 points in the range R = 0. 3933 - 4. 0067 a_0 with step size

0.0067 a_0. The matrix elements were then calculated by a 541 point trapezoidal rule integration. For this integration the polarizabilities and quadrupole moment were calculated by third order interpolation (Bessel's formula) of the tabulated values of Kolos and Wolniewicz.[4, 57] The eigenvalues and matrix elements determined this way are in good agreement with values determined by Wolniewicz and Kolos using a more elaborate method.[63, 4]

The α, α', and Q matrix elements are given in Table V.

4. Scattering Calculations (without exchange)

From equations (32) and (35) we obtain, with $s = \frac{1}{2}q$,

$$N_{v'v} = \alpha_{v'v} N_{\alpha} + N^{C}_{v'v} \tag{39}$$

where

$$N_{\alpha} = q^{-2} \int r^{-3} g(r) \sin qr \, dr \tag{40}$$

$$N^{C}_{v'v} = 2 q^{-1} \int R^2 \psi^{*}_{v'}(R) \psi_{v}(R) F_0(R, Z(R), q) \, dR \tag{41}$$

$$F_0(R, Z(R), q) = \left(\frac{2Z^2 + s^2}{2sR}\right) \frac{\sin sR}{(Z^2+s^2)^2} \tag{42}$$

and

$$M_{v'v} = \alpha'_{v'v} M_{\alpha'} + Q_{v'v} M_Q + M^{C}_{v'v} \tag{43}$$

where

$$M_{\alpha'} = -\int r^{-2} g'(r) j_2(qr) \, dr \tag{44}$$

$$M_Q = -\int r^{-1} f(r)\, j_2(qr)\, dr \tag{45}$$

$$M^C_{v'v} = 2\int R^2 \psi^*_{v'}(R)\, \psi_v(R)\, F_2(R, Z(R), q)\, dR \tag{46}$$

$$F_2(R, Z(R), q) = \frac{5(2Z^2 + s^2)}{2s^3R^3(Z^2+s^2)^2}\, [(s^2R^2 - 3)\sin sR + 3sR\cos sR] \tag{47}$$

Several of the integrals N_α, $M_{\alpha'}$, and M_Q can be done analytically and the resulting expressions are given in Appendix B. The others were done numerically using Romberg quadrature.[64] The integrals (41) and (46) were done numerically as described in section B.3 but with 253 points and step size 0.0143 a_0 for the range R = 0.3857-4.0143 a_0. The resulting amplitudes at 50 evenly spaced values of q in the range 0-4.9 a_0^{-1} were fit to series of a form suggested to us by analogy with the work of Lassettre:[65]

$$N^C_{v'v} = \frac{1}{s(Z_e^2 + s^2)^2} \sum_{i=0}^{5} a_{v'v,i} \left(\frac{s^2}{Z_e^2 + s^2}\right)^i \tag{48}$$

$$M^C_{v'v} = \frac{2}{(Z_e^2 + s^2)^2} \sum_{i=0}^{4 \text{ or } 5} b_{v'v,i} \left(\frac{s^2}{Z_e^2 + s^2}\right)^i \tag{49}$$

with $Z_e \equiv 1.18 \cong Z(R_e)$. For $M^C_{v'v}$ the first data point for the fit is at q = 0.05 a_0^{-1} instead of q = 0.0 for numerical reasons. The a and b coefficients are given in Table VI. These equations and equations (31) and (34) were used to calculate the differential cross sections. The integral cross sections were

computed using equation (23) and a 49 point Weddle's Rule integration (unequal steps).

5. Inclusion of Exchange

There have not been many examples in electron scattering which compared the scattering with and without exchange in a calculation where the long range forces are explicitly included (one exception is by Stone and Reitz[66] for cesium). Application of the Ochkur and Ochkur-Rudge approximations to electron scattering without electronic excitation has previously been carried out by Rudge[6] and others[67, 7]--but only for atoms. Further, these methods have never been tested for scattering processes with long-range potentials except by Bely in his application to electron scattering from ions.[68] He did not study angular distributions. In the absence of polarization, the DCS in the prior Born-Ochkur-Rudge approximation (BOR, or, to emphasize the neglect -X- of polarization -P-, BORXP)[7] consists in subtracting an exchange amplitude $g_{p'p}$ from the direct amplitude $f_{p'p}$ of equation (25) where[69]

$$g_{p'p}(\theta) = -\frac{E_2}{2\pi} \int d\underset{\sim}{R}\, \psi^*_{v'J'M'}(\underset{\sim}{R})\, \psi_{vJM}(\underset{\sim}{R})$$

$$\int d\underset{\sim}{r}\, V^e(\underset{\sim}{r}, \underset{\sim}{R}) \exp[\, i(\underset{\sim}{k} - \underset{\sim}{k}') \cdot \underset{\sim}{r}\,] \qquad (50)$$

where $E_2 = q^2/2(k' - i\sqrt{2I})^2$, I is the ionization potential, and V^e is defined in equation (4). We do a multipole expansion of V^e and retain only the spherically symmetric term for the calculation of the exchange amplitude. Then

$$V^e(\underset{\sim}{r}, \underset{\sim}{R}) \cong V_0'(r, R) - V_0^n(r, R) \tag{51}$$

where

$$V_0^n(r, R) = \begin{cases} -\frac{2}{r} & r > R/2 \\ -\frac{4}{R} & r < R/2 \end{cases} \tag{52}$$

We substitute (51) - (52) into (50) and perform the $\hat{r}$ and $\hat{R}$ integrals to obtain (with $s = \frac{1}{2} q$)

$$g_{p'p}(\theta) = 2s E_2 [N^C_{v'v} - (\frac{1}{s^3}) G_{v'v}] \delta_{J'J} \delta_{M'M}$$

where

$$G_{v'v} = \tfrac{1}{2} \int \psi^*_{v'}(R)\, s^{-1} \sin sR\, \psi_v(R)\, R\, dR .$$

$G_{v'v}$ is evaluated numerically as discussed in section 4 and fit to a series

$$G_{v'v} = \sum_{i=0}^{4} c_{v'v,i}\, s^{2i}$$

in the range $q = 0.0 - 4.9\, a_0^{-1}$. The fit is generally accurate to better than 0.1%. The coefficients $c_{v'v,i}$ are given in Table VI. Including exchange in this way finally amounts to replacing $N_{v'v}$ in Eq. (39) by

$$(1 - E_2) N^C_{v'v} + E_2 s^{-3} G_{v'v} . \tag{53}$$

It is more difficult to account for exchange and polarization simultaneously. As a first order approximation to the exchange adiabatic approximation (EAA) we will consider the scattering off the polarization potential to be only direct scattering; i. e., we calculate the direct and exchange scattering from the static potential as described in section 4 and the present section and then correct the direct scattering for polarization as described in section 4. This procedure (like the EAA) cannot be derived variationally and neglects exchange polarization terms[71, 44] which can be important in quantitative work. It will be called the polarized Born-Ochkur-Rudge approximation (BOR/P).

C. INCLUSION OF DISTORTION IN THE FIRST TWO PARTIAL WAVES

The scattering particle wave function can be expanded in a series of partial waves, each of which is characterized by its angular momentum quantum numbers including ℓ (the orbital angular momentum of the electron with respect to the center-of-mass of the molecule). Distortion of the ℓ =0 and 1 partial waves (s and p waves) might be important at any energy and should have a strong effect on the large angle scattering. We will give the equations for a simple treatment of this distortion (neglecting electron exchange) which could be used as an improvement over the polarized Born approximation just considered. In this treatment, the distorted partial waves are taken to be the regular solutions $\chi_{\ell c}$ of

$$\frac{d^2\chi_{\ell c}(r)}{dr^2} + \left[k_c^2 - 2V_{o,cc}(r) - \frac{\ell(\ell+1)}{r^2}\right] \chi_{\ell c}(r) = 0 \qquad (54)$$

where the potential is defined in (29) and

$$k_c^2 = k_o^2 - |\Delta E_{co}| \qquad (55)$$

where ΔE_{co} is the vibrational excitation energy of the v′ = c state. Thus the distorting effect of the spherically averaged potential is included but the distortion due to the anisotropic part of the potential is not. This approximation[72, 53] has been called[73] the restricted distorted wave approximation and is an important practical simplification because it means the potential that is used to calculate the distorted

waves depends neither on the rotational quantum numbers nor on the angular coordinates of the scattering electron. This saves computer time and also allows us to analytically perform averages over M and sums over J' and M'.

Another interpretation of the restricted distorted wave approximation is possible if only terms proportional to $P_0(\hat{r}\cdot\hat{R})$ and $P_2(\hat{r}\cdot\hat{R})$ are important in the potential--as in the present case. Then the distorting potential is the one seen by an electron whose trajectory is at a 54.7° angle with the internuclear axis when the molecule does not rotate appreciably during the collision.

This approximation of obtaining the distorted waves from scattering off the spherically symmetric part of the potential was used and justified by Sampson and Mjolsness[53] for rotational excitation in $e^- - H_2$ and $e^- - N_2$ collisions and by Davison[74] for rotational excitation in $H_2 - H_2$ collisions. Arthurs and Dalgarno[26] did model calculations on $e^- - H_2$ scattering and concluded orientation-dependent distortion is not important for the integral cross sections. Also, Roberts,[75] who did not use this approximation for his $He - H_2$ rotational excitation calculations, argued it would be a good approximation; i.e., he argues from analysis of his results that the role of V_2 in the transition matrix element where it is not neglected is more important by far than its role in distortion. The approximation should be even better for vibrational excitation.

In equation (25) we defined the (polarized) Born approximation scattering amplitude $f^B_{p'p}$. We now define the sums of the partial scattering amplitudes for the s and p partial waves as ${}^{sp}f^B_{p'p}$ and ${}^{sp}f^{DW}_{p'p}$ in the (polarized) Born and (polarized) restricted distorted wave approximations, respectively. The s wave amplitude includes final

states with $\ell' = 0$ and 2 and the p wave amplitude includes final states with $\ell' = 1$ and 3. We define

$$f'_{p'p}(\theta) = {}^{sp}f^{DW}_{p'p} - {}^{sp}f^{B}_{p'p} \tag{56}$$

so that the scattering amplitude in the (polarized) restricted sp-distorted wave approximation is

$$f^{DW}_{p'p}(\theta) = f^{B}_{p'p} + f'_{p'p} \quad . \tag{57}$$

Then the differential cross section for vibrationally elastic scattering ($v = v'$) or vibrational excitation from level v to level v′ (averaged over initial rotational magnetic substates and summed over final rotational states) is

$$\sigma^{DW}_{vJv'} = \frac{k_{v'}}{k_v} \frac{1}{(2J+1)} \sum_{J'M'M} \left| f^{DW}_{p'p}(\theta) \right|^2 \tag{58}$$

$$= \sigma^{B}_{vv'} + \frac{k_{v'}}{k_v} H_{vv'} \tag{59}$$

where $\sigma^{B}_{vv'}$ is given by equation (38). We obtain

$$\begin{aligned} H_{vv'} = {} & H_1^2 + \tfrac{1}{5}H_2^2 + H_1H_3 + \tfrac{1}{5}H_2H_4 \\ & + [6(2H_2+H_4)H_5/25] \cos\theta + (36H_5^2/125)\cos^2\theta \\ & + (108H_6^2/125)\sin^2\theta \end{aligned} \tag{60}$$

where

$$H_1 = -2\left[I_{0v'v_{00}} + 3\cos\theta\, I_{0v'v_{11}}\right] \tag{61}$$

$$H_2 = 2\, I_{2v'v20} \tag{62}$$

$$H_3 = -4\int_0^\infty (r/q)\sin qr\, V_{0,v'v}(r)dr \tag{63}$$

$$H_4 = -4\int\left[\frac{\sin qr}{qr} - \frac{3\sin qr}{(qr)^3} + \frac{3\cos qr}{(qr)^2}\right] V_{2,v'v}(r)r^2dr \tag{64}$$

$$H_5 = 3I_{2v'v31} - 2I_{2v'v11} \tag{65}$$

$$H_6 = I_{2v'v31} + I_{2v'v11} \tag{66}$$

$$I_{Lv'v\ell'\ell} = \int_0^\infty \chi_{\ell'v'}(r)\, V_{L,v'v}(r)\, \chi_{\ell v}(r)r^2\, dr \tag{67}$$

$$- \int_0^\infty j_{\ell'}(k_{v'}r)\, V_{L,v'v}(r)\, j_{\ell}(k_v r)r^2\, dr \tag{68}$$

and $j_{\ell'}$ is a spherical Bessel function of order ℓ'. Note that the vibrational excitation cross sections turn out to be independent of J to this approximation.

In summary, in the (polarized) restricted sp-distorted wave approximation the s and p partial waves are calculated in the (polarized) restricted distorted wave approximation and all the higher partial waves are calculated in the (polarized) Born approximation. This will give more realistic results for small angle scattering than distorted wave or close coupling calculations which calculate the lowest few partial waves and neglect the others; it will be more accurate for predicting large angle scattering than plane wave calculations.

D. THE EFFECTS OF VARIOUS PARTS OF THE POTENTIAL ON THE SCATTERING CROSS SECTIONS

We will now consider the effects on the cross sections of including the amplitudes for scattering off various terms in the interaction potential one-at-a-time and in combinations to determine the energy and angle range in which each type of interaction is important. We will indicate which amplitudes (see section B. 1) are included in a cross section in parentheses; for example, when form B′ is used for f, the integral elastic cross section in the Born approximation (BXP) is denoted $Q_{0\,0}(S_0 S_2 Q_2^{B'})$ and in the Born-Ochkur-Rudge approximation (BORXP) is denoted $Q_{00}(S_0 E_0 S_2 Q_2^{B'})$. Note that because of interference terms the contributions from the different interaction terms of the same angular symmetry are not additive. All the considerations in this section are based on the plane wave approximation calculations.

1. Integral Elastic Cross Sections

Figures 5 and 6 show the integral elastic cross sections for scattering by the symmetric and asymmetric parts of the electron-H_2 interaction potential for the potential parameters of DS 1. Since $Q_{00}(S_2 Q_2^{B'} P_2^{D5})$ is at most about 15% of $Q_{00}(S_0 E_0 P_0^{D5})$ for the whole range of impact energies we studied (1 eV to 912 eV), the integral elastic cross section is determined primarily by the symmetric parts of the potential.

S_0 alone gives a relatively low cross section which decreases monotonically with increasing energy. The addition of exchange

$[Q_{00}(S_0 E_0)]$ or polarization $[Q_{00}(S_0 P_0)]$ increases the scattering by comparable factors in the 5 to 100 eV range. At higher energies $Q_{00}(S_0 E_0)$ converges to $Q_{00}(S_0)$ while $Q_{00}(S_0 P_0^{D5})/Q_{00}(S_0)$ converges to a nearly constant value of 2.13 (for DS 1) for E = 60-912 eV. $Q_{00}(S_0 P_0$ is a steep, decreasing function of energy, e.g., at 1 eV, $Q_{00}(S_0 P_0^{D5}$, DS 1) = 125 a_0^2. The addition of exchange to $Q_{00}(S_0 P_0)$ increases the cross section for impact energies above 10 eV. At higher energies $Q_{00}(S_0 E_0 P_0)$ converges to $Q_{00}(S_0 P_0)$ and is within 13% (D5 form for g, DS 1) of it above 100 eV. The addition of the quadrupole and/or polarization interaction terms to the asymmetric short range potential increases the cross section at all energies. At energies above 100 eV, the quantities $Q_{00}(S_2 Q_2^{B'} P_2^{D5})$: $Q_{00}(S_2 Q_2^{B'})$: $Q_{00}(S_2)$ reach the constant ratio 1.4:1.2:1.0 for D51.

The cutoff radius a_P = 2.1 a_0 of data set 1 is larger than that generally used in the past. For smaller cutoff radii, the potentials become much deeper. For example, decreasing a_P to 1.7 a_0 deepens the polarization potentials (any form) by a factor of 1.53. The A, B, or C form of the potential is then about 3.3 times deeper than the Lane-Henry NP′ potential. For any cutoff a_P, the A, B, and C forms of the polarization are 1.46 times deeper than the D5 potential and 1.58 times deeper than the D7 potential. Decreasing the cutoff parameter a_P increases $Q_{00}(P_0)$ as expected. Decreasing a_P from 2.1 a_0 to 2.0 a_0 increases $Q_{00}(P_0)$ for all forms of g by the same factor of 1.21 at energies above 20 eV. However, this same change raises $Q_{00}(S_0 P_0)$ by

only a factor of about 1.09 at the same energies. A change of a_P from 2.1 a_0 to 1.7 a_0 increases $Q_{00}(P_0)$ for all forms of g by a factor of about 2.32. At lower energies, decreasing a_P has an even greater effect on the integral cross sections.

Figure 7 shows the scattering due to the spherical component of the polarization potential alone for DS 1. $Q_{00}(P_0)$ has essentially the same energy dependence for all the forms of g that we examined. For energies higher than about 20 eV, the quantities $Q_{00}(P_0^B)$: $Q_{00}(P_0^{D5})$: $Q_{00}(P_0^C)$: $Q_{00}(P_0^A)$ attain a nearly constant proportionality at 1.71:1.00:0.55:0.34 for a_P = 2.1 a_0 to 1.2 a_0. Above about 6 eV, the scattering from V_0^C dominates that from the polarization potential (for any form of g), and, for energies above 45 eV, $Q_{00}(S_0)/Q_{00}(P_0^{D5})$ $\cong$ 2.65 for a_P = 2.1 a_0. $Q_{00}(P_2)$ has a prominant peak at about 6 eV in contrast to the monotomic decrease of $Q_{00}(P_0)$ in this region.

2. Elastic Differential Cross Sections

The elastic DCS's for scattering by various combinations of the symmetric and asymmetric parts of the interaction potential for the parameters of DS 1 are shown in Figs. 8-11 (E = 20 eV), Fig. 12 (E = 35 eV), and Figs. 13-15 (E = 60 eV).

The characteristics of the angular distributions for scattering by the various parts of the potential can be interpreted qualitatively by recalling that the scattering amplitude is closely related to the Fourier transform of the potential--see equation (25). For spherically symmetric potentials, this reduces to a Fourier sine transform--see equation (32)--and DCS's due to scattering by potentials confined to

smaller regions of space are appreciable over wider ranges of q than those due to scattering by potentials extending over longer ranges. This is clearly illustrated, for example, by comparing $\sigma_{00}(S_0)$ with $\sigma_{00}(P_0^{D5})$ in Fig. 8. In effect, the shape and magnitudes of the DCS's at large q (and hence, high energies and large scattering angles) are determined primarily by short range interactions while those at small q depend to a larger extent on the long range forces. Further, in cases where the DCS's are highly forward peaked, the integral cross sections are determined by small angle scattering (small q) and hence these, too, are determined by the long range potentials.

In plane wave approximations, DCS's due to scattering from the symmetric parts of the potential often peak at $\theta = 0^\circ$ and decrease with increasing θ, becoming steeper at higher energies. Those from the asymmetric parts generally increase with increasing θ (for small θ) and peak at larger angles, but at higher energies they peak at lower angles and are smaller at larger ones. This large-energy decrease in large angle scattering is not nearly as great as is the similar decrease of the large angle scattering due to the symmetric part of the potential. As a result, the large angle DCS depends much more on the asymmetric parts of the potential at higher energies than it does at lower ones.

We note, however, that scattering due to the quadrupole interaction and the asymmetric part of the polarization potential is relatively unimportant at larger angles at high energies (compare $\sigma_{00}(S_2)$ and $\sigma_{00}(S_2Q_2P_2)$ in Fig. 14). At lower energies these interactions contribute appreciably to $\sigma_{00}(S_2Q_2P_2)$ as shown in Fig. 10, but the

scattering from the whole asymmetric potential is less important at any angle at these energies. Thus, the most important asymmetric interaction is the short range one at any energy above about 10 eV.

Figure 12 shows the DCS's at 35 eV due to scattering from the quadrupole and asymmetric polarization potentials, using for the cut-off functions the theoretically most justifiable forms (DS 1) and for the extreme case of form F. The strong short range attraction of form F leads to a large angle DCS which exceeds that of forms B′ or D5 by several orders of magnitude. It is interesting to note that $\sigma_{0\,0}(Q_2^F) = 2.08 \times 10^{-2}\ a_0^2/\text{sr}$ for any energy or angle.

The small angle scattering is dominated by the symmetric part of the potential. The most important effect of adding exchange to S_0 is to increase the DCS at small angles (except at low energy--see Section F). For example, at 30 eV and $\theta = 0^\circ$, $\sigma_{00}(S_0 E_0)/\sigma_{00}(S_0) = 1.43$ while at 180° this ratio is 1.19. (Including P_0^{D5} changes these figures to 1.10 and 1.21, respectively, for DS 1.) At higher energies, the importance of exchange at small angles decreases (as does its contribution to the integral cross sections). At 70 eV $\sigma_{00}(S_0E_0)/\sigma_{00}(S_0) = 1.32$ at 0° and 1.09 at 180°. Adding polarization to S_0 or S_0E_0 increases the small angle DCS. This increase extends to larger angles at lower energies. In addition, the large angle scattering is reduced somewhat, more so at lower energies.

The steepest low angle DCS's are those which include polarization, and a calculation which includes only P_0 will predict

too steep a DCS. However, since the various forms of the polarization potential differ only for small r and at small r differ from each other much less than they differ from V_0^C, the angular dependence of the scattering from these forms differs appreciably only for large θ. $\sigma_{00}(P_0)$ exhibits sharp dips to zero for forms B, C, and Dn but not for A. The positions of these zeroes are correlated with the position of the minimum in the potential. Decreasing a_P causes the potential to reach its minimum at smaller r and the zeroes in $\sigma_{00}(P_0)$ to occur at larger angles. The number of minima in $\sigma_{00}(P_0)$ and their positions are also related to the incident energy--there are more at higher energies and they occur at lower angles. Analogously the minimum at $r = 0.7\ a_0$ in V_0^C causes $\sigma_{00}(S_0)$ to have a zero at large angles for energies greater than 60 eV. These zeroes are artifacts of the Born approximation with these simple potential forms.

3. Integral Vibrational Excitation Cross Sections for $v' = 1$

It is known from previous calculations[5,76] that the short range interactions are much less effective in causing vibrational excitation than they are for elastic scattering. A direct numerical verification of this fact is given in Table VII. This table gives several values of the ratio $\mathcal{R}_{01}$ where

$$\mathcal{R}_{v'v''} \equiv Q_{0v''}/Q_{0v'} \quad . \tag{69}$$

The ratios are obtained by including various complete and incomplete

sets of interactions from the theoretically most justifiable potential in the calculation. All of the $\mathcal{R}_{01}$ are much less than one and the smallest are those which include S_0. The table also shows that the asymmetric potential is relatively effective for vibrational excitation: $\mathcal{R}_{01}(S_2)$ is larger than $\mathcal{R}_{01}(P_0)$ and $\mathcal{R}_{01}(P_2)$ is the largest ratio of all.

Breig and Lin have suggested that the vibrational excitation is dictated primarily by the longer range interactions and hence they neglected the short range ones. Since both have been included in the present calculation, we are able to test the validity of their procedure. Table VIII shows the ratios $Q_{01}(Y)/Q_{01}(Z)$ for several combinations Y and Z of scattering amplitudes. In particular, the table shows that the long range forces alone ($P_0Q_2P_2$) account for less than half of the polarized Born integral vibrational excitation cross section above about 13 eV. Recall, however, that for the elastic scattering, $Q_{00}(P_0Q_2P_2)/Q_{00}(S_0P_0S_2Q_2P_2)$ is less than 0.2 for $E \geq 10$ eV.

Figures 16 and 17 show the integral $0 \rightarrow 1$ vibrational excitation cross sections for scattering as calculated using the parameters of DS 1. Scattering by the asymmetric part of the potential is relatively more important for vibrational excitation than it is for elastic scattering. It accounts for about 30% of the polarized Born cross section (DS 1) for $v' = 1$ above 20 eV.

The addition of exchange to the polarized Born approximation changes Q_{01} relatively little, even below 10 eV. Evidently, the effective exchange potential implied by the Ochkur-Rudge method is not very dependent on the internuclear separation.

Tables IX and X show cross sections which have been calculated using several different forms and cutoffs of the quadrupole and polarization potentials for an impact energy of 20 eV. In general, decreasing the cutoff parameter increases the depth of these potentials and increases the cross section. In particular, changing the cutoff in P_0^Y (Y = A, B, C, or D5) from a_p to b_p changes Q_{01} (P_0^Y) by nearly a factor $(a_p/b_p)^4$ as was the case for elastic scattering.

We have taken the polarization and quadrupole interaction potentials to be products of a function of r and a function of R. For the polarization potentials there is no better information available and for the quadrupole interaction potential this is compensated by the way we treat the short range static potential V_2^C. This product form of these potentials has the effect that the predicted energy and angle dependencies of the cross sections determined from any interaction (e.g., P_0, P_2, or Q_2) are very similar for elastic scattering and for excitation of the different vibrational levels. For example, if the variable of integration θ in equation (23) is changed to q in the usual way, then the only differences in $Q_{01}(Y)$ and $Q_{00}(Y)$ for Y = P_0, P_2, or Q_2 are small changes in the limits of integration q_{min} and q_{max} in equation (23) and in k′ in equation (24) and the changes in the values of the quantities in Table V. The changes in the interference terms

for scattering off the various potentials and in the terms representing scattering off this short range potential are more complicated, however, and the scattering off the whole potential is thereby allowed to be much different.

4. Differential Vibrational Excitation Cross Sections for $v' = 1$

The differential cross sections for excitation of the first vibrationally excited level of H_2 for several combinations of the various interaction potentials for data set 1 are shown in Figs. 18 and 19 for ($E \doteq 13.6$ eV) and in Fig. 20 ($E = 60$ eV). The comparison of the polarized Born approximation with the Born approximation in Figs. 19 and 20 shows that both the magnitude and shape of the low angle DCS's are determined by the polarization potential. Polarization has relatively little effect on the higher angle DCS's, becoming less important at higher energies.

Including the exchange interaction raises the high angle DCS's by only a small amount, even at lower energies where it is most important (e.g., see Figs. 18 and 20). Increasing the depth of the polarization potential has an effect on the integral cross sections which is similar to that of exchange. However, their respective effects on the angular distributions are quite different.

Scattering by the asymmetric parts of the potential contributes most to the DCS at intermediate angles in the present calculations. At higher impact energies this scattering is negligible at both high and low angles, but at lower energies it becomes increasingly more important at higher angles.

Comparing the BXP and S_0S_2 curves indicates that the quadrupole interaction is most significant at lower energies. At higher energies it has practically no effect on high-angle scattering but does modify the low and intermediate angle DCS's. These effects are shown more clearly in Fig. 21.

Figures 22 and 23 show the effect on B/P of changing the cutoffs and forms of the polarization and/or quadrupole interaction potentials at 13.6 and 60 eV. The shapes of the various distributions at each energy are similar, but they differ considerably in magnitude.

Figures 24 and 25 show some DCS's for which the far-field forms of the asymmetric part of the polarization and quadrupole interactions are used. Although these forms of the potentials seem unrealistic, they are sometimes used by other workers. It is interesting to note that they increase the high angle scattering. This change is in the same direction as the change due to the inclusion of distortion in the scattering electron wave function.

5. Cross Sections for Excitation of the Higher Vibrational Levels

For scattering off each of the terms in equations (21) - (22) considered separately, we find $Q_{03} < Q_{02} < Q_{01} < Q_{00}$ for any choice of potential forms we have studied. Some examples of this trend are shown in Tables XI and XII. The ratios $\mathcal{R}_{v'v''}$ (see Eq. (69)) for $v' < v''$ are generally smallest if they are calculated using only the long range forces. This is because the matrix elements in

Table V decrease rapidly with increasing v′. Thus, although the short range potentials are less effective than the long range ones in causing the 0 → 1 transition at low energies, they are more important for excitation of the higher vibrational states. For elastic scattering $Q_{00}(S_0S_2)$ exceeds $Q_{00}(P_0Q_2P_2)$ above about 2.5 eV. For 0 → 1 transitions, this is true only for E > 48 eV, but for 0 → 2 transitions it holds for E > 25 eV. For 0 → 3 transitions, $Q_{03}(S_0S_2)$ exceeds $Q_{03}(P_0Q_2P_2)$ at all energies. As an example of the trends, at E = 25 eV, $\mathcal{R}_{12}(S_0S_2)$ is 3.7 times $\mathcal{R}_{01}(S_0S_2)$ while $\mathcal{R}_{12}(P_0^{D5}Q_2^{B'}P_2^{D5})$ is 0.43 times $\mathcal{R}_{01}(P_0^{D5}Q_2^{B'}P_2^{D5})$ for DS 1. At E = 5 eV, the long range forces ($P_0Q_2P_2$, DS 1) contribute only about 36% of the scattering predicted by the polarized Born approximation for the 0 → 2 excitation. In addition, Tables XIII and XIV show that the contribution to $Q_{0v'}$ of the short range forces increases relative to the contribution of the long-range forces as the energy increases. In conclusion, the use of only a polarization potential (Breig and Lin's procedure) to calculate $Q_{0v'}$ would be a poor approximation for $v' > 1$ at any E.

Tables VIII, XIII, and XIV show that $Q_{0v'}(S_2Q_2P_2)/Q_{0v'}^{B/P}$ is a decreasing function of v′ at low energies and an increasing function of v′ at high energies.

The integral cross sections Q_{02} and Q_{03} calculated using data set 1 are shown in Figs. 26-29. Figures 26 and 28 show that the addition of exchange in the prior Born-Ochkur-Rudge approximation to the polarized Born approximation changes the v = 0, v′ = 2 and 3 integral cross sections very little above about 20 eV. We note, however, that the contribution of exchange scattering at

lower energies increases with increasing v'. For example, using DS1 at 13.6 eV the BOR/P cross section is about 5% larger than the B/P one for v' = 1, 9% larger for v' = 2, and 18% larger for v' = 3.

The Q_{02} cross sections calculated with data set 1 in the B/P (D5) and B/P(B) approximations are monotonically decreasing functions of E over the whole range we calculated them (1.8-912 eV). Both the B/P(A) and B/P(C) calculations exhibit broad local maxima in the region of 60-70 eV.

The polarized Born calculations of Q_{03} for data sets 1 and 2.0 (with B' form for f and A, B, C, or D5 forms for g and g') show broad minima in the vicinity of 45 eV, are increasing at 100 eV, and are decreasing by E = 500 eV.

Table V shows that the sign of α'_{30} is such that scattering off the asymmetric polarization potential interferes with the other scattering differently in the case of 0 → 3 excitation than in the other cases. Figure 29 shows one effect of this. $Q_{03}(S_2Q_2^{B'}P_2^{D5})$ is less than $Q_{03}(S_2Q_2^{B'})$ and very nearly equals $Q_{03}(S_2)$.

Tables XV to XVIII show cross sections which have been calculated using several different forms and cutoffs of the quadrupole and polarization potentials. Comparing columns 2 and 3 of Table XVII shows that increasing the depth of the asymmetric part of the polarization potential, with a constant a_Q, generally increases the Q_{02} cross section by a small amount (~ 1%). The

same comparison in Table XVIII shows that Q_{03} is reduced 16-20% for the same change in the polarization potential. The $Q_{0v'}(S_2Q_2^{B'}P_2^A)$ appear to be exceptions in that the effect of changing $a_{P'}$ is in the opposite direction to that for other cutoff function forms in each case ($v' = 1 - 3$).

Figures 30 and 31 show $v = 0$, $v' = 2 - 3$ differential cross sections at 20 eV calculated using several combinations of the various interaction potentials for DS 1. The low angle DCS's are determined primarily by the polarization potential for both the $0 \rightarrow 2$ and $0 \rightarrow 3$ excitations. At high angles, the B/P $0 \rightarrow 2$ DCS's are a little larger than the BXP ones while this order is reversed for the $0 \rightarrow 3$ DCS's.

The exchange effect becomes relatively more important with increasing v'. This is consistent with the fact that the scattering by the short range forces contributes proportionately more to DCS's for large v' than for small v'.

Scattering by the asymmetric part of the potential considerably exceeds that by the symmetric part at higher angles. Adding the asymmetric term in the polarization potential to the static potential decreases the $0 \rightarrow 3$ scattering because of the destructive interference between the scattering by these parts of the asymmetric potential. A comparison of the DCS's calculated in the Born approximation with those calculated using only the short range forces (Carson's method) shows that the quadrupole interaction is unimportant at low angles, like the rest of the asymmetric part of the potential, and it is

somewhat more effective in increasing the high angle scattering for $0 \rightarrow 3$ than for $0 \rightarrow 2$.

Figures 32 and 33 show DCS's for excitation of the $v' = 2$ and 3 levels calculated in the polarized Born approximation at 20 eV using several choices of potential forms and data sets. The curves in each figure exhibit the same general shape with rather large differences in magnitude. An example of a calculation using a far-field form of the asymmetric polarization and/or quadrupole potential is also shown in each figure. The enhancement in large angle scattering due to use of form F for f (with $g' = 0$) is larger than that resulting from the inclusion of exchange for $v = 0$, $v' = 2$ above 13 eV. Similarly, this is true for the high angle $0 \rightarrow 3$ DCS's but only for energies above about 25 eV.

Figure 34 shows the effect of exchange on the $0 \rightarrow 3$ DCS and also how large an error would be made by following the Breig and Lin procedure (long range forces only) for this transition.

E. HIGH ENERGY SCATTERING

Figures 35 to 37 show comparisons of the Born and polarized Born calculations using data set 1 with the experiments of McMillen,[17] Arnot,[18] and Webb[20] at impact energies 150 to 912 eV. At 150 eV, the McMillen experiment yields $\sigma_{00}(36^\circ)/\sigma_{00}$

$(10°) \cong 0.147$. For data set 1, this same ratio is 0.032, 0.033, 0.136, and 0.127 in the B/P, BOR/P, BXP, and BORXP approximations, respectively. Thus the uncorrected Born approximation (BXP) is in excellent agreement with the experimental angular dependence at this energy. Over the angular range where experimental data are available (see Fig. 36), the B/P decreases 4 and 5 times as much as experiment and the BXP decreases 2 and 4 times as much as experiment at 412 and 812 eV, respectively. This fact and the comparison of large angle scattering in Figs. 37 and 38 show that, as expected, the plane wave approximation used here fails to predict the gradual flattening out of the high energy DCS's at large scattering angles[21b] and large momenta transfers.[69] (The failure is due to neglect of distortion of the scattering wave.[21b] It could probably be corrected to a large degree by using the formalism of section C.) This means that for Born calculations at high energies, the predicted scattering can be used only at small angles to judge the appropriateness of the potential. Further, the maximum angle at which the inclusion of polarization in a calculation makes a significant difference decreases with increasing energy to the extent that very little of the previous experimental data is relevant to this point. Nevertheless, examination of the small angle scattering shows that sometimes the data are fit better by including polarization and sometimes by neglecting it. Considering together all these results and the possible inaccuracies of the data, it is probable that the true

angular dependence at small angles lies somewhere between that predicted by the B/P and BXP calculations. This conclusion is in qualitative agreement with the recent study of elastic electron-helium atom scattering for E = 100 - 400 eV by La Bahn and Callaway.[77] They included distortion in the scattering waves and compared their calculation with normalized experimental DCS's. They also found that the experimental small angle DCS lies between the one calculated without polarization (their SE calculations) and the one calculated with a polarization potential corrected at small r for nonadiabatic effects.

To complete our comparison with all the available high-energy (E > 100 eV) experimental differential cross sections, Fig. 38 shows our calculated differential cross sections at E = 125 eV for comparison with the experiments of Mohr and Nicoll at θ = 50°-160°. In this case, in the angular range $\theta \geq 50°$, the polarization correction in the B/P calculation is less than 11%. The figure shows that theory and experiment disagree at very large angles, evidently due to neglect of distortion (as discussed above).

Table XIX gives computed integral cross sections Q_{00} at high energies for various types of polarization potentials. These are of interest since the Born approximation should be fairly accurate at these energies. There are no data available for comparison with these numbers at this time, but from the discussion earlier in this section, we expect the accurate values to lie between the Born

approximation neglecting polarization and the calculation including polarization in the most reasonable way, i.e., between the BXP and the B/P(D5) calculations, but closer to the former at the highest energies and to the latter below 100 eV.

Tables XX and XXI give high energy integral cross sections for vibrational excitation computed by various methods. These should be only a little less accurate than the elastic scattering cross sections and provide values of the cross sections in an energy region where their experimental measurement would be difficult (because they are so small). Vibrational excitation cross sections at lower energies will be considered again in paper III.

F. LOW ENERGY ELASTIC SCATTERING

Figure 39 compares integral cross sections from calculations in the BORXP and BXP approximations for the data set 1 static potentital with those from four continuum Hartree-Fock (includes exchange) and continuum Hartree (neglects exchange) calculations of Wilkins and Taylor,[8] Tully and Berry,[9] and Henry and Lane.[10] The calculations of the last two sets of authors are even more recent than the present ones. These four calculations, unlike the present ones, did not assume plane wave scattering states. The comparison of the present calculations which include exchange and neglect polarization (BORXP) with the calculations of these authors for the same interactions (HF) and the comparison of the Born approximation (BXP) with the corresponding numerical calculations (H) of Wilkins and Taylor, show what

errors are introduced by the plane wave approximation in our treatment of the short range and quadrupole interactions. The figure also includes the present calculations which include scattering off the theoretically most justified polarization potential (DS 1), the calculations of Henry and Lane[10] which include polarization, and the experimental results for total scattering (uncorrected) of Golden, Bandel, and Salerno.[15] The older experiments of Ramsauer and Kollath[78] (not shown) are in good agreement with the ones shown. The figure shows that the present simple calculations, especially the B/P ones, are remarkably accurate (the comparison of curves 1 and 3 and curves 2 and 4 shows that only a small error is caused by the plane wave approximation when polarization is important) above 2 eV but untrustworthy at energies below that. The present calculations were not expected to be valid at very low energies because of the plane wave approximation. For completeness of the comparison, Fig. 40 shows experimental[16] and theoretical[8,9] differential cross sections at 3.4 - 3.5 eV. The inclusion of exchange correctly lowers the forward peak at low energy but good agreement with experiment is hard to obtain.

Figure 41 shows some other calculations of integral elastic scattering in the 5 - 20 eV range. The Q_{00} calculated in the B/P approximation using data set 2 (with B′ form for f and D7 forms for g and g′) and data set L (with B′ form for f) are both shown; they are both lower

than the values calculated using DS1 but are within 11% of those values in this energy range. This is an indication that our fitting procedures are adequate since all three of these potentials are fits to the Lane-Henry potential but with different restrictions (see section B.1). Figure 41 also shows a calculation in the B/P approximation using data set 1.7 (with B′ form for f and D5 forms for g and g′). This curve shows that using a cutoff radius that is too small (which is what has usually been done) leads to large overestimates of the cross sections.

Another curve on the figure represents the calculations of Fisk.[11] Fisk's calculation is an (exact) partial wave solution in the static approximation (no exchange) for the scattering off a semi-empirical potential expressed in spheroidal coordinates. The potential does not correspond to that of two point charge protons and an electronic charge cloud. This calculation yields cross sections which are too small at energies above about 1 eV.

Nagahara[12] obtained the (exact) partial wave solution (lowest few partial waves only) for a static potential calculated from Inui's H_2 wave function. His results, shown in Fig. 41, are in good agreement with experiment. Hara[14] calculated the partial wave solution for scattering off a potential which included the static interactions, a semiempirical polarization potential (A form for g), and

a potential to represent the exchange interaction. He empirically adjusted the cutoff radius a_p in his polarization potential to get agreement with experiment for Q_{00}. This yielded $a_p = 1.6\ a_0$ and an A form polarization potential with a depth of 0.406h at r = 0. This polarization potential is not attractive enough at medium r. Figure 42 shows a plot of the B/P approximation for a case where the spherically symmetric part of the polarization potential has A form with $a_p = 1.7\ a_0$. The agreement with Hara's calculation is good.

Elastic scattering at intermediate energies will be considered in paper II.

G. SUMMARY

We present a quantum mechanical theory of electron scattering by a homonuclear diatomic molecule in which the molecule is considered to be a polarizable, aspherical, rotating, anharmonic oscillator with a realistic electronic ground state charge distribution. Real electronic excitation is neglected, but virtual electronic excitation is included by means of the dipole polarizability. We consider the static electron-molecule potential, which includes the long-range quadrupole interaction and electron exchange and the polarization potential.

The theory assumes plane waves for the scattering electron wave functions and includes electron exchange by the Born-Ochkur-Rudge approximation. Formulas are derived for all possible

rovibrational excitations and for vibrational excitations averaged over the initial rotational states and summed over the final ones. The latter are applied to the calculation of elastic scattering and excitation of the first, second, and third vibrational states of H_2. For these calculations the vibrational excitation transition moments of the polarizability and static interaction potential are evaluated numerically.

We examine the effects of the various interaction potential terms and electron exchange on the integral and differential scattering cross sections to learn in which energy and angular regions each is most important. The calculations show that the relative contribution of the static interaction to the integral cross sections increases with increasing energy, is smaller for Q_{01} than for Q_{00}, and otherwise increases with increasing v'. Conversely, scattering by the polarization potential contributes appreciably to Q_{01} at low energies and relatively little to Q_{03} at high energies. The effect of exchange is predicted to be small at energies above about 20 eV, to decrease rapidly with increasing energy, and to be smaller for vibrational excitation than for elastic scattering. The shape and magnitude of the low angle DCS's for elastic scattering and vibrational excitation are determined primarily by scattering by the polarization potential. At high angles, the static interaction is dominant.

The calculations are in fair agreement with the high energy ($E > 100$ eV) experimental elastic scattering data at low angles (considering the errors in the experiments), but the inclusion of

distortion of the scattering wave functions is apparently necessary to correctly predict the high angle DCS's. We show how to improve the present calculations to include distortion of the lowest two partial waves while retaining the plane wave scattering approximation for all higher ones. Our high-energy integral elastic scattering and vibrational excitation cross sections, calculated without distortion, should be the best estimates available of the cross sections in that energy range.

The present calculations are also compared with previous theoretical and experimental low-energy elastic cross sections. The polarized Born approximation is in good agreement with experiment above about 5 eV and the polarized Born-Ochkur-Rudge approximation is in good agreement with experiment above about 1 eV.

In two subsequent articles, calculations using the present method will be compared with all available intermediate energy elastic scattering DCS's for H_2 and with all available cross section data for vibrational excitation of H_2.

APPENDIX A: PROPERTIES OF Dn POTENTIALS

The Dn potential is given by

$$\nu_L^D(n,r) = -\frac{\alpha_L}{2r^4}\left[1 - \exp(-r^n/a_L^n)\right] \qquad \text{(A1)}$$

For a given n, increasing a_L yields a potential which is broader, less attractive, and has its minimum at larger r. For a fixed a_L, increasing n gives a potential which is narrower with little change in depth and a minimum at larger r. The shape of the potential as a function of r can be characterized by defining a dimensionless potential

$$\mu_L^D(n,r) \equiv \frac{2a_L^4}{\alpha_L}\,\nu_L^D \quad , \qquad \text{(A2)}$$

which implies

$$\mu_L^D = -\rho_L^{-4}\left[1 - \exp(-\rho_L^n)\right] \qquad \text{(A3)}$$

where $\rho_L \equiv r/a_L$. The minimum value of μ_L^D, its full-width at half-minimum, and the position of its minimum are presented in table A1 for n equal 3 to 10. It is then a simple procedure to calculate these same quantities for any ν_L^D given n, a_L, and α_L.

Table A1. Properties of the dimensionless potential μ_L^D defined in Eq. (A3). ρ_L^{min} is the value of ρ_L at the minimum of μ_L^D. $(\Delta\rho_L)_{1/2}$ is the full-width at half-minimum of μ_L^D.

n	ρ_L^{min}	$(\Delta\rho_L)_{1/2}$	$-\mu_L^D(n,\rho_L^{min})$
3	0.0	-	∞
4	0.0	1.5936	1.0000
5	0.8450	0.9541	0.6865
6	0.9559	0.7584	0.6392
7	1.0044	0.6438	0.6322
8	1.0289	0.5682	0.6382
9	1.0421	0.5146	0.6489
10	1.0493	0.4745	0.6613

APPENDIX B: ANALYTIC EXPRESSIONS FOR SCATTERING AMPLITUDES

Analytic expressions are given below for $N_\alpha(Y)$, $M_{\alpha'}(Y)$, and $M_Q(Y)$ where Y indicates the form used for g, g′, or f in Eqs. (40), (44), or (45), respectively. Si is the standard notation for the sine integral; $C = qa_P$, $qa_{P'}$, and qa_Q for N_α, $M_{\alpha'}$, and M_Q, respectively.

$$N_\alpha(A) = \frac{\pi}{4c} \exp(-c)$$

$$N_\alpha(C) = \frac{1}{2c^2} (\sin c + c \cos c) + Si(c)/2 - \pi/4$$

$$N_\alpha(B) = N_\alpha(C) + \left(\frac{1}{c^4}\right) (\sin c - c \cos c)$$

$$M_{\alpha'}(A) = \left(\frac{1}{4c^4}\right) [-6q\pi + q\pi (c^3 + 3c^2 + 6c + 6) \exp (-c)]$$

$$M_{\alpha'}(C) = \left(\frac{q}{16c^4}\right) [(2c^2 - 12) \sin c + (2c^3 + 12c) \cos c + c^4 (2Si(c) - \pi]$$

$$M_{\alpha'}(B) = M_{\alpha'}(C) + \left(\frac{1}{c^4}\right) [4q \sin c - cq \cos c - 3qSi(c)]$$

$$M_Q(C) = \left(\frac{1}{c^3}\right) (c \cos c - \sin c)$$

$$M_Q(B') = M_Q (C) + \left(\frac{1}{c^3}\right) [4 \sin c - c \cos c - 3Si(c)]$$

$$M_Q(B) = M_Q (C) + \left(\frac{1}{c^4}\right) [5c \sin c + 8 (\cos c - 1) - c^2 \cos c]$$

The expression $N_{\alpha}(C)$ was first given by Breig and Lin.[3] They also gave expressions for M when the far-field (F) forms (f = g = 1) are used, viz., $M_{\alpha'}(F) = -\pi q/16$ and $M_{Q}(F) = -(1/3)$.

Table I. Comparison of model potential V_2^1 with the accurate static potential of Ardill and Davison for $R = R_e$.

Form	Best a_Q[a] (a_0)	Max. deviation[b] (%)	Ave. deviation[b] (%)
B′	2.0	11	7
B	1.9	13	9
C	1.5	30	17

[a]The deviations listed in the third and fourth columns both increase if any one of these a_Q is changed by $0.1\ a_0$.

[b]In the range $0.2\,a_0 \leq r \leq 2.0\,a_0$.

Table II. Properties of the Lane-Henry NP′ polarization potentials, $V_L^{NP'}(r, R_e)$; r_{min} is the position of the minimum in $V_L^{NP'}$, $\Delta r_{1/2}$ is the full-width at half-minimum.

L	r_{min} (a_0)	$\Delta r_{1/2}$ (a_0)	$V_L^{NP'}(r_{min})/\beta_L$ (a.u.)
0	1.5	1.4_7	-0.0182
2	1.5	1.4_3	-0.0248

[a] β_L is determined such that $V_L^{NP'} = -\beta_L/(2r^4)$ at $r = 5.0\ a_0$.

Table IIIa. Properties of the D potentials ν_0^D employed in the present work; r_{min} is the value of r at the minimum of ν_0^D and $\Delta r_{1/2}$ is the full-width at half-minimum. Column seven is the average percent absolute deviation of the Lane-Henry NP′ potential from $\nu_0^D(n, r)$ (see Eq. A1) over the range $1.0\,a_0 \leq r \leq 4.0\,a_0$ where α_0 is determined so that ν_0^D equals the NP′ potential at $r = 5.0\,a_0$.

Data set	n	a_0 (a.u.)	r_{min} (a.u.)	$\Delta r_{1/2}$ (a.u.)	$-\nu_0^D(r_{min})$ (a.u.)	Average % Deviation
1	5	2.10	1.77	2.00	0.0176	22
2	7	2.00	2.01	1.29	0.0198	37
3	5	1.70	1.44	1.62	0.0411	71
2.0	5	2.00	1.69	1.91	0.0214	29
1.7	6	1.70	1.62	1.29	0.0383	60
1.7	8	1.70	1.75	0.97	0.0382	52
1.2	6	1.20	1.15	0.91	0.154	204
1.2	8	1.20	1.23	0.68	0.154	193

Table IIIb. Properties of the D potentials ν_2^D (n, r) employed in the present work. (Refer to Table IIIa.)

Data set	n	a_2	r_{min}	$\Delta r_{1/2}$	$\frac{-\nu_2^D(r_{min})}{\alpha_2}$	Average % Deviation
1	5	1.80	1.52	1.72	0.0327	24
2	7	1.80	1.81	1.16	0.0301	20
3	5	1.70	1.44	1.62	0.0411	36
2.0	5	2.00	1.69	1.91	0.0214	11
1.7	6	1.70	1.62	1.29	0.0383	27
1.7	8	1.70	1.75	0.97	0.0382	26
1.2	6	1.20	1.15	0.91	0.154	141
1.2	8	1.20	1.23	0.68	0.154	131

Table IV. Parameters in the potential energy (a.u.).

Data set	a_Q	a_P	$a_{P'}$
1[a]	2.0	2.1	1.8
2	2.0	2.0	1.8
3	1.7	1.7	1.7
2.0	2.0	2.0	2.0
1.7	1.7	1.7	1.7
1.2	1.2	1.2	1.2
L	2.0	b	b

[a]In addition, "data set 1" implies form B′ for f and D5 for g and g′ unless explicitly stated otherwise.

[b]Special fit to Lane-Henry potential (see text, section B.1).

Table V. Vibrational matrix elements of the quadrupole moment and polarizability[a]. The number in parentheses, if any, is the power of ten by which the preceding number is to be multiplied.

v′	v	$Q_{v'v}$	$\alpha_{v'v}$	$\alpha'_{v'v}$
0	0	9.6777(-1)	5.4118	1.3482
1	0	1.7580(-1)	7.3878(-1)	4.0627(-1)
2	0	-2.2370(-2)	-7.1167(-2)	-8.1422(-3)
3	0	3.1210(-3)	9.9493(-3)	-3.7168(-3)

[a] in atomic units. The phase of the vibrational wave functions is chosen so that they are positive at large R.

Table VI. Coefficients for calculating scattering off the short range potential by equations (48), (49), (53). The number in parentheses denotes the power of ten by which the preceding number is to be multiplied.

v'v	00	10	20	30
i		$a_{v'v,i}$		
0	1.43 15(0)	6.00727(-2)	-1.32878(-2)	3.94784(-3)
1	-3.61175(-1)	1.47877(-1)	4.38564(-2)	-4.39155(-2)
2	3.66834(0)	-5.12082(0)	-3.77004(-1)	5.18085(-1)
3	-1.83074(1)	1.99999(1)	1.93515(0)	-2.19092(0)
4	3.38465(1)	-3.35461(1)	-3.66333(0)	3.72918(0)
5	-2.51615(1)	1.89624(1)	2.68402(0)	-2.27471(0)
i		$b_{v'v,i}$		
0	3.45352(-4)	-3.48046(-3)	9.155021(-5)	-3.39928(-5)
1	-1.45861(0)	1.65779(-1)	-3.75235(-3)	1.00812(-2)
2	-2.38204(0)	-1.11926(1)	2.83195(-1)	-1.56768(-1)
3	4.16715(0)	5.52215(1)	-9.18101(-1)	6.55858(-1)
4	-1.36967(1)	-1.05550(2)	1.39810(0)	-8.16063(-1)
5	0.0(0)	6.76053(1)	0.0(0)	0.0(0)

Table VI, continued.

v'v	00	10	20	30
i		$c_{v'v,i}$		
0	4.99990(-1)	1.63241(-6)	-5.95354(-7)	-1.02851(-6)
1	-1.77043(-1)	-4.09983(-2)	2.22216(-3)	-2.45187(-4)
2	1.97217(-2)	9.26648(-3)	9.46006(-4)	-1.56290(-4)
3	-1.05692(-3)	-7.48189(-4)	-1.88839(-4)	4.64519(-6)
4	2.68733(-5)	2.48411(-5)	9.40457(-6)	6.28837(-7)

Table VII. Ratios $\mathcal{R}_{01} = Q_{01}(Y)/Q_{00}(Y)$ of predicted integral cross sections when the terms Y are included in the scattering amplitude calculated using DS1. Numbers in parentheses are powers of 10 by which preceding numbers are to be multiplied.

Y \ E(eV)	5	10	50	100
S_0	9.31(-4)	8.30(-4)	5.07(-3)	6.43(-3)
S_2	9.81(-2)	7.44(-2)	2.91(-2)	2.03(-2)
S_0S_2	1.32(-3)	1.79(-3)	7.62(-3)	8.52(-3)
P_0^{D5}	1.85(-2)	1.86(-2)	1.86(-2)	1.86(-2)
P_2^{D5}	8.50(-2)	8.89(-2)	9.08(-2)	9.08(-2)
$P_0^{D5}P_2^{D5}$	1.87(-2)	1.90(-2)	1.92(-2)	1.92(-2)
$S_0P_0^{D5}$	6.39(-3)	5.70(-3)	7.77(-3)	8.40(-3)
$S_2Q_2^{B'}$	5.17(-2)	5.37(-2)	3.20(-2)	2.49(-2)
$Q_2^{B'}P_2^{D5}$	4.53(-2)	4.85(-2)	5.05(-2)	5.05(-2)
$S_2Q_2^{B'}P_2^{D5}$	5.83(-2)	6.02(-2)	3.84(-2)	3.01(-2)
$S_0E_0P_0^{D5}$	9.40(-3)	6.06(-3)	6.95(-3)	7.72(-3)
$S_0E_0P_0^{D5}S_2Q_2^{B'}P_2^{D5}$	1.03(-2)	7.46(-3)	9.16(-3)	9.81(-3)
$S_0P_0^{D5}S_2Q_2^{B'}P_2^{D5}$	7.08(-3)	7.12(-3)	1.03(-2)	1.07(-2)
$Q_2^{B'}$	3.18(-2)	3.27(-2)	3.30(-2)	3.30(-2)
S_0E_0	2.01(-3)	1.29(-3)	4.86(-3)	6.09(-3)
$P_0^{D5}Q_2^{B'}P_2^{D5}$	1.93(-2)	2.00(-2)	2.05(-2)	2.05(-2)
$S_0S_2Q_2^{B'}$	2.18(-3)	2.99(-3)	8.74(-3)	9.55(-3)

Table VIII. $Q_{01}(Y)/Q_{01}(Z)$ for DS1.

Y/Z \ E(eV)	1	5	10	50	100
$P_0Q_2P_2/S_0P_0S_2Q_2P_2$	0.661	0.595	0.541	0.342	0.322
$P_0P_2/P_0Q_2P_2$	0.984	0.939	0.909	0.890	0.890
$S_0S_2Q_2/S_0P_0S_2Q_2P_2$	0.043	0.101	0.171	0.420	0.454
$P_0P_2/S_0P_0S_2Q_2P_2$	0.650	0.559	0.492	0.304	0.287
$S_0P_0/S_0P_0S_2Q_2P_2$	0.986	0.890	0.779	0.689	0.701
$S_0S_2/S_0P_0S_2Q_2P_2$	0.036	0.060	0.099	0.354	0.393
$S_0S_2/S_0S_2Q_2$	0.828	0.592	0.580	0.843	0.864
$S_0P_0Q_2P_2/S_0E_0P_0S_2Q_2P_2$	0.965	0.912	0.947	0.950	0.964

Table IX. Q_{01} (Y) in units of 10^{-2} a_0^2 at E = 20 eV.

a_P \ Z	A	B	C	D5	D7 (or L)
			$Y = P_0^Z$		
2.1	1.84	9.15	2.90	5.36	4.31
2.0	2.24	11.11	3.53	6.50	5.22
1.7	4.29	21.23	6.68	12.39	9.90[a]
1.2	16.97	85.13	25.51	49.72	
L					4.08(L)
			$Y = S_0P_0^Z$		
2.1	4.41	14.25	6.73	9.81	8.70
2.0	4.90	16.44	7.73	11.24	9.95(D7)
1.7	7.23	27.08	12.14	17.92	15.61
L					7.95(L)

[a] For D8, the result is 9.32.

Table X. $Q_{01}(S_2Q_2{}^{Y}P_2{}^{Z})$ in units of 10^{-2} $a_0{}^2$ at E = 20 eV. All distances in atomic units.

Y, Z \ $a_Q, a_{P'}$	2.0, 2.0	2.0, 1.8	2.0, L	1.7, 1.7
B'A	3.07	2.94		3.65
B'B	4.15	4.55		5.20
B'C	3.32	3.63		4.20
B'D5	3.75	4.08		4.69
B'D7	3.62	3.95		4.55
B'L			3.78	
BB	4.31	4.72		5.36
BC	3.46	3.78		4.33
BD5	3.90	4.24		4.83
BD7	3.76	4.11		4.69
BL			3.93	
CC	2.81	3.09		3.66
CD5	3.20	3.50		4.11
CD7	3.08	3.38		3.99
CL			3.22	

TABLE XI. Ratios $\mathcal{R}_{12} = Q_{02}(Y)/Q_{01}(Y)$ of predicted integral cross sections when the terms Y are included in the scattering amplitude calculated using data set 1.

Y \ E(eV)	10	50	100	a
S_0	6.03	2.27	4.21	-2
S_2	0.303	3.18	6.27	-2
S_0S_2	2.93	2.64	4.95	-2
P_0^{D5}	9.20	9.26	9.27	-3
P_2^{D5}	3.93	4.02	4.02	-4
$P_0^{D5}P_2^{D5}$	8.95	8.91	8.92	-3
$S_0P_0^{D5}$	1.69	1.64	2.39	-2
$S_2Q_2^{B'}$	0.633	2.53	4.70	-2
$Q_2^{B'}P_2^{D5}$	6.12	5.75	5.76	-3
$S_2Q_2^{B'}P_2^{D5}$	0.420	1.76	3.25	-2
$S_0E_0P_0^{D5}$	1.78	1.69	2.44	-2
$S_0E_0P_0^{D5}S_2Q_2^{B'}P_2^{D5}$	1.48	1.71	2.68	-2
$S_0P_0^{D5}S_2Q_2^{B'}P_2^{D5}$	1.41	1.68	2.64	-2
$Q_2^{B'}$	1.60	1.62	1.62	-2
S_0E_0	5.04	2.26	4.09	-2
$P_0^{D5}Q_2^{B'}P_2^{D5}$	8.83	8.75	8.76	-3
$S_0S_2Q_2^{B'}$	2.07	2.40	4.43	-2
$S_0E_0S_2Q_2^{B'}$	2.38	2.37	4.34	-2

(TABLE XI continued)

E(eV) / Y	10	50	100	a
$S_0P_0^AS_2Q_2^{B'}P_2^A$	1.77	2.13	3.58	-2
$S_0P_0^BS_2Q_2^{B'}P_2^B$	1.38	1.58	2.35	-2
$S_0P_0^CS_2Q_2^{B'}P_2^C$	1.35	1.78	3.06	-2

[a]Power of 10 by which the other numbers in that row are to be multiplied.

TABLE XII. Ratios $\mathcal{R}_{23} = Q_{03}(Y)/Q_{02}(Y)$ of predicted integral cross sections when the terms Y are included in the scattering amplitude calculated using data set 1. All the ratios in this table have been multiplied by 100.

E(eV) / Y	10	45	100
S_0	9.87	5.10	5.69
S_2	0.128	3.48	7.03
S_0S_2	9.32	4.31	6.30
P_0^{D5}	1.93	1.95	1.95
P_2^{D5}	20.4	20.8	20.8
$P_0^{D5}P_2^{D5}$	1.95	1.98	1.99
$S_0P_0^{D5}$	4.42	3.74	4.67
$S_2Q_2^{B'}$	0.886	3.07	6.59
$Q_2^{B'}P_2^{D5}$	0.546	0.482	0.486
$S_2Q_2^{B'}P_2^{D5}$	0.294	2.80	6.40
$S_0E_0P_0^{D}5$	4.80	3.72	4.81
$S_0E_0P_0^{D5}S_2Q_2^{B'}P_2^{D5}$	4.54	3.45	5.36
$S_0P_0^{D5}S_2Q_2^{B'}P_2^{D5}$	4.15	3.45	5.30
$Q_2^{B'}$	1.92	1.95	1.94
S_0E_0	9.43	4.74	5.78
$P_0^{D5}Q_2^{B'}P_2^{D5}$	1.82	1.81	1.81
$S_0S_2Q_2^{B'}$	7.85	4.02	6.12
$S_0E_0S_2Q_2^{B'}$	8.06	3.96	6.14

(TABLE XII continued)

Y \ E(eV)	10	45	100
$S_0P_0{}^AS_2Q_2{}^{B'}P_2{}^A$	5.13	3.82	5.73
$S_0P_0{}^BS_2Q_2{}^{B'}P_2{}^B$	3.80	3.32	5.02
$S_0P_0{}^CS_2Q_2{}^{B'}P_2{}^C$	4.59	3.65	5.63

TABLE XIII. $Q_{02}(Y)/Q_{02}(Z)$ for data set 1.

Y/Z \ E(eV)	10	50	100
$S_0S_2Q_2/S_0P_0S_2Q_2P_2$	0.251	0.600	0.761
$P_0Q_2P_2/S_0P_0S_2Q_2P_2$	0.339	0.178	0.107
$P_0P_2/P_0Q_2P_2$	0.921	0.907	0.907
$S_0P_0/S_0P_0S_2Q_2P_2$	0.934	0.673	0.633
$S_0S_2/S_0S_2Q_2$	0.821	0.929	0.966
$S_0P_0S_2Q_2P_2/S_0E_0P_0S_2Q_2P_2$	0.892	0.932	0.953

TABLE XIV. $Q_{03}(Y)/Q_{03}(Z)$ for data set 1.

Y/Z \ E(eV)	10	45	100
$S_0S_2Q_2/S_0P_0S_2Q_2P_2$	0.475	0.657	0.845
$P_0Q_2P_2/S_0P_0S_2Q_2P_2$	0.149	0.102	0.036
$P_0P_2/P_0Q_2P_2$	0.988	0.993	0.993
$S_0P_0/S_0P_0S_2Q_2P_2$	0.995	0.747	0.564
$S_0S_2/S_0S_2Q_2$	0.975	0.981	0.995
$S_0P_0S_2Q_2P_2/S_0E_0P_0S_2Q_2P_2$	0.815	0.930	0.942

TABLE XV. $Q_{02}(Y)$ $(10^{-4}a_0^2)$ at E = 45 eV.

a_P \ Z	A	B	C	D5
		$Y = P_0^Z$		
2.1	0.760	3.78	1.22	2.21
2.0	0.924	4.60	1.48	2.69
1.7	1.77	8.81	2.80	5.15
1.2	7.14	35.3	11.2	20.6
		$Y = S_0P_0^Z$		
2.1	5.87	11.4	5.90	8.65
2.0	6.22	12.8	6.46	9.60
1.7	7.83	19.4	9.44	14.0
1.2	15.2	51.3	24.2	34.9

TABLE XVI. $Q_{03}(Y)$ $(10^{-5}\ a_0^2)$ at E = 20 eV.

a_P \ Z	A	B	C	D5	D7
		$Y = P_0^Z$			
2.1	0.330	1.64	0.519	0.960	0.772
2.0	0.402	2.00	0.631	1.17	0.937
1.7	0.771	3.83	1.20	2.23	1.78
		$Y = S_0 P_0^Z$			
2.1	5.16	8.46	4.83	6.59	5.83
2.0	5.44	9.32	5.18	7.17	6.32
1.7	6.69	13.3	6.84	9.85	8.59
		$Y = S_0 E_0 P_0^Z$			
2.1	5.81	9.10	5.54	7.26	6.52
2.0	6.09	9.95	5.88		7.01
1.7	7.31	13.8	7.53		9.25

TABLE XVII. $Q_{02}(S_2Q_2^{Y}P_2^{Z})$ $(10^{-4}\ a_0^2)$ at E = 45 eV.

Y, Z \ $a_Q, a_{P'}$	2.0, 2.0	2.0, 1.8	1.7, 1.7	1.2, 1.2
B′A	3.83	3.82	4.29	5.67
B′B	3.92	3.99	4.47	6.15
B′C	3.78	3.80	4.25	5.79
B′D5	3.86	3.91	4.37	5.97
BB	4.15	4.22	4.72	6.40
BC	4.00	4.03	4.50	6.03
BD5	4.09	4.14	4.63	6.21
CC	3.27	3.30	3.53	4.90
CD5	3.35	3.39	3.64	5.06

TABLE XVIII. $Q_{03}(S_2Q_2^{Y}P_2^{Z})$ $(10^{-6}\ a_0^2)$ at E = 20 eV.

Y, Z \ $a_Q, a_{P'}$	2.0, 2.0	2.0, 1.8	1.7, 1.7
B′A	0.865	0.930	1.05
B′B	0.507	0.421	0.543
B′C	0.768	0.659	0.843
B′D5	0.612	0.520	0.670
BB	0.588	0.489	–
BC	0.881	0.760	0.945
BD5	0.709	0.604	0.757
CC	0.440	0.376	0.507
CD5	0.347	0.300	0.394

Table XIX. Integral elastic cross sections (a_0^2) computed without exchange with data set 1, the B'form for f, and the indicated forms, if any, for g and g'.[a]

E (eV)	S_0	$S_0P_0^{D5}$	BXP	B/P(D5)	B/P(A)	B/P(B)	B/P(C)
90	1.70	3.62	2.05	4.04	3.24	5.17	3.05
100	1.53	3.26	1.86	3.64	2.92	4.66	2.76
125	1.22	2.61	1.50	2.93	2.36	3.75	2.22
150	1.02	2.17	1.26	2.45	1.97	3.13	1.86
200	0.766	1.63	0.977	1.84	1.48	2.36	1.40
350	0.439	0.934	0.551	1.06	0.852	1.35	0.804
412	0.373	0.793	0.467	0.899	0.724	1.15	0.684
600	0.256	0.545	0.319	0.618	0.498	0.788	0.470
820	0.187	0.399	0.234	0.452	0.364	0.576	0.343
912	0.168	0.358	0.210	0.406	0.327	0.518	0.309

[a]Columns 4-8 include a small contribution from rotational excitation as discussed in section B.2.

Table XX. Integral 0 → 1 vibrational excitation cross sections ($10^{-2}a_0^2$) computed as in Table XIX.

E (eV)	S_0	$S_0P_0^{D5}$	BXP	B/P(D5)	B/P(A)	B/P(B)	B/P(C)
90	1.076	3.02	1.95	4.31	2.78	5.45	3.31
100	0.982	2.74	1.77	3.90	2.52	4.93	3.00
125	0.798	2.20	1.45	3.15	2.05	3.98	2.42
150	0.668	1.84	1.23	2.65	1.73	3.33	2.04
200	0.503	1.38	0.952	2.02	1.32	2.53	1.56
350	0.287	0.790	0.565	1.18	0.777	1.46	0.914
412	0.244	0.670	0.484	1.00	0.664	1.25	0.781
600	0.168	0.460	0.335	0.690	0.459	0.859	0.538
820	0.123	0.337	0.245	0.505	0.336	0.629	0.395
912	0.110	0.303	0.221	0.454	0.302	0.566	0.356

Table XXI. Integral 0 → 2 vibrational excitation cross sections ($10^{-4}a_{0_2}^2$) computed as in Table XIX.

E (eV)	S_0	$S_0P_0^{D5}$	BXP	B/P(D5)	B/P(A)	B/P(B)	B/P(C)
90	4.16	6.82	8.02	10.76	9.33	12.14	9.48
100	4.13	6.53	7.84	10.3	9.02	11.57	9.17
125	3.92	5.83	7.22	9.20	8.17	10.22	8.25
150	3.62	5.21	6.55	8.20	7.34	9.04	7.38
200	3.03	4.23	5.37	6.61	5.97	7.24	6.01
350	1.91	2.60	3.33	4.03	3.66	4.39	3.69
412	1.64	2.23	2.85	3.46	3.14	3.76	3.16
600	1.15	1.55	1.98	2.40	2.18	2.61	2.20
820	0.844	1.14	1.46	1.76	1.60	1.91	1.61
912	0.760	1.02	1.31	1.58	1.44	1.72	1.45

REFERENCES

1. The next paper in the series is S. Trajmar, D.G. Truhlar, and J.K. Rice, J. Chem. Phys., to be published, and paper III is S. Trajmar, D. G. Truhlar, J. K. Rice, and A. Kuppermann, J. Chem. Phys., to be published.
2. K. Takayanagi, J. Phys. Soc. Japan 20, 562 (1965).
3. E.L. Breig and C.C. Lin, J. Chem. Phys 43, 3839 (1965).
4. W. Kolos and L. Wolniewicz, J. Chem. Phys. 46, 1426 (1967).
5. T.R. Carson, Proc. Phys. Soc. (London)A 67, 909 (1954).
6. M.R.H. Rudge, Proc. Phys. Soc. (London) 86, 763 (1965).
7. D.G. Truhlar, D.C. Cartwright, and A. Kuppermann, Phys. Rev. 175, 113 (1968).
8. R.L. Wilkins and H.S. Taylor, J. Chem. Phys. 47, 3532 (1967).
9. J.C. Tully and R.S. Berry, J. Chem. Phys. 51, 2056 (1969).
10. R.J.W. Henry and N.F. Lane, Phys. Rev. 183, 221 (1969).
11. J.B. Fisk, Phys. Rev. 51, 25 (1937).
12. S. Nagahara, J. Phys. Soc. Japan 9, 52 (1952).
13. S.P. Khare and B.L. Moisiewitsch, Proc. Phys. Soc. (London) 85, 821 (1965).
14. S. Hara, J. Phys. Soc. Japan 22, 710 (1967).
15. D.E. Golden, H.W. Bandel, and J.A. Salerno, Phys. Rev. 146, 40 (1966).

16. H. Ehrhardt, L. Langhans, F. Linder, and H.S. Taylor, Phys. Rev. 173, 222 (1968).

17. J.H. McMillen, Phys. Rev. 36, 1034 (1930).

18. F.L. Arnot, Proc. Roy. Soc. A133, 615 (1931).

19. C.B.O. Mohr and F.H. Nicoll, Proc. Roy. Soc. 138, 469 (1932).

20. G.M. Webb, Phys. Rev. 47, 384 (1935).

21. N.F. Mott and H.S.W. Massey, "The Theory of Atomic Collisions," 3rd ed., Oxford at the Clarendon Press (1965); (a) Chapter V, §3. 2, (b) Chapter XVI, §5.

22. E. Gerjuoy and S. Stein, Phys. Rev. 97, 1671 (1955); 98, 1848 (1955).

23. K. Takayanagi and S. Geltman, Phys. Rev. A138, 1003 (1965).

24. E.N. Lassettre, Scientific Report 1 for Contract No. AF19 (122)-642, Technical Report Nos. AFCRC-TN-57-244 and AD-133822 (The Ohio State Research Foundation, Columbus, Ohio, 1957), unpublished.

25. J.D. Craggs and H.S.W. Massey, "Handbuch der Physik," edited by S. Fluegge (Springer-Verlag, Berlin, 1959) 37, 314, 333f.

26. A.M. Arthurs and A. Dalgarno, Proc. Phys. Soc. A256, 540 (1960).

27. A. Dalgarno and R.J. Moffett, Proc. Natl. Acad. Sci. India A33, 511 (1963).

28. K. Takayanagi, JILA Report No. 11 (University of Colorado, Boulder, 1964), unpublished.

29. J.M. Peek, Phys. Rev. 134, 877 (1964) and S.P. Khare, ibid. 149, 33 (1966).

30. A. Temkin and V. Vasavada, Phys. Rev. 160, 109 (1967).

31. D.C. Cartwright and A. Kupperman, Phys. Rev. 163, 86 (1967).

32. O.H. Crawford, A. Dalgarno, and P.B. Hays, Molecular Physics 13, 181 (1967).

33. M. Weinberg, R.S. Berry, and J.C. Tully, J. Chem. Phys. 49, 122 (1968).

34. C.J. Lenander, Air Force Report No. SSD-TR-66-91 with Aerospace Report No. TR-1001 (2240-20)-1 (Aerospace Corporation, 1966), unpublished.

35. N.F. Lane and S. Geltman, Phys. Rev. 160, 53 (1967).

36. J. Callaway, R.W. LaBahn, R.T. Pu, and W.M. Duxler, Phys. Rev. 168, 12 (1968).

37. We use Hartree atomic units. In these units the energy is in hartrees (1 h = 27.210 eV), distance is in first Bohr radii a_0, and differential cross sections are in a_0^2/steradian.

38. R.W. B. Ardill and W.D. Davison, Proc. Roy. Soc. (London) A304, 465 (1968).

39. The importance for vibrational excitation of the R-dependence of the atomic orbital exponents was first pointed out by H.S.W. Massey, Trans. Faraday Soc. 31, 556 (1935).

40. D.G. Truhlar, unpublished calculation (1966).

41. See ref. 36 and footnotes 1-7 therein.

42. V.M. Martin, M.J. Seaton, and J.G.B. Wallace, Proc. Phys. Soc. (London), 72, 701 (1958).

43. M.H. Mittleman and K.M. Watson, Phys. Rev. 113, 198 (1959); M.H. Mittleman, Ann. Phys. (New York) 14, 94 (1961); M.H. Mittleman and J.L. Peacher, Phys. Rev. 133, 160 (1968).

44. A. Temkin, Phys. Rev. 116, 358 (1959).

45. L.A. Vainshtein, in "Atomic Collisions," edited by V. Ya. Veldre (Academy of Sciences of the Latvian SSR, Riga, 1963). [English translation by M.I.T. Press, Cambridge, Mass., 1966, see p. 63];

46. C.J.Kleinman, Y. Hahn, and L. Spruch, Phys. Rev. 165, 53 (1958).

47. N.F. Lane and R.J.W. Henry, Phys. Rev. 173, 183 (1968).

48. For a review, see P.G. Burke, in "Atomic Physics," edited by V.W. Hughes. B. Bederson, V.W. Cohen, and F.J. Pichanick, (Plenum Press, New York, 1969), p. 265.

49. S.P. Khare and B.L. Moisiewitsch, in "Atomic Collision Processes," edited by M.R.C. McDowell, North-Holland Publishing Co., Amsterdam, 1964, p. 49.

50. R.J. Drachman, Phys. Rev. 144, 25 (1966).

51. R.T. Pu and E.S. Chang, Phys. Rev. 151, 31 (1966).

52. S.P. Khare, Proc. Phys. Soc. 86, 25 (1965).

53. D.H. Sampson and R.C. Mjolsness, Phys. Rev. 140, A1466 (1965).

54. For the NP potentials of Lane and Henry, good overall fits to the shape are obtained with n = 5, $a_{P'} = a_P = 2.4\ a_0$ or n = 7, $a_P = a_{P'} = 2.2\ a_0$.

55. See, for example, G. Karl and J.D. Poll, J. Chem. Phys. 46, 2944 (1967) and G. Karl, Can. J. Phys. 46, 1973 (1968).

56. A.R. Edmonds, "Angular Momentum in Quantum Mechanics," (Princeton University Press, Princeton, 1957), pp. 46, 50, 53. In equation (3.7.3) there is a misprint; the corrected factor is $(2j_3 + 1)^{-1/2}$.

57. W. Kolos and L. Wolneiwicz, J. Chem. Phys. 43, 2429 (1965).

58. "Handbook of Mathematical Functions," edited by M. Abramowitz and I.A. Stegun (N.B.S. Applied Mathematics Series No. 55, 1964), Eq. 25.3.23.

59. J. Ortega, in "Mathematical Methods for Digital Computers," Vol. II, edited by R. Ralston and H.S. Wilf (John Wiley and Sons, New York, 1967), p. 94.

60. D.J. Diestler and V. McKoy, J. Chem. Phys. 47, 454 (1967); N.W. Winter, D.J. Diestler, and V. McKoy, J. Chem. Phys. 48, 1879 (1968).

61. D.G. Truhlar and A. Kuppermann, to be published.

62. D.G. Rush, Trans. Faraday Soc. 64, 2013 (1968).

63. L. Wolneiwicz, J. Chem. Phys. 45, 515 (1966).

64. R. Bulirsch and J. Stoer, Numer. Math. 8, 1 (1966).

65. E.N. Lassettre, J. Chem. Phys. 43, 4479 (1965).

66. P.M. Stone and J.R. Reitz, Phys. Rev. 131, 1201 (1963).

67. S.N. Banerjee, R. Jha, and N.C. Sil, Indian J. Physics 40, 489 (1966).

68. O. Bely, Nuovo Cimento 49b, 66 (1967).

69. D.G. Truhlar, J.K. Rice, A. Kupperman, S. Trajmar, and D.C. Cartwright, Phys. Rev., to be published. This paper reviews the derivation of Eq. (50) and relevant references.

70. B.H. Bransden, A. Dalgarno, T.L. John, and M.J. Seaton, Proc. Phys. Soc. 71, 877 (1958).

71. V.M. Martin, M.J. Seaton, and J.B.G. Wallace, Proc. Phys. Soc. (London) 72, 701 (1958).

72. K. Takayanagi, Progr. Theor. Phys. 11, 557 (1954), p. 584.

73. C.F. Curtiss and R.B. Bernstein, J. Chem. Phys. 50, 1168 (1969).

74. W.D. Davison, Discussions Faraday Soc. 33, 71 (1962).

75. C.S. Roberts, Phys. Rev. 131, 209 (1963).

76. H.S.W. Massey, Trans. Faraday Soc. 31, 556 (1935).

77. R.W. LaBahn and J. Callaway, Phys. Rev. 180, 91 (1969).

78. C. Ramsauer and R. Kollath, Ann. Phys. 4, 91 (1929).

FIGURE CAPTIONS

Fig. 1. Terms and sums of terms in the "theoretically most justifiable" semiempirical electron-molecule potential (for $R = 1.0$, 1.4, and $1.8\ a_0$) as functions of the electron-molecule separation distance. All quantities are in atomic units: (a) asymmetric Carson-type short-range potential V_2^C; (b) asymmetric static potential V_2^1; (c) whole asymmetric potential V_2; (d) symmetric Carson-type short-range potential V_0^C; (e) whole symmetric potential V_0. Part b also includes (as circles) the Ardill-Davison potential (for $R = 1.4\ a_0$) for comparison.

Fig. 2. Equicharacteristic lines for specific values of the characteristics r_{min}, $\nu_{min} = \mu_L^D(n, \rho_L^{min})$, and $\Delta r_{1/2}$ of reduced Dn polarization potentials (see Eq. (A3) as functions of the parameters of a_L and n.

Fig. 3. Polarization potentials (for $R = 1.4\ a_0$) as a function of the distance of the electron from the center-of-mass of H_2. The forms of the potential are indicated. The solid curves are the symmetric potentials with $a_P = 2.1\ a_0$ and the dotted ones are the asymmetric potentials with $a_P = 1.8\ a_0$. The circles and triangles are the NPS′ polarization potentials from Lane and Henry. The polarizabilities used for the curves are determined such that $V_L^{NPS'} = \alpha_L/(2r^4)$ at $r = 5.0\ a_0$.

Fig. 4. The potential $V(\underset{\sim}{r}, \underset{\sim}{\underset{\sim}{R}})$ for $R = 1.4\ a_0$ and its negative as a function of the position of the electron with respect to the center-of-mass of the H_2 molecule. Only one quadrant of the plane through the molecule is represented. The left side is a perspective view of the surface with spherical polar coordinate viewing angles $\Theta = 60°$ and $\phi = 30°$. The right side is a view of the negative of the same function from $\theta = 70°$ and $\phi = 80°$.

Fig. 5. Integral elastic cross sections as a function of impact energy for the parameters of data set 1. Each curve is calculated using the indicated amplitudes for scattering off the symmetric parts of the potential.

Fig. 6. Same as Fig. 5 except that it is for the asymmetric parts of the potential.

Fig. 7. Integral elastic cross sections as a function of impact energy calculated for scattering off the symmetric part of the polarization potential with $a_P = 2.1\ a_0$ and the asymmetric polarization potential with $a_{P'} = 1.8\ a_0$. The scattering predicted by the L forms for the polarization potentials is also shown.

Fig. 8. Elastic differential cross sections for $E = 20$ eV. Each curve is calculated using the indicated amplitudes for scattering off

the symmetric parts of the potential. Data set 1 was used. It is not shown that σ_{00} (P_0^{D5}) has a zero near 75°.

Fig. 9. Same as Fig. 8. Note that the predicted scattering off form A of the polarization potential is a monotonically decreasing function of angle over the whole angular range, reaching 1.55×10^{-4} a_0^2/sr at 180°. σ_{00} (P_0^{C}) decreases to 5.52×10^{-5} a_0^2/sr at 180°.

Fig. 10. Elastic differential cross sections for E = 20 eV calculated using data set 1 for the indicated amplitudes.

Fig. 11. Elastic differential cross sections calculated at E = 20 eV using data set 1 and the B′ form for f. Two calculations including polarization are shown with the forms used for g and g′ indicated. The Born approximation neglecting polarization is also compared with a calculation for which the quadrupole interaction term is omitted.

Fig. 12. Elastic differential cross sections at E = 35 eV. Each curve is calculated using the indicated amplitudes for scattering off the asymmetric long-range parts of the potential. Form B′ is used for f with $a_Q = 2.0\, a_0$, and form D5 is used for g′ with $a_p' = 1.8 a_0$. σ_{00} ($Q_2^{B'}$) has a zero near 155° and then rises to $7.20 \times 10^{-7} a_0^2$/sr at 180°.

Fig. 13. Elastic differential cross sections at E = 60 eV. Each curve is calculated using the indicated amplitudes with $a_P = 2.1\ a_0$ except for one curve for which $a_P = 1.2\ a_0$. $\sigma_{00}\ (P_0^{D5})$, which is shown to 90°, has a second zero near 100°, rises to a peak of 2.66×10^{-5} a_0^2/sr at 120° and then decreases monotonically to 2.02×10^{-6} a_0^2/sr at 180°. $\sigma_{00}\ (P_0^{B})$, which is shown to 40°, has a zero near 48°, rises to a peak of 4.86×10^{-3} a_0^2/sr near 65°, falls to zero again near 100°, rises to a second peak of 3.22×10^{-4} a_0^2/sr near 125° and then decreases monotonically to 1.12×10^{-4} a_0^2/sr at 180°. $\sigma_{00}\ (P_0^{A})$, which is shown to 75°, decreases monotonically to 8.94×10^{-8} a_0^2/sr at 180°.

Fig. 14. Elastic differential cross sections at E = 60 eV. Each curve is calculated using the indicated amplitudes for scattering off the asymmetric parts of the potential. Data set 1.2 is used for the upper curve and data set 1 for the others. $\sigma_{00}\ (P_2^{D5})$ has a zero near 130°, rises to a peak of 1.30×10^{-7} a_0^2/sr near 155°, and then decreases to 1.25×10^{-7} a_0^2/sr at 180°.

Fig. 15. Elastic differential cross sections at E = 60 eV. Each curve is calculated using the indicated amplitudes with data set 1. σ_{00} (S_0S_2) is within about 7% of σ_{00} (BXP) over the whole angular range. σ_{00} (S_0) decreases monotonically to 8.68×10^{-5} a_0^2/sr at 180°.

Fig. 16. Integral 0 → 1 vibrational excitation cross sections as a function of impact energy calculated using various combinations of the interaction potentials for data set 1.

Fig. 17. Same as Fig. 16.

Fig. 18. Differential cross sections for v = 0, v′ = 1, E = 13.6 eV. These are calculated with data set 1 using the approximations or sets of amplitudes indicated.

Fig. 19. Differential cross sections for v = 0, v′ = 1, E = 13.6 eV. These are calculated with data set 1 using the sets of amplitudes indicated.

Fig. 20. Differential cross sections for v = 0, v′ = 1, E = 60 eV. The curves are calculated using data set 1 with the indicated amplitudes. The insert compares the B/P and BOR/P DCS's with the same angle scale as the other curves.

Fig. 21. Differential cross sections for v = 0, v′ = 1, E = 45 eV. The curves are calculated using the indicated amplitudes for scattering by the asymmetric parts of the potential with data set 1.7 except as noted.

Fig. 22. Differential cross sections in the polarized Born approximation for v = 0, v′ = 1; E = 13.6 eV. Each curve is labeled by the form used for f, the form used for g and g′, and the data set, respectively. Changing the form of f alone makes only a small change (less than 15% for data set 1.7 with form B for g and g′) and does this only at large angles ($\theta \gtrsim 60°$). The incomplete curve shown for the D7 polarization potential goes to 0.00498 a_0^2/sr at $\theta = 180°$.

Fig. 23. Differential cross sections calculated in the polarized Born approximation for v = 0, v′ = 1, E = 60 eV. Each curve is labeled by the forms used for f, the form used for g and g′, and the data set, respectively.

Fig. 24. Differential cross sections for v = 0, v′ = 1, E = 60 eV. These are calculated using the sets of amplitudes and the data sets shown.

Fig. 25. Differential cross sections for v = 0, v′ = 1, E = 13.6 eV. These are calculated with data set 1.7 using the sets of amplitudes indicated.

Fig. 26. Integral cross sections for v = 0, v′ = 2 calculated using the indicated approximations or amplitudes for DS1. The letters A, B, and C refer to the form of g and g′ used in the polarized Born calculations shown in the insert.

Fig. 27. Integral cross sections for v = 0, v′ = 2 calculated using the indicated approximations or amplitudes for DS1.

Fig. 28. Same as Fig. 27 except v = 0, v′ = 3.

Fig. 29. Same as Fig. 27 except v = 0, v′ = 3.

Fig. 30. Differential cross sections for v = 0, v′ = 2, and E = 20 eV, calculated using DS1 and the indicated amplitudes or approximations. Different ordinate scales, different by a factor of 20, are used on either side of $\theta = 60°$. σ_{02} (P_0^{D5}), which is not shown above 60°, drops to zero near 75°, rises to a peak of 1.00×10^{-6} a_0^2/sr near 110°, and then decreases monotonically to 4.81×10^{-7} a_0^2/sr at 180°. The BOR/P is not shown for $\theta < 60°$.

Fig. 31. Differential cross sections for v = 0, v′ = 3, and E = 20 eV calculated using DS1 and the indicated amplitudes or approximations. The minima in σ_{03} ($S_2Q_2{}^{B'}P_2{}^{D5}$) and σ_{03} (S_0) are near 100° and 140°, respectively.

Fig. 32. Differential cross sections for v = 0, v′ = 2, and E = 20 eV calculated using the polarized Born approximation. The curve labeled FF is calculated with form F for f, D7 for g, and F for g′ with DS2. The other curves are calculated with form B′ for f and the indicated form for g and g′ and data set, respectively.

Fig. 33. Differential cross sections for v = 0, v′ = 3, and E = 20 eV. The curve labeled F is σ_{03} ($S_0P_0{}^{D5}S_2Q_2{}^{F}$) calculated with DS1. The other curves are calculated in the polarized Born approximation with form B′ for f and the indicated form for g and g′ and indicated data set, respectively.

Fig. 34. Differential cross sections for v = 0, v′ = 3, and E = 20 eV calculated using the indicated approximations, amplitudes, and data sets. The BOR/P calculations use form B′ for f and the indicated form for g and g′. The BORXP calculation uses form B′ for f.

Fig. 35. Differential cross sections for elastic scattering. The curves are calculated in BXP approximations at 150, 421, and 812 eV using the B′ form with $a_Q = 2.0\ a_0$ for the quadrupole term. The effect of exchange on these curves is neglected but was calculated to be less than 4%. The diamonds are the experimental results of

McMillen at 150 eV and the circles are the experimental results of Arnot at 412 and 812 eV. For plotting purposes, all three experiments were arbitrarily normalized to the BXP curves at $\theta = 20°$.

Fig. 36. Differential cross sections for elastic scattering. The curves are calculated for data set 1 for an impact energy of 200 eV with various combinations of terms included in the interaction potential; in order of increasing magnitude at 40°, they include: $S_0S_2Q_2$, $S_0P_0S_2Q_2P_2$, S_0, S_2Q_2, S_2. One effect of adding exchange to the B/P calculation is to decrease the cross section 9% at 30°. The triangles are the experimental results of Webb at 200 eV and the circles are the experimental results of Arnot at 205 eV. For the plot, both experiments were arbitrarily normalized to the B/P curve at 30°.

Fig. 37. Differential cross sections for elastic scattering. The curves are calculated for data set 1, both adding and neglecting polarization for impact energies of 350, 600, and 912 eV. For each energy, the higher curve at the smallest angles is the B/P approximation. The triangles are Webb's experimental results at these same energies, arbitrarily normalized to the BXP curve at 20° in each case.

Fig. 38. Differential cross sections for elastic scattering at an impact energy of 125 eV. The shaded region covers the results predicted by the B/P calculation with data set 1 when either the B′ or the B or the C form is used for f and the D5 form is used for g and g′. The dots are the experiments of Mohr and Nicoll, arbitrarily normalized at a scattering angle of 50° to the calculation in which the B′ form is used for f. The lower curve shows the calculated results when just three long-range terms are included in the calculation (using data set 1, the B′ form for f, and the D5 form for g and g′).

Fig. 39. Integral elastic (including rotational excitation) cross sections for electron scattering from the ground state of H_2. The squares are the experiments of Golden, Bandel, and Salerno. The curves are quantal calculations in the following approximations: 1 - polarized Born, 2 - polarized Born-Ochkur-Rudge, 3 - calculation of Henry and Lane, including polarization but neglecting exchange, 4 - same as 3, except including exchange, 5 - Born, 6 - Born-Ochkur Rudge, 7 - calculation of Wilkins and Taylor neglecting polarization and exchange, 8 - same as 7, except including exchange, 9 - same as 8, except by Tully and Berry, 10 - same as 8, except by Henry and Lane.

Fig. 40. Low-energy differential cross sections. The circles are the experimental results of Ehrhardt et al. (Ref. 16) and the curves are calculated results (see Fig. 39) at E = 3.5 eV, except for curves 7, 8, and

9 which are at E = 3.4 eV. The DCS's from Refs. 8 and 9 were calculated with a program kindly supplied by Dr. John Tully.

Fig. 41. Integral elastic scattering cross sections as a function of energy. The lower dotted curve is the calculation of Fisk, the x's are the calculation of Nagahara, and the dashed curve is the calculation of Hara. The other curves are the present calculations using the theoretically justified static potential (B′ form for f) and various polarization potentials. The curve labeled DSL uses the special fit to the Lane-Henry potential for g and g′; and is in the B/P approximation. The remaining three curves are also in the B/P approximation and are labeled by the data set name and the form of cutoff function used for g and g′.

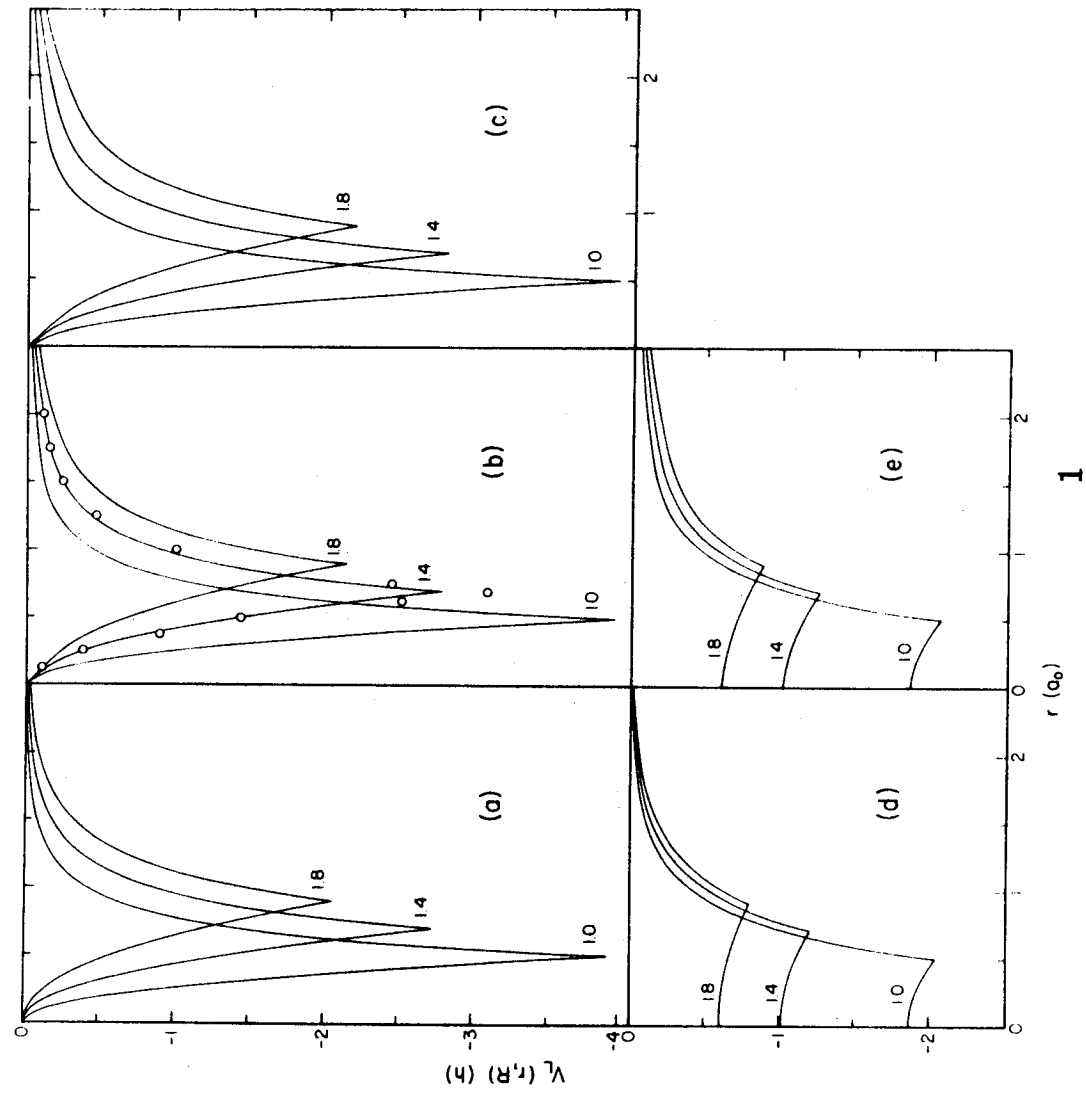

1

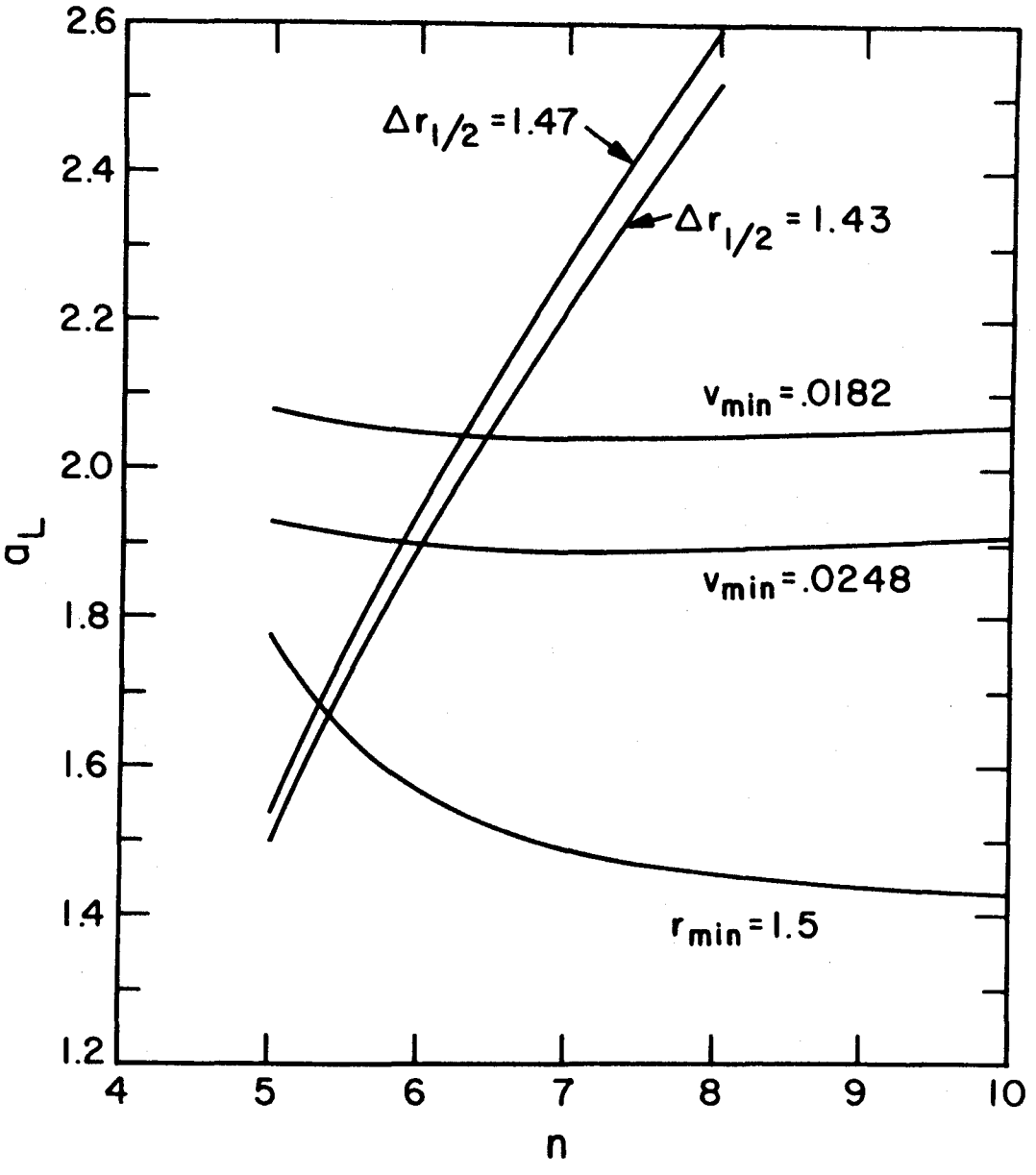
2.6
2.4
2.2
2.0
1.8
1.6
1.4
1.2
σ_L
4
5
6
7
8
9
10
n
$\Delta r_{1/2} = 1.47$
$\Delta r_{1/2} = 1.43$
$v_{min} = .0182$
$v_{min} = .0248$
$r_{min} = 1.5$

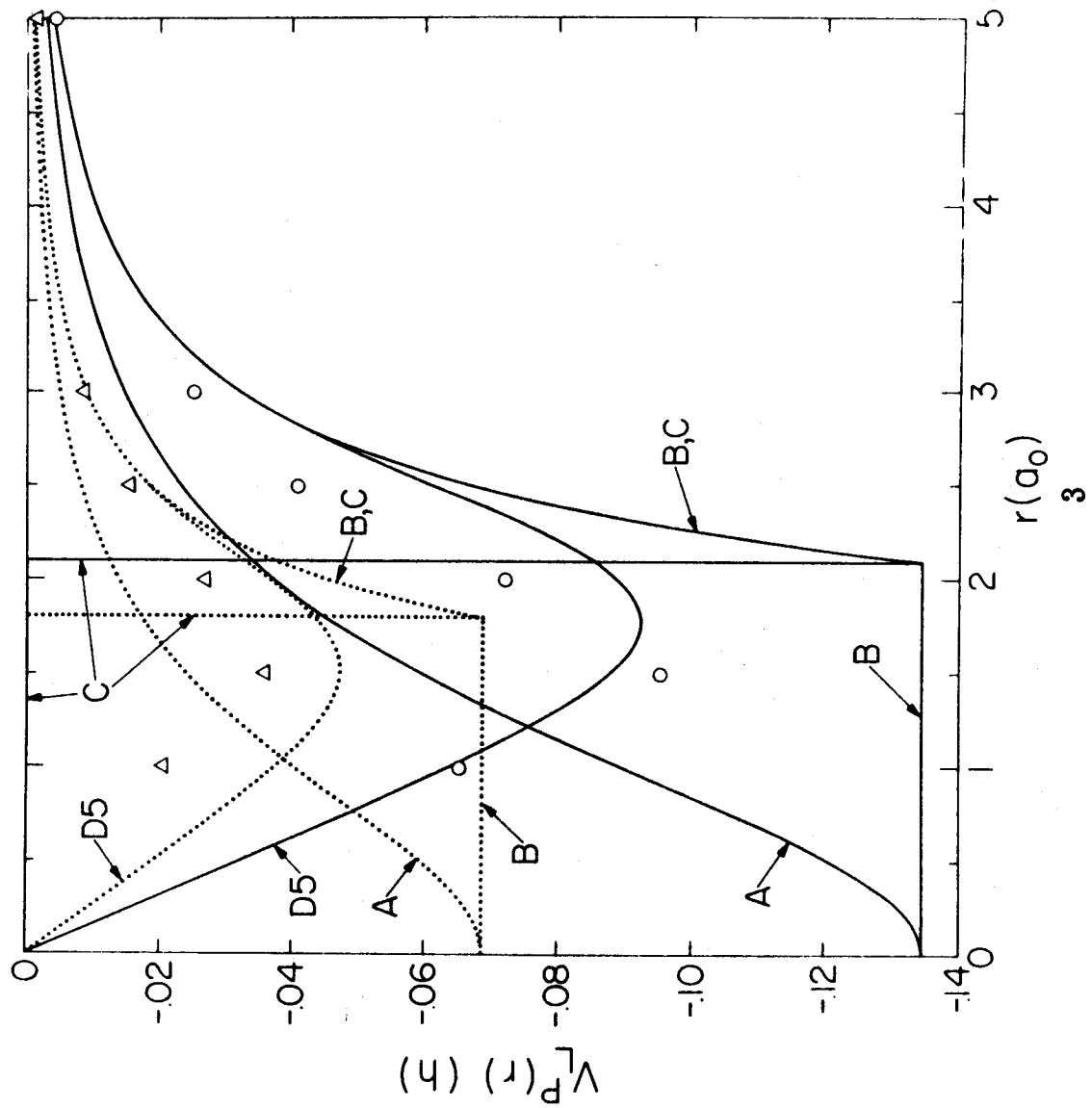
$V_L^P(r)$ (h)
0
-.02
-.04
-.06
-.08
-.10
-.12
-.14
0
1
2
3
4
5
$r(a_0)$
B,C
B,C
B
A
A
B
D5
D5
C
C

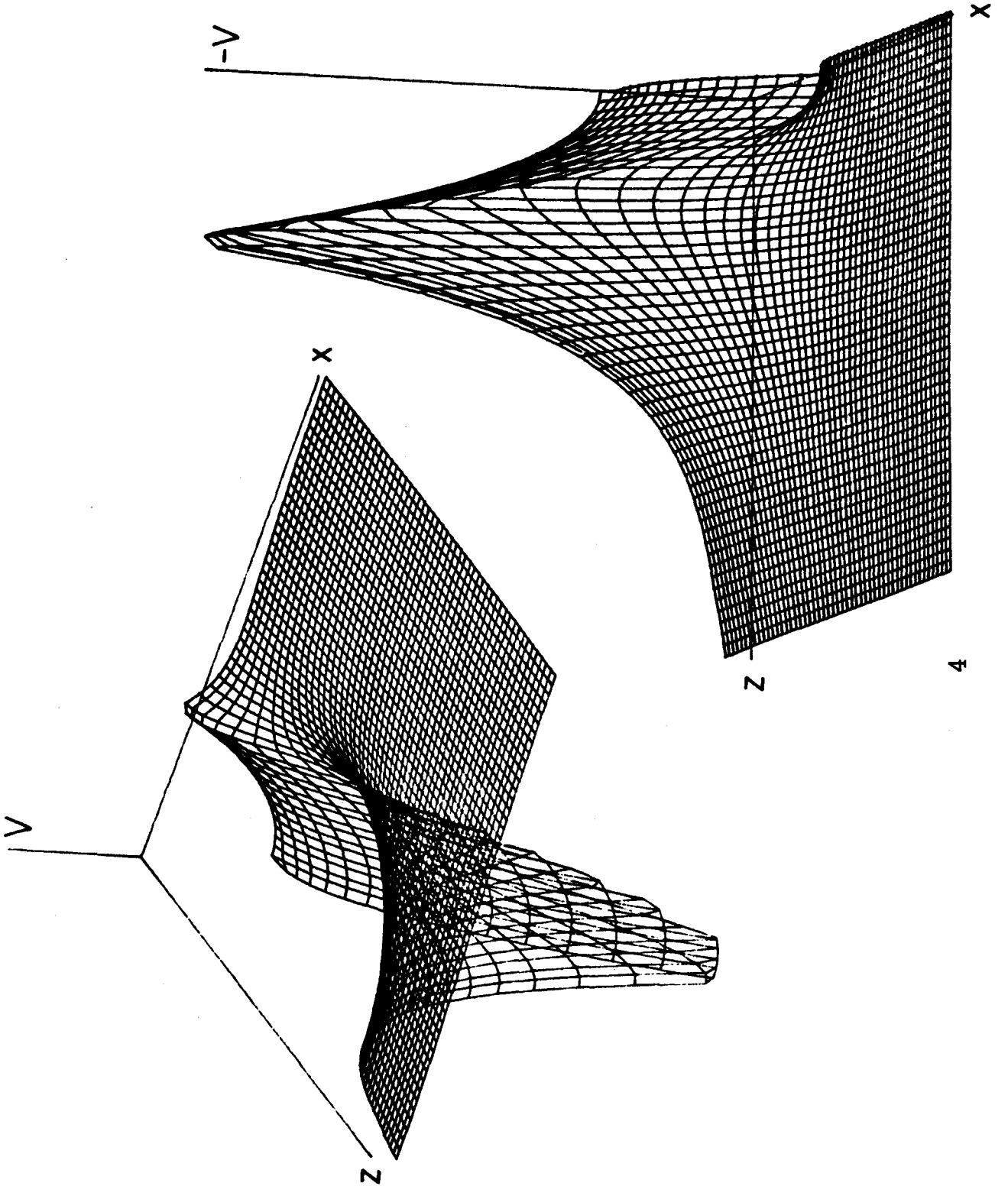
-V
X
Z
4
X
V
Z

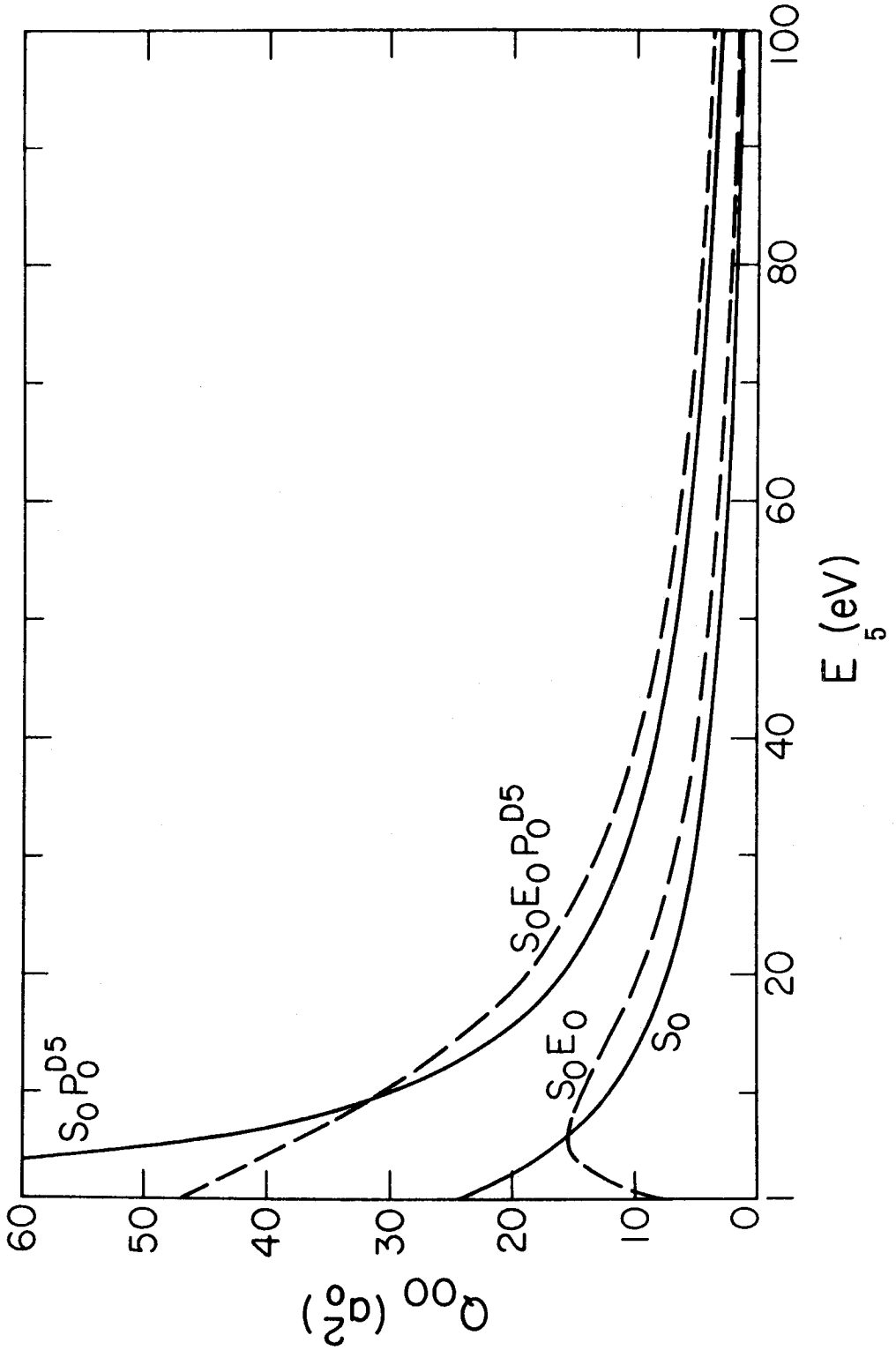
Q_{00} (a_0^2)
E_5 (eV)
$S_0P_0^{D5}$
$S_0E_0P_0^{D5}$
S_0E_0
S_0
0
10
20
30
40
50
60
20
40
60
80
100

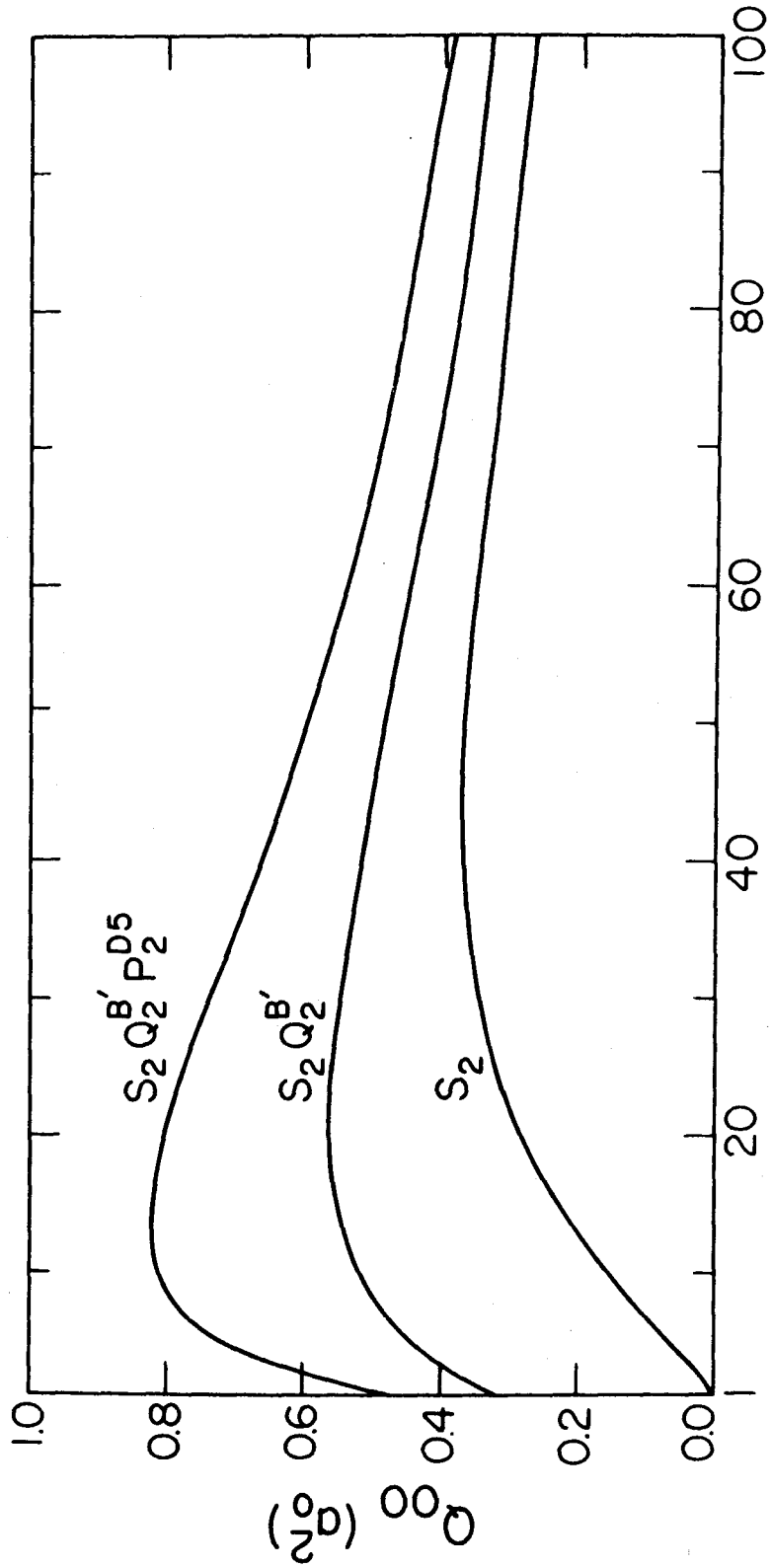
Q_{00} (a_0^2)
1.0
0.8
0.6
0.4
0.2
0.0
$S_2 Q_2^{B'} P_2^{D5}$
$S_2 Q_2^{B'}$
S_2
20
40
60
80
100
E_6 (eV)

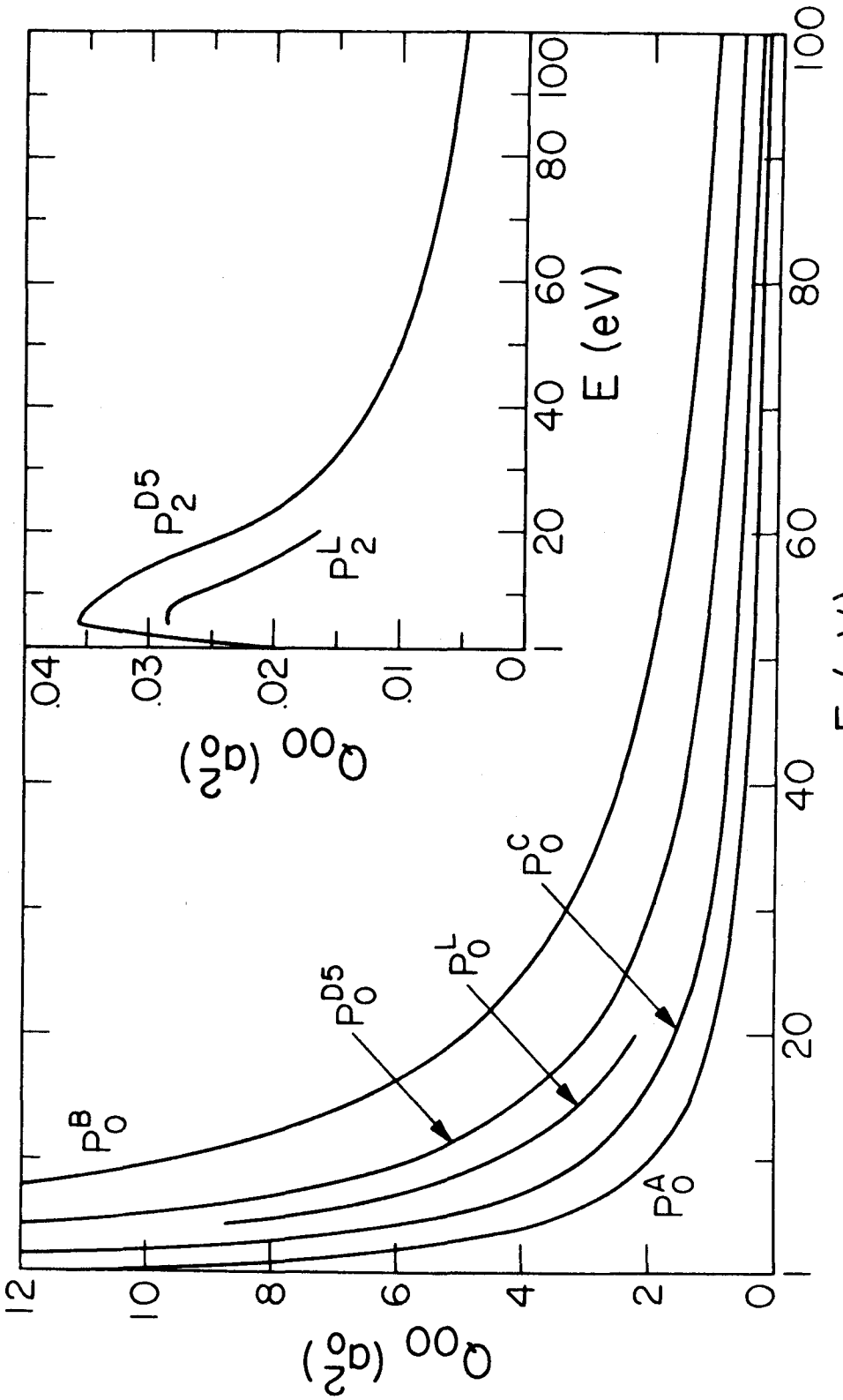

7

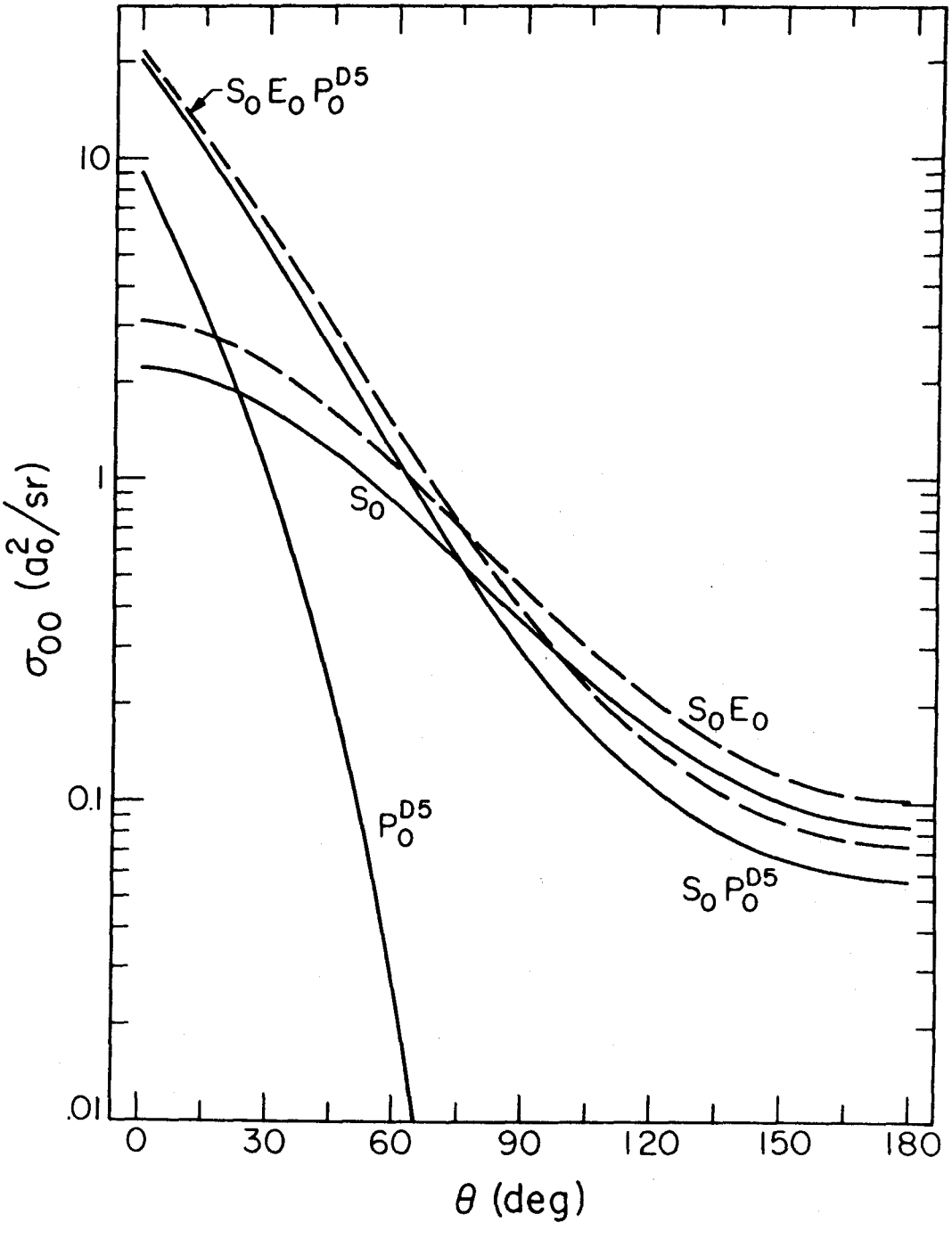
$S_0 E_0 P_0^{D5}$
10
1
0.1
.01
σ_{00} (a_0^2/sr)
S_0
$S_0 E_0$
P_0^{D5}
$S_0 P_0^{D5}$
0
30
60
90
120
150
180
θ (deg)

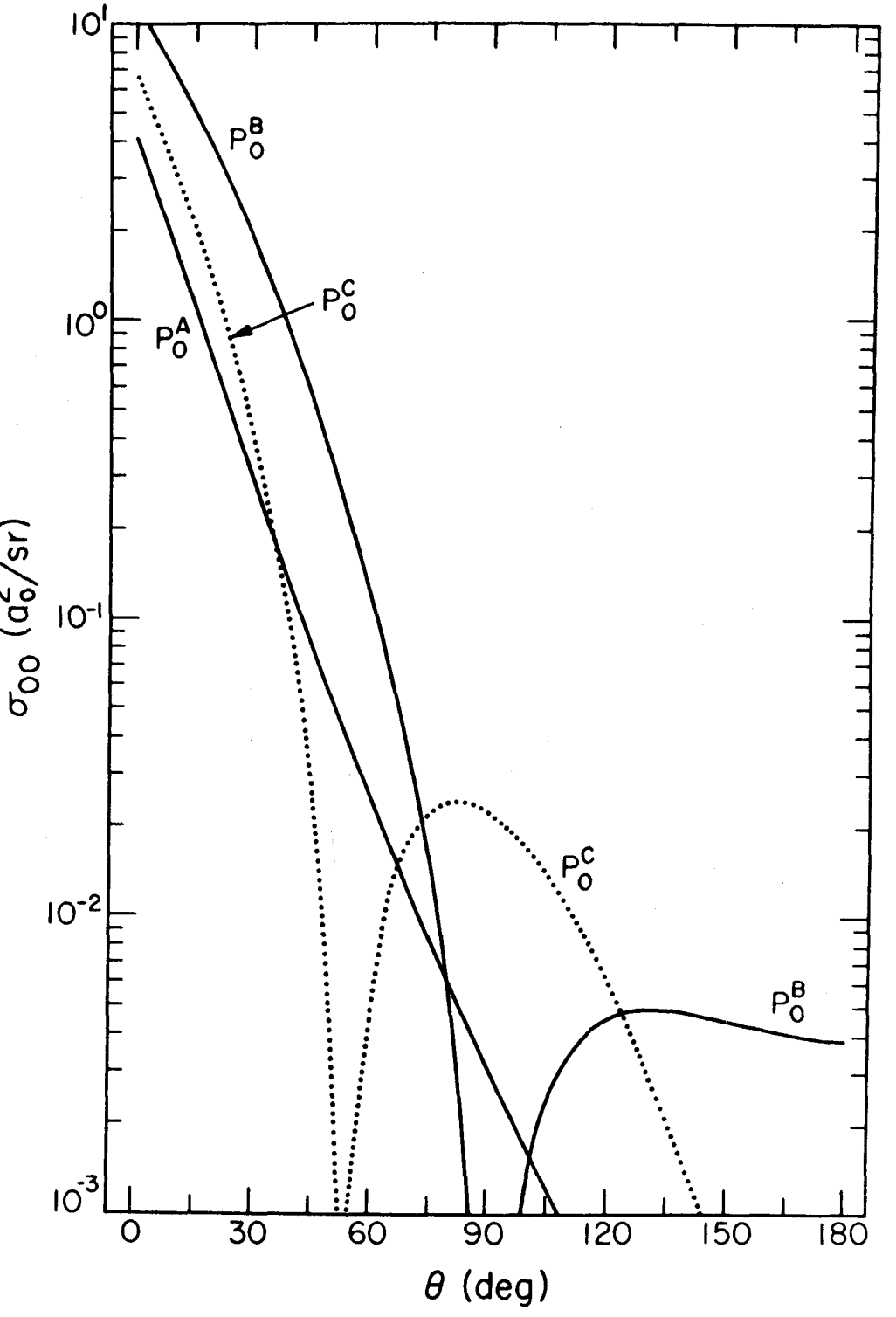
10^1
10^0
10^{-1}
10^{-2}
10^{-3}
σ_{00} (a_o^2/sr)
P_0^B
P_0^C
P_0^A
P_0^C
P_0^B
0
30
60
90
120
150
180
θ (deg)

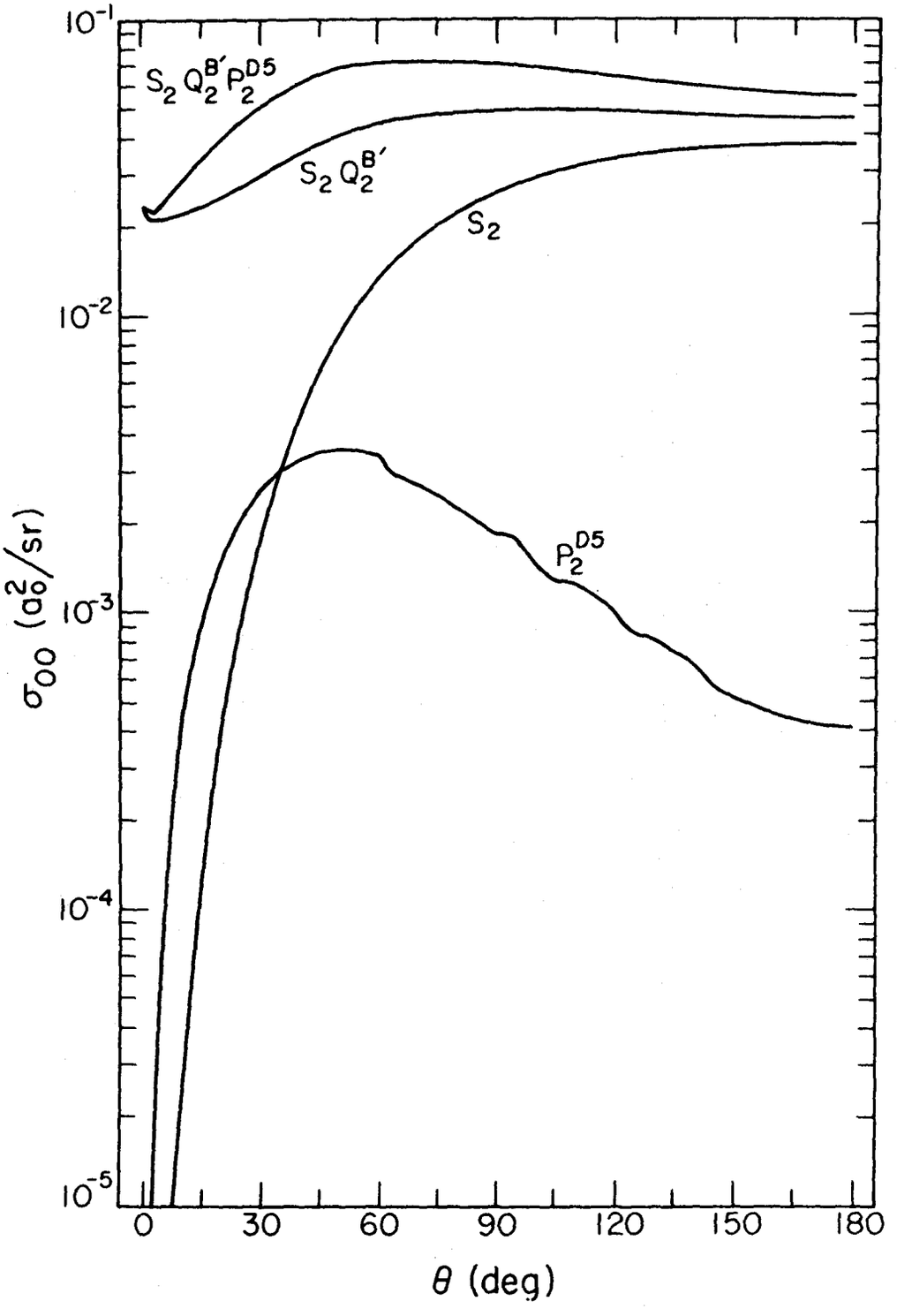
10^{-1}
10^{-2}
10^{-3}
10^{-4}
10^{-5}
σ_{00} (a_0^2/sr)
$S_2\,Q_2^{B'}\,P_2^{D5}$
$S_2\,Q_2^{B'}$
S_2
P_2^{D5}
0
30
60
90
120
150
180
θ (deg)

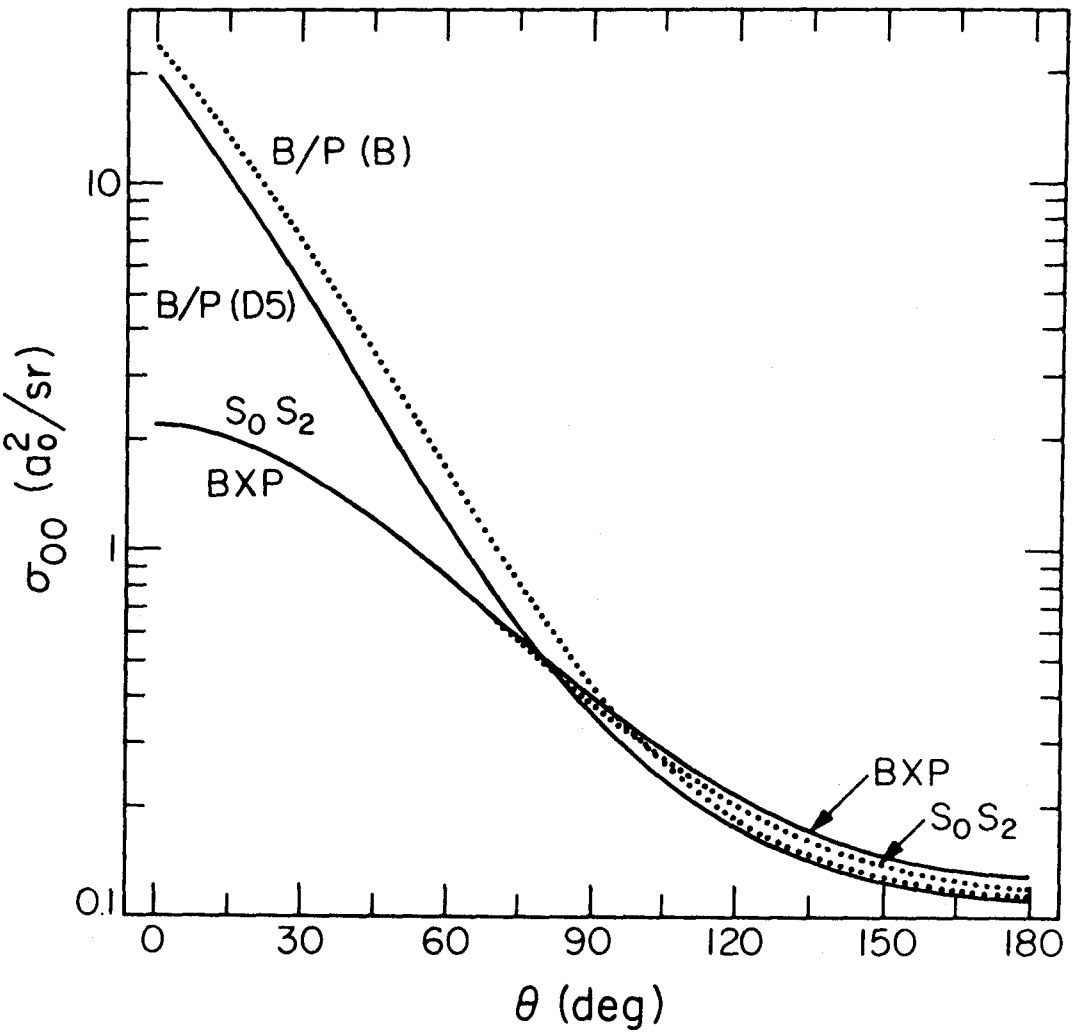
B/P (B)
B/P (D5)
$S_0 S_2$
BXP
BXP
$S_0 S_2$
10
1
0.1
σ_{00} (a_0^2/sr)
0
30
60
90
120
150
180
θ (deg)

11

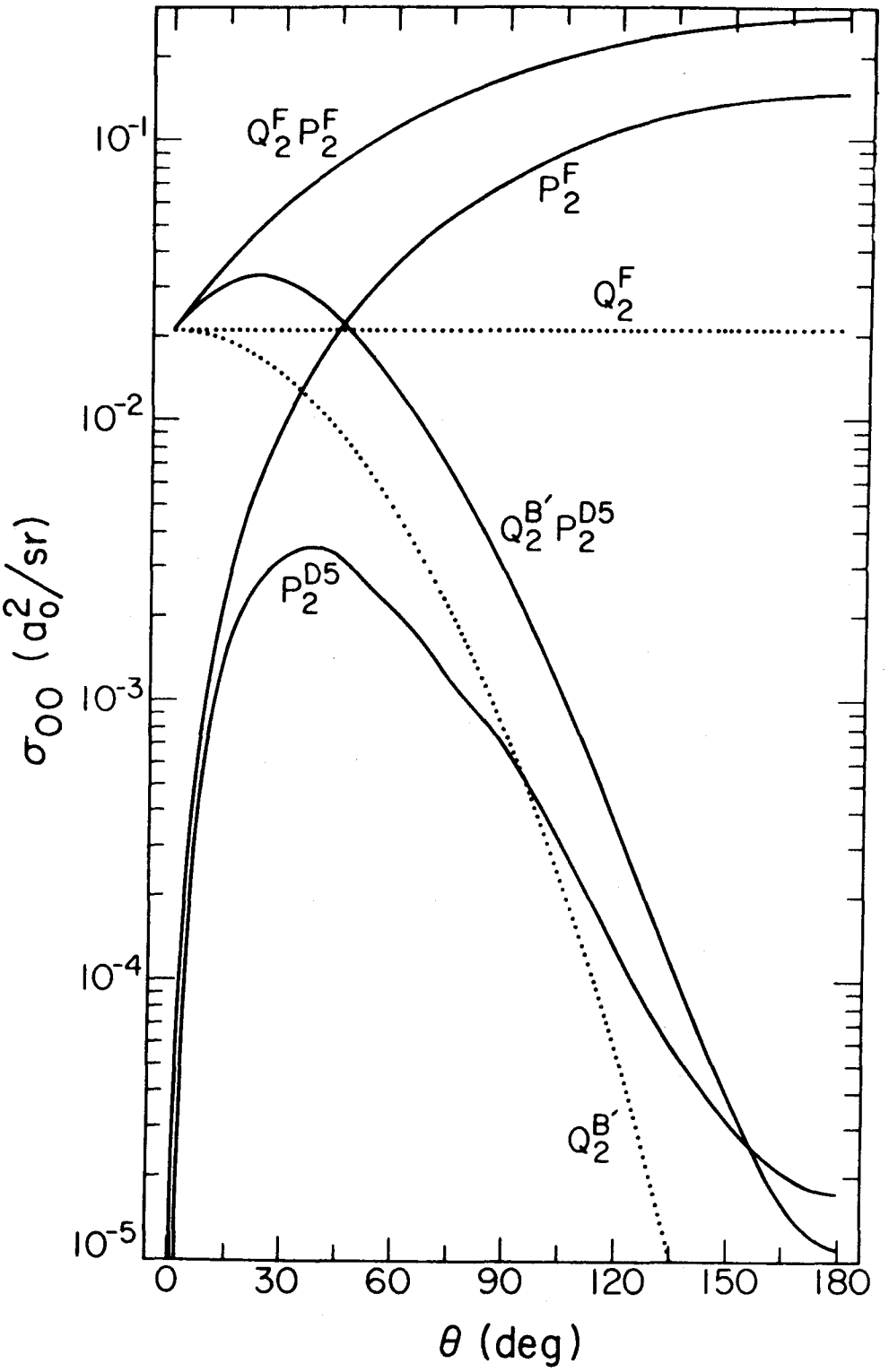
$Q_2^F P_2^F$
P_2^F
Q_2^F
$Q_2^{B'} P_2^{D5}$
P_2^{D5}
$Q_2^{B'}$
10^{-1}
10^{-2}
10^{-3}
10^{-4}
10^{-5}
σ_{00} (a_o^2/sr)
0
30
60
90
120
150
180
θ (deg)

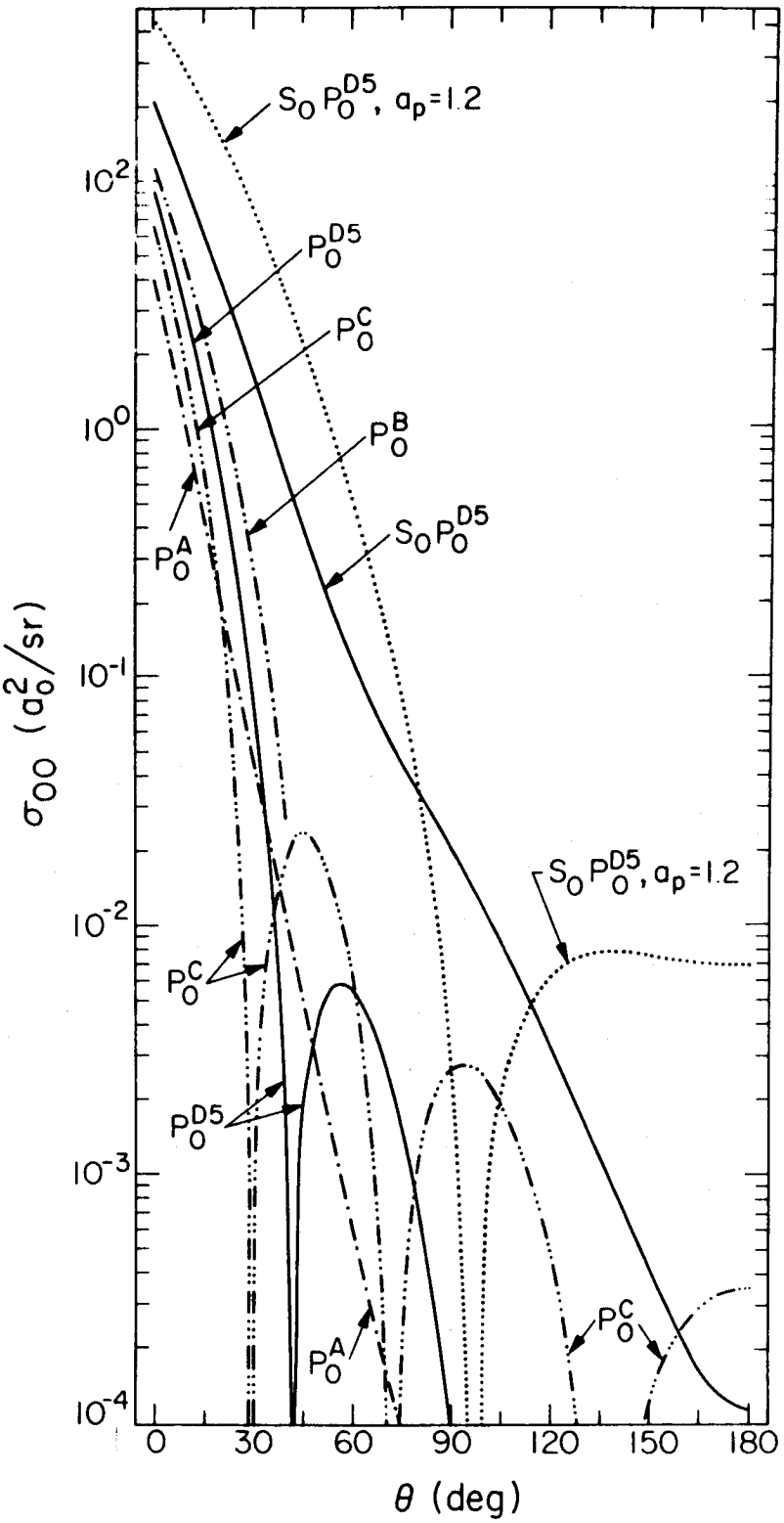
$S_0 P_0^{D5}$, a_p=1.2
P_0^{D5}
P_0^C
P_0^B
$S_0 P_0^{D5}$
P_0^A
$S_0 P_0^{D5}$, a_p=1.2
P_0^C
P_0^{D5}
P_0^A
P_0^C
10^2
10^0
10^{-1}
10^{-2}
10^{-3}
10^{-4}
σ_{00} (a_0^2/sr)
0
30
60
90
120
150
180
θ (deg)

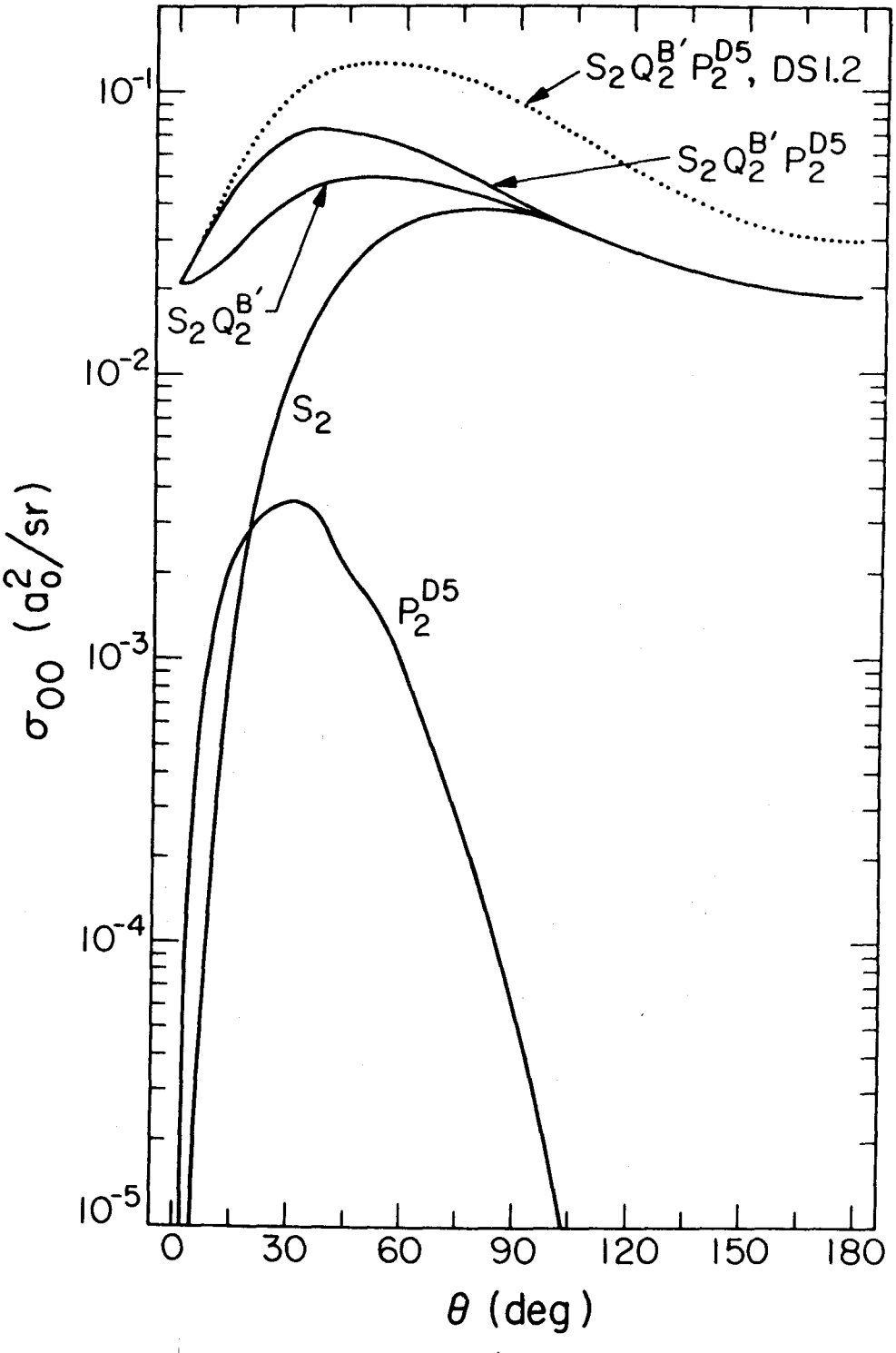
$S_2 Q_2^{B'} P_2^{D5}$, DS1.2
$S_2 Q_2^{B'} P_2^{D5}$
$S_2 Q_2^{B'}$
S_2
P_2^{D5}
10^{-1}
10^{-2}
10^{-3}
10^{-4}
10^{-5}
σ_{00} (a_0^2/sr)
0
30
60
90
120
150
180
θ (deg)

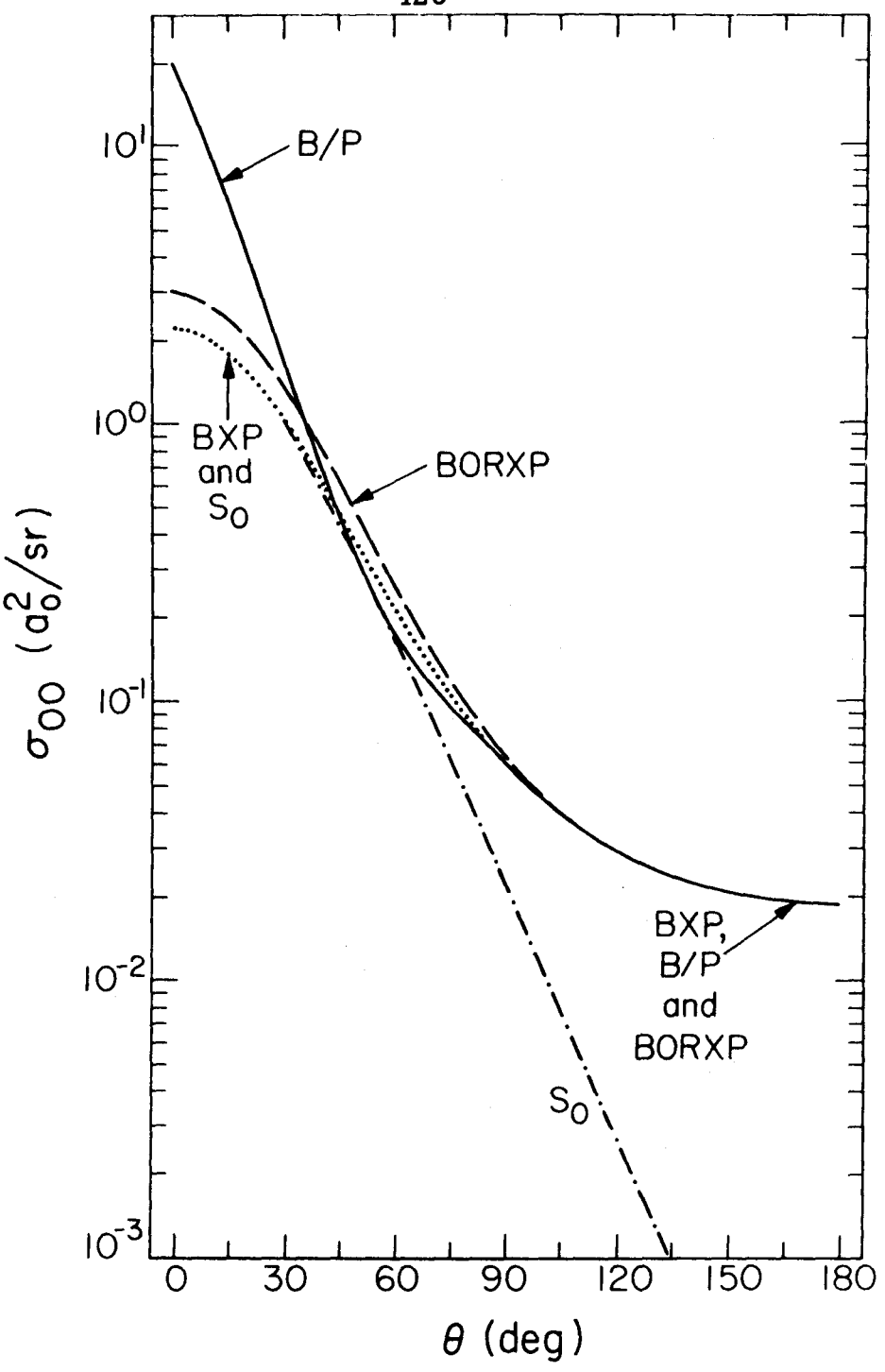
B/P
BXP
and
S_0
BORXP
BXP,
B/P
and
BORXP
S_0
10^1
10^0
10^{-1}
10^{-2}
10^{-3}
σ_{00} (a_0^2/sr)
0
30
60
90
120
150
180
θ (deg)

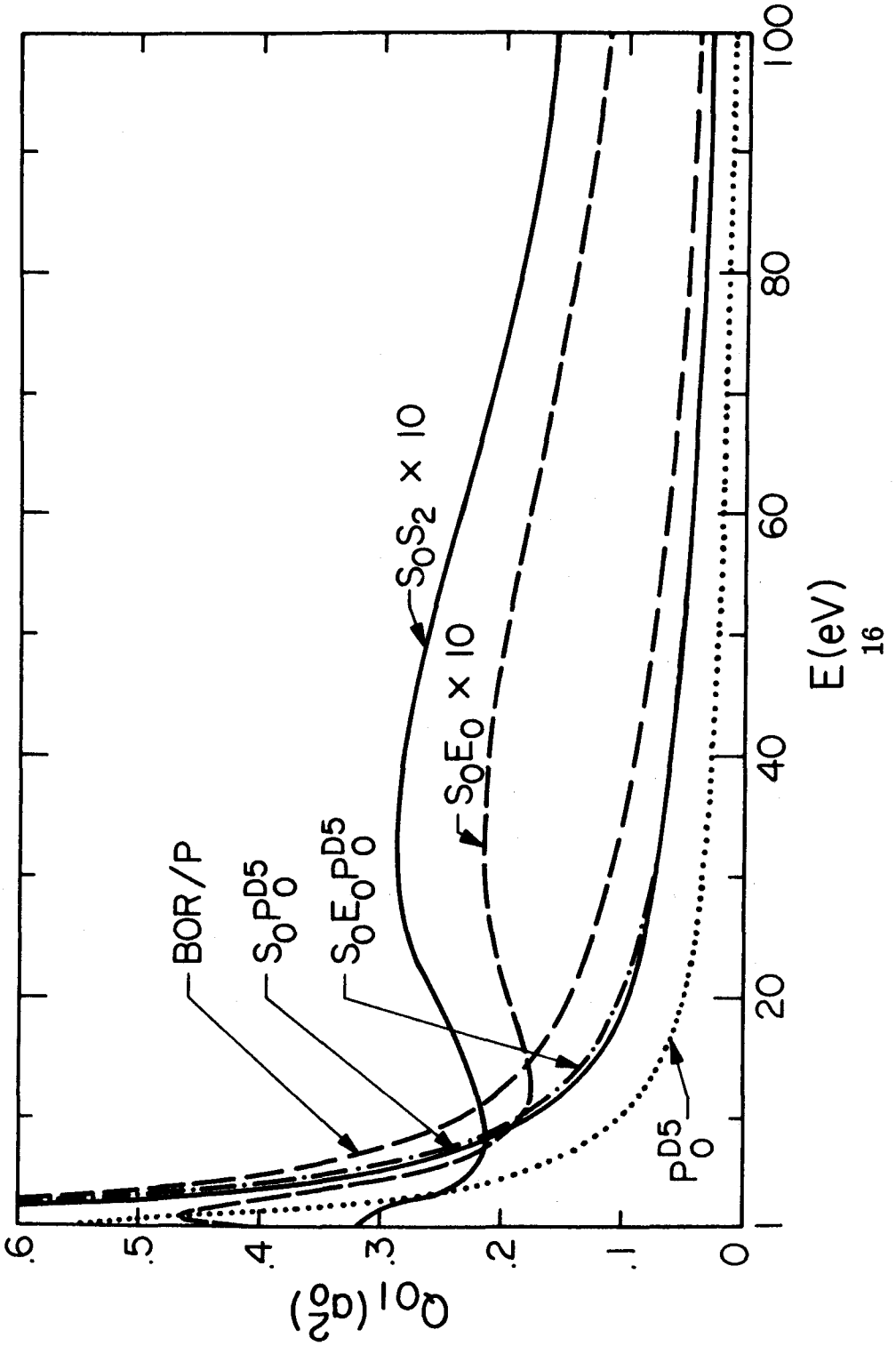
$Q_{01}(a_0^2)$
E(eV)
$S_0S_2 \times 10$
$S_0E_0 \times 10$
BOR/P
$S_0P_0^{D5}$
$S_0E_0P_0^{D5}$
P_0^{D5}
0
.1
.2
.3
.4
.5
.6
20
40
60
80
100

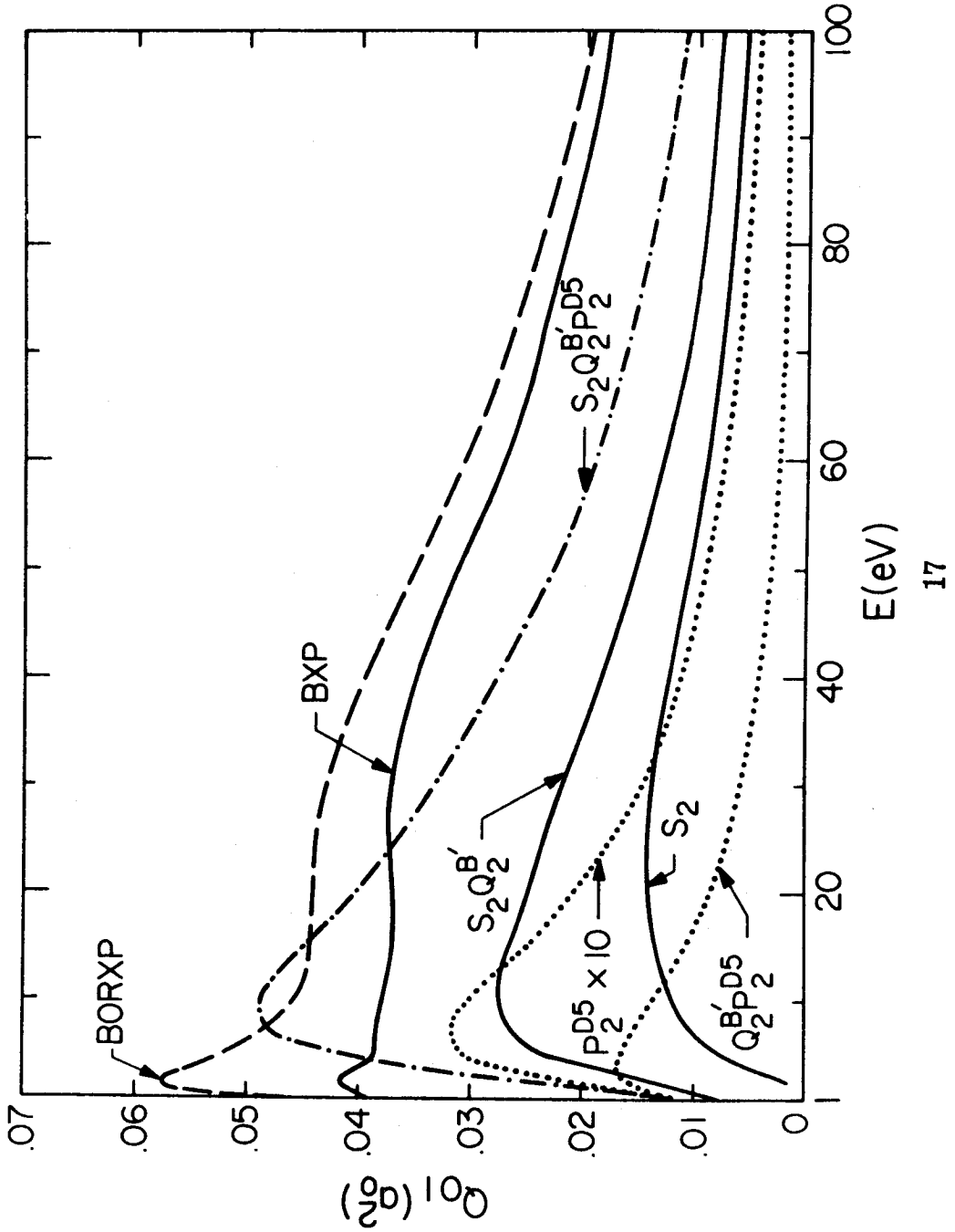
BORXP
BXP
$S_2Q_2^{B'}P_2^{D5}$
$S_2Q_2^{B'}$
P_2^{D5} x 10
S_2
$Q_2^{B'}P_2^{D5}$
$Q_{01}(a_0^2)$
.07
.06
.05
.04
.03
.02
.01
0
20
40
60
80
100
E(eV)

17

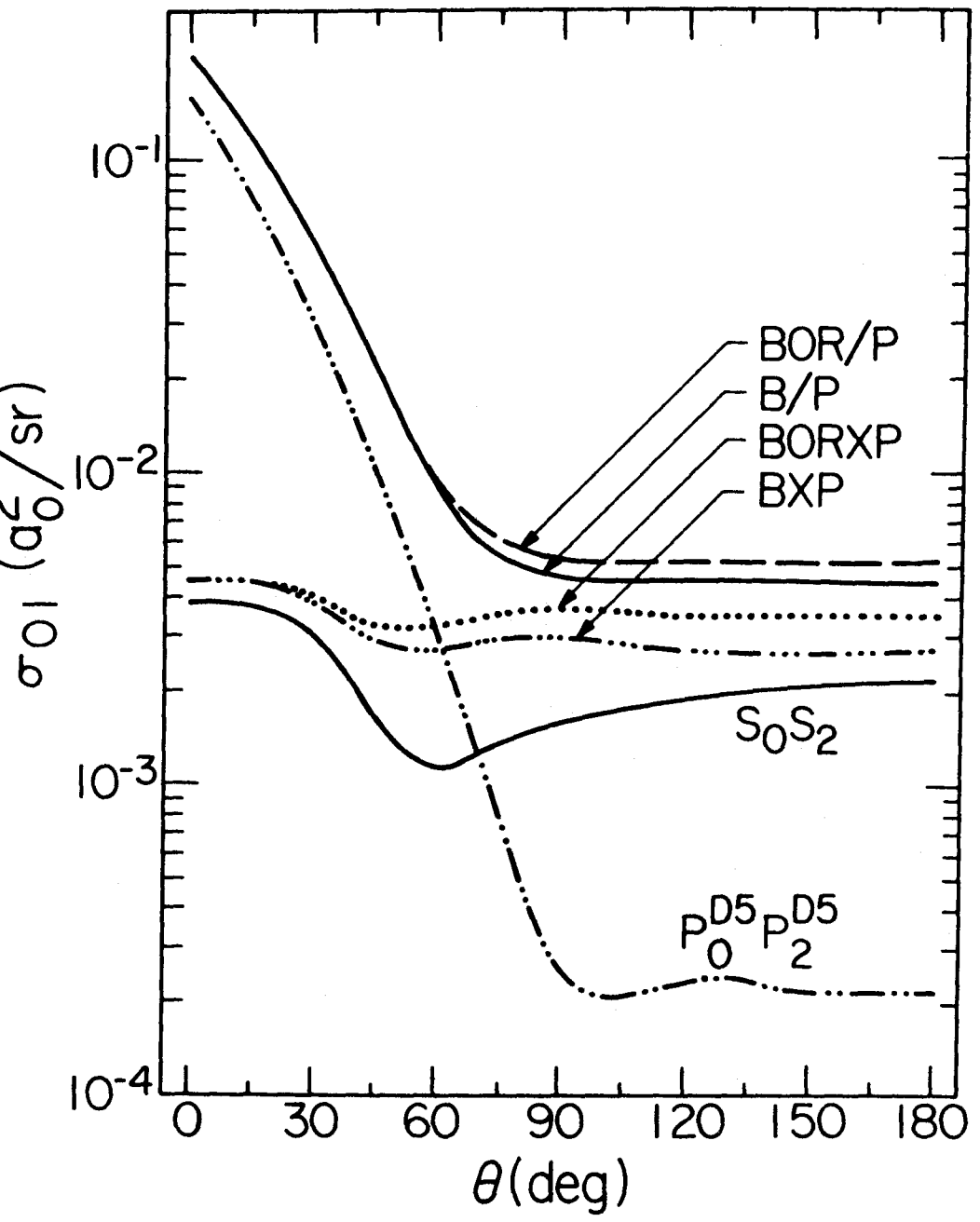
10^{-1}
10^{-2}
10^{-3}
10^{-4}
σ_{01} (a_0^2/sr)
0
30
60
90
120
150
180
θ(deg)
BOR/P
B/P
BORXP
BXP
S_0S_2
$P_0^{D5}P_2^{D5}$

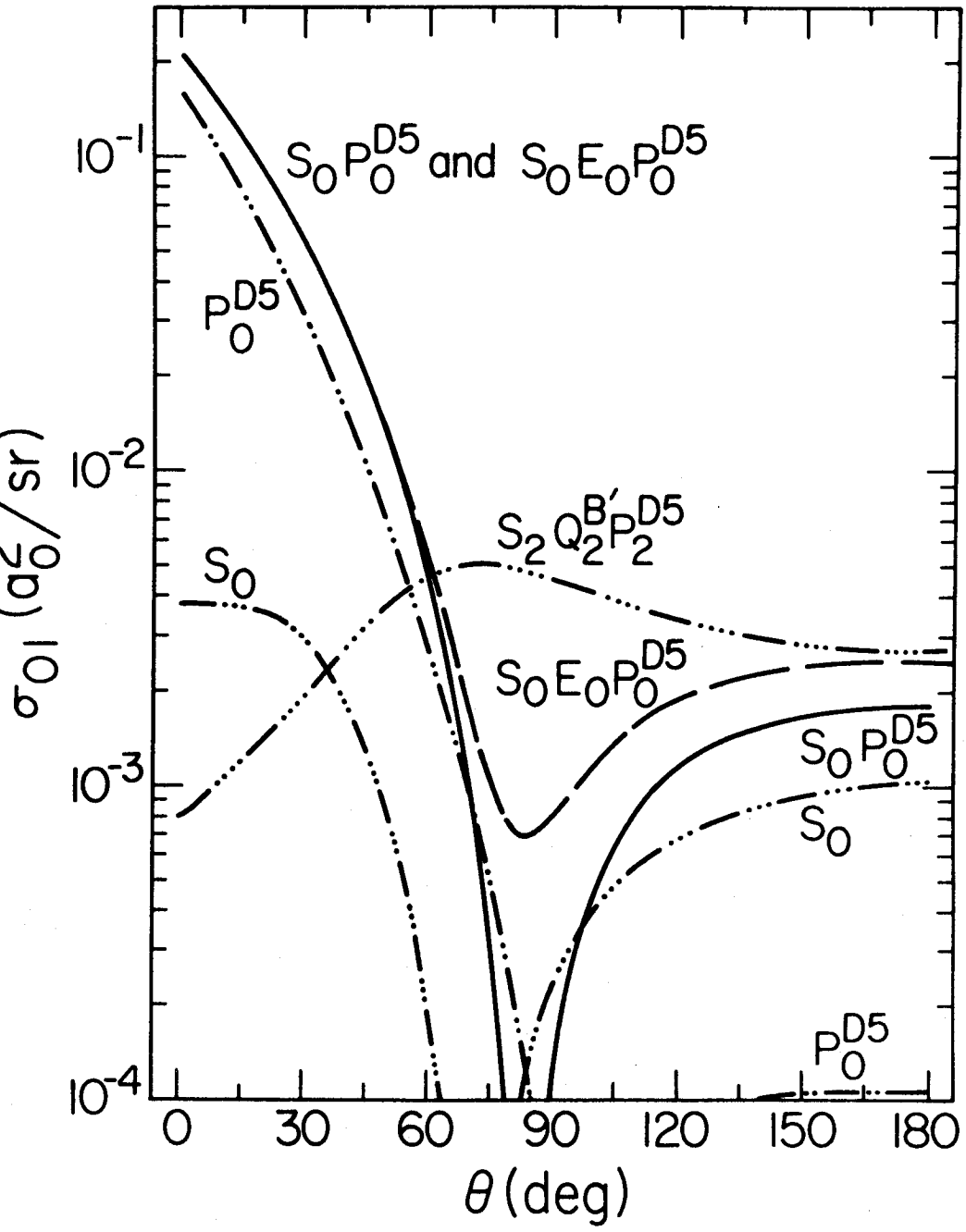
$S_0 P_0^{D5}$ and $S_0 E_0 P_0^{D5}$
P_0^{D5}
$S_2 Q_2^{B'} P_2^{D5}$
S_0
$S_0 E_0 P_0^{D5}$
$S_0 P_0^{D5}$
S_0
P_0^{D5}
10^{-1}
10^{-2}
10^{-3}
10^{-4}
σ_{01} (a_0^2/sr)
0
30
60
90
120
150
180
θ (deg)

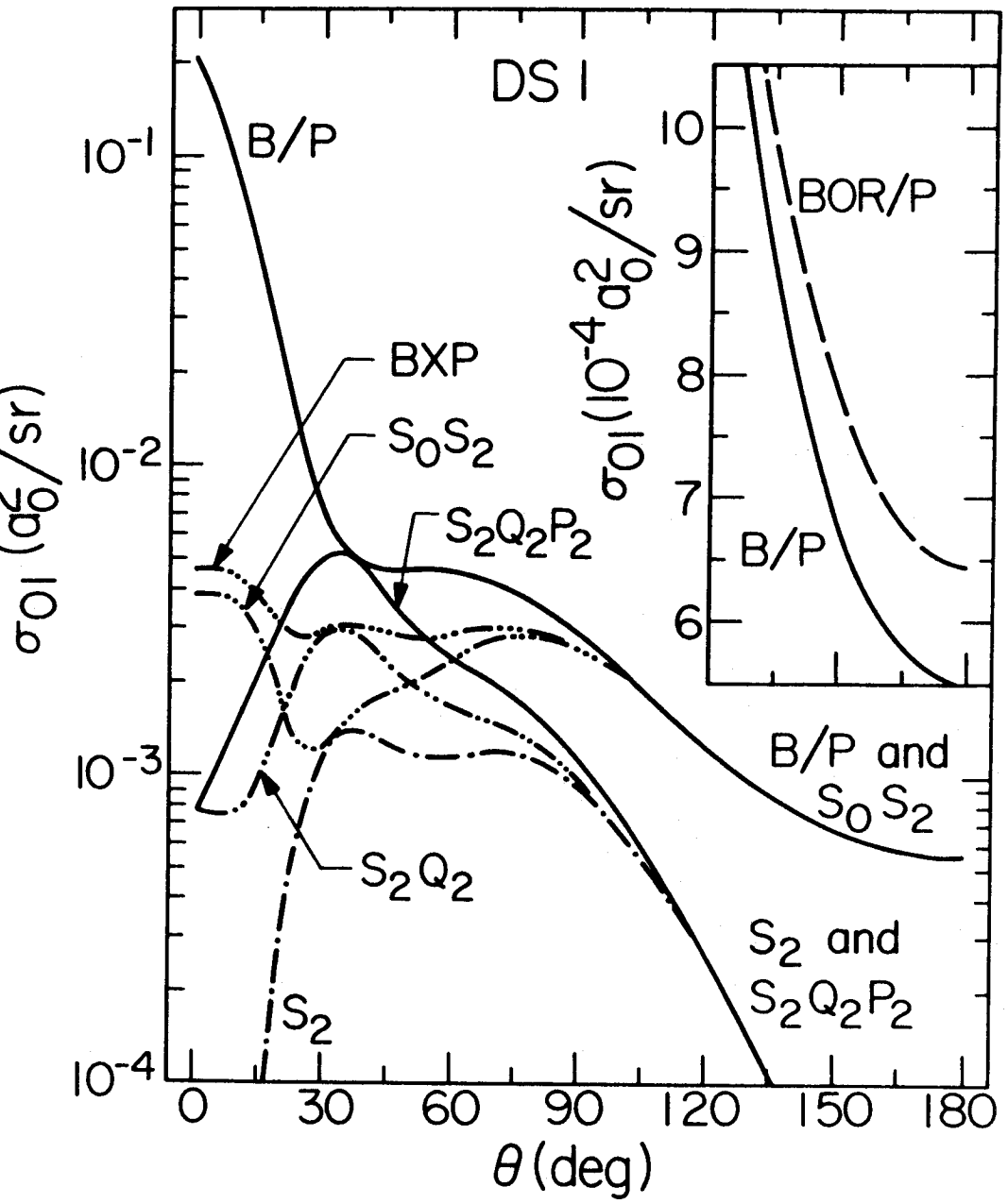
DS I
B/P
BXP
S_0S_2
$S_2Q_2P_2$
S_2Q_2
S_2
B/P and S_0S_2
S_2 and $S_2Q_2P_2$
BOR/P
B/P
σ_{01} (a_0^2/sr)
σ_{01} ($10^{-4}a_0^2$/sr)
θ (deg)
10^{-1}
10^{-2}
10^{-3}
10^{-4}
0
30
60
90
120
150
180
10
9
8
7
6

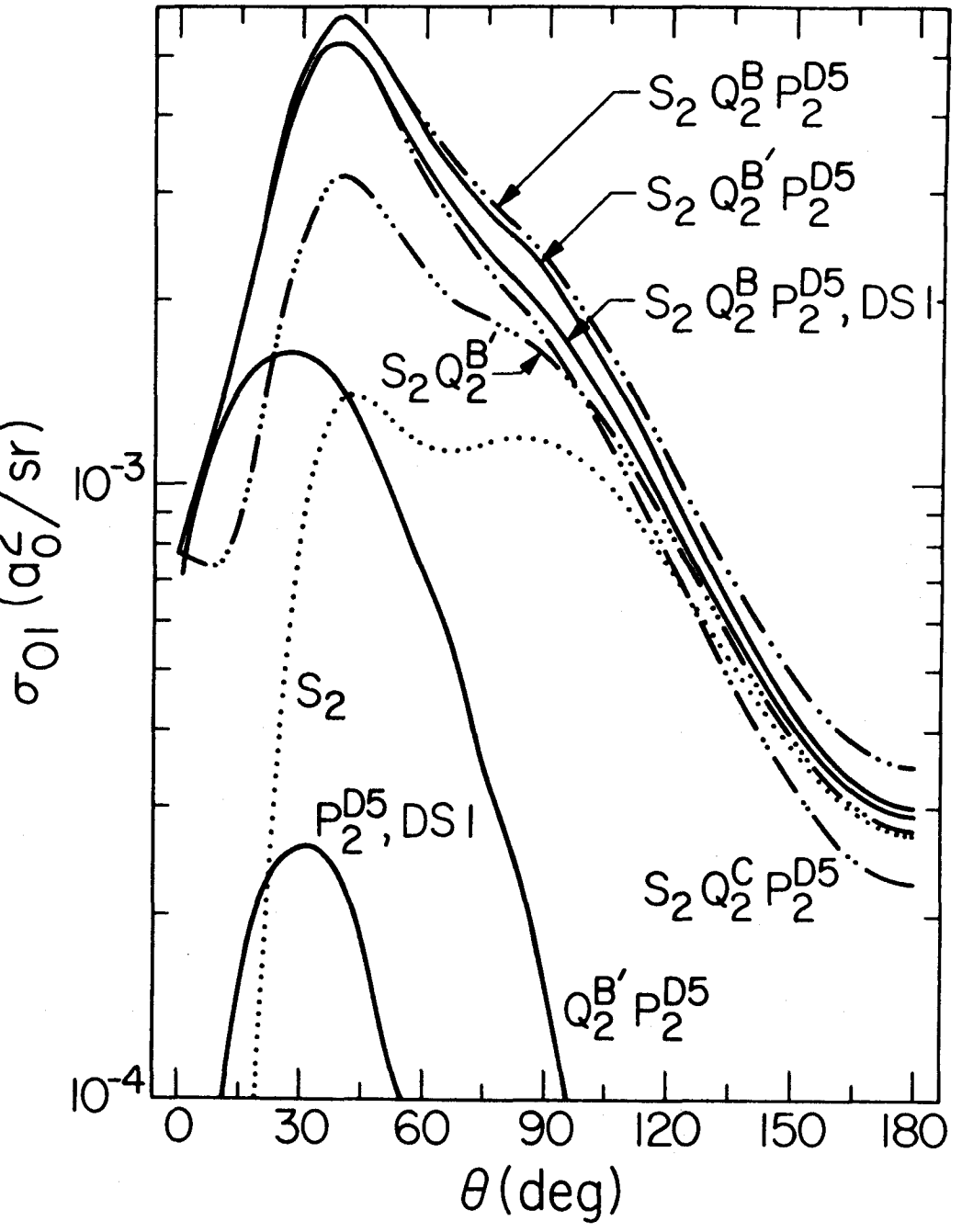
$S_2\, Q_2^B\, P_2^{D5}$
$S_2\, Q_2^{B'}\, P_2^{D5}$
$S_2\, Q_2^B\, P_2^{D5}$, DS 1
$S_2\, Q_2^{B'}$
S_2
P_2^{D5}, DS 1
$S_2\, Q_2^C\, P_2^{D5}$
$Q_2^{B'}\, P_2^{D5}$
$\sigma_{01}\,(a_0^2/sr)$
10^{-3}
10^{-4}
0
30
60
90
120
150
180
θ (deg)

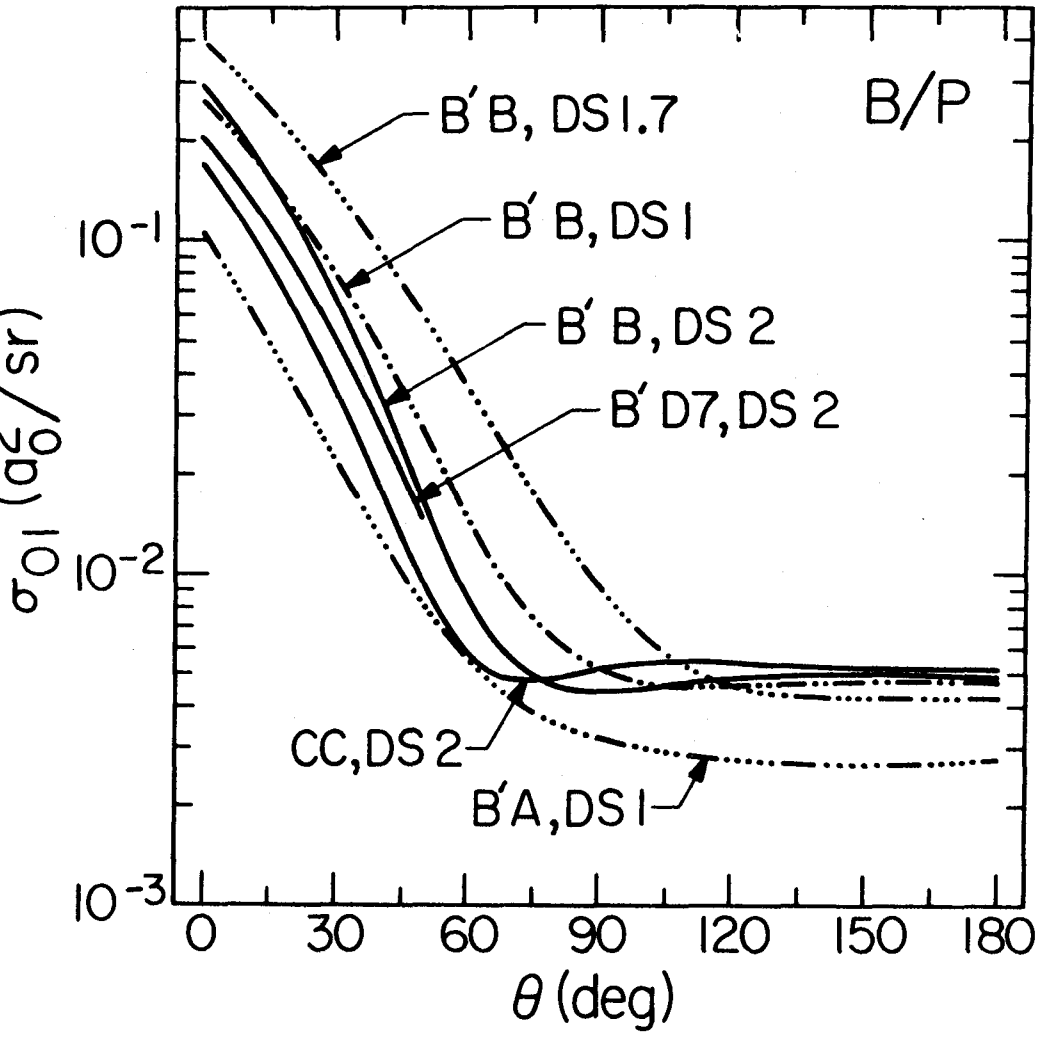
B′B, DS1.7
B/P
B′B, DS1
B′B, DS 2
B′D7, DS 2
CC, DS 2
B′A, DS1
10^{-1}
10^{-2}
10^{-3}
σ_{01} (a_0^2/sr)
0
30
60
90
120
150
180
θ (deg)

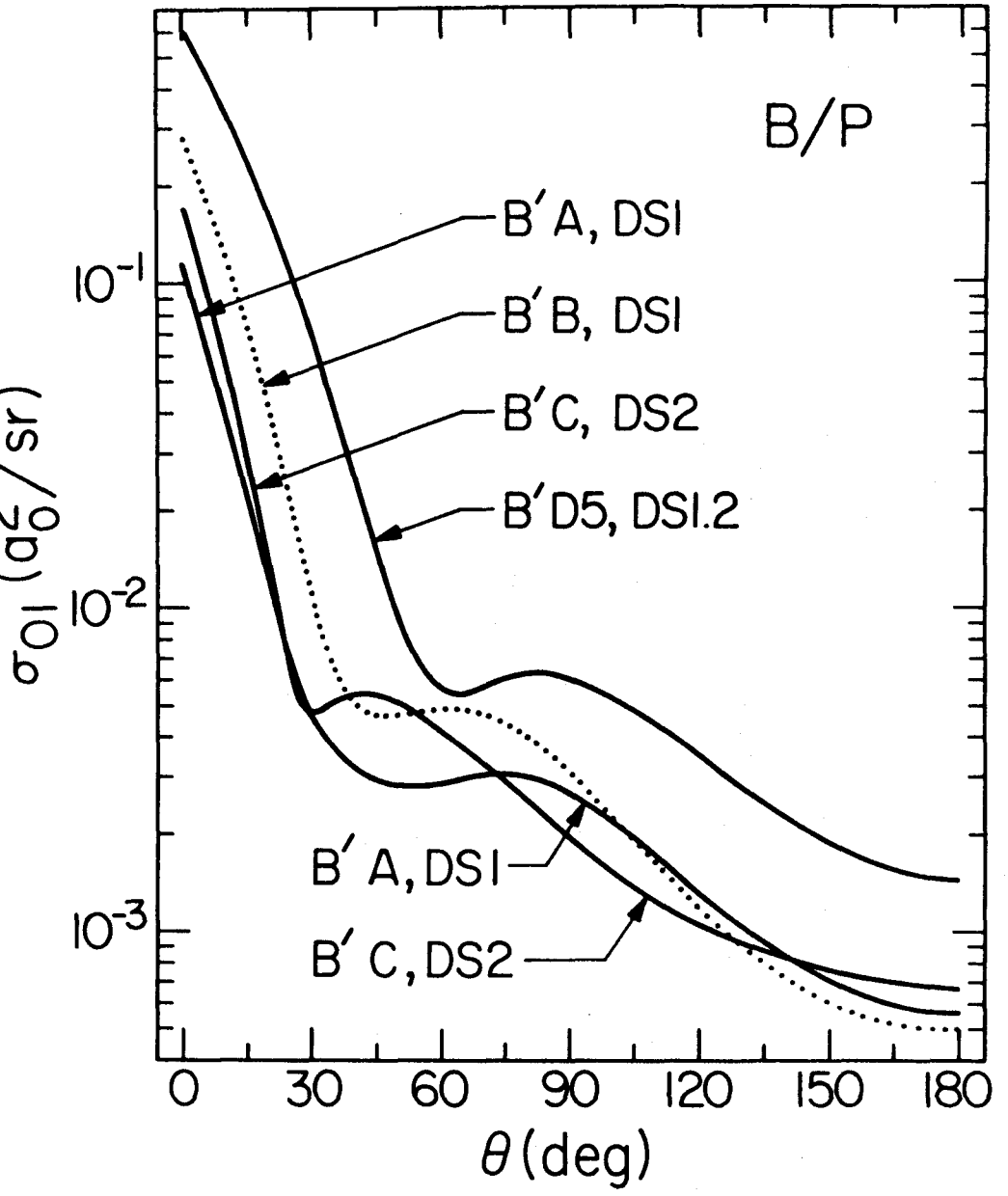
B/P
B′A, DSI
B′B, DSI
B′C, DS2
B′D5, DSI.2
B′A, DSI
B′C, DS2
10^{-1}
10^{-2}
10^{-3}
$\sigma_{01}(a_0^2/sr)$
0
30
60
90
120
150
180
θ(deg)

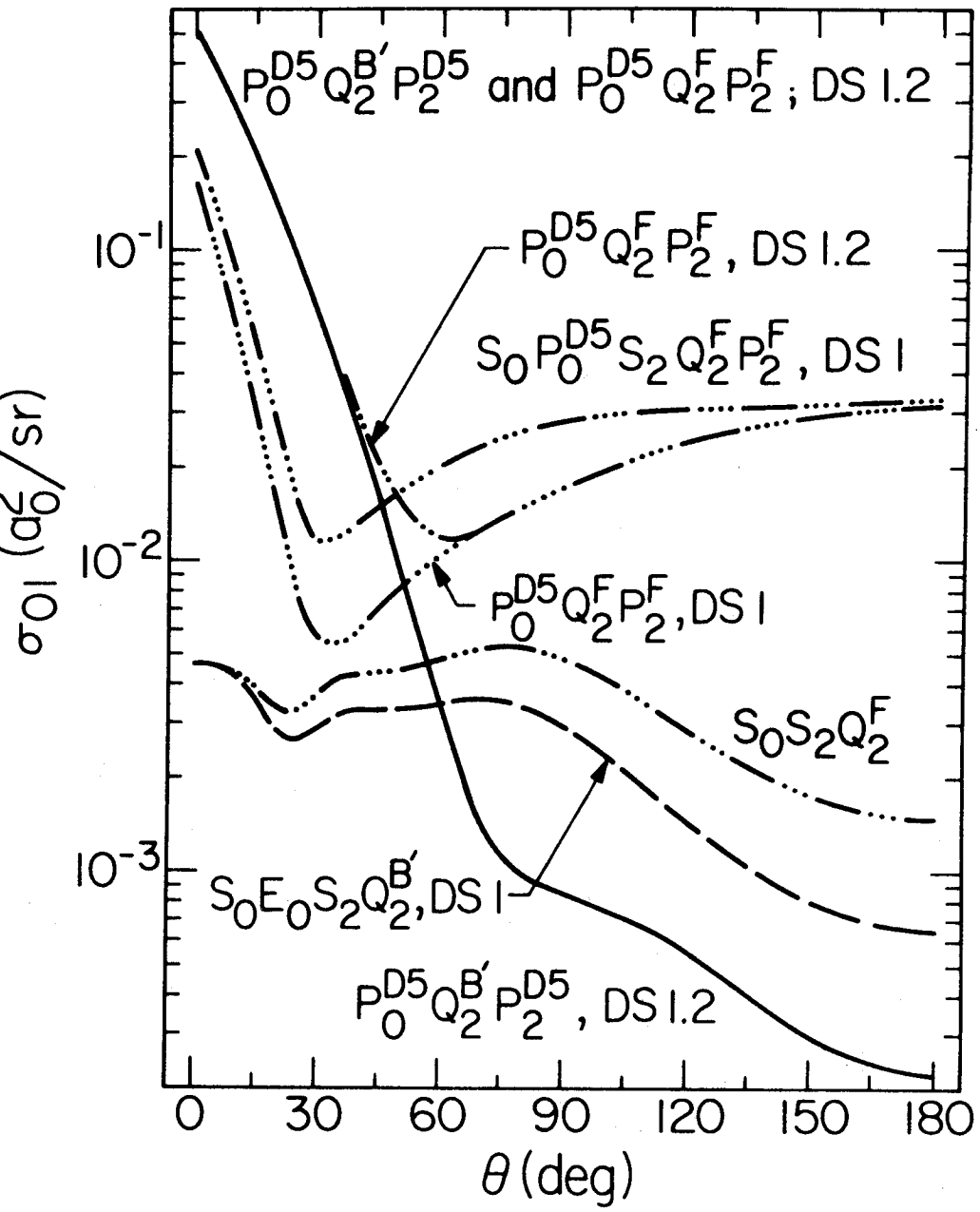
$P_0^{D5} Q_2^{B'} P_2^{D5}$ and $P_0^{D5} Q_2^F P_2^F$; DS 1.2
$P_0^{D5} Q_2^F P_2^F$, DS 1.2
$S_0 P_0^{D5} S_2 Q_2^F P_2^F$, DS 1
$P_0^{D5} Q_2^F P_2^F$, DS 1
$S_0 S_2 Q_2^F$
$S_0 E_0 S_2 Q_2^{B'}$, DS 1
$P_0^{D5} Q_2^{B'} P_2^{D5}$, DS 1.2
10^{-1}
10^{-2}
10^{-3}
σ_{01} (a_0^2/sr)
0
30
60
90
120
150
180
θ (deg)

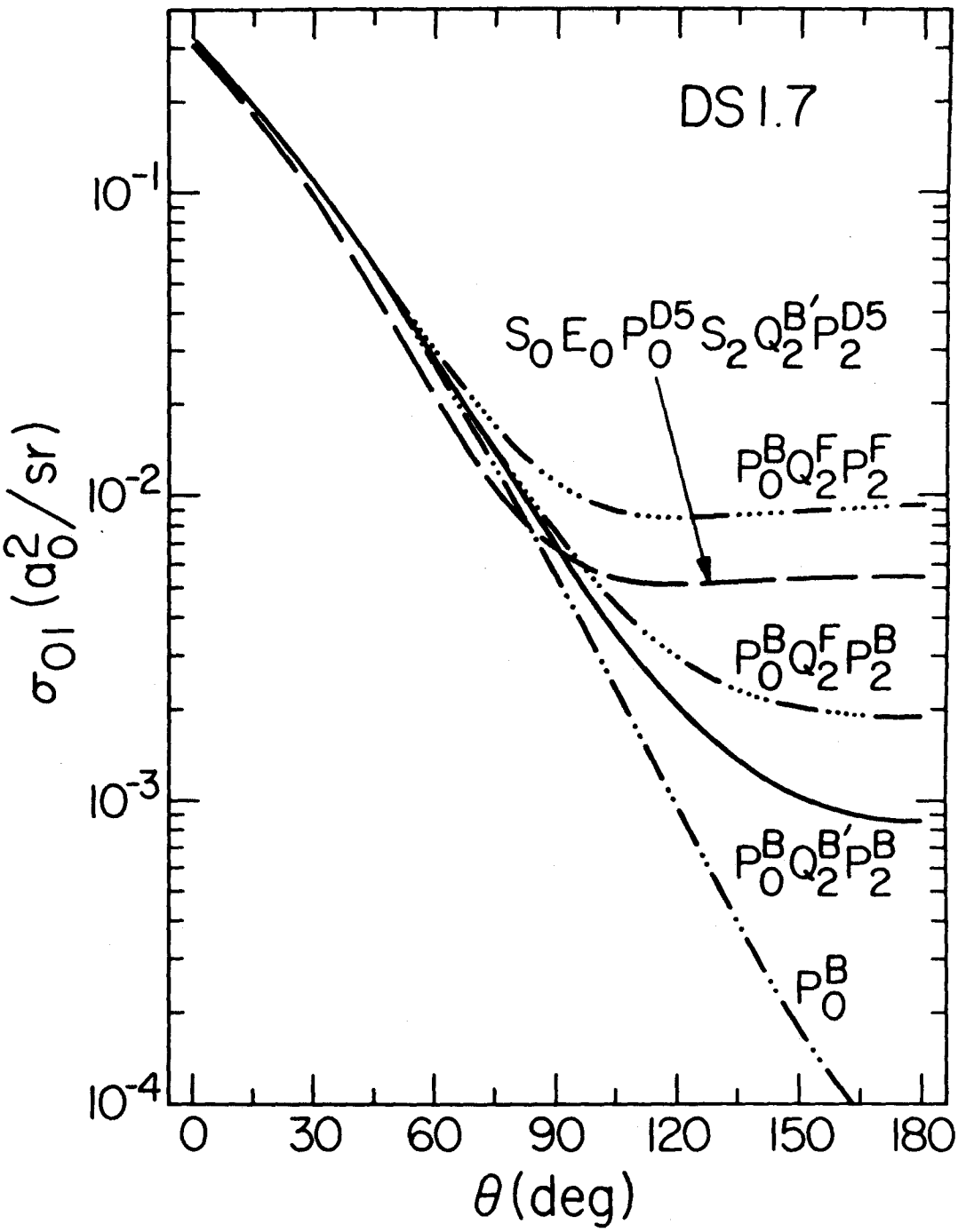
DS 1.7
$S_0 E_0 P_0^{D5} S_2 Q_2^{B'} P_2^{D5}$
$P_0^B Q_2^F P_2^F$
$P_0^B Q_2^F P_2^B$
$P_0^B Q_2^{B'} P_2^B$
P_0^B
$\sigma_{01}\,(a_0^2/sr)$
10^{-1}
10^{-2}
10^{-3}
10^{-4}
0
30
60
90
120
150
180
θ (deg)

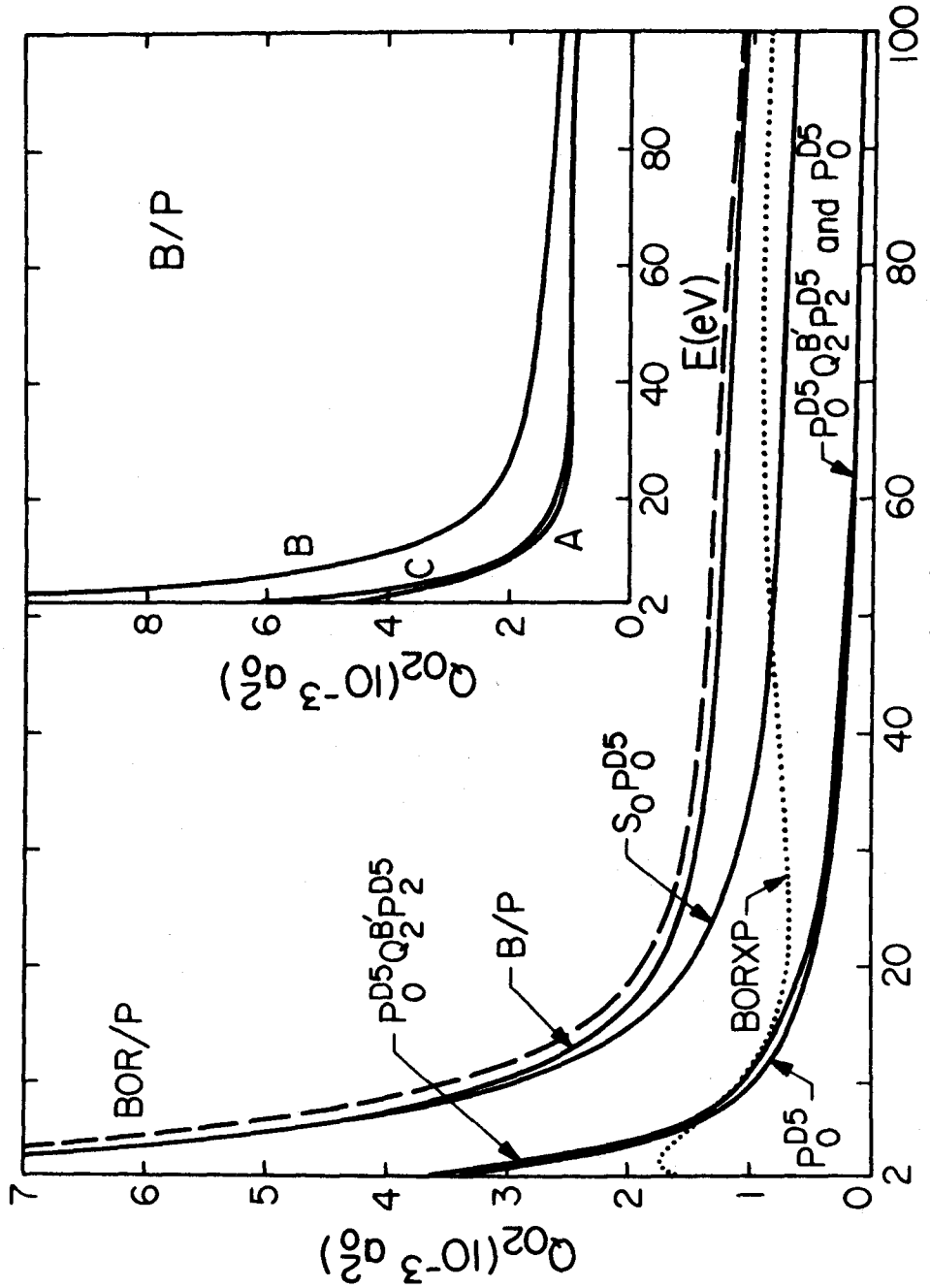
B/P
B
C
A
$Q_{02}(10^{-3}\ a_0^2)$
E(eV)
BOR/P
$P_0^{D5}Q_2^{B'}P_2^{D5}$
B/P
$S_0P_0^{D5}$
BORXP
P_0^{D5}
$P_0^{D5}Q_2^{B'}P_2^{D5}$ and P_0^{D5}
$Q_{02}(10^{-3}\ a_0^2)$
E(eV)

26

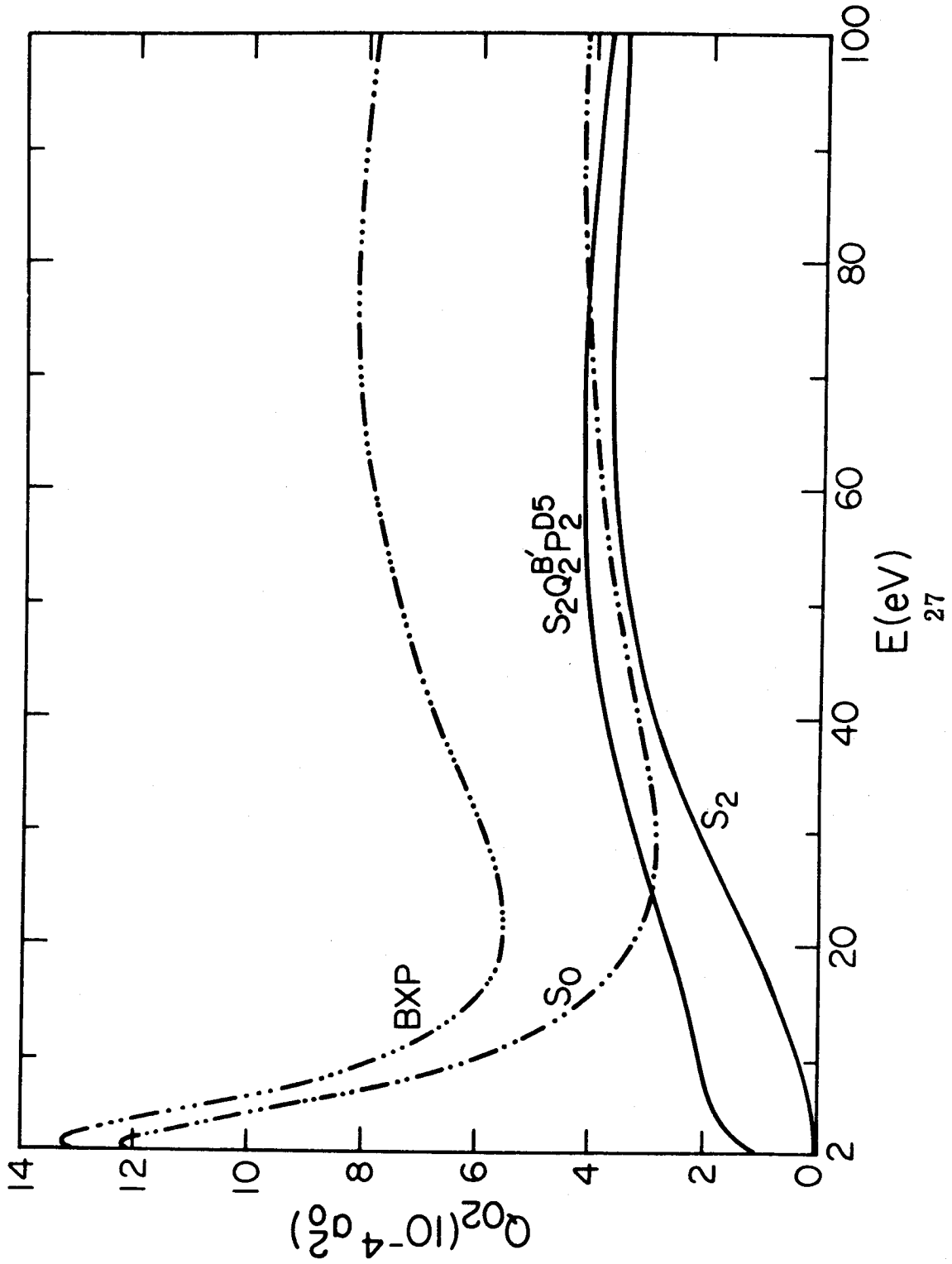
$Q_{02}(10^{-4}a_0^2)$
14
12
10
8
6
4
2
0
2
20
40
60
80
100
E(eV)
27
BXP
S_0
S_2
$S_2Q_2^{B'}P_2^{D5}$

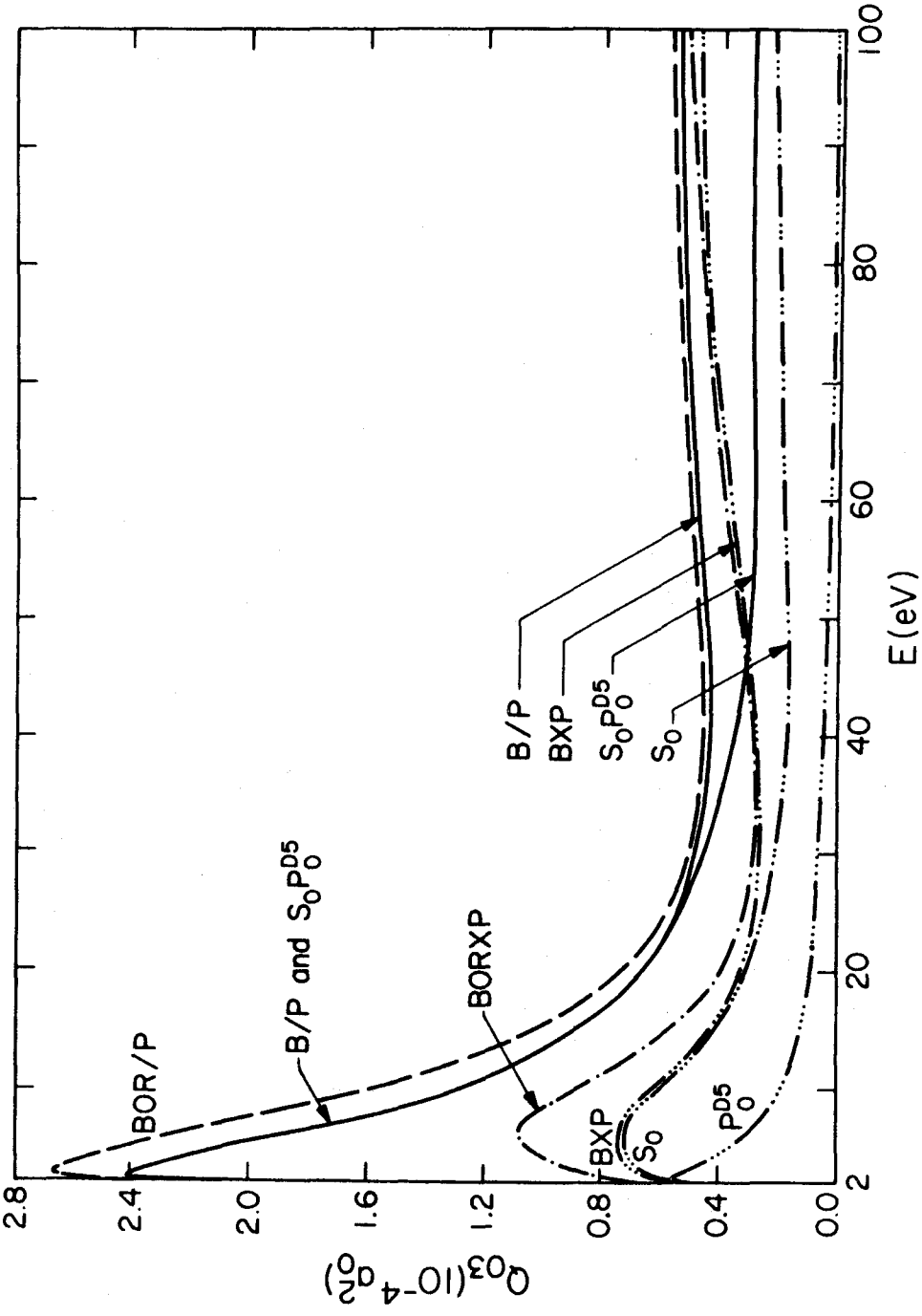
$Q_{03}(10^{-4}a_0^2)$
E(eV)
BOR/P
B/P and $S_0P_0^{D5}$
BORXP
B/P
BXP
$S_0P_0^{D5}$
S_0
BXP
S_0
P_0^{D5}
2.8
2.4
2.0
1.6
1.2
0.8
0.4
0.0
2
20
40
60
80
100

28

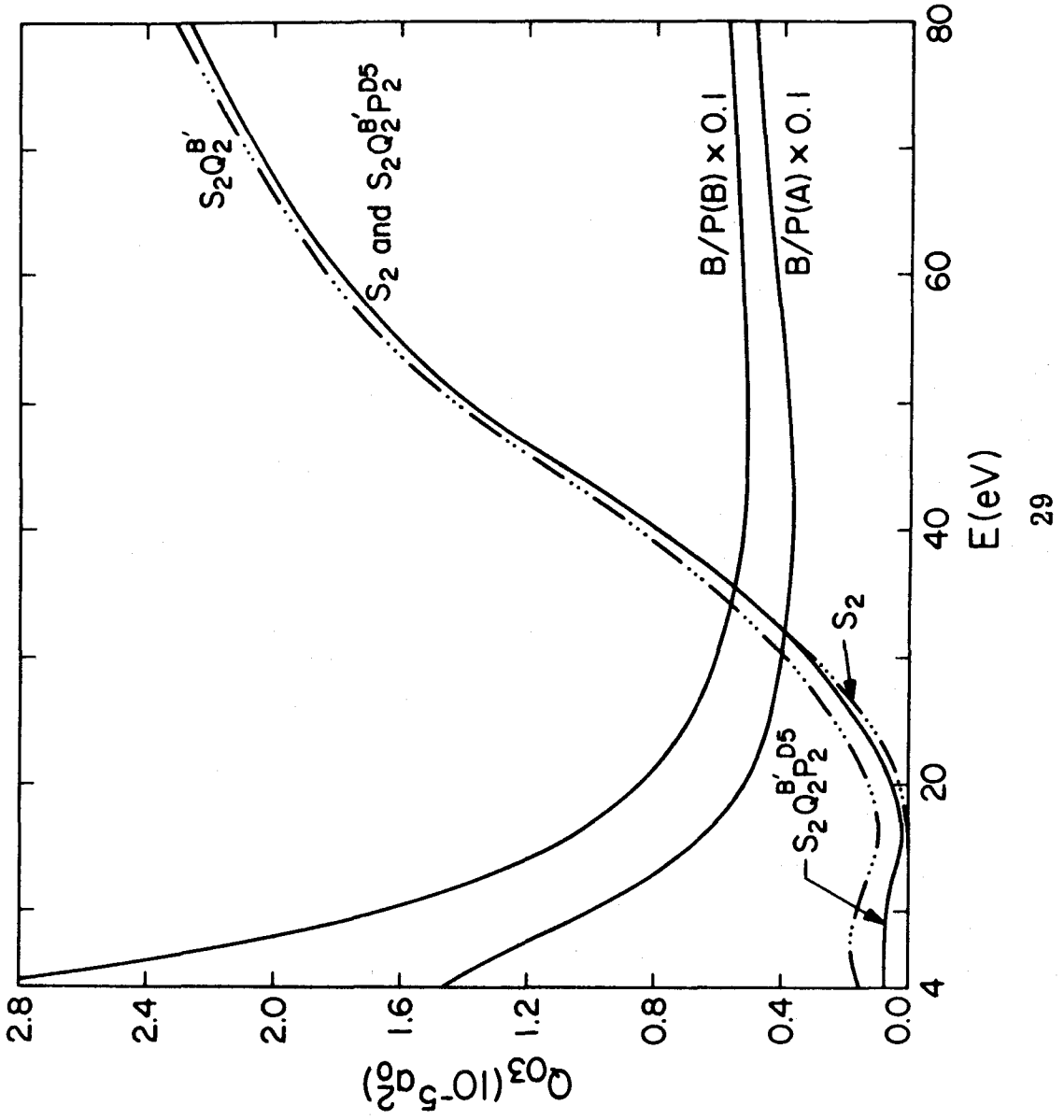
$S_2Q_2^{B'}$
S_2 and $S_2Q_2^{B'}P_2^{D5}$
B/P(B) x 0.1
B/P(A) x 0.1
S_2
$S_2Q_2^{B'}P_2^{D5}$
$Q_{03}(10^{-5}a_0^2)$
E(eV)
2.8
2.4
2.0
1.6
1.2
0.8
0.4
0.0
4
20
40
60
80

29

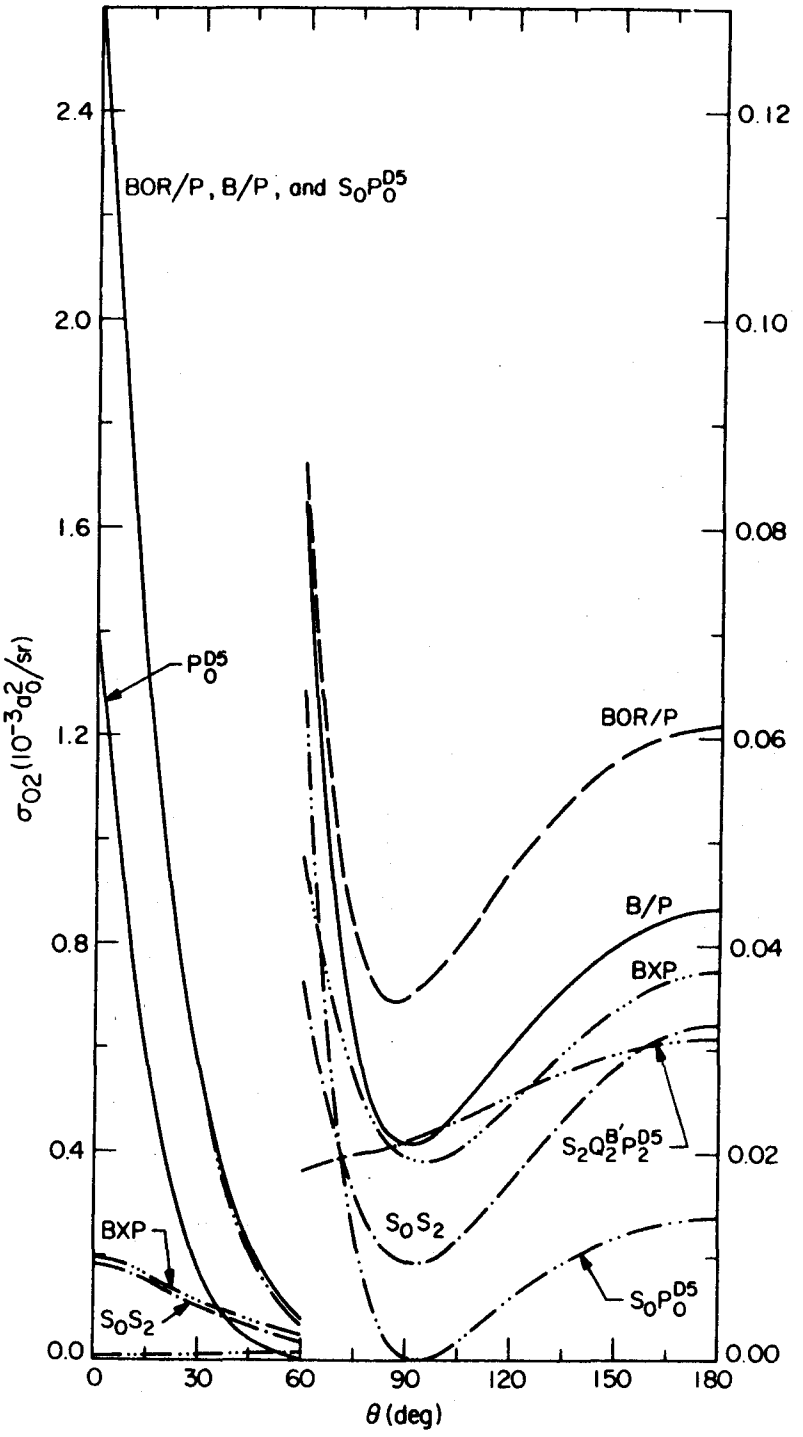
BOR/P, B/P, and $S_0P_0^{D5}$
P_0^{D5}
BOR/P
B/P
BXP
$S_2Q_2^{B'}P_2^{D5}$
S_0S_2
BXP
S_0S_2
$S_0P_0^{D5}$
$\sigma_{O2}(10^{-3}a_0^2/sr)$
θ (deg)
0.0
0.4
0.8
1.2
1.6
2.0
2.4
0.00
0.02
0.04
0.06
0.08
0.10
0.12
0
30
60
90
120
150
180

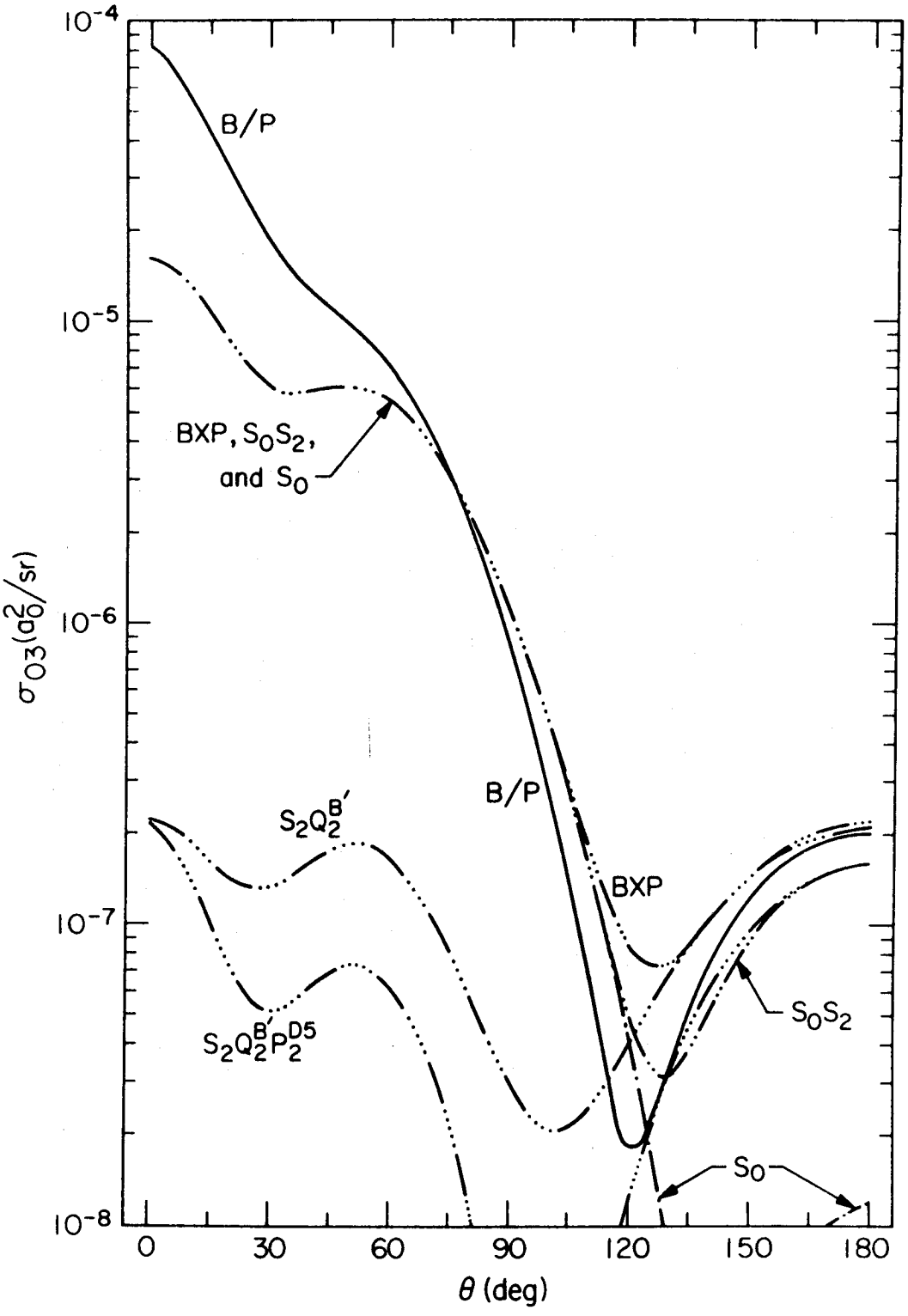
10^{-4}
10^{-5}
10^{-6}
10^{-7}
10^{-8}
$\sigma_{03}(a_0^2/sr)$
B/P
BXP, S_0S_2,
and S_0
$S_2Q_2^{B'}$
B/P
BXP
S_0S_2
$S_2Q_2^{B'}P_2^{D5}$
S_0
0
30
60
90
120
150
180
θ (deg)

31

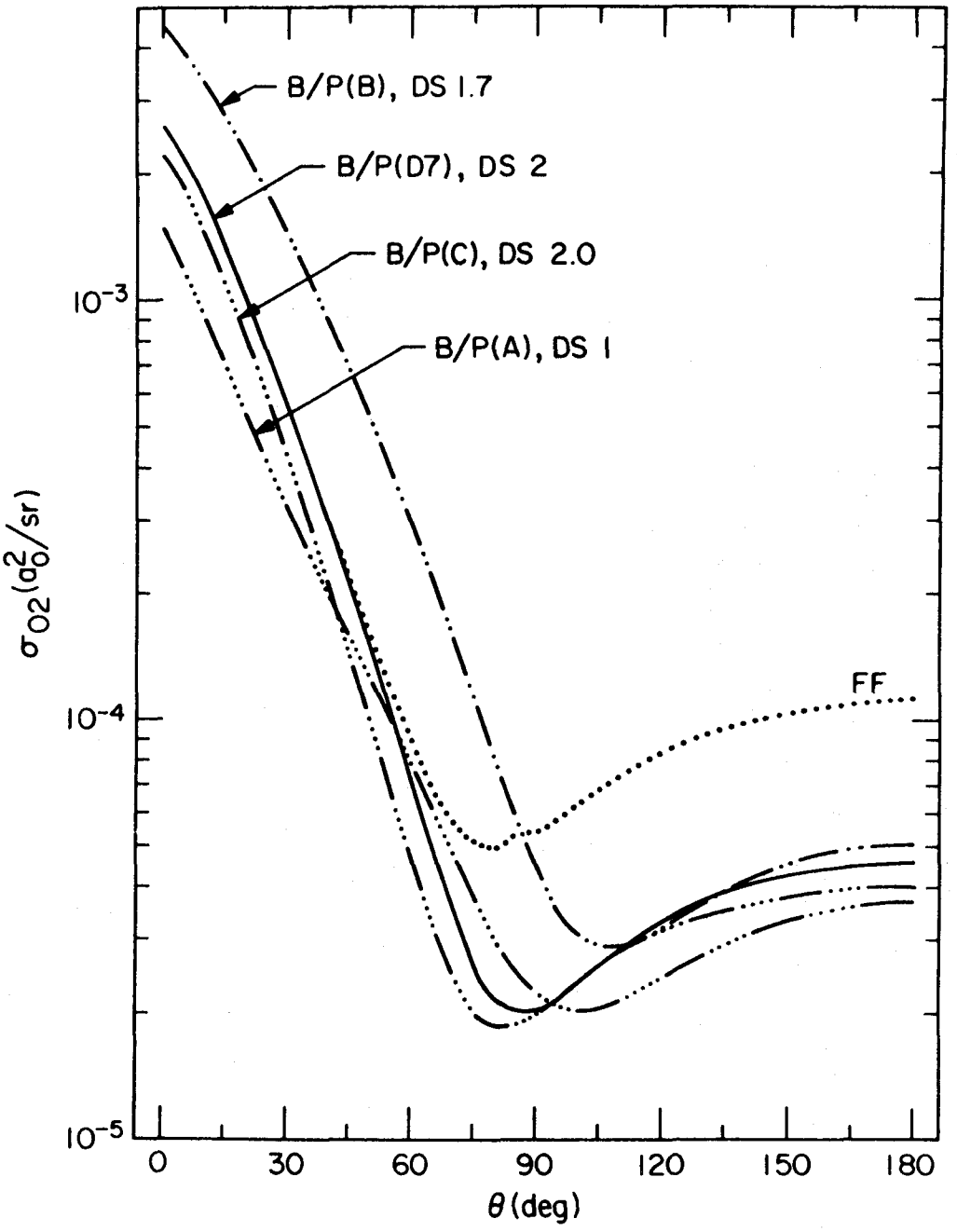
B/P(B), DS 1.7
B/P(D7), DS 2
B/P(C), DS 2.0
B/P(A), DS 1
FF
10^{-3}
10^{-4}
10^{-5}
$\sigma_{02}(a_0^2/sr)$
0
30
60
90
120
150
180
θ (deg)

32

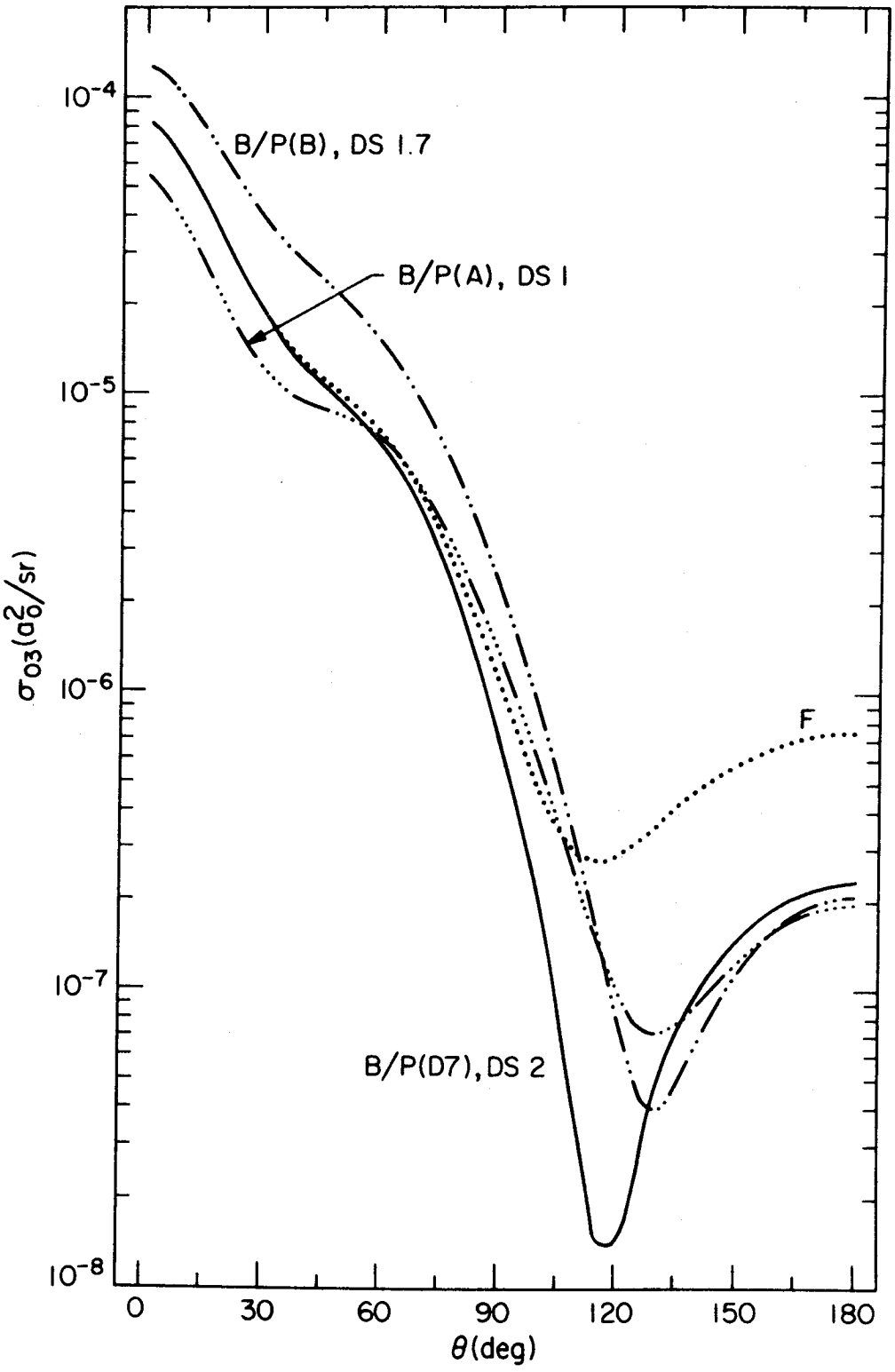
B/P(B), DS 1.7
B/P(A), DS 1
F
B/P(D7), DS 2
10^{-4}
10^{-5}
10^{-6}
10^{-7}
10^{-8}
$\sigma_{03}(a_0^2/sr)$
0
30
60
90
120
150
180
θ(deg)

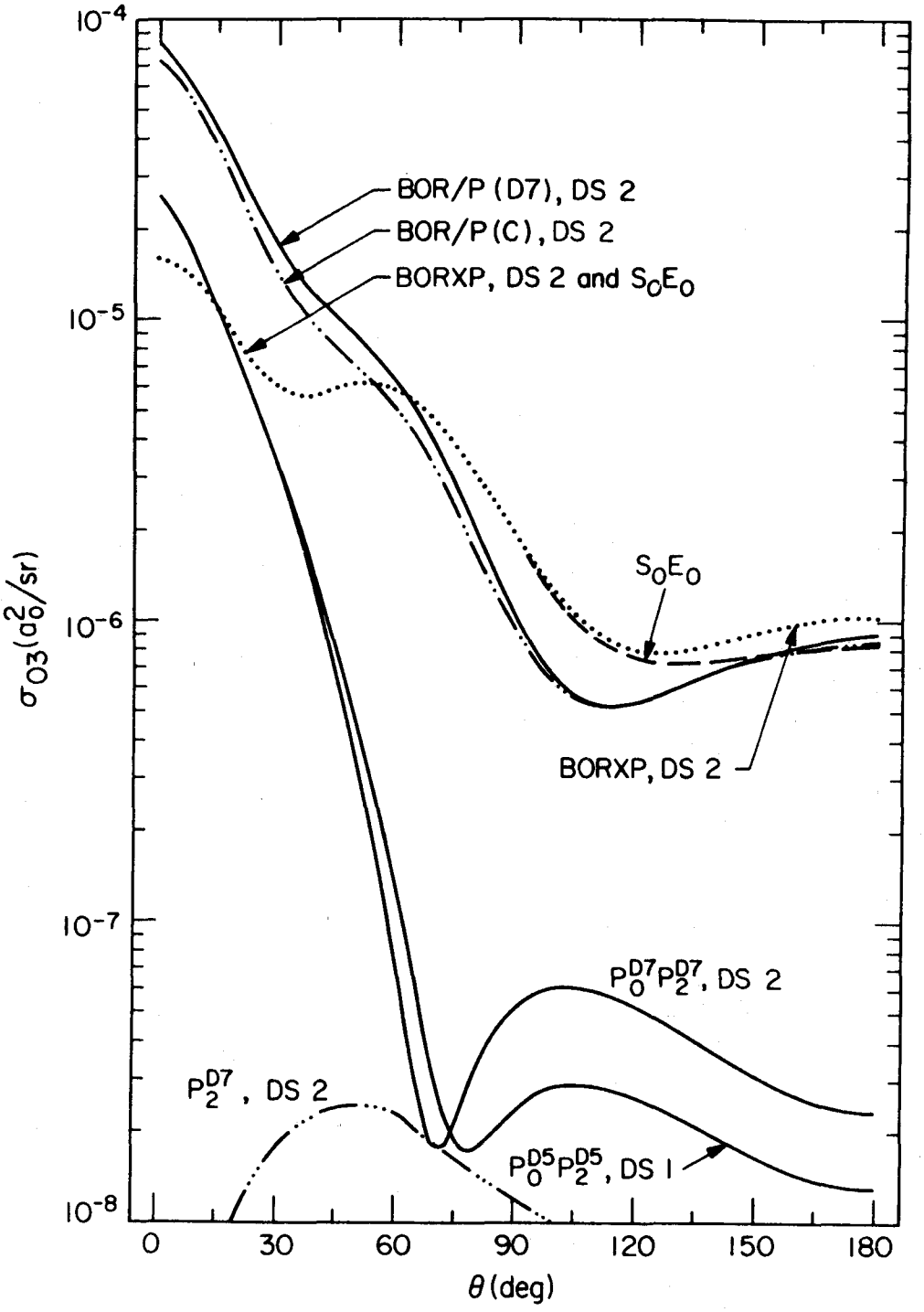
10^{-4}
10^{-5}
10^{-6}
10^{-7}
10^{-8}
$\sigma_{03}(a_0^2/sr)$
BOR/P (D7), DS 2
BOR/P (C), DS 2
BORXP, DS 2 and S_0E_0
S_0E_0
BORXP, DS 2
$P_0^{D7}P_2^{D7}$, DS 2
P_2^{D7}, DS 2
$P_0^{D5}P_2^{D5}$, DS 1
0
30
60
90
120
150
180
θ (deg)

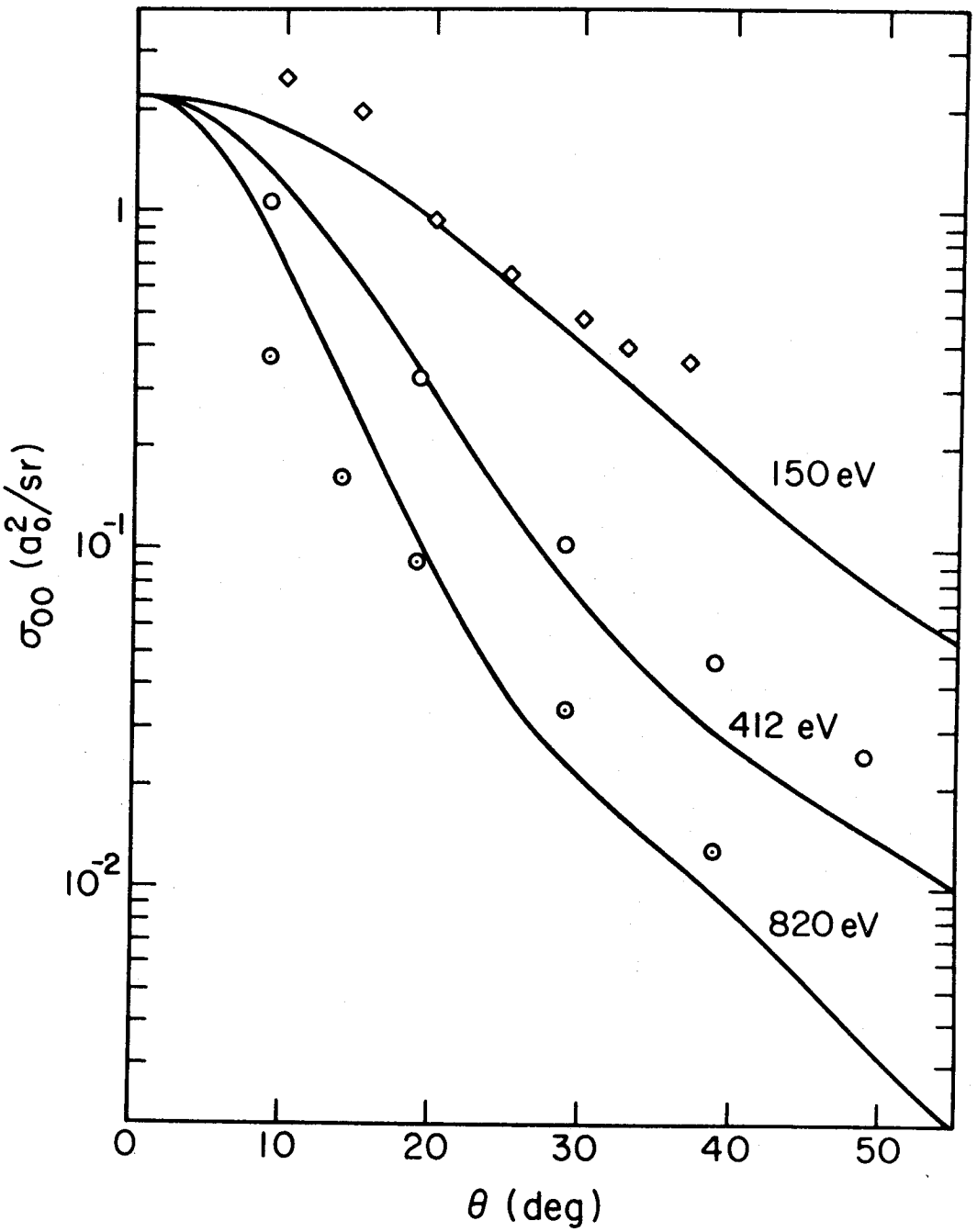
1
10^{-1}
10^{-2}
σ_{00} (a_0^2/sr)
150 eV
412 eV
820 eV
0
10
20
30
40
50
θ (deg)

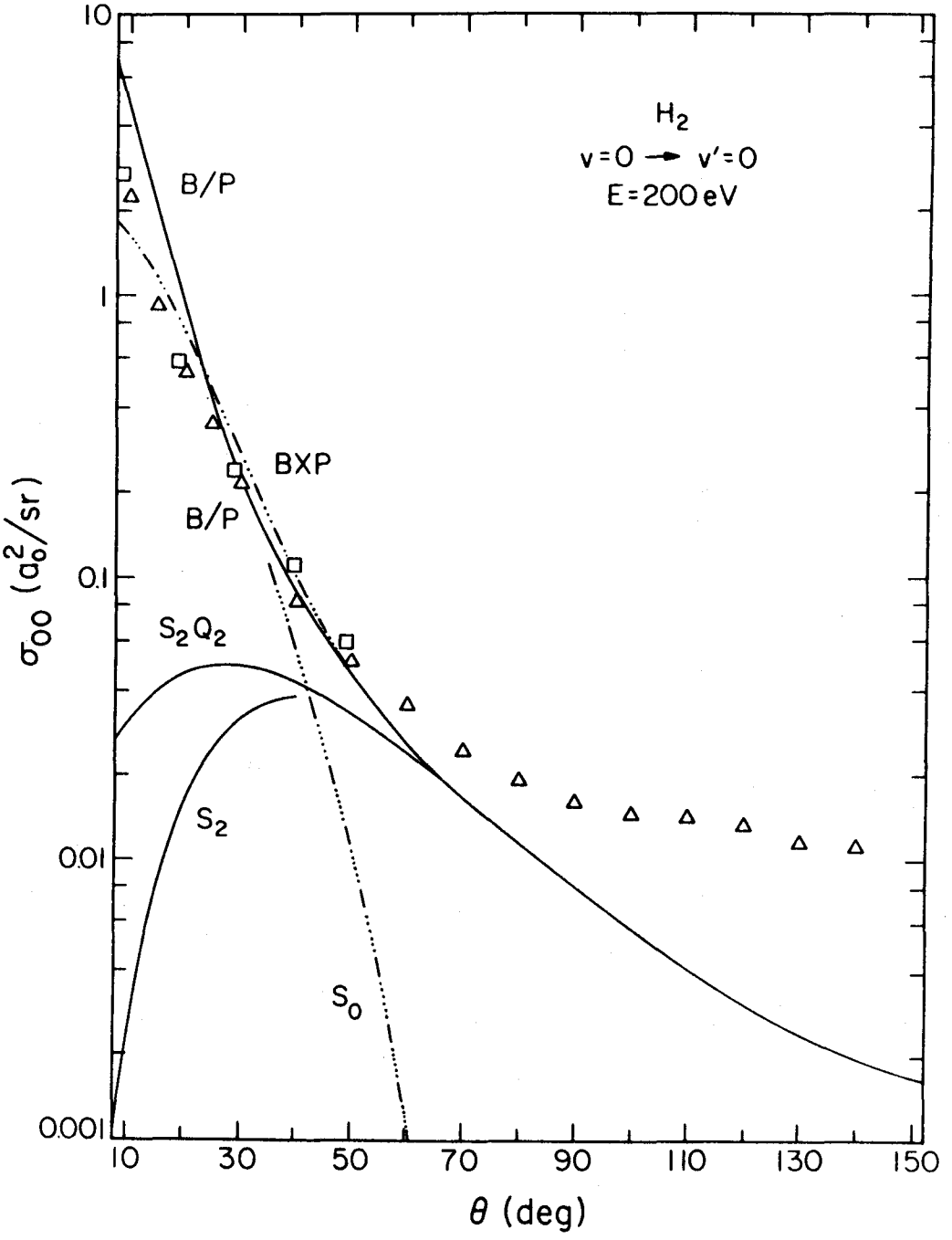
H2
v=0 → v'=0
E=200 eV
B/P
BXP
B/P
S2Q2
S2
S0
σ00 (a0²/sr)
θ (deg)
10
1
0.1
0.01
0.001
10
30
50
70
90
110
130
150

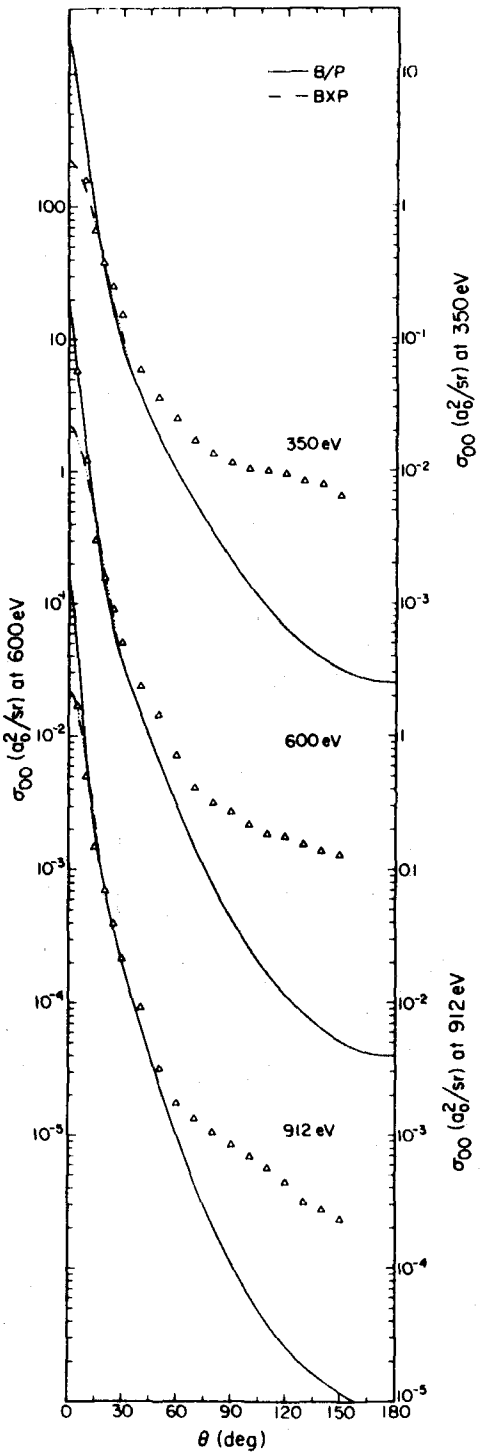
B/P
B×P
350 eV
600 eV
912 eV
σ_{00} (a_0^2/sr) at 600 eV
σ_{00} (a_0^2/sr) at 350 eV
σ_{00} (a_0^2/sr) at 912 eV
θ (deg)
0
30
60
90
120
150
180

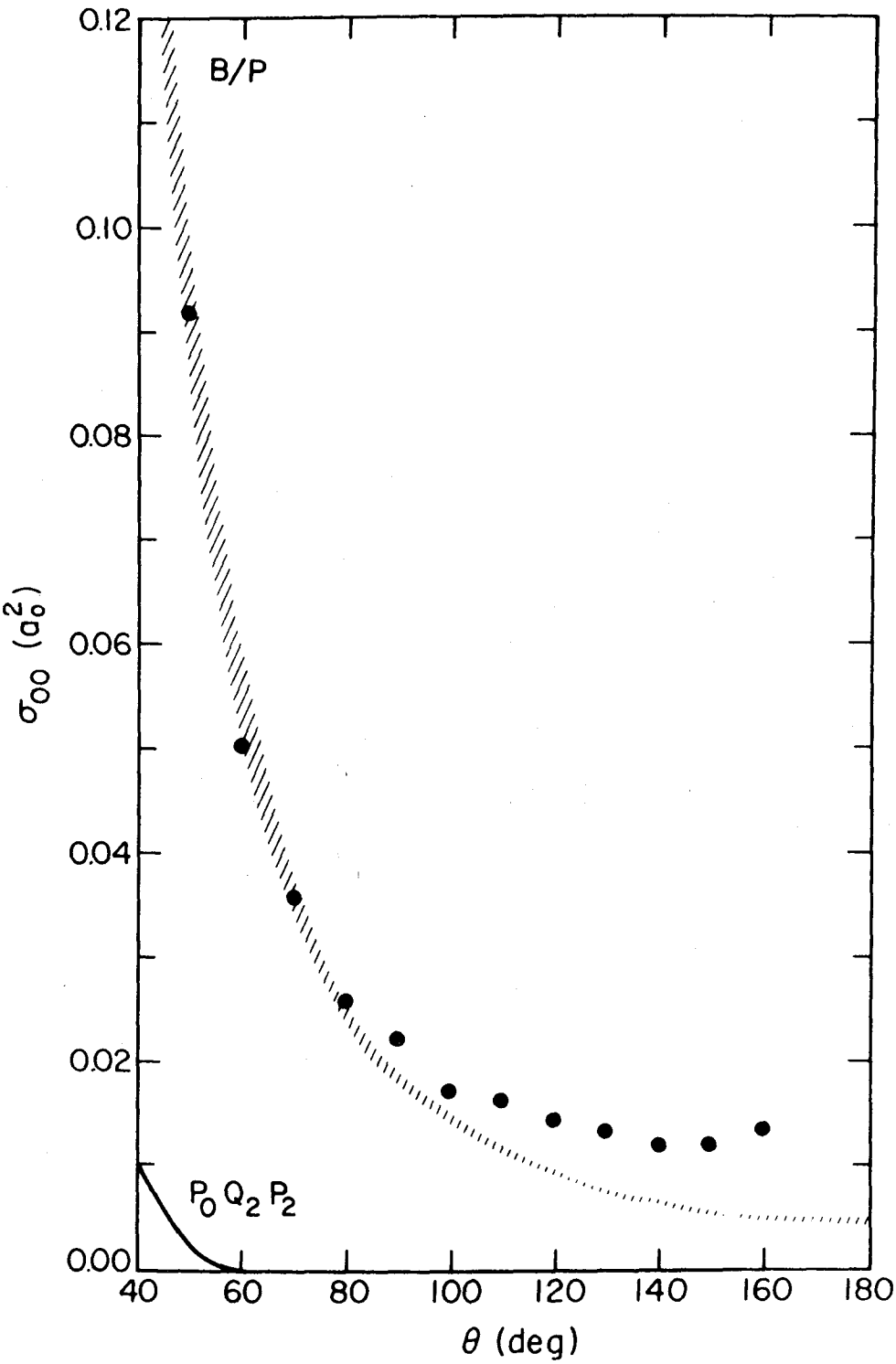
0.12
0.10
0.08
0.06
0.04
0.02
0.00
B/P
$P_0 Q_2 P_2$
σ_{00} (a_0^2)
40
60
80
100
120
140
160
180
θ (deg)

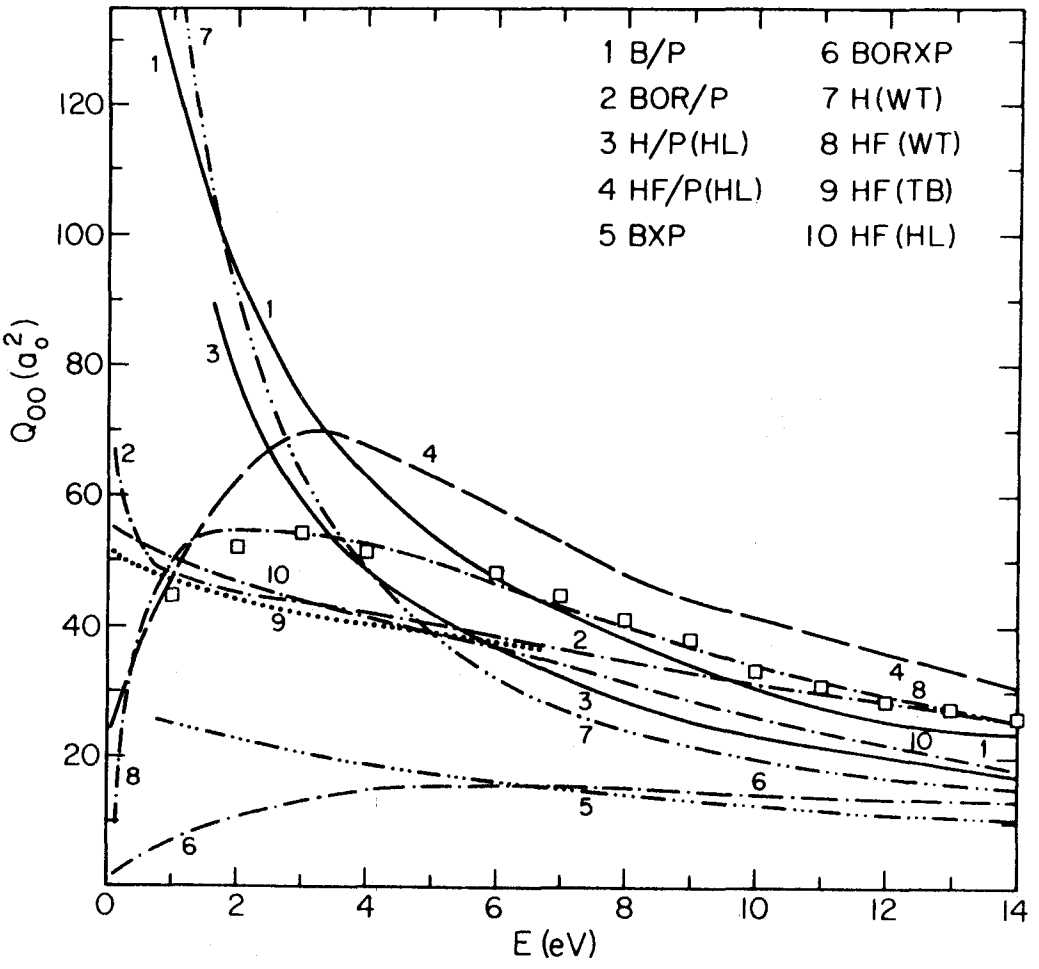
1 B/P
2 BOR/P
3 H/P(HL)
4 HF/P(HL)
5 BXP
6 BORXP
7 H(WT)
8 HF (WT)
9 HF(TB)
10 HF (HL)
$Q_{00}(a_o^2)$
E (eV)
0
2
4
6
8
10
12
14
20
40
60
80
100
120

39

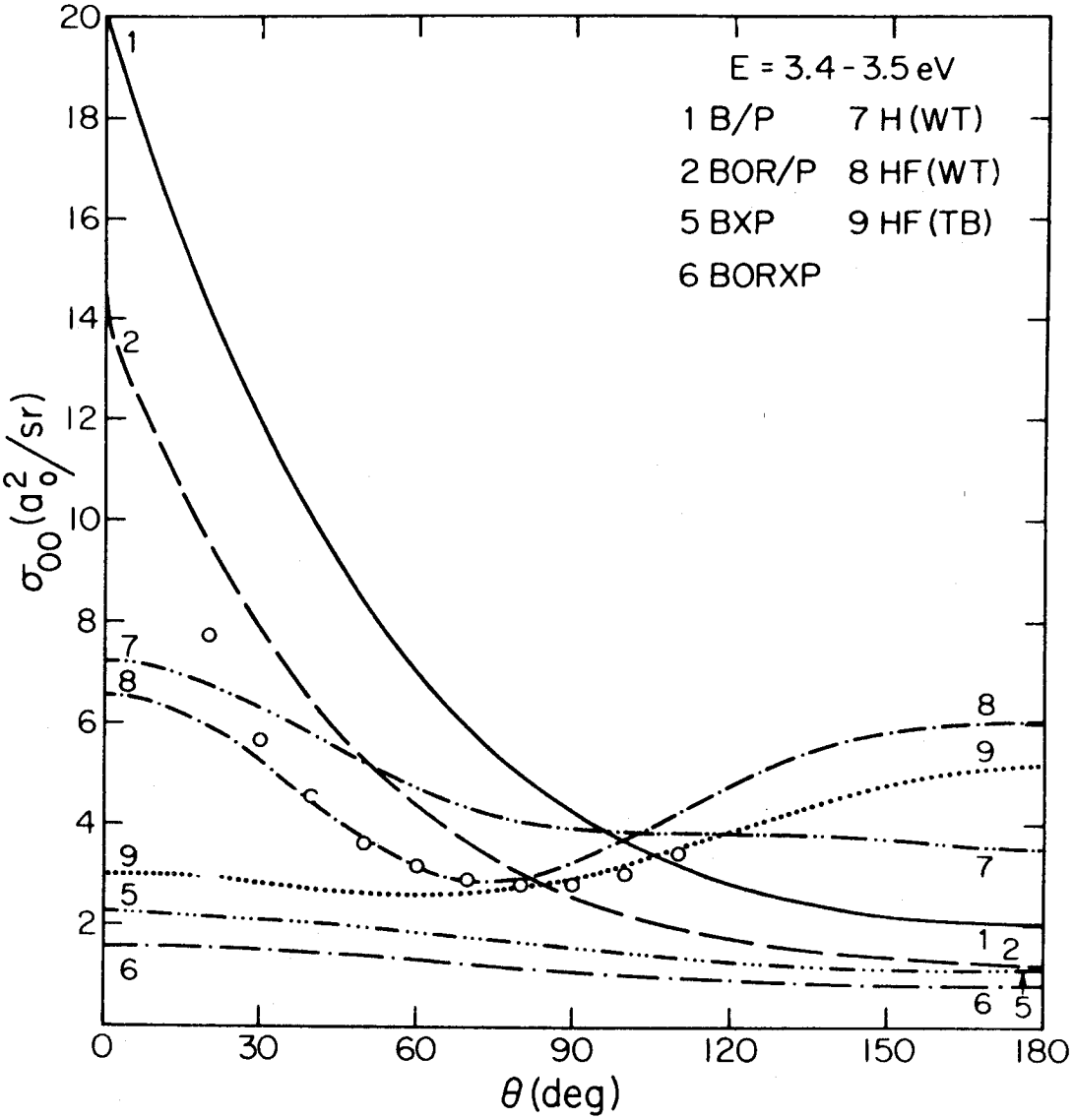
E = 3.4 - 3.5 eV
1 B/P
2 BOR/P
5 BXP
6 BORXP
7 H (WT)
8 HF (WT)
9 HF (TB)
$\sigma_{00}(a_o^2/sr)$
θ (deg)
0
30
60
90
120
150
180
2
4
6
8
10
12
14
16
18
20

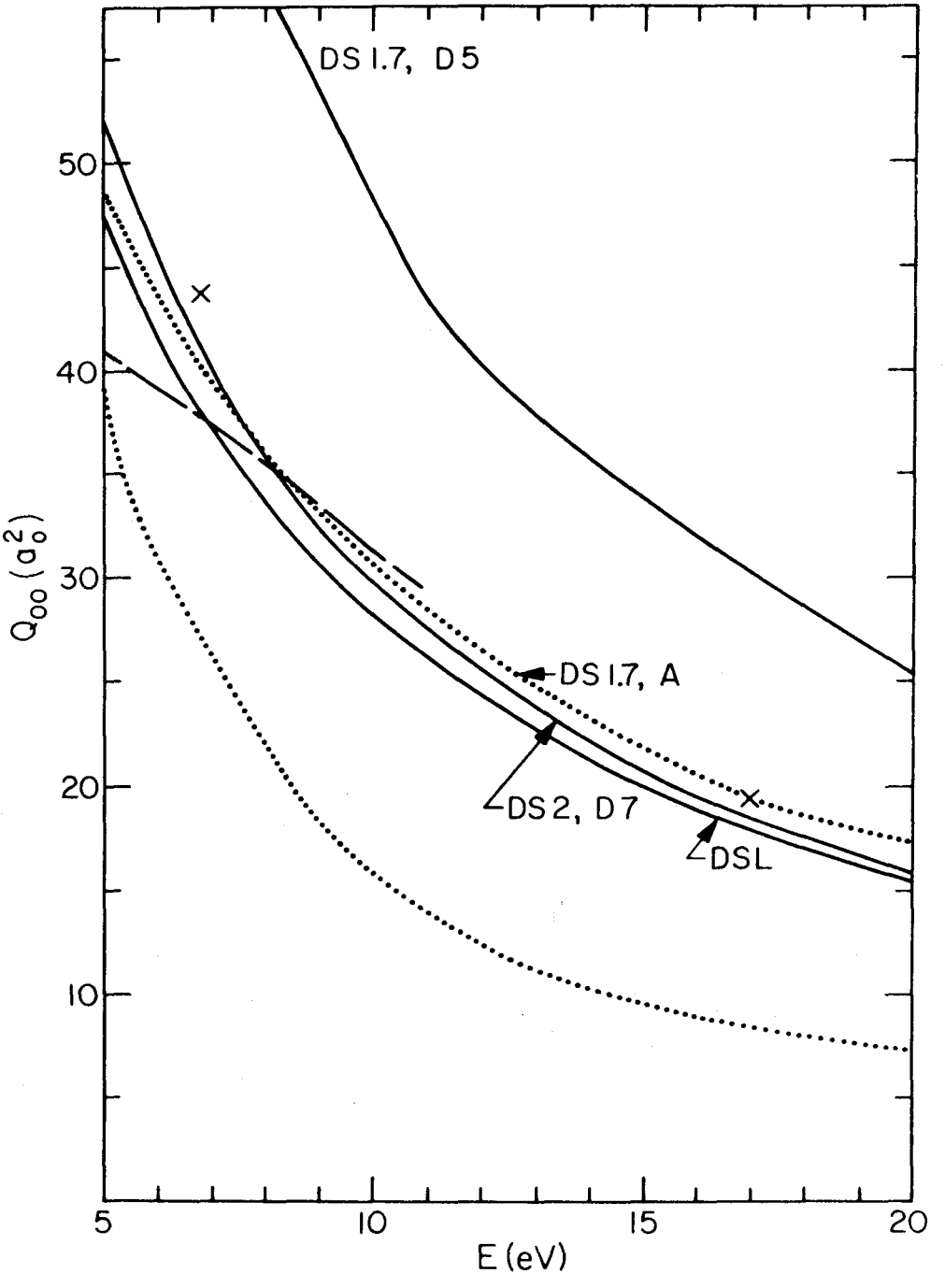
DS 1.7, D5
DS 1.7, A
DS 2, D7
DSL
50
40
30
20
10
5
10
15
20
E (eV)
$Q_{00}(a_0^2)$

II. EXPERIMENTAL AND THEORETICAL STUDY OF ELASTIC SCATTERING*

---

* This is an article by S. Trajmar, D. G. Truhlar, and J. K. Rice.

A. Introduction

Scattering of electrons by H_2 is one of the simplest electron-molecule scattering processes and is therefore of fundamental importance. The elastic scattering has been studied over a wide range of impact energies (E) and scattering angles (θ).[1] Total,[2,3] momentum transfer,[4] and relative differential elastic cross sections[5-13] for this process have been measured at several energies ranging from less than 1 eV to 25 keV.

Our investigation is concerned with the intermediate energy range (defined as approximately 10 to 100 eV). Differential cross sections (DCS's) have been determined for elastic scattering from 10^{o} to 80^{o} at 7, 10, 13.6, 20, 45, 60, and 81.6 eV impact energies. The quantum mechanical theory presented in a previous article (I)[14] is applied here to the calculation of differential and integral elastic cross sections in the whole angular range for impact energies between 0.2 to 100 eV. Because of insufficient apparatus resolution, all of the experimental elastic scattering cross sections reported here include pure rotational excitation contributions. Therefore, we include rotational excitation in our quantum mechanical calculations of elastic scattering. The experimental cross sections have been normalized using the total e - H_2 scattering cross sections of Golden, Bandel, and Salerno[3] at 20 eV and below. Above 20 eV, our integral elastic cross sections (the integral cross section Q is the DCS integrated over all solid angles of scattering) calculated by the Born plus polarization approximation served as the standard for normalization. (The justification for this procedure is discussed in Section D.1.)

We compare our results with previous theoretical[15-18] and experimental[5-11,13] differential cross sections. All previous experimental DCS's have been given in arbitrary units. The previous work is summarized in Tables I and II together with the present one.

B. Experimental and Theoretical Methods

Our electron impact spectrometer is the same type as the one designed by Simpson[19] and Kuyatt and Simpson.[20] The original version of the apparatus has been described earlier.[21,22] Since then, the electron optics have been improved to increase the sensitivity and to make it less dependent on energy loss. This was achieved by introducing several new lens elements. The spectrometer consists of an electron gun, two hemispherical electrostatic energy selectors (monochromator and analyzer), a scattering chamber and a detector system. Figure 1 shows the schematic diagram of the apparatus. An energy-selected electron beam with a distribution of energies centered around the required impact energy E is introduced into the scattering chamber which contains the gaseous molecular target at a pressure of about 10^{-3} torr. Electrons that lose a certain amount of energy and undergo scattering by a specific angle are passed by the analyzer and are detected. The specific energy loss for which electrons can pass through the analyzer to the detector is determined by an analog voltage signal V_2 which is generated by the 1024-channel detector system. The magnitude of V_2 is linearly related to the channel number of the detector memory into which the signal is accumulated and

to the difference between the impact energy E and the energy of the scattered electron. For an ideal experimental setup, V_2 would be zero for the detection of elastically scattered electrons. Due to contact potentials of the order of ± 1 eV, however, this V_2 has a nonzero value and, furthermore, since the electron beam is not completely monoenergetic, a sweep in V_2 over the energy distribution of the electron beam is necessary. The scattering angle stays fixed during one measurement, but it can be set to any angle between -30^{o} and $+90^{o}$ with respect to the direction of the incoming electron beam. All the measurements reported here were taken for positive scattering angles; however the symmetry of the scattering around zero angle and therefore the alignment of the apparatus has been previously verified.

The scattered signal intensities were measured at a given impact energy and scattering angle to obtain an energy loss spectrum. We found that the line shape in the spectrum was not a function of scattering angle; therefore the peak height was taken to be proportional to the scattered intensity at that angle. From spectra taken at one impact energy and several scattering angles, one can obtain the corresponding DCS. An accurate determination of the elastic DCS requires that (a) the experimental conditions remain unchanged for the measurements at all angles, (b) the efficiency of the instrument be independent of scattering angle, and (c) a proper correction for the change of "effective path length" with scattering angle be known and taken into account. The satisfaction of these requirements was ascertained experimentally (a) by measuring the beam intensity and target gas pressure before and after

each experiment, and (b) by comparing our angular distributions of e - He scattering to the ones measured by other investigators.[23]

Geometrical considerations show that the effective path length correction can be made by multiplying the signal at each scattering angle by sin θ provided that θ is much larger than the beam divergence angle. In some of our experiments this was not the case and a more elaborate correction procedure has been applied to all our measurements. The incoming electron beam has been considered as a cone with a truncated Gaussian electron density distribution, having its maximum along the cone axis. A view cone is defined by two apertures at the exit of the scattering chamber. Scattered electrons can reach the detector from the volume defined by the intersection of the two cones. The volume elements within the scattering volume have been weighted for electron density and for the solid angle subtended at the exit apertures. The integration has been performed numerically within the limits which are defined by the intersecting cone surfaces. The measured intensities at each angle are then divided by the value of this integral to bring the differential cross sections to the same arbitrary scale. This method of correcting for the change of effective path length has been discussed previously.[22] A weighting factor that takes into account the change of DCS with scattering angle within the view cone is also included in the computer program; however, since most of the data reported here are for $\theta \geq 20^{o}$, this additional correction was not made. The error introduced in this way is small compared to other uncertainties.[24]

With the present electron optics the measurement of signal intensities corresponding to elastic scattering below 10^{o} is not feasible. The signal for zero energy loss at these low angles is the sum of scattered and direct beam intensities. The separation of the total signal into the two components cannot be done with satisfactory accuracy with the present instrument. (This problem does not exist for the inelastic features because of the energy selection capability of the analyzer and therefore the inelastic signal intensities can be studied down to zero scattering angle.) Experiments with no gas in the scattering chamber show that for a typical case with the present apparatus, the signal (in this case corresponding only to the direct beam) drops by five orders of magnitude when the scattering angle increases from zero to 10^{o}; however at the latter angle it is still about equal to the elastic scattering intensity. Increasing the scattering angle further, the beam-to-elastic signal intensity ratio decreases sharply, and at 20^{o} the direct beam contribution is about a factor of ten less than the scattered elastic signal. Our experimental elastic results at $\theta \leq 10^{o}$ can, therefore, be subject to large errors.

The impact energies have not been calibrated and could be in error by about ± 1 eV due to contact potentials.

The quantum mechanical calculations were performed using the procedures of paper I.[14] In particular, we use four approximate scattering theories which assume the scattering wave functions are

plane waves: the Born approximation (BXP), the prior formulation of the Born-Ochkur-Rudge approximation (BORXP), the polarized Born approximation (B/P), and the Born approximation with corrections both for exchange in the prior formulation of the Ochkur-Rudge approximation and for polarization (BOR/P). When any parameters in the analytic forms used for the potentials are not explicitly specified, they are taken from data set 1 (DS1), and when the forms used for the cutoff functions in the potentials are not explicitly stated, the polarization potential is of form D5 and the quadrupole term has B' form.[14] This is our theoretically most justifiable approximation to the effective e - H_2 interaction potential.

C. Normalization of Experimental Cross Sections

The experimental procedure which was described in the previous section yields the DCS in arbitrary units. A calibration based on measuring all quantities that relate measured signal intensities to DCS is not feasible with our present apparatus. Although the pressure, the incoming electron beam current, and scattered signal intensities could be quantitatively measured, the absolute determination of the effective scattering path length is subject to considerable error, and the instrument's overall efficiency is not known at all. We have used known integrated cross sections to achieve the normalization.

In order to obtain the integral elastic cross sections from our experimental DCS, the curves had to be extrapolated from 10^{o} to 0^{o} and from about 80^{o} to 180^{o}. This extrapolation procedure may at first seem to introduce unreasonably large uncertainties into the calibration; however a more careful examination shows that this is

not the case. For extrapolation to 0^{o} the experimental curve has been simply extended as a straight line (on a logarithmic DCS scale) whose slope is determined by the data between 20^{o} and 30^{o}. This procedure does not appear to introduce more than a couple of percent error. Two alternative extreme methods of extrapolation: (a) zero slope and (b) five times as steep slope as the one measured between 20^{o} and 30^{o} yield integral cross sections which deviate by less than 5% from the values obtained as above. The extrapolation to 180^{o} is more uncertain; however it does not introduce too large an error into the integral cross section since: (1) the DCS is much smaller at angles above 80^{o} than at low angles, where the experimental values are available; (2) the DCS curve is smooth and almost flat at around 80^{o}; (3) the uncertainty in extrapolating the curves increases as one approaches 180^{o}, but the elements of solid angle corresponding to large scattering angles are small (the sin θ factor in the integral) so that scattering at very large angles contributes less to the integral cross sections.

Three methods of extrapolation were tried for the 80^{o} to 180^{o} region:

Type 1 $$\text{DCS}\ (\theta) = \frac{C_1}{q^n}$$

Type 2 $$\text{DCS}\ (\theta) = \text{DCS}\ (\theta_{max})$$

Type 3 $$\text{DCS}\ (\theta) = C_2\ e^{-C_3\theta}$$

where the q is the momentum transfer and θ_{max} is the maximum scattering angle at which we measured experimental DCS. The constants n, C_1, C_2,

and C_3 were determined from two experimental data points (usually at 70^o and 80^o). In each case the choice of which method of extrapolation to use was made after studying the early elastic scattering data which extends to large scattering angles.[6-11] At 7, 10, and 13.6 eV impact energies Type 1 extrapolation was accepted as the most reasonable one, while at the higher energies Type 2 was used. The error due to the extrapolation procedure is estimated to be less than 20% for each integrated elastic cross section. This estimation is based on the deviation that could be introduced into the integrated cross sections by using the different types of extrapolations. On the right-hand side of Figures 2-8, the extrapolated values of the cross sections at the highest angle occurring on each figure are shown.

Golden, Bandel and Salerno[3] measured the total e - H_2 scattering cross sections (Q_{TOT}) from 0.2 to 15 eV with an estimated accuracy of about 3% by measuring the loss of intensity of an electron beam passing through a scattering chamber containing H_2. Their results have been used to calibrate our DCS at impact energies 7, 10, and 13.6 eV, and with extrapolation at 20 eV. The total scattering cross section is the sum of the integrated elastic ($Q_{elastic}$), pure rotational (Q_{rot}), rovibrational ($Q_{ov'}$), and rovibronic (Q_e) excitation cross sections. Table III summarizes the contributions from the different channels that are open at each particular energy. Rotational structure is not resolved in our spectra; hence rotational excitation is mixed into the elastic, vibrational excitation, and vibronic excitation features in our spectra and into those cross sections in Table III. At 7 eV no electronic

excitation channel is open. At higher energies, the integrated cross sections for excitation of the triplet electronic states and ionization are taken from the measurements of Corrigan.[25] The contributions from excitation of the B and C singlet states have been estimated from Khare's calculations.[26] Possible contributions from other weaker electronic transitions have been neglected. The integrated vibrational excitation cross sections have been obtained in the same arbitrary units as the elastic one by the method described in the following article (III).[27] At and below 20 eV the sum of these integral elastic and vibrational excitation cross sections have been normalized to the total e - H_2 scattering cross section of Ref. 3 after the subtraction from the latter of the proper electronic contributions. Above 20 eV no absolute measurements are available for any cross section that could serve to normalize our data. It is believed, however, that our calculated integral elastic cross sections calculated with the polarized Born approximation (B/P) are fairly accurate at these energies (see Section D.1) and they have been used as a standard for normalization of the experimental cross sections. If more accurate integral elastic cross sections Q_{oo} become available, the 45, 60 and 81.6 eV cross sections can be renormalized by multiplying them by the factors $\frac{Q_{oo}}{7.86}$, $\frac{Q_{oo}}{5.97}$, and $\frac{Q_{oo}}{4.44}$, respectively.

The error bars on our experimental absolute values (±35% for E = 7, 10, 13.6 and 20 eV) have been estimated by summing all uncertainties in the extrapolation, in the effective path length correction, in the experimental measurements, and in the absolute measurement used for normalization. For the 45, 60 and 81.6 eV DCS the error (±12%) does not include the errors associated with the normalization to absolute scale. For a given

impact energy, the errors in the relative DCS are only about ±12% which includes errors due to reproducibility, to effective path length correction, and to counting statistics. Uncertainties associated with the electronic contributions to the total cross sections are not considered. (A renormalization of the data can, however, be easily carried out if better values of these contributions become available.) Errors in the vibrational contributions were neglected since these contributions themselves are small compared to the elastic cross sections.

D. Results and Discussion

1. Angular Dependence

Figures 2-11 show the angular dependence of the elastic DCS at different impact energies. In the figures, curves always refer to results of calculations and symbols to experimental data. Table I summarizes the quantum mechanical calculations, and Table II, the measurements on the angular distribution of the elastic scattering in the 6 to 100 eV impact energy range. All the experimental DCS published so far in the literature have been given in arbitrary units; we have normalized them to our experimental values or to our B/P calculations (when an experimental value is not available) at 40^{o} for McMillen[5] and at 60^{o} for Arnot,[6] for Bullard and Massey,[7] for Ramsauer and Kollath,[8] for Mohr and Nicoll,[9] for Hughes and McMillen,[10] for Webb,[11] and for Ehrhardt et al.[13]

In general, there is fairly good agreement among the experimental angular distributions. For the most recent comparison, Ehrhardt et al. claim 10% uncertainty in their relative values. It is evident from Fig. 2

that their measured angular distribution (which was measured only for $\theta \geqslant 20^{o}$) is in excellent agreement with our measurements at 7 eV.

Khare and Moiseivitsch[15] calculated the elastic cross sections in the BEISA approximation (direct scattering calculated in the Born approximation, exchange scattering calculated by the first-order exchange method with the separated atom approximation, and polarization neglected). They used a minimum basis set molecular orbital wave function for H_2 and evaluated some integrals in spheroidal coordinates by expanding the plane wave in spheroidal functions. Their results at 50 and 100 eV are shown in Figures 10-11 (curves marked by KM). Their cross sections are too low at small angles due to the neglect of polarization and too high at intermediate angles (perhaps due to the improper treatment of exchange). At high angles, their cross section, like many other Born calculations, falls monotonically with increasing angle, contrary to experimental observations. Curves marked by R in Figures 2-8 and 11 represent Rozsnyai's Born calculation (BXP approximation).[16] Rozsnyai's calculation neglects exchange and polarization and uses a Heitler-London-like wave function for H_2. This calculation gives cross sections which are too low at all energies and at any energy the deviation from experimental results is most serious at low scattering angles where polarization is most important. Rozsnyai's calculation represents an improvement in numerical technique by expanding the plane wave first into spherical coordinates and making the change to spheroidal coordinates subsequently. This improvement should be significant at low momentum transfers where the existing tables of spheroidal functions cease to be sufficiently

accurate. His calculation, however, doesn't include exchange and is therefore not directly comparable to the KM curve.

Khare and Moiseivitsch[15] also made some calculations without exchange (BXP approximation). These can be directly compared to some other BXP calculations of Rozsnyai[16] which used a molecular orbital wave function for H_2 and to our BXP calculation which uses what we consider to be our theoretically most justifiable approximation to the static potential.[14] The comparison at two energies is shown in Figure 12. This figure shows that there is very good agreement between the three sets of electronic transition moments which determine these DCS's despite the entirely different calculational methods.

Wilkins and Taylor[17] calculated phase shifts for elastic scattering by solving numerically the static exchange equations for an electron moving in the potential field of the neutral homonuclear diatomic hydrogen molecule. This potential field is that calculated using a Hartree-Fock wave function for the scatterer. While such a wave function doesn't include correlation, it is expected, because of Brillouin's theorem, that it gives accurate values for one-electron properties[28] like the potential field. Their treatment (denoted by WT/E) takes full account of electron exchange, but neglects the effect of polarization. Their calculated integral elastic cross sections are in good agreement with experimental results. (See Fig. 13.) (This agreement, however, is completely lost in calculations where they intentionally neglected exchange (WTXE).) We have interpolated their calculated phase shifts and computed differential cross sections from them at 7, 10,

and 13.6 eV impact energies (curves marked by WT/E on Figs. 2-4) by a method described by Temkin and Vasavada[29] and Tully and Berry.[18] These differential cross sections include s and p waves and their interference with each other and with the d wave, but do not include terms quadratic in the d phase shifts or of any order in the higher phase shifts.[18] These differential cross sections are in good agreement with experiment at high scattering angles. At lower scattering angles, however, the agreement is poor and the reason for this discrepancy seems to be the neglect of the polarization.

Tully and Berry[18] carried out calculations at low energies similar to those of Wilkins and Taylor with some improvements (a better bound state wave function and better numerical methods for the scattering), but they also neglected polarization. We have extrapolated their phase shifts to 7 eV and transformed them into DCS by the method mentioned in the previous paragraph. The curve marked by TB/E on Fig. 2 shows these cross sections. The two curves TB/E and WT/E are nearly identical above 70^{o}. At lower angles, however, the TB/E curve lies appreciably under the WT/E curve, which is quite surprising. One would not expect such a large deviation from the differences in the computational methods. Tully and Berry concluded that, if the old DCS data of Ramsauer and Kollath[8] are substantially correct, then the calculations of Wilkins and Taylor must be wrong at low energy. Therefore, it is interesting to note that our experimental confirmation of the RK DCS results at slightly higher energies gives credence to all the RK DCS data.

Hara[30] performed calculations similar to those of Wilkins and Taylor except he made extra simplifying approximations. However, he also included polarization. An example of his calculations is given in Fig. 3; it predicts an angular distribution similar to that predicted by the calculations of Wilkins and Taylor. That the large forward peak that we find due to the polarization potential was not completely obtained by Hara is probably due to the fact that he (like Wilkins and Taylor and Tully and Berry) retained only the first three partial waves in the expansion of the wave function. Our calculation includes all the partial waves.

Curves B/P and BOR/P (see, e.g., the B/P and BOR/P cross sections in Fig. 3) represent the results of our Born and Born-Ochkur-Rudge calculations, respectively, with the theoretically most justifiable potential (data set 1), including polarization. This potential is calibrated against the a priori potentials of Ardill and Davison[31] and Lane and Henry[32] as explained in Paper I. These calculations give good agreement with experiment in the 7 to 81.6 eV energy and 10^{o} to 90^{o} angular range (see Figs. 2-8). In fact, the present calculations are in better agreement with experiment than any of the previous ones. We have to emphasize again that at 7, 10, 13.6 and 20 eV impact energies the experimental cross sections have been normalized independently of any calculation and the agreement, both in magnitude and angular distribution, is significant. Above 20 eV no experimental data are available for calibration; therefore we assumed that our calculated integral elastic cross sections are correct and we used them for the normalization. This assumption is

supported by two things: (a) the B/P calculation gives good agreement with experimental (absolute) integral cross sections from 5 to 15 eV (Fig. 13) and with DCS (both magnitude and angular distribution) at 7, 10, 13.6 and 20 eV (Figs. 2-5); (b) at the higher energies, the plane wave approximation which is made in the calculations should be even more reliable, and it is found that the angular distributions are in excellent agreement with experiment.

Changing the short range part of the polarization potential, which is the part of the whole potential which is least well known, has a more noticeable effect on the magnitude of the DCS than on its angular dependence at small angles. This has been discussed in Paper I and a few more cases are shown in Fig. 6. For example, retaining a polarization potential which is zero at r = 0 (r is the separation of the electron from the molecule) but which has a deeper potential well (this is the direction in which older calculations using a polarization potential were usually wrong) predicts a DCS which is steeper, in worse agreement with experiment at 45 eV, but larger. Since the D5 polarization potential and the parameters of DS1 are most justifiable a priori and do agree with experiment, we will continue to use this potential to interpret the experiments.

The inclusion of polarization terms in the potential increases the cross sections at low angles and makes the agreement between the calculated and experimental values good down to 10^{o} (the lowest angle investigated experimentally). It is interesting to note that the plane

wave calculation with the semiempirical potential that includes polarization gives better overall agreement with experiment than more rigorous calculations which neglect polarization. At higher angles the effect of polarization is much smaller because our polarization potential is a long range potential located mainly outside the region of the bound charge distribution. At 100 eV the B/P and BOR/P curves rise too fast below 30^{o}. This discrepancy may be due to the fact that we calculated our polarization terms in the interaction potential from the static polarizabilities. At high electron velocities one has to use the dynamic polarizabilities; these quantities are, however, difficult to calculate. (See Paper I for more detailed discussion.) Neglecting the polarization effect altogether gives better angular distributions at 100 eV (dash-single dot and dash-triple dot curves on Fig. 11), seemingly indicating that polarization is not important at this energy. In Paper I we also found that the BXP curve agreed better with experiment than the B/P one at 350, 412, 820, and 912 eV. But the data, especially at 200 and 600 eV, also showed that polarization may still be important at high energies, but that accurate differential cross sections at $\theta \leq 10^{o}$ are necessary to judge this at high energy. The D5 and C polarization potentials are zero at $r = 0$ and are approximations to potentials which include nonadiabatic effects at small r, but the A and B polarization potentials are finite at the origin like the adiabatic one. Figures 4, 8 and 11 show scattering off the A, B, C, and D5 polarization potentials (with $a_p = 2.1\ a_o$ and $a_{p'} = 1.8\ a_o$) in the B/P scattering approximation. These figures show

that, even at high enough energies for the plane wave approximation to be good, there are small differences between the angular dependences of the resulting differential cross sections, and very accurate experimental data could be used to distinguish between them.

The inclusion of exchange by our approximate theory (see Paper I) usually improved the agreement with experiment. It lowered the cross section over the whole angular range at 7 eV and over the 0-48° angular range at 10 eV; at energies of 13.6 eV and greater, the BOR/P DCS is greater than the B/P one at all angles. The effect of exchange becomes smaller with increasing impact energy and it is small at around 100 eV. Due to the known difficulties in trying to include exchange in first-order theories,[33,34] we believe that the error in the treatment of exchange may sometimes be as large as the difference between the B and BOR calculations. The Ochkur-Rudge (OR) approximation for exchange does have the advantage that it usually predicts approximately the correct magnitude of the exchange effect.[33,35,36] Since the OR approximation predicts that exchange is not a major effect for the processes and energies (at least above 10 eV) considered in this paper, we then feel safer to be using only the BOR approximate theory for calculating the exchange contributions.

Massey and Mohr[37] used the Born approximation (BXP) to calculate elastic DCS's and compared their results with experimental angular distributions. Reasonable agreement in angular dependence with the data of Arnot was claimed at energies at 80 eV and higher. However, the theory and experiment at 80 eV were compared only for $\theta \geq 20^{\circ}$. Figure 8

shows that for scattering angles greater than 20^{o} the BXP approximation does agree well in shape with Arnot's experimental data if theory and experiment are normalized at 20^{o}, but at 10^{o} the BXP approximation fails to predict the experimentally observed forward peak which is correctly predicted by the B/P approximation. The BXP agrees well with our data above 40^{o} but is about a factor of 3 smaller at 10^{o}. At higher energies polarization may also be important (see Paper I), although the lack of adequate low angle data precludes a definite conclusion.

Massey and Mohr also conclude that the Born approximation fails to predict the correct shape of the DCS at 30 eV. This is confirmed in Fig. 9. The BXP approximation predicts a DCS which is too small at low angles (by a factor of about 6 at 5^{o}) and is in reasonable agreement with the data at angles between 50^{o} and 90^{o}. The inclusion of polarization (B/P) yields a DCS of the correct shape for all angles up to about 90^{o}.

At very high scattering angles, the curves B/P and R merge into each other. This is expected since the effect of polarization here is negligible, but it also indicates that our Born calculation carried out with the semiempirical Carson potential (see Paper I) augmented by a quadrupole term gives just as good results as the more rigorous Born calculation of Rozsnyai (who used the potential generated by a complete valence bond wave function). The polarized Born calculation is in good agreement with the experimental angular distributions up to 90^{o}, but it continues to drop steadily at higher angles, while the experimental curves reach a minimum at around 100^{o} and then increase with increasing scattering

angle to form a local maximum at around 160°, as shown by Hughes and McMillen's data,[10] which extends to 165°. This phenomenon, which is due to scattering in the lowest partial waves (including the interference terms),[6,9,38] is not predicted by the Born or Born-Ochkur-Rudge theories with the present approximation to the potential.

2. Energy Dependence

Figure 13 shows integral elastic cross sections as a function of incident energy. The "experimental" values are determined from the data of Ramsauer and Kollath[8] (Δ) and Golden, Bandel, and Salerno[3] (o) by the procedure used for Table III (see Section C). The curves are from the calculations of Wilkins and Taylor[17] and Tully and Berry[18] in the static exchange approximation and from the present calculations. The four x's are from the calculations of Nagahara[39] in the static approximation (without exchange) in spheroidal coordinates. At energies above 5 eV, our B/P and BOR/P calculations predict an energy dependence in agreement with experiment and with the Wilkins-Taylor calculation. However, Fig. 13 shows that the cross sections predicted by the present calculations are not reliable below 2 eV or below 5 eV if exchange is neglected, evidently because the plane wave approximation made in these calculations is not valid at low energies. Further, the angular dependence of the cross sections (as discussed in Paper I and Section D.1 of this paper) also indicates that our treatment of the static and polarization potentials is at least qualitatively correct at energies above 5 eV.

Figure 13 also shows a comparison with the results of Arnot. Arnot measured the DCS over a 100° angular range at 29 eV and 83 eV in the same arbitrary units. He also integrated his experimental DCS over all scattering

angles to obtain integral cross sections. We normalized his Q_{oo} at 83 eV to our B/P calculation, and with this normalization factor we obtained Q_{oo} in atomic units from his experiments at 29 eV. The figure shows that this energy dependence is in disagreement with the more recent results.

Table IV gives a comparison of our integral cross sections with the calculations (RXE) of Rozsnyai which were already discussed. Also given are some unpublished calculations (R/E) of Rozsnyai which include exchange in the Ochkur approximation. The difference between the BXP and RXE results is due to the different approximations used for the effective static charge distribution of H_2. The table also shows that the OR method predicts a greater effect of exchange than does the Ochkur method.

Since our measurements are normalized, it is possible to investigate the energy dependence of the differential cross sections. Theoretical calculations in the past have been compared to total electron-molecule or integrated elastic and inelastic scattering cross sections. It is a more critical test of scattering theories, models, and approximations, however, to see how well they can predict angular and energy dependencies of differential cross sections. In Figs. 14-21, DCS at 10^{o}, 20^{o}, 30^{o}, 40^{o}, 60^{o}, 70^{o}, 80^{o}, and 110^{o} are shown as a function of impact energy. The crosses are our experimental values; the solid and dashed lines are our B/P and BOR/P calculations, respectively. The dotted curves show the values calculated from the phase shifts of Tully and Berry.[18] The agreement between our experimental values and the B/P calculation is

very good above 10 eV, as we have already seen for the angular dependence of the DCS at each impact energy. The BOR/P calculations are in good agreement with experiment at all energies. The only other measurement on the energy dependence of the elastic DCS for H_2 is given by Ehrhardt et al.[13] in the 1 to 10 eV energy range at 20^o, 40^o, 70^o, 90^o, and 110^o (arbitrary units). We have normalized their values to our experimental ones at 10 eV for the 20^o, 40^o, and 70^o cases and to the calculation of Tully and Berry at 7 eV for the 110^o case, and their normalized values are shown in Figs. 15, 17, 19, and 21. In the 10 to 100 eV region, the DCS monotonically decreases with increasing energy at all angles. The decrease is small at low angles (about a factor of two at 10^o). As the scattering angle increases, the DCS versus energy curve becomes steeper and at 80^o the value of the DCS decreases by about two orders of magnitude from 10 eV to 100 eV. The data of Ehrhardt et al. shows that the DCS curve has a peak below 7 eV for angles 20^o to 70^o.

E. Conclusions

In summary, first-order calculations with theoretically justified static and polarization potentials predict the elastic cross sections for e - H_2 scattering approximately correctly. Not only the magnitude of the integrated cross sections, but also the angular and energy dependence of the elastic differential cross sections are obtained in good agreement with experiments in the 10^o to 80^o angular and 10 eV to 81.6 eV (intermediate) energy range. Below 10 eV, the agreement is less satisfactory. Contrary to previous work[15,17] we find that inclusion of polarization is essential for getting the good agreement with experiment, particularly with the DCS at low scattering angles, and use of the static polarizability appears to be adequate at least up to 82 eV. At higher energies, however,

the nonadiabatic corrections may become too large to use only the static polarizability to calculate the polarization potential, and one would need to consider the dynamic polarizability. Below about 5 eV, the Born calculations (with polarization) without exchange, as well as the more rigorous calculation of Wilkins and Taylor without exchange, give unreasonably large cross sections and the inclusion of exchange is necessary to correct for this failure. The introduction of exchange transforms the monotonically increasing Q_{oo} curve (Fig. 13) into one that has a maximum at intermediate energies. This is qualitatively the right feature; the quantitative agreement with experiment is also fairly good for $E > 2$ eV for our approximate treatment of the exchange. Above 50 eV, the calculated exchange contribution is small (less than 20% of the integral cross section), and it becomes even smaller (about 13%) by 100 eV. The angular distributions predicted by our B/P calculations are in good agreement with experiments up to about 90^{o}. Above this angle, the plane wave theories we examined do not predict the proper angular behavior, evidently because of neglect of distortion of the scattering electron wave function.

The 35-40 year old experimental data on electron-hydrogen molecule elastic scattering are found to be generally, but not always, reliable. There is good agreement between the present results and the low energy cross sections of Ehrhardt et al.[13] There is no comparable previous work on the energy dependencies of the cross sections in the intermediate energy range.

TABLE I. Summary of the Theoretical Work on the Angular Dependence of e - H_2 Elastic DCS[a]

Ref. No.	Abbr.	E(eV)	Method[e]	Fig. No.	Symbol
15	KM-B	50, 100	BXP-MO	12	------
	KM	50, 100	BXP/E-MO[f]	10, 11	------
16	R-HL[g]	7 - 81.6[b]	BXP-HL	2 - 8, 11	—·—·
	R-MO	50, 100	BXP-MO	12	—··—
17	WT	7 - 13.6	NXP/E-MO	2 - 4	-------
18	TB	7[c]	NXP/E-W	2	.....
30	H	10.9	N/P/E-MO	3	-------
This paper[d]		7 - 100	B/P	2 - 11	——— ··—— ···— ····—
		7 - 100	BOR/P	2 - 11	— —
		30 - 100	BXP	8, 9, 11, 12	—·· ·····
		60 - 81.6	BORXP or $(BORXP)_o$	7, 8	·····

[a] Only the 7 to 100 eV impact energy range is included.

[b] The DCS was calculated as a function of momentum transfer for $q = 0 - 2\ a_o^{-1}$.

[c] Extrapolated phase shifts.

[d] Present calculation.

[e] The following notation is used: B = Born; BOR = Born-Ochkur-Rudge; N = numerical solution for scattering wave function; / means plus; X means without; E = exchange; P = polarization; HL = valence bond bound state wave function; MO = molecular orbital bound state wave function; W = Weinbaum bound state wave function.

[f] This calculation by Khare and Moiseivitsch is sometimes called BE1SA.

[g] This is sometimes called R or RXE.

TABLE II. Summary of Experimental Work on the Angular Dependence of e - H_2 Elastic DCS[a]

Ref. No.	Abbr.	E(eV)	θ(deg)	Fig. No.	Symbol
5	M	50, 100	10 - 40	10, 11	◇
6	A	29, 83	10 - 120	9, 8	○
7	BM	10, 20, 30	20 - 120	3, 5, 9	□
8	RK	7.4, 10	15 - 167.5	2, 3	▲
9	MN	63	45 - 165	7	●
10	HM	35, 50, 100	43.5 - 170	9 - 11	■
11	W	30, 50, 100	5 - 150	9 - 11	△
13	ELLT	7	20 - 110	2	○
This paper[b]		7, 10, 13.6 20, 45, 60, 81.6	10 - 80	2 - 8	x

[a] Only the 6 to 100 eV impact energy range is included.

[b] Present results.

TABLE III. Contributions of Various Transitions to Total e - H_2 Scattering Cross Sections (a_o^2) at Different Impact Energies

Transition\Energy (eV)	7	10	13.6	20	45	60	81.6
A. Total Scattering	42.1[a]	33.7[a]	26.9[a]	20.0[a]			
B. Electronic Excitation:							
Triplets and Ionization[b]	0.0	0.73[b]	2.87[b]	3.73[b]			
$B^1\Pi$ and $C^1\pi$	0.0	0.0	0.4[c]	1.5[c]			
C. A minus B	42.1	33.0	23.6	14.8			
D. Elastic Scattering	41.5[d]	32.6[d]	23.4[d,*]	14.7[d,*]	7.86[f]	5.97[f]	4.44[f]
E. Vibrational Excitation:							
(Sum of excitations to all vibrationally excited levels)	0.60[e]	0.35[e]	0.11[e]	0.05[e]	0.05[g]	0.03[g]	0.03[g]

[a] Experiments of Ref. 3 (cross section at 20 eV is our extrapolation).

[b] Dissociation cross section from Ref. 25. This is approximately equal to the sum of all triplet excitation cross sections and the ionization cross section.

[c] Estimated from quantum mechanical calculations in the Born-Ochkur approximation by S. P. Khare (Ref. 26). (75% of his calculated value was taken.)

[d] Obtained by multiplying the cross section in row C by our experimental results (from Article III) for the ratio D/(D + E) — i.e., the ratio of the integral elastic and rotational excitation cross sections to the sum of these and the vibrational excitation cross sections.

[e] C minus D.

[f] Present calculation in the Born plus polarization approximation.

[g] Obtained from experimental integral vibrational excitation to elastic scattering cross section ratios (Article III) and from the calculated elastic integral cross sections in row D.

* Our calculated (Born approximation plus polarization) elastic scattering cross sections for 13.6 eV and 20 eV are 23.75 a_o^2 and 16.76 a_o^2, respectively.

TABLE IV. Integral Elastic Cross Sections (a_o^2)

E (eV)	B/P	BOR/P	BXP	BORXP	RXE[a,b]	R/E[b]
30	11.52	13.83	5.57	7.38	4.68	5.46
50	7.11	8.43	3.53	4.52	3.01	3.56
60	5.97	7.00	2.99	3.75	2.54	3.01
70	5.15	5.98	2.59	3.20	2.23	2.95
80	4.52	5.20	2.29	2.78	1.88	2.36
90	4.04	4.60	2.05	2.46	1.76	2.10
100	3.64	4.12	1.86	2.20	1.60	1.92

[a] Ref. 16.

[b] B. F. Rozsnyai, private communication (1969). These results were obtained with the Heitler-London-like wave function with exponent 1.18.

References

1. L. J. Kieffer, Bibliography of Low Energy Electron Collision Cross Section Data. NBS Misc. Publications 289, March 10, 1967.

2. H. S. W. Massey and E. H. S. Burhop, Electronic and Ionic Impact Phenomena, 1st ed., Clarendon Press, Oxford, p. 206 (1952).

3. D. E. Golden, H. W. Bandel, and J. A. Salerno, Phys. Rev. 146, 40 (1966).

4. A. G. Engelhardt and A. V. Phelps, Phys. Rev. 131, 2115 (1963).

5. J. H. McMillen, Phys. Rev. 36, 1034 (1930).

6. F. L. Arnot, Proc. Roy. Soc. (A) 133, 615 (1931).

7. E. C. Bullard and H. S. W. Massey, Proc. Roy. Soc. (A) 133, 637 (1931).

8. C. Ramsauer and R. Kollath, Ann. Phys. (Leipzig) 4, 91 (1929) and 12, 529 (1932).

9. C. B. O. Mohr and F. H. Nicoll, Proc. Roy. Soc. 138, 469 (1932).

10. A. L. Hughes and J. H. McMillen, Phys. Rev. 41, 39 (1932).

11. G. M. Webb, Phys. Rev. 47, 384 (1935).

12. J. Geiger, Z. Physik 181, 413 (1964).

13. H. Ehrhardt, L. Langhans, F. Linder, and H. S. Taylor, Phys. Rev. 173, 222 (1968).

14. D. G. Truhlar and J. K. Rice, to be published. This article will be referred to as I. A study of elastic scattering at energies above 100 eV is contained in this article.

15. S. P. Khare and B. L. Moiseivitsch, Proc. Phys. Soc. 85, 821 (1965).

16. B. F. Rozsnyai, J. Chem. Phys. 47, 4102 (1967).

17. R. L. Wilkins and H. S. Taylor, J. Chem. Phys. 47, 3532 (1967).

18. J. C. Tully and R. S. Berry, J. Chem. Phys. 51, 2056 (1969).

19. J. A. Simpson, Rev. Sci. Instr. 35, 1698 (1964).

20. C. E. Kuyatt and J. A. Simpson, Rev. Sci. Instr. 38, 103 (1967).

21a. S. Trajmar, J. K. Rice and A. Kuppermann, JPL Tech. Memo. No. 33-373 (1968).

21b. J. K. Rice, Ph.D. Thesis, California Institute of Technology (1968).

22. S. Trajmar, D. C. Cartwright, J. K. Rice, R. T. Brinkmann, and A. Kuppermann, J. Chem. Phys. 49, 5464 (1968).

23. J. A. Simpson, M. G. Menendez, and S. R. Mielczarek, Phys. Rev. 150, 76 (1966). In this work there is little uncertainty in the volume correction since narrow beams were used. Their inelastic angular distributions may suffer from double scattering at higher scattering

angles [see G. E. Chamberlain, J. A. Simpson, S. R. Mielczarek, and C. E. Kuyatt, J. Chem. Phys. 47, 4266 (1967)]. Thus, we limited the comparison to small angles ($\theta \lesssim 30^{o}$) which is just the region in which the volume correction is most critical in our work.

24. S. Trajmar, J. K. Rice, D. G. Truhlar, R. T. Brinkmann, and A. Kuppermann, The VI International Conference on the Physics of Electronic and Atomic Collisions, Cambridge, Mass., July 28 - August 2, 1969.

25. S. J. B. Corrigan, J. Chem. Phys. 43, 4381 (1965).

26. S. P. Khare, Phys. Rev. 149, 33 (1966).

27. S. Trajmar, D. G. Truhlar, J. K. Rice, and A. Kuppermann, J. Chem. Phys. , (1970), following article. This article will be referred to as III.

28. See, for example, M. Cohen and A. Dalgarno, Proc. Phys. Soc. (London) 77, 748 (1961).

29. A. Temkin and K. V. Vasavada, Phys. Rev. 160, 109 (1967).

30. S. Hara, J. Phys. Soc. Japan 22, 710 (1967).

31. R. W. B. Ardill and W. D. Davison, Proc. Roy. Soc. (London), A 304, 465 (1968).

32. N. F. Lane and R. J. W. Henry, Phys. Rev. 173, 183 (1968).

33. D. G. Truhlar, D. C. Cartwright, and A. Kuppermann, Phys. Rev. 175, 113 (1968).

34. D. G. Truhlar, J. K. Rice, A. Kuppermann, S. Trajmar, and D. C. Cartwright, Phys. Rev. (to be published).

35. M. R. H. Rudge, Proc. Phys. Soc. 86, 763 (1965).

36. D. C. Cartwright and A. Kuppermann, Phys. Rev. 163, 861 (1967).

37. H. S. W. Massey and C. B. O. Mohr, Proc. Roy. Soc. (London) A 135, 258 (1932).

38. N. F. Mott and H. S. W. Massey, The Theory of Atomic Collisions, 3rd ed., Clarendon Press, Oxford (1965), pp. 464-467.

39. S. Nagahara, J. Phys. Soc. Japan 9, 52 (1954).

Figure Captions

Fig. 1 Schematic diagram of the electron impact spectrometer.

Fig. 2 Elastic DCS at E = 7 eV. The curves are calculated results as listed in Table I. The symbols refer to various experimental results as listed in Table II. The RK and ELLT data are normalized to those of the present work at $\theta = 60^{o}$(*). The x's at $\theta = 180^{o}$ are the type 1, 2, and 3 extrapolated DCS values.

Fig. 3 Elastic DCS at E = 10 eV. Refer to Tables I and II for definitions of the curves and symbols. The BM and RK data are normalized to those of the present work at $\theta = 60^{o}$. The x's at $\theta = 180^{o}$ are the type 1, 2, and 3 extrapolated DCS values. Hara did not report the DCS for $\theta \leq 11^{o}$.

Fig. 4 Elastic DCS at E = 13.6 eV. Refer to Tables I and II for definitions of the curves and symbols. The B/P scattering is shown for three types of polarization potentials at small angles. At these angles the B/P(B) cross section is within 10% of the BOR/P(D5) one. The x's at $\theta = 180^{o}$ are the type 1, 2, and 3 extrapolated DCS values for the experimental data.

Fig. 5 Elastic DCS at E = 20 eV. Refer to Tables I and II for definitions of the curves and symbols. The BM data are normalized to those of the present work at $\theta = 60^{o}$. The x's at $\theta = 180^{o}$ are the type 1, 2, and 3 extrapolated DCS values.

Figure Captions (Cont.)

Fig. 6 Elastic DCS at E = 45 eV. Refer to Tables I and II and text for definitions of the curves and symbols. The *'s at $\theta = 140^{\circ}$ are the type 1, 2, and 3 extrapolated DCS values at $\theta = 140^{\circ}$. The data set and the type of cutoff function used for the two polatization terms are shown in parentheses.

Fig. 7 Same as Fig. 6 except that E = 60 eV and the MN data are presented and normalized to those of the present work at $\theta = 60^{\circ}$. The dotted line is the BORXP calculation when only the spherically symmetric part of the potential is used.

Fig. 8 Elastic DCS at E = 81.6 eV. Refer to Tables I and II for definitions of the curves and symbols. At small angles the B/P approximation is shown for four different choices of the polarization potential. The BORXP approximation is also shown in this region. At $\theta = 60^{\circ}$, the four curves would all lie within 24% of the B/P(D5) one. The calculations are all for data set 1 with a B' form for the quadrupole term cutoff function. The Arnot data are normalized to those of the present work at $\theta = 60^{\circ}$. The *'s at $\theta = 140^{\circ}$ are the type 1 and 2 extrapolated DCS values at $\theta = 140^{\circ}$.

Fig. 9 Elastic DCS at E = 30 eV. Refer to Tables I and II for definitions of the curves and symbols. The A, BM, HM, and W data are normalized to the B/P curve at $\theta = 60^{\circ}$(*).

Figure Captions (Cont.)

Fig. 10 Elastic DCS at E = 50 eV. Refer to Tables I and II for definitions of the curves and symbols. The HM and W data are normalized to the B/P curve at $\theta = 60^{o}$. The M data are normalized to those of W at $\theta = 40^{o}$.

Fig. 11 Elastic DCS at E = 100 eV. Refer to Tables I and II for definitions of the curves and symbols. Four B/P curves are shown just as in Fig. 8. The HM and W data are normalized to the B/P curve at $\theta = 60^{o}$. The M data are normalized to those of W at $\theta = 40^{o}$.

Fig. 12 Elastic DCS at E = 50 and 100 eV. Comparison of three Born calculations which neglect polarization and exchange. The curve marked BXP is from the present calculations, the curve marked R-MO is Rozsnyai's calculation with an MO wave function, and the curve marked KM-B is the BXP calculation of Khare and Moiseiwitsch.

Fig. 13 Integral elastic cross sections as a function of impact energy. Refer to Table I for definitions of the curves. The circles are obtained from the experimental total cross section measurements of Golden, Bandel, and Solerno by subtracting the integral vibrational excitation cross sections of Ehrhardt, Langhans, Linder, and Taylor from raw C of Table III. The triangles are obtained from the data of Ramsauer and Kollath the same way; squares are obtained from the measurements of Arnot as discussed in Section D.2. The x's are cross sections calculated by Nagahara.

Figure Captions (Cont.)

Fig. 14 The differential cross section at 10^{o} is shown as a function of impact energy. The curve TB/E represents the calculation of Tully and Berry. The curves B/P and BOR/P are our calculations, and our experimental results are indicated by crosses.

Fig. 15 Same as Fig. 14 except $\theta = 20^{o}$, and the results of Ehrhardt et al. (Ref. 13) are also shown (as circles).

Fig. 16 Same as Fig. 14 except $\theta = 30^{o}$.

Fig. 17 Same as Fig. 15 except $\theta = 40^{o}$ for the experimental data and 42^{o} for the calculations.

Fig. 18 Same as Fig. 14 except $\theta = 60^{o}$.

Fig. 19 Same as Fig. 15 except $\theta = 70^{o}$.

Fig. 20 Same as Fig. 14 except $\theta = 80^{o}$.

Fig. 21 The differential cross section at 110^{o} as a function of impact energy. The curve TB/E represents the calculation of Tully and Berry, and the curve WT/E represents the calculation of Wilkins and Taylor. The curves B/P and BOR/P are the present calculations, and the experimental results of Ehrhardt et al. (Ref. 13) are indicated by circles.

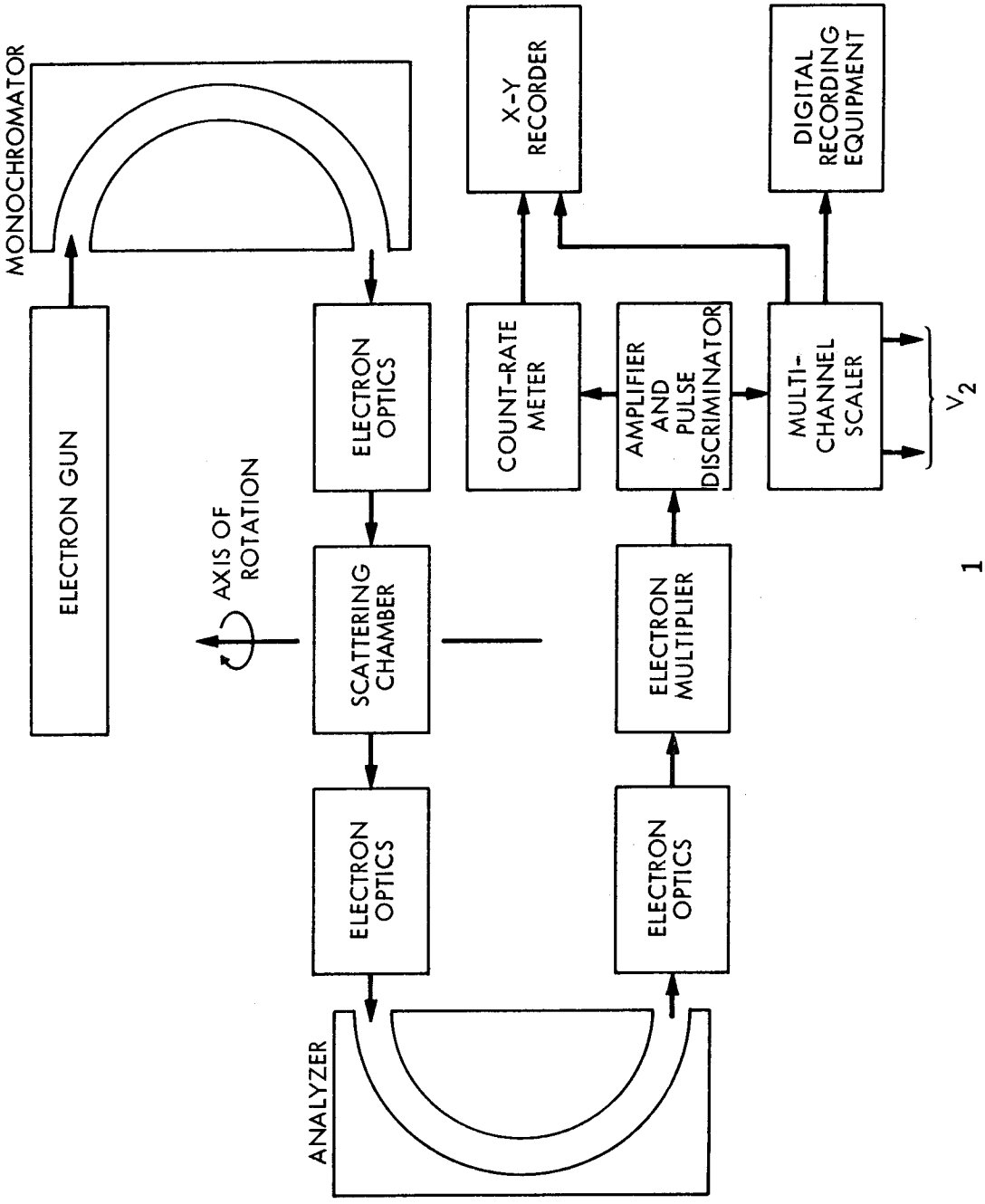
MONOCHROMATOR
ELECTRON GUN
ELECTRON OPTICS
AXIS OF ROTATION
SCATTERING CHAMBER
ELECTRON OPTICS
ANALYZER
ELECTRON OPTICS
ELECTRON MULTIPLIER
COUNT-RATE METER
AMPLIFIER AND PULSE DISCRIMINATOR
MULTI-CHANNEL SCALER
X-Y RECORDER
DIGITAL RECORDING EQUIPMENT
V_2
1

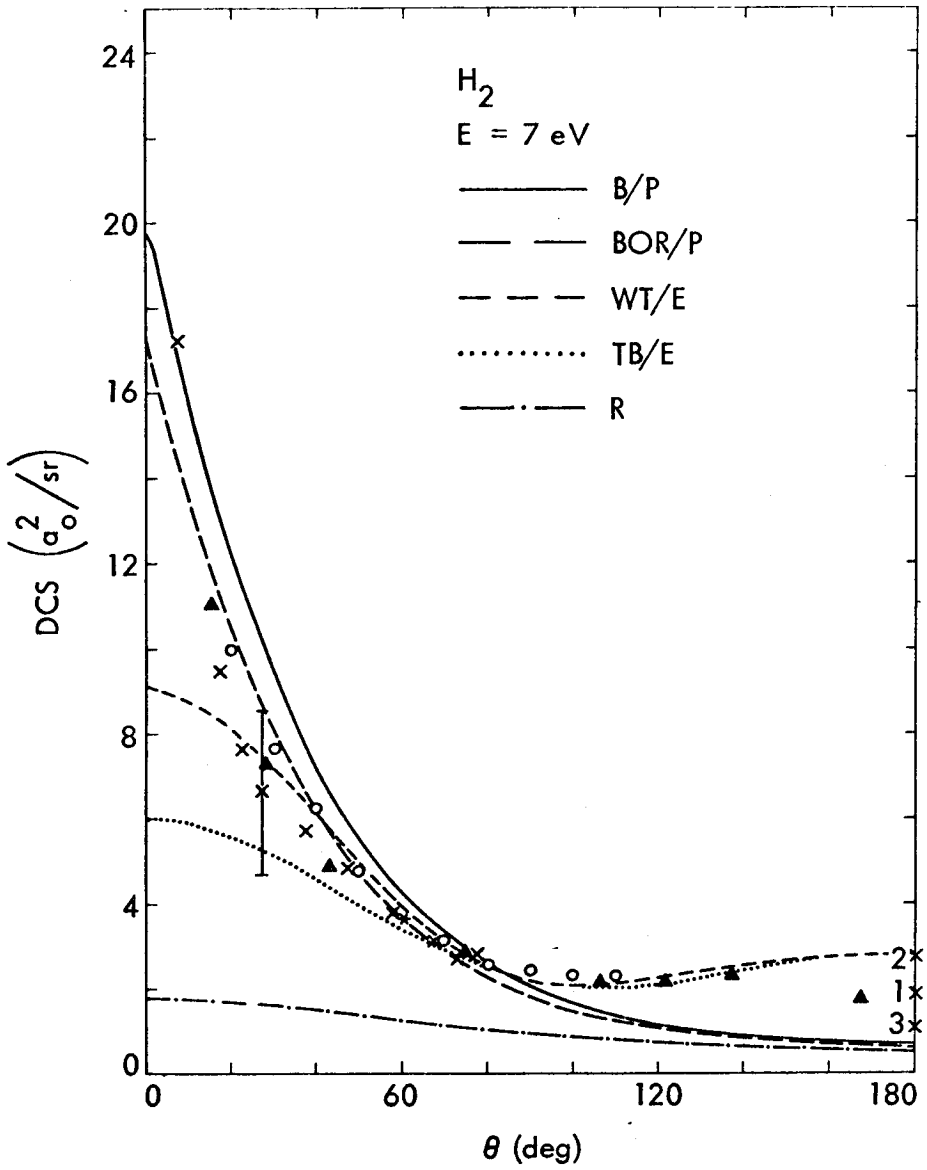
H_2
E = 7 eV
B/P
BOR/P
WT/E
TB/E
R
DCS $\left(a_o^2/sr\right)$
24
20
16
12
8
4
0
0
60
120
180
θ (deg)
2×
1×
3×

2

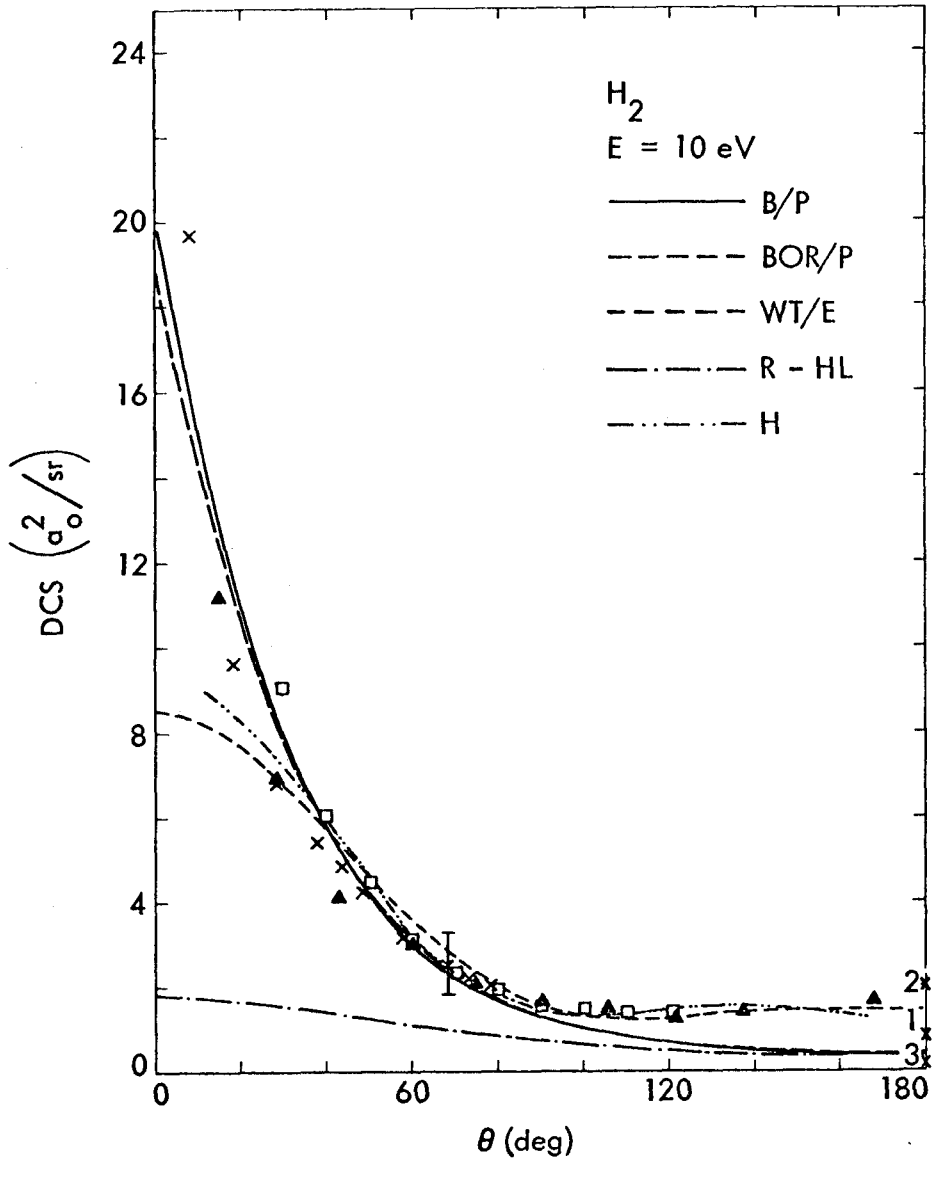
H2
E = 10 eV
B/P
BOR/P
WT/E
R - HL
H
DCS (a0^2/sr)
θ (deg)
0
4
8
12
16
20
24
0
60
120
180
1
2
3

3

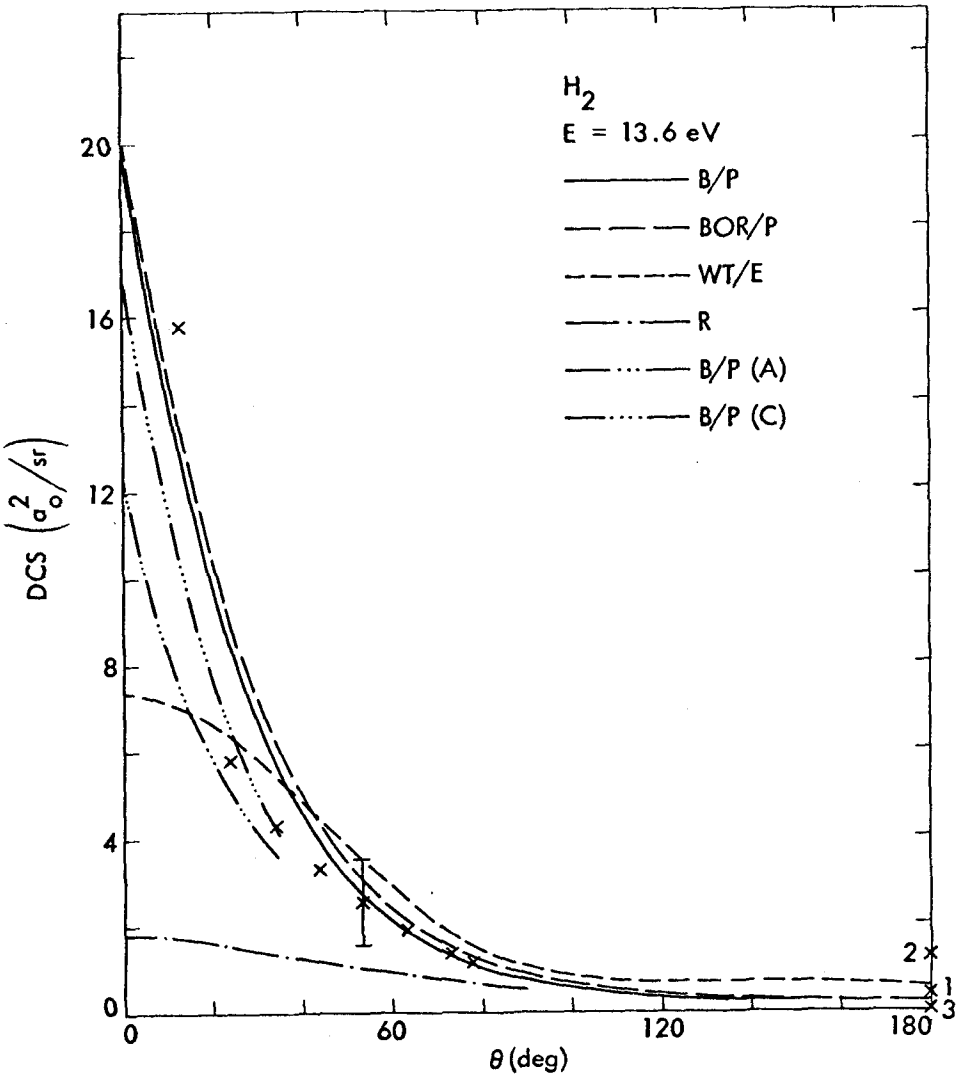
H2
E = 13.6 eV
B/P
BOR/P
WT/E
R
B/P (A)
B/P (C)
DCS (a0²/sr)
θ (deg)
0
4
8
12
16
20
0
60
120
180
1
2
3

4

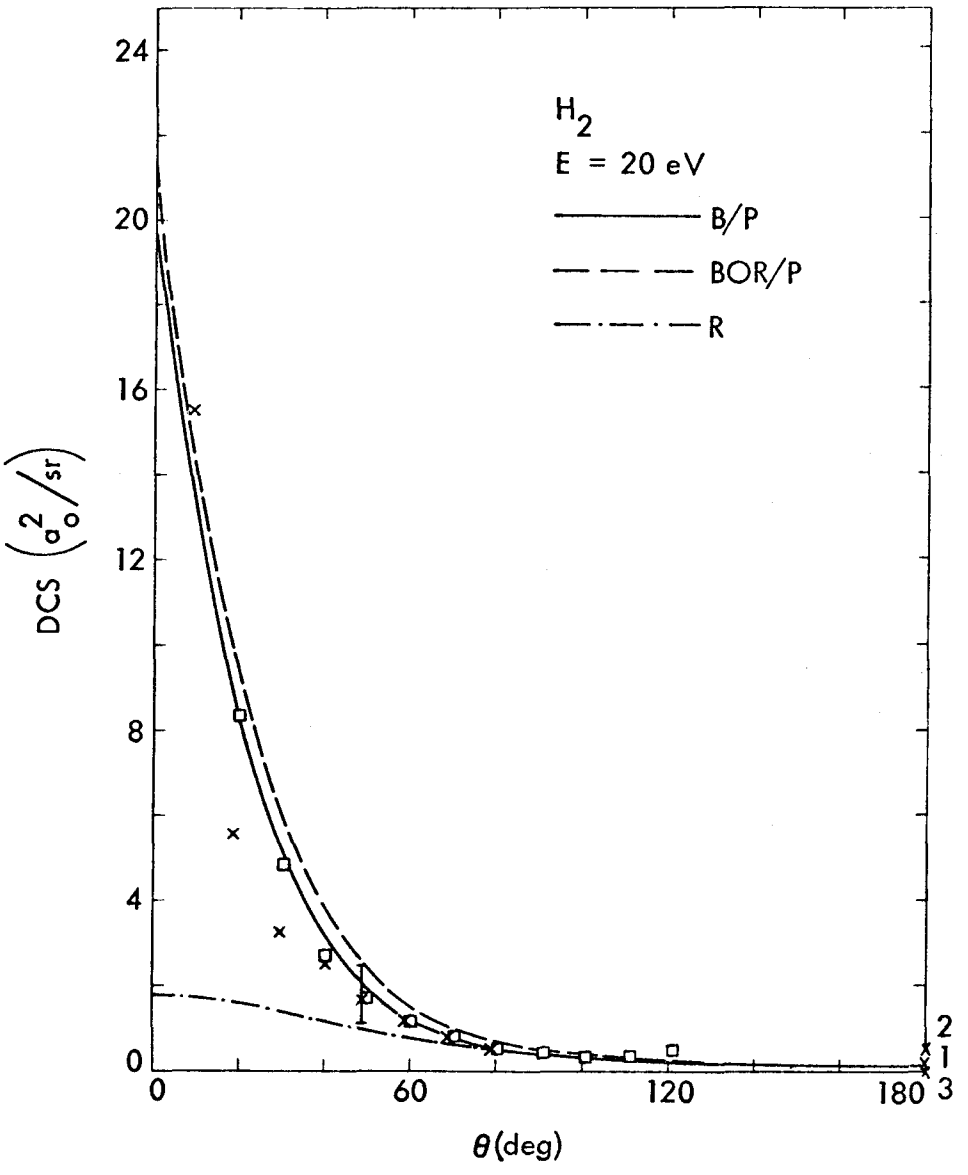
H_2
E = 20 eV
B/P
BOR/P
R
DCS $\left(a_o^2/sr\right)$
24
20
16
12
8
4
0
0
60
120
180
θ(deg)
1
2
3

5

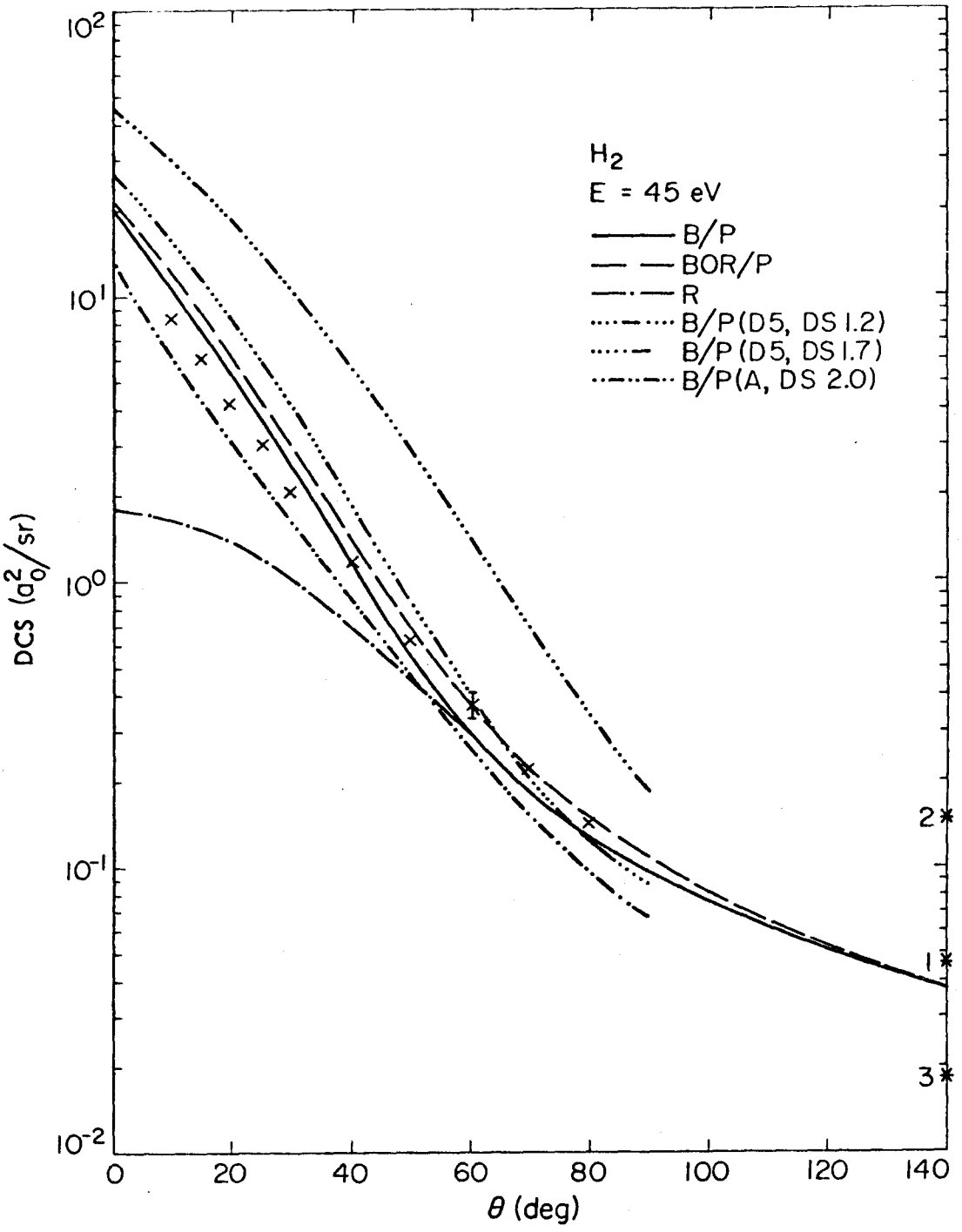
H_2
E = 45 eV
B/P
BOR/P
R
B/P(D5, DS 1.2)
B/P(D5, DS 1.7)
B/P(A, DS 2.0)
DCS (a_0^2/sr)
10^2
10^1
10^0
10^{-1}
10^{-2}
0
20
40
60
80
100
120
140
θ (deg)
1
2
3

6

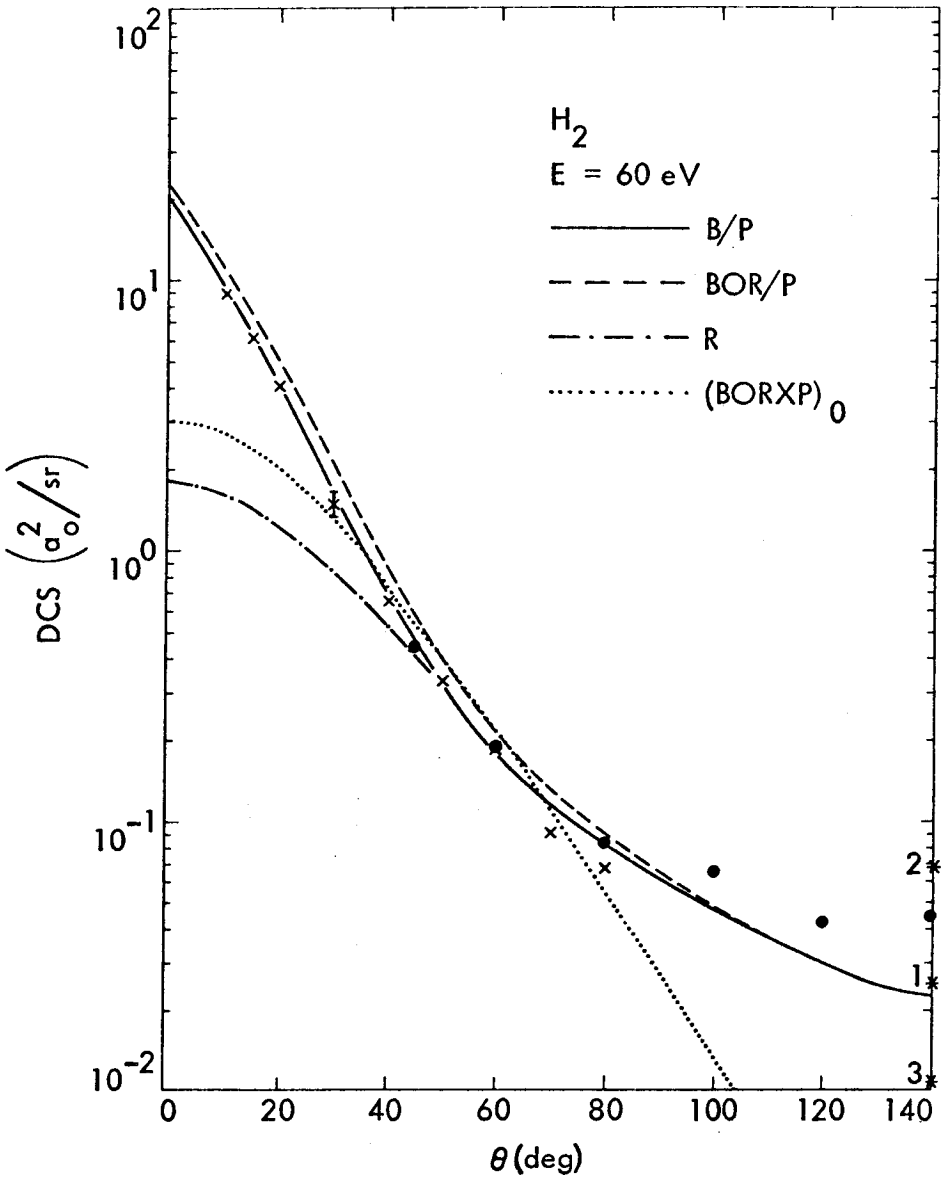
H_2
E = 60 eV
B/P
BOR/P
R
$(BORXP)_0$
DCS $\left(a_o^2/sr\right)$
10^2
10^1
10^0
10^{-1}
10^{-2}
0
20
40
60
80
100
120
140
θ (deg)
1
2
3

7

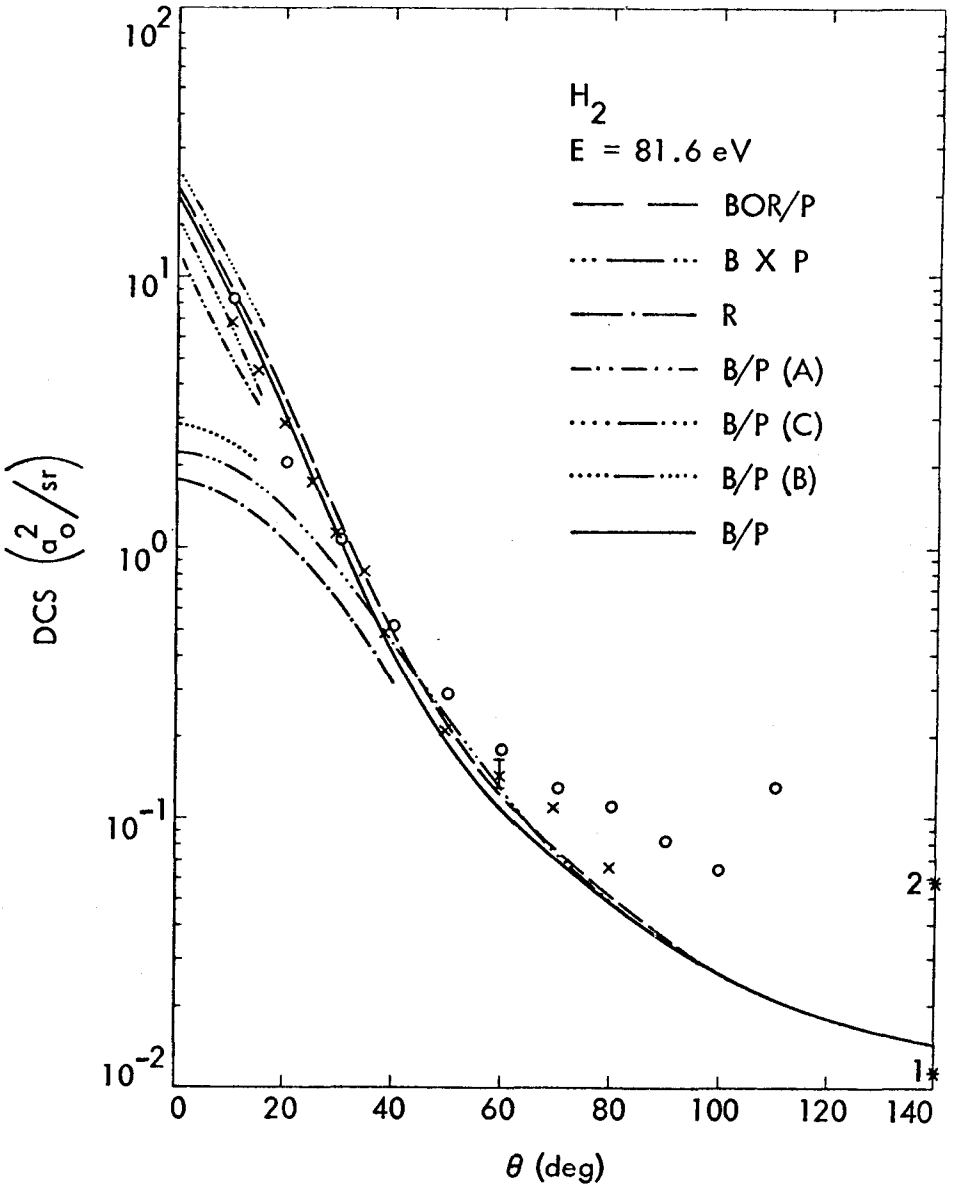
H_2
E = 81.6 eV
BOR/P
B X P
R
B/P (A)
B/P (C)
B/P (B)
B/P
DCS $\left(a_o^2/sr\right)$
10^2
10^1
10^0
10^{-1}
10^{-2}
0
20
40
60
80
100
120
140
θ (deg)
1
2

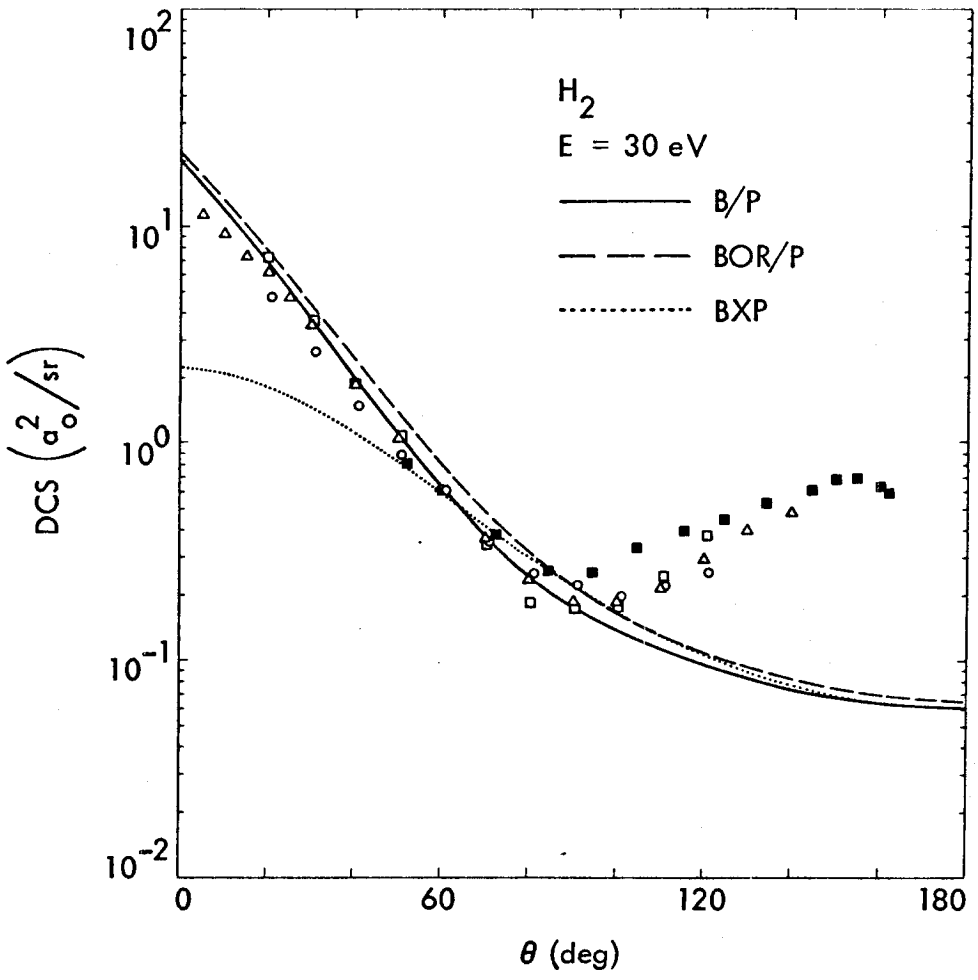
10^2
10^1
10^0
10^{-1}
10^{-2}
DCS $\left(a_o^2/sr\right)$
H_2
E = 30 eV
B/P
BOR/P
BXP
0
60
120
180
θ (deg)

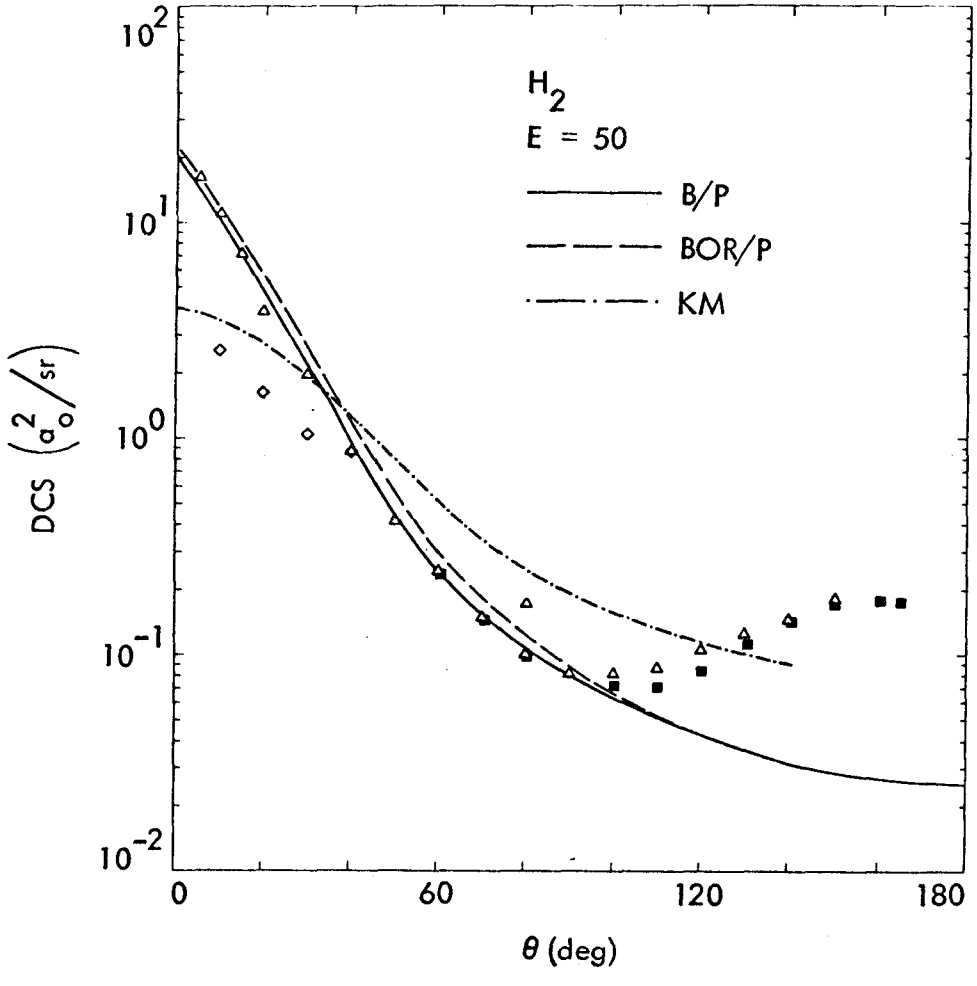
H_2
E = 50
B/P
BOR/P
KM
10^2
10^1
10^0
10^{-1}
10^{-2}
DCS $\left(a_o^2/sr\right)$
0
60
120
180
θ (deg)

10

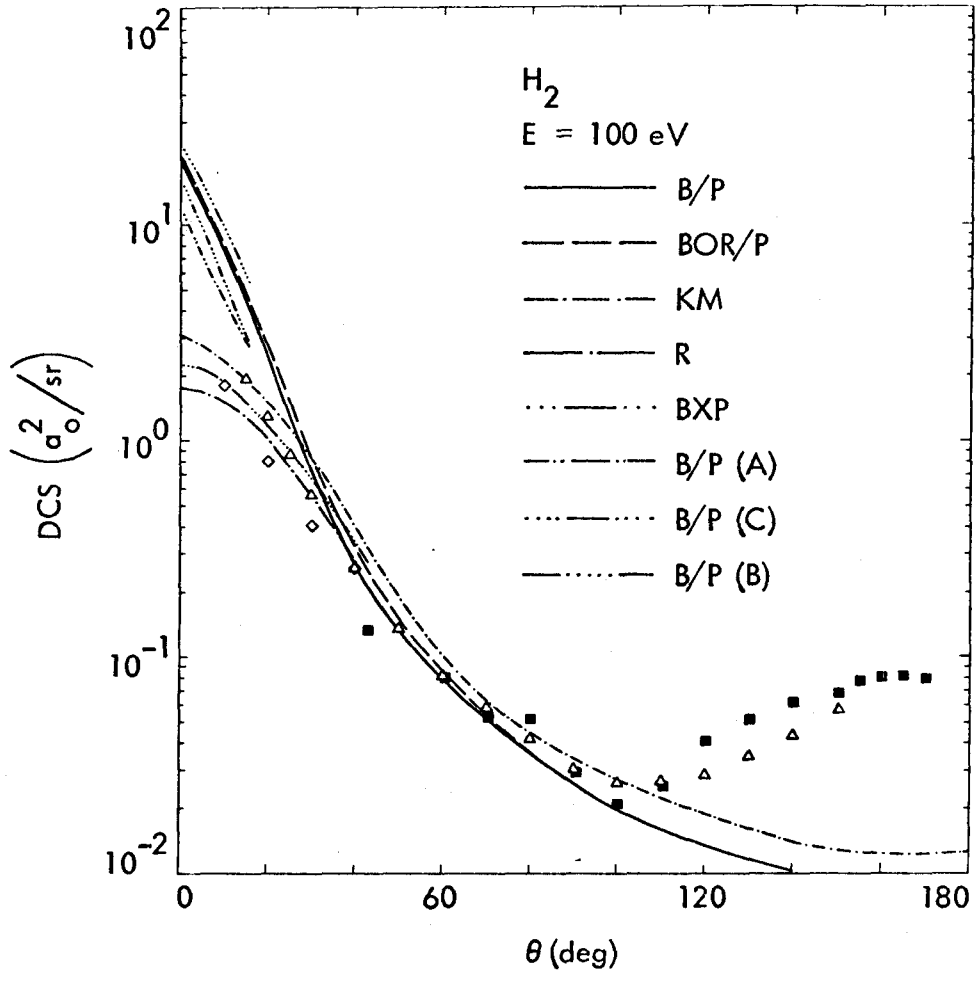
H_2
E = 100 eV
B/P
BOR/P
KM
R
BXP
B/P (A)
B/P (C)
B/P (B)
DCS $\left(a_o^2/sr\right)$
10^2
10^1
10^0
10^{-1}
10^{-2}
0
60
120
180
θ (deg)

11

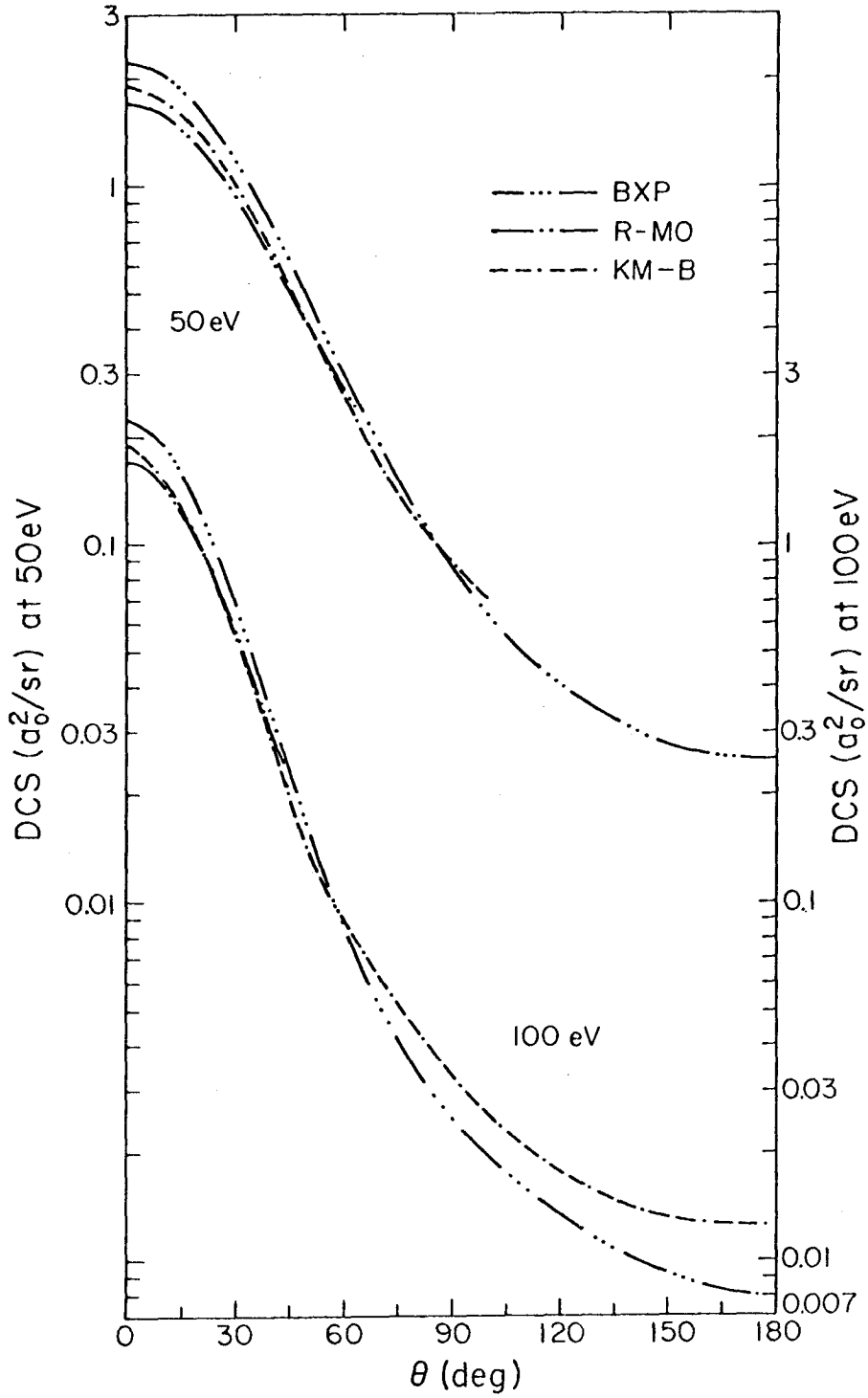
BXP
R-MO
KM-B
50 eV
100 eV
DCS (a_0^2/sr) at 50eV
DCS (a_0^2/sr) at 100eV
θ (deg)
3
1
0.3
0.1
0.03
0.01
0.007
0
30
60
90
120
150
180

12

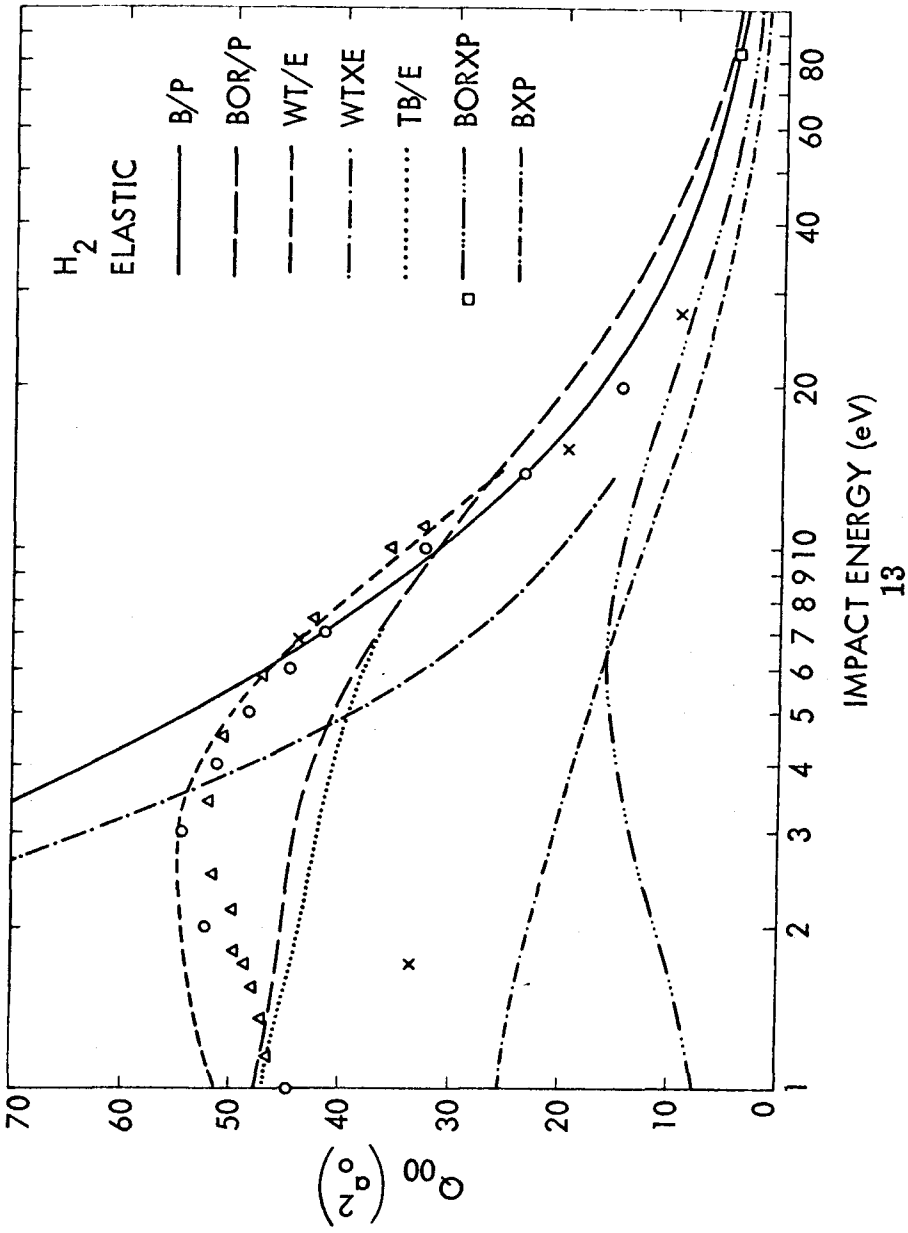
H_2
ELASTIC
B/P
BOR/P
WT/E
WTXE
TB/E
BORXP
BXP
σ_{00} (πa_0^2)
0
10
20
30
40
50
60
70
1
2
3
4
5
6
7
8
9
10
20
40
60
80
IMPACT ENERGY (eV)

13

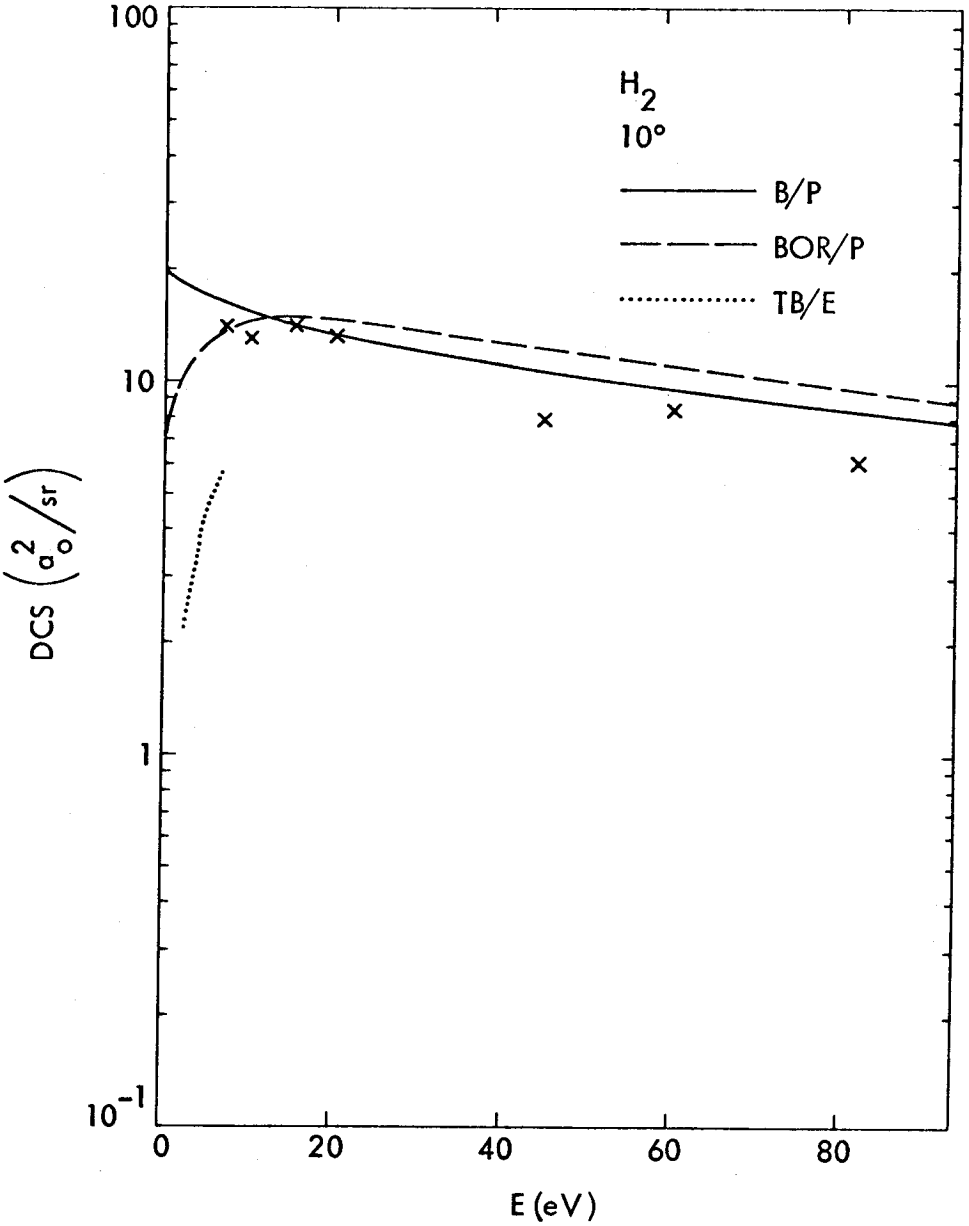
100
10
1
10^{-1}
H_2
10°
B/P
BOR/P
TB/E
DCS $\left(a_o^2/sr\right)$
0
20
40
60
80
E (eV)

14

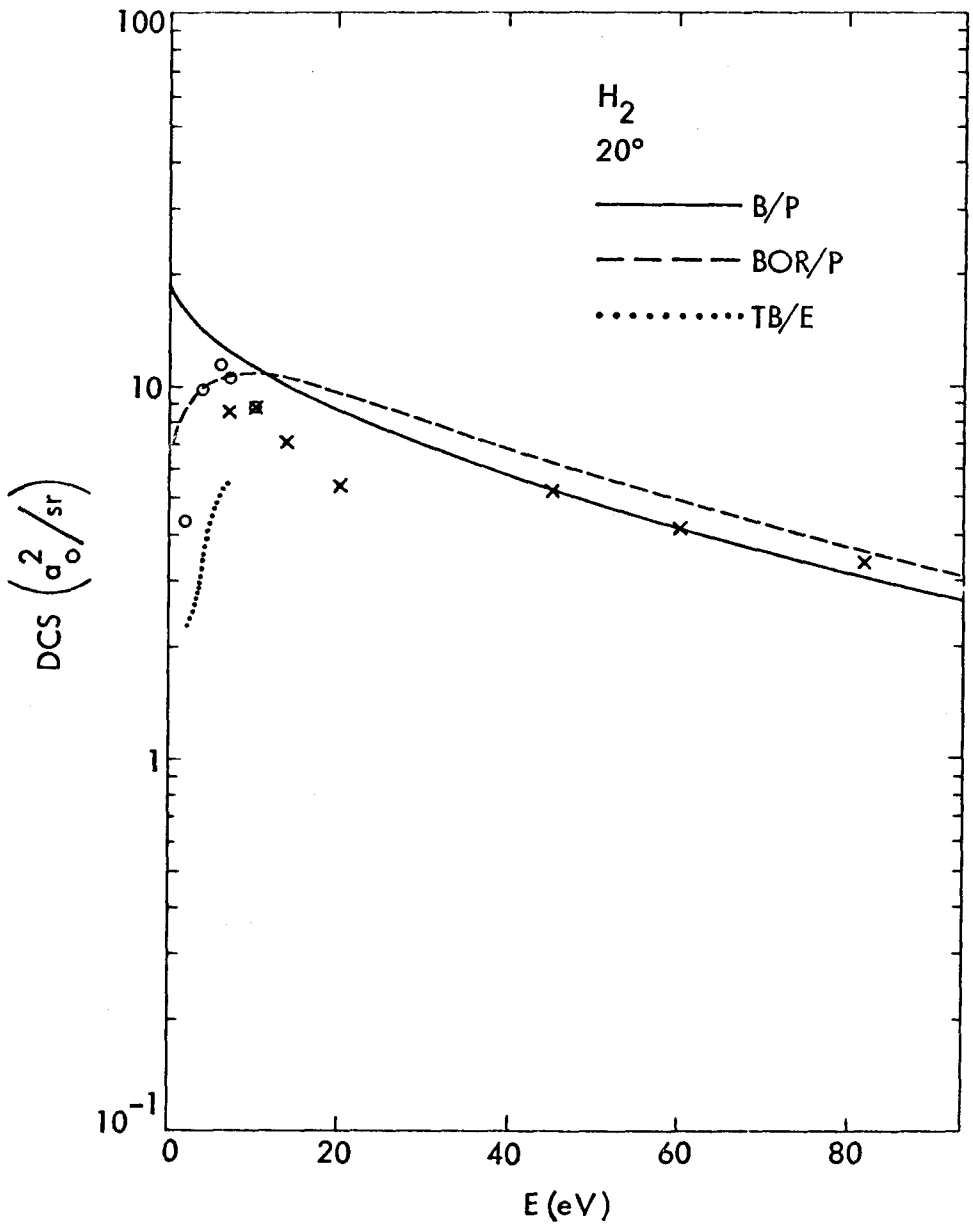
100
10
1
10^{-1}
H_2
20°
B/P
BOR/P
TB/E
DCS $\left(a_o^2/sr\right)$
0
20
40
60
80
E (eV)

15

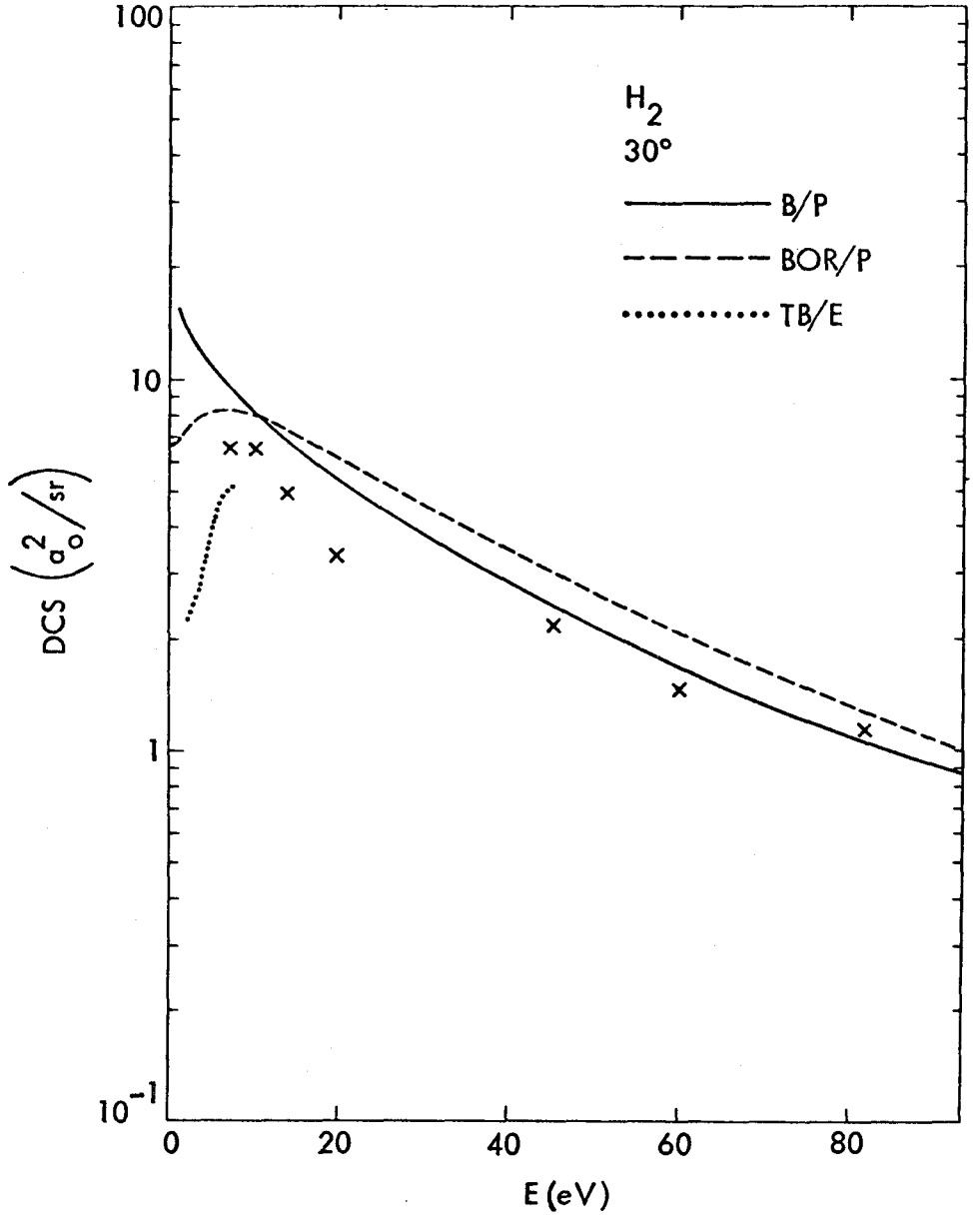
100
10
1
10^{-1}
H_2
30°
B/P
BOR/P
TB/E
DCS $\left(a_o^2/sr\right)$
0
20
40
60
80
E (eV)

16

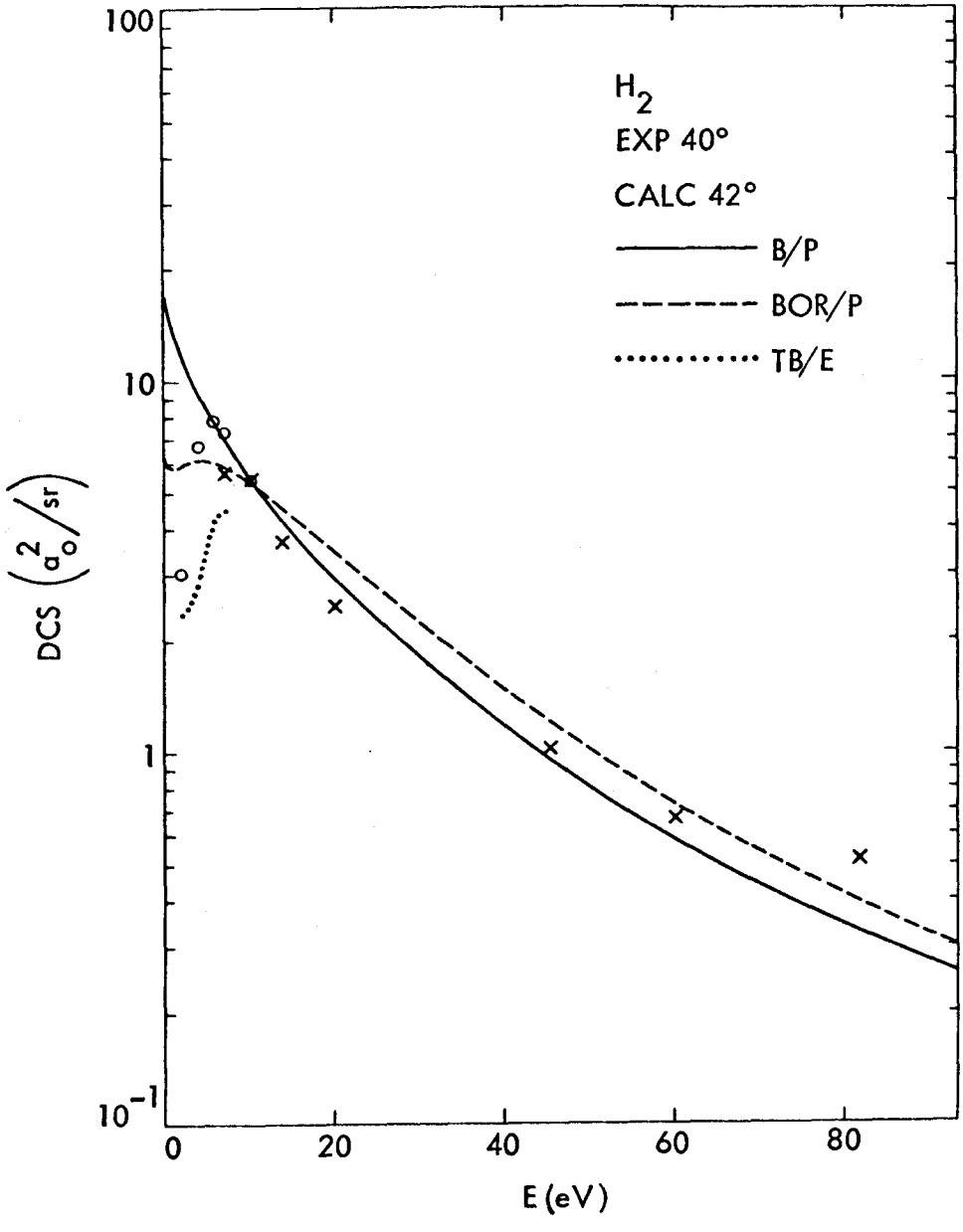
100
10
1
10^{-1}
DCS $\left(a_o^2/sr\right)$
0
20
40
60
80
E (eV)
H_2
EXP 40°
CALC 42°
B/P
BOR/P
TB/E

17

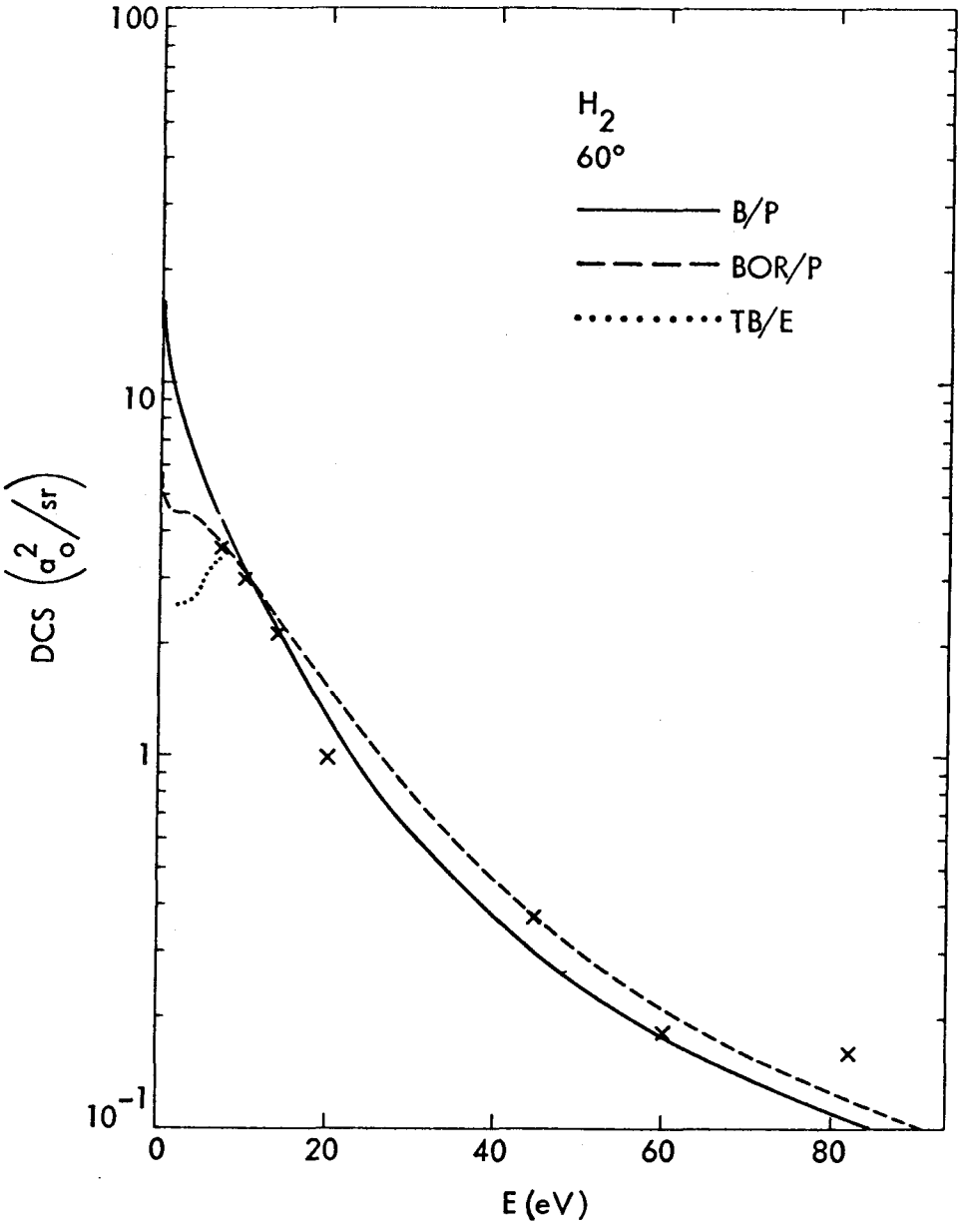
100
10
1
10^{-1}
0
20
40
60
80
DCS $\left(a_o^2/sr\right)$
E (eV)
H_2
60°
B/P
BOR/P
TB/E

18

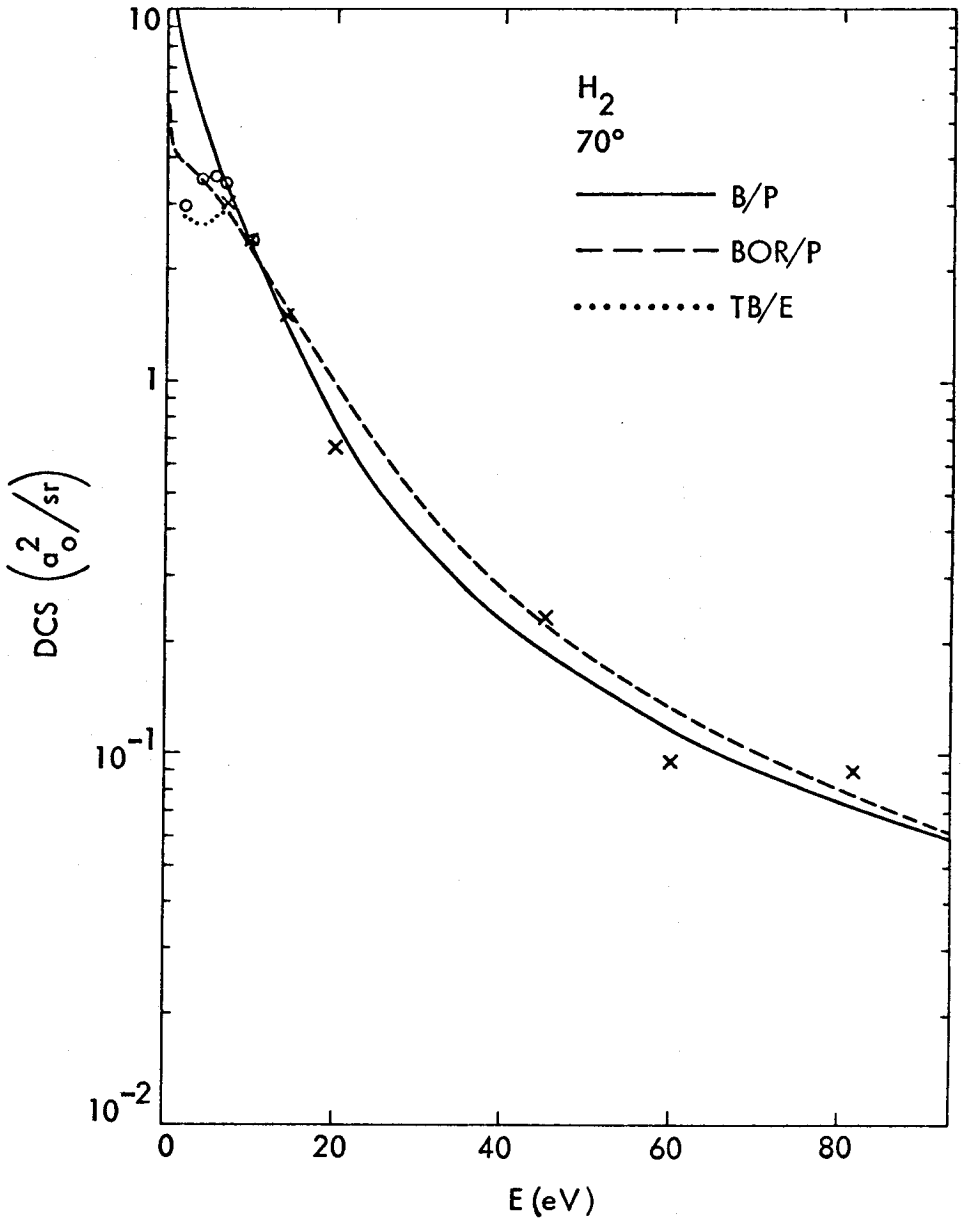
10
1
10^{-1}
10^{-2}
0
20
40
60
80
E (eV)
DCS $\left(a_o^2/sr\right)$
H_2
70°
B/P
BOR/P
TB/E

19

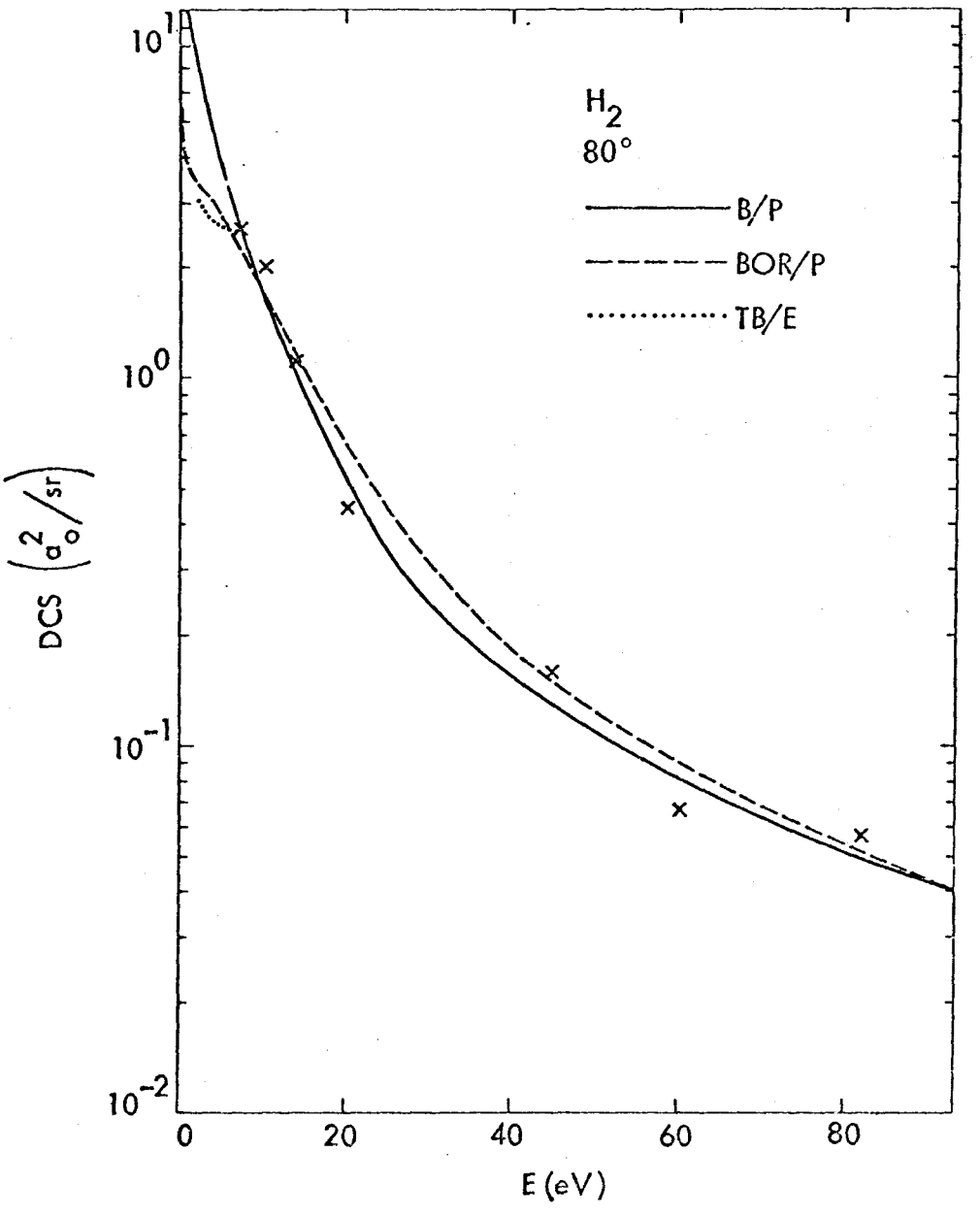
10^1
10^0
10^{-1}
10^{-2}
DCS $\left(a_o^2/sr\right)$
H_2
80°
B/P
BOR/P
TB/E
0
20
40
60
80
E (eV)

20

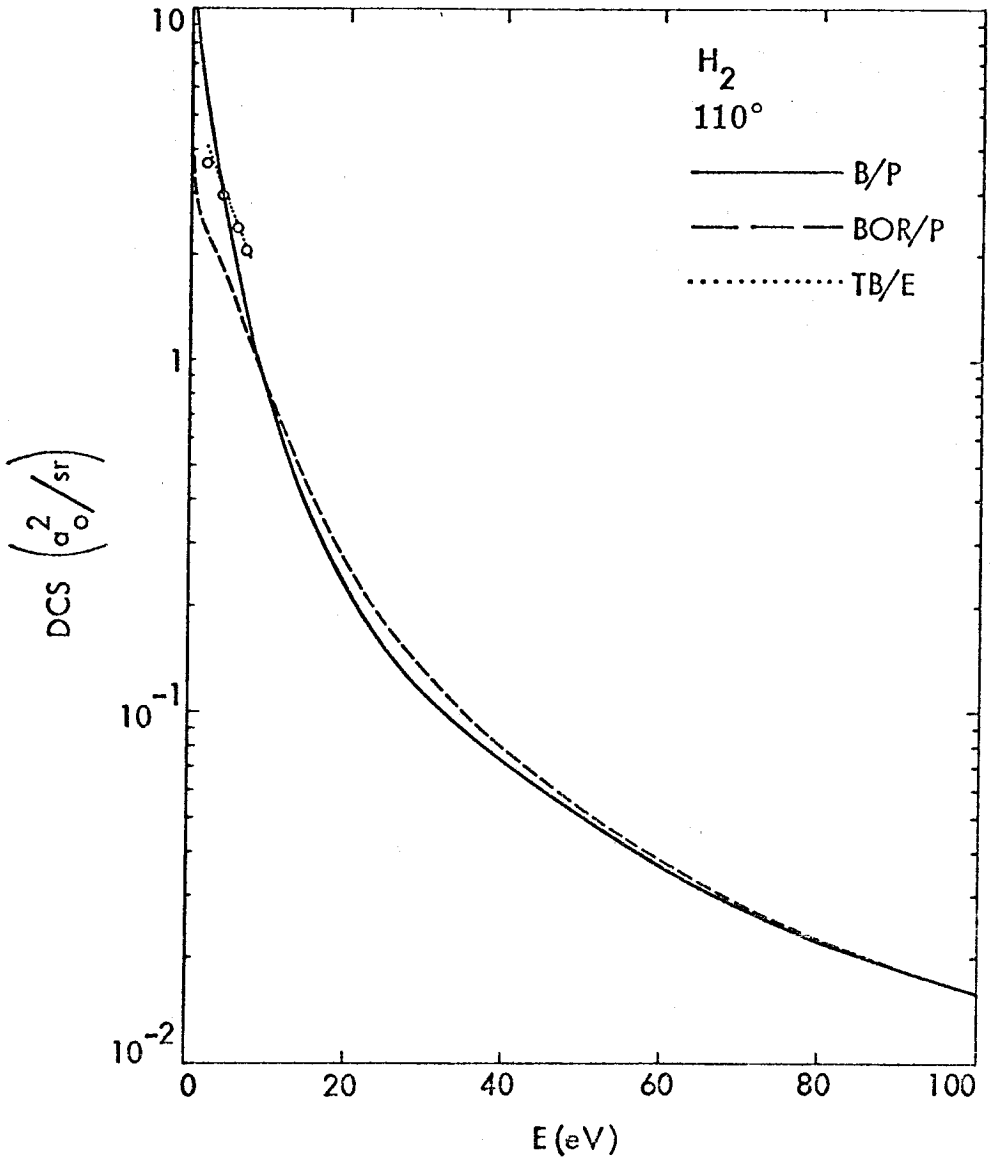
H_2
110°
B/P
BOR/P
TB/E
DCS $\left(a_o^2/sr\right)$
10
1
10^{-1}
10^{-2}
0
20
40
60
80
100
E (eV)

21

III. EXPERIMENTAL AND THEORETICAL STUDY OF INELASTIC SCATTERING*

---

* This is an article by S. Trajmar, D. G. Truhlar, J. K. Rice, and A. Kuppermann.

A. Introduction

Diffusion[1] and swarm[2,3] experiments carried out since the early 1930's have indicated the importance of vibrational excitation of molecular gases by low-energy electrons. However, the actual observation of discrete vibrational transitions and the detailed study of this phenomenon have become possible only recently with the advances of electron beam techniques.

Vibrational excitation of H_2 by low-energy electrons (below 10 eV) has been observed and studied by Schulz,[4] Menendez and Holt,[5] and Ehrhardt et al.[6] The scattering cross section was observed to have a maximum between about 2 and 4 eV and the energy dependence[6-8] and angle dependence[6,9-11] of the cross section have been explained by resonance models at these low energies. Vibrational excitation of H_2 by electrons in the 11-13 eV range has been studied experimentally by Menendez and Holt[5] and others;[12] this scattering could be explained as due to contributions from higher energy resonances superimposed on a potential scattering background. Vibrational excitation in H_2 is optically forbidden and has not been observed at very high energies (35 keV)[13] where the first Born approximation predicts that optical electric dipole selection rules are approximately valid.

Our investigation is concerned with low energy scattering at 7 and 10 eV and with the intermediate energy range (from 10 to 100 eV). The vibrational excitation in the intermediate energy range is expected to be due to potential scattering, but there have been no previous experimental investigations of it in this range. The ratio of the intensity of electrons scattered after causing a transition to a specific vibrational

level of the ground electronic state of H_2 to the intensity of electrons scattered without having caused either vibrational or electronic excitation has been measured for scattering angles $\theta = 10^o$ to 80^o, for impact energies E = 7 to 81.6 eV, and for final vibrational levels $v' = 1$ to 3. From these measurements and from the elastic differential cross sections[14] the vibrational differential cross sections have been obtained. By extrapolating the differential cross sections (DCS's) to 0^o and 180^o, the integral vibrational excitation cross sections were determined. The experiments do not resolve the rotational structure of the energy loss processes.

We have also calculated the vibrational excitation cross sections by the quantum mechanical method described in paper I.[15] Our experimental and theoretical values are compared with the measurements of Ramien[1] (E = 3.5 eV to 7.2 eV), Schulz[4] (E = 3 eV to 8 eV), and Ehrhardt et al.[6] (E = 1 eV to 10 eV), and with the calculational methods (low energy) of Breig and Lin[16] and Takayanagi.[17]

B. Experimental Methods and Data Handling

Measurement of scattered signal intensities corresponding to vibrational excitation in H_2 requires a moderately high energy-loss resolution (about 0.1 eV or better) and a very sensitive detector. The first vibrational energy-loss feature is separated by only 0.52 eV from the elastic peak in the energy-loss spectrum, and the latter is in some cases 10^4 times stronger. The results presented here were obtained with the same electron impact spectrometer used in II. The H_2 pressure was kept constant at about 10^{-3} torr as measured by an uncalibrated ion gauge. At this pressure the effect of double scattering is negligible

for the type of DCS which occurs in the present case. While obtaining one spectrum, the electron impact energy (E) and scattering angle (θ) are fixed, and the energy-loss range from -0.2 to +1.6 eV is scanned. The sweep is repeated many times and the scattered intensities from each sweep are accumulated to form the final energy-loss spectrum. On the average about 10 hours of multichannel scaling were necessary at each θ and E to build up an acceptable signal-to-noise ratio in the vibrational excitation part of the spectrum. A typical energy-loss spectrum is shown on Fig. 1. Study of the angular and energy dependence of the cross sections requires the collection of many spectra over a period of months. It cannot be expected that the instrumental conditions remain unchanged during these long data collecting periods. In order to minimize the errors introduced by the changing instrumental conditions, the following experimental procedure was used.

1. Each spectrum is a superposition of many repetitive energy-loss scans, where each scan has a duration of about 10 minutes. (Since the instrument is very stable for a few hours, the different parts of the spectrum are produced under identical conditions.)
2. From each spectrum the ratios $R_{v'} = I_{v'}/I_o$ are measured for $v' = 1$, 2, and 3, where $I_{v'}$ is the scattered intensity corresponding to excitation of the v' vibrational state and I_o is the elastic scattering intensity. These ratios are the quantities that are least subject to experimental errors and are directly comparable at all angles.

3. The elastic DCS's determined separately (paper II) are then utilized to obtain the vibrational DCS's. The measurement of the elastic angular distribution[14] takes only about 3 hours, during which the change in the experimental conditions can be made negligible.

As Fig. 1 shows, there is some contribution from the tail of the elastic peak to the vibrational intensities. This tail contribution, however, is a smoothly varying function of energy loss and is interpolated and subtracted from the composite signal. A practically complete resolution of the elastic scattering and vibrational excitation features would have been possible; this, however, would have appreciably increased the time required for the experiments. (The spectrometer is capable of about 0.030 eV resolution and can measure a signal that corresponds to one electron in every 20 seconds.)

The spectrum accumulated in the detector memory was smoothed by averaging over three neighboring channels, and the intensity ratios R_v, were calculated from the peak heights of the energy-loss features after subtraction of the background. Using the peak heights as a measure of intensity is acceptable since it was found that the line shape was independent of scattering angle. It was also experimentally established that the instrument efficiency was independent of energy-loss over the spectral range of interest here. (The gun, the energy selector, and entrance optics to the scattering chamber were tuned to generate the required electron beam and the second half of the apparatus was tuned to get the optimum elastic peak (maximum intensity at the required resolution) at 40°. With these settings, energy loss features about 6-8 eV away from

the elastic peak were recorded at several lower and higher scattering angles and then an attempt was made to reoptimize the second half of the instrument to give maximum signal for the inelastic features at the same resolution. In all cases it was found that no improvement was possible and that the optimum tuning conditions for the elastic feature were also the optimum conditions for the inelastic ones. This was not true for inelastic features about 15-20 eV from the elastic peak.) Since the factors relating the peak intensities to their respective DCS's are the same for every energy-loss feature in any one spectrum, $R_{v'} = DCS_{ov'}/DCS_{oo}$, where we denote the DCS for excitation of the v' vibrational state by $DCS_{ov'}$, and the elastic DCS by DCS_{oo}. Multiplication of $R_{v'}$ by the elastic DCS, which was determined previously (paper II), gives the DCS for vibrational excitation in the 10^{o} to 80^{o} angular range at each of seven individual impact energies. The incident energy scale was not calibrated and hence E can be in error by about ±1 eV due to contact potentials. An angular extrapolation and integration procedure similar to the one described in the previous article (II) for the elastic scattering was applied to the $DCS_{ov'}$ to obtain the integrated vibrational excitation cross sections $Q_{ov'}$. Type 1 extrapolation[14] was used to calculate $Q_{ov'}$ for Table III of Paper II and for this paper. The error bars shown on the figures are typical values obtained by summing up all the estimated errors in the experimental and calibration procedures. Their values are approximately 10% for R_1, 20% for R_2, 30% for R_3, 45% for the DCS_{01}, 55% for the DCS_{02}, and 65% for the DCS_{03}.

C. Calculation Methods

A calculation procedure using plane wave scattering wave functions, accurate unperturbed molecular vibrational wave functions, and model potentials based on quantum mechanical considerations of the electronic charge distributions has been described in I.[15] This procedure represents an improvement over earlier less complete methods used by Carson,[18] Breig and Lin,[16] and others (see I for references). One method we use is to calculate in first order perturbation theory the transition probability between unperturbed initial and final vibrational states, i.e., the Born approximation (BXP). In addition, we sometimes make corrections to account for exchange effects; this gives the prior Born-Ochkur-Rudge approximation (BORXP). For accurate results, however, this method might have to be carried to at least second order in the scattering to include the distortion of the scattering electron wave function and/or to include the polarization of the electronic wave function of the bound states of H_2. In I, we describe a method of including polarization by adding to the static perturbation potential an effective (nonadiabatic) polarization potential based on variational calculations.[19] This is a common technique and it corresponds to a partial summation of the electronic polarization terms in the perturbation series. The results are the polarized Born approximation (B/P) and when we include exchange effects the polarized BOR approximation (BOR/P). Because the conditions for validity of the Ochkur-Rudge method of including exchange are not known, we generally present the results of both calculations. These methods neglect back coupling, the direct effect of distortion (which was considered by Takayanagi[17]), most of the effect of distortion on the

exchange correction, and some other higher order effects which might be important. The present calculations also do not include resonance effects. To test these methods, they were applied to calculate the elastic scattering cross sections for H_2 and shown in II to give good agreement with the experimental integral and differential elastic cross sections at and above 10 eV when the model potential (data set 1) which is considered theoretically most justified (see Paper I) is used in the calculation. Thus, in the present article we will continue to use this model. We will use data set 1 (DS1) except where explicitly stated otherwise. DS1 implies the use of a D5 form for the polarization potential cutoff functions and the B′ form for the quadrupole interaction cutoff function.[16] Sometimes calculations using A or B forms of the polarization potentials (with the cutoff radii the same as for DS1) are also shown for comparison.

D. Results and Discussion

1. Angular Dependence of Intensity Ratios

The experimentally measured R_v's are not subject to uncertainties introduced by the effective path length correction, the normalization procedures, and changes in instrumental conditions which are slow with respect to the sweep-time for one energy-loss scan. We pointed out in Section B that these ratios are equal to the corresponding cross section ratios. The experimental and calculated intensity ratios as a function of scattering angle are given in Figs. 2 through 10. On Figs. 4 and 7, several separate measurements of R_1 taken over periods of up to half a year are shown to demonstrate the reproducibility.

At scattering angles 10^o - 15^o and below the direct beam contribution to the elastic scattering signal can be important;[14] therefore, the errors in the ratios and DCS's can be considerably greater at 10^o than at larger angles.

Other experimental R_v's in this energy region with which our measurements can be compared are those which we can obtain from the measurements of Schulz[4] and of Ehrhardt et al.[6] Schulz's data is considered in Section D.3. Ehrhardt et al. give $Q_{ov'}$ for $v' = 1$, 2, and 3 as a function of impact energy from about 1 eV to 10 eV. They found that the shapes of the angular distributions for $20^o \leq \theta \leq 110^o$ for the $v' = 1$ and 2 (and presumably for the $v' = 3$) channels were the same and were independent of impact energy from about 1 eV to 10 eV within their experimental errors (about 10%). Therefore, the ratios DCS_{02}/DCS_{01} and DCS_{03}/DCS_{01} should be independent of angle and equal to $Q_{01}/Q_{02} = 8.3$ and $Q_{01}/Q_{03} = 1.0 \times 10^2$. These ratios combined with our ratio R_1 at several angles yield the values representing their R_2 and R_3 in Fig. 2. The agreement with our experimental values for R_2 is good.

At E = 7, 10, and 13.6 eV, the calculated R_1 curves agree fairly well with the measured ones both in magnitude and shape. As one goes to higher impact energies, the experimental ratio curves develop deep minima around 20^o - 40^o scattering angles. At these energies the calculated curves are in poorer agreement as they do not reproduce the dips quantitatively. There is, however, still an order of magnitude agreement with experiment, and the experimentally observed shift of the minimum in the ratio curves to lower angles with increasing impact energy is properly predicted by the calculations. The BOR/P curves give somewhat better agreement with experiment than the B/P ones. The difference, however, is not always significant and becomes negligible at some energies.

At low angles the term which has the largest effect on the calculated scattering cross section is the polarization potential, as expected from its long range nature. This is shown on Figs. 5 and 7 and in Paper I.

The calculated values for R_2 and R_3 are about a factor of ten less than the experimental ones at 7 and 10 eV, but at higher energies the agreement for R_2 is much better. The discrepancies at 7 and 10 eV probably are due to inaccuracies in the vibrational excitation DCS calculation and will be discussed in Sections D.2 and D.5. The calculated R_3 curves are also shown above 10 eV, although at the present time no experimental data are available for comparison.

Figures 7 and 9 show the R_1 values calculated by the BOR model with form A for the polarization potential[15] [curve BOR/P(A)] and when polarization is neglected (Curve BORXP). (See Paper I for further discussion of these methods.) These curves show that the polarization potential is necessary for producing the deep dip in the R_1 ratio but that the exact form of the polarization potential for small electron-H_2 distances (r) is not crucial in determining the shape of the curve in the vicinity of the dip. This is true at all energies above 10 eV except that at energies of several hundred eV the dip appears prominently in the calculation even without polarization and the effect of including the polarization potential is to make it deeper.

2. Angular Dependence of the DCS

The vibrational excitation DCS's as a function of scattering angle are shown in Figs. 11-21. Calculations using the B/P and BOR/P approximations are shown. When only the former is indicated, the BOR/P curve

would not deviate noticeably from the B/P one. The absolute values for the experimental measurements were obtained from the normalized elastic cross sections (Paper II) and from the experimentally determined R_v, as described in Section B. On the right-hand side of each figure, the values of the DCS at the highest angle shown on that figure are given as obtained by the three different extrapolation methods described in II. Type 1 extrapolation has been used to calculate the integral cross sections.

Figure 13 also shows the angular distribution measured by Ehrhardt et al.[6] for the first vibrational excitation at 10 eV. Their cross section was given in arbitrary units and for purposes of display has been normalized to our experimental one at 60^{o}. The two experimental angular distributions are in excellent agreement. The dash-dot curve on Fig. 13 is obtained from the expression $DCS(\theta) \propto (1 + 2\cos^2\theta)$ by normalizing it to experiment at 40^{o}. This type of angular behavior is predicted by resonance theories for scattering by means of a $^2\Sigma_u^+$ intermediate negative ion state.[6,9,10] Although the predicted angular distribution of the resonance model is in good agreement with experiment above 40^{o}, at the lowest angles there is a considerable disagreement. O'Malley and Taylor[9] suggested that the deviation could be due to scattering by higher partial waves, e.g., f waves. In our model the strong forward scattering is due to scattering in many higher partial waves by the polarization potential. The direct scattering model (B/P) curve gives just as good or better agreement with experiment as the resonance model and requires no empirical scale adjustment.

As noted in Section D.1, Ehrhardt et al.[6] found that the shapes of the angular distributions for vibrational excitation of the $v' = 1$ and 2 states were independent of energy from about 1 eV to 10 eV and were the same for both states. Our 7 and 10 eV measurements do not eliminate this as a possibility within the limits of experimental errors. In fact, if the angular distribution of Ehrhardt et al. for $v' = 1$ at E = 10 eV and our four DCS's for E = 7 and 10 eV and $v' = 1$ and 2 are all normalized at 36^{o}, a median DCS can be obtained and all the data points of these five DCS's in the 8^{o} - 80^{o} range fall within 20% of it. Within the limits of our much larger 42% estimated error for the shape of DCS_{03}, even these points are consistent with the median DCS. Ehrhardt et al.[6] argued that the excitation cross section must be dominated by resonance scattering at all energies up to 10 eV since the shape of the angular distribution is practically independent of impact energy in that range. While it is true that pure resonance scattering would lead to a DCS whose shape is exactly the same over the whole width of the resonance, it is possible that the shape of the angular distribution due to potential scattering would also be fairly independent of impact energy over some energy range. Since we have shown in the previous paragraph that a potential scattering explanation of the $v' = 1$ vibrational excitation is not precluded in the 7 - 10 eV energy range, this could be an example of inelastic scattering with an appreciable contribution from potential scattering which still exhibits a DCS whose shape does not change much with energy. Further support for such a possibility comes from the calculations for potential scattering in

the B/P approximation shown in Table I. The shape of the DCS from 0^{o} to 120^{o} does not change much between 7 and 10 eV. Such a phenomenon could also occur in more accurate calculations. Another example is the excitation of the $2^{1}P$ state of helium by electrons with energies in the 34 - 55.5 eV range. The DCS's for this process have been determined in the $10^{o} \leq \theta \leq 70^{o}$ region and their shape changes only slightly more than experimental error in this non-resonance energy range.[20] These examples indicate that approximate energy-independence of the DCS shape is a necessary but not sufficient criterion for pure resonance scattering.

Above 10 eV the experimental DCS_{01} exhibits a gradual change in shape. A minimum and a maximum develop in the 10^{o} - 80^{o} range and they shift progressively to lower angles with increasing impact energies.

The B/P (or BOR/P) calculation is in good agreement with measurements at 7 and 10 eV for the excitation of the fundamental vibration. At higher energies, however, the agreement becomes poor and the minimum found in the experimental angular distributions is not reproduced quantitatively by the calculations. (This is the source also for the disagreement in the experimental and calculated R_1 curves at the higher energies.) The polarized Born approximation evidently overestimates the potential scattering cross section for excitation of the first excited vibrational level of H_2.

For the excitation of the first overtone ($v' = 2$) at 7 and 10 eV the calculated cross sections are about a factor of ten smaller than the experimental ones. At 13.6 eV this factor is only about two and

from 20 eV on the calculated and measured cross sections are in good agreement. This discrepancy at low energy is also present in the R_2 ratio versus scattering angle curves discussed previously and seems to be due to resonance contributions. Although the peak of the resonance is in the 2 to 4 eV impact energy range and its half width is about 3 eV,[6] the resonance tail contribution is apparently still the dominant part of the overtone excitation cross section up to over 10 eV impact energy. Thus the resonance is more important for σ_{02} than for σ_{01}. This is discussed further in Section D.5. Figure 14 compares the DCS_{02} with the $1 + 2\cos^2\theta$ angular distribution predicted by the resonance model (see above). The agreement at lower angles is poor.

There is only a limited amount of experimental data on the second overtone excitation. At 10 eV we find experimentally that the ratio DCS_{02}/DCS_{03} is about 4 and that DCS_{03} looks somewhat more isotropic than either DCS_{02} or DCS_{01}. This qualitative behavior is also shown by the calculation, but the calculated cross section is about ten times smaller. The quantitative disagreement is again probably due to resonance contributions.

Figure 21 shows the results of calculations at 81.6 eV with form A of the polarization potential [BOR/P(A)], with a potential where the polarization terms were omitted (BORXP), and with a potential where both polarization and quadrupole terms were neglected (BORXPXQ). At this high impact energy it is hard to decide which of the calculations gives better agreement with experiment. This also has been found in some cases for the elastic scattering (see Papers I and II) and is attributed

to the partial failing of the static polarizability model at high impact energies. More accurate experimental differential cross sections for $\theta \leq 10^{o}$ would provide a more critical test of this point.

3. Energy Dependence of the Intensity Ratios

It is of some interest to look at the energy dependence of the intensity ratios in a more explicit form. Figures 22 through 27 show the ratios R_1 and R_2 at 20^{o}, 30^{o}, 40^{o}, 60^{o}, 70^{o} and 80^{o} scattering angles as a function of impact energy. The experimental R_1 curves have a minimum as a function of impact energy. This minimum becomes more pronounced and shifts to lower impact energies as the scattering angle increases. The agreement between the calculations and experiments is poor at low angles but reasonably good above 40^{o}. The minimum and its shift to lower energies with increasing angle is properly predicted by the calculations. The R_2 curves behave similarly to the R_1 curves, but for the former the experimental data extend only to 40 eV at 20^{o} and 30^{o} and only to 20 eV at higher angles.

Figure 26 shows the intensity ratios R_1 measured by Schulz[4] at 72^{o} scattering angle. He gave the integral cross section for the fundamental vibrational excitation as a function of impact energy (Fig. 11 of Ref. 4). He obtained these cross sections from his measured ratios of vibrational excitation to elastic scattering intensities at 72^{o} and from the total electron-hydrogen molecule scattering cross sections of Ramsauer and Kollath[21] by assuming the angular dependences of the elastic and inelastic cross sections to be the same. Since DCS_{oo} and DCS_{o1} are now known not to have exactly the same shape (or else our ratios R_1 would

be independent of angle), the most meaningful results from Schulz's measurements are the ratios R_1 at 72^o. We have back-calculated his intensity ratios and they are shown in Fig. 26. The agreement with our measurements is excellent. This is a most significant check on the measurements since these ratios were obtained directly from two different instruments and since, as mentioned previously, the ratios are the quantities least subject to experimental errors.

At E = 3.4 eV and $\theta = 72^o$, Schulz also observed excitation of the $v' = 2$ vibrational level.[4] From Fig. 11 of his paper one gets $\left[\frac{DCS_{02}(72^o)}{DCS_{01}(72^o)}\right] = \frac{Q_{01}}{Q_{02}} = 0.20$, while the value of the same ratio is 0.074 from Fig. 5 of Ref. 6. For a wide range of choices of scattering potential (and with and without exchange and/or polarization) we calculate values of this quantity in the range 0.013 - 0.040 with 0.0145 for the theoretically most justifiable potential including polarization. This discrepancy indicates either that potential scattering contributions are proportionately much less important for $v' = 2$ than for $v' = 1$ even at E = 3.4 eV (which is very near the nominal "resonance energy") and/or that our first order calculation is very bad, even for the nonresonance part of the cross section at this low energy. From the discussions in Sections D.2 and D.5, it appears that the former alternative may be correct.

4. Energy Dependence of the Differential Cross Sections

The energy dependencies of the present experimental and theoretical differential cross sections are shown explicitly in Figs. 28-34. Ehrhardt et al.[6] also measured the energy dependence (for $E \leq 10$ eV) of the differential cross section at 20^o. We compare the two sets of results in

Figure 28; for the comparison we normalize Ehrhardt's data such that his DCS_{01} (20^{o}) is equal to ours at E = 10 eV. The agreement of the different experiments is seen to be good.

These figures show explicitly what follows from the comparison of the calculated and experimental elastic cross sections and scattering intensity ratios; e.g., that for the first vibrational excitation the calculated and experimental cross section versus energy curves differ considerably at low angles, but the agreement is good at high angles. For the overtone vibration, the angle-analyzed excitation functions seem to be very similar to the ones corresponding to the fundamental vibration. The experimental data are, however, limited to low energies for the overtone.

It is noteworthy that the experimental DCS_{01} is an increasing function of energy at energies near 60 eV. This behavior is especially striking in the 30^{o} - 60^{o} range. While this behavior is not predicted quantitatively by the calculations, the BXP cross section, which peaks very close to threshold, is again an increasing function of energy at least one higher energy range at any angle. The B/P calculations also show minima, but they are smaller. The minima in the experimental DCS_{01} as functions of energy move to lower energies at higher angles. The BXP calculations are in approximate qualitative agreement with this trend at higher energies, but the present calculations do not predict this feature accurately.

5. Energy Dependence of the Integral Cross Sections

The excitation functions $Q_{01}(E)$, $Q_{02}(E)$, and $Q_{03}(E)$ are shown on Figs. 35-36.

The experimental values of Ramien[1] and Ehrhardt et al.[6] are in good agreement with our measurements. Ramien's data are from multiple-scattering experiments in which he obtains the ratio of the number of inelastic collisions (with energy loss 0.5 eV) to the total number of collisions, i.e., approximately $Q_{01}/(Q_{00} + Q_{01})$. From this ratio, we obtained and plotted Q_{01} by using the cross sections of Golden, Bandel, and Salerno.[22] The differences between the results of Ehrhardt et al. and our data are within the combined errors of the experiments and the extrapolations of the DCS's to 180°. The B/P and BOR/P calculations yield Q_{01}'s which agree within a factor of 3 with experiment over the 1.5 - 100 eV energy range.

For the overtone vibrational excitations, the two sets of experimental integral cross sections are in agreement within their error limits. The calculated cross sections are also in agreement with experiment at 20 and 40 eV; at the lower energies, however, they are about an order of magnitude smaller than the experimental values. This discrepancy is discussed at the end of this section.

Since there is very little information available for the excitation of the second overtone, our calculated integral cross sections for this process are given in Table II. The BOR/P calculation is the most reliable estimate of these cross sections presently available.

It has long been known that the static potential alone cannot account for the order of magnitude of the vibrational excitation cross sections at low energies. Figure 35 shows the calculated cross sections for vibrational excitation ($v' = 1$) due to scattering off the static potential ($S_0 S_2 Q_2^{B'}$) and off the spherically symmetric component of this potential (S_0). Our experimental and theoretical results show that the static potential becomes so much more important at higher energies that it cannot be neglected even

for qualitative work above 20 eV. Breig and Lin did plane wave calculations below 10 eV using only the spherically symmetric part of the polarization potential P_o^{D5} for the scattering.[16] They showed that this calculation could predict scattering of the correct order of magnitude. In Fig. 35 we show a calculation which uses only our DS1 polarization potential. Breig and Lin showed that it is possible using just the polarization potential to get more quantitative agreement with experiment at low energies by empirically increasing the potential's depth. This led to a D8 polarization potential with $a_p = 1.3\ a_o$ (using the notation of Paper I). Such a potential has a depth of 0.604 h^{23} at $r = 1.34\ a_o$. This potential appears unrealistic because the Lane-Henry polarization potential (see Paper I and Ref. 19) has a maximum depth of 0.095 h at $r = 1.50\ a_o$, while the deeper static potential is deepest at $r = 0.70\ a_o$. Breig and Lin's incomplete procedure also leads to the prediction of qualitatively incorrect DCS's (see Paper I). Takayanagi did distorted wave calculations for the spherically symmetric part of the polarization potential.[17] His calculations, like Breig and Lin's, were exploratory and cannot be used for quantitative estimation of cross sections because he used an oversimplified potential and unrealistic values for the cutoff radius. Nevertheless, his calculations do show that the distorted wave and plane wave treatments agree fairly well at low energies when compared for similar potentials and values of the cutoff radius.

Ehrhardt et al.[6] showed that at very low energies the vibrational excitation cross sections can be qualitatively explained using resonance theory. The resonance can be seen, for example, on Fig. 35. This resonance is a shape resonance in the $p\sigma$ partial wave and is associated with the $^2\Sigma_u^+$ state of H_2^- ion[24]. Our discussion of the 7-10 eV differential cross

sections, however, has shown that potential scattering can account at least approximately for the $v' = 1$ excitation cross section. It is interesting therefore to attempt a crude breakdown of the low energy scattering into resonance and potential scattering contributions. Bardsley[25] showed that the integral cross section curve $Q^{RES}_{m\ell,pp'}$, for excitation of state p' (= $v'J'M'$) of the electronic ground state g from state p (= vJM) of the same electronic state by means of temporary formation of the vibrational states n of the intermediate electronic state (resonance state) d having $\ell = 1$, $m = 0$ ($^2\Sigma^+_u$) is given by

$$Q^{RES}_{o1,pp'} = \frac{4\pi}{k_p k_{p'}} \left| \Sigma_n f^{gd}_{p'n} f^{gd}_{pn} \left(\frac{1}{\epsilon_n + i} \right) \right|^2 \qquad (1)$$

where ℓ and m refer to the orbital angular momentum of the scattering electron and to the component of this angular momentum along the internuclear axis, respectively. The f's are the Franck-Condon factors, k_p and $k_{p'}$ are the wave numbers of the incident and scattered electron.

$$\epsilon_n = \frac{E - E_n}{\frac{1}{2}\Gamma} \qquad (2)$$

E is the impact energy, E_n is the energy of the resonance state with respect to the ground state of H_2 and a separated electron, and Γ is the width of the resonance. Bardsley *et al.*[7] have estimated theoretically that $\frac{1}{2}\Gamma = 4.5$ eV, but we will use the value $\frac{1}{2}\Gamma = 3$ eV estimated by Ehrhardt *et al.*[6] from their experiments. If we assume that the rotational state doesn't change and that only one vibrational state r

of the resonance contributes, we can rewrite (1) as

$$Q^{RES}_{01,vv'} = \frac{A(v,v',r)}{k_v k_{v'}(\epsilon_r^2+1)} \tag{3}$$

where the numerator A is independent of impact energy. Finally, without making a partial wave decomposition of the potential scattering cross section $Q^{POT}_{vv'}$, the simplest approximation we can use for the full (resonance + potential scattering) integral cross section is

$$Q_{vv'} = Q^{RES}_{vv'} + Q^{POT}_{vv'} \tag{4}$$

This amounts to neglecting terms due to interference of the resonance and potential scattering in the $\ell = 1$ partial wave. We will further make the approximation that $Q^{POT}_{vv'}$ can be estimated from our B/P calculations (with data set 1).

For this one state resonance model, we estimate from the cross sections of Ehrhardt et al.[6] that $E_r = 3.5$ eV. Using eq. (4), we also obtain from their data estimates of $Q^{RES}_{01,0v'}$ at E = 3.5 eV. Then we use eqs. (2) and (3) to calculate empirical values for A(0, v', r) for v' = 1, 2, and 3.

Next, eq. (3) with the value of A determined above is used to predict $Q^{RES}_{01,0v'}$ at energies above 3.5 eV. Finally, the model's predictions for the full $Q_{0v'}$ are calculated from eq. (4) and these cross sections are compated with experiment in Table III. In view of the approximations involved, these results can be considered only as qualitative estimates of the true situation. For the v' = 1 case this crude

model gives good agreement with experiments up to 10 eV and indicates that above about 7 eV the contribution from potential scattering is comparable to or larger than the one from resonance scattering.

For the excitation $v = 0 \rightarrow v' = 1$, a more realistic model would include at least the $r = 0$ and $r = 1$ vibrational states of the resonance. The disagreement of the model and experiment for the energy dependence of Q_{01} would be lessened for a 2 vibrational-state resonance model because the added resonance state would raise the cross section more at 5 eV than at 10 eV. Ehrhardt *et al.*[6] interpreted the unsymmetrical shape of the Q_{01} curve as meaning that several states of the negative ion are important. It seems more probable, however, that only the lowest $(v' + 1)$ states are very important and that the rest of the tail in the Q_{01} curve is due to contributions from potential scattering. For the higher v', the agreement between the predictions of this model and the experiments becomes progressively worse. The table indicates that excitation of these states is much closer to being pure resonance scattering than is the $v' = 1$ excitation. The one-state model predicts that the cross sections decrease too rapidly with energy. Since we probably have not underestimated the potential scattering (the comparison of theory and experiment in the nonresonant regions indicates that our theoretical treatment overestimates the potential scattering cross section), this error is probably due to our oversimplified treatment of the resonance. One defect of the model is that the $n = 2$ and 3 states, which it neglects, probably are more important for excitation of these higher vibrational states. Also, perhaps the results indicate that a half-width larger than 3 eV should be used. Both these corrections would raise the predicted cross sections at energies above 3.5 eV.

E. Conclusions

The differential cross sections for vibrational excitation of $v' = 1$ level of H_2 are strongly decreasing functions of scattering angle in the 10^o - 30^o region for E = 7 - 81.6 eV. At energies above 20 eV they show a deep minimum near 30^o. The polarized Born and polarized prior Born-Ochkur-Rudge calculations are in qualitative agreement with experiment except that they do not give a deep enough minimum in the differential cross section. The energy and angle dependence of the quantum mechanical cross sections is quantitatively very good in the 50^o - 80^o range. For the integral cross sections, theory and experiment agree only within a factor of about 3, and the calculations seem to overestimate the nonresonance contributions to the cross sections in the intermediate energy range.

While Taylor and co-workers[6,9] interpreted the excitation of the $v' = 1$, 2, and 3 levels at 10 eV impact energy as due mainly to resonance contributions, we find that the potential scattering (or direct interaction) contributions to the $v' = 1$ excitation cross section are appreciable at 10 eV. However, these contributions decrease more rapidly with increasing v' than do those predicted by a resonance mechanism so that excitation of the $v' \geq 2$ levels is evidently due primarily to resonance scattering even at 10 eV (about 7 eV away from the nominal resonance energy). (It has been known for a long time that resonance scattering often leads to appreciable cross sections for processes with large Δv.[27]) However, at higher energies (E = 20-45 eV) our first order calculations account quantitatively for the magnitude of the $v' = 2$ cross sections. Both experimentally and theoretically, the shapes of the differential cross sections for exciting the $v' = 1$ and the $v' = 2$

levels are similar to each other as compared to the shapes of the DCS's for elastic scattering[14] or excitation of the $b^3\Sigma_u^+$ or the $a^3\Sigma_g^+$ states.[26]

TABLE I. Differential cross sections (a_0^2/sr) for vibrational excitation due to potential scattering (calculated in the polarized Born approximation) at low energies.

v'	1	1	1	1	1	1	1	1	1
Data Set[a]	1	1	1	1	1	1	L	L	L
θ(deg) \ E(eV)	1.8	3.4	5	7	10	25	5	7	10
0	0.164	0.187	0.195	0.201	0.206	0.214	0.169	0.174	0.178
12	0.151	0.157	0.154	0.147	0.138	0.106	0.131	0.125	0.117
24	0.129	0.123	0.112	0.100	0.086	0.045	0.093	0.083	0.071
36	0.109	0.095	0.080	0.066	0.051	0.016	0.066	0.054	0.041
48	0.092	0.072	0.056	0.042	0.028	0.007	0.046	0.034	0.023
60	0.077	0.055	0.039	0.026	0.015	0.005	0.031	0.021	0.012
75	0.063	0.039	0.024	0.014	0.008	0.005	0.020	0.012	0.007
90	0.051	0.028	0.015	0.009	0.005	0.005	0.013	0.007	0.005
105	0.042	0.020	0.010	0.006	0.005	0.004	0.009	0.006	0.004
120	0.035	0.015	0.008	0.005	0.005	0.004	0.007	0.005	0.004
v'	2	2	2	2	2	2	3	3	3
Factor*	10^2	10^2	10^2	10^2	10^2	10^2	10^4	10^4	10^4
Data Set	1	1	1	1	1	1	1	1	1
θ(deg) \ E(eV)	1.8	3.4	5	7	10	25	3.4	7	10
0	0.145	0.200	0.222	0.234	0.245	0.262	0.552	0.710	0.759
12	0.140	0.181	0.188	0.187	0.180	0.145	0.517	0.595	0.586
24	0.128	0.150	0.144	0.133	0.118	0.068	0.440	0.425	0.375
36	0.115	0.120	0.108	0.092	0.074	0.030	0.358	0.288	0.231
48	0.101	0.096	0.080	0.063	0.046	0.012	0.284	0.198	0.155
60	0.089	0.076	0.059	0.043	0.028	0.005	0.226	0.147	0.118
75	0.076	0.057	0.041	0.027	0.015	0.002	0.174	0.114	0.093
90	0.065	0.044	0.029	0.017	0.008	0.002	0.141	0.095	0.071
105	0.057	0.035	0.021	0.011	0.005	0.003	0.120	0.081	0.050
120	0.050	0.028	0.016	0.008	0.003	0.004	0.107	0.067	0.033

[a] See Paper I.

* The factor, if given, is the number by which the cross sections have been multiplied.

TABLE II. Calculated integral vibrational excitation cross sections (10^{-5} a_o^2) for $v' = 3$.

E(eV)	10	20	45	60	81.63	100	500
B/P	12.9	6.6	4.3	4.7	5.3	5.5	2.1
BOR/P	15.9	7.3	4.7	5.0	5.6	5.8	
BXP	6.1	3.3	2.8	3.6	4.5	4.8	2.0
BORXP	8.9	4.0	3.2	3.9	4.7	5.1	

TABLE III. Summary of estimated resonance and potential scattering contributions to the integral cross sections (a_o^2).

v'	E(eV)	Calculation			Experiment	
		Res.	Pot.[a]	Sum.	ELLT[b]	TTRK[c]
1	3.5	1.256[e]	0.504	1.760[d]	1.76	
1	5	0.699[f]	0.380	1.079[g]	1.32	-
1	7	0.260[f]	0.290	0.550[g]	0.80	0.57
1	10	0.075[f]	0.221	0.296[g]	0.31	0.32
2	3.5	0.13[e]	0.007	0.137[d]	0.14	
2	5	0.069[f]	0.006	0.075[g]	0.12	-
2	7	0.025[f]	0.004	0.029[g]	0.096	0.050
2	10	0.007[f]	0.003	0.010[g]	-	0.034
3	3.5	0.015[e]	0.0002	0.0152[d]	0.014	
3	5	0.0055[f]	0.0002	0.0057[g]	0.012	-
3	7	0.0025[f]	0.0002	0.0027[g]	0.008	-
3	10	0.0005[f]	0.0001	0.0006[g]	-	(0.014)

[a] Present B/P calculation (DS1).

[b] Reference 5.

[c] Present results.

[d] Taken as equal to column 6.

[e] Taken as column 5 minus column 4.

[f] Calculated from eq. (3)

[g] Taken as sum of column 3 and column 4.

References

1. H. Ramien, Z. Physik 70, 353 (1931).

2. V. A. Bailey, Phil. Mag. 13, 993 (1932).

3. A. G. Engelhardt and A. G. Phelps, Phys. Rev. 131, 2115 (1963); A. V. Phelps, Rev. Mod. Phys. 40, 399 (1968).

4. G. J. Schulz, Phys. Rev. 135, A988 (1964).

5. M. G. Menendez and H. K. Holt, J. Chem. Phys. 45, 2743 (1966).

6. H. Ehrhardt, L. Langhans, F. Linder, and H. S. Taylor, Phys. Rev. 173, 222 (1968).

7. J. N. Bardsley, A. Herzenberg, and F. Mandl, Proc. Phys. Soc. 89, 305, 321 (1966).

8. J. N. Bardsley and F. Mandl, Rep. Prog. Phys. 31, 471 (1968).

9. T. F. O'Malley and H. S. Taylor, Phys. Rev. 176, 207 (1968).

10. F. H. Read, J. Phys. B (Proc. Phys. Soc. [2]) 1, 893 (1968); J. N. Bardsley and F. H. Read, Chem. Phys. Letters 2, 333 (1968).

11. H. S. Taylor, Advances in Chemical Physics, Vol. 18 (to be published).

12. J. Comer, F. R. Read, 6th Int. Conf. on the Physics of Electronic and Atomic Collisions: Abstracts of Papers, edited by I. Amdur (M.I.T., Cambridge, 1969), p. 86; A. Weingartshofer, H. Ehrhardt, and F. Linder, ibid., p. 91.

13. J. Geiger and K. Wittmaack, Z. Physik 187, 433 (1965).

14. S. Trajmar, D. G. Truhlar, and J. K. Rice, J. Chem. Phys. 00, 0000 (1970), preceding article, paper II.

15. D. G. Truhlar and J. K. Rice, (to be published). This article will be referred to as I.

16. E. L. Breig and C. C. Lin, J. Chem. Phys. 43, 3839 (1965).

17. K. Takayanagi, J. Phys. Soc. Japan 20, 562 (1965).

18. T. R. Carson, Proc. Phys. Soc. A67, 909 (1954).

19. N. F. Lane and R. J. W. Henry, Phys. Rev. 173, 183 (1968).

20. D. G. Truhlar, J. K. Rice, A. Kuppermann, S. Trajmar, and D. C. Cartwright, Phys. Rev., submitted for publication.

21. C. Ramsauer and R. Kollath, Ann. Phys. (Leipzig) 4, 91 (1929) and 12, 529 (1932).

22. D. E. Golden, H. W. Bandel, and J. A. Salerno, Phys. Rev. 146, 40 (1966).

23. 1 h = 1 hartree = 27.210 eV = 4.3592×10^{-11} ergs.

24. H. S. Taylor, G. V. Nazaroff, and A. Golebiewski, J. Chem. Phys. 45, 2872 (1966).

25. J. N. Bardsley, Chem. Phys. Letters 2, 329 (1968).

26. S. Trajmar, D. C. Cartwright, J. K. Rice, R. T. Brinkmann, and A. Kuppermann, J. Chem. Phys. 49, 5464 (1968).

27. G. J. Schulz, Phys. Rev. 125, 229 (1962).

Figure Captions

Fig. 1 Energy-loss spectrum of H_2 at E = 10 eV and $\theta = 58.5^{o}$ (before smoothing). The spectrum is a superposition of 58 scans with 1 sec dwell time (time spent in one channel during each scan accumulating the scattered signal intensity) and 1.75 MeV increments between adjacent channels.

Fig. 2 The ratios R_v, of the vibrational excitation to elastic scattering intensities as a function of scattering angle at E = 7 eV. The indices 1, 2, and 3 on R_v, refer to final vibrational quantum number $v' = 1$, 2, and 3, respectively. The symbols x and * are our measured values for R_1 and R_2, respectively, and the symbols o and □ show the values obtained for R_2 and R_3, respectively, by using the data of Ehrhardt et al.[6] and the procedure described in Section D.1 of the text. The curves are the results of the present calculation.

Fig. 3 The ratios R_v, of the vibrational excitation to elastic scattering intensities as a function of scattering angle at E = 10 eV. The symbols x, *, and Δ are our measured values for R_1, R_2, and R_3, respectively. The curves are the results of the present calculation.

Fig. 4 Same as Fig. 3, except E = 13.6 eV and the symbols +, x, and o represent three measurements of R_1 taken at different times. No experimental R_3 ratios are available.

Figure Captions (cont'd.)

Fig. 5 Same as Fig. 3, except E = 20 eV.

Fig. 6 Same as Fig. 3, except E = 45 eV.

Fig. 7 The ratios R_v, of the vibrational excitation to elastic scattering intensities as a function of scattering angle at E = 60 eV. The symbols + and x are two separate measurements of R_1 and the symbol * is a measured R_2 value. The curves are the results of the present calculation. (See Section D.1 of the text for an explanation of the curves.)

Fig. 8 The calculated values of R_3 as a function of scattering angle at E = 60 eV.

Fig. 9 The ratios R_v, of the vibrational excitation to elastic scattering intensities as a function of scattering angle at E = 81.6 eV. The symbols x are our measured values for R_1. The curves are the results of the present calculation. (See text for explanation of curves.)

Fig. 10 The calculated values of R_3 as a function of scattering angle at E = 81.6 eV.

Fig. 11 Differential cross sections for the excitation of the fundamental vibration ($v' = 1$) in H_2 by 7 eV electrons. The symbols x are our measured values and the curves are our calculated values. The asterisks at 180^o show the values of the DCS predicted there by the three methods of extrapolation discussed in Section C of Paper II.

Figure Captions (cont'd.)

Fig. 12 Differential cross sections for the excitation of the first overtone vibration ($v' = 2$) in H_2 by 7 eV electrons. The symbols x are our measured values and the curve is from our calculations. The asterisks at 180^o are explained in Fig. caption 11.

Fig. 13 Differential cross sections for the excitation of the fundamental vibration ($v' = 1$) in H_2 by 10 eV electrons. The open circles and crosses are the measurements of Ehrhardt et al. (Ref. 6) and the present measurements, respectively. The curve labelled RESONANCE is proportional to $(1 + 2 \cos^2\theta)$ and is normalized to experiment at 40^o. The solid and the dashed curves are the results of the present calculation. The asterisks at 180^o are explained in Fig. caption 11.

Fig. 14 Differential cross sections for the excitation of the first ($*$) and second (Δ) overtone vibrations in H_2 by 10 eV electrons. The resonance curve corresponds to a $(1 + 2 \cos^2\theta)$ angular distribution and is normalized to experiment at 50^o. The other curves are the results of the present calculation. (See text for explanation of the curves.)

Fig. 15 Differential cross sections for the fundamental vibrational excitation in H_2 by 13.6 eV electrons. The x's are the present experiments, the curves are the present calculations, and the asterisks are explained in Fig. caption 11.

Figure Captions (cont'd.)

Fig. 16 Differential cross sections for the excitation of the first overtone vibration in H_2 by 13.6 eV electrons. The *'s below 80^o are the present experiments and the asterisks at 180^o are explained in Fig. caption 11. The curve is the result of the present calculation.

Fig. 17 Same as Fig. 15, except E = 20 eV.

Fig. 18 Same as Fig. 16, except E = 20 eV.

Fig. 19 Differential cross sections for the excitation of the fundamental (x) and first overtone (*) vibrations in H_2 by 45 eV electrons. The asterisks at 180^o represent possible extrapolations of the $v' = 1$ experiments. The curves are the results of the present calculation.

Fig. 20 Same as Fig. 19, except E = 60 eV.

Fig. 21 Differential cross sections for the excitation of the fundamental and first overtone vibrations in H_2 by 81.6 eV electrons. The symbols are as in Fig. 19. The results of a BOR calculation without polarization and quadrupole interaction terms in the potential are also shown (BORXPXQ). The curves are the results of the present calculation. (See text for explanation of the other curves.)

Fig. 22 Intensity ratios as a function of impact energy at 20^o scattering angle. Crosses and open circles are the experimental R_1 and R_2 values, respectively; the curves are the results of our calculations. (See text for explanation of the curves.)

Figure Captions (cont'd.)

Fig. 23 Same as Fig. 22, except $\theta = 30^{o}$.

Fig. 24 Same as Fig. 22, except $\theta = 40^{o}$.

Fig. 25 Same as Fig. 22, except $\theta = 60^{o}$.

Fig. 26 Same as Fig. 22, except $\theta = 70^{o}$. The R_1 values measured by Schulz at 72^{o} are also shown as boxes.

Fig. 27 Same as Fig. 22, except $\theta = 80^{o}$.

Fig. 28 The energy dependence of the 20^{o} differential cross sections for the fundamental, first, and second overtone excitation in H_2 (Δ, o, and $\square$, respectively). The low energy values indicated by filled-in symbols represent the measurements of Ehrhardt et al. The curves are the results of the present calculation.

Fig. 29 The energy dependence of the DCS at 30^{o} for the excitation of the fundamental (Δ) and first overtone (o) vibrations. The symbols are the present experiments and the curves are the results of the present calculation (two typical error bars are shown).

Fig. 30 The energy dependence of the DCS for vibrational excitation. The Δ and the o are the present experimental results at $\theta = 40^{o}$ for $v' = 1$ and $v' = 2$, respectively. The curves are the present calculations at $\theta = 42^{o}$.

Fig. 31 Same as Fig. 29, except $\theta = 60^{o}$.

Fig. 32 Same as Fig. 29, except $\theta = 70^{o}$, and the results of the BXP calculation for DCS_{01} and DCS_{02} are also shown. The BXP cross sections are the lower solid curves.

Figure Captions (cont'd.)

Fig. 33 Same as Fig. 29, except $\theta = 80^{o}$.

Fig. 34 The energy dependence of the DCS at $\theta = 120^{o}$ for excitation of the fundamental vibration as calculated in the polarized B/P and BOR/P approximations. The inclusion of polarization in the calculation makes less than 18% difference above 35 eV.

Fig. 35 Integral cross sections for the excitation of the fundamental vibrations ($v' = 1$) as a function of impact energy. The symbols x, o, and ◇ represent the results of this paper, of Ehrhardt *et al.*, and of Ramien, respectively. The curves are the present calculations using data set 1. The dotted curves are calculated using only the amplitudes indicated (in the notation of Paper I).

Fig. 36 Integral cross sections for the excitation of the first two overtone vibrations ($v' = 2$ and 3) as a function of impact energy. Experimental cross sections are obtained from Ehrhardt *et al.* (o for $v' = 2$, □ for $v' = 3$) and from the present measurements (* for $v' = 2$, Δ for $v' = 3$). Typical error bars are shown on some of our results. Theoretical cross sections are shown only for $v' = 2$ because the theoretical curves for $v' = 3$ are too small to fit on scale.

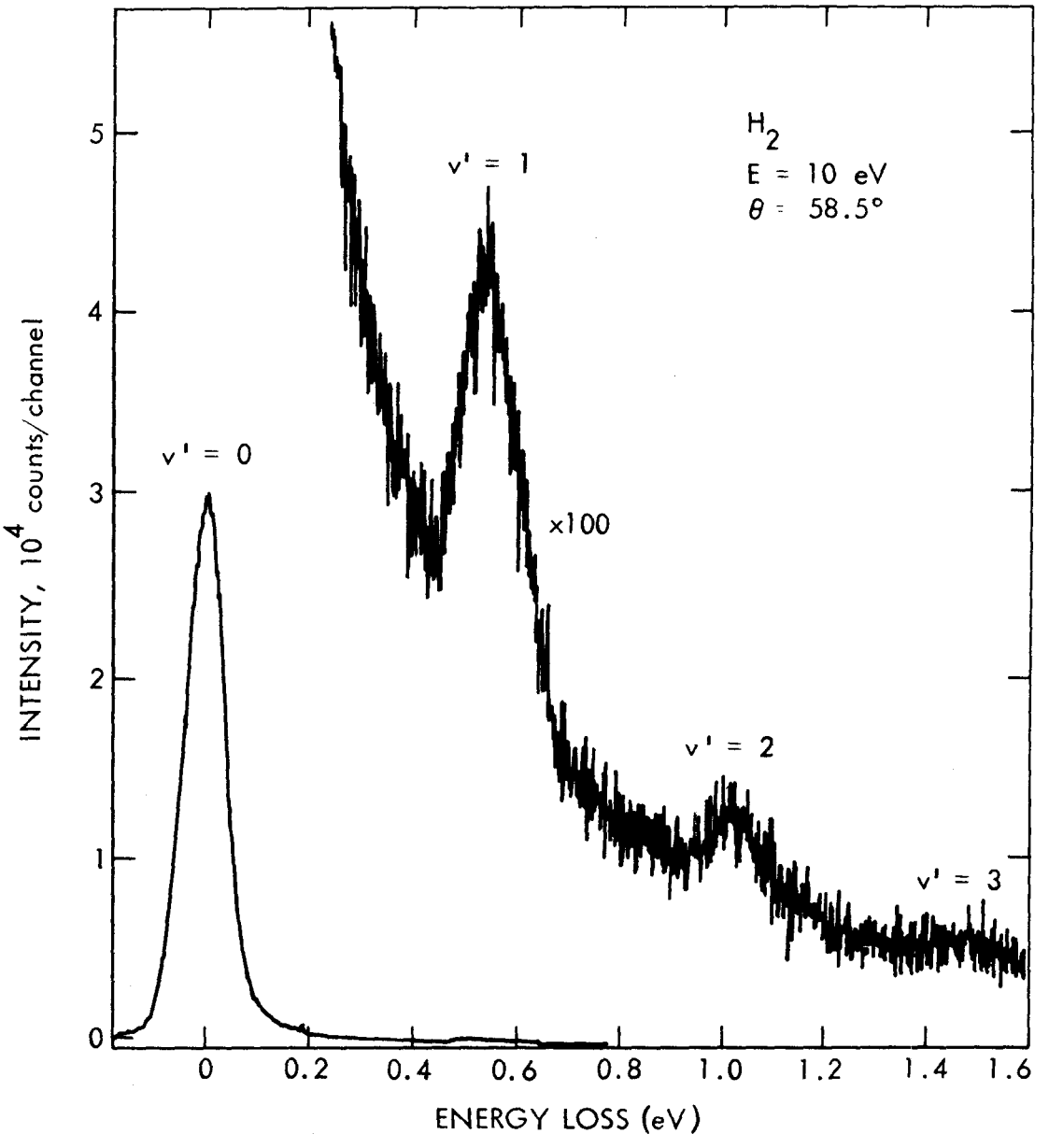
H2
E = 10 eV
θ = 58.5°
v' = 0
v' = 1
v' = 2
v' = 3
x100
INTENSITY, 10^4 counts/channel
ENERGY LOSS (eV)
0
1
2
3
4
5
0
0.2
0.4
0.6
0.8
1.0
1.2
1.4
1.6

1

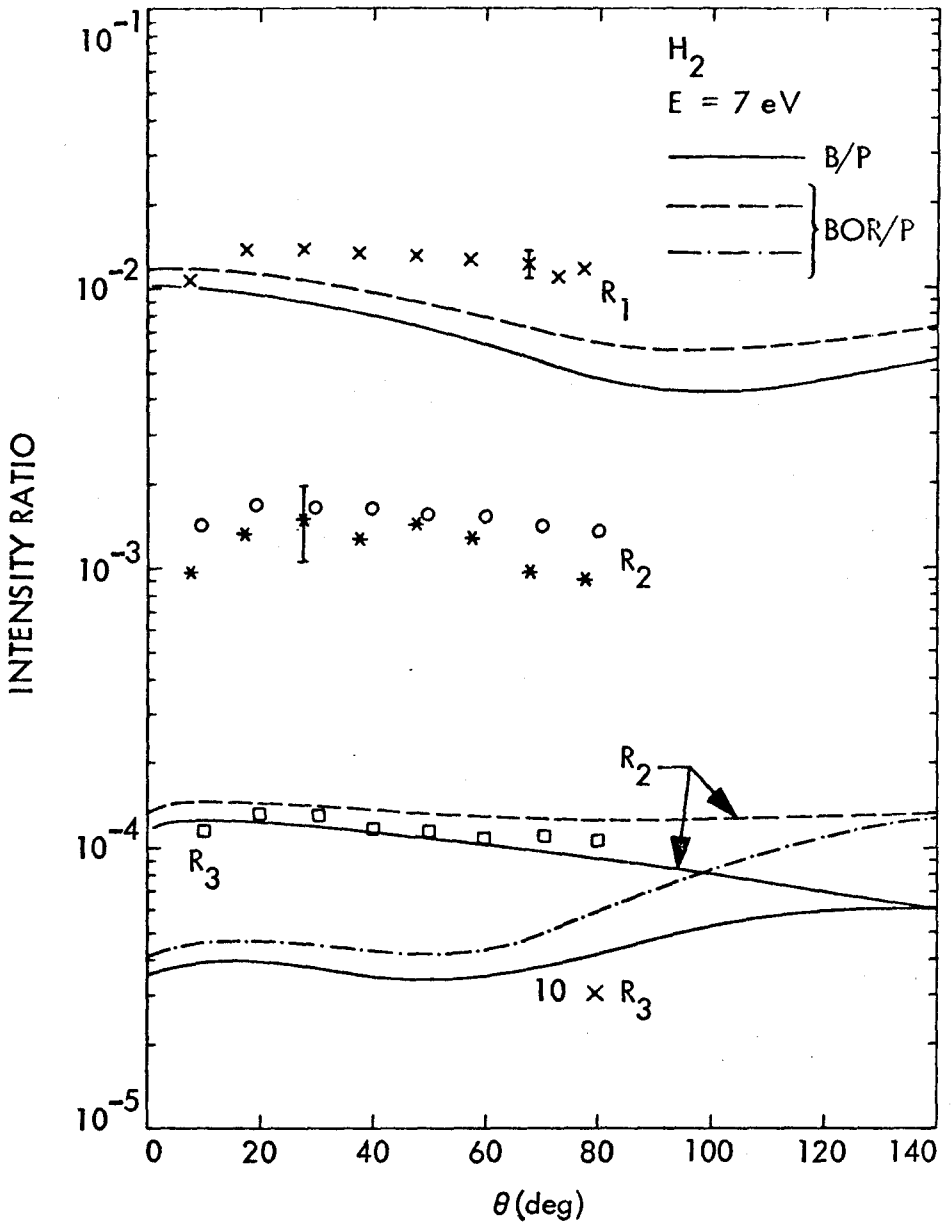
H_2
E = 7 eV
B/P
BOR/P
R_1
R_2
R_2
R_3
10 × R_3
INTENSITY RATIO
10^{-1}
10^{-2}
10^{-3}
10^{-4}
10^{-5}
0
20
40
60
80
100
120
140
θ (deg)

2

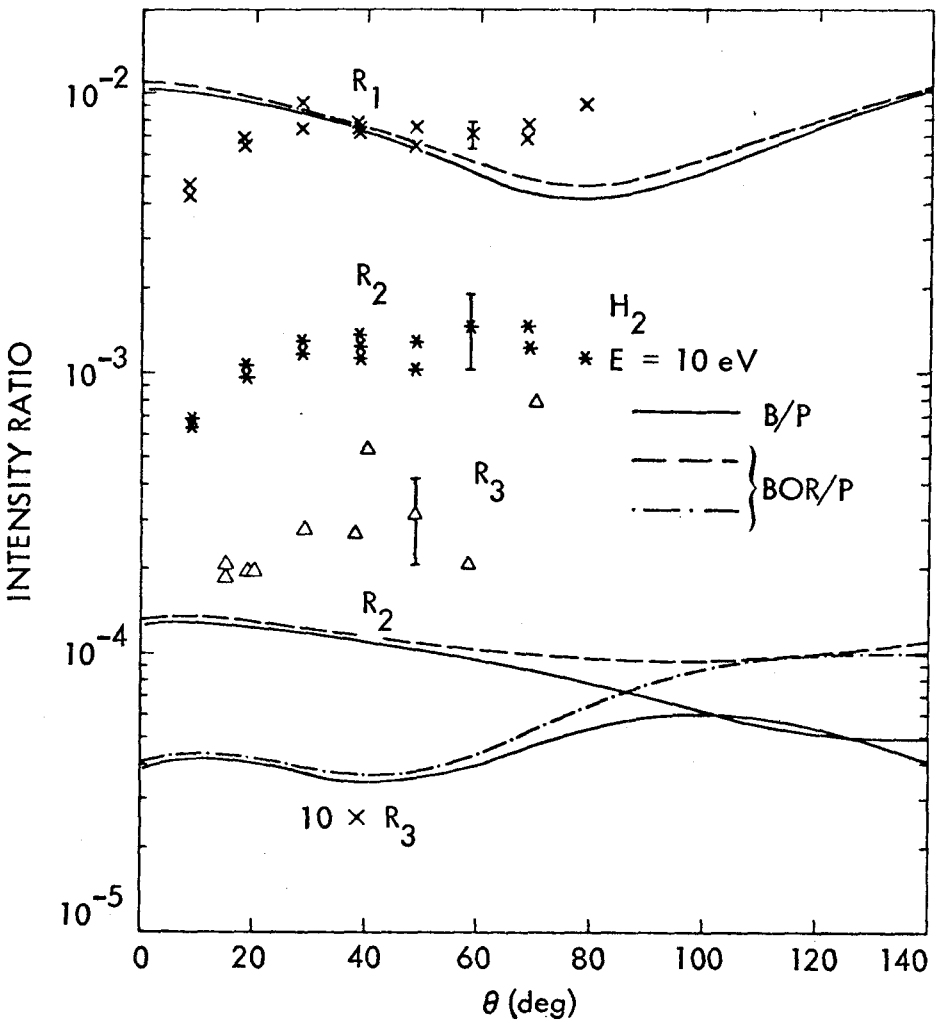
INTENSITY RATIO
10^{-2}
10^{-3}
10^{-4}
10^{-5}
R_1
R_2
H_2
* E = 10 eV
B/P
BOR/P
R_3
R_2
10 × R_3
0
20
40
60
80
100
120
140
θ (deg)

3

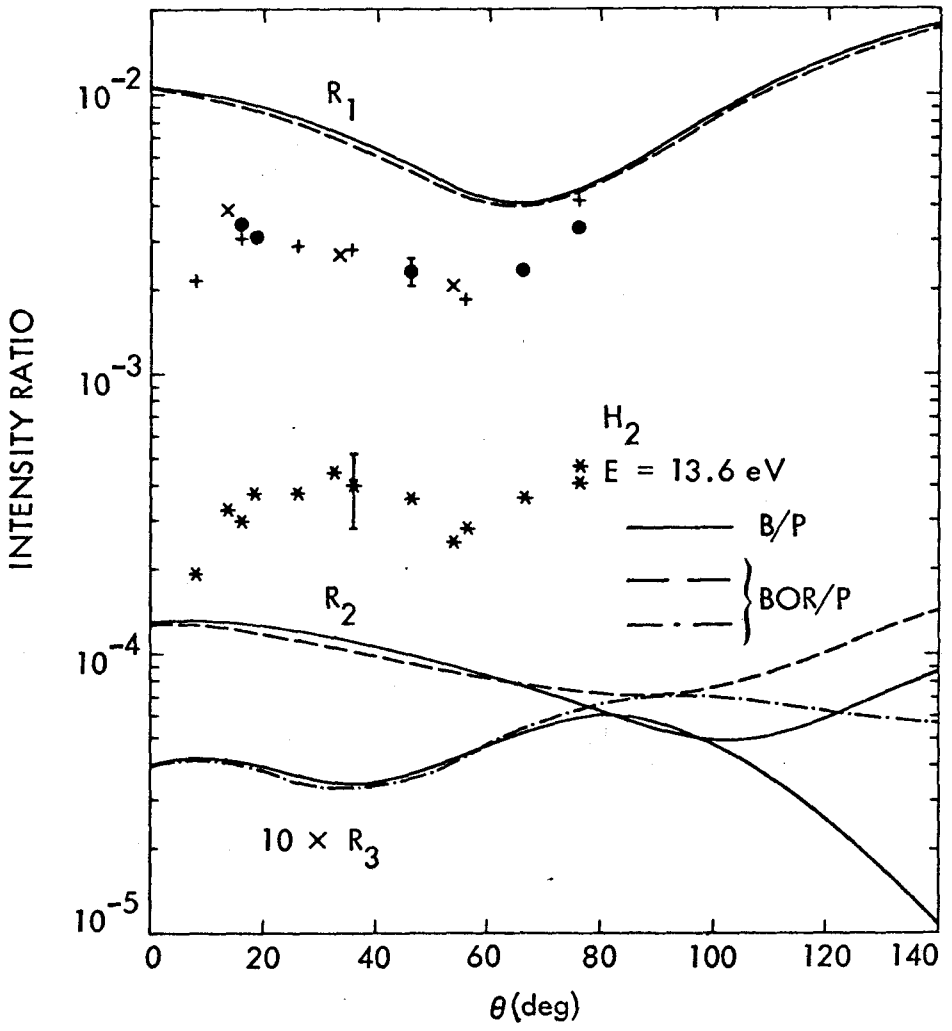
INTENSITY RATIO
10^{-2}
10^{-3}
10^{-4}
10^{-5}
R_1
R_2
$10 \times R_3$
H_2
E = 13.6 eV
B/P
BOR/P
0
20
40
60
80
100
120
140
θ(deg)

4

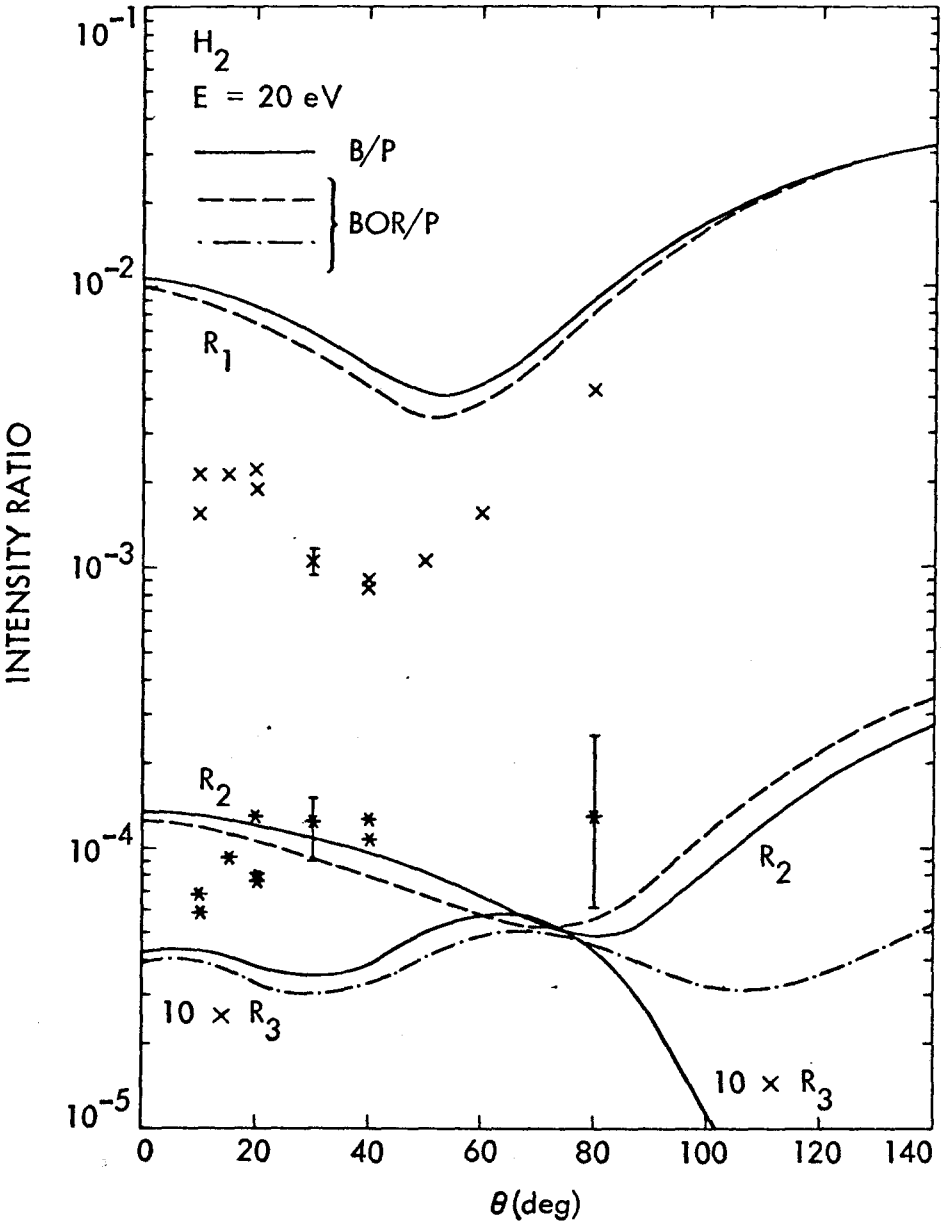
H_2
E = 20 eV
B/P
BOR/P
R_1
R_2
$10 \times R_3$
R_2
$10 \times R_3$
INTENSITY RATIO
10^{-1}
10^{-2}
10^{-3}
10^{-4}
10^{-5}
0
20
40
60
80
100
120
140
θ(deg)

5

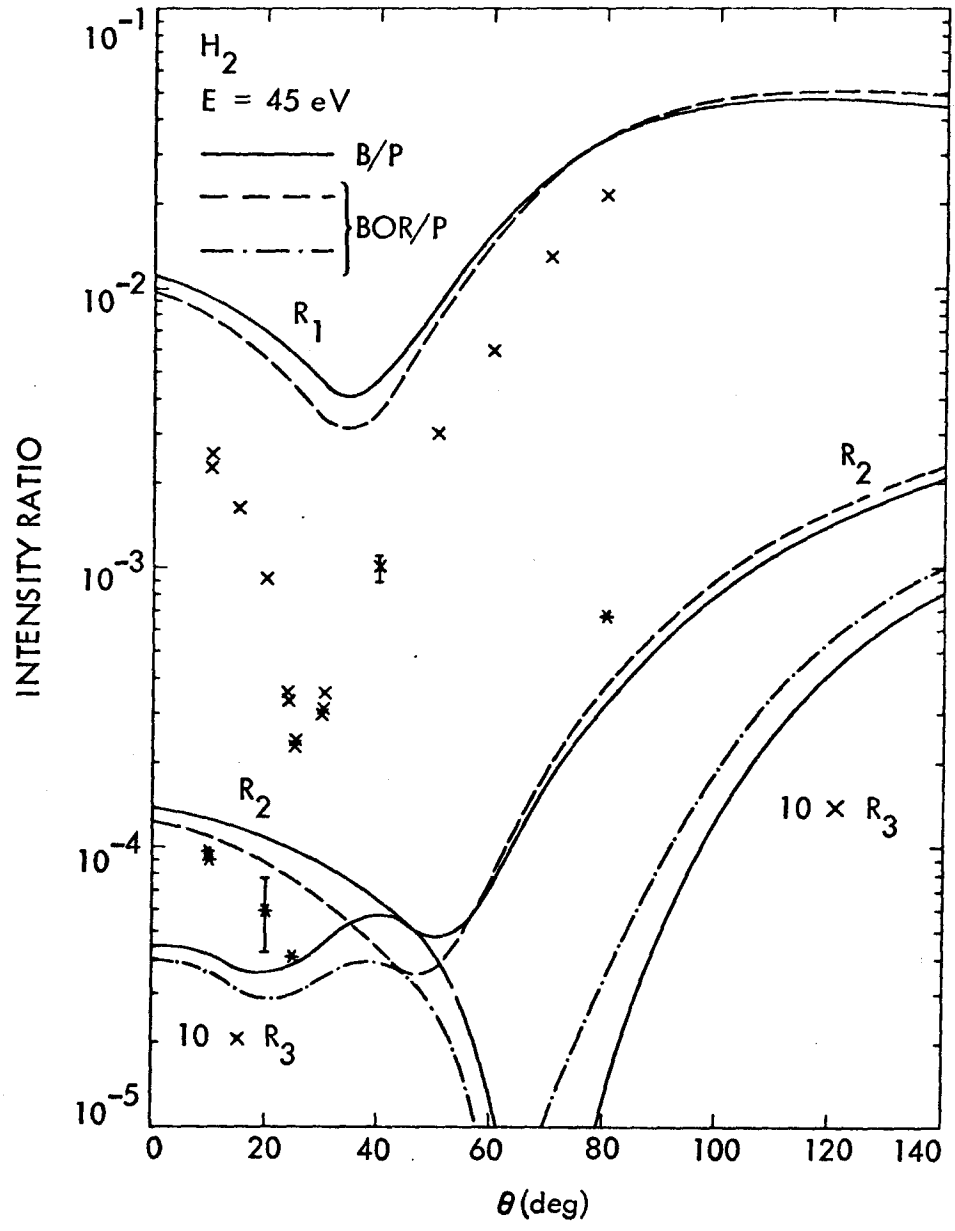
10^{-1}
10^{-2}
10^{-3}
10^{-4}
10^{-5}
H_2
E = 45 eV
B/P
BOR/P
R_1
R_2
R_2
10 × R_3
10 × R_3
INTENSITY RATIO
0
20
40
60
80
100
120
140
θ (deg)

6

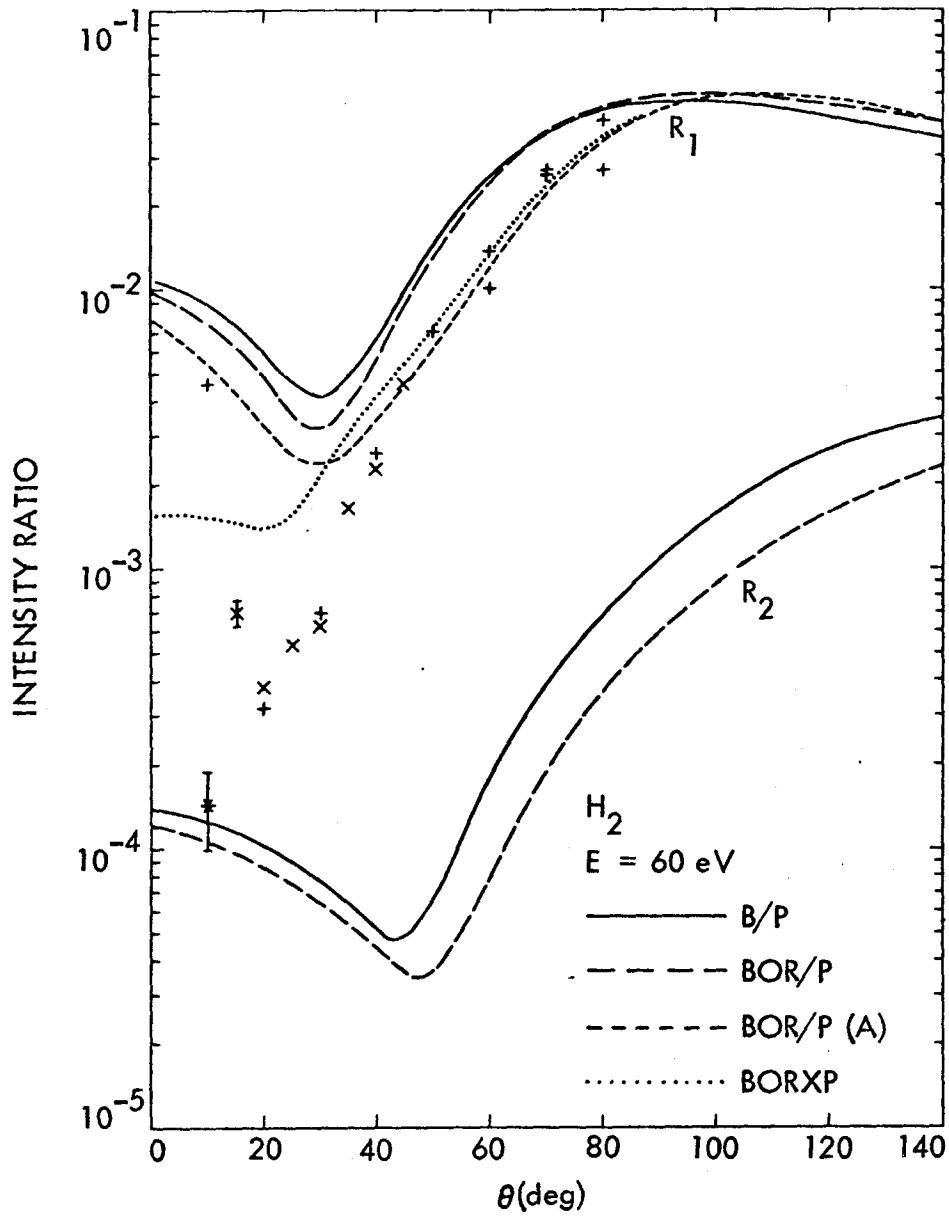
INTENSITY RATIO
10^{-1}
10^{-2}
10^{-3}
10^{-4}
10^{-5}
0
20
40
60
80
100
120
140
θ(deg)
R_1
R_2
H_2
E = 60 eV
B/P
BOR/P
BOR/P (A)
BORXP

7

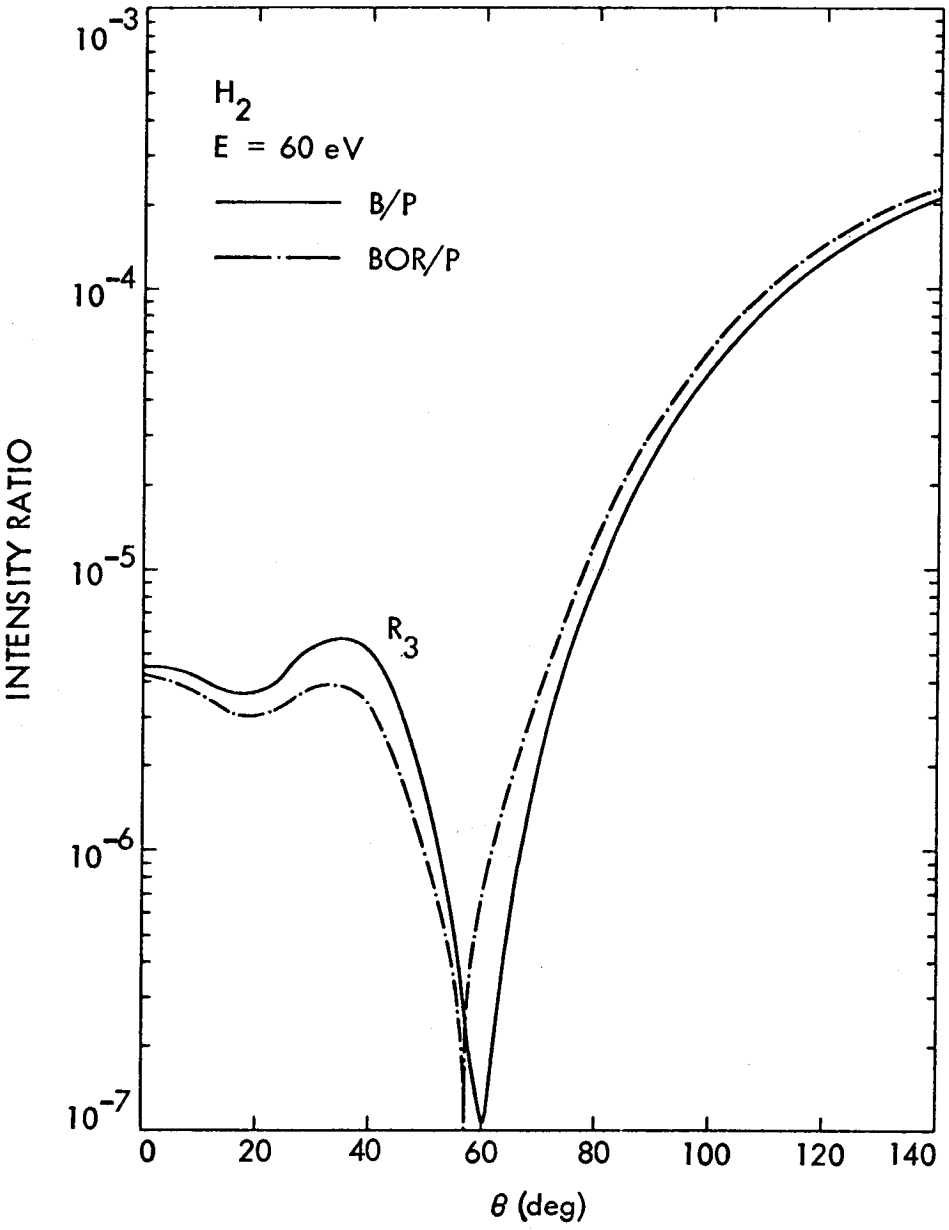
10^{-3}
10^{-4}
10^{-5}
10^{-6}
10^{-7}
INTENSITY RATIO
H_2
E = 60 eV
B/P
BOR/P
R_3
0
20
40
60
80
100
120
140
θ (deg)

8

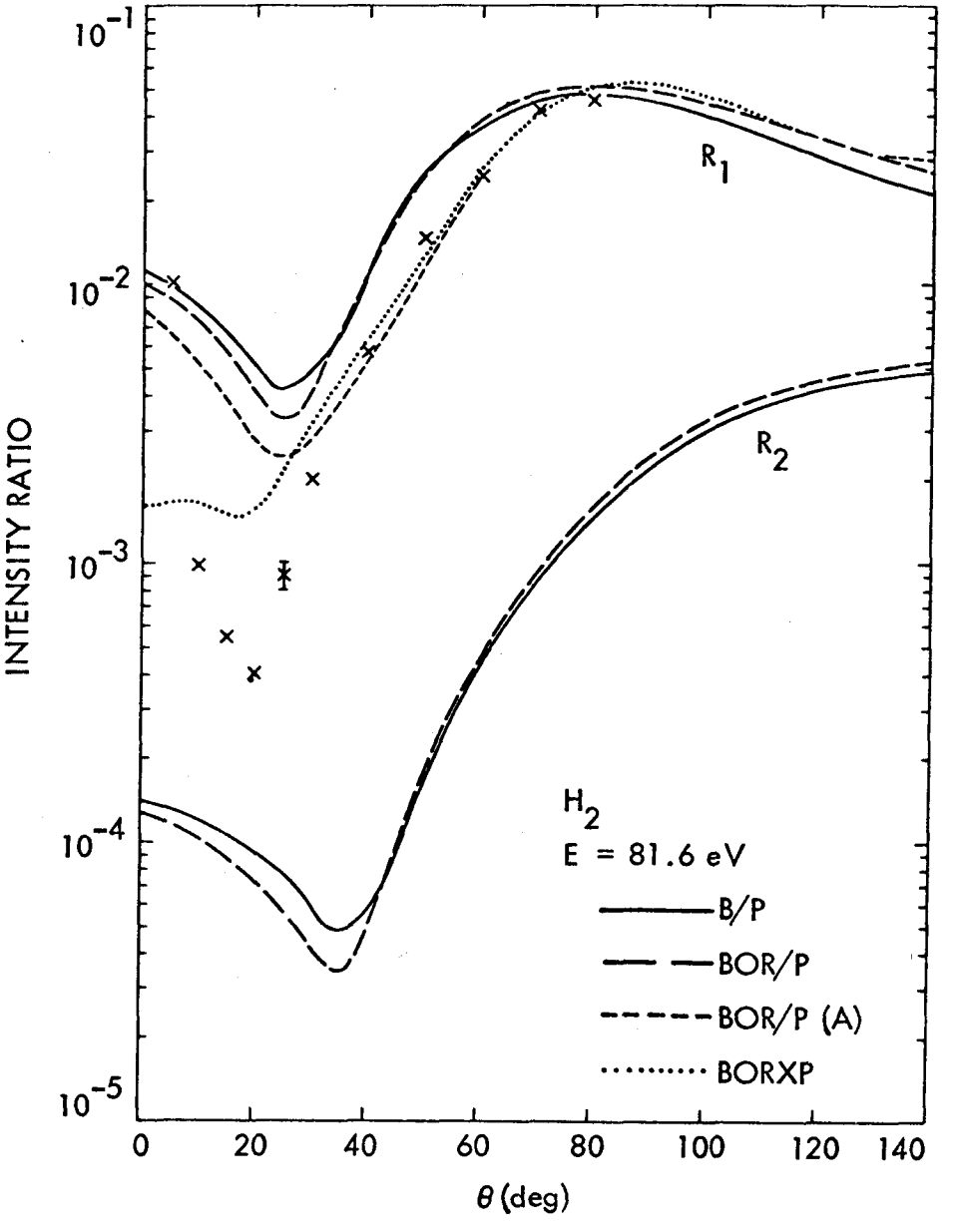
INTENSITY RATIO
10^{-1}
10^{-2}
10^{-3}
10^{-4}
10^{-5}
R_1
R_2
H_2
E = 81.6 eV
B/P
BOR/P
BOR/P (A)
BORXP
0
20
40
60
80
100
120
140
θ (deg)

9

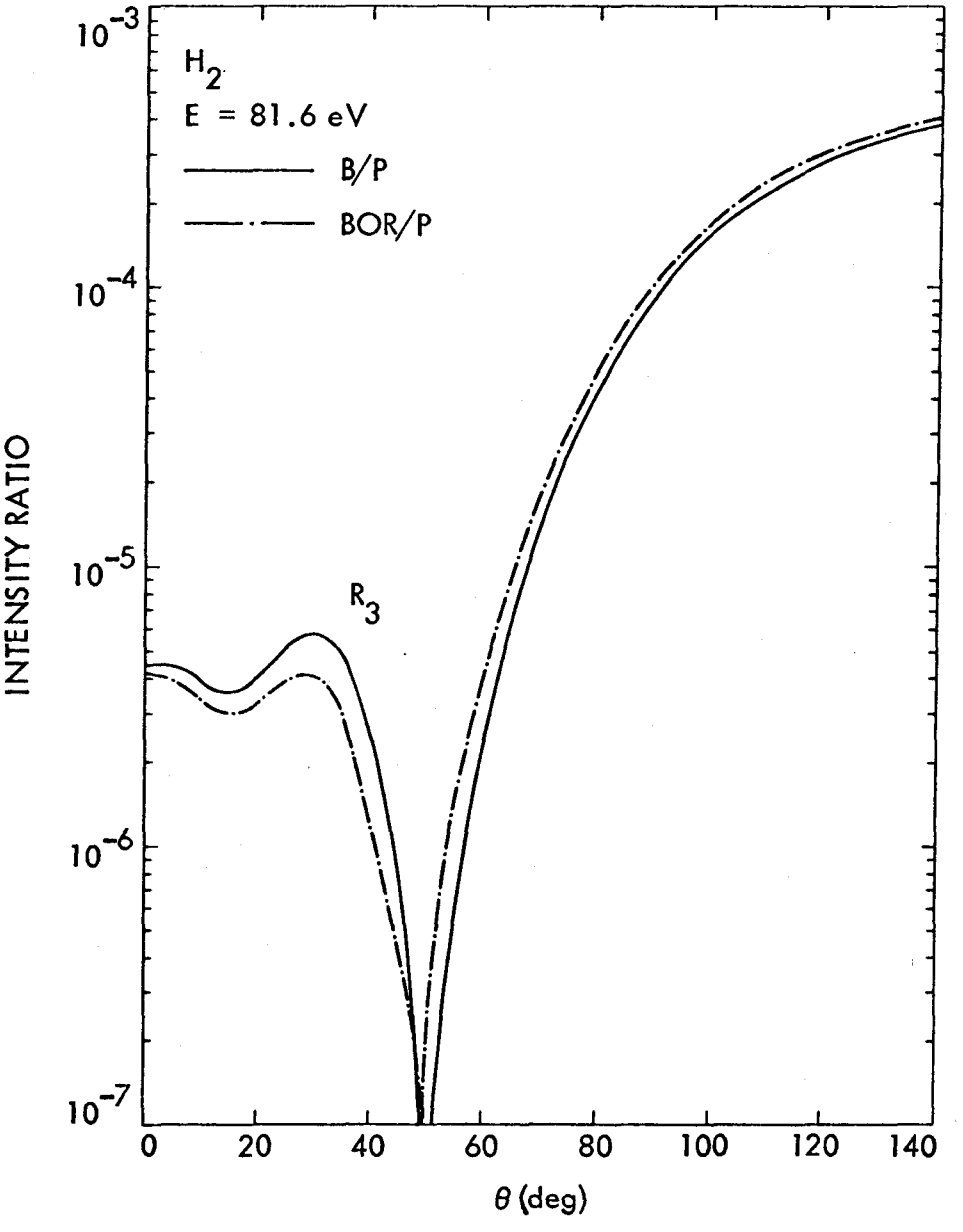
10^{-3}
10^{-4}
10^{-5}
10^{-6}
10^{-7}
H_2
E = 81.6 eV
B/P
BOR/P
R_3
INTENSITY RATIO
0
20
40
60
80
100
120
140
θ (deg)

10

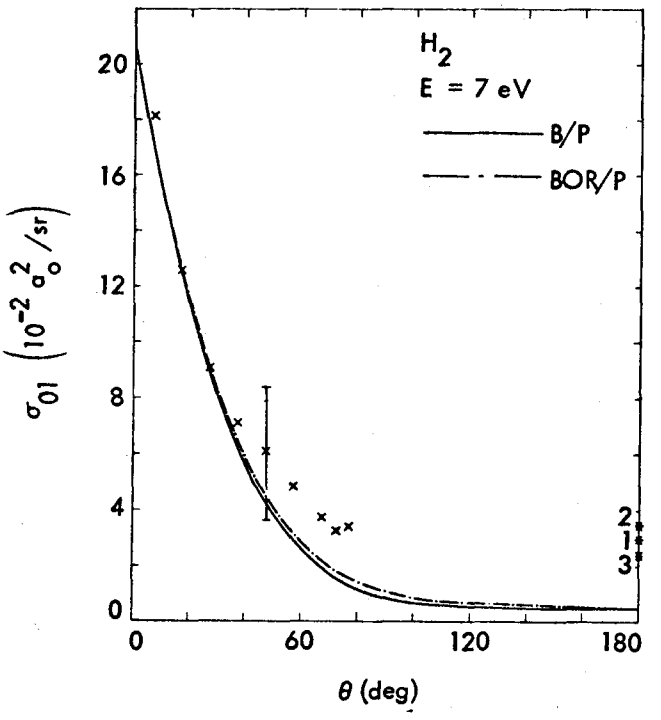

11

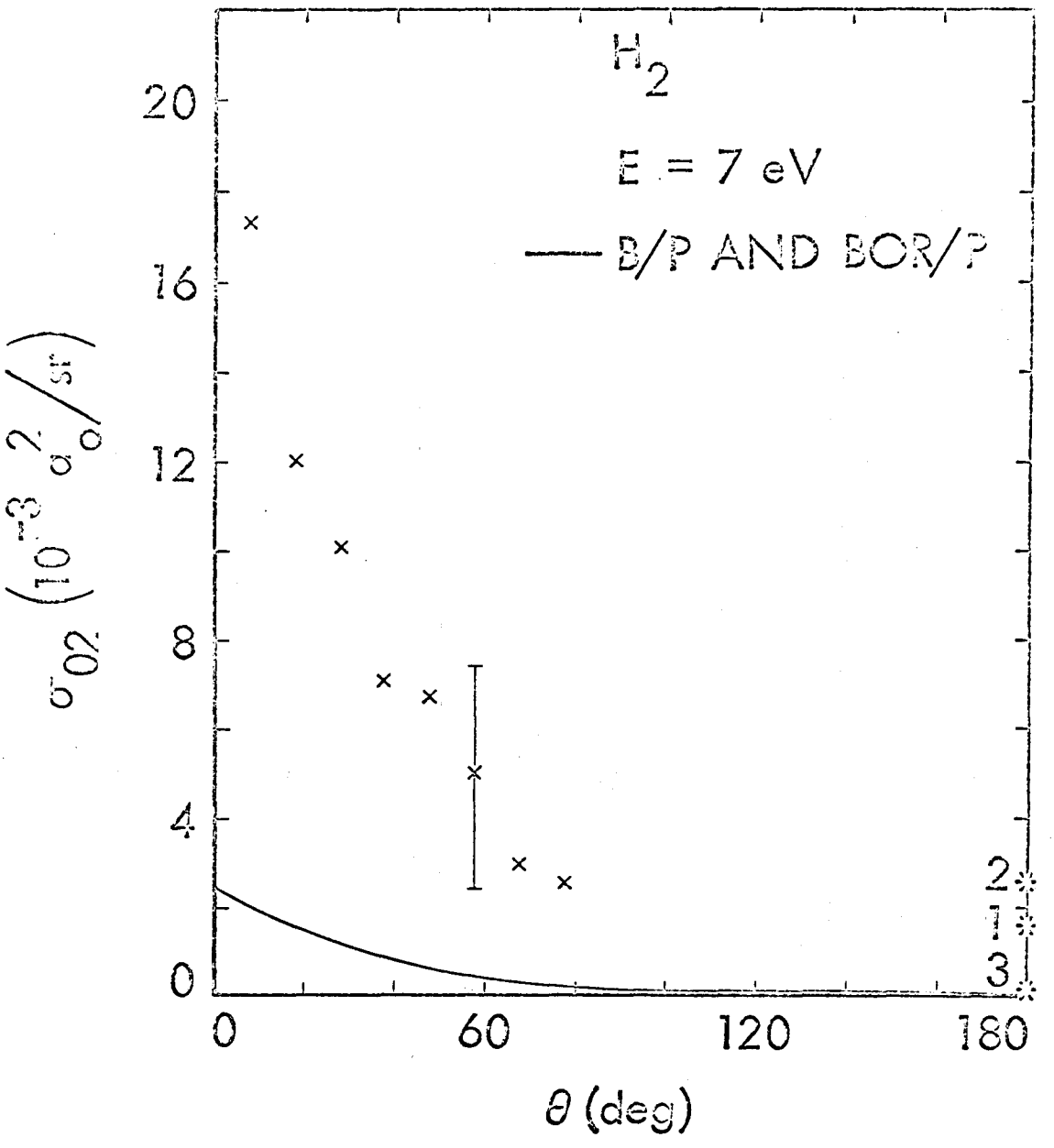
H_2
E = 7 eV
B/P AND BOR/P
$\sigma_{02}\ (10^{-3}\ a_o^2/sr)$
20
16
12
8
4
0
0
60
120
180
θ (deg)
2
1
3

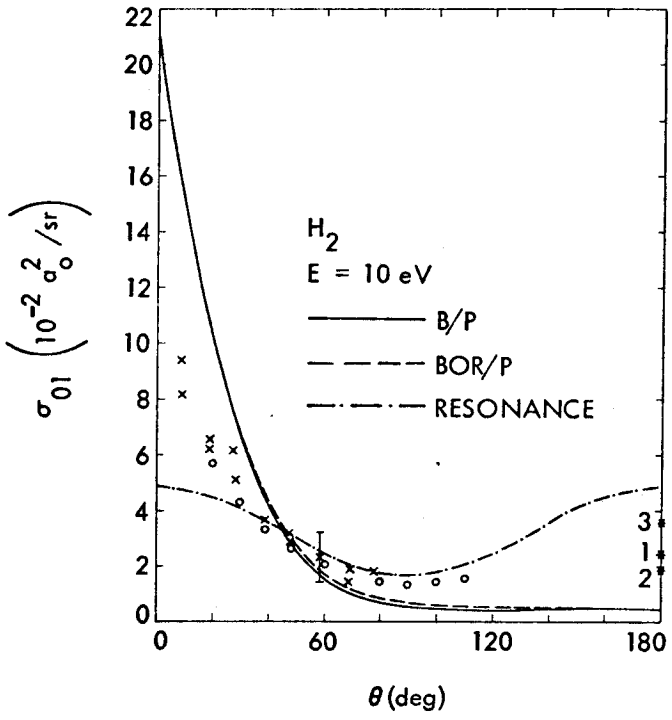
$\sigma_{01}\left(10^{-2}\,a_o^2/sr\right)$
22
20
18
16
14
12
10
8
6
4
2
0
0
60
120
180
θ (deg)
H_2
E = 10 eV
B/P
BOR/P
RESONANCE
3
1
2

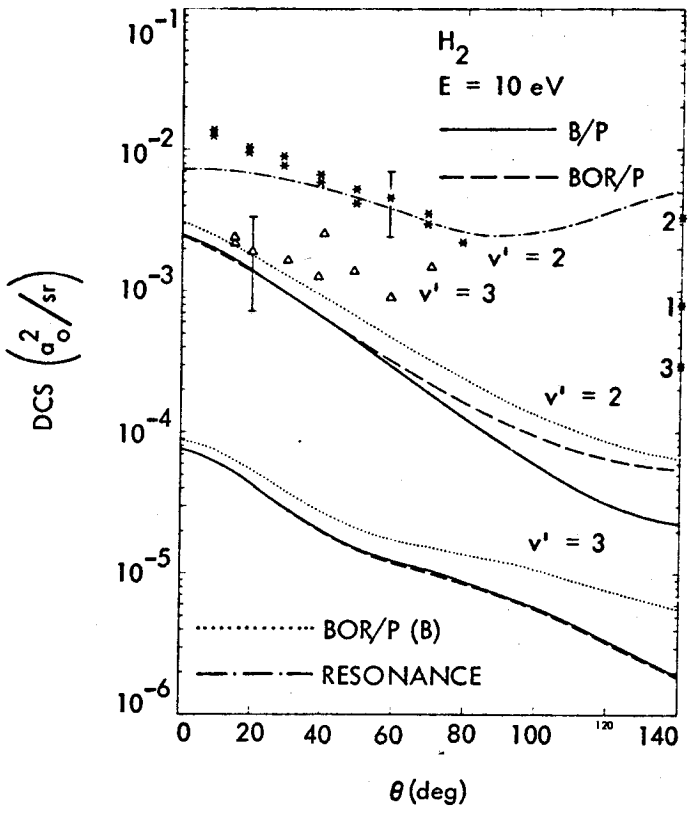
H_2
E = 10 eV
B/P
BOR/P
v' = 2
v' = 3
v' = 2
v' = 3
BOR/P (B)
RESONANCE
DCS $\left(a_o^2/sr\right)$
10^{-1}
10^{-2}
10^{-3}
10^{-4}
10^{-5}
10^{-6}
0
20
40
60
80
100
120
140
θ (deg)
2
1
3

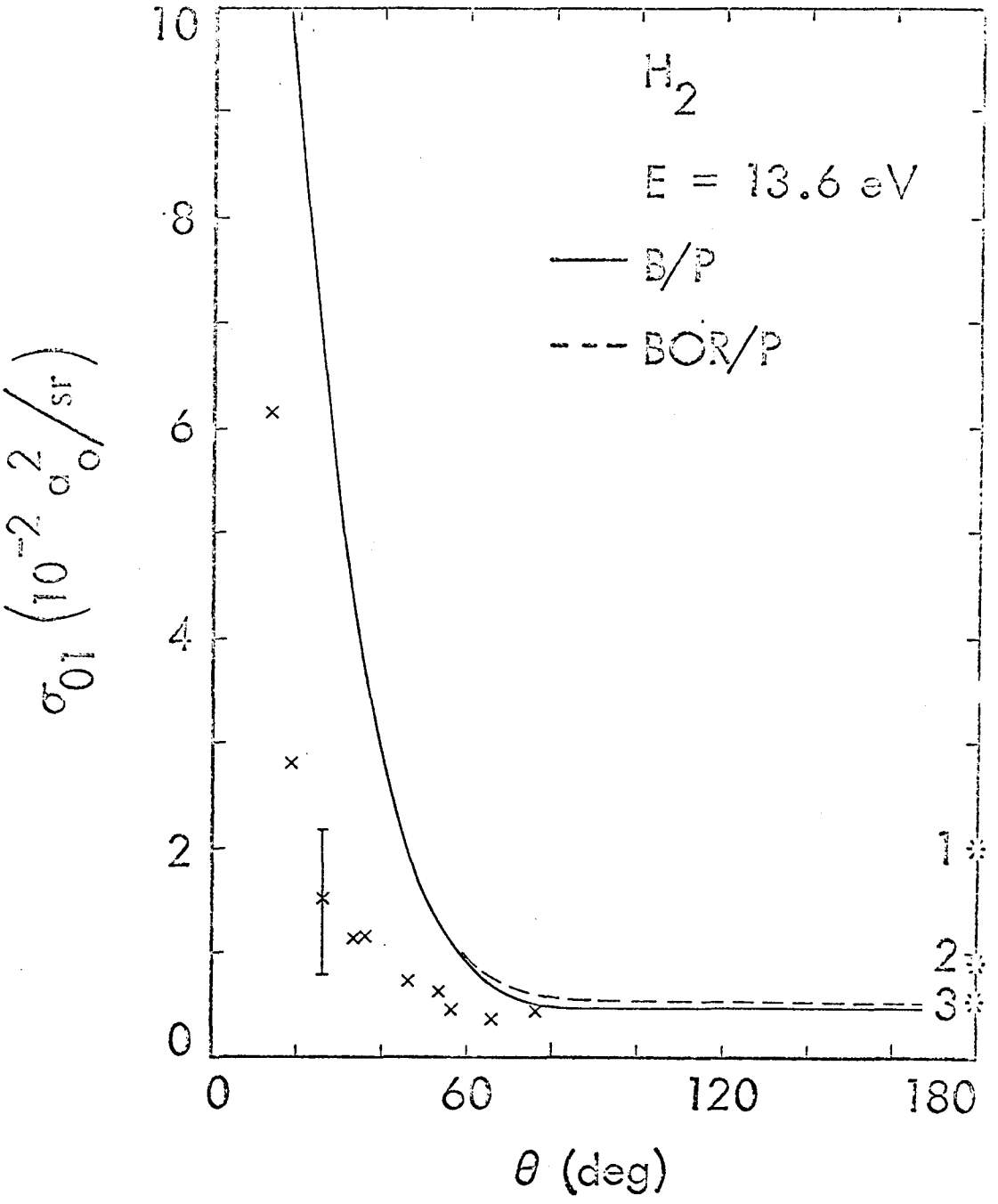
H_2
E = 13.6 eV
B/P
BOR/P
σ_{01} (10^{-2} a_o^2/sr)
θ (deg)
0
2
4
6
8
10
0
60
120
180
1
2
3

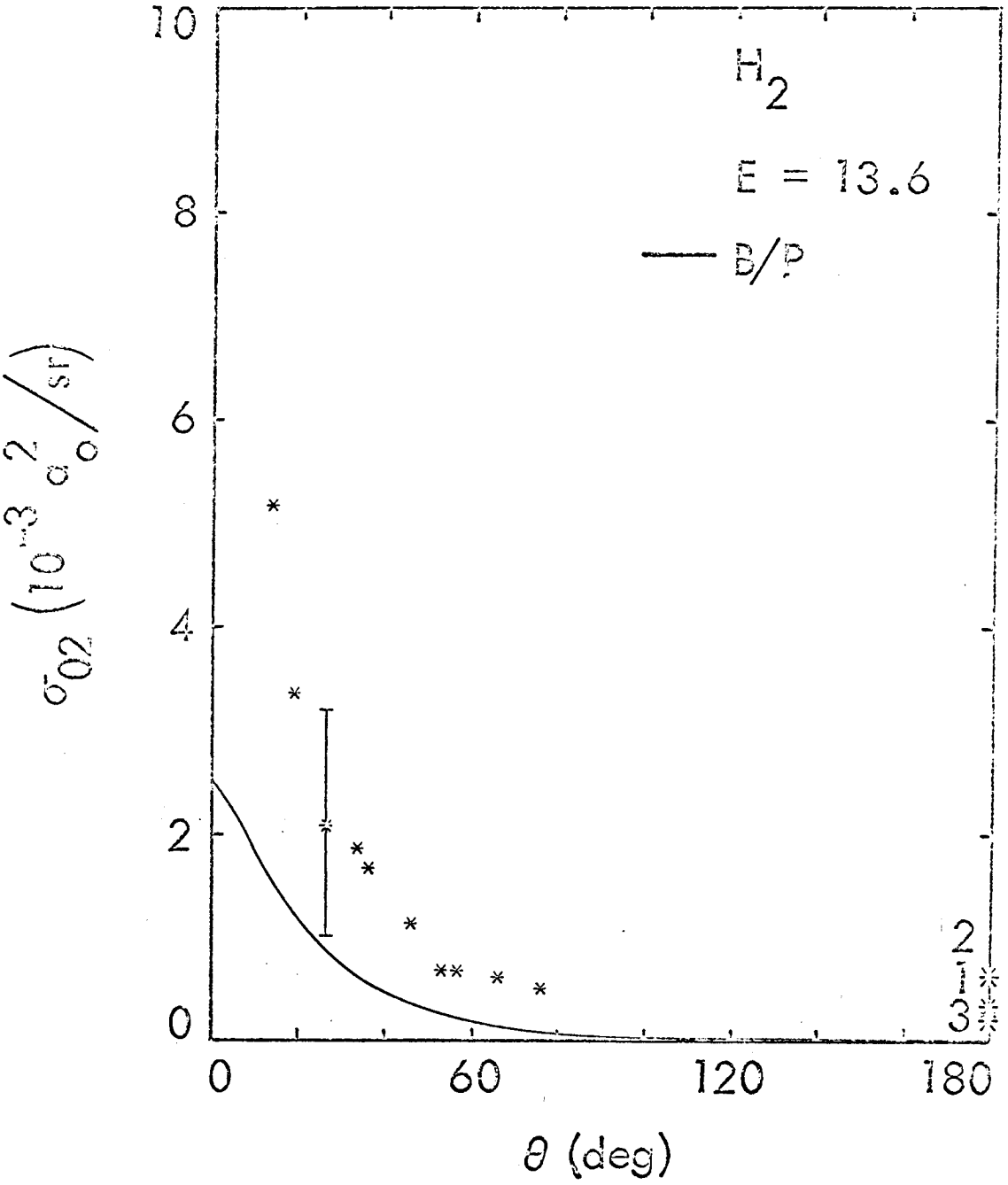
H_2
E = 13.6
B/P
$\sigma_{02}\left(10^{-3}\ a_o^2/sr\right)$
10
8
6
4
2
0
0
60
120
180
θ (deg)

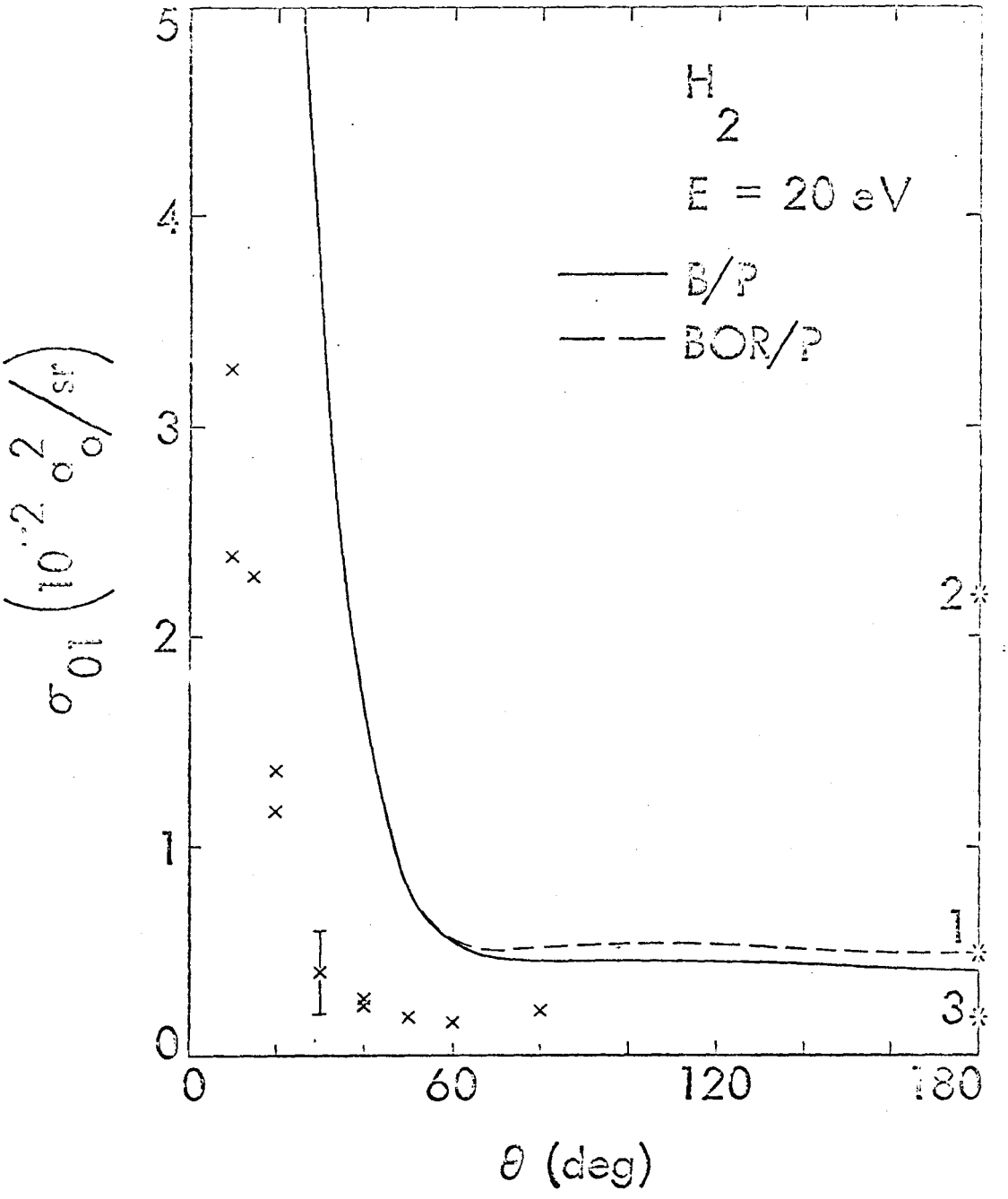
H
2
E = 20 eV
B/P
BOR/P
$\sigma_{01}\left(10^{-2}\ a_o^2/sr\right)$
ϑ (deg)
0
60
120
180
1
2
3
4
5

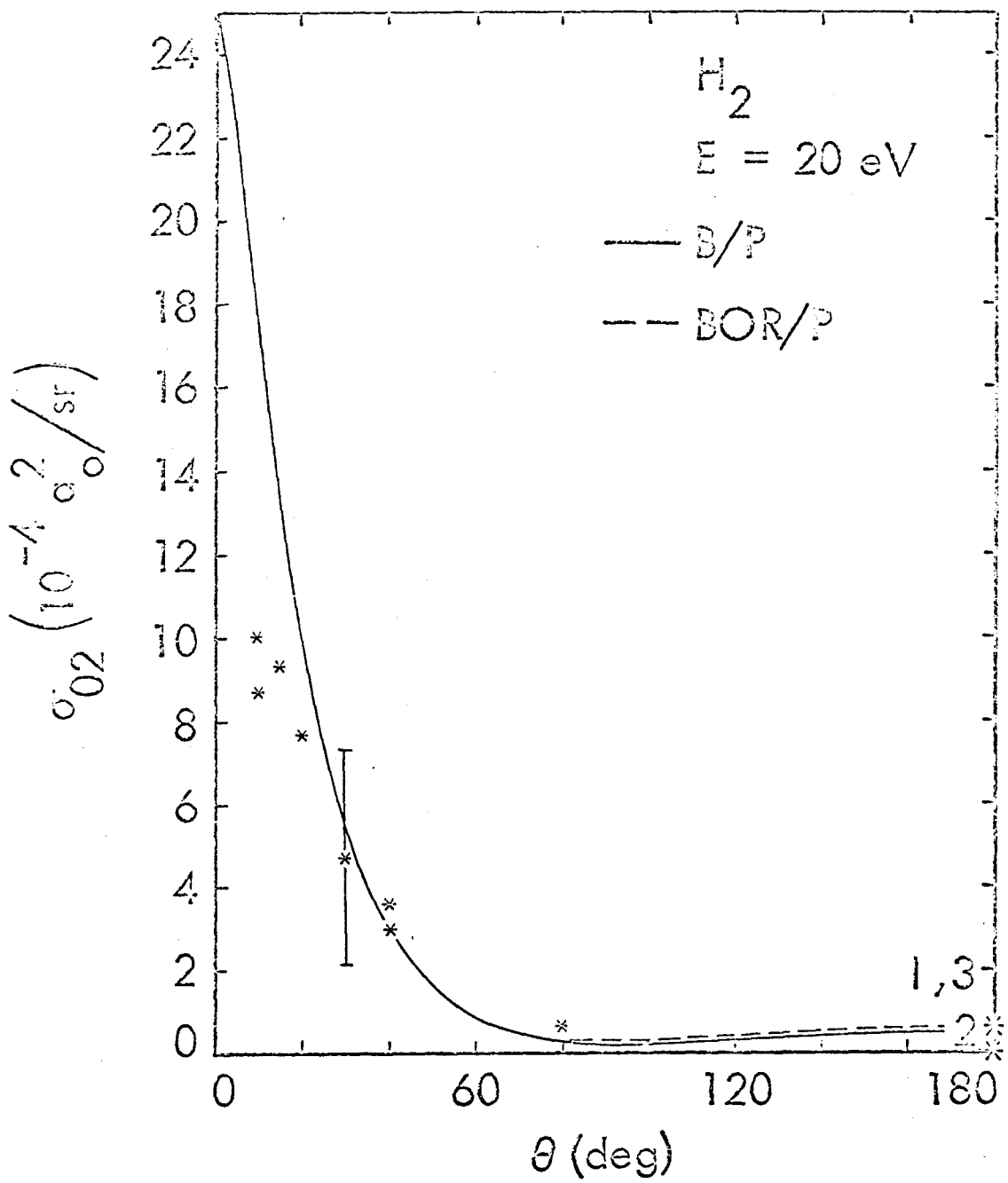
H_2
E = 20 eV
S/P
BOR/P
1,3
2
σ_{02} $(10^{-4}$ a$_o^2$/sr)
ϑ (deg)
0
60
120
180
0
2
4
6
8
10
12
14
16
18
20
22
24

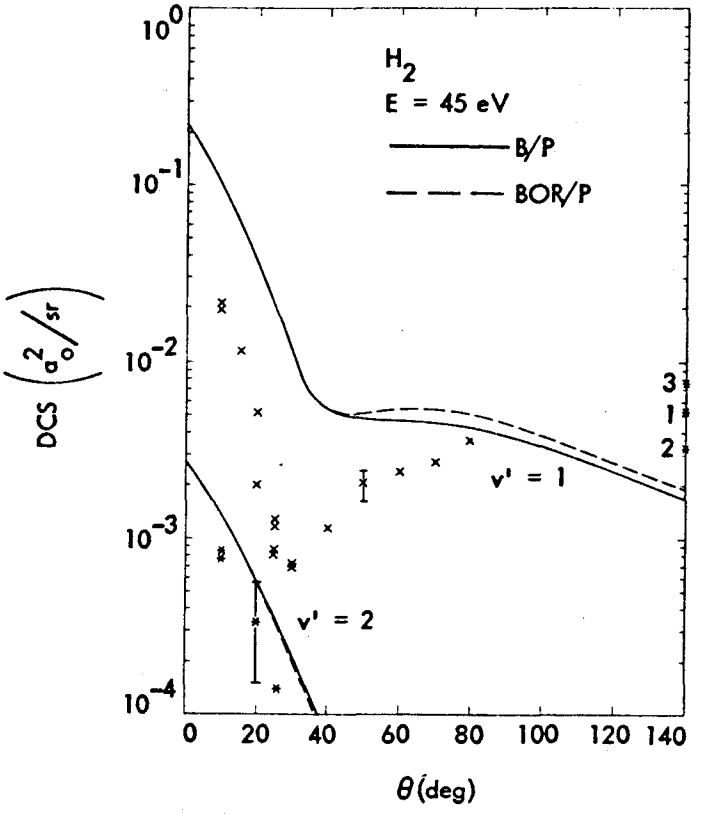
H_2
E = 45 eV
B/P
BOR/P
v' = 1
v' = 2
3
1
2
DCS $\left(a_o^2/sr\right)$
10^0
10^{-1}
10^{-2}
10^{-3}
10^{-4}
0
20
40
60
80
100
120
140
θ(deg)

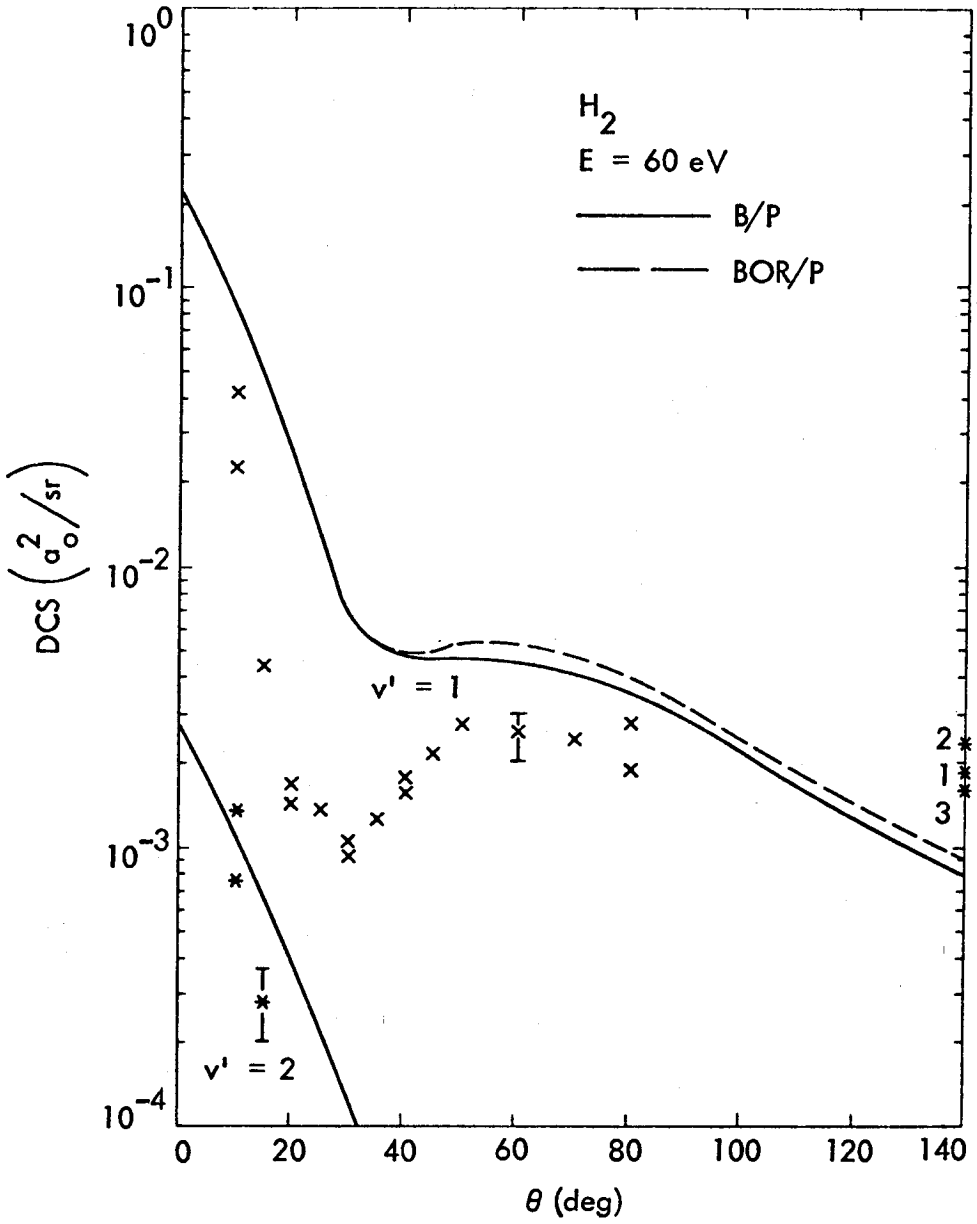
H_2
E = 60 eV
B/P
BOR/P
v' = 1
v' = 2
2
1
3
DCS $\left(a_o^2/sr\right)$
10^0
10^{-1}
10^{-2}
10^{-3}
10^{-4}
0
20
40
60
80
100
120
140
θ (deg)

20

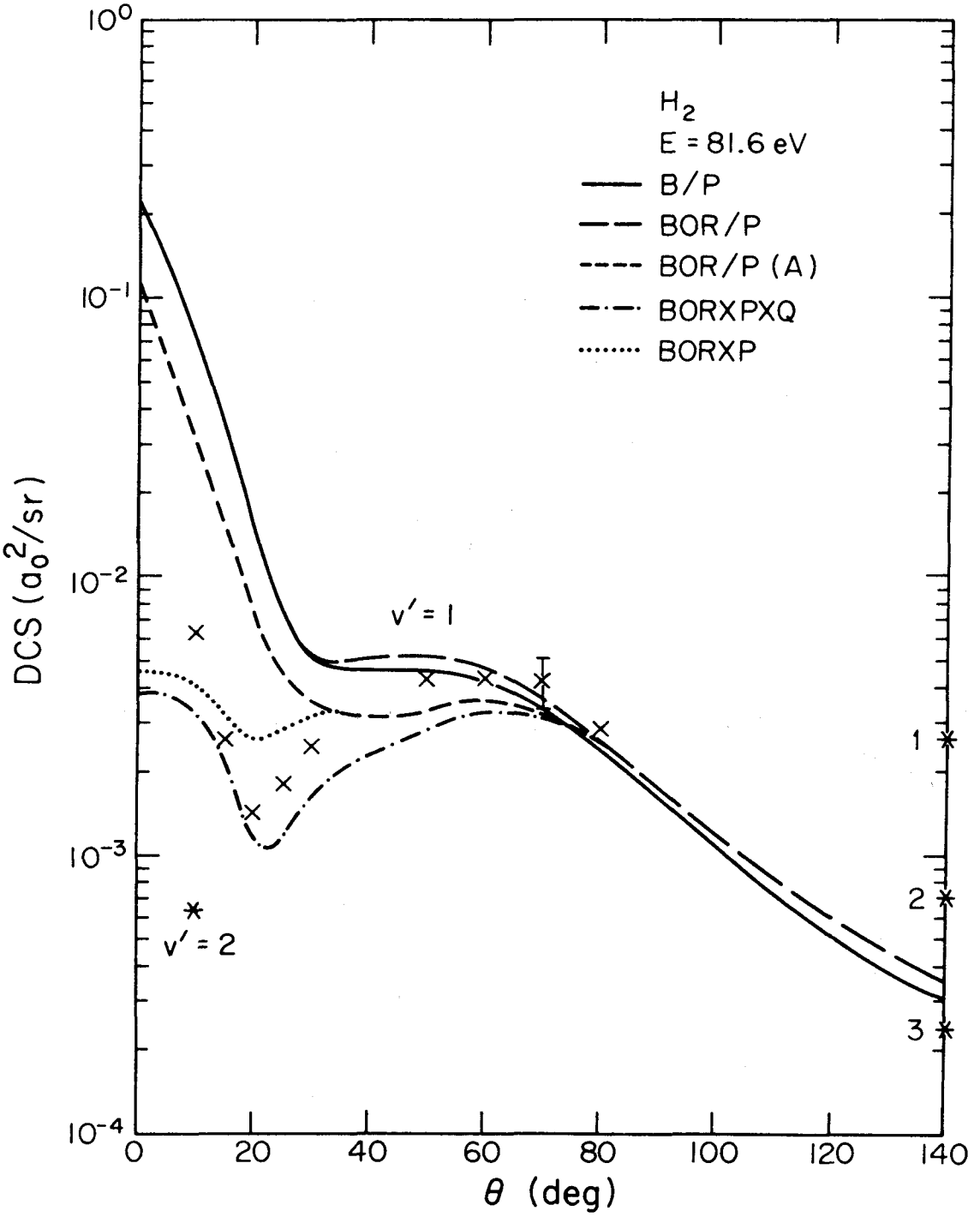
10^0
10^{-1}
10^{-2}
10^{-3}
10^{-4}
DCS (a_0^2/sr)
H_2
E = 81.6 eV
B/P
BOR/P
BOR/P (A)
BORXPXQ
BORXP
v′ = 1
v′ = 2
1
2
3
0
20
40
60
80
100
120
140
θ (deg)

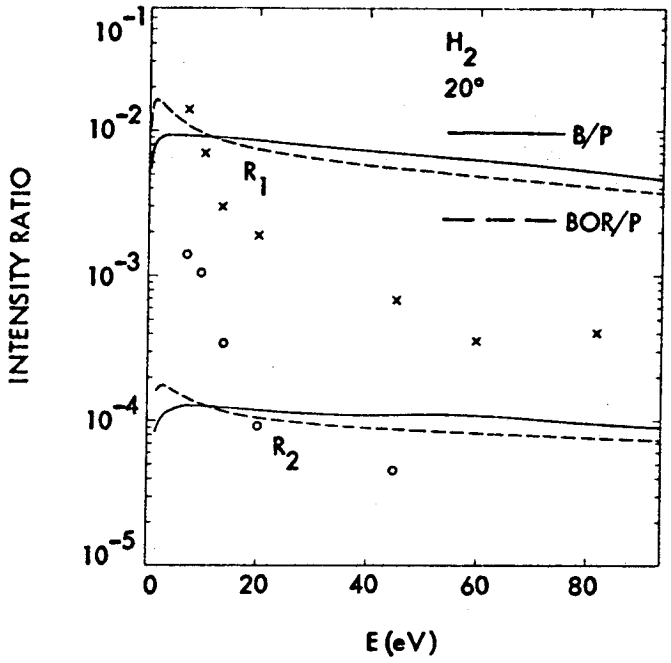
10^{-1}
10^{-2}
10^{-3}
10^{-4}
10^{-5}
INTENSITY RATIO
H_2
20°
B/P
BOR/P
R_1
R_2
0
20
40
60
80
E (eV)

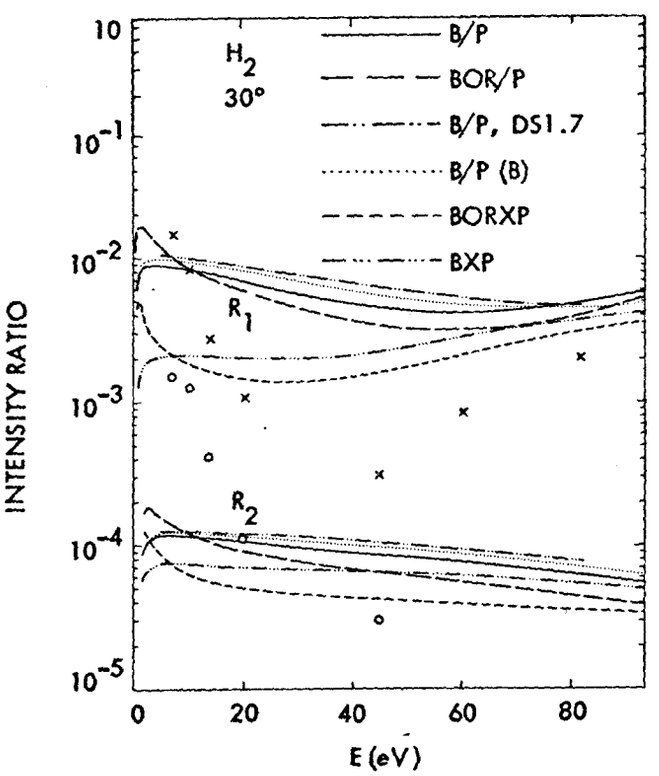
10
10^{-1}
10^{-2}
10^{-3}
10^{-4}
10^{-5}
INTENSITY RATIO
H_2
30°
B/P
BOR/P
B/P, DS1.7
B/P (B)
BORXP
BXP
R_1
R_2
0
20
40
60
80
E (eV)

23

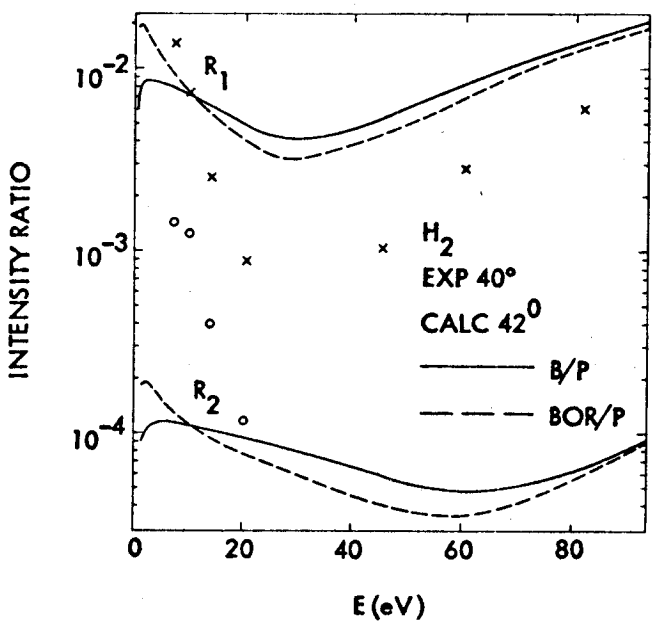
INTENSITY RATIO
10^{-2}
10^{-3}
10^{-4}
R_1
R_2
H_2
EXP 40°
CALC 42°
B/P
BOR/P
0
20
40
60
80
E (eV)

24

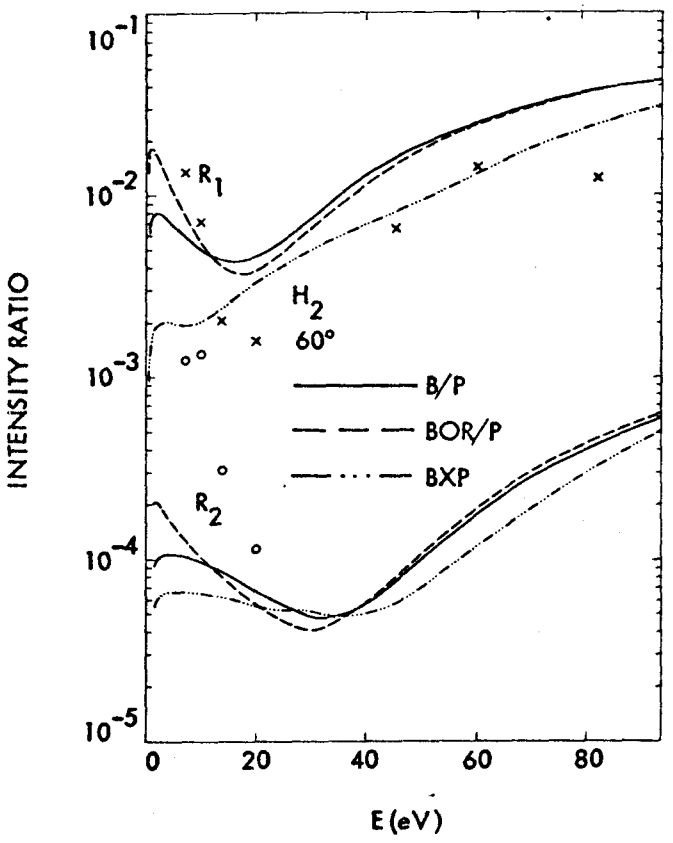
INTENSITY RATIO
10^{-1}
10^{-2}
10^{-3}
10^{-4}
10^{-5}
R_1
R_2
H_2
60°
B/P
BOR/P
BXP
0
20
40
60
80
E(eV)

25

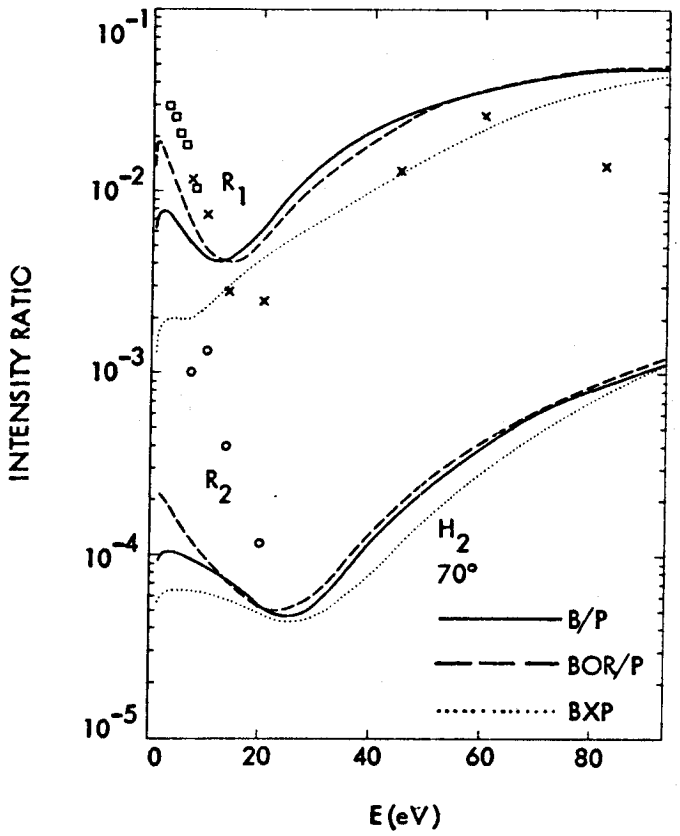
INTENSITY RATIO
10^{-1}
10^{-2}
10^{-3}
10^{-4}
10^{-5}
R_1
R_2
H_2
70°
B/P
BOR/P
BXP
0
20
40
60
80
E(eV)

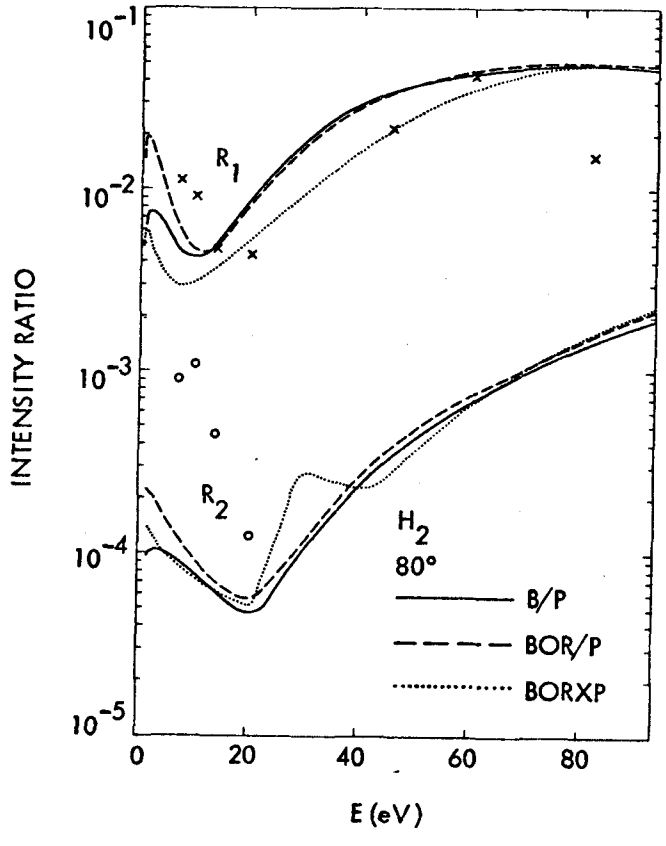
INTENSITY RATIO
10^{-1}
10^{-2}
10^{-3}
10^{-4}
10^{-5}
R_1
R_2
H_2
80°
B/P
BOR/P
BORXP
0
20
40
60
80
E (eV)

27

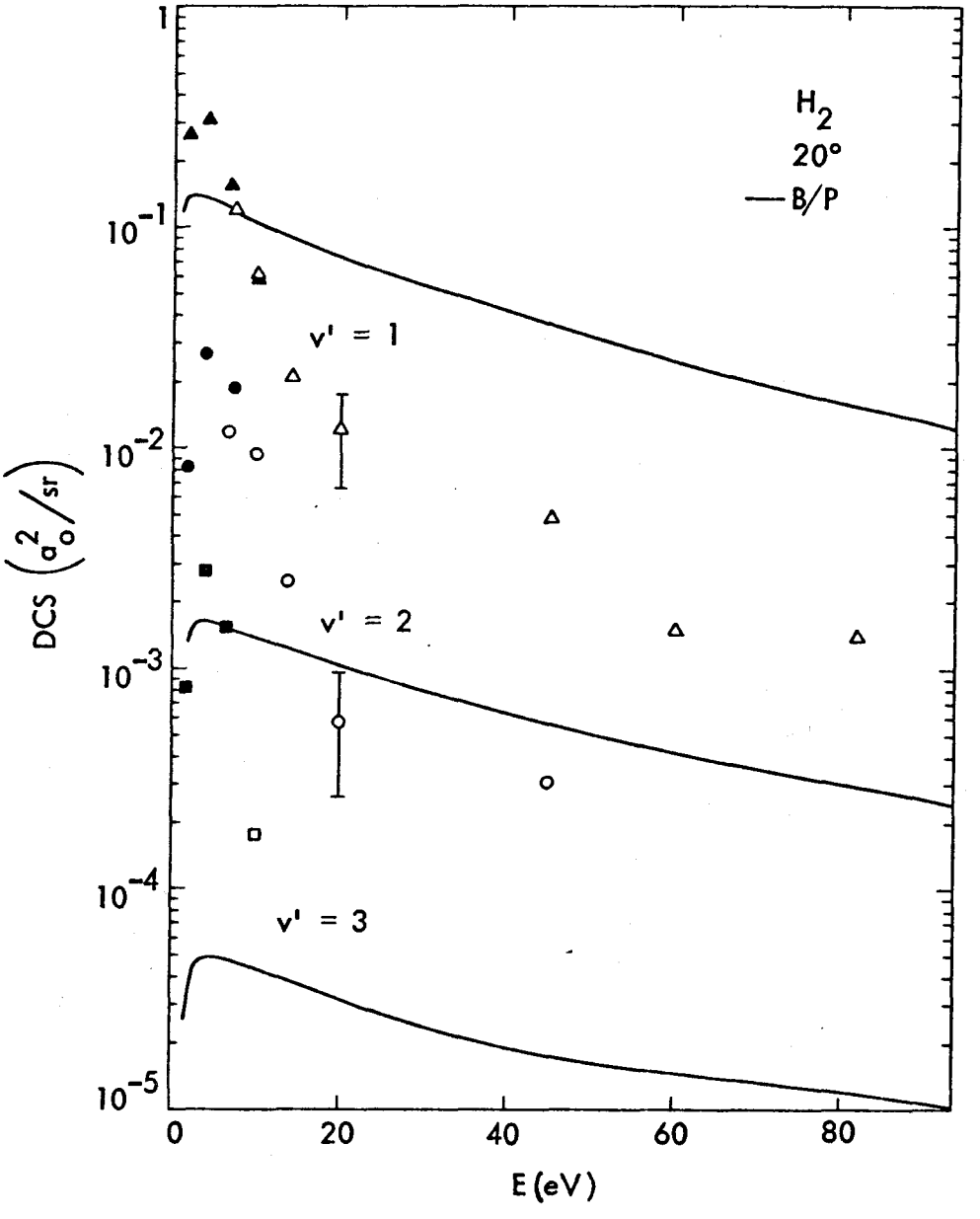

28

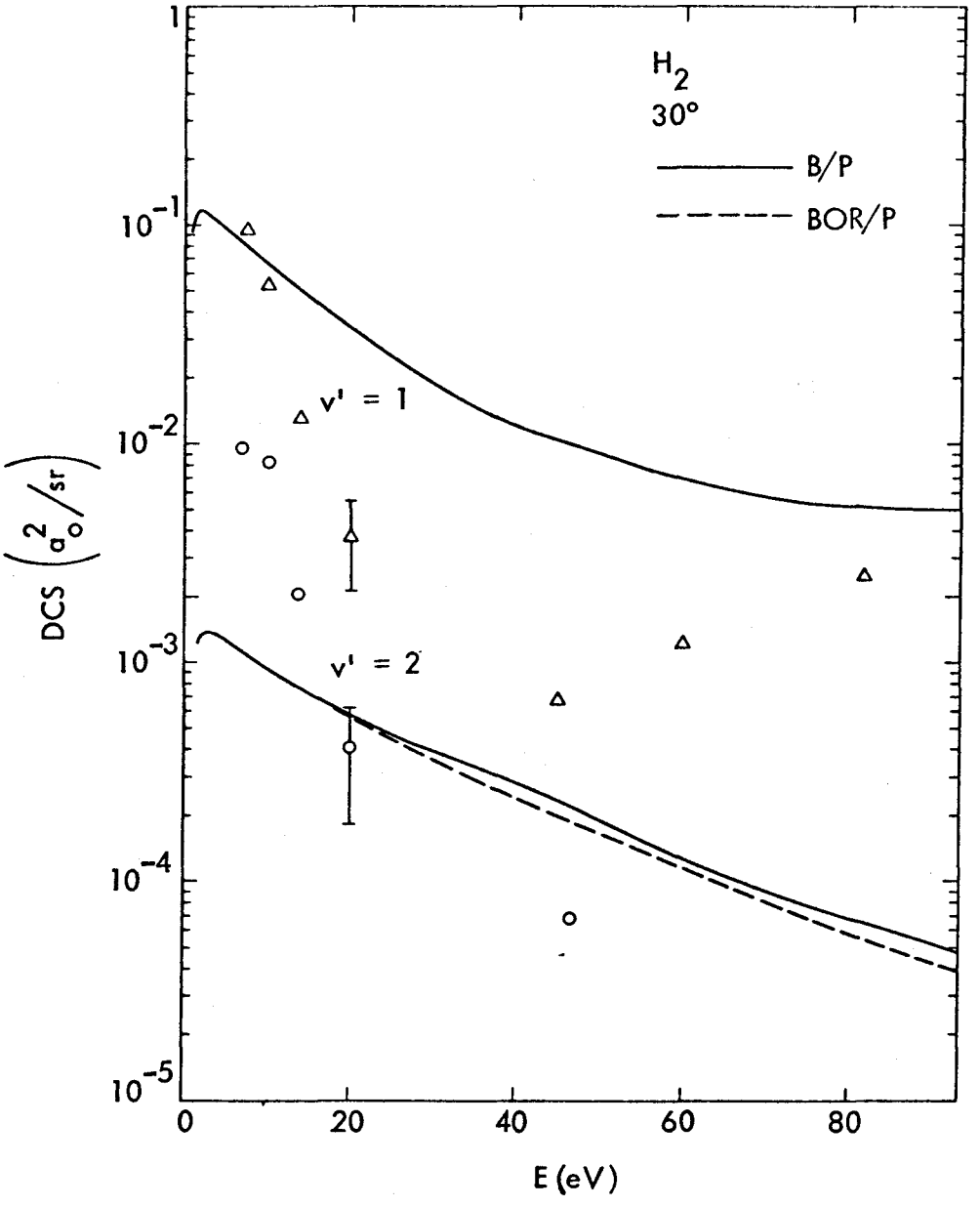
H2
30°
B/P
BOR/P
v' = 1
v' = 2
DCS (a0²/sr)
E (eV)
1
10⁻¹
10⁻²
10⁻³
10⁻⁴
10⁻⁵
0
20
40
60
80

29

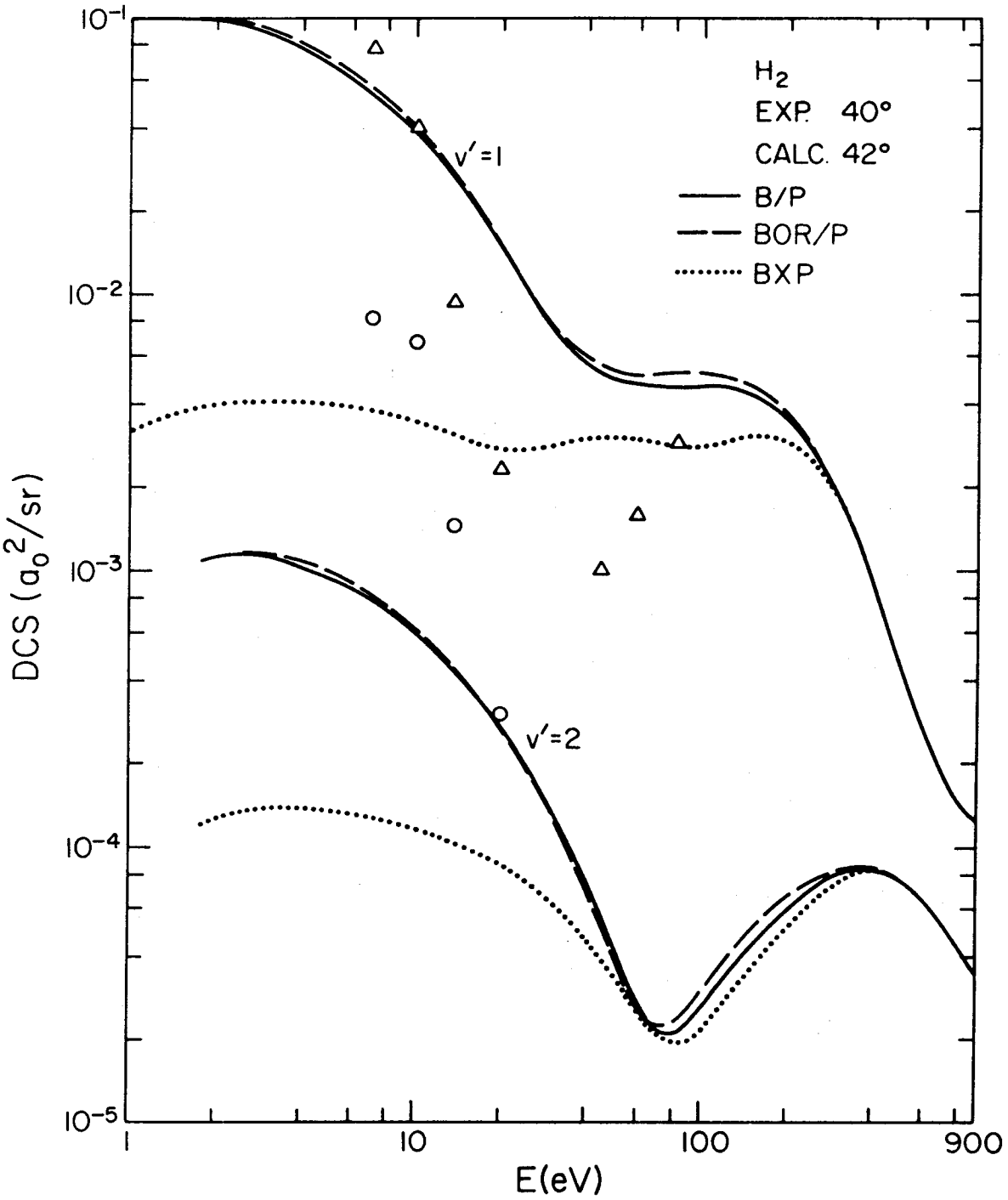
10^{-1}
10^{-2}
10^{-3}
10^{-4}
10^{-5}
DCS (a_0^2/sr)
1
10
100
900
E(eV)
H_2
EXP. 40°
CALC. 42°
B/P
BOR/P
BXP
v′=1
v′=2

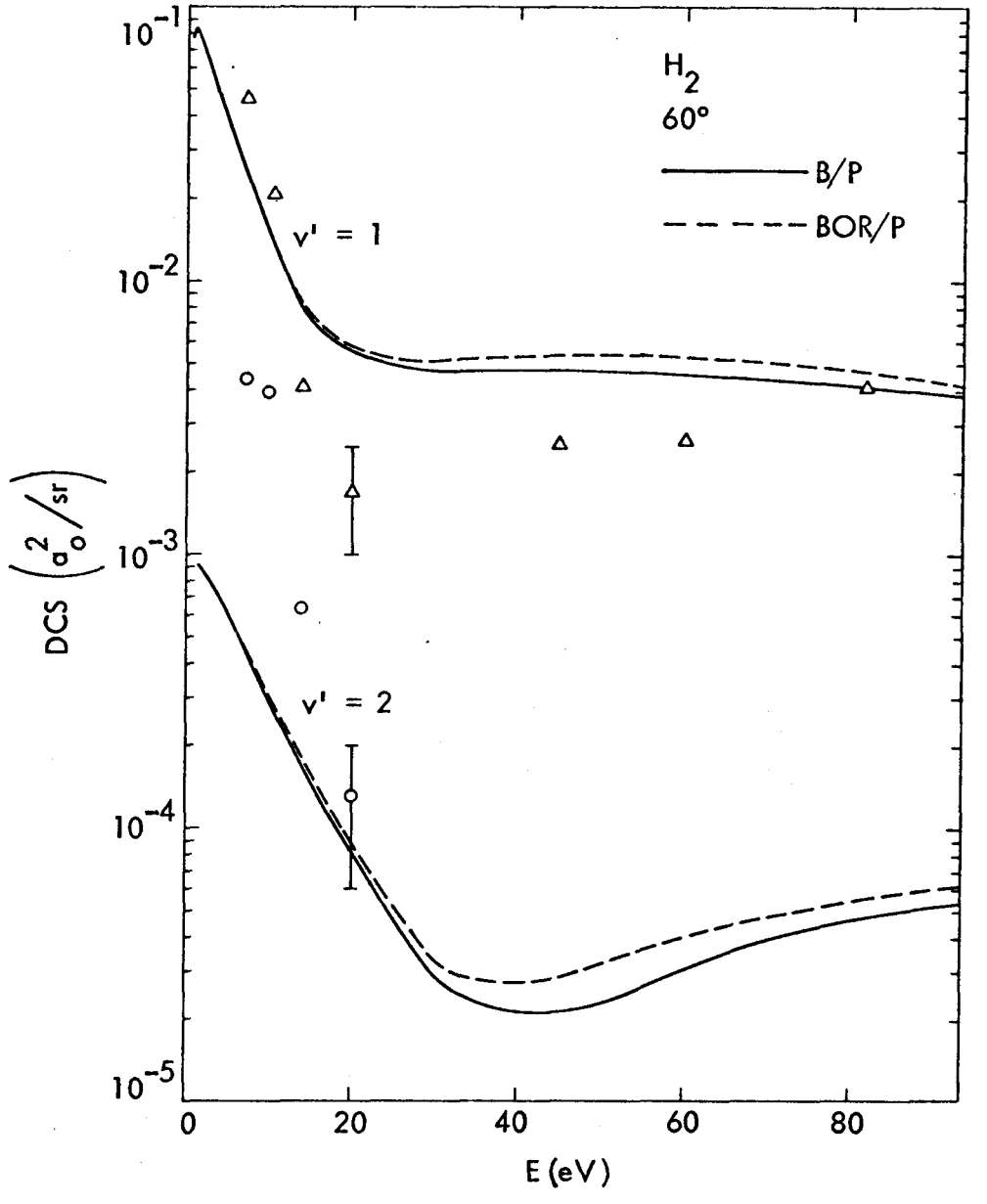
10^{-1}
10^{-2}
10^{-3}
10^{-4}
10^{-5}
DCS $\left(a_o^2/sr\right)$
H_2
60°
B/P
BOR/P
v' = 1
v' = 2
0
20
40
60
80
E (eV)

31

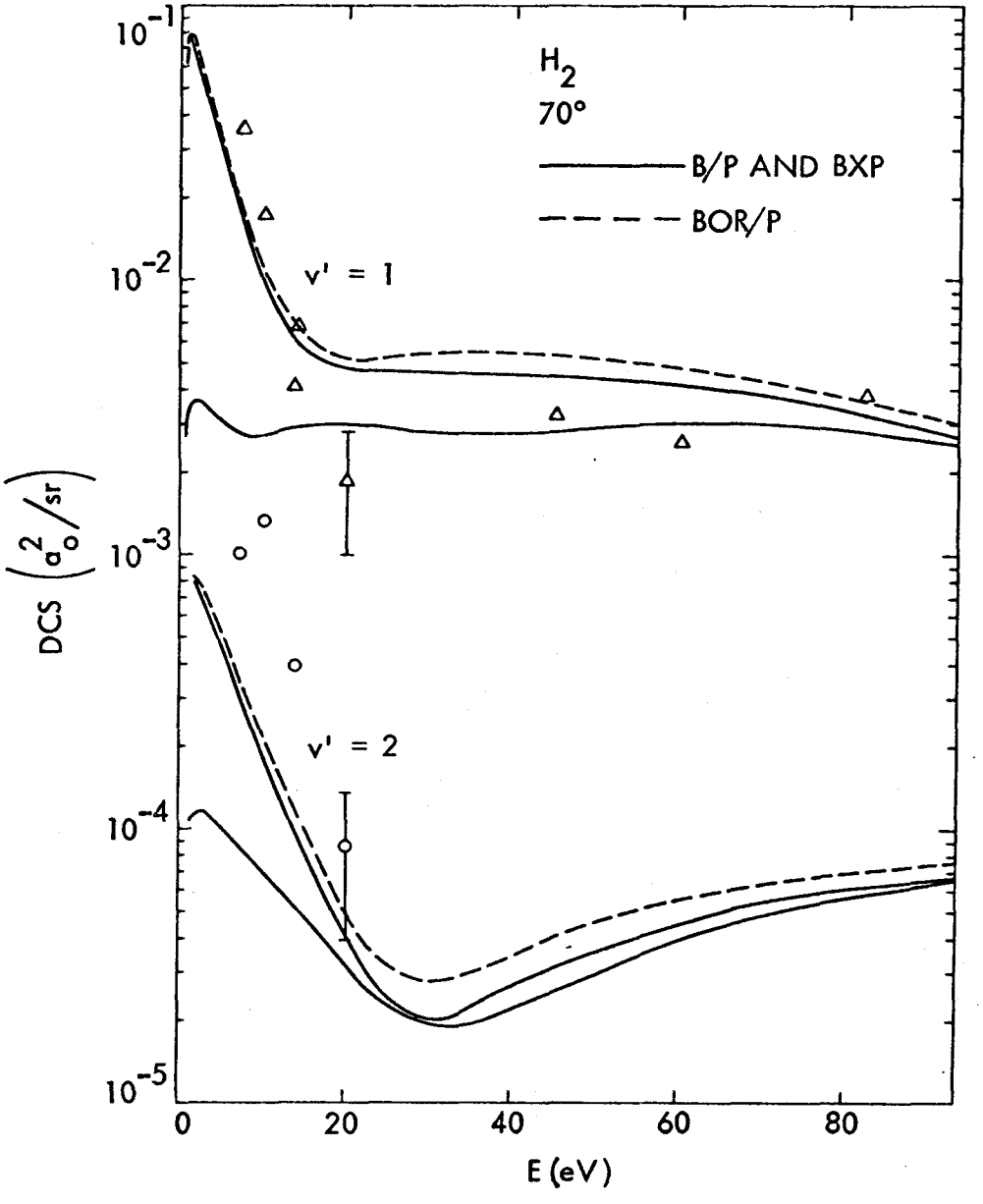
H_2
70°
B/P AND BXP
BOR/P
v' = 1
v' = 2
DCS $\left(a_o^2/sr\right)$
10^{-1}
10^{-2}
10^{-3}
10^{-4}
10^{-5}
0
20
40
60
80
E (eV)

32

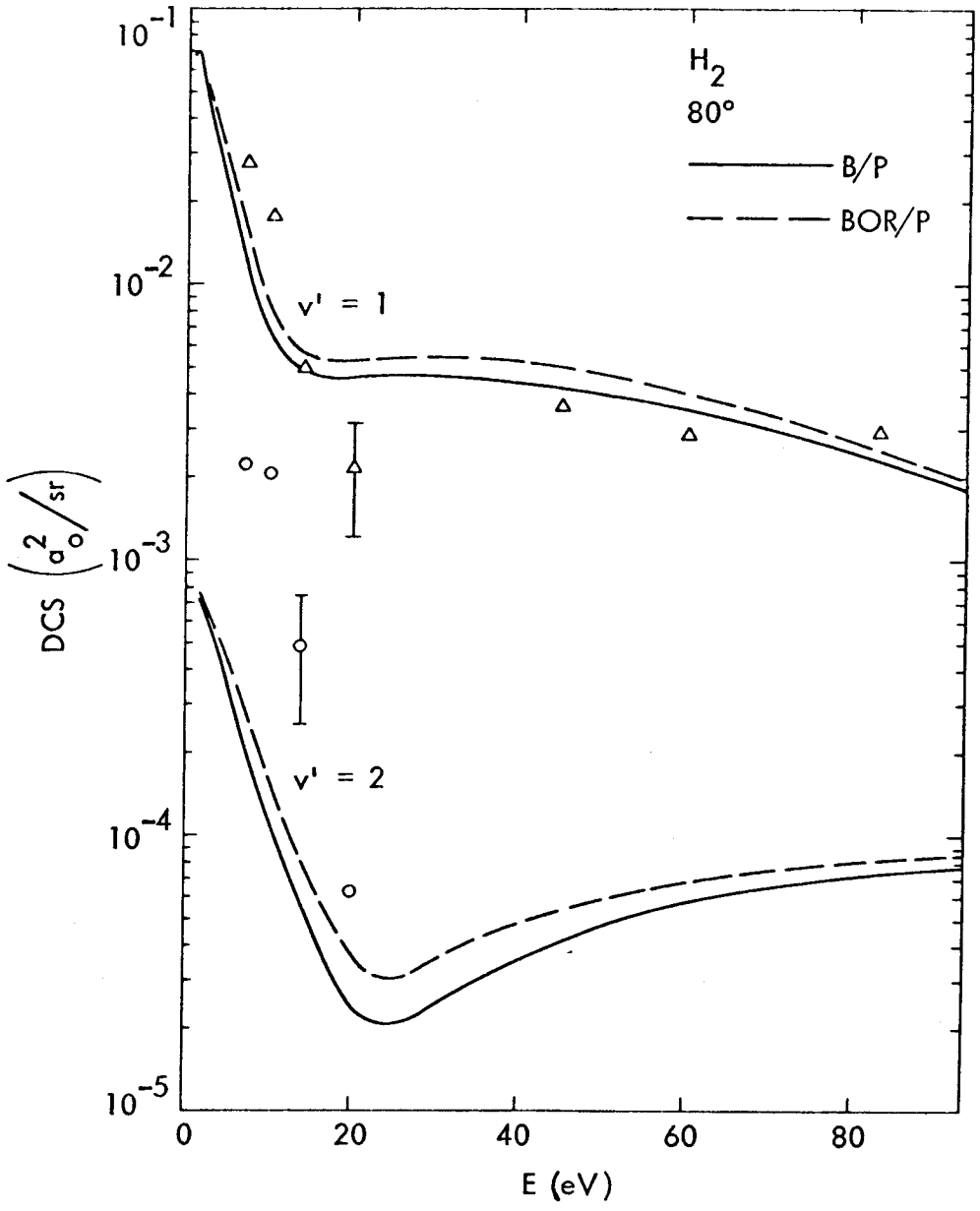
10^{-1}
10^{-2}
10^{-3}
10^{-4}
10^{-5}
DCS $\left(a_o^2/sr\right)$
H_2
80°
B/P
BOR/P
v' = 1
v' = 2
0
20
40
60
80
E (eV)

33

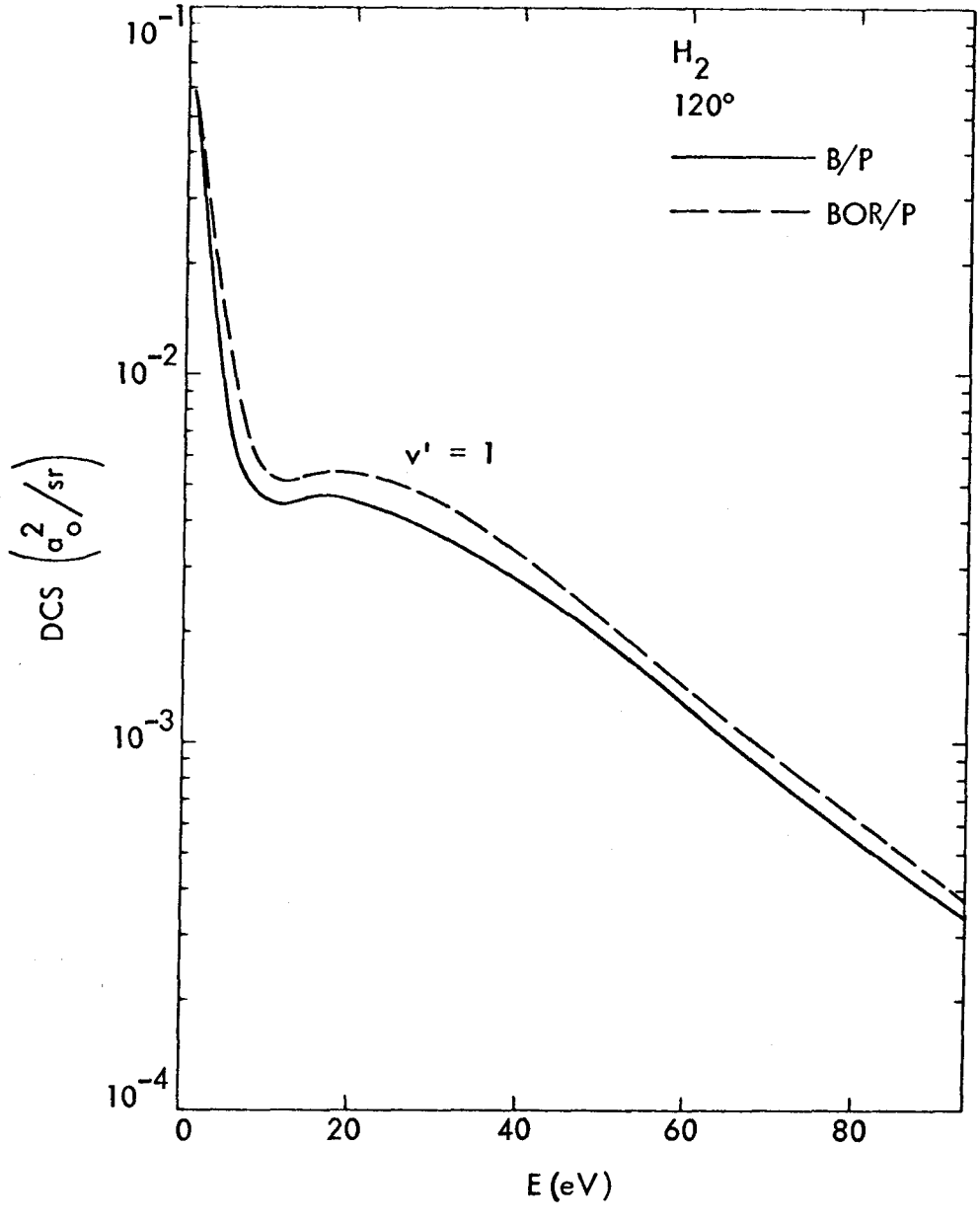
H_2
120°
B/P
BOR/P
v' = 1
DCS $\left(a_o^2/sr\right)$
10^{-1}
10^{-2}
10^{-3}
10^{-4}
0
20
40
60
80
E (eV)

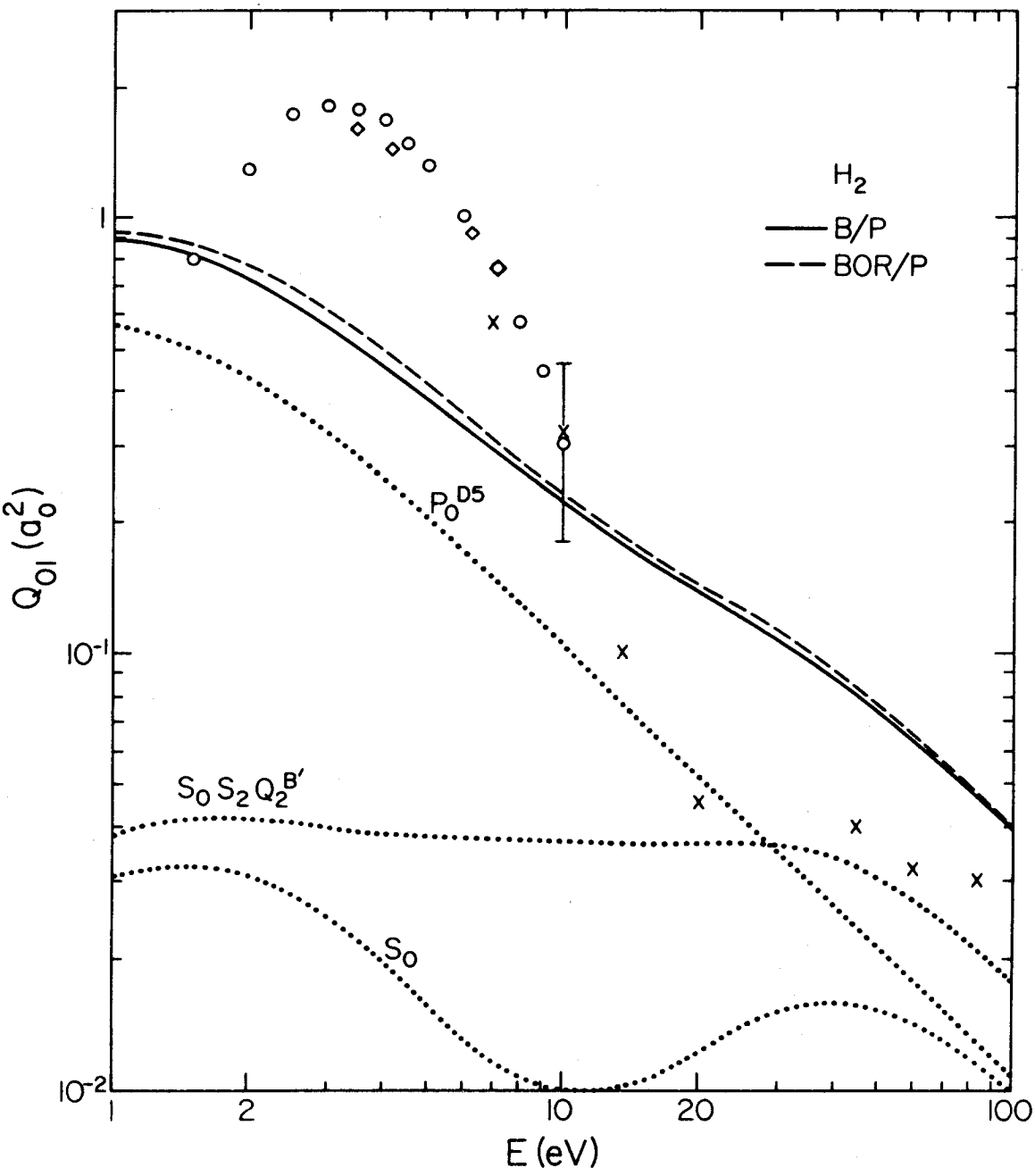
H2
B/P
BOR/P
P0 D5
S0 S2 Q2 B'
S0
Q01 (a0^2)
E (eV)
1
10^-1
10^-2
1
2
10
20
100

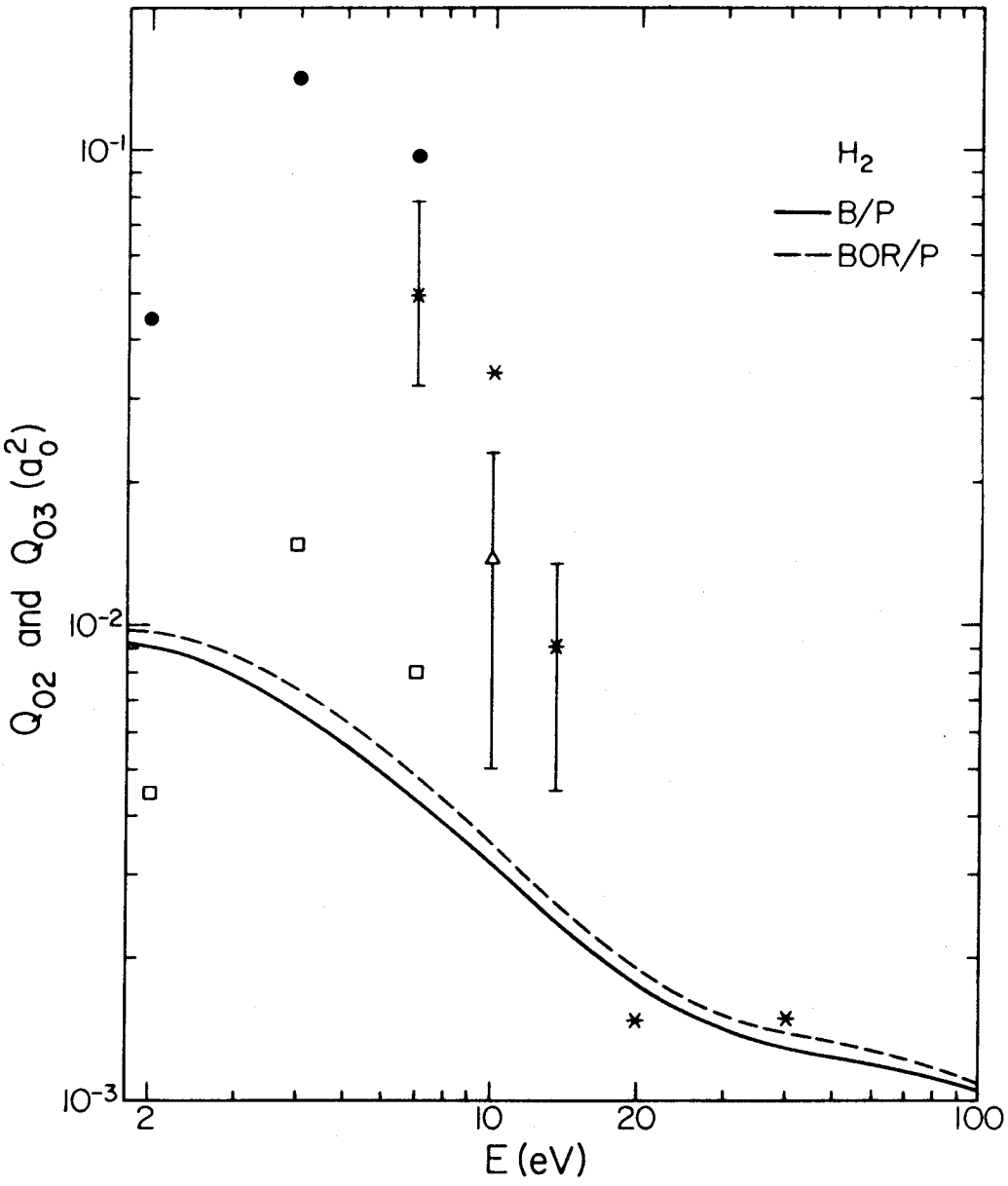
10^{-1}
10^{-2}
10^{-3}
Q_{02} and Q_{03} (a_o^2)
H_2
B/P
BOR/P
2
10
20
100
E (eV)

PROPOSITIONS

ABSTRACTS

I. The quantum mechanical statistical phase space theory of Pechukas, Light, and Nikitin is used to calculate the cross sections for the endothermic ion-molecule reaction $C^+ + D_2 \rightarrow CD^+ + D$ in the energy range 0-4 eV. The statistical theory threshold law is predicted to be valid only for a region less than 0.1 eV from threshold. Two different types of dependence of the reaction probability on incident impact parameter are distinguished and one is used to explain the magnitude of the predicted cross section in this case.

II. It is proposed to make an experimental search for infrared chemiluminescence in the 8,000-18,000 Å range in diffusion flames of alkali metals with methyl halides.

III. A variation-perturbation method is proposed to obtain approximate eigenvalues of oscillators with the potential energy function

$$V(x) = ax^4 + cx^2 .$$

Numerical results are presented showing that the analytic solution of a cubic equation can often yield energy differences between the levels accurate to better than 0.001%. The method is accurate for both high and low quantum numbers.

IV. It is shown that the singlet excited states of the water molecule cannot be adequately represented by an a priori calculation (no semiempirical elements) using a valence-like basis set of Slater orbitals. The implications for the applicability of simple molecular orbital theory of the type used by Mulliken, Walsh, and Pople is discussed briefly.

V. The method of Shuler and Zwanzig for calculating vibrational excitation in atom-molecule collisions with a hard sphere interaction potential is known to lead to numerically ill-conditioned equations. In many cases, this ill-conditioning prevents us from including enough vibrator eigenfunctions in the expansion of the scattering wave function for the solutions to converge. An alternative method of solving for the scattering wave function is proposed and tested. Suggestions for future work on this problem are given.

PROPOSITION I

INTRODUCTION

Recently Maier has measured the cross section curve (reaction cross section vs. initial translational energy E_i) for the hydrogen atom transfer reaction[1] $C^+ + D_2 \rightarrow CD^+ + D$. Because the initial states of the reactants are well known (the C^+ atoms are all in their ground state for these experiments,[2] but with some other experimental techniques the ionic reactants have a poorly characterized internal energy distribution), this presents an opportunity for an important test of the statistical phase space theory of reactions.[3] The comparison of a theoretical model with experiment for this reaction is important because of the doubt about how well translational energy can be used to cause reaction in such systems.[4,5] Further, Maier has shown[1] that, for the first 0.25 eV excess energy (excess energy E_{ex} is the excess translational energy above threshold, i.e., $E_i - E_{threshold}$), the cross section curve is approximately consistent with the statistical theory threshold law $\sigma \propto E_{ex}^{5/4}$ derived by Nikitin, Pechukas, and Light.[3,6] The experimental reaction cross sections fit this curve "only slightly less well" than a linear curve. It is interesting to test whether the statistical theory also predicts the correct magnitude for the cross section near threshold and whether it predicts the shape and/or magnitude of the cross section curve at higher energies.

Morrison has written, "One difficulty in assessing theoretical calculations of threshold behavior is the fact that it is seldom stated over how great an energy range the predicted laws are expected to hold."[7] We try to shed light on this difficulty here by using the complete statistical theory (from which the threshold law was derived) to calculate the cross section at a number of different energies just above threshold. This answers the question of how far the threshold law is predicted to hold.

REVIEW OF THRESHOLD LAWS[8,9,3]

One type of threshold law (how the reaction cross sections for endothermic processes depend on excess translational energy E_{ex}) is generally derived by assuming the kinematic factors in the initial state and the dynamic factors of the reaction vary slowly with incident energy in the threshold region for the new process. Then the critical factor becomes the ability of the products to separate (i. e., the amount of phase space in the final state). This depends on the long range nature of the interaction potential, in particular on any part of the potential which dies off as r^{-2} or slower. Thus the threshold behavior depends on the orbital angular momentum in the final state. Usually, at and just above the threshold the products must be formed in an s wave. For a two-body collision yielding two products with no r^{-2} or longer range interactions (e. g., an ion and a molecule whose long range potential energy dies off as r^{-4}), this gives the Wigner threshold law[8] $\sigma \propto E_{ex}^{1/2}$. Although this

quantum mechanical threshold law is sometimes useful for collisions involving free electrons in the final state, it holds in a region smaller than 0.01 eV for typical atomic and molecular processes. For these cases the masses are large enough that quantization of the final orbital angular momentum is not crucial for higher energies, and we want a classical threshold law.[9,3,10] This is obtained by summing over a set of final partial waves (or integrating over a set of final impact parameters). Since the upper limit of the sum depends on the long range force law for any range of potential, the threshold law depends on the exact nature of the potential. For the attractive r^{-4} potential of interest here, the classical threshold law is[3,6] $E_{ex}^{5/4}$.

This type of threshold law, which is derived on the basis of available phase space in the final channel, is not valid for reactions in which the threshold behavior is controlled by the change of reaction transition probabilities due to dynamic effects. Thus, for example, many neutral-neutral reactions have threshold behavior controlled by the tunneling through a potential energy barrier in a critical region of configuration space. For these reactions the assumption that dynamic factors are not changing rapidly with energy for energies near the threshold is incorrect. However, such barriers are not generally expected to play an important role in ion-molecule reactions, and, in particular, they do not appear to be important for $C^+ + D_2$. Thus the attempt to use the statistical phase space theory threshold law is justified in this case.

COMPUTATION

Calculations were carried out using the quantum mechanical statistical theory formulas[3, 11] and a modification of programs developed earlier.[12] The vibrational energy levels were calculated from D_e, ω_e, and the Morse potential model as in Ref. 12. The nuclear spin degeneracy factors for odd and even rotational levels were included properly. The long range potential is the r^{-4} polarization potential due to the interaction of the charge and the induced dipole. The r^{-3} charge-quadrupole interaction is much smaller for these reactants and products and was neglected.[13] The data necessary for the calculations (except for the masses) are shown in Table I. The data for CD^+ ($^1\Sigma^+$) were chosen so that the reaction is 0.4 eV endothermic[1] for reactants without internal excitation. The data for CD^+ ($^3\Pi$) are also uncertain and were estimated from the calculations of Moore, Browne, and Matsen.[14] The program provides an automatic check in the entrance and exit channels on the requirements[12] imposed on the orbital angular momentum limits ($L_{i_{max}}$, $L_{f_{max}}$) by the gas kinetic cross sections. However, no corrections to L_{max} were required in the present case.

Table II gives the arrangement numbers (used for subscripts) and state degeneracy factors for the three arrangement channels. The degeneracy of a particular vibrational-rotational state (with rotational angular momentum $M_f\hbar$) is taken as $(2M_f + 1)g$ where g accounts for electronic and nuclear spin degeneracies and electronic orbital degeneracy.

In judging the possible validity of a statistical approach it may be of interest to know how many quantum states are involved. Thus Table III lists the maximum values for $N(E_T, K\ K_z)$[11] which occurred in a sample group of calculations. $N(E_T, K, K_z)$ is the number of quantum states which can be formed upon decomposition of a strongly coupled compound system of total energy E_T and total angular momentum $K\hbar$. This table also explains why computing times rise as E_T rises.

The phase space program was written in FORTRAN IV and run on the IBM 7094. The average execution time per cross section (over the whole energy range) was less than 20 seconds. This was achieved by saving intermediate results for $n(f, E_T, K, K_z)$, in the notation of Ref. 12, and using them without recomputation when they reappeared in subsequent partial waves. In some of the runs only every third partial wave was computed and the others were obtained by interpolation. In every case this caused errors of much less than one per cent.

RESULTS AND DISCUSSION

The dependence of the reaction cross section on initial rotational energy was examined and found to be small. Table IV shows some results at $E_i = 0.7$ eV (at this energy, the electronically excited state of CD^+ is not accessible). The reaction cross section σ_F, the per cent of vibrational excitation in the product ($PCVE_F$), and the quantum number of the highest rotational state of the product that is

formed ($M_{f_{max}}$) are predicted to be insensitive to the quantum number of the initial rotational state (M_i). The table also shows the results when all partial cross sections are averaged over a Boltzmann distribution of rotational states at 300° K (room temperature conditions corresponding to Maier's experiment[1]). This result agrees closely with the result for $M_i = 2$, the most highly populated state of D_2 at this temperature. Thus in the rest of the article we will consider only reactions from the $M_i = 2$ state of D_2.

Figure 1 shows the results of the calculation for the reaction cross section curve. This general agreement in size and shape of this curve with Maier's experimental curve is very good. Neglecting a possible systematic error in the collection efficiencies of product ions, one can estimate from Maier's discussions[15] experimental error limits of about 60% for the absolute calibration and 15% for the shape. Then the present calculations are within experimental error except for the shape above 2 eV (discussed below). The fact that collection efficiencies of secondary ions are not unity is expected[11] to make the experimental reaction cross section too small at higher energies. Since the statistical theory almost always predicts reaction cross sections that are too large,[16] the close agreement of experiment with the present calculation may indicate that this is not a great source of error for this case (the error is expected to be small when the product ion is heavy compared to the product neutral, as in the present reaction).

The energy of the lowest excited electronic state of CH^+ is in doubt and the value used here (taken from the calculations of Moore,

Browne, and Matsen[14]) may be in error by as much as an eV. In addition to the full calculation, Fig. 1 shows the result of omitting this electronic state from the calculation. The resulting curve is then in better agreement for both magnitude and shape. The plateau in this second calculation is due to two competing factors. The total capture cross section is decreasing with increasing E_i but the fraction of captures leading to CD^+ is rising because of the availability of new channels. The improved agreement of theory and experiment when the triplet state is omitted has at least three possible interpretations: (1) the excitation energy of the $^3\Pi$ electronically excited state may be higher than the estimate used here; (2) the excited state may be energetically accessible in this region with the statistical theory overestimating the magnitude of the cross section for its production; (3) other errors in the statistical theory treatment may have canceling effects so that the improved agreement of theory and experiment when production of $^3\Pi$ CD^+ above 1.4 eV is omitted is not meaningful. Resolution of these possibilities will require further experimental and/or theoretical work.

The statistical theory predicts that the reaction cross section rises rapidly from threshold and that there is no "delayed onset." This behavior is expected for ion-molecule reactions in general because the strong attraction between the charge of the ion and the induced dipole in the neutral should dominate over any small repulsive forces so that there are no small electronic energy barriers to reaction (exceptions occur in special cases where curve crossing is important). This contrasts a typical behavior for neutrals.[17] This

expectation is built into the statistical theory used here[3] in the criterion for whether a collision with certain parameters can form a strong coupling complex. Thus the prediction is not surprising and is not new. The agreement with experiment for the shape of the cross section curve in this whole region is some evidence that the prediction is correct. This fast rising of the cross section curve had to be assumed by Maier in interpreting his data (but the assumption did not affect the shape of the curve).

The statistical theory predicts that the threshold law energy dependence $E_{ex}^{5/4}$ is valid for less than a tenth of an eV above threshold. This is because one of the conditions for the threshold law to hold (as pointed out by Pechukas and Light[3]) is that $L_{f\,max} \ll L_{i\,max}$ [$L_{i\,max}$ ($L_{f\,max}$) is the highest orbital angular momentum (in units of $\hbar$) of relative motion in the incident (exit) channel for which the reactants (products) can pass over the barrier in the effective potential energy]. Near this threshold $L_{i\,max} = 64$ and this condition is fulfilled only in a very small energy range. For reactants in the $M_i = 2$ rotational state, the threshold is 0.3799 eV and the complete statistical calculation fits the curve $\sigma = (26.3\ \text{Å}^2\ \text{eV}^{-5/4})\ E_{ex}^{5/4}$ within 15% up to 0.47 eV. In this range the complete statistical calculation fits the $E_{ex}^{5/4}$ law much better than a linear E_{ex} law. This threshold law, however, predicts a cross section which is 98% higher than the statistical theory calculation at 0.6 eV. Thus, while the experiments are consistent with the statistical theory threshold law up to 0.6 eV, they are not consistent with the full statistical theory in this range. In the range 0.41 - 0.5 eV the statistical calculations can be fit

within 6% by the curve $\sigma = (11.7\ \text{Å}^2\ \text{eV}^{-1})\ E_{ex}$. This curve predicts a cross section 29% higher than the statistical theory calculation at 0.6 eV. Thus one of the disadvantages of the threshold law is that it holds, even within the realm of the statistical model, only for a very small region near threshold (the exact size of the region depends on the molecules and states involved and can be estimated, but only roughly, without doing a full statistical calculation). This problem of a small region of validity[10] or an uncertain region of validity[18, 7, 19] has been a difficulty with other threshold laws in the past.

The statistial theory not only assumes that the various transition probabilities have their mean values (and that these mean values can be predicted by considering only the conservation laws and the amount of phase space available) but also implicitly assumes that we can ignore fluctuations of these transition probabilities about their mean values (this is partly justified theoretically because we consider averaged properties of the collision which depend on large numbers of transition probabilities). However, Moldauer pointed out[20] that the fluctuation of the transition probabilities (henceforth called the width fluctuation effect) may cause a systematic error which is especially important near threshold. Making further assumptions which were known to be reasonable for nuclear physics, he showed that the correction factor for the width fluctuation effect always tends to decrease the cross sections for reactions and increase the cross section for compound elastic scattering. The correction factor approaches 1 (becomes unimportant) when many channels are open. Tucker, Wells and Meyerhof[21] studied inelastic neutron-nucleus scattering within

0.3 MeV of various thresholds for neutron impact energies 0.65 - 2.5 MeV. They found that in this region the width fluctuation correction factor can lower the statistical cross section by 50%. They found much better agreement with experiment when the correction was included. It is unknown how important this type of correction to the statistical theory can be for chemical processes.

The general agreement with experiment for the shape of the cross section curve for the reaction $C^+ + D_2$ is quite significant because the predicted cross section curve does not have the same shape as the Langevin cross section[22] for orbitting collisions in this case. Also the magnitudes of the two curves are different. This is illustrated in Fig. 2, which also shows the predictions for the reaction cross section at higher energies. Although new arrangement channels open for this reaction above 3.3 eV, they were not included in these calculations because there are no experiments in that energy range yet.

A better understanding of the predicted cross section curves can be obtained by studying the probability of reaction as a function of initial orbital angular momentum $L_i\hbar$. Semiclassically this is equivalent to studying the probability of reaction as a function of the impact parameter. For this reaction the reduced mass μ_i in the reactant channel ($C^+ + D_2$) is larger than the reduced mass μ_f in the product channel ($CD^+ + D$). Thus the same orbital angular momentum produces a larger centrifugal barrier for the separating products than for the approaching reactants. Also the reaction endothermicity means there is less energy available in the product channel

than in the reactant one. All reactants with $L_i \geq L_{i_{max}}$ pass over the initial centrifugal barrier and make a strongly coupled collision. However, because of the two facts just mentioned many of these collisions still do not have enough energy to pass over the product channel centrifugal barrier; these systems then decompose entirely into various rovibrational states of $C^+ + D_2$. Table V compares $L_{i_{max}}$ with L_{iF}^{max}, where L_{iF}^{max} is defined as the highest L_i which actually leads to products in arrangement channel F. Reactants incident in partial waves with L_i just a little less than L_{iF}^{max} can form product F only in a few internal states. These are the reasons for the shapes of the curves in Fig. 3a for the probability of reaction as a function of impact parameter. In summary, the statistical theory predicts that $\mu_i > \mu_f$ and/or a large endothermicity leads to the reaction cross section being much less than the collision cross section.[23] For comparison we show a contrasting case ($H + HI \rightarrow H_2 + I$)[24] in Figs. 3b and 3c. This reaction is exothermic and has a higher reduced mass for relative motion for the products than for the reactants. Thus for this reaction the centrifugal barrier which most limits the cross section is in the entrance channel. Another example where the more important centrifugal barrier is in the reactant channel is $CD^+ + D \rightarrow C^+ + D_2$.

Although it may not be necessary for the validity of the statistical theory that a long-lived complex is formed, such a complex leads to one possible way of attempting theoretical justification for the theory. Because CD_2^+ can be held together by strong valence forces, it may be a small system in which such a complex is formed. Usually,

however, it requires many degrees of freedom (hence polyatomic systems are required) for such a complex to be favored. It is an interesting but unsolved question whether such long-lived collisions contribute to the success of the theory shown here. It is also possible that an improved theory would have to take account of these valence forces in the calculational criteria for the occurrence of a strongly coupled collision.

Talrose and Karachevtsev have reviewed some studies of isotope effects in ion-molecule reactions.[25] Klein and Friedman studied intramolecular isotope effects in HDX^+ systems where X is a rare gas atom.[26] They found that at low energies the isotope effect could be explained by a crude collision complex model which included two types of complexes and three adjustable parameters. We have calculated the isotope effect for the reactions

$$C^+ + HD \xrightarrow{4} CD^+ + H$$
$$C^+ + HD \xrightarrow{5} CH^+ + D$$

by using the statistical phase space theory (which contains no adjustable parameters). The predictions are given in Table VI. These numbers can be compared with experiment fairly easily and will provide another test of the theory for a property for which it is expected to work well. The table also gives the predicted ratio of the reaction cross section for $C^+ + HD$ to that for $C^+ + D_2$ when both HD and D_2 are in the $M_i = 2$ rotational state.

CONCLUSIONS

The statistical phase space theory is fairly successful in predicting the magnitude and energy dependence of the cross section for the reaction $C^+ + D_2 \rightarrow CD^+ + D$. This lends further support to the now generally expected reliability[16, 12] of the theory for these properties for simple molecular rearrangement reactions. Further tests for these properties will require further experiments or a more definitive treatment of the triplet state of CD^+. Finally, it is shown that the threshold law is predicted to be valid for an even shorter range than the experiments would have indicated.

Because of the success of theory for the integral cross sections, it would be interesting to see how well the internal energy distributions and the angular differential cross sections can be predicted in this way. A check against experiment of the predictions for product excitation would start to answer the question of whether the statistical reaction cross section is too large because it predicts too much excitation or because it overestimates the total cross section for strongly or moderately strongly coupled collisions. Since the experimental determination of these properties has not yet been made, we did not include the product excitation predictions in this report.

TABLE I. Data

Molecule	D_e(eV)	$r_e(a_0)$	$\omega_e(cm^{-1})$	$\alpha(Å^3)$
D_2	4.7475	1.4011	3118.46	0.7749
$CD^+(^1\Sigma^+)$	4.2774[a]	2.137	2011.3	- -
$CD^+(^3\Pi)$	3.2774	2.23	1650.	- -

[a]A better value can be obtained from F. Jenc, Collection Czech. Chem. Commun. 5, 121 (1963). But see text.

TABLE II. Product labels and degeneracy factors.

F	Parity of M_F	g odd	g even
1	$C^+ + D_2(^1\Sigma_g^+)$	2	4
2	$CD^+(^1\Sigma^+) + D$	2	2
3	$CD^+(^3\Pi) + D$	12	12

TABLE III. Maximum $N(E_T, K, K_Z)$ which occur in some calculations on $C^+ + D_2$.

E_i (eV)	M_i	n_i[a]	max N
0.2	2	1	184
0.5	2	1	764
0.7	2	1	1634
1.2	2	1	5546
2.5	2	1	73276
4.8	2	1	557661
0.8	2	1	2308
0.8	9	1	4630
0.8	2	2	5318
0.8	9	2	10256

[a] n_i is the vibrational quantum number.

TABLE IV. Reaction results at E_i = 0.7 eV.

M_i	$\sigma_2(\text{Å}^2)$	$PCVE_2$	$M_{2\,max}$
0	2.32	6.8	17
1	2.40	7.6	17
2	2.49	9.7	17
3	2.70	12.0	18
4	2.99	15.0	19
5	3.13	17.8	20
10	5.03	37.9	26
300° K*	2.58	9.3	

*The integration over rotational energy Boltzmann factors was done using a 7 pt. generalized Gauss-Laguerre-Radau scheme.

TABLE V. Maximum incident partial waves which lead to strongly coupled complexes and which lead to reactive transitions.

E_1 (eV)	L_{1max}	L_{12max}[a]	L_{13max}[b]
0.20	54	--	--
0.39	64	20	--
0.40	65	24	--
0.50	68	39	--
0.70	75	52	--
1.00	82	62	--
1.50	90	77	41
2.50	103	96	79
3.50	112	109	98
4.80	121	121	115

[a] For formation of CD^+ ($^1\Sigma^+$).

[b] For formation of CD^+ ($^3\Pi$).

TABLE VI. Intramolecular (C^+ + HD) and intermolecular (C^+ + HD, D_2) isotope effects.

E_i (eV)	σ_5/σ_4 [a]	$(\sigma_5+\sigma_4)/\sigma_2$ [b]
0.45	0.565	1.78
0.55	0.802	1.27
0.70	0.826	1.16
0.95	0.893	1.12
1.00	0.917	1.06
1.15	0.927	1.06
1.30	0.932	1.04

[a] $(CH^+)/(CD^+)$ for C^+ + HD.

[b] $\sigma(C^+ + D_2)/\sigma(C^+ + HD)$.

REFERENCES

1. W. B. Maier II, J. Chem. Phys. 46, 4991 (1967).
2. Additional evidence on the electronic states of C^+ beams produced by 26 - 32 eV electron impact is given in R. C. C. Lao, R. W. Rozett, and W. S. Koski, J. Chem. Phys. 49, 4202 (1968).
3. P. Pechukas and J. C. Light, J. Chem. Phys. 42, 3281 (1965).
4. V. L. Talrose, Pure and Applied Chem. 5, 455 (1962), esp. p. 462.
5. M. J. Henchman, Ann. Reports Progress Chem. (London) 62, 39 (1965), esp. p. 50 f.
6. E. Nikitin, Teor. i Eksperim. Khim. 1, 135 (1965). [English transl.: Theor. and Exper. Chem. 1, 831 (1965).]
7. J. D. Morrison, J. Chem. Phys. 40, 2488 (1964).
8. E. P. Wigner, Phys. Rev. 73, 1002 (1948).
9. R. Karplus, in Energy Transfer in Gases, 12th Solvay Conference, edited by R. Stoops (Interscience Publishers, Inc., New York, 1962), pp. 458-460.
10. T. F. O'Malley, Phys. Rev. 150, 14 (1966).
11. P. Pechukas, J. C. Light, and C. Rankin, J. Chem. Phys. 44, 794 (1966). We use the notation of this paper and of Ref. 12 wherever possible.
12. D. G. Truhlar and A. Kuppermann, J. Phys. Chem. 73 (1969).
13. See also F. A. Wolf, J. Chem. Phys. 44, 1619 (1966), esp. Ref. 13.

14. P. L. Moore, Ph. D. thesis, University of Texas (Austin, 1964), esp. p. 80.

15. W. B. Maier II, J. Chem. Phys. (a) 39, 739 (1963); (b) 42, 1790 (1965).

16. See J. C. Light, Discussions Faraday Soc. 44, 14 (1968) for a review of most previous calculations using the statistical theory.

17. See, for example, the delayed onset in the reactions of K with hydrogen halides [D. Beck, E. F. Greene, and J. Ross, J. Chem. Phys. 37, 2895 (1962; M. Ackerman, E. F. Greene, A. L. Moursand, and J. Ross, ibid. 41, 1183 (1964)] and H + H_2 [M. Karplus, R. N. Porter, and R. D. Sharma, J. Chem. Phys. 43, 3259 (1965); 45, 3871 (1966)].

18. E. Baranger and E. Gerjuoy, Phys. Rev. 106, 1182 (1957).

19. C. Lifshitz, Israel J. Chem. 4, 47p (1966).

20. P. Moldauer, Phys. Rev. 123, 968 (1961).

21. A. B. Tucker, J. T. Wells, and W. E. Meyerhof, Phys. Rev. 137, B1181 (1965).

22. G. Gioumousis and D. P. Stevenson, J. Chem. Phys. 29, 294 (1958).

23. The case $\mu_i \gg \mu_f$ was previously singled out by D. R. Herschbach, Adv. Chem. Phys. 10, 319 (1966), p. 350, because it is a case where most of the available angular momentum appear as rotation of the product molecule.

24. The data and methods used for this calculation were the same as in Ref. 12.

25. V. L. Talrose and G. V. Kasachevtsev, Advances in Mass Spectrometry 3, 211 (1966).

26. F. S. Klein and L. Friedman, J. Chem. Phys. 41, 1789 (1964).

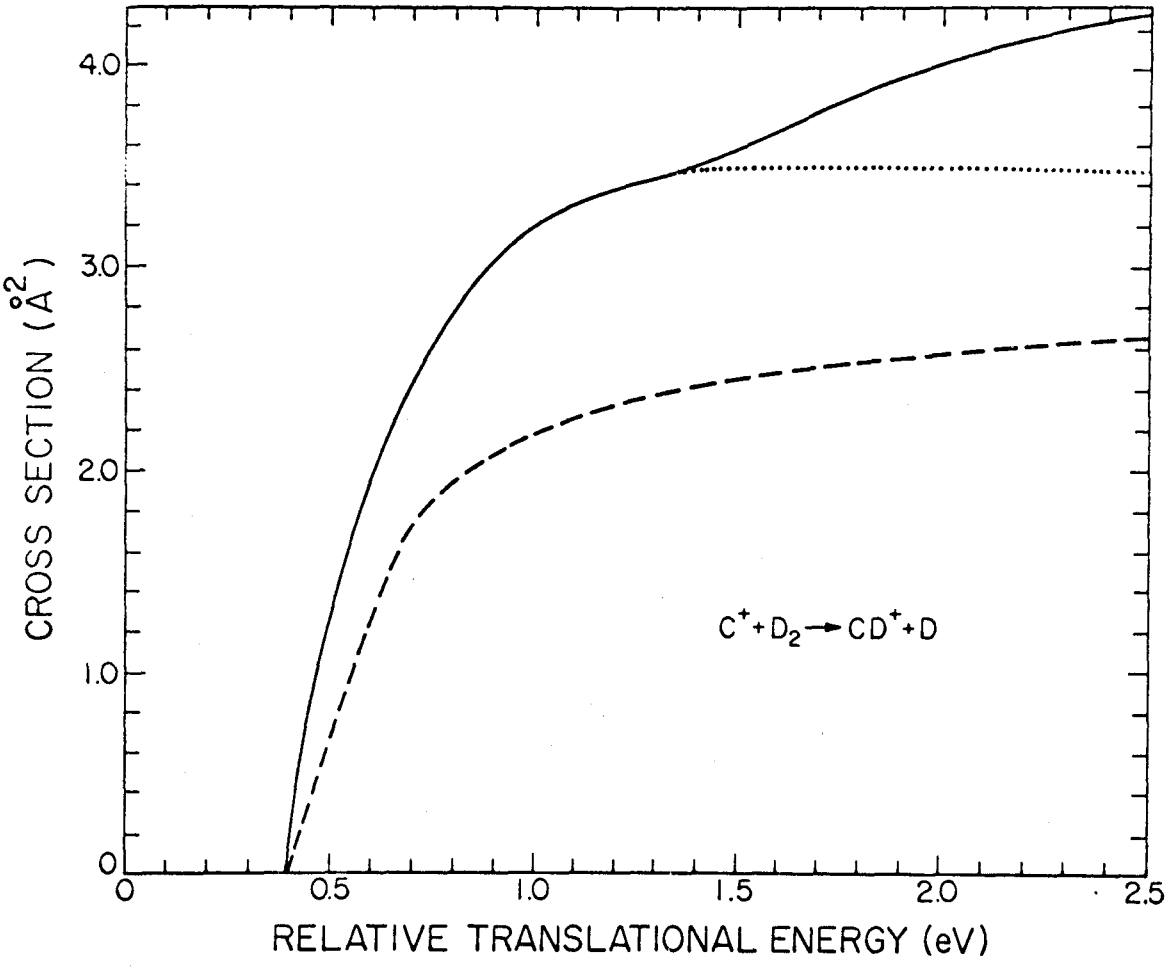

Fig. 1. Cross section for $C^+ + D_2 \rightarrow CD^+ + D$ as a function of the relative kinetic energy of the reactants. Dashed line is the experiment of Maier with a kinetic energy resolution which is probably better than 1%. Solid line is the present calculation (for D_2 in the ground vibrational state and the $M_i = 2$ rotational state). Dotted line is the present calculation when production of the triplet electronically excited state of CD^+ is arbitrarily excluded.

Fig. 2. Reaction cross sections as a function of initial relative kinetic energy. The curve L gives the Langevin cross section (the total cross section for formation of the strongly coupled complex). The other curves are the results of the present statistical phase space calculations when the triplet state formation is and is not included.

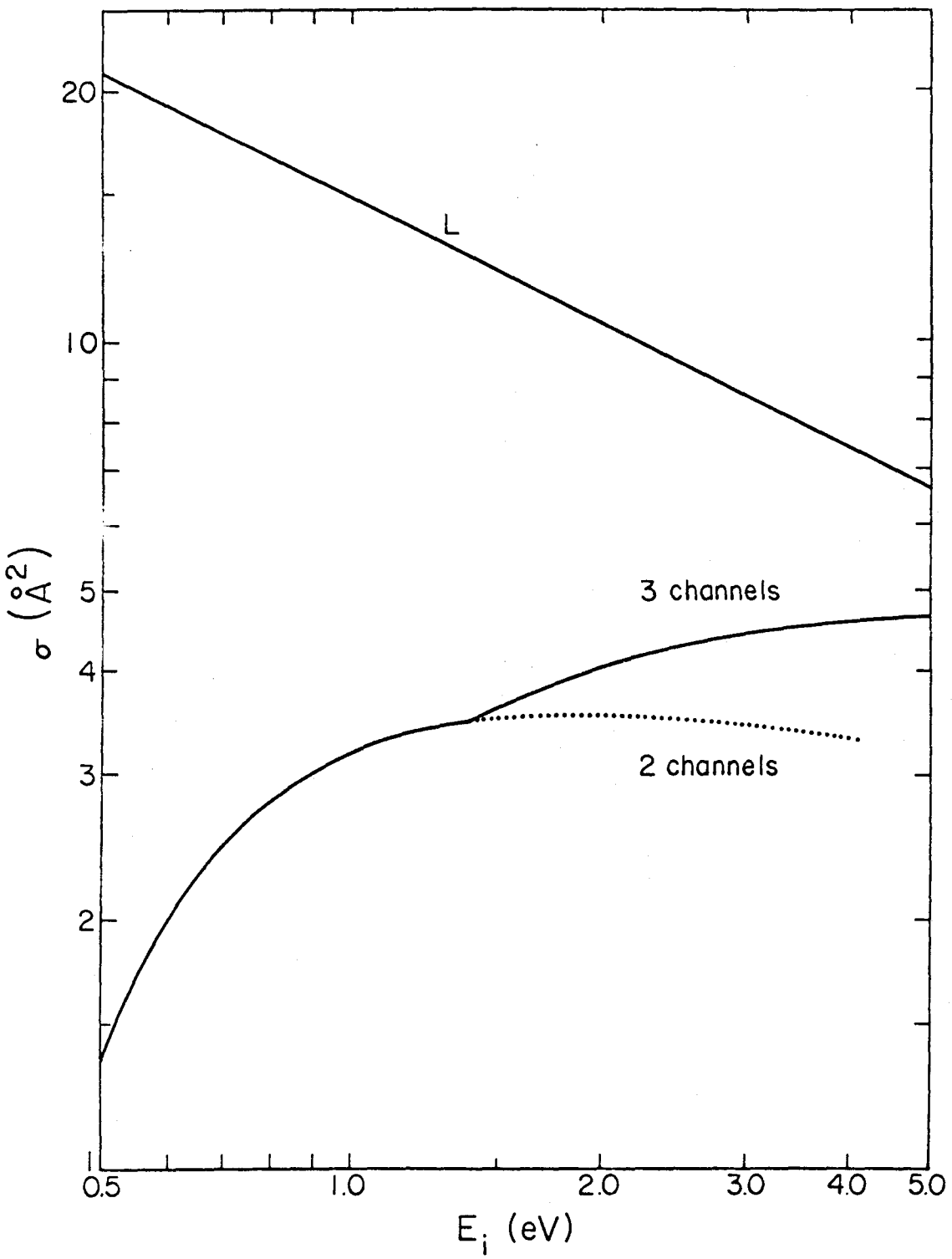

2

Fig. 3. Probability of reaction as a function of initial relative orbital angular momentum in atomic units. For each curve, except the lowest in (a), the incident kinetic energy E_i is given in eV. For the unlabellet curve $D_i = 0.385$ eV. (a) $C^+ + D_2 (M_i = 2) \rightarrow CD^+ + D$. (b) $H + HI$ $(M_i = 2) \rightarrow H_2 + I(^2P_{3/2})$. (c) $H + HI\,(M_i = 2) \rightarrow H_2 + I(^2P_{1/2})$. The two dotted curves have 0.1 added to them so that they can be seen better.

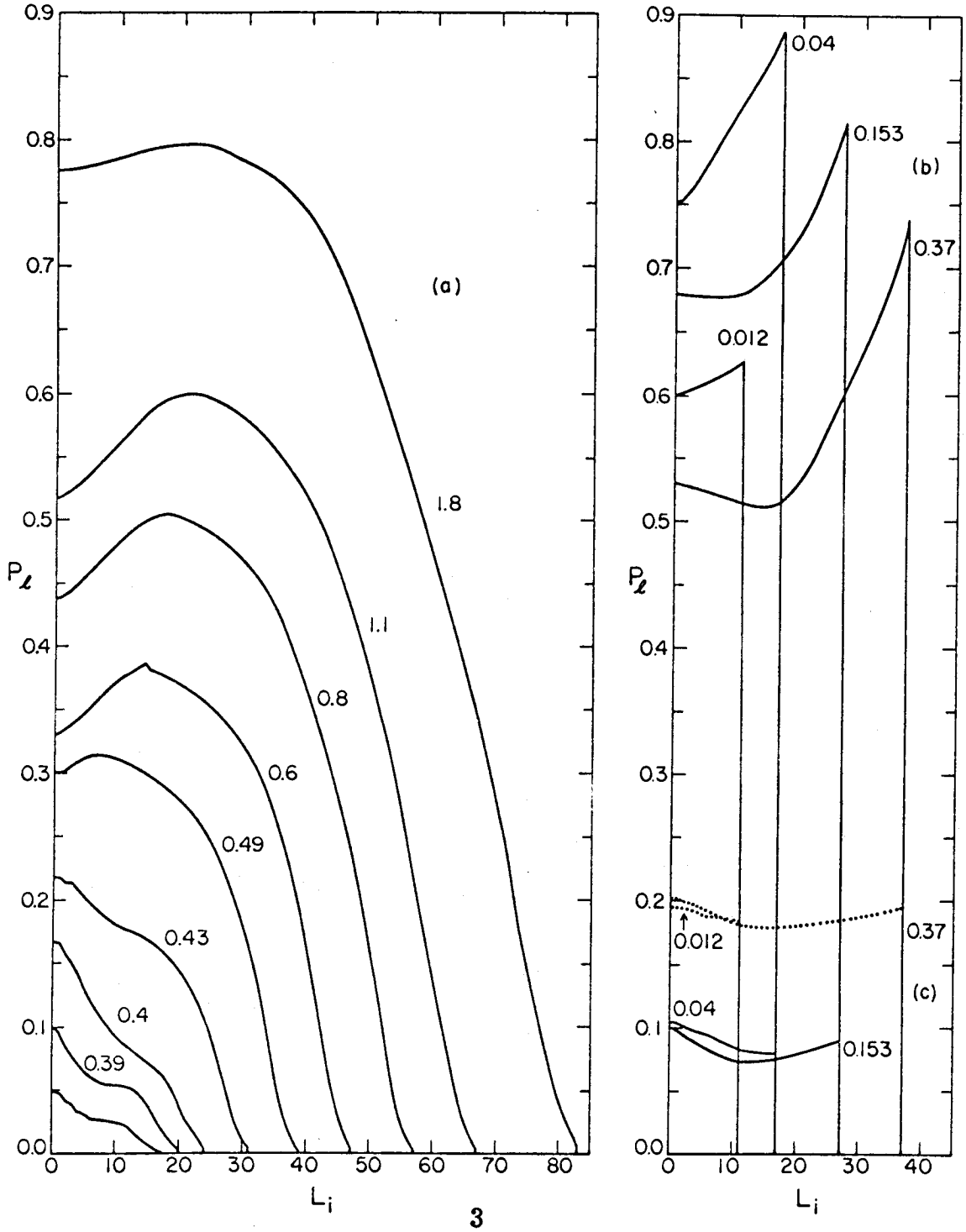
0.9
0.8
0.7
0.6
0.5
0.4
0.3
0.2
0.1
0.0
P_ℓ
(a)
1.8
1.1
0.8
0.6
0.49
0.43
0.4
0.39
0 10 20 30 40 50 60 70 80
L_i
(b)
0.04
0.153
0.37
0.012
(c)
0.012
0.37
0.04
0.153
0 10 20 30 40
L_i

3

PROPOSITION II

Electronically excited atoms and molecules are often produced in flames. Because flames are so complicated, the mechanism is generally known only very incompletely and the particular reactions responsible for producing the electronically excited species are often not known.[1] Nevertheless, the progress that is made in understanding flames and the chemical reactions occurring in them is very exciting and much effort has been spent on understanding the chemical kinetics of flames using spectroscopic and other techniques.[2-9] These studies have had much success.

Chemiluminescent emission from flames of Na and K atoms with inorganic and organic halides has been well studied.[10-24] In many flames with methyl halides such as K + CCl_4, $CHCl_3$, or CBr_4 and Na + CCl_4 a blue emission is seen in the region around 5,000 Å.[21,23] This emission has been identified as being the C_2 Swan bands ($A\,^3\Pi_g \rightarrow X\,^1\Sigma_g^+$) by Palmer and Miller.[22,23] They suggested that electronically excited C_2 is produced by reactions like

$$C + CCl \rightarrow C_2(A\,^3\Pi_g) + Cl \quad . \tag{1}$$

They studied the distribution of intensity coming from the different rovibrational states of electronically excited C_2 and speculated on the dynamics of reaction (1). Reaction (1) was an important part of the mechanism they used to interpret the flame kinetics. This mechanism, for example, gave an indication that disproportionation reactions of the radicals were important in these flames.

While the emission of visible light from flames of alkali metals and metal and organic halides has been studied for a long time (since 1922), it appears that no search has ever been made for infrared chemiluminescence.

Fourgere and Nesbet carried out extensive configuration interaction calculations on the electronic wave functions of C_2.[25] Their results indicate that there are probably six excited states of C_2 that have lower excitation energies than the $A\ ^3\Pi_g$ state. Downward transitions allowed by electric-dipole selection rules from previously unobserved $^1\Sigma_g^+$ and $^1\Delta_g$ states are predicted to lie in the 9,000-12,000 Å spectral region. In addition, the previously observed Ballik-Ramsay and Phillips band systems lie in the 11,600-25,000 Å spectral range. It seems likely that whatever mechanism in the alkali flames with methyl halides is responsible for the production of the $A\ ^3\Pi_g$ upper state of the Swan bands will also produce at least one of the four lower energy upper states of these four electronic transitions. For example, if the reaction C + CCl is really responsible for the production of the Swan bands in the K + CCl_4 system, then we expect it will also lead to C_2 molecules in some of the other lower energy electronically excited states. Observation of infrared chemiluminescence due to any of these electronic transitions would lead to information about the energies of the previously unobserved excited states, the chemical kinetics of the flames, or both. Using modern techniques infrared chemiluminescence has already been observed from chemical reaction products in other systems.[26] It would be interesting to look for it in the flame reactions of sodium and potassium with methyl halides.

REFERENCES

1. See, e.g., A. Fontijn, J. Chem. Phys. 43, 1829 (1965); W. Brennen and T. Carrington, J. Chem. Phys. 46, 7 (1967).
2. M. Polanyi, Atomic Reactions (Williams and Northgate, London, 1932).
3. A. G. Gaydon, Quart. Revs. 4, 1 (1950).
4. K. J. Laidler and K. E. Shuler, Chem. Revs. 48, 153 (1951).
5. K. J. Laidler, The Chemical Kinetics of Excited States (Clarendon Press, Oxford, 1955).
6. A. G. Gaydon, The Spectroscopy of Flames (Chapman and Hall, London, 1957).
7. R. R. Fristrom and A. A. Westenberg, Flame Structure (McGraw-Hill, New York, 1965).
8. Eleventh Symposium (International) on Combustion (The Combustion Institute, Pittsburgh, 1967) and also the other Combustion Symposia.
9. A. G. Gaydon, Dissociation Energies, 3rd Edition (Chapman and Hall, London, 1968), pp. 159ff.
10. F. Haber and W. Zisch, Z. Physik. 9, 302 (1922).
11. R. L. Hasche, M. Polanyi, and E. Vogt, Z. Physik. 41, 583 (1927).
12. M. Polanyi and G. Schay, Z. Physik. 47, 814 (1928).
13. H. Beutler and M. Polanyi, Z. physik. Chem. B1, 1 (1928).
14. S. v. Bogdandy and M. Polanyi, Z. physik. Chem. B1, 28 (1928).
15. H. V. Hartel and M. Polanyi, Z. physik. Chem. B11, 97 (1930).
16. R. A. Ogg, Jr. and M. Polanyi, Trans. Faraday Soc. 31, 1375 (1935).

17. W. Heller and M. Polanyi, Trans. Faraday Soc. 32, 633 (1936).

18. C. E. H. Bawn and R. F. Hunter, Trans. Faraday Soc. 34, 608 (1938).

19. C. E. H. Bawn and W. J. Dunning, Trans. Faraday Soc. 35, 185 (1939).

20. J. N. Haresnape, J. M. Stevels, and E. Warhurst, Trans. Faraday Soc. 36, 465 (1940).

21. E. D. Kaufman and J. F. Reed, J. Phys. Chem. 67, 896 (1963).

22. H. B. Palmer and W. J. Miller, J. Chem. Phys. 40, 3201 (1964).

23. W. J. Miller and H. B. Palmer, J. Chem. Phys. 40, 3701 (1964).

24. D. W. Naegeli and H. B. Palmer, J. Chem. Phys. 48, 2372 (1968).

25. P. F. Fougere and R. K. Nesbet, J. Chem. Phys. 44, 285 (1966).

26. See, e. g., J. K. Cashion and J. C. Polanyi, J. Chem. Phys. 29, 455 (1958); F. D. Findlay and J. C. Polanyi, Can. J. Chem. 42, 2176 (1964); K. G. Anlauf, P. J. Kuntz, D. H. Maylotte, P. D. Pacey, and J. C. Polanyi, Discussions Faraday Soc. 44, 183 (1968).

PROPOSITION III

Considerable work has been done obtaining approximate eigenvalues and eigenfunctions of potentials of the form

$$U = \tfrac{1}{2} kx^2 + bx^4 \quad . \tag{1}$$

Chan, Stelman, and Thompson[1] (CST) have discussed both several attempts to solve the numerical problem and the theoretical basis for expecting mixed harmonic-quartic potential functions to occur in specific cases. It is desirable to have a method of obtaining the eigenvalues of such systems without resorting to lengthy machine calculations. The problem is most easily attacked by considering the quartic term as a perturbation of a harmonic oscillator. Unfortunately it is known[1,2] that perturbation theory fails badly for systems of interest. For example, for $b/k = 0.25$, the energy to the second order is off by 80% for the ground state and of the wrong sign for all other states. CST and Reid[3] were able to obtain accurate solutions but only by a linear variational method involving 20 basis functions. McWeeny and Coulson[4] suggested as a first approximation on a treatment with a single harmonic oscillator basis function including a variable scale factor. The results (for typical cases) are accurate to about 0.5%. Following the observation of CST that the quartic oscillator representation is a more suitable basis system for mixed potentials with moderately large anharmonicities, the present paper considers a treatment based on a single quartic oscillator basis function with a variable scale factor. A simple derivation of the scale factor method is

given. This makes clear the generality of the method and its limitations to problems where the first order perturbation energy is nonzero. Numerical results are presented showing that the analytic solution of a simple cubic equation can often yield energy differences between the levels accurate to better than 0.001%. Further, it is shown that the scale factor method, unlike either conventional perturbation theory or linear variational methods with a small number (5) of basis functions, is accurate for both high levels and large perturbations.

In 1947 Kohn[5] considered the Schröedinger Equation for the Hamiltonian

$$H = T(x) + V(x) + cv(x) \tag{2}$$

where T(x) is the kinetic energy and V(x) and v(x) are potentials (such as electrostatic potentials) with the property

$$U(x/\lambda) = \lambda U(x) \quad . \tag{3}$$

The particular example he chose was the helium atom where the perturbation v(x) is the electron-electron repulsion term. By using the unperturbed wave function with a variable scale factor as a trial function for the perturbed Schröedinger equation, he obtained (by the variational method) a lower bound for the second order perturbation energy in terms of the unperturbed and first order energies. My method is essentially an extension of Kohn's method to the oscillator problem.

Consider the Hamiltonian

$$H = T(x) + V(x) + v(x) \tag{4}$$

where $$T(x) = \frac{-\hbar^2}{2m^2}\frac{\delta^2}{\delta x^2}$$

$$V(x) = ax^4 \tag{5}$$

and $$v(x) = cx^2 \quad .$$

Then $$T(x/\lambda) = \lambda^2 T(x)$$

$$V(x/\lambda) = \lambda^{-4} V(x) \tag{6}$$

and $$v(x/\lambda) = \lambda^{-2} v(x) \quad .$$

Let us take as trial function $\lambda^{\frac{1}{2}}\psi_0(\lambda x)$ where $\psi_0(x)$ is the solution to the unperturbed quartic oscillator. Then the energy is given by

$$\begin{aligned} W &= \int \psi_0^*(\lambda x)H(x)\,\psi_0(\lambda x)\lambda\,dx \\ &= \int \psi_0^*(\lambda x)H(x)\,\psi_0(\lambda x)d(\lambda x) \\ &= \int \psi_0^*(x)H(x/\lambda)\,\psi_0(x)dx \\ &= \lambda^2 \int \psi^*{}_0(x)T(x)\,\psi_0(x)dx \\ &\quad + \lambda^{-4} \int \psi_0^*(x)V(x)\,\psi_0(x)dx \\ &\quad + \lambda^{-2} b \int \psi_0^*(x)v(x)\,\psi_0(x)dx \quad . \end{aligned} \tag{8}$$

Now by the quantum mechanical virial theorem, for the unperturbed problem

$$\langle T \rangle = \tfrac{2}{3} W_n^0 \tag{9}$$

and $$\langle V \rangle = \tfrac{1}{3} W_n^0$$

so that (8) becomes

$$W_n = \tfrac{2}{3}\lambda^2 W_n^0 + \tfrac{1}{3}\lambda^{-4} W_n^0 + c\lambda^{-2}\langle x^2\rangle \tag{10}$$

where $\langle x^2\rangle$ is the first order perturbation energy ϵ_1^Q. Letting $dW/d\lambda = 0$ we obtain

$$\lambda^6 - 3y\lambda^2 - 1 = 0 \tag{11}$$

where $y = c\epsilon_1^Q/2W_n^0$. The cubic can be solved for λ^2, giving one real positive root, which is, for the usual case $y^3 > \frac{1}{4}$,

$$\lambda^2 = 2y \cos(\tfrac{1}{3}\arccos(1/2y^{3/2})) \quad . \tag{12}$$

The energy obtained in this quartic oscillator representation by using equations (10) and (12) is called W^Q. The W_n^0 and ϵ_1^Q are available.[6] The units are equivalent to CST η units with $c = \eta$.

One may also solve the problem of potential (1) by considering the quartic term as a perturbation and taking the trial function as a scaled harmonic oscillator function. One then obtains

$$W_n^H = \tfrac{1}{2}\lambda^2 W_n^0 + \tfrac{1}{2}\lambda^{-2} W_n^0 + \lambda^{-4} b\epsilon_1^H \tag{13}$$

where λ^2 is a solution of

$$\lambda^6 - \lambda^2 - 4b\epsilon_1^H/W_n^0 = 0 \quad . \tag{14}$$

Here the first order perturbation energy ϵ_1^H is the matrix element of x^4 in the harmonic oscillator representation. Convenient units, denoted h, are obtained by taking $\hbar = m = k = 1$ in equations (1) and (5). These units are such that W_n^H has one-fourth the value it has in the CST ξ units,

where $\xi = b$. The calculation of W_n^0 and ϵ_1^H in this representation is a textbook problem.[7] The resulting W_n^H are identical numerically to those obtained by the method of McWeeny and Coulson.

The results of equations (10) and (13) are compared with several other approximate solutions [upper bounds to eigenvalues (UB), lower bounds to eigenvalues (LB), and perturbation theory energies (P1-first order and P2-second order)] in Tables I, II, and III. The values of Reid[3] and his answers (E for exact since his UB and LB are equal to each other to the precision indicated) using twenty basis functions and double precision. He used the partitioning technique of Löwdin.[8] The Bazley-Fox calculations[2] use a five function basis set. Their UB is obtained by the method of intermediate Hamiltonians and their LB by using a five function linear variational scheme in the harmonic oscillator representation. The UB values of CST were obtained using twenty basis functions and a perturbed quartic oscillator representation. Also listed is a LB calculated by Reid using the method described above but limiting himself to a five function basis set and single precision.

Table III is particularly interesting because it compares energy differences--which are the experimental observables. The calculations by the new method are superior to perturbation theory and in many cases also to the McWeeny-Coulson method and a five function variational method. The method works well for large perturbations and excited states. It is felt that the model is accurate enough to be of practical importance for mixed harmonic-quartic potential wells and also for double minimum wells of the type[9]

$$V = -dx^2 + bx^4 \quad .$$

In cases where the energy or eigenfunction is not deemed accurate enough, a basis set composed of these easily calculated scaled functions should be more quickly convergent than the unscaled function set and result in a considerable saving of computer time.

We have emphasized the goodness of the eigenvalues we obtained. The eigenfunction obtained by the method discussed here is probably not as accurate as the eigenvalue.

TABLE I. Approximate energies in units h.

Calculation Type		W^H	Reid E^H	Reid LB^H	Bazley LB^H	Bazley UB^H	CST UB^Q
No. of functions		1	20	5	5	5	20
n	b						
0	0.125	0.5725	0.5710				0.5710
	0.25	0.6240	0.6209	0.5209	0.621	0.621	
	0.50	0.7017	0.6962	0.6961	0.696	0.697	
1	0.125	1.8246	1.8197				1.8197
	0.25	2.0350	2.0260				
	0.50	2.3391	2.3244				
2	0.125	3.2498	3.2504				3.2504
	0.25	3.6965	3.6985	3.6960	3.629	3.700	
	0.50	4.3235	4.3275	4.2765	4.164	4.345	
4	0.125	6.4773	6.4955				6.4955
	0.25	7.5385	7.5684	5.9978	7.277	7.984	
	0.50	8.9838	9.0288	1.6773	8.815	10.871	
7	0.125	12.0208	12.0750				12.0750
	0.25	14.2408	14.323				
	0.50	17.2029	17.32				
9	0.125	16.0847	16.1678				16.1678
	0.25	19.1939	19.32				
	0.50	23.3104	23.4				

TABLE II. Approximate energies in η units.

Calculation Type		W^Q	CST E	W^H	CST $P1^Q$	CST $P2^Q$	CST UB^H
No. of functions		1	20, 40	1	1	1	20
n							
n	c						
0	4.0	4.5899	4.5676	4.5797	4.9706	4.4185	4.5676
	1.5	3.4713	3.4659		3.5340	3.4563	3.4659
1	4.0	14.5898	14.5579	14.5969	15.2994	14.3797	14.5580
	1.5	11.6095	11.6028		11.7214	11.5921	11.6028
2	4.0	25.9640	26.0037	25.9986	26.6906	25.9451	26.0037
	1.5	21.6400	21.6488		21.7509	21.6461	21.6499
3	4.0	38.4872	38.5346	38.4659	39.2349	38.4814	38.5343
	1.5	32.9400	32.9492		33.0524	32.9465	32.9563
4	4.0	51.9103	51.9642	51.8187	52.6708	51.9202	51.9644
	1.5	45.2491	45.2590		45.3624	45.2568	45.2758
5	4.0	66.1140	66.1722	65.9391	66.8835	66.1337	66.1733
	1.5	58.4158	58.4262		58.5296	58.4242	58.4870
6	4.0	81.0114	81.0724	80.7429	81.7873	81.0385	81.0863
	1.5	72.3358	72.3463		72.4500	72.3447	74.0662
7	4.0	96.5370	96.6004	96.1660	97.3182	96.5697	96.6192
	1.5	86.9320	86.9427		87.0404	86.9411	92.3540
8	4.0	112.6392	112.7045	112.1580	113.4245	112.6764	112.8655
	1.5	102.1445	102.1553		102.2592	102.1541	125.0946
9	4.0	129.2760	129.3429	128.6775	130.0647	129.3167	130.0799
	1.5	117.9254	117.9364		118.0402	117.9351	157.8429

TABLE III. Energy differences in η units.

Calculation		W^Q	E	W^H
Transition	c			
0-1	4.0	9.9999	9.9903	10.0172
	1.587401	8.2073	8.2058	8.2523
	1.5	8.1382	8.1369	
1-2	4.0	11.2742	11.4458	11.4016
	1.587401	10.0780	10.0951	10.0008
	1.5	10.0305	10.0460	
2-3	4.0	12.5232	12.5309	12.4674
	1.587401	11.3432	11.3437	11.2447
	1.5	11.3000	11.3004	
3-4	4.0	13.4231	13.4296	13.3528
	1.587401	12.3483	12.3491	12.2418
	1.5	12.3091	12.3098	
4-5	4.0	14.2037	14.2080	14.1204
	1.587401	13.2032	13.199	13.0888
	1.5	13.1667	13.1672	
5-6	4.0	14.8974	14.9002	14.8038
	1.587401	13.9543	13.96	13.8326
	1.5	13.9200	13.9201	
6-7	4.0	15.5256	15.5280	15.4231
	1.587401	14.6288	14.63	14.5003
	1.5	14.5962	14.5964	
7-8	4.0	16.1022	16.1041	15.9919
	1.587401	15.2437	15.2	15.1091
	1.5	15.2125	15.2126	
8-9	4.0	16.6368	16.6384	16.5195
	1.587401	15.8109		15.6705
	1.5	15.7809	15.7811	

Note: These correspond to values of b of 0.125, 0.5, and 0.54433105.

REFERENCES

1. S. I. Chan, D. Stelman, and L. E. Thompson, J. Chem. Phys. 41, 2828 (1964).
2. N. W. Bazley and D. W. Fox, Phys. Rev. 124, 483 (1961).
3. C. E. Reid, J. Chem. Phys. 43, S186 (1965).
4. R. McWeeny and C. A. Coulson, Proc. Cambridge Phil. Soc. 44, 413 (1948).
5. W. Kohn. Phys. Rev. 71, 635 (1947).
6. S. I. Chan and D. Stelman, J. Mol. Spect. 10, 278 (1963).
7. A. M. Shorb, R. Schroeder, and E. R. Lipponcott, J. Chem. Phys. 37, 1043 (1962).
8. P. -O. Löwdin, J. Chem. Phys. 43, S175 (1965).
9. R. L. Somorjai and D. F. Hornig, J. Chem. Phys. 36, 1980 (1962); C. F. Bunge and A. Bunge, J. Chem. Phys. 43, S194 (1965).

PROPOSITION IV*

The ground state of the water molecule has been well studied in quantum chemistry.[1-9] Although some of the excited states were discussed in terms of molecular orbital theory by Mulliken[10] in 1935 and Walsh[3] in 1953, there had been only two ab initio calculations[11-12] on the excited states of the water molecule until the last two years. Quite recently, however, much interest has been directed to the calculation of wave functions for the excited states of this molecule.[13-18] The interest in this problem is further accentuated by the interesting new experimental spectra obtained by the techniques of electron impact spectroscopy.[19-22]

The present work is an examination of how well ab initio LCAO molecular orbital calculations using basis sets appropriate for the ground state can be used to predict the energies and order of the excited states of molecules. Since all the excited states of water are Rydberg states,† we might expect that the description of the wave functions will require the use of expanded basis functions. Thus this is a stiff test for the use of valence-like functions. Hopefully the results, while not completely general, will at least be indicative of the situation which exists for Rydberg states of other polyatomic molecules. Further, it

---

*The calculations reported here were all done in collaboration with Thomas H. Dunning, Jr.

†We use the definition here that if the excited orbital of a state has a principal quantum number n greater than the principal quantum numbers in the united-atom limit of all the orbitals occupied in the ground state, the excited state is a Rydberg state. Other definitions of Rydberg states may be more appropriate in other cases.

has been common for chemists to use simple LCAO molecular orbital theory to visualize almost all low-lying (in energy) excited states of molecules in terms of orbitals of similar spatial extent to the orbitals occupied in the ground state. Two examples follow. Roothaan[23] suggested that excited states could be described acceptably well by using the virtual orbitals arising from a ground state calculation using a minimum basis set of atomic orbitals appropriate to the g round states of the atoms. Walsh[3] interpreted the lowest singlet excitation ($^1B_1$) of water to be an excitation to an antibonding orbital of "intra-valency shell" type. He apparently considered this to be a nonexpanded orbital. Many semiempirical schemes also implicitly assume that the excited state orbitals are not diffuse. For example, in the CNDO/2 method[24] the parameters are chosen so that the calculations agree as well as possible with a priori molecular orbital calculations on the ground states of diatomic molecules. The parameters are thus appropriate for valence orbitals and not for diffuse orbitals. Yet these calculations have been applied to molecular excited states.[25]

It was shown nine years ago that the inclusion of expanded orbitals in the basis set is necessary to obtain even a qualitative description of Rydberg states of diatomic molecules.[26-27] Recently it has been shown that this is also true for polyatomic molecules.[14, 16, 28] The results given here are part of the present evidence for the case of polyatomic molecules.

We have done calculations using excitation operator methods and programs developed previously.[28] All of the molecular integrals

are accurate. The methods have been adequately discussed elsewhere.[23, 28-34] Nevertheless we give a brief review of the methods here:

1. Restricted virtual orbital approximation (RVO).[23, 28] This method is also called the single-transition approximation. The ground state wave function is approximated as the restricted Hartree-Fock single Slater determinant. The wave function for the excited state is constructed by replacing the product of doubly occupied orbitals for electrons (m - 1) and m

$$\phi_i(m-1)\alpha(m-1)\phi_i(m)\beta(m) \tag{1}$$

in the Slater determinant by

$$\left[\phi_i(m\text{-}1)\phi_j(m) \pm \phi_j(m\text{-}1)\phi_i(m)\right]\left[\frac{\alpha(m\text{-}1)\beta(m) \mp \beta(m\text{-}1)\alpha(m)}{\sqrt{2}}\right] \tag{2}$$

where the excitation is from orbital ϕ_i to the virtual orbital ϕ_j from the ground state calculation. In Eq. (2), the upper signs are for the singlet and the lower signs are for the triplet. Since the orbital ϕ_i corresponds physically to an electron moving in field of a neutral molecule instead of a positive ion, the restricted virtual orbital approximation is expected to be very bad.[35, 16, 28]

2. Tamm-Dancoff approximation (TDA).[30, 28] In this method, the ground state is again represented by the Hartree-Fock wave function. The excited state wave functions and energies are those obtained from a configuration interaction calculation which includes all the configurations which can be formed from the ground state wave function by

making single excitations of the kind which are used in the restricted-virtual-orbital approximation. In practice, the configuration interaction Hamiltonian matrix factors into blocks corresponding to different symmetries of the excited state. Since solution of the configuration interaction problem is a linear variational method, the Tamm-Dancoff approximation is a variational one.

3. The random-phase approximation (RPA).[29,28] In this method the ground state is represented by a superposition of configurations including the Hartree-Fock wave function and configurations obtained from the Hartree-Fock wave function by double excitations. The excited state wave function is represented by a superposition of configurations which includes single excitations and single deexcitations from the ground state. The determination of the coefficients in these wave functions is not done variationally but by a series of approximations. This method has its origins in the theory of an infinite electron gas and in solid-state and nuclear physics.

In addition to these methods used here we compare our results with results from some other methods:

4. Improved-virtual-orbital approximation (IVO).[16,28] This is also called the improved single-transition-approximation. It corresponds to including in the Tamm-Dancoff approximation only those configurations which correspond to excitation from any one orbital. It also corresponds to using the Hartree-Fock ground state and obtaining the excited state by solving the Hartree-Fock self-consistent-field equation for the excited orbital in the field of the core orbitals (the

core orbitals are the orbitals in the ground state wave function which are unchanged upon excitation).

5. Hartree-Fock self-consistent-field approximation (HF).[36] In this method, the wave functions for the ground and excited states are obtained by separate Hartree-Fock calculations. This method, when compared to the improved-virtual-orbital approximation, allows for relaxation of the core. Since the correlation energy (defined here as the difference between the Hartree-Fock energy and the real energy) is expected to be less for the excited state than for the ground state, the self-consistent-field approximation is expected to yield excitation energies too low. If the neglect of core relaxation in the improved-virtual-orbital approximation gives a cancellation of errors, the improved-virtual-orbital approximation will be in better agreement with experiment than the self-consistent-field approximation.

Three basis sets were used:

a. Minimum basis set with Slater values for the exponents. The calculations with this basis set were carried out for a geometry with an O-H distance of 1.8103 a_0 and an H-O-H angle of 105°. It gives a ground state Hartree-Fock energy of -75.65559 a.u.

b. Optimized minimum basis set. The calculations with this basis set were carried out for the same geometry as for basis set a. The basis set is optimized for the ground state Hartree-Fock wave function and gives a ground state energy of -75.70313 a.u. in the Hartree-Fock approximation.

c. Almost double zeta basis set. The calculations with this

basis set are for a geometry with an O-H distance of 1.8111 a_0 and a bond angle of 104° 27′. This basis set was created by dropping the d functions in basis set III of Aung, Pitzer, and Chan.[8] It lacks a second 1s function on the oxygen atom from being a double zeta basis set. It is a very good basis set for the ground state, for which it gives a Hartree-Fock energy of -75.95800 a.u.

The results of the calculations for the excitation energies of the predicted lowest two states of each symmetry are given in Table I. The calculated excitation energies are all too high. The excitation energies for the minimum basis set with exponents optimized for the ground state are higher than those for the set with Slater exponents. The Slater exponents are a more reasonable basis to use for excitation energy calculations since they are not optimum for either state. The minimum basis set has only two virtual orbitals. The use of a bigger basis set allows more freedom to the excited state orbital and allows more configurations to interact to lower the excited state energy. The results in Table I for the larger basis set, however, indicate that this basis set, which is a valence set appropriate for the molecular ground state, improves the ground and excited states to about the same extent from the optimized minimum basis set and does not remove the error of using a basis set optimized for the ground state. (The conclusions drawn here are similar to those of Lefebvre-Brion, Moser, and Nesbet[26,27] who found they could not use valence-like double zeta basis sets for Rydberg excited states of diatomic molecules.) Based on these conclusions, we will consider further only the results with the unoptimized basis set a. Because Table I shows that the random-phase

approximation does not give significant improvement over the Tamm-Dancoff approximation, we will not consider it further.

Table II compares the results of the present calculations using basis set a to the calculations of Hunt and Goddard,[16] Hunt, Goddard, and Dunning,[17] and Segal and Claydon[18] and to some experimental results. The authors of references 16 and 17 used Gaussian type functions (GTF's) and arrived at their basis sets by adding expanded orbitals to good ground state basis sets. In each case they added at least one GTF with an exponent less than 0.004. The calculations in the restricted-virtual-orbital approximation are hard to interpret because this method is so crude (see above); the restricted-virtual-orbital approximation will not be discussed further. The improved-virtual-orbital calculations of Ref. 16 are in much better agreement with experiment if the comparison is made of stabilities instead of excitation energies.[16] However, we are not interested here in that aspect of their results. Since Hunt and Goddard's basis set is much more appropriate for the description of the excited states of water, their calculations are more appropriate for interpreting the observed spectra. We will limit ourselves here to an examination of the errors caused by the use of a minimum basis set. This is a test of the model of the excited states of water as nonexpanded (or valence-like) states.

We compare the Hunt-Goddard calculations in the improved-virtual-orbital approximation with the present results in the Tamm-Dancoff approximation. The first conclusion is that the present calculations, because of the small valence-like basis set, are not at all appropriate for the description of excited states which are not the lowest

state of that symmetry. This was entirely expected. The second conclusion is that the present results are much more appropriate for the triplets than for the singlets. The triplets which are the lowest states of their symmetry seem to be described approximately correctly. The error due to not having expanded orbitals in the basis set appears to be a few tenths of an eV. It is difficult to be quantitative about this because of the sensitivity of the results to the exponents in this small basis set. It is possible that the Slater values of the exponents are accidently better for the excited triplet states than for the ground states and that this makes the excitation energies fortuitously accurate. The actual excited state energies from the Hunt-Goddard calculation are much lower than those from the present calculation. The present calculations give excitation energies about $1\frac{1}{2}$ eV too high for the excited singlet states. [Hunt and Goddard did find (private communication) that the excited singlet states are more expanded than the excited triplet states. This is expected because the exchange integral K_{ij} makes the effective potential for the excited orbital more attractive in the triplet state than in the singlet state.] The present calculations appear to have only minimal use in predicting even the qualitative aspects of the H_2O excited state spectrum.

The conclusion that the minimum basis set calculation is not a qualitatively correct treatment of the excited states of polyatomic molecules means that many of Walsh's arguments[3, 37] and similar arguments about the spectra of small molecules are untrustworthy. While this could also have been concluded from the work of Hunt, Goddard,[16] and Dunning,[28] more calculations are needed to provide

adequate descriptions of the excited states of molecules and to properly classify the excited states and systematize their interpretation.

It had been argued that the antibonding valence-like orbitals of molecules such as methane and ammonia have nodal properties and spatial extent similar to the diffuse Rydberg orbitals of the central atom.[38] Our conclusion is that these antibonding orbitals are not diffuse enough.

Finally we conclude that the semiempirical calculations such as CNDO/2, which use nonexpanded orbitals, must be interpreted in terms of the empirical nature of the energy quantities which enter the calculations rather than in terms of the orbitals.

The author is grateful to Dr. Thomas H. Dunning, Jr. for his collaboration on this project and to Dr. Sandor Trajmar for stimulating his interest in the excited states of the water molecule. The author and Dr. Dunning are grateful to Professor Russell M. Pitzer, Professor William E. Palke, Dr. Soe Aung, Professor Sunney I. Chan, Professor William A. Goddard III, and Mr. C. Woodrow Wilson for use of their integral values or programs and for advice on various aspects of the calculations. The author is grateful to Mr. Steve L. Guberman, Mr. William J. Hunt, Professor Goddard, Professor Gerald A. Segal, and Dr. Charles R. Claydon for discussions of their calculations on the water molecule and excited states of other molecules.

TABLE I. Virtual excitation energies (eV) of the water molecule.

Basis Set	a	a	a	b	b	b	c	c	c
Method	RVO	TDA	RPA	RVO	TDA	RPA	RVO	TDA	RPA
State									
$^3B_1$	8.15	8.15	8.08	11.71	11.71	11.67	12.42	12.15	12.02
							48.47	47.89	47.68
$^1B_1$	10.29	10.29	10.24	13.76	13.76	13.76	13.99	13.78	13.70
							50.47	50.31	50.24
$^3A_1$	10.10	9.40	8.45	14.39	13.87	13.36	14.41	13.75	---
	14.12	14.32	13.77	20.36	20.28	19.89	18.79	18.49	---
$^1A_1$	13.09	12.48	12.39	17.99	17.22	17.12	16.96	16.20	---
	23.19	23.56	22.82	28.58	29.01	28.42	25.96	25.25	---
$^3A_2$	10.33	10.33	10.31	14.26	14.26	14.24	14.33	14.04	13.93
							58.51	58.35	58.17
$^1A_2$	11.56	11.56	11.54	15.52	15.52	15.51	15.21	14.97	14.90
							59.32	59.31	59.21
$^3B_2$	11.35	10.35	9.50	16.29	15.51	14.97	---	---	---
	12.82	13.43	13.31	17.97	18.38	18.26	---	---	---
$^1B_2$	15.64	14.90	14.82	20.02	19.47	19.41	---	---	---
	16.96	17.66	17.44	21.94	22.44	22.33	---	---	---

TABLE II. Experimental and theoretical excitation energies (eV) for water. All the calculations except those from Ref. 18 are based on accurate evaluation of the integrals. The calculations of Ref. 18 approximated the integrals using the CNDO/2 method.

Reference	Present	16	Present	16	18	17	
Method	RVO	RVO	TDA	IVO*	HF	HF	Experiment
State							
$^3B_1$	8.15	11.70	8.15	7.88 (3s) 11.24 (3p)	6.20	--	--
$^1B_1$	10.29	11.71	10.29	8.53 (3s) 11.32 (3p)	7.43	-- --	7.50 10.00
$^3A_1$	10.10 14.12	13.35 12.64	9.40 14.32	9.82 (3s) 11.01 (3p)	8.67	8.12	-- --
$^1A_1$	13.09 23.19	13.37 12.65	12.48 23.56	10.75 (3s) 11.42 (3p)	10.85	8.75	9.75 10.16
$^3A_2$	10.33	12.48	10.33	9.98 (3p)	7.49	--	--
$^1A_2$	11.56	12.48	11.56	10.35 (3p)	8.03	--	--
$^3B_2$	11.35	--	10.35	--	9.43	--	--
$^1B_2$	15.64	--	14.90	--	11.06	--	--

*These authors classified their improved virtual orbitals as ns-like or np-like. Their classification is included in parentheses. The classification applies approximately to the whole row in this table.

REFERENCES

1. L. Pauling, J. Amer. Chem. Soc. 53, 1367 (1931); J. C. Slater, Phys. Rev. 37, 481 (1931); 38, 1109 (1931); F. Hund, Z. Physik 73, 565 (1932).
2. R. S. Mulliken, J. Chem. Phys. 3, 506 (1935).
3. A. D. Walsh, J. Chem. Soc. 1953, 2260 (1953).
4. L. Pauling, The Nature of the Chemical Bond, 3rd Edition (Cornell University Press, Ithaca, N. Y., 1960), Sections 3-5 and 4-3; M. W. Hanna, Quantum Mechanics in Chemistry (W. A. Benjamin, New York, 1965), pp. 181-183; R. Dandel, Electronic Structure of Molecules (Pergamon Press, Oxford, 1966), Chapter VI; and other textbooks.
5. J. C. Slater, Quantum Theory of Molecules and Solids: Electronic Structure of Molecules (McGraw-Hill Book Co., New York, 1963), pp. 221-226.
6. M. Krauss, "Compendium of ab initio Calculations of Molecular Energies and Properties," Technical Note 438, National Bureau of Standards (1967).
7. D. Neumann and J. W. Moskowitz, J. Chem. Phys. 49, 2056 (1968).
8. S. Aung, R. M. Pitzer, and S. I. Chan, J. Chem. Phys. 49, 2071 (1968).
9. R. M. Pitzer and D. P. Merrifield, "Minimum Basis Set Wave Functions for Water," preprint.
10. R. S. Mulliken, J. Chem. Phys. 3, 506 (1935).

11. F. O. Ellison and H. Shull, J. Chem. Phys. 23, 2348 (1955).

12. S. R. LaPaglia, J. Chem. Phys. 41, 1427 (1964).

13. Y. Harada and J. N. Murrell, Mol. Phys. 14, 1531 (1968).

14. T. F. Lin and A. B. F. Duncan, J. Chem. Phys. 48, 866 (1968).

15. J. A. Horsley and W. H. Fink, J. Chem. Phys. 50, 750 (1969).

16. W. J. Hunt and W. A. Goddard, Chem. Phys. Letters 3, 414 (1969).

17. W. J. Hunt, T. H. Dunning, and W. A. Goddard, Chem. Phys. Letters 3, 606 (1969).

18. G. A. Segal and C. F. Claydon, unpublished.

19. G. J. Schulz, J. Chem. Phys. 33, 1661 (1960).

20. R. N. Compton, R. H. Huebner, P. W. Reinhardt, and L. G. Christophorou, J. Chem. Phys. 48, 901 (1968).

21. A. Skerbele, M. A. Dillon, and E. N. Lassettre, J. Chem. Phys. 49, 5042 (1968).

22. S. Trajmar, unpublished.

23. C. C. J. Roothaan, Rev. Mod. Phys. 23, 69 (1951).

24. J. A. Pople and G. A. Segal, J. Chem. Phys. 44, 3289 (1966).

25. A review is H. H. Jaffe, Accounts Chem. Res. 2, 136 (1969).

26. H. Lefebvre-Brion, C. M. Moser, and R. K. Nesbet, J. Chem. Phys. 33, 931 (1960).

27. H. Lefebvre-Brion, C. M. Moser, and R. K. Nesbet, J. Chem. Phys. 35, 1702 (1961); J. Mol. Spectry. 13, 418 (1964).

28. T. H. Dunning, Ph. D. Thesis, California Institute of Technology (Pasadena, 1970).

29. P. L. Altick and A. E. Glassgold, Phys. Rev. 133, 632 (1964).

30. A. Herzenberg, D. Sherrington, and M. Suveges, Proc. Phys. Soc. (London) 84, 465 (1964).

31. T. H. Dunning and V. McKoy, J. Chem. Phys. 47, 1735 (1967).

32. T. H. Dunning and V. McKoy, J. Chem. Phys. 48, 5263 (1968).

33. R. K. Nesbet, J. Math. Phys. 6, 621 (1965).

34. H. Gutfreund and W. A. Little, Phys. Rev. 183, 68 (1969).

35. R. K. Nesbet, J. Chem. Phys. 43, 4403 (1965).

36. C. C. J. Roothaan, Rev. Mod. Phys. 32, 179 (1960); and other papers on open-shell Hartree-Fock theory.

37. A. D. Walsh, J. Chem. Soc. 1953, 2266 (1953), and following papers.

38. R. S. Mulliken, J. Amer. Chem. Soc. 86, 3183 (1964).

PROPOSITION V

The first scattering problem in molecular physics for which an essentially exact numerical solution was obtained was the linear collision of an atom A with a diatomic vibrator BC for the case where the atom interacts with the vibrator according to a hard sphere potential.[1] We will consider this problem.

We consider a case considered by Riley[2] in reduced coordinates x and y and reduced units. The reduced units and their interpretation in terms of a linear atom-diatomic molecule collision are discussed elsewhere.[2,3] The Schröedinger equation is[2]

$$[H_0(y) - \frac{\partial^2}{\partial x^2} + V_I^{HS}(x,y) - E]\ \Psi_i(x,y) = 0 \qquad (1)$$

where i labels the degenerate solutions, $H_0(y)$ is the internal Hamiltonian of the diatomic molecule in reduced units,

$$V_I^{HS}(x,y) = \begin{cases} 0 & x > y \\ \infty & x \leq y \end{cases} \qquad (2)$$

is a hard sphere interaction between A and B and E is the total energy. The diatomic molecule potential is a square well (of width π in reduced units) with the orthogonal eigenfunctions $\varphi_n(y)$. The boundary conditions on the wave function are

$$\Psi_i(y,y) = 0 \qquad (3)$$

$$\Psi_i(x,y) = e^{-ik_i x}\varphi_i(y) + \sum_{n=1}^{\infty} D_{ni}\, e^{ik_n x}\varphi_n(y) \qquad x \geq y \qquad (4)$$

where the D_{ni} are as yet undetermined and

$$H_0(y)\varphi_n(y) = n^2 \varphi_n(y) \tag{5}$$

$$k_n = \sqrt{(E - n^2)} \tag{6}$$

for $n = 1, 2, \ldots$ and the probability of scattering from the state i to the state f is

$$P_{if} = \frac{k_f}{k_i} |D_{ni}|^2 \qquad n = 1, 2, \ldots, N \tag{7}$$

The number of open channels is M where M is the highest n for which the radicand in (6) is positive. To obtain the scattering probabilities we must solve for the upper left $M \times M$ subblock of the D matrix. The Shuler-Zwanzig method of solving for D is to approximate Ψ_i by

$$\Psi_i^N = e^{-ik_i x} \varphi_i(y) + \sum_{n=1}^{N} D_{ni} e^{ik_n x} \varphi_n(y) \tag{8}$$

where $N > M$ and to obtain N equations for the D_{ni}, $i = 1, 2, \ldots, N$ by requiring Eq. (3) to be true for the approximate scattering solution in the space spanned by $\{\varphi_j | j = 1, 2, \ldots, N\}$, i.e.,

$$\langle \varphi_j(y) | \Psi_i^N(y, y) \rangle = 0 \qquad j = 1, 2, \ldots, N \tag{9}$$

Equation (9) for all j is equivalent to the $N \times N$ matrix equation[2]

$$\underset{\sim}{U}\,\underset{\sim}{D} = -\underset{\sim}{U}^* \tag{10}$$

where

$$U_{jn} = \langle \varphi_j(y) | e^{ik_n x} \varphi_n(y) \rangle \quad . \tag{11}$$

Schuler and Zwanzig[1] applied their method to the collision of an atom and a diatomic molecule with a harmonic potential. They considered cases $M \leqslant 4$ and used $9 \leqslant N \leqslant 21$. They were able to obtain accurate scattering probabilities this way but for $N > 21$ they had computer overflow. This meant they could not go to higher energies where $N > 21$ would be required for accurate solutions. Grimaldi, Endres, and Wilson[4] applied the method to the collision of an atom with a triatomic molecule with nearest-neighbor harmonic-potential atom-atom interactions. They included 25 to 49 terms in the sum of reflected waves and exponentially decreasing virtual solutions in their approximate wave function corresponding to Eq. (8), and they considered cases with up to 11 open channels. They found that their matrix corresponding to $\underset{\sim}{U}$ was often ill-conditioned* so that the results depended sensitively on round-off errors even for double precision arithmetic. In some cases they could not obtain even approximately accurate results. They found that the possible accuracy depended on the atomic mass ratios and the vibration frequencies. Endres[5] applied the method to the collision of an atom with a diatomic Morse oscillator. He considered cases with $M \leqslant 5$ and used $N = 15$ for his published results. He checked that these were accurate by varying N

*An ill-conditioned matrix is one that is hard to invert numerically.

to prove the results had converged. His accuracy was limited by inaccuracies in computing the U_{jn} rather than by lack of convergence or by inversion problems. Diestler and McKoy[6] applied the method to the collision of a diatomic harmonic oscillator with another diatomic harmonic oscillator. They found upon increasing the number of terms in their approximate wave function that numerical instability set in before the scattering probabilities converged. Grimaldi, Endres, and Wilson[7] considered the same problem. They had no problems with ill-conditioned matrices, convergence, or instability. They considered cases with $M \leq 13$ and obtained accurate results with 37 to 50 terms in their approximate scattering wave function. Riley[2] applied the method to the collision of an atom and a diatomic molecule with an infinite square well binding potential (the case considered here). He found $\underset{\sim}{U}$ could seldom be inverted for $N > 11$. He obtained accurate results by extrapolating the results computed for different N to $(1/N) = 0$. At least two other attempts[8, 9] to use the Shuler-Zwanzig method had led to severe problems due to ill-conditioned matrices. In summary, the biggest difficulties in the Shuler-Zwanzig procedure seem to be that the matrix $\underset{\sim}{U}$ is ill-conditioned and that the scattering probabilities converge to the exact results only slowly as $N \to \infty$. However, these difficulties are not fully understood.

Secrest and Johnson[3] and Riley[2, 2a] have obtained accurate solutions for the atom-diatomic vibrator collision problem by methods which are equivalent to solving the close coupling equations. Riley[2] found for the case considered here that for a given number N of

states included in the approximate wave function the close coupling method was more accurate than the Shuler-Zwanzig method. Nevertheless, there are reasons for continuing to study the Shuler-Zwanzig method. First, Riley[2] found that it was three times faster in computer time than the close coupling method in his calculations. Second, the procedure of projection used in Eq. (9) is a general one which can be used in many problems and it is important to understand the sources of the difficulties it engenders.

There is simplicity to recommend the Shuler-Zwanzig procedure of obtaining N conditions on the approximate scattering wave function Ψ_i^N by requiring it to satisfy Eq. (3) in the space spanned by the lowest N eigenfunctions of the vibrator. Since this leads to ill-conditioned equations, we tested the effect of varying the weight with which each of the N conditions enters in the determination of the D matrix. Thus we replaced Eq. (9) by

$$\langle \varphi_j(y)[H_0(y) - E] \,|\, \Psi_i^N(y,y)\rangle = 0 \qquad j = 1, 2, \ldots, N \tag{12}$$

which leads to

$$\underset{\sim}{U}^H \underset{\sim}{D} = -\underset{\sim}{U}^{H*} \tag{13}$$

in analogy with Eq. (10). The quantity $[H_0(y) - E]$ is a weighting function w_j. This procedure was programmed using single precision arithmetic on the IBM 7094. Particular attention was paid to arranging the computations to minimize round-off error. The system (13) was solved by Gaussian elimination with row interchanges. For $N > 12$ we could not obtain accurate solutions. A study of the matrix $\underset{\sim}{U}^H$

convinced us that this inaccuracy was due to $\underset{\sim}{U}^{H}$'s ill-conditioning for high N. For $N \leq 11$ our results were similar to those obtained by Riley using the Shuler-Zwanzig procedure. We feel that this procedure deserves further study and that a weighting function which puts more weight in the higher j equations in Eq. (12) will lead to better conditioned matrices. However, these weighting functions may be less appropriate physically than the Shuler-Zwanzig functions $w_j = 1$. Thus the probabilities might be less accurate for a given N. This should be tested.

A second suggestion is to use the approximate wave function Ψ_i^N and obtain the N equations for the D_{ni} by the delta function projector in

$$\left\langle \frac{2}{\pi} \delta\left(y - \frac{j}{N+1}\pi\right) \middle| \Psi_i^N \right\rangle \qquad j = 1, 2, \ldots, N \quad . \tag{14}$$

A test of this method showed the equations were much better conditioned but that their solution did not yield very accurate scattering probabilities. This method should be studied further.

To understand the difficulties in these methods, it is suggested we plot $\Psi_i^N(y, y)$ as a function of y and see how big the errors are, where this function is large, and whether it oscillates rapidly. Then we can choose a new set of basis functions $\varphi_j'(y)$ which are most well suited to minimizing $\max_{0 \leq y \leq \pi} \Psi_i^N(y, y)$. The trial function will then be

$$\Psi_i^{N, N'} = e^{-ik_i x} \varphi_i(y) + \sum_{j=1}^{N} e^{ik_j x} \varphi_j(y) + \sum_{j=N+1}^{N'} e^{-|k_j| x} \tilde{\varphi}_j(y) \tag{15}$$

where $N > M$. The $\tilde{\varphi}_j(y)$ are orthogonal to $\{\varphi_j(y) | j = 1, 2, \ldots, N\}$ and are obtained from the $\varphi'_j(y)$ by (i) orthogonalizing the $\varphi'_j(y)$ to $\{\varphi_j(y) | j = 1, 2, \ldots, N\}$ and (ii) diagonalizing the matrix representation of H_0 for these orthogonalized functions. Then

$$H_0(y)\tilde{\varphi}_j(y) = W_j \tilde{\varphi}_j(y) \tag{16}$$

and

$$k_j = \sqrt{(E - W_j)} \tag{17}$$

In this way we utilize our freedom to represent the closed channels in the most efficient possible way. The $\varphi_j(y)$ have the form $\sin jy$. An example of the type of functions which might be useful as basis functions are functions which are nonzero over only a finite range of y which is smaller than $0 \leq y \leq \pi$, e.g., spline functions or bell-shaped functions. Another example is

$$\varphi'_j(y) = (\tfrac{1}{2}\pi)^{2p} - (y - \tfrac{1}{2}\pi)^{2p} \tag{18}$$

where p is an integer. It may be necessary to include functions with high W_n in order to get a good representation of the end effects (the end is where x is just a little longer than y) in the wave function. These end effects could be important because of the nature of the hard sphere interaction. Once we have chosen the N'-parameter trial function $\Psi_i^{N, N'}$, we can obtain N' conditions by

$$\langle \varphi_j^P(y) w_j(y) | \Psi_i^{N, N'}(y, y) \rangle = 0 \qquad j = 1, 2, \ldots, N' \tag{19}$$

where the $\varphi_j^P(y)$ may be the N functions $\varphi_j(y)$ and the $(N'-N)$ functions $\tilde{\varphi}_j(y)$ and the w_j may be 1 or the $\varphi_j^P(y)$ and $w_j(y)$ may be chosen in any of the other ways suggested above. Hopefully these generalized trial functions will increase the convergence as N increases with fixed $(N'-N)$ or as N' increases with fixed N.

The author is grateful to Dr. Dennis J. Diestler for stimulating discussions.

REFERENCES

1. K. E. Shuler and R. Zwanzig, J. Chem. Phys. 33, 1778 (1960).
2. M. E. Riley, Ph. D. Thesis, California Institute of Technology (Pasadena, 1968), pp. 104-112, (a.) pp. 112-114.
3. D. Secrest and B. R. Johnson, J. Chem. Phys. 45, 4556 (1966).
4. J. J. Grimaldi, P. F. Endres, and D. J. Wilson, J. Chem. Phys. 50, 1627 (1969).
5. P. F. Endres, J. Chem. Phys. 51, 477 (1969).
6. D. J. Diestler and V. McKoy, J. Chem. Phys. 48, 2941 (1968).
7. J. J. Grimaldi, P. F. Endres, and D. J. Wilson, J. Chem. Phys. 51, 611 (1969).
8. M. E. Riley and A. Kuppermann, unpublished.
9. D. J. Diestler, unpublished.